

N O T I C E

THIS DOCUMENT HAS BEEN REPRODUCED FROM
MICROFICHE. ALTHOUGH IT IS RECOGNIZED THAT
CERTAIN PORTIONS ARE ILLEGIBLE, IT IS BEING RELEASED
IN THE INTEREST OF MAKING AVAILABLE AS MUCH
INFORMATION AS POSSIBLE

NI

AGT-102 Automotive Gas Turbine

Summary Report

Chrysler Corporation Advance Powerplant Engineering
and
Williams Research Corporation

(NASA-CR-165353) AGT-102 AUTOMOTIVE GAS
TURBINE Summary Report (Chrysler Corp.)
434 p HC A19/MF A01

June, 1981

CSCL 13I

N82-12444

Prepared for
National Aeronautics and Space Administration
Lewis Research Center
Cleveland, Ohio 44135
Under Contract DE-AC02-76-CS 52749

Unclas
G3/37 08331

for
U. S. Department of Energy
Conservation and Solar Energy
Office of Transportation Programs



DOE/NASA/2749-81/1
NASA CR-165353

AGT-102

Automotive Gas Turbine

Summary Report

Chrysler Corporation Advance Powerplant Engineering
and
Williams Research Corporation

June, 1981

Prepared for
National Aeronautics and Space Administration
Lewis Research Center
Cleveland, Ohio 44135
Under Contract DE-AC02-76-CS 52749

for
U. S. Department of Energy
Conservation and Solar Energy,
Office of Transportation Programs

TABLE OF CONTENTS

<u>Section</u>	<u>Title</u>	<u>Page</u>
1.0	FOREWORD	1
2.0	SUMMARY	3
3.0	INTRODUCTION	5
4.0	RPD DESCRIPTION	7
4.1	<u>Powertrain</u>	7
4.2	<u>Vehicle Installation</u>	8
4.3	<u>Vehicle Performance</u>	12
5.0	POWERTRAIN DESIGN AND DEVELOPMENT PROGRESS	13
5.1	<u>Basic Engine</u>	13
5.1.1	Overall Design	13
5.1.2	Engine Performance	18
5.1.3	Thermal Model	20
5.1.4	Compressor	22
5.1.5	Turbine	33
5.1.6	Combustor	41
5.1.7	Regenerator and Seal System	58
5.1.8	Inner Hsg. (with Thermal Emissivity Effects)	63
5.1.9	Rotor System	66
5.1.10	Recuperator	67
5.2	<u>Materials</u>	70
5.2.1	Ceramic Components	70
5.2.2	Metallic Components	73
5.2.3	Regenerator and Seal System	74
5.2.4	Ceramic Wheel Shaft Attachment	77
5.2.5	Insulation (also Low Emissivity Coatings)..	80
5.2.6	Ceramic Development Testing	82
5.2.7	Ceramic Interfacing	83
5.2.8	Brazing to Ceramics	84
5.2.9	Materials Status Summary	86
5.3	<u>Drivetrain and Control</u>	86
5.3.1	Reduction Gearing	86
5.3.2	Continuously Variable Transmission	90
5.3.3	Response Assist Flywheel	96
5.3.4	Parasitic Losses	99
5.3.5	Control System (incl. Torque Sensor Des.) .	101
5.4	<u>Vehicle Performance and Fuel Economy</u>	105
5.4.1	Fuel Econ. Studies (incl. Warm-up Fuel Sens.)	105
5.4.2	Performance Studies	107
5.4.3	Accel Model	109
5.4.4	Decel Model (with Compressor Bleed)	111
6.0	CONCLUDING COMMENTS	115

TABLES		ff
FIGURES		ff
APPENDIX A	Program Goals, Schedule, and Program Tasks	A-1
APPENDIX B	AGT-102 Basic Engine Characterization	B-2
APPENDIX C	Preliminary Bearing-Rotor Design - MTI	C-1
APPENDIX D	Van Doorne Belt Analysis - Battelle	D-1

ABBREVIATIONS

AGT	Advanced Gas Turbine
ANSYS	Finite Element Computer Programs: Stress, Thermal, Dynamics
AS	Aluminum Silicate Ceramic
ATF	Automatic Transmission Fluid
CDT	Compressor Discharge Temperature
CINDA	Finite Difference Computer Programs: Heat Transfer
CVT	Continuously Variable Transmission
DBTT	Ductile-to-brittle Transition Temperature
DDA	General Motors, Detroit Diesel Allison Division
DOE	U. S. Department of Energy
DN	Bearing Parameter: Diameter Times Speed (mm-rpm)
EDX	Energy Dispersive X-ray
EPA	U. S. Environmental Protection Agency
EPD	Experimental Powertrain Design of AGT
LAS	Lithium Aluminum Silicate Ceramic
LPP	Lean, Pre-mixed, Pre-vaporized Combustion
M	Weibull Slope; Statistical Distributor
NACA	National Advisory Committee for Aeronautics (now NASA)
NASA	National Aeronautics and Space Administration
NASTRAN	Finite Element Computer Programs: Stress, Thermal, Dynamics
NISA	Finite Element Computer Programs: Stress, Thermal, Dynamics
NNEP	Gas Turbine Performance Computer Program
RAF	Response Assist Flywheel
RBSC	Reaction Bonded Silicon Carbide Ceramic
RPD	Reference Powertrain Design of AGT
SI	Standard Spark Ignition Reciprocating Engine
SiC	Silicon Carbide Ceramic
SMD	Sauter Mean Diameter; Droplet Size
TET	Turbine Exit Temperature
TFSR	Turbulent/Laminar Flame Speed Ratio
TIT	Turbine Inlet Temperature
TZM	Molybdenum-Titanium-Zirconium Alloy
VIGV	Compressor Variable Inlet Guide Vanes
WRC	Williams Research Corporation-became Williams International Corporation, July 1981.

1.0 FOREWORD

This report covers work performed by Chrysler Corporation and Williams Research Corporation under DOE Contract DE-AC02-76CS-52749 (Mod M015) on the initial development of an advanced gas turbine (AGT), powertrain concept, the AGT-102. The work was funded by the Department of Energy (DOE) Office of Transportation Programs under the Automotive Technology Development Division's Gas Turbine Highway Vehicle Systems Program. Technical management was provided by the Gas Turbine Project Office of the NASA Lewis Research Center through an inter-agency agreement with DOE.

Team Project Managers were Mr. C. E. Wagner of Chrysler and Mr. W. I. Chapman of Williams. Mr. James N. Deyo of NASA Lewis was the Contract Project Officer.

Preceding this work both Chrysler and Williams participated in the 1978-1979 initial study phase of the DOE/NASA AGT program, Williams under NASA Contract DEN 3-13 and Chrysler under Mod M006 of the Upgraded Gas Turbine Engine Program, DOE Contract DE-AC02-76CS-52749. In November of 1978 Chrysler and Williams signed a memorandum of understanding which established a partnership for future participation in the ongoing DOE-NASA AGT program.

The initial effort of this team was preparation of a proposal submitted in April 1979 in response to a competitive contract solicitation by NASA Lewis for a five year AGT development and demonstration program. The proposed AGT powertrain concept consisted of a high temperature recuperated single shaft engine coupled to a two range synchronous shift metal belt continuously variable transmission and packaged for a rear wheel drive vehicle. Other concepts were proposed by AiResearch/Ford and GM (Detroit Diesel Allison/Pontiac) teams. NASA was authorized to make two awards and selected the AiResearch and DDA proposals as offering lower risk approaches for achieving the program objectives.

In November 1979, Congress acted to broaden and lower the risk of the overall AGT effort by providing funding for DOE to award a third contract. Chrysler-Williams was determined to be the sole available source for such an effort and in December of 1979 NASA established guidelines for a directed procurement action. These were that the proposed concept should minimize use of high risk technology such as a ceramic recuperator and catalytic combustor and that fundamental development of ceramic materials should be minimized through reliance on results of ceramic development being conducted by other existing contractors. Also, with this third program being both complementary and partially dependent on DDA and AiResearch efforts, the powertrain concept would be developed in a single phase and would be expected to require less overall effort than the two prime programs. Basic program goals relating to emissions, fuel economy and other AGT program objectives would remain intact.

In revising the original Chrysler-Williams concept within these guidelines, particular emphasis was placed on a design which would be received by automotive management as having significant potential for

future high volume production. Accordingly, the concept had to exhibit simplicity, light weight, driveability, producibility, packageability and competitive overall cost in future front wheel drive vehicles.

The powertrain which was structured to meet these guidelines consisted of a single shaft engine with a ceramic inner shell for containment of hot gases and support of twin regenerators. The ceramic inner housing was contained within an outer sheet metal housing with the space between housings filled with insulation. The rotor consisted of an aluminum radial compressor wheel and ceramic radial turbine wheel supported by an air-lubricated journal bearing adjacent to the turbine wheel and oil lubricated ball bearings adjacent to the reduction gear pinion, remote from the hot section of the engine. The burner was a lean premixed pre-vaporized fixed geometry concept. The engine was sized for about 78 horsepower at 2300F turbine inlet temperature and with a rotor speed of 99,500 RPM.

The entire turbine section was ceramic, but if delays were encountered in development of the relatively high risk ceramic wheel, an interim engine could rely on use of a metal superalloy wheel by limiting temperature to 2100F and accepting an engine output of about 66 horsepower. By coupling the engine to a vehicle through a continuously variable transmission (CVT), performance comparable to the 90 HP standard reference SI reciprocating engine was expected. The CVT proposed was a repackaged version of the two range synchronous shift variable metal compression belt unit proposed for the rear wheel drive in the original AGT proposal. A response assist flywheel was proposed as part of the reduction gear train to achieve acceptable levels of engine response even with use of a metal turbine wheel.

Overall, the package could be installed readily in Chrysler's K cars, and acceptably in Omni-Horizon size compartments with ample room for accessories, intake and exhaust and at about a 100 pound weight advantage compared to the normal spark ignition (SI) engine powertrain.

Technical design and development of this concept, designated the AGT-102, began in January of 1980 and was continued under Mod 15 of Chrysler's Upgraded Engine Contract. In parallel with the Mod 15 effort a revised proposal for an ongoing five year NASA Contract was prepared and submitted in December 1980.

Subsequently, in February 1981, administrative decisions were reached within DOE to reduce the scope of the AGT program and to withhold further funding of the AGT-102. Accordingly, close-out activities were begun in early March 1981 which included preparation of this final summary report.

2.0 SUMMARY

This summary report covers the work accomplished by Chrysler-Williams during the start-up phase of the AGT-102, Advanced Gas Turbine Powertrain Development Program. Ultimate program goals were to demonstrate at least a 30 percent fuel economy improvement over a comparable SI reciprocating engine, operation within .41 HC, 3.4 CO, and .40 NOx grams per mile emissions levels, and the ability to use a variety of alternate fuels.

The powertrain concept consists of a single-shaft engine with a ceramic inner shell for containment of hot gasses and support of twin regenerators. It uses a fixed-geometry, lean, premixed, prevaporized combustor, and a ceramic radial turbine rotor supported by an air-lubricated journal bearing. The engine is coupled to the vehicle through a wide-range continuously-variable transmission (CVT), which utilizes gearing and variable-ratio metal compression belt. A response assist flywheel (RAF) is used to achieve acceptable levels of engine response. The package offers a 100 lb. weight advantage in a Chrysler K Car front-wheel-drive installation.

Initial layout studies, preliminary transient thermal analysis, ceramic inner housing structural analysis, and detailed performance analysis were carried out for the basic engine.

Following is a brief summary of accomplishments and conclusions resulting from this initial phase of work on the AGT-102 gas turbine powertrain development program.

1. Reference Powertrain Design (RPD) studies indicate that minimization of the engine's warm-up fuel requirement and parasitic power losses are essential to the achievement of program goal drive cycle fuel economy levels.
2. Design and thermal analysis studies of the overall engine have not progressed far enough to confirm that an aluminum impeller can withstand shutdown soakback temperatures without some form of after-cooling system.
3. An initial design study showed that a radial-axial variable inlet guide vane (VIGV) configuration should have greater range and efficiency than an axial cascade, but recommended verification tests. However, further studies showed that VIGV's are ineffective in reducing flow and pressure ratio with a backswept compressor impeller because of its rising slip factor characteristic; the concept was therefore dropped from the RPD.
4. Aerodynamic design analysis of the ceramic radial turbine gave good performance characteristics with maximum efficiency of 86 percent. Preliminary stress analysis indicated reasonable stress levels, but rigorous analysis including thermal transients and comparison with realistic strength data from equivalent ceramic structures is required to finalize the design and determine practicality.
5. Design analysis of electromagnetically forming a molybdenum sleeve over a ceramic wheel shaft stub indicates that this concept of providing a transition part for connecting a ceramic wheel to a metal shaft is practicable.

6. Analytical studies confirm that a fixed geometry lean premixed pre-vaporized (LPP) combustor can meet the very low program goal emission standards. The most critical requirement is that of developing small droplet size fuel injectors.
7. Conventional elastomeric retention of the regenerator drive gear can be utilized at AGT-102 temperature levels with proper design.
8. Lithium aluminum silicate (LAS) with 3/8 in. walls can safely be used as an initial ceramic inner housing material. To reduce warm-up mass of the inner housing, thinner wall designs in SiC should be investigated. A system for applying a low friction wear coating on a SiC regenerator platform was established. Promising approaches were demonstrated for establishing such a coating on LAS.
9. An analytically sound air bearing shaft system has been configured.
10. Extensive ceramic/ceramic and ceramic/metal interfacing studies have shown that zirconia can generally be used to prevent adhesion.
11. The theoretical basis for brazing a ceramic wheel to a metal shaft has been established.
12. A method of analytically characterizing the metal compression belt for the continuously variable transmission (CVT) was developed which agrees closely with test data.
13. A detailed design layout of the continuously variable transmission (CVT) and a preliminary design of the response assist flywheel (RAF) were completed. Both components appear to meet practical automotive design criteria.
14. A simple stable control logic was developed for fuel, transmission ratio, compressor bleed, and flywheel energy flow through use of a transmission input torque sensor.
15. Performance studies show that initial experimental engines using metal turbine wheels and limited to 2100F TIT should have acceptable driveability and experience no more than 1/2 MPG loss in fuel mileage. However, the use of metal turbine wheels would require a dependence on strategic materials which would restrict application to low volume production.

These conclusions and accomplishments were developed as part of the initial effort to establish the Reference Powertrain Design (RPD) for the AGT-102. Overall the RPD concept appeared to be capable of ultimately achieving the goals of the DOE/AGT program at the time work was terminated due to government funding reductions. This report details the work that was accomplished up to the funding termination.

3.0 INTRODUCTION

This summary report covers the work accomplished by Chrysler-Williams during the start-up phase of the AGT-102 Advanced Gas Turbine Powertrain Development Program. Major goals were to demonstrate at least a 30 percent fuel economy improvement over a comparable SI reciprocating engine, operation within .41 HC, 3.4 CO, and .40 NOx grams per mile emissions levels, and the ability to use a variety of alternate fuels. Detailed goals, schedule, and task description for this five-year planned effort are contained in Appendix A. Curtailment of Government funding resulted in termination of the program following approximately one year of work which was funded on an interim basis by Mod M015 of Chrysler's Upgraded Gas Turbine Engine Contract DE-ACO2-76CS-52749. Funding of the full program was to be through a contract from the NASA Lewis Gas Turbine Project Office which was being negotiated at the time of this termination.

The program was structured around the establishment and updating of a Reference Powertrain Design (RPD) capable of meeting program goals and objectives. Specific component development tasks were derived from this design with results to be used interactively in RPD updating. The combined RPD and component tasks provide the basis for the design and development of a complete experimental powertrain system. The Experimental Powertrain Design (EPD) would approach the RPD as closely as possible within the limits of component technology status and manufacturing practicability. Accordingly, the initial EPD would rely on items such as a metallic rather than a ceramic turbine wheel, a fabricated rather than a stamped outer housing, and gearing machined from available cutting tools. The EPD and RPD would converge as the program progressed toward full vehicle demonstration.

The primary thrust of the initial program phase was establishment of an initial RPD. Work on the basic engine of the RPD included overall layout studies, a preliminary transient thermal analysis, structural studies of the ceramic inner housing and detailed engine performance analysis. Engine component work was targeted towards definition of the regenerator system, a fixed geometry lean premixed prevaporized (LPP) combustor, aero-mechanical design of the compressor and turbine section and analysis of the high speed bearing and shaft system. Work on the drivetrain included reduction gear design, preliminary designs of the continuously variable transmission (CVT) and response assist flywheel (RAF), definition of auxiliary and accessory requirements and analysis of parasitic losses. Also included were layout studies of the vehicle installation and detailed analysis of vehicle performance and drive cycle fuel economy. The program was terminated two months before a scheduled RPD design review, the first major program milestone.

Work outside the RPD task included design and procurement of component rigs, fundamental development of ceramic materials, and characterization testing of the variable ratio metal compression belt.

In carrying out this team effort, Chrysler as prime contractor maintained responsibility for the overall powertrain system. Williams Research Corporation (WRC) had direct responsibility for the basic en-

gine, but utilized Chrysler for support in the areas of the combustor, regenerator, and ceramic materials engineering. Carborundum Company and Corning Glass Works provided subcontractor support in ceramic component design, and Mechanical Technology Incorporated provided subcontractor support in the design of the air bearing high speed shaft system.

Chrysler had direct responsibility for design and development of the drivetrain, control and vehicle systems. The drivetrain consisted of the reduction gearing, response assist flywheel (RAF), accessory drive, and the continuously variable transaxle (CVT). Orshansky Transmission Company provided subcontractor support in the CVT design, and Battelle Laboratories provided subcontractor support in design analysis of both the RAF unit and the variable belt unit of the CVT.

Section 4.0 of this report describes the overall status of the Reference Powertrain Design (RPD). The powertrain as currently defined is described with respect to concept, automotive product potential, vehicle installation and performance, fuel economy and emissions.

Section 5.0 details progress made in the design and development of specific subsystems and components. The report is by subject, and within each subject work relating both to the target RPD system and the developmental or experimental systems leading to the RPD are described.

Section 5.1 describes work done on the basic engine and its components. Section 5.2 describes work performed in the area of advanced materials technology. Section 5.3 describes design and development of the system drivetrain and includes subsections on the reduction gearing, response assist flywheel (RAF), continuously variable transmission, parasitic losses and control system. Vehicle performance analysis is contained in Section 5.4.

Conclusions and assessments resulting from these efforts are presented in Section 6.0.

4.0 RPD DESCRIPTION

4.1 POWERTRAIN

The ACT-102 reference powertrain design reflects a design philosophy that combines gas turbine technology with the requirement for mechanical simplicity for automotive manufacturability. It consists of a single-shaft regenerative gas turbine engine, a continuously variable transmission and a response assist flywheel. A cutaway of the RPD is shown in Figure 1. The four major components used on the engine are the single-stage centrifugal compressor, single stage ceramic radial turbine, the ceramic LPP combustor, and the ceramic regenerator. The single-shaft engine uses a continuously variable ratio steel belt drive transmission to power and control the vehicle. Maximum turbine inlet temperature is 2300F.

There is no variable geometry on the engine. The two turbomachines are radial-flow types which are inherently and traditionally less costly than axial-flow components. The outer housing is of a simple geometric shape. The regenerator cores run directly on the ceramic inner housing platforms which results in a seal system much simpler than on past engines. Except for the high-speed reduction gear, the RAF, and the CVT belt and pulleys, the drivetrain contains machine elements familiar to automotive design.

A key feature of the dual-regenerator engine is the ceramic inner housing. The uncooled bulkhead separating the turbine inlet and exit zones is integrated with the regenerator crossarms and with the turbine rotor shroud. Past practice with metallic housings required that the bulkhead be insulated from high temperature gas and that it be further protected by a double wall with cooling air flow. In addition, the separate shroud required sealing at high pressure and temperature. The ceramic inner housing, as shown in Figure 1, eliminates these needs; it also significantly reduces weight and mechanical complexity.

The aerodynamic designs of the compressor and turbine are based on technology used for higher massflow components. The specific speeds are consistent with high efficiency. However, the fuel economy goal of this program demands significant development to preserve high efficiency in these low massflow components. The turbine volute, nozzle and rotor are made of ceramic. High-volume use of ceramics will require both the development of consistent material properties and practical, high yield manufacturing processes.

The engine uses a conventional ceramic regenerator system, which is based on the many years of Chrysler/WRC experience with these units. The LPP combustor is considered near-term technology which can be achieved within the time-frame of the program. This type of combustor has demonstrated the potential for very low emissions and high efficiency and the capability of handling a wide variety of fuels.

It is generally agreed that the single-shaft engine is more efficient than a two-shaft engine, but for an automotive application it must

be coupled to the vehicle through an efficient CVT. The CVT design selected for the RPD uses a steel compression belt combined with a synchronous shift range extending planetary gear system. This design is based on demonstrated technology and is capable of good low power efficiency. The belt concept is the primary choice because it has been judged to be potentially quieter and lower in cost than hydromechanical or traction drive types.

Vehicle driveability is dependent upon engine response and powertrain control. To achieve engine response comparable to the baseline SI engine, a response assist flywheel has been incorporated into the powertrain. It connects with the first reduction gear shaft and spins counter to the main turbine shaft. Charging is through a step up planetary gear set with final speed and charging rate controlled through a slip clutch. The step up planetary gear set also allows the flywheel to maintain speed by tapping engine power. To achieve nearly instantaneous changes in engine speed, flywheel energy is discharged directly into the gear train through a second slip clutch.

By providing flywheel energy, the need for added fuel flow during engine acceleration is reduced, thereby simplifying the design of the LPP combustor. Also, the need for the hot turbomachinery to withstand momentary overtemperature is reduced.

The control system activates the clutches for the response assist flywheel system and for the CVT during launch (initial vehicle movement from a standing start). Control of engine power at idle is accomplished by reduction in engine speed. Controls change belt ratio during launch, acceleration and deceleration, correlate flywheel speed with engine speed, and reduce power during braking by compressor bleed.

Studies of performance during vehicle launch from a standing start show that values for one second and five second distances and the time to accelerate to 60 MPH are comparable to the values expected of the 1985 vehicle with an SI engine. To achieve this level of performance, energy is discharged from the flywheel during the first second of launch time.

4.2 VEHICLE INSTALLATION

4.2.1 General Arrangement

The conversion of the front-wheel-drive K-body to the AGT-102 engine is planned to require few modifications to the base vehicle. The powertrain installation is shown in Figures 2, 3, and 4. A preliminary mock-up is shown in Figures 5. The transverse powertrain arrangement is retained with the engine to the right side and transmission on the left. No changes are needed in structures, steering, or suspension geometry. The radiator is deleted. No exterior restyling is necessary. Driver controls are retained in their familiar location.

4.2.2 Auxiliary Considerations

4.2.2.1 Intake and Filter

The engine intake is located near the center of the engine compartment. The inlet air is ducted from the left front fender, ahead of the wheel opening, where an intake grill must be added. This location has proven acceptable in the past as a relatively clean body area. It lends itself well to multiple turns in the duct needed to provide intake noise control as well as effective water separation (road splash).

The filter element is chosen from available, commercial, replaceable elements. It is a pleated paper cylinder with high air flow and dirt retention capacities.

4.2.2.2 Exhaust System

The dual engine exhausts are joined in Y-pipe fashion within the engine compartment. A single exhaust of about 10in² flow area is placed in the existing body tunnel and extends to beneath the rear seat area. Past experience has been satisfactory with pipe termination at this location both with respect to avoiding undue heating of the fuel tank and fumes entering the passenger compartment. A fuel tank modification would be necessary to extend a pipe of this size to the rear of the vehicle.

The entire exhaust system is made of aluminum sheet metal for light weight and long life. An insulative liner provides additional sound absorption without requiring baffles in the exhaust. The regenerator matrix provides most of the exhaust noise control.

4.2.2.3 Fuel Supply

A single electric pump with integral pressure relief at the fuel tank will supply the combustor system through a filter, pressure regulator and control valves in the engine compartment. A return line will provide by-pass and/or cooling flow return to the tank.

4.2.2.4 Engine Mounts

The three production engine mounts will be retained as nearly as possible in their production locations. Mount location in a unibody is critical with respect to control of noise, vibration, drive loads and road shock and in securing the powertrain as an integral part of the crash structure. Slight relocations, to provide accessory clearances or improve support bracket designs, are considered acceptable.

As is current practice, rubber isolators are procured in a variety of stiffnesses. The final choice of isolator stiffness is made by vehicle evaluation on the basis of sound and feel.

4.2.2.5 Electrical System

A conventional electrical system consisting of starter, alternator, battery, and wiring harness is planned for the AGT-102. (The ignition system is included with the combustor description.)

The starter is a 12 volt DC motor connected to the gearbox through a V-belt drive and overrunning clutch. The belt drive has proven effective in absorbing initial shock loads, and provides a convenient range of drive ratios. The overrunning clutch prevents the engine from driving the starter into an overspeed condition. A 1.5HP starter motor can provide acceptable start times with the relatively low inertia of a ceramic turbine rotor.

The alternator is sized for a 65 amp. capability to handle the expected engine and vehicle electrical loads. Since only a 2:1 speed range is required, idle alternator speed is selected to provide full charging capacity. Actual current generation is regulated by the state of battery charge and actual electrical loads.

A conventional, but unique, wiring harness is necessary. Such harnesses are normally developed experimentally on the basis of appearance, accessibility and other factors and then recorded on drawings, rather than being designed in advance.

4.2.2.6 Lubrication System

One oil system supplies the complete powertrain lubrication and actuator requirements. The variable displacement pump and regulation valves are included in the transmission assembly. Automatic transmission fluid (ATF) is utilized. An inlet filter (internal) protects the system from build contamination and potential failure-generated debris. There would be no need for routine filter replacement or oil changes. Provision is made for an external oil cooler with thermostatic control, though these items are not expected to be necessary. Adequate cooling should result from the transmission housing surfaces alone. Cold ambient operation with "overcooled" oil should not be a problem since high speed journal bearings are not used and the ATF oil maintains a reasonably low viscosity at cold temperatures.

4.2.2.7 Vehicle Controls

Driver controls for the AGT-102 will be the same as the SI baseline vehicle: a steering wheel, ignition switch, shift lever, and multipurpose switch (signal lights, dimmer, and wiper control); accelerator and brake pedals. Displays other than speedometer, oil pressure and alternator have not yet been determined.

4.2.2.8 Auxiliary Air Pump

No air pump is currently planned with the LPP combustor concept. A starter-driven or accessory-belt driven pump could be adapted if required for special circumstances such as cold climate operation with heavy fuels.

4.2.2.9 Engine Cooling

The AGT-102 is designed as a self-cooled power plant. The bulk of the heat rejection is in the exhaust gas stream. Underhood losses will be comparable to the baseline SI vehicle system. No radiator, fan, coolant, or pump is required for engine temperature control.

Localized cooling of the fuel atomizers will be provided by fuel recirculation and minimal use of compressor discharge air.

4.2.3 Vehicle Accessory Systems

4.2.3.1 Heater

Details of the RPD heater system have not yet been developed. However, rather than using a hot gas to water unit adaptable to a conventional in-dash heater-defroster unit, the system developed for the AGT powertrain will most likely utilize a direct gas-to-air heat exchanger for reduced weight, cost and electrical load and for elimination of the antifreeze mixture.

4.2.3.2 Air Conditioner System

The air conditioning system would be conventional except for changes relating to use of a gas to air reheat system and for the substitution of pressure for vacuum controls. The compressor is re-located and driven at a slightly lower speed, offset by improved condenser effectiveness due to elimination of the radiator. An electric fan cools the condenser when the compressor is running. Refrigerant plumbing is arranged such that engine/transmission repair/replacement can be conducted without system discharge. Air conditioning controls are the same as the baseline SI system, with provision to deactivate the compressor clutch during start, acceleration, and WOT operation as desired.

4.2.3.3 Power Steering

A conventional power steering system is included with the pump belt-driven from the reduction gear box accessory shaft.

4.2.3.4 Power Brakes

Because conventional vacuum-boosted power brakes would require a separate vacuum supply, the RPD vehicles will probably utilize very similar hardware but adapted for use with regulated engine air pressure.

4.3 VEHICLE PERFORMANCE

Table 1 shows the predicted vehicle performance and Federal Drive Cycle fuel economy of the RPD compared to the projected 1985 SI vehicle.

The projected fuel economy gain of the AGT at this stage of its design is 17%. To obtain the 30% program goal, the RPD needs to achieve 36.1 MPG. One approach to improving fuel economy would be to reduce the performance of the AGT by downsizing to comparable SI vehicle performance levels. This was examined but did not yield much improvement in fuel economy because of the increased levels of aerodynamic and mechanical losses with smaller size and higher speed. Analysis indicates that the most practicable approach to achieving the goal would be to reduce parasitic losses by about 15% and warm-up fuel by about 30%. In calculating Federal Drive Cycle fuel economy, 43 percent of the warm-up fuel requirement is used in the determination of city cycle mileage.

Design work did not progress far enough to evaluate whether these reductions could be fully achieved. Optimization of gears, clutches and bearings was still in progress. Major changes in gear train configuration, clutch requirements and bearing sizes had evolved but the final configuration of the machine elements was not completed.

Studies had not yet begun with the thermal model to optimize the engine structure for minimum heat loss and heat storage. However, it is apparent that to achieve a warm-up heat reduction of 30% would require a significant reduction in mass of the various hot section components.

The emission targets were (in grams/mile): 0.41 HC, 3.4 CO and 0.40 NOx. With the LPP dual stage fixed geometry combustor it was projected that CO emissions would be under 2.0 grams/mile. HC was expected to be a small fraction of 0.41 grams/mile. It was expected that NOx could be met with diesel fuel (about 0.2 grams/mile), but it was not clear whether it could be met with all possible fuels, including unleaded gasoline. The estimate for NOx emissions from diesel fuel assumes atomization comparable to the NASA high-temperature, ultra-lean combustion rig referred to in Section 5.1.6.

5.0 POWERTRAIN DESIGN AND DEVELOPMENT PROGRESS

5.1 BASIC ENGINE

5.1.1 Overall Design

5.1.1.1 Engine Arrangement

The basic engine for the Reference Powertrain Design (R2D) is a regenerated single rotor gas turbine with centrifugal compressor and radial inflow turbine (Figures 6, 7, 8). The rotor assembly is supported on a gas bearing located between the turbine rotor and the compressor impeller, and it is piloted into the output drive pinion mounted on two ball bearings at the compressor inlet.

Dual rotary regenerators are provided to recover heat from the turbine exhaust gas. They are mounted on each side of the turbomachinery, with their axes perpendicular to the rotor. This symmetrical arrangement simplifies the ducting and provides balanced flow passages to and from each regenerator. The flow passages have ample flow area and are shaped to provide good flow distribution across the regenerator rotor segments.

The engine uses a lean, premixed prevaporized combustor for high efficiency and low emissions, with the capability of handling many types of fuel. The can-type combustor is located at the bottom of the engine, feeding the radial turbine nozzle through a volute.

The engine housing is a simple, two-piece construction, with an outer steel shell and an inner ceramic housing. The inner housing is basically a cylinder between the two regenerator rotors, with a vertical bulkhead between the turbine inlet and exhaust. The regenerator inner seals and turbine shroud are integral parts of the inner housing. Radial keys on the front flange, where the turbomachinery assembly is inserted, locate the turbine shroud axially and concentrically to the rotor.

The inner housing is inserted into the outer housing through the regenerator openings. The space between the housings is filled with insulation, and no bulkhead cooling is required. These factors minimize heat loss and reduce engine compartment cooling requirements.

The turbine section, combustor, inner housing, and regenerator cores are fabricated from ceramic for high temperature capability and the potential for low material cost.

5.1.1.2 Compressor Section

The centrifugal compressor described in Section 5.1.4, is based on a 36 degree backswept impeller, using an aluminum alloy casting for low inertia and low cost. VIGV's were eliminated in the course

of the design. The impeller discharges into a parallel-walled diffuser located between the front and back sections of the compressor housing. These sections are bolted together for assembly. Nineteen triangular diffuser vanes are pinned and/or brazed to the inlet section, which is cast with deep ribs to minimize deflection and weight. The back section contains the air bearing and shaft seals. Retention provisions for the ceramic inner housing are a part of both sections. The front has four cast bosses that house a spring retention mechanism and the back section has four precision ground keyways that mate to the inner housing.

An aluminum front housing connects the basic engine to the drivetrain. It provides the compressor inlet flow passage, supports the high speed pinion assembly, and houses the reduction gear. A dead air gap between the air flowpath and high speed pinion support reduces heat input to the compressor inlet. The flow contour permits space for possible shaft damping.

5.1.1.3 Turbine Section

The turbine section of the RPD is all ceramic. Aeromechanical details are discussed in Section 5.1.5. The initial turbine inlet volute and nozzle assembly assumes use of a permanently bonded multipiece alpha silicon carbide assembly. The combustor enters the volute tangentially at a 30 degree declination from the engine centerline with no tilt fore or aft. The volute area decreases linearly for 360 degrees from the combustor entrance. The nozzle is full entry with constant section vanes. Nozzle throat size is controlled at assembly to minimize tolerance requirements and/or costly machining for flow sizing. This would be achieved initially through a development discussed under Materials in Section 5.2.1 in which the nozzle vanes are fixtured within the flowpath by molybdenum pins, so that they are accurately located in place before bonding of the assembly.

The turbine shroud is machined integral with the ceramic inner housing, and the volute and nozzle assembly are positioned axially and radially from a flange on the shroud. An "E" seal ring loads the nozzle against the flange. During operation, the nozzle and turbine pressure differentials apply additional loading.

A variety of fabrication techniques are projected for use in volute and nozzle manufacture, with slip cast constant wall thickness flowpath components being permanently bonded together with injection molded nozzle vanes.

The ceramic RPD turbine rotor is initially designed for fabrication from injection molded alpha silicon carbide, integral or permanently bonded from two or more pieces. The blading is radial, with deep scallops in the back face to control thermal gradients and stress.

Initial experimental engines would utilize metallic superalloy components. Of particular concern is development of a ceramic turbine wheel in time for final vehicle evaluation, although a demonstration of program goals would be possible with a metallic wheel running with maximum turbine inlet temperature reduced to 2100F. Under such conditions overall performance would be at the low end of the acceptable band (discussed in Section 5.4), but fuel economy would be about the same as when running the engine at 2300F maximum temperature. The flywheel provided for the RPD could be modified to assure adequate vehicle response with the higher inertia metal wheel.

5.1.1.4 Combustor Section

The combustor concept for the RPD is a fixed geometry, lean, premixed, prevaporized (LPP) design with all high temperature components fabricated from silicon carbide.

This subsystem (described in detail in Section 5.1.6) consists of a ceramic premixer/prevaporizer with fuel injector, a simple igniter, and the combustor tube. The function of the premixer/prevaporizer is to prepare a lean, homogeneous mixture for the reaction zone. A prefilming airblast atomizer is used to obtain homogeneity before autoignition, which occurs very rapidly at these high cycle temperatures. The airblast atomizer will flow all of the primary zone air to ensure good mixing.

The combustor tube is a well-stirred reactor, convectively cooled with ample residence time to allow completion of the combustion.

5.1.1.5 Regenerator Section

The dual regenerator cores are made from an aluminum silicate (AS) matrix with triangular flow passages, wound around a ceramic hub. The rim section is modified and filled to control stresses and leakage.

The inner surface of the regenerator core runs directly on the theta-shaped seal platforms integral with the ceramic inner housing. The seal platforms are coated for reduced friction and wear, and finished flat to minimize leakage. The outer surface of the regenerator core is sealed by a floating D-shaped rubbing seal, connected to the regenerator cover by a static seal.

Each regenerator core is housed in a regenerator cover, a formed sheet steel shell with a welded or brazed flange. The core is surrounded by compressor discharge air, with the exhaust discharging through one-half of each core.

The regenerator core is supported on a shaft cantilevered from the regenerator cover with a graphite bushing to handle drive loads

at the low (20 RPM maximum) core speed. A ring gear is mounted with high temperature elastomer to the outer diameter of the core. The ring gear is driven by a pinion mounted on dry bushings from the regenerator cover. The pinions and connecting cross shaft are driven through a wormgear assembly with chain or belt drive from the reduction gear.

5.1.1.6 Outer Housing

The outer structure of the engine consists of an outer housing closed off by regenerator covers, burner cover, and compressor housing. It is formed of a sheet metal shell with welded or brazed flanges. It is shaped to withstand compressor discharge pressure with minimum distortion.

5.1.1.7 Inner Housing

The ceramic inner housing directs engine airflow from the high pressure side of the regenerator into the combustor, through the turbine, and into the low pressure side of the regenerator. The housing provides a sealing surface for the regenerator cores and a bulkhead that separates the high-pressure regenerated air from the low-pressure turbine exit air. The inner housing is located relative to the compressor housing by four radial keys at the interface between these two components; this maintains good control of turbine rotor tip clearance. Spring loaded retainers, aided by pressure load when operating, hold the inner housing in place.

The basic geometry of the initial RPD design is a right angle intersection of two cylinders. This configuration should expedite manufacturing, control stress and thermal patterns, and allow placement of retention features on the outside surface for assembly and maintenance. The regenerator flanges are flared in-board to expose the inner faces of the flanges to high temperature air and thus reduce thermal gradients, stresses, and deflections.

The inner housing is inserted into the outer housing through the regenerator openings, and the space between the housings is filled with insulation. No bulkhead cooling is required, thus reducing heat loss and reducing engine compartment cooling requirements.

Candidate ceramics for this component are reaction bonded SiC, sintered alpha SiC and lithium aluminum silicate (LAS). LAS was selected for initial experimental engine parts because Corning has experience with fabrication of similar parts, and also because the very low thermal expansion of the material essentially eliminates thermal stress considerations. Its drawbacks are a relatively low strength (10 ksi level), which results in thicker walls, a high warm-up mass, and, as with all candidate materials, an uncertain high volume cost outlook. Dimensional control of critical surfaces and fits will be obtained, where necessary, by machining the green

cast parts and/or machining after sintering. Areas of primary concern are the mating surfaces with the scroll, the four radial mounting keyslots, the regenerator seal surfaces, and the turbine shaft. Close dimensional control of the last item is necessary to maintain close running clearances.

Due to the relative complexity of the inner housing and scroll, these components might be assembled from two or more slip cast and/or injection molded parts that are either bonded or mechanically joined. Assembly of individual parts would require a compromise between design and manufacturing. Choice of bonded or mechanical joints would depend on the thermal and structural analyses. Tests with SiC have shown that some joints are as structurally sound as the parent material. Corning's experience with LAS, however, is that joining results in structural weakness, and consequently, as described in Section 5.1.8, the initial experimental engine unit was designed in one piece.

5.1.1.8 Rotor System

The ceramic turbine rotor requires attachment to a steel shaft. The primary joining method proposed and researched by Chrysler Corporation is a molybdenum sleeve inertially welded to a 400 series stainless steel shaft, electromagnetically formed to the ceramic turbine stub shaft. Axial serrations and a circumferential groove on the turbine stub shaft were also to be considered for increased strength. After forming, the displaced metal and contacting ceramic is loaded radially and axially in bearing. Concentricity control during joining is critical in that material removal from the shaft area directly adds to rotating unbalance. For initial experimental engines with metal wheels, the shaft would be inertially welded directly.

The compressor impeller assembly is mounted on the turbine shaft, and the assembly is clamped together by tensioning the turbine quill shaft. The pinion gear has been excluded from the clamp group to decrease bearing alignment requirements.

An air bearing, 1.375 inch diameter by 1.5 inch long, supports the rotor assembly between the turbine rotor and compressor impeller. The bearing is a Mechanical Technology Incorporated design using three pads with corrugated bump foils and single wrap top foils.

A typical journal finish of 2 to 6 rms is required. The bearing is press fit into the diffuser and radially located to prevent shaft static contact at the foil attachment. Cooling air to the bearing is metered from the compressor backface. The bearing is discussed further in Section 5.1.9 along with the dynamic analysis.

The compressor end of the rotor is piloted into the output drive pinion, with a spline coupler for torque transmittal. The drive pinion is straddle mounted in two 104 size angular contact

ball bearings for accurate pinion location and low gear noise and axial positioning of the compressor and turbine rotors. With an operating rotational speed of 99,500 rpm, the DN value is approximately two million. The bearings are presently shown as separate components assembled onto the pinion; however, future incorporation of the inner races into the pinion could be a production cost advantage. With either design, the pinion and bearings are preassembled into a modular unit for installation and service advantages.

A shaft seal prevents oil loss by isolating the pinion area from the compressor inlet. The seal package is a controlled gap seal using two carbon seal rings. Compressor discharge guard air is used between the seal rings, and ample space is provided in this area to add damping to the shaft, possibly in combination with the seal package. The seal package is modular for installation and service advantages.

A second carbon seal ring behind the compressor impeller reduces air recirculation, so that the bearing cooling air is also used effectively for turbine rotor and shaft attachment cooling. The air bearing greatly simplifies the bearing housing and sealing system compared to conventional oil lubricated bearings.

5.1.2 Engine Performance

5.1.2.1 Engine Performance Simulation Model

The WRC digital computer engine performance simulation program is shown schematically in Figure 9.

The program requires that a complete description of each individual rotating component be provided in the form of a performance map. These maps cover the operating range of the component and define these characteristics at any speed and flow within the engine operating range. Compressor maps define the pressure ratio and efficiency as a function of corrected speed and corrected flow rate. The maps also define the surge and choke limits of operation. Turbine maps define efficiency and inlet flow parameter as a function of corrected speed and expansion ratio. The maps are generated analytically using methods that have been verified by previous testing. The simulation program predicts the performance of the engine at the output shaft for any given set of specified operating conditions. It also defines the operating pressures and temperatures, mass flow rates, corrected speeds, and other required design parameters at defined stations throughout the engine flow path. The program will provide matched gas turbine operating data for specified inputs of turbine inlet or exhaust temperature, compressor surge margin, or shaft output power.

The model includes gas leakages, heat losses, pressure losses, and parasitic power losses, as well as the performance of the individual components. Leakage flows may be removed from the cycle completely (such as an external leak or intentional bleed) or may be reintroduced to the gas path at another location. The effect of the

reintroduced leakage is accounted for by calculating a mixed enthalpy for the gas at that point. The mixed flow condition is calculated by mass averaging the enthalpies of the main stream and the leakage at the station where the leakage is introduced. Heat losses/leakages are calculated by decreasing the temperature of the station that loses heat. As with flow path leakage, some heat leakages are lost to the cycle, such as heating of the oil used for lubrication, while other heat leakages result in a redistribution of gas and material temperatures within the engine. Other parasitic losses such as bearing frictional losses, oil pump, alternator, and reduction gearing, are treated as power extracted from the engine.

Pressure losses for ducting, such as the inlet, exhaust diffuser, burner, and tailpipe, are varied as a function of the square of the local stream velocity head. The pressure losses for the heat exchanger are calculated using a coefficient of friction, and therefore reflect laminar or turbulent flow conditions. The pressure losses associated with manifolds that carry flow to and from the heat exchanger are also included in the pressure losses attributed to the heat exchanger.

The performance of the regenerator is calculated by a subroutine which uses the heat exchanger geometry as input and calculates the off-design performance of the heat exchanger. Input items include frontal areas, hydraulic diameters, length, and flow rates. Output parameters are effectivenesses, pressure losses for hot and cold side, and outlet temperature. The regenerator drive is considered a parasitic power loss.

5.1.2.2 Engine Performance Analysis

Detailed performance print-outs are contained in Appendix B, both for the 2300F RPD concept and for a 2100F cycle limited by use of a metallic wheel. Results of applying this simulation to the overall powertrain/vehicle system are described in Section 5.4.

The calculated SFC versus horsepower characteristic for the current RPD is shown on Figure 10. It includes a comparison of two approaches to controlling idle power. As shown, maintaining temperature and reducing engine speed uses less fuel than holding speed and reducing temperature.

Figure 11 shows the results of an earlier study which included the option of controlling idle power with variable inlet guide vanes (VIGV) or controlling with the vehicle brakes. Again, a speed variation is shown to be the most fuel efficient approach.

The engine performance analysis program was also used to determine engine starter motor requirements. A curve of engine motoring as a function of engine speed was calculated and is shown on Figure 12. The 1.5 HP RPD starter motor is shown to be capable of motoring the engine to 20,000 RPM without light-off. With light-off, the engine is estimated to self sustain at 30,000 RPM, where starter cut-off would occur.

An information flow chart for a dynamic engine simulation was prepared as a preliminary step in developing the engine transient performance computer model (see Figure 13). The computer model for transient performance was to use the NASA Navy Engine Program (NNEP) as its base. This program was obtained from NASA for simulation of the AGT cycle. The program is operational on the WRC system, being able to simulate the AGT at design point, but requires installation of modified regenerator, heat loss, and flow leakage routines. The potential decrease in computer run time and the increased flexibility in going from the current cycle simulation program to NNEP makes NNEP a valuable tool for dynamic and off-design simulation studies.

VIGV performance tradeoff studies were conducted for axial, radial-axial, and radial VIGV designs. The radial-axial design was predicted to provide ten percent power augmentation versus six percent for the all-axial and two percent for the all-radial. However, subsequent studies, described in Section 5.4, concluded that the small performance gain with VIGV's, for an engine which was already superior in performance with respect to the baseline SI engine, did not warrant their increased cost and complexity.

5.1.3 Thermal Model

Because of its high temperature operation and mix of ceramic and metallic parts, the complete engine was computer modeled for thermal analysis. Studies were conducted to:

1. Evaluate engine soak-back temperatures and the effectiveness of proposed methods for minimizing temperatures.
2. Provide engine component boundary conditions for steady-state and transient heat transfer analyses and for thermal growth analysis
3. Determine the amount of heat rejection for the SFC estimate and of heat storage for the warm-up fuel estimate (cf. Section 5.4.1).

The soak-back problem is a consequence of designing for low SFC and high specific power through the use of temperature. After engine shutdown, the stored heat within the highly insulated ceramic hot section flows through the shaft system to the cold section. There are three critical areas. The first is the turbine rotor attachment, where differential thermal expansion between the metal sleeve and the ceramic hub could unload the joint such that an engine start at the critical time may cause separation. The second is the air bearing, which has a steady-state operating temperature limit of 1000F and a never-exceed temperature of 1200F (heat treat effect). The third is the compressor impeller. Without adequate heat shunting or active cooling, the structural integrity of the aluminum impeller may be endangered.

Heat transfer analyses are required to evaluate stresses under steady-state and transient conditions. For the design of certain high-strength ceramic parts, it is critical to minimize thermal gradients. For metal parts, low thermal gradients are important, but the first consideration must be to maintain temperature levels commensurate with material strength. The thermal model provides the boundary conditions for components throughout the engine as well as an analytical tool for making local changes for thermal relief.

Besides providing information for stress analysis, the thermal model also provides running clearance data. Differential growth of the static and the rotating parts will result in either a closure or an opening of the cold clearances. Since running clearances have a significant impact on engine performance, growth studies based on the thermal model temperatures will set the minimum cold clearances, axial and radial, to accommodate expected operating extremes and ambient temperatures.

Heat rejection is of two forms. The first is ambient heat loss from engine exterior surfaces. This loss represents a direct cycle penalty in terms of SFC. The thermal model identifies the magnitude of this external heat loss and guides the selection of insulation types and thicknesses for optimum performance. The second form of heat rejection occurs within the engine itself. For example, heat flow from the ceramic inner housing to the compressor outlet will reduce cycle efficiency and increase SFC.

All significant engine components are included in the finite element model. Figures 14 through 16 detail the element network. A finer mesh was used on the rotor system components than other areas. Sufficient detail was included such as tiebolt spacers to increase the accuracy of the critical soakback results. Special attention was paid to closely approximate the actual mass of the individual components.

Superimposed onto the geometric element network is a fluid network. Since the internal fluids (air and oil) undergo considerable temperature change during soakback and have a pronounced influence on the calculated temperatures, the only analytical approach to accurately predict engine thermal behavior after shutdown is to use a full fluid analysis. In the analysis of steady-state operation the fluid elements were linked one to another and the velocities established from the engine mass flow rate. The fluid elements are actually boundaries whose temperature changes depend on heat transfer to or from the flow passage or adjacent structure. Heat generation applied to the appropriate fluid elements simulates compressor work, combustor temperature rise, turbine work, and bearing power losses.

Depending on the engine component and the local aerothermodynamic conditions, heat transfer coefficients were estimated from the following types of models: modified duct, modified flat plate impingement, cylinder in cross flow, non-luminous gas radiation, abrupt expansion, rotating disk, rotating cylinder and hot-structure

surface-to-surface radiation. Free convection was to be used after shutdown. Heat extraction during rundown was to be included in the analysis.

At the time of program close-out, the geometric portion of the thermal model as described had been assembled. The boundary conditions input was approximately 50 percent complete. The computer program had been debugged for limited boundary conditions. The basic planned analyses included:

- a. Steady-state at full and part power.
- b. Transient from idle to full power.
- c. Shutdown from part power and soak.

After the basic analyses were completed and key element temperatures were defined, design alternatives to solve soak-back problems were to be explored. They included:

- a. Passive cooling of the shaft system through natural convection to ambient air via both the shaft and bearing support section of the compressor housing.
- b. Active cooling using forced air or oil.
- c. Selection of component materials to withstand soak-back temperatures.

In support of the thermal model, testing was performed on an air bearing test rig to determine the heat transfer coefficient across the foils of the air bearing.

Figure 17 shows a schematic of the test set-up along with plots of test results and analyses. Figure 18 is a close-up view of the encapsulated simulated air bearing. Heat source for the test was supplied by two 500 watt quartz lamps controlled by a variable power supply.

The experimental shaft temperatures were computed on a CINDA thermal model of the fixture. The heat transfer coefficient across the foils in the model was then adjusted until the bearing cartridge model temperatures agreed with experimental temperatures. The heat transfer coefficient was determined to be $43 \text{ BTU/hr/ft}^2/\text{°F}$. In an air gap of the same width as the gap across the foils, the coefficient was calculated to be $28 \text{ BTU/hr/ft}^2/\text{°F}$.

5.1.4 Compressor

The compressor activity consisted of defining the flowpath, configuring variable inlet guide vanes and the blades for the impeller, and estimating the performance characteristics. In general, the methodology followed procedures common in compressor design.

Unique to this compressor, however, was the plan to examine the design of the VIGV system and its integration with the impeller blade leading edge. Although it was ultimately decided not to utilize the VIGV system in the RPD, the analysis is summarized in this section because of the uniqueness of the effort undertaken and the results obtained. At the time of program close-out, the non-VIGV impeller blade shape definition had just begun.

5.1.4.1 Design Objectives

The original compressor design was based on the following requirements:

- * Impeller. Design suitable for high production rate casting in aluminum with minimum cleanup.
- * Impeller shroud. Running clearances appropriate to mass production.
- * Diffuser. Suitable for one-piece casting, a brazed assembly, or combination.
- * Inlet Guide Vanes. Suitable for mass production assembly, movable between $+60^\circ$ to -30° .

The compressor 100 percent corrected speed design point was:

Corrected Flow, $W\sqrt{\theta}$, 0.6459 lbm/sec.

Pressure Ratio (T-T), 4.260

Zero Inlet Swirl

The compressor was designed to be operated with as much prewhirl as possible at 100 percent corrected speed in order to gain maximum pressure ratio and flow augmentation for vehicle acceleration. At the same time, design requirements included stable operation at match TIT down to 50 percent speed, and compatibility with high positive VIGV prewhirl for reducing pressure ratio and flow at idle power, while maintaining efficiency.

5.1.4.2 Centrifugal Compressor Design System

The WRC centrifugal compressor design system consists of a series of linked computer programs leading from preliminary design to tooling drawings.

Preliminary Design - During preliminary design, decisions are made for values of the important parameters in the detailed segment of the aerodynamic design. From the preliminary design computer program, key parameters are examined by empirically based models for each of the compressor components in the program. This results in

identification of the best compressor for a given application at a chosen design point based on cycle requirements at full and part speed. The program was modified by the addition of inlet swirl angle input capability to assist in evaluation of the effect of swirl on various parameters.

Models for the various compressor design parameters have been matched to actual centrifugal compressor test data. For instance, the impeller efficiency routine uses loss models of Galvas (Reference 1) along with others developed at WRC which are adjusted through the use of fixed multipliers to match all available impeller test data over a broad range of flows and pressure ratios. Radial diffuser modeling is done through test data based correlations based primarily on Runstadler's data (Reference 2).

The preliminary design program supports trade-off and parametric studies leading to selection of the optimum number of impeller blades and diffuser vanes, and determination of the preliminary diffuser flowpath and maximum radius requirement. Parameters examined included shroud relative velocity ratio, inducer tip relative Mach number, hub/tip radius ratio, impeller inertia, compressor exit conditions, and vaned diffuser inlet conditions.

Impeller Aero Design Program - The aerodynamic analysis used is of the axisymmetric, compressible, inviscid, radial equilibrium type. The program interfaces with a blade generator that uses the intersection in space of the calculation station lines and the streamlines, to generate the geometric blade definition having the specified thickness distributions, incidence and deviation. Pressure and suction surface Mach number and interim blade geometry are type-writer plotted for each program pass to support rapid development of the flowpath, blading, and energy addition parameters. Output includes data files for direct input to the NASTRAN stress analysis program, permitting rapid but detailed stress and vibratory analyses of preliminary impellers.

Radial Diffuser Program - Radial diffuser design is conducted (based upon the preliminary design results) by use of the Stanitz vaneless space analysis (Reference 3) and a vaned diffuser computer program which uses vane meanline metal angle and thickness to generate the vane shape to a diffuser area ratio and length to inlet-width between vanes ratio selected from the Runstadler data (Reference 2).

Off Design Analysis - A number of published and WRC experimental compressor maps were available for machines of the 4:1 pressure ratio class. These maps were combined to produce the predicted zero inlet swirl map. In addition, compressor maps for impellers with variable inlet guide vanes were also available to provide a basis for the compressor predicted performance with variable IGVs.

The following sections outline the work performed and the results obtained for the preliminary design, for the aerodynamic analysis of the blading of the impeller and the VIGV, and for the estimates of compressor performance characteristics.

5.1.4.3 Preliminary Design Analysis

Approach - The preliminary design phase considered the use of three VIGV flowpath configurations. These flowpaths were pure axial, pure radial and a combination of axial and radial, called semi-axial.

The prime candidate was the VIGV in an axial flowpath since more data on that flowpath type is available. It also gives mechanically simpler VIGV installation. The semi-axial VIGV configuration showed promise based on detailed flowpath studies. Both configurations were analyzed in detail and the advantages and disadvantages of each configuration determined. It also became obvious that even with common rotor inlet and exit coordinates, identical impeller blading could not be used for both configurations since different inducer inlet flow profiles existed as a result of the differences in inlet swirl and flowpath. Thus, each VIGV flowpath and impeller configuration had to be designed as an integrated system. It was determined, however, that a pure radial inlet and VIGV configuration could use the impeller from the semi-axial configuration without significant compromise. This meant that design effort on the two selected VIGV configurations did not preclude possible testing of a radial VIGV inlet with the impeller design for the semi-axial VIGV.

Preliminary Impeller Design - The compressor selected is a single-stage, backswept centrifugal compressor. The design is based on requirements for a highly efficient stage that possesses broad operating range, low inertia, and mass producibility. The resultant design was the product of the combined experience of both the Chrysler and WRC compressor design teams.

The compressor rotational speed was selected to optimize both compressor and turbine efficiency while maintaining acceptable levels of shaft inertia and disk stress. A low hub-to-tip ratio was selected to minimize disk inertia and impeller shroud inlet relative Mach number, thus providing maximum opportunity for high speed compressor augmentation through the VIGV. Impeller shroud diffusion ratio (inducer exit relative velocity divided by inlet shroud relative velocity) was set at 0.55. This value has proven to be a good preliminary design criterion based on previously successful development work. Impeller backsweep angle was specified to be about 36° in an effort to minimize inertia while still retaining broad operating range and high levels of efficiency in a region that is well removed from the compressor surge line.

Resultant impeller preliminary design parameters became:

	<u>AXIAL INLET FLOWPATH</u>	<u>SEMI-AXIAL INLET FLOWPATH</u>
Inlet Shroud Blade Angle	61.28°	59.38°
Exit Absolute Mach No.	0.975	0.991
Exit Relative Mach No.	0.456	0.485
Exit Relative Flow Angle	48.2°	44.5°
Impeller Efficiency (T-T)	0.883	0.883
Impeller $\Delta T/T$	0.64	0.64

Inlet R _{hub}	0.490"	0.490"
Inlet R _{tip}	1.125"	1.125"
Exit R _{tip}	1.9594"	1.9594"
Exit blade width	0.1486"	0.1486"

VIGV Concept Assessment - Use of VIGV's with centrifugal impellers has typically been with axial inlet flowpaths where a major loss-producing mechanism at large flap deflections would be the increasing gap between the flap and the cylindrical hub flowpath surface. Hub region air turning would also reach a limit because of this gap. In addition, cascade suction surface pressure loading at large flap deflection would contribute to large pressure losses and air turning limitations. Large wakes from partly-separated flaps flowing into a close-proximity inducer would produce a distortion pattern that could excite inducer vibratory modes. It was therefore felt that design improvements could be made.

The intended approach to improving the performance of VIGV in an axial flowpath is summarized as follows:

- * Use increased cascade solidity and flowpath convergence (probably on OD) to minimize cascade loading and thereby improve pressure losses and turning.
- * Use through-the-blade radial equilibrium streamline analysis to support vane profile selection and for prediction of local streamline choke.
- * Displace flapped VIGV upstream of impeller to allow wake dissipation to the maximum extent possible.
- * Consider the possibility of articulating the VIGV leading edge as well as the flap in order to better match the cascade to minimum loss incidence at large flap angles.
- * Produce a VIGV radial swirl distribution (more swirl at the hub than the tip) tailored to properly match inducer incidence requirements as computed by radial equilibrium analysis with entropy gradients.
- * Be realistic in the estimation of VIGV pressure losses since they affect impeller performance and overall compressor efficiency, pressure ratio, and choke margin.

Figure 19 shows the tentative axial inlet flowpath. Table 2 summarizes the advantages and disadvantages of this flowpath.

The installation of VIGV in a semi-axial flowpath is shown in Figure 20. The use of spherical flowpath surfaces produces a constant endwall clearance at all flap deflections. This feature should improve pressure loss and turning performance and permit larger flap deflections. The VIGV are in a lower Mach number region of the flowpath which should reduce pressure losses at all flap

deflections and delay cascade choking at high flap deflections. Flowpath area convergence through the VIGV is obtained at constant passage height due to the reduction in mean flowpath radius.

Through conservation of angular momentum, the tangential velocity and swirl angle increase as the streamline radius decreases. The primary design risk involves increased changes for inlet flow separation due to flowpath curvatures. Additional analysis of this problem is required using viscous flow computational techniques. Experimental work must ultimately validate the computational model of the complex flow field of this curved, inward-flowing annulus with swirl. Table 3 summarizes the semi-axial VIGV inlet approach.

The pure radial location of the VIGV eliminates the requirements for spherical surfaces at the flap location since the VIGV would lie between parallel plane surfaces. A shorter overall compressor flowpath results, but the flowpath curvature near the inducer inlet would be more severe than that of the semi-axial design case. Figure 21 shows a preliminary version of the radial inlet flowpath. Because a radial VIGV can be designed to produce the same inducer inlet swirl pattern as a semi-axial VIGV, it can be considered as a special case of the semi-axial flowpath. Since only two compressor rig variants were to be built and tested, the radial flowpath was dropped in favor of the axial and semi-axial designs. Table 4 summarizes the radial VIGV flowpath design advantages and disadvantages.

5.1.4.4 Performance Projections

Figures 22 and 23 show the predicted performance of the basic compressor as designed for no inlet guide vanes. The performance represents production hardware expectations following a limited development effort with current state-of-the-art design techniques.

Figures 24 and 25 show the predicted performance of the compressor designed for variable inlet guide vanes and an axial inlet flowpath. The 100 and 50 percent speed lines are shown with the VIGV in the zero swirl position and the positions estimated to produce the maximum augmentation at full speed and maximum deaugmentation at idle speed (50 percent). The estimated pressure losses of the VIGV cascade have been applied to these performance maps. Inlet guide vane losses based on those published by Serovy (Reference 6) and the experience of Chrysler (Reference 10) have been used for this estimate, although losses may be reduced by further development.

Design analysis of the semi-axial inlet compressor with variable inlet guide vanes was also completed and performance maps generated. These maps also represent production-type cast rotor hardware with production tolerances and clearances, following a modest compressor development program. Figure 26 shows the 100 percent speed line with 0, -20, -30, and -40 degree flap settings. The dashed line shows the estimated performance of the axial inlet

flowpath design from Figure 24. The semi-axial inlet design is considered to be potentially superior to the axial inlet design in performance because:

- * The VIGV is in a lower Mach location, resulting in reduced pressure losses.
- * The spherical endwalls produce a constant, minimum endwall clearance which reduces endwall losses and turbulence.
- * The flowpath converges in area through the vanes, reducing pressure losses and wakes.
- * The swirl angle produced by the vanes is amplified due to the radius change between the vanes and the inducer inlet, thus producing the required swirl at lower flap angles.

Experimental data, of course, will be required in order to verify:

- * VIGV turning correlations
- * VIGV loss predictions
- * VIGV and inlet aerodynamic blockage assumptions, and
- * Swirl augmentation predictions and flow performance of the curved inlet.

Figure 27 shows the estimated performance of the semi-axial inlet configuration compressor at 50 percent corrected speed and +55 degree flap angle. The results of the axial inlet design performance prediction are overplotted for comparison. Additional reduction in flow is obtained at the same VIGV angle with the VIGV in the semi-axial flowpath due to reduced deviation and the positive effects of swirl augmentation. Deviation is the difference between the VIGV exit air angle and the flap angle.

5.1.4.5 Impeller/IGV Design

In order to begin the design analysis, an optimum zero swirl impeller was generated to match the preliminary design criteria for both the axial and semi-axial flowpaths.

Number of Blades	26 (13 main, 13 splitter)
Impeller Exit Deviation Angle	8.6 ^o
Inlet Aero Blockage Factor	0.96
Impeller Exit Blockage Factor	0.90

Impeller Inlet Tip Radius	1.125 in.
Impeller Exit Average Blade Angle	40° Axial Flowpath 36.5° Semi-axial Flow- path
Impeller Efficiency	0.883
Impeller Total Pressure Ratio	4.839
Impeller Inlet Tip Relative Flow Angle	62° Axial Flowpath 59.4° Semi-Axial
Absolute flow angle	71.8° Axial
Relative Inlet Shroud Mach No.	1.04 Axial 1.08 Semi-Axial
Shroud Relative Velocity Ratio W_2/W_1	0.55 Axial 0.57 Semi-Axial

Blading thickness appropriate to minimum castability in aluminum was used, 0.050 inch at the inlet hub, and 0.020 inch at the inlet tip.

The design was biased toward increased choke margin by:

- * Limiting inlet shroud relative flow angle
- * Larger than normal inlet hub/shroud radius ratio
- * Lower inlet shroud relative Mach number
- * Control of inlet blade passage shape by careful specification of angular momentum (energy addition, RV_U)
- * Minimizing number of inducer blades

Through adjustment of the impeller flowpath and rate of streamline energy addition (RV_U), a satisfactory preliminary impeller was generated for both the axial and semi-axial inlet flowpaths. This blading, designed for free entry incidence, was fixed and the design point choke margin documented for each streamline. In order to estimate the range of incidence through which the impeller would be expected to operate without massive inducer stall, it was assumed that the impeller could operate at the predicted compressor map stall line down to 50 percent corrected speed, the selected idle speed. The inducer incidence and choke margin at various operating points were determined by running the compressor aero program at fixed preliminary blade geometry and streamline loss characteristic using the speeds and flows of the selected map operating points. Program runs were made at 50, 90, 100, and 110 percent speed for surge, operating line, and choke flow conditions.

VIGV Swirl Optimization - At 100 percent corrected speed, various combinations of average swirl level, radial swirl patterns, and augmented flow values (flows greater than the zero swirl compressor design flow at 100 percent speed) were evaluated in the aero design program using the fixed preliminary blade geometry. The goal was to closely match the design inducer radial incidence patterns while preserving choke margin, thereby determining the optimum swirl pattern to maintain satisfactory incidence, as well as to predict the additional flow which the inducer would pass. The VIGV passages were monitored to preclude VIGV choking prior to inducer choke. The resultant compressor flow, pressure ratio, and efficiency provided a point on the 100 percent speed augmented compressor map. By reducing flow at the augmented flap setting until impeller surge incidence was obtained, the surge point for the augmented conditions was estimated. The estimated radial pressure losses of the flapped VIGV were included in the augmented performance prediction. This system of estimating VIGV augmented compressor performance using design point analytical programs is only an analytical approach, and must be verified and updated with experimental data.

Axial VIGV - The desired swirl pattern for 100 percent corrected speed is shown in Figure 28. The resulting flap angle was -37 degrees. It was based on rate of change of loss coefficient versus flap angle from Figure 29 and passage choking considerations. The radial variation of loss coefficient initially selected for the flap was based on the Serovy data correlation of Figure 29. However, since the VIGV configuration resembled the Chrysler design of Reference 10, the Chrysler loss data was used and is reflected in the increase of predicted loss coefficients shown in Figure 28. Figure 30 shows a comparison of the two sets of loss data. While it was felt that an improved VIGV with low pressure losses could be designed even in the axial inlet flowpath, performance prediction data was based on best available experimental data.

With the VIGV tentatively designed for the 100 percent corrected speed augmentation conditions, the performance evaluation was made at 50 percent speed and maximum deaugmentation. At the low corrected flows compatible with 50 percent corrected speed (Figure 25), VIGV passage choke was not a factor, and even with the substantial pressure loss coefficients compatible with large flap deflection angles, the absolute level of VIGV pressure loss was small. A 55 degree flap angle was selected for design analysis, contingent on validation during rig testing. The resulting swirl angle (Figure 28), was used to determine the compressor performance effect.

The resulting inducer incidence at 50 and 100 percent speed with the VIGV set to the appropriate position is indicated in Figure 31 with a dashed line. The average incidence at 100 percent speed augmented is greater than that for 100 percent speed with zero VIGV swirl in order to produce the additional impeller work necessary to attain the augmented pressure ratio at the increased compressor flow. The inability to obtain good hub VIGV turning because of the endwall gap is part of the reason that the inducer incidence near the hub is larger than for the zero swirl angle values at 100 per-

cent speed, as shown in Figure 31. Figure 32 shows the resultant inducer choke margin (dashed line) for the 100 percent speed augmented operating line conditions. Impeller tip region choke margin is increased compared to the zero swirl case because of the additional work in the inducer due to the increased incidence.

After the determination of the apparent optimum swirl for 100% speed augmentation, the VIGV cascade was selected which would produce that swirl, and VIGV pressure loss coefficients reestimated. The preliminary axial inlet VIGV design is shown in Figure 33. Based on a stress and critical speed analysis of the preliminary impeller, the number of acceptable VIGVs was established at fewer than 12 or more than 22 vanes. The philosophy was to keep the VIGV chord length enough so that minimum vane thicknesses were appropriate to manufacturing tolerances, but small enough so that the inducer was several chord lengths downstream in order to minimize vane wake effects.

For the axial inlet flowpath configuration, eleven vanes were selected, as shown in Figure 33. Since the VIGV flap was required to turn the flow in both directions from axial, a zero-cambered symmetrical NACA 63-series airfoil was tentatively selected. This bladeform is commonly utilized for VIGV, and several published design and test reports are available (References 7, 8, and 11), including one employing a flapped configuration (Reference 7). The flap effectiveness factor (FEF) of 1.0 was for a movable flap length equal to 70 percent VIGV chord (identical to Serovy's design, Reference 6), and permitted use of Carter's rule-type turning correlation of Figure 34. The circular arc meanline curve was the best fit for the Serovy-type flap data. If the movable VIGV flap were to become zero in length, the air would not be deflected at all, hence an FEF value of zero. A linear relationship between the FEF values of 1.0 and 0.0 was assumed for Figure 33. For the axial inlet flowpath configuration, a further reduction in air turning was assumed to account for the effects of the large hub endwall-flap clearance (Figure 28).

Semi-Axial VIGV - The design approach for the semi-axial inlet flowpath VIGV and impeller followed the same pattern as for the axial inlet flowpath configuration, although the design effort was not as far along at the time of project close-out. Twenty-three vanes were selected and design pressure losses were based on Serovy's (Reference 6) mid and tip data (Figure 29), since no large hub endwall clearance existed.

The effect of the various VIGV angles on impeller incidence is shown by the dashed lines in Figure 35. The effect on choke margin is shown by the dashed lines in Figure 36. The predicted flow angles and loss coefficients are shown in Figure 37.

5.1.4.6 VIGV Assessment

Shortly before termination of the program it was decided that VIGVs would not be included in the RPD design. The performance gain to be expected, based on the analysis completed, did not appear to be sufficient to warrant the added cost and complexity of using VIGVs.

REFERENCES

Section 5.1.4

1. Galvas, M. R. "Fortran Program for Predicting Off-Design Performance of Centrifugal Compressors," NASA-TN-D-7437, 1973.
2. Runstadler, P. W., "Pressure Recovery Performance of Straight-Channel Single Plane Divergence Diffusers at High Mach Numbers," USAAVLABS Technical Report 69-56, Contract No. DAAJ02-67-C-0106, October 1969.
3. Stanitz, J. D., "One-Dimensional Compressible Flow in Vaneless Diffusers of Radial and Mixed-Flow Centrifugal Compressors, Including Effects of Friction, Heat Transfer, and Area Change," NACA TN 2610, January 1952.
4. Johnson, I. A. and Bullock, R. D., Editors, "Aerodynamic Design of Axial-Flow Compressors", NASA SP-36, 1965.
5. Wheeler, W. R., "Experimental Determination of Turbine Angle and Losses of Axial Compressor Inlet Guide Vanes," Naval Post Graduate School, December, 1972.
6. Serovy, G. K. et al., "Experimental Performance in Annular Cascades of Variable Trailing Edge Flap Axial Flow Compressor Inlet Guide Vanes", ASME 70-GT-106.
7. Jones, B. A., "Single Stage Experimental Evaluation of Variable Geometry IGVs and Stator Blading," NASA CR-54559, Part IV, 1970.
8. Sawyer, C. W. III, "Evaluation of a Low Aspect Ratio Small Axial Compressor Stage," NASA CR-135240, November, 1977.
9. Doyle, M.D.C., and Shaw, R., "Pressure Distribution on Axial Flow Compressor Blading," VKI Proceedings, March, 1965, Part I.
10. Pampreen, R. C., "The Use of Variable Inlet Guide Vanes for Automotive Gas Turbine Engine Augmentation and Load Control," SAE 760285, 1976.
11. Dunavant, J. C., "Cascade Investigation of a Related Series of Six Percent Thick Guide Vane Profiles and Design Charts," NACA RM L54102, 1954.

5.1.5 Turbine

The turbine system for the AGT-102 consists of an inlet scroll, inlet nozzle, radial inflow turbine, and an exhaust diffuser. The turbine was designed with several key features in mind while keeping within structural, packaging, and material constraints. All turbine system components were designed for ceramic materials. The inlet scroll was designed to fit within the regenerator high pressure outlet cavity without presenting any major flow distortion to the regenerator, while providing sufficient flow area from the combustor to the inlet nozzle. The nozzle was optimized for the thickness requirements of ceramic materials.

The radial inflow turbine was designed to achieve peak efficiencies at 80 percent speed while still maintaining the power and flow requirements at the 100 percent speed point. This design point selection was chosen to provide the highest overall operating efficiencies over the range of normal engine operating speeds. The rotor design was optimized within the constraints as defined by the requirements for thick root blading for the ceramic materials, extensive backface disk scalloping, low rotor hub diameter, and the specification of radial blade elements. Bore holes are shown, but would be eliminated to reduce hub stresses if permitted by the ceramic fabrication process. The 80 percent speed point was designed with near zero exit swirl, to balance the magnitude of exit swirl at idle and maximum speed points. The exhaust diffuser featured a 2:1 area ratio and is a conical type.

The design requirements for the turbine at 100 percent speed are shown in Table 5. It is designed to operate close to the optimum values of specific speed and the blade-jet speed ratio parameters, thus insuring the likelihood of attaining the predicted performance goals.

Electromagnetic forming was to be the primary approach for attaching the ceramic rotor to the gas generator shaft. The complete assembly would consist of a metallic sleeve electromagnetically formed around the ceramic rotor stub shaft which would, in turn, be inertia welded to the gas generator shaft. This attachment method offers the greatest potential for both early demonstration and eventual high volume production.

5.1.5.1 Preliminary Design

The WRC design system for radial turbines combines the available literature and data in the industry, in addition to in-house developed or refined correlations, studies, and computer programs to form a comprehensive base of design techniques from the preliminary design stages to the design of templates needed for manufacturing.

Inlet Scroll - The inlet scroll was designed as a single piece ceramic part (Figure 38). The scroll cross-section was constrained

at the combustor exit to minimize the radius and allow sufficient flow area leaving the regenerator. A simple constant change in effective area was maintained with duct flowpath length. This provides a uniform inlet velocity and pressure at all inlets to the nozzle vanes.

Nozzle - The preliminary design for the nozzle was based on a radial inlet and an exit vane angle of 76 degrees. The inlet angle will change from radial when the inlet scroll design is finalized. The exit angle selected was the optimum value based on turbine specific speed correlations. The number of nozzle vanes chosen (19) held the nozzle aerodynamic loading to a moderate level. A smooth area schedule was specified through the nozzle channel to help maintain uniform acceleration along the blade surfaces while minimizing diffusion.

Rotor Preliminary Design - The preliminary rotor design took a number of important factors into consideration. Inputs from the various related groups (e.g., performance, stress, and dynamics) were used to establish the general characteristics required for the rotor. Early in the design work it became clear that the stress requirements of the rotor and disk would have the primary influence on the design.

A study was performed to compare three rotor designs with tip speeds of 2158, 2220, and 2300 fps. Initially the optimum value was 2300 fps as indicated by specific speed correlations. The 2158 fps version best met initial stress level targets but proved to have an unacceptable efficiency penalty. The 2300 fps version had excessive stress levels. The 2220 fps version was configured with acceptable stress levels and even higher efficiencies at the low-end speed range compared to the 2300 fps version. The higher low-speed efficiency was the result of matching this stage at the 80 percent speed point. Figure 39 shows performance comparisons.

The blade thickness and disk profile were established where the maximum blade stress was approximately the same as that of the disk. Stress levels of 26 ksi were obtained for both locations when using a solid disk for the 2220 fps tip speed.

This was considered a reasonable stress level for the preliminary design, based on the average strength of 66.6 ksi and Weibull modulus at 6.7 (Section 5.2.1.1).

The number of rotor blades selected was a compromise between high aerodynamic blade loading and the structural concern for excessive disk stress levels. Twelve blades were eventually chosen as opposed to fourteen, which would be the number chosen from the Stanitz slip factor criterion. The use of splitter blades to reduce inlet loading levels was not mechanically possible due the backface disk scalloping requirements. Their effect on performance improvement is, in any case, somewhat suspect. In one study conducted by

NASA (Reference 1), it was concluded that the losses incurred in the use of splitter blades from additional blade surface friction were offset by the losses incurred from excessive loading levels without splitter blades. Thus, performance levels with or without splitters proved nearly the same.

Obtaining balance in the blade and disk stress levels resulted in a rotor design with extensive backface disk scalloping and a low rotor exit hub diameter. It has been observed in the large majority of experimental studies performed (References 2, 3, 4, and 5) that the additional clearance losses associated with scalloping are balanced by the reduction in disk windage losses. Little, if any, efficiency loss is therefore expected to result. The effect of low rotor exit hub diameter on turbine performance is a relatively high blade surface diffusion rate. An increased hub diameter, however, results in higher exit passage velocities, and thus, poorer diffuser performance. The hub diameter was chosen to balance both concerns.

Radial blade elements were specified in the rotor design to minimize blade bending stresses. This "no lean" condition restricts the degree of freedom in specifying the flow characteristics of the rotor in the radial direction.

Design Point Velocity Triangles - The predicted velocity triangles at 100 percent speed for the hub, mean, and tip streamlines are shown in Figure 40. Good rotor reaction can be observed at all stations. The rotor exit swirl is moderately high in backspin ranging from approximately -16 degrees at the hub to -26 degrees at the tip. The amount of swirl specified was the result of careful consideration in matching the swirl schedule at the different operating speeds with the exhaust diffuser performance. Table 6 shows a summary of the rotor and nozzle design parameters.

5.1.5.2 Rotor Geometric and Aerodynamic Design

The preliminary design of the system established the basic dimensional requirements for the rotor. From this point, a rotor flowpath contour is then generated using superellipse curve fitting. The flowpath contour is divided into equally-spaced meridional calculation stations as shown in Figure 41. Initial estimates are made on the blade thickness and blade angle distributions. In the case of the former, a polynomial expression with a high taper ratio was used to describe the thickness contour. The use of a thick root section tapering rapidly to thin shroud sections keeps centrifugal blade stresses to a minimum. The blade thickness and angle distributions used are shown in Figures 42 and 43. The blade coordinate data are also automatically generated in such a form as to allow direct input into stress analysis programs.

The aero analysis program used is essentially a modification of the program used for centrifugal impellers. It is described in Section 5.1.4 for the compressor design.

The results of the aero analysis at the 100 percent speed point for the hub, mean, and shroud streamlines are shown in Figures 44, 45, and 46, respectively. In general, the analysis indicates reasonable blade loadings at all stations. The established criterion for blade loadings (uniformly increasing mid-channel velocities and minimum blade surface diffusion) have been met for the most part. Moderately high loading at the rotor inlet is unavoidable because of the stress requirement for a relatively small number of blades. The inlet loading, however, is within the levels observed in previously designed radial turbines in the industry (most notably Reference 6). There is also a moderate amount of suction surface diffusion at the hub streamline which, as earlier explained, is due to the low exit rotor hub diameter dictated by stress considerations.

5.1.5.3 Exhaust Diffuser

A conical-type diffuser with an L/D of 1.433 and an area ratio of 2:1 was designed for the turbine exit (Figure 47). The diffuser length was set by packaging constraints. The area ratio selected was one which would offer the maximum average pressure recovery attainable within the range of varying flowfield conditions observed at different operating speeds. Conditions of inlet swirl, blockage, velocities, and rotor exit geometries were considered in the selection of area ratio. The diffuser serves to minimize flow distortions into the regenerators by keeping velocity levels within the feed cavity as low as possible.

5.1.5.4 Performance Projections

The performance of the radial inflow turbine was designed to achieve the good part-load efficiency desired in automotive applications while still maintaining adequate performance for maximum rated power. The predicted turbine performance is shown in Figure 48 as efficiency and flow parameter versus pressure ratio. At the 50, 80 and 100 percent design speed points, the predicted turbine total-to-total efficiencies are approximately 81.9, 87.7 and 87.6 percent, respectively. The turbine was designed to be most efficient at the 80 percent speed point. This approach had the effect of minimizing exit swirl at points below and above the target speed, as can be seen in Figure 49. The swirl levels are +30 degrees at 50 percent speed, -6 degrees at 80 percent speed, and -20 degrees at 100 percent speed.

5.1.5.5 Aerodynamic Design Status

- a. Rotor - Design is essentially complete. Rotor blade z-sections and r-sections have been generated.
- b. Nozzle - Preliminary airfoil design complete. Nozzle radial inlet could change slightly depending upon further analysis of scroll flow characteristics. Number of nozzles also subject to change pending results from further dynamic analyses.

- c. Scroll - Scroll design is complete, and has been submitted for vendor's final ceramic fabrication technique and quotation.
- d. Diffuser - Design is complete. Alternate types of diffuser proposed (e.g., radial and hybrid) have not been studied.

5.1.5.6 Turbine Rotor Mechanical Analysis

The design requirements for the ceramic turbine rotor are a turbine inlet temperature (TIT) of 2300F and an operating speed of 99,500 rpm. The ceramic material assumed is alpha silicon carbide. The design requirements for the uncooled metal turbine rotor are a TIT of 2100F and an operating speed of 99,500 rpm. The metal turbine rotor is cast MAR-M 247.

Both turbine designs were investigated with the aid of finite element analysis. A heat transfer analysis and a structural analysis were performed on each design. The details and results of these analyses are described in this section.

Turbine Rotor Heat Transfer Analysis - A 2-D finite element model and the ANSYS computer code were used to determine the operating temperatures of the ceramic turbine wheel in a steady-state 2300F TIT environment. The model is axisymmetric, so the blade element material properties have to be scaled to account for the thickness of the blades.

Heat transfer coefficients and bulk temperatures were applied as boundary conditions to the model, using the exhaust gas temperature and compressor discharge temperature (CET) obtained from performance data. The convection coefficients for the gas path elements were based on channel theory. Since the model is axisymmetric, these coefficients are modified to account for actual gas path surfaces. The convection coefficients on the faces of the hub are based on free convection from a rotating disk.

The turbine rotor temperature distribution resulting from the heat transfer analysis is shown with isothermal lines in Figure 50. Note the effect of air bearing cooling air which discharges on the backface of the hub.

The heat transfer analysis for the metal turbine rotor was also performed using a 2-D finite element model and the ANSYS computer code. The model is axisymmetric as in the ceramic turbine analysis, so the blade element conductivities are scaled to reflect the blade thicknesses.

Convection coefficients and bulk temperatures for a 2100F TIT steady-state condition are applied to the model as boundary conditions. The heat transfer coefficients are determined in the same manner as those for the ceramic turbine.

The resulting rotor temperatures are given in Figure 51 as lines of constant temperature.

Turbine Rotor Stress Analysis - The 2-D finite element model of the ceramic turbine rotor used in the heat transfer analysis was used in the stress analysis. A plane stress element with thickness input was used for the blades. This element provides a reasonable stress picture of the blade and was used to determine a preliminary thickness distribution (Figure 52). This element also simulates the centrifugal load of the blades on the hub.

The temperatures determined in the preceding heat transfer analysis are used in the stress analysis. Maximum speed centrifugal and thermal loads are applied to the turbine rotor. The resulting maximum principal blade stress is 26 ksi. This model provided partial bores in both faces of the hub to aid sintering of the alpha silicon carbide. This increased the tangential stress at the disk center to 31 ksi, Figure 53. Development of the ceramic rotor fabrication process may permit a solid hub with a corresponding reduction in hub stress.

A 3-D finite element analysis was then performed using a sector model of the turbine rotor constructed with 8-node brick elements (Figure 54). This model yields more accurate results in the blade than the 2-D analysis. Static load due to design speed only was applied to the model. The resulting peak stresses, shown on Figure 54, correlate well with the 2-D analysis of the turbine rotor.

The stress analysis of the metal turbine rotor was performed with the same finite element model that was used in the heat transfer analysis. The metal rotor blade is a preliminary 2150 fps tip speed design. The 2220 fps tip speed design had not yet been modeled for the metal turbine. A plane stress element with thickness input was used for the blades. This element provides a reasonable stress picture of the blade and was used to determine a preliminary thickness distribution (Figure 55). This element also simulates the centrifugal load of the blades on the hub.

The rotor temperatures determined in the heat transfer analysis were used in the stress analysis. The resulting stresses in the rotor at design speed are given in Figure 56. The maximum equivalent stress in the disk, 100 ksi, occurs at the center. The estimated temperature at this location is 1566F. This combination of stress and temperature results in a stress-rupture life of only 10 hours. This was considered acceptable for a limited-life turbine for initial engine development. This is especially true if early engine testing is speed-limited or temperature-limited for initial mechanical and aerodynamic evaluation and development. Design modifications, better material, or cooling could be considered for longer life.

5.1.5.7 Turbine Rotor Shaft Attachment

Considerable effort was expended on design analysis of the attachment of the ceramic turbine rotor to the shaft. Primary effort made use of a dual-property shaft electromagnetically formed to the hub of the ceramic rotor. The shaft consisted of a molybdenum sleeve inertia-welded to a steel shaft and then electromagnetic-formed to the ceramic (Figure 57).

A critical property of the sleeve material for electromagnetic forming is high electrical conductivity. In addition, the sleeve must possess suitable elevated temperature strength and relatively low thermal expansion to maintain adequate clamping force on the ceramic stub shaft through thermal cycling. The alloy chosen for the RPD is molybdenum (see Section 5.2.4).

The design effort addressed two basic problems:

- * Stress levels at the inertia welded joint.
- * Stresses and fit of the ceramic-molybdenum interface.

A finite element model of the shaft joint shown in Figure 58 was used in this analysis. The joint location was chosen at a distance from the ceramic rotor that had no influence on the stresses in the joint. Primary stresses are then only a function of the temperature of the shaft. Steady-state temperatures were used assuming no residual stresses developed during the inertia welding. The maximum equivalent stress was 94,425 psi in the molybdenum sleeve and 41,460 psi in the steel shaft. Primary cause of the difference in stresses between the molybdenum and steel is the difference in the modulus of elasticity between the two materials (42,500,000 psi for the molybdenum versus 27,200,000 psi for steel at 500F). The joint appears to be satisfactory at this design condition, based on a yield strength of 121,000 psi for the molybdenum and 105,000 psi for steel. Fatigue and fracture mechanics were not considered in this evaluation.

An interference fit up to the yield strength of the sleeve can be achieved by electromagnetic forming. This maximum interference fit is required between the ceramic rotor and molybdenum sleeve in order to maintain a positive attachment during the operating cycle of the engine. This includes thermal transients, steady-state, and soakback after the engine is shut down.

Several configurations were investigated as follows:

- a. Molybdenum sleeve with shrink fit onto the ceramic turbine.
- b. Same as above but with a layer of zirconium oxide between to act as a thermal barrier.

- c. Same as "a" but with a stainless steel compliant material between them.
- d. Steel shaft with cooling air passing between the shaft sleeve and ceramic rotor.

After consideration, the first configuration was chosen as the most applicable. A layer of zirconium oxide between the sleeve and ceramic is proposed but to be used as a diffusion limiter rather than thermal barrier.

The molybdenum sleeve shrunk onto the ceramic provides a compressive stress of 130,000 psi at room temperature which is the yield strength of the material. Results of the thermal and stress analyses are shown in Figures 59 through 63.

REFERENCES

Section 5.1.5

1. Futural, S. M. and Wasserbauer, C. A., "Experimental Performance Evaluation of a 4.59-Inch Radial-Inflow Turbine With and Without Splitter Blades", NASA TN D-7015, 1970.
2. Rodgers, C., "Efficiency and Performance Characteristics of Radial Turbines," SAE 660754, 1966.
3. Vershure, R. W., Large, G. D., and Meyer, L. J., "A Cooled Laminated Radial Turbine Technology Demonstration," AIAA-80-0300, 1980.
4. Monson, D. S. and Ewing, B. A., "High Temperature Radial Turbine Demonstration" USAAVRADCOM-TR-79-2106, April, 1980.
5. Kidwell, J. R. and Large, G. D., "Advanced Technology Components for GTP-305-2 APU," AFAPL-TR-79-2106, 1979-1980.
6. Calvert, G. S., Beck, S. C., and Okapuu, V., "Design and Experimental Evaluation of a High-Temperature Radial Turbine," USAAVLABS Technical Report 68-69, AD688164, January, 1969.

5.1.6 Combustor

5.1.6.1 Combustor Analysis and Modeling

The major design problems associated with the lean, premixed, prevaporized (LPP) combustor stem from the nature of a mass-production automotive component. The combustor must combine the sophisticated technical demands of low emissions, multifuel capability and minimal total pressure drop with the restrictions of low cost, compactness, and reliability.

In order to resolve these often conflicting goals, it was necessary to carefully quantify all aspects of the combustor. This was done by first conducting an intensive study of published reports and papers on each of the various combustion phenomena (turbulent flame speed, mixing losses, and many, many others) and then selecting the data base for each subject which was judged to be closest to the AGT-102 combustor operating conditions. A mathematical model of the data was then constructed. Finally, these various models were combined with basic fluid flow and thermodynamic equations to create a complete combustor model. The model can simulate operation of the combustor, including off-design points, and predict driving cycle emissions.

The sections below briefly summarize all of the important individual modeling tasks. Details of the complete computer program and its output are available in Section 5.1.6.3, which traces the development of the final design. Section 5.1.6.3 also provides quantitative answers for the final combustor design behavior when the models explained in this section are applied.

Although the phrase LPP combustor is used throughout the report, it will become apparent that pure LPP operation represents an ideal behavior which can only be approached under AGT operating conditions.

Autoignition - The ignition of a fuel/air mixture solely because of its inherent high-temperature/high-pressure thermodynamic state is well known in spark-ignition engines as "spark knock" or detonation. It is the "modus operandi" of the diesel engine. An automotive gas turbine can operate with the fuel spray igniting before evaporation and mixing with the combustion air is completed, but such diffusion flame combustion will (as in a diesel engine) produce high nitrogen oxide (NOx) emissions. The high NOx problem results from preferential combustion in a stoichiometric vapor-air diffusion zone adjacent to each droplet. This results in very high local temperatures even with an overall lean fuel-air ratio where there is excess air and a low average temperature. To design a low NOx combustor, evaporation and mixing of the fuel spray must be achieved before autoignition begins. Therefore, a design model is needed of the influence of fuel type, air temperature, and pressure upon the time available before autoignition.

Numerous references were found in the literature which could be used to formulate such a model, but most of the experiments were performed at air temperatures lower than the AGT-102 operating conditions. Additionally, sprays of much coarser droplets (or even large single drops) were used instead of the very fine sprays expected for the LPP combustor. There are some excellent studies underway such as the work L. J. Spadaccini of United Technologies (Reference 1) that should provide excellent reference material for the future.

Ultimately, the extensive data base of B. P. Mullins of the National Gas Turbine Establishment (British) was selected in spite of its 1950's vintage (Reference 2). The major arguments in its favor are: air temperatures up to 2300R, a gas-turbine-like spray (Sauter mean diameters as low as 50 microns), and a check of a great variety of fuels.

Although the data were obtained in oxygen-deficient air (due to precombustion), an experimentally derived correction factor was obtained to adjust the data to standard air. Figure 64 reveals typical ignition delay data. As might be expected, it is exponential in temperature. The Figure 64 data are not corrected for standard oxygen concentration. Performing the correction reduces the autoignition time to well under one millisecond at AGT-102 inlet air temperature.

The data were taken at atmospheric and subatmospheric pressure, and a modification for the moderate (up to 4 atmospheres) pressures of the AGT-102 cycle was also required. A study of the Mullins data plus other information leads to a correction that is linearly inverse with pressure. Thus, at two atmospheres, autoignition occurs in half the measured time for one atmosphere. Results from the NASA high temperature, ultra-lean test rig confirm the reality of very rapid autoignition, and the modified Mullins data are believed to be quite accurate.

Equations were computed for six fuels (heptane, iso-octane, kerosene, turbine fuel, iso-dodecane and ethanol) with the following form:

$$t = (P/14.7)^{-1.0} 10^{m_1/T + C_1}$$

where m_1 and C_1 are fuel dependent. The autoignition time is denoted by t ; T and P are gas temperature and pressure (both are static properties). The form of the equation follows directly from the Mullins' data. The values of m_1 and C_1 (after applying Mullins' correction to standard air) are given below:

<u>Fuel</u>	<u>M_1</u>	<u>C_1</u>
Heptane	23567.744	-11.202185
Iso-Octane	13858.943	- 6.326877
Kerosene	18174.517	- 8.438687
Turbine Fuel	18821.349	- 8.663272
Iso-Dodecane	19526.472	- 8.955744
Ethanol	17018.785	- 7.794519

Autoignition times for one of the fuels (kerosene) are computed below for approximate cycle conditions at engine speeds of 50%-80%. The results illustrate the rapidity of the autoignition reaction under AGT-102 conditions.

<u>Speed</u>	<u>Temp. (^oR)</u>	<u>Press. (PSIA)</u>	<u>Time (Millisecs.)</u>
50%	2200	22	0.44
60%	2200	27	0.36
70%	2200	32	0.31
80%	2200	40	0.24

Droplet Evaporation - The evaporation of a single droplet of fuel in a gaseous environment by conduction and diffusion processes is a well-researched topic and is expertly explained by D. B. Spalding in Reference 3. A description of the equations would be fairly lengthy and will not be repeated here. In brief, evaporation time is proportional to the square of the droplet diameter. It also depends on the gas density, molecular diffusion coefficient and the transfer number, all of which are functions of temperature.

Droplets that are moving relative to their surroundings undergo an additional evaporation augmentation--convection. A recent paper (Reference 4) relates aerodynamic factors and Prandtl and Reynolds numbers to a convective correction. This work aided the Reference 3 characterization effort to provide a complete description of the evaporation phenomena.

Given an autoignition time, one can compute the diameter of the largest droplet to evaporate before autoigniting. Since autoignition time decreases exponentially with temperature while evaporation increases with only a low power of temperature, it is clear that very high temperature environments (such as the AGT-102 combustor inlet air) will require very small droplets to complete evaporation before autoignition.

Figure 65 underscores the difficulty of designing an LPP combustor as the inlet air temperature increases. Spray requirements are modest at the 1200-1300F temperatures accompanying previous gas turbine cycles, but they become severe at AGT-102 conditions. Also, as shown, the type of fuel is a significant factor.

Any real spray will have a distribution of droplet sizes which can be described by a parameter such as Sauter mean diameter (SMD). Knowledge of the distribution of droplet sizes for a given SMD will allow the calculation of the mass fraction of the total spray that will autoignite before evaporating. A great many spray distribution functions have been proposed. Two recent papers by H. C. Simmons (References 5 and 5a) review previous work and present a method for calculating the mass fraction of the spray that is equal to or

smaller than λ given diameter when the spray SMD is specified. One can enter an array of SMD likely to correspond to different atomizers and have the spray mass fraction burning as droplets predicted for each atomizer. As will be seen later, the SMD required is quite small.

Fuel Atomization - A Russian textbook on atomization (Reference 6) serves as a good overview of the diversity of atomization techniques available. A thorough investigation of the SMD performance and fuel-air mixing characteristics of atomizers was undertaken since the success of the LPP combustor depends upon the atomizer accomplishing two functions: it must achieve an SMD small enough that only a modest amount of any type of fuel will burn as droplets, and it must thoroughly and almost instantaneously mix the fuel with all of the combustor primary air to insure that lean combustion keeps the flame temperature under the range where high NOx concentrations would develop. This section provides a brief overview of the atomization problem.

Equations for SMD can be often arranged into the following form for different types of atomizers. The values of the exponents usually vary somewhat with the type of atomizer. This equation is similar but not identical to a universal atomizer equation derived by H. C. Simmons (Reference 5a).

$$SMD = \sigma_l^{1/2} L^{1/2} \rho_a^{-1} V_{l-a}^{-1} (1 + W_l/W_a) + f(\mu)$$

σ_l	Droplet surface tension
L	Atomizer characteristic length
ρ_a	Air density
V_{l-a}	Droplet velocity relative to air
W_l	Mass flow liquid
W_a	Mass flow air
$f(\mu)$	Fuel viscosity correction function

SMD is almost inversely related to the relative velocity between the spray and the surrounding gas. The functions of surface tension or air density are fuel or operating-condition dependent and thus largely out of the control of the atomizer. SMD increases with the square root of some characteristic length of the atomizer. For airblast or air-assist atomizers there is an effect due to relative fuel and air massflow rates. Finally, there exists a second order term that depends upon the fuel viscosity. Clearly, the way to create a small SMD is to move the fuel or air (or both in opposite directions) at very high velocity. Data in Reference 7 show that SMD's of only 5-6 microns are possible if supersonic air velocities are used.

The practical problems are obvious. Very high fuel pressures (and very small holes that are prone to plugging) are needed if one desires high fuel velocities. High air velocities are easy to achieve, but they result in lengthy combustors and high diffusion losses during deceleration.

The major types of atomizers investigated were: pressure (Simplex), airblast, air-assist, rotating disk, vaporizing, ultrasonic, and electrostatic. Although very fine values of SMD could be produced with high-speed rotating disks or ultrasonic devices, these techniques do not achieve rapid dispersion of the fine fuel droplets into the large amount of primary air used in an LPP combustor. Because of autoignition, there is simply insufficient time for the necessary mixing processes to occur. The vaporizing systems suffer from the same defect.

The pressure (swirl chamber type) atomizers do not meet either criterion: mixing is insufficient and the spray is too coarse for reasonable fuel pressures (100 psi).

Most of the potential fuels (except alcohols) do not have the polar charge on a molecule that is required for electrostatic atomization techniques.

The air-assist devices may achieve fine sprays with some air intermixed with the fuel, but since the cycle limits the amount of air that one can bleed from the compressor, a large mixing problem remains.

Ultimately, one selects the fuel-air preparation method recommended by Prof. LeFebvre of Purdue University: send all of the primary air through an airblast atomizer. This technique insures intimate (and rapid) mixing of the air and fuel. However, calculation of the values of SMD for conventional airblast atomizers (see Reference 8) at AGT-102 operating conditions yields sizes of about 20 microns. As is shown in the combustor design discussion (Section 5.1.6.3), lower values of SMD are probably required. Figure 66 from Reference 9 shows one of the best of the conventional airblast atomizer designs. This design impacts the fuel (20) with air from both sides (17 and A1). There are swirl vanes in all three passages (22, 16, and 25). Acceleration is used in the air passages to reduce boundary layer growth. The fuel exit region (12 and 13) is designed to prevent a fuel boundary layer from developing when the air is added. Further details are carefully explained in the patent.

While one can increase air velocities (and get smaller SMD values), greater total pressure losses and increased combustor sizes result. The NASA high temperature, ultra-lean rig (Reference 10) uses air moving at around 900 feet/sec to obtain SMD values of approximately 12 microns. It is suspected that a modified airblast design (starting from Reference 9) could achieve similar performance at lower air velocities since the NASA design uses a simple tube to inject the fuel.

Residence Time - Calculation of the residence time in the primary zone of the reactor tube, which is essential for some emissions estimates, required calculation of the diffusion/combustion cone within the cylindrical tube. (The final design uses a sudden expansion from the atomizer tube into the end of a cylindrical flame tube. This arrangement results in a free jet which expands in the downstream direction). A jet cone expansion angle of 23° was calcu-

lated based upon the fluid mechanics of diffusion and 38° - 71° based upon inlet velocity and turbulent flame speed ratios.

The 23° cone angle was obtained by establishing the same velocity deceleration rate tolerated in conventional diffuser designs, taking into account the density changes due to heat addition.

The 38° - 71° cone angle was obtained by simply taking the arc-tangent of the predicted turbulent flame speed to the inlet velocity. Here, the radial velocity is assumed to arise from flame propagation only.

It was decided to use 23° as the angle to provide a conservative (i.e., minimum) estimate of residence time. Using this approach, a residence time is calculated by integrating along the flow length using the velocity deceleration achievable in a conventional conical diffuser. This technique was used in Reference 10.

Emissions - Combustor emissions consist of carbon monoxide (CO), nitrogen oxide (NOx), unburned hydrocarbons (HC), and smoke/odor. Automotive gas turbines that meet CO standards almost always meet the hydrocarbon standard, and the ceramic combustor (with no film cooling air) at a high cycle temperature will easily meet the HC goals provided that the startup behavior is reasonable. Also, smoke and odor are likely to be only startup concerns with this high-temperature LPP concept. Thus, the two emissions that were studied in detail were CO and NOx.

The approach used to predict emissions over a driving cycle was to consider the process as quasi-steady-state (a summation of time at steady-state engine conditions) and then somewhat arbitrarily double the results to allow for the problems of startup, accelerations and unknown factors. This technique has been used successfully on past turbine power plants, but since the AGT-102 uses a flywheel assist for acceleration, it is likely to have more safety margin on emissions than past engines. The table below gives the breakdown of engine speeds and their times for the EPA driving cycle (urban) determined by AGT-102 vehicle performance analysis. These times were used by the combustor program to calculate driving cycle emissions.

<u>Engine Speed</u>	<u>Cycle Time</u>
42% (Idle)	623 Secs.
50% ± 2½%	348
55% ± 2½%	162
60% ± 2½%	133
65% ± 2½%	72
70% ± 2½%	22
75% ± 2½%	6
80% ± 2½%	<u>6</u>
TOTAL	1372 Secs.

Three different methods are used to estimate the driving cycle emissions. The first relies on the data from the NASA high tempera-

ture, ultra-lean combustion rig (Reference 10). Figure 67 plots the emissions index for CO and NO_x as a function of adiabatic flame temperature and residence time. The inlet air temperature of 1200K (1700F) is very close to the values entering the combustor (1722F to 1745F) over the idle to 80% speed range encountered during the driving cycle. The residence times also span typical values for the AGT-102 combustor. Fuel flow at the various engine speeds can be used with the times from the table above to easily compute the driving cycle emissions (based upon flame temperatures at each condition).

The second emission calculation procedure uses the characteristic time method promoted by Prof. A. M. Mellor of Purdue University. It computes a characteristic residence time based on combustor geometry. It is ratioed to a chemical kinetics time for the pollutant species, and this ratio is linearly related to an emission index. See Figure 68 for a sample correlation using the JT9D engine.

The following equations were proposed for general purpose use:

$$NO_x - EI = 4.5 \tau_{(sl, NO_x)} / \tau_{NO_x} \quad (\text{gms/kg fuel})$$

$$CO - EI = 35 \tau_{CO} / \tau_{(sl, CO)} \quad (\text{gms/kg fuel})$$

EI Emissions index

$\tau_{(sl, NO_x)}$ Residence time in shear layer, NO_x

τ_{NO_x} Chemical kinetics time, NO_x

$\tau_{(sl, CO)}$ Residence time in shear layer, CO

τ_{CO} Chemical kinetics time, CO

Figure 68 and the above equations are discussed in Reference 11. The NO_x correlation is for a diffusion flame, and hence it was used with the estimate of fuel mass fraction that autoignited (while still in droplet form) to get estimates of the SMD needed from the atomizer. The CO calculation was modified, after discussion with Prof. Mellor, to allow for a premixed flame. CO is strongly dependent upon the inlet air temperature.

The third emissions estimate resulted from running the NASA chemical kinetic computer program (Reference 12). The lengthy run time (approximately one minute) for this program, when about 20 different oxidation and NO_x equations are input, restricted its use. In general, the bulk of the fuel energy is released in about 4 cm of distance. The remainder of the combustor length oxidizes CO and, unfortunately, creates NO_x. An ultimate goal was to run the program for only the final combustor geometry at its various operating conditions, but time did not permit this activity before program close-out.

As is clear from Figure 67, there is a range of flame temperatures between which the standards for CO and NO_x are both met. However, the wide range of AGT-102 operating conditions spans a much

wider band of flame temperatures. The desire to avoid a variable geometry combustor while meeting the emissions standards led to a dual stage approach that is described in Section 5.1.6.3. Detailed emissions predictions will also be presented in Section 5.1.6.3.

Flashback and Turbulent Flame Speed - Turbulent flame speed is often computed by multiplying the laminar flame speed by a factor which depends upon Reynolds number, turbulence intensity or some other fluid mechanic parameter. Hence a considerable effort was expended to achieve an accurate laminar flame speed model. Reference 13 presents the data which were chosen because they were taken with inlet mixture temperatures up to 1460R, and thus the extrapolation needed was smaller than that needed for other sources. The equation to provide an analytic model is:

$$S_{LAM,MAX} = 0.55655 \exp(0.001874T(^{\circ}R))$$

It has a correlation coefficient of 0.997 through temperatures of 560R, 860R, 1160R, and 1460R. The form of the equation and the excellent fit suggest that extrapolation to 2160R should not be overly risky.

Computation of the turbulent/laminar flame speed ratio (TFSR) is not as straightforward. The best investigation appears to be the work by Ballal and LeFebvre in Reference 14. Using the criteria in their paper, it is likely that the AGT-102 combustor would operate in region one of their 3-region model (see Figure 69). The region one selection results from relating the laminar flame speed to the inlet velocity r.m.s. fluctuating velocity level. The turbulence intensity and integral scale of turbulence are not known, but reasonable guesses for them indicate that a turbulent/laminar flame speed ratio of around 4.0 would be likely. Hence, that value was used in the program. One then enters a safety factor to insure that the flame will not propagate upstream. This approach is discussed in Section 5.1.6.3, Engine Combustor Design.

A second method of predicting flashback is presented in Reference 15. This Russian work relates a flashback Reynolds number to a laminar flame speed-thermal diffusivity ratio. It predicts 3.9 to 4.1 for TFSR, which confirms the previous estimate.

Lean Limit Prediction - Three methods were used to estimate the conditions under which the mixture would be too lean to maintain stable combustion. The first approach is simply the well-known White criterion that the flame temperature is 2372F at the lean limit, regardless of inlet temperature. The second scheme uses the equation developed in Reference 16 by Ballal and LeFebvre. It inputs blockage, turbulence intensity, initial temperature and pressure, and mixture velocity. The results were surprisingly close to the White criterion under most conditions, as indicated in Section 5.1.6.3, Engine Combustor Design.

The final lean limit estimate draws on the NASA ultra-lean, high temperature rig data (Reference 10). It shows a lean limit temperature of 2050F to 2100F, which is well below the other methods. Thus there appears to be more margin at very high inlet temperatures than traditional approaches indicate. It was a design goal to achieve some safety margin by not violating either of the first two methods.

Pressure Drop - Three sources of total pressure drop through the combustor were considered: 1) an atomization loss through the atomizer into the primary, 2) the fundamental pressure loss due to heat addition to a flowing fluid and an increase in area (sudden expansion loss), and 3) dilution and mixing losses in the secondary region. Each loss source is discussed separately.

A constant loss of 0.75% was selected as an acceptable limit for fuel/air atomization. While this value is generous for a high-pressure-ratio gas turbine, it is a significant pressure drop for an engine with only a 4:1 pressure ratio. Airblast atomization nozzle vendors considered it marginal but probably acceptable if the start up mode was handled using a pressure-type atomizer.

The fundamental total pressure loss can be found in any text on combustors or compressible fluid flow. It is small due to the high inlet air temperature provided to the combustor and the overall lean combustion which limits peak temperatures before dilution. A loss of about 1% was typical for this combustor. This loss also accounts for the expansion of the high-velocity fluid from the premixer/prevaporizer exit (flashback orifice) into the liner.

The mixing and dilution losses were handled as explained by Profs. LeFebvre and Norster in Reference 17. It bases the calculation on annular to liner pressure differences, and it includes curves for the calculation of dilution hole area and number. Losses ranged from around 1% to slightly over 2% depending upon the engine speed.

Flame Stabilization - The area ratio from the flashback orifice to the main liner is input. In general, sudden expansions of 3 or 4 to 1 (or more) aid stability by creating recirculation regions. Other methods are discussed in the design section. The startup process where velocities are low is most critical for stability.

Heat Transfer Through Liner - Prof. L'Ecuyer of Purdue has created an extensive calculation procedure to predict inside and outside liner temperatures. The method allows for conduction, convection, radiation, and film cooling (if present). His work includes data on flame luminosities and various measured coefficients. See Reference 18 for details. Since liner temperatures were not needed during

each phase of the combustor design effort, this heat transfer routine was coded separately and only used to analyze the final design under various operating points.

Miscellaneous - Flame temperatures were computed using the data of Reference 19, which also provides internal energy, specific heat, and gas constant.

5.1.6.2 Combustor Test Rig

Design Features - The combustor test rig (see Figure 70) uses bleed (about 25%) from a modified Baseline Engine as the high-temperature, variable-pressure-level air supply. All of the components of the rig were designed at the time of program close-out. This included three ceramic parts. Carborundum Corporation was consulted regarding the design of the ceramic parts. Two of them were to be fabricated from standard ceramic tubing and the third from a slip-cast component.

The gas turbine uses ceramic regenerator cores and a remote-control modulating valve to meter the rig airflow. The pressure level is coupled to the engine speed in the usual manner.

The rig incorporates a quartz viewing window at the right-angle elbow to the engine. This feature allows closed-circuit video viewing of the combustion process and optical pyrometer measurements. A smaller quartz window mounted directly in the combustor dome permits observation of the startup process.

Standard water-cooled probes are used to measure emissions following techniques previously developed on LPP combustors.

Development Items - The performance of different types of atomizers, and their emissions behavior using various fuels, was the primary task for the combustor test rig. The design allows rapid interchange of atomizers, and the test cell can provide several different fuels, although most of the development will use research grade unleaded gasoline because of its well-defined composition. As mentioned in Section 5.1.6.1, airblast atomizers are believed to hold the most promise, and a variety of them would be investigated.

A second task for the combustor test rig would be the development of a reliable startup system using a ceramic glowbar ignitor and a pressure-atomizing startup nozzle (see design section). This work would involve optimizing the location of these startup components, defining the temporal characteristics of their operation, and interfacing the startup system with the switch-over to operation using the main atomizer.

An additional task of the combustor test rig would be the development of a geometry which minimizes the total pressure drop

through the combustor. Metal combustor liners would be used to allow rapid modification of the shape, and the hence, many possibilities could be explored. Tests would be run using a ceramic combustor only after a final geometry had been determined and a complete structural analysis (including a probabilistic failure analysis) had been performed.

5.1.6.3 Engine Combustor Design

Design Philosophy - A basic ground rule for the combustor design was that variable geometry would be totally out of character with low-cost, reliable, high-volume production, automotive technology. A variable geometry combustor requires rapid response actuating hardware and a precision non-binding mechanism. Both of these components would be costly and likely candidates for failure. It was therefore decided to rule out variable geometry, keep all other options open, and let the final design geometry evolve.

The initial work considered using a torch which would burn continuously at low values of fuel flow; this concept had proven itself useful on past Chrysler LPP combustors. Further investigation, however, revealed that the torch was not needed. At the high AGT-102 combustor inlet temperatures, the combustor will automatically relight by autoignition if the fuel or air supplies are interrupted. A torch could also be a significant source of emissions and it is a fuel economy loss if it utilizes compressor discharge air for atomization or cooling.

The fueling arrangement selected is based on a well-established approach to wide-range LPP combustion: parallel-circuit fuel splitting. The design employs two parallel primary air circuits, each flowing the same airflow. The amount of fuel (if any) sent to a stage depends upon the engine speed. At idle, fuel is supplied to only one stage, and this stage runs lean enough so that CO is just held under control by means of a moderate flame temperature. Increasing the engine speed (and hence, power) results in increased fuel flow to this stage up to 60% engine speed. At this power level, continued increases in fuel flow (and hence, flame temperature) would begin to produce substantial NOx. Consequently, some of the fuel is metered to the second stage. The fuel split is unequal. This technique provides greater stability since the first (hotter) stage can stabilize the second. For engine speeds above 80%, the first stage again begins to produce high NOx. However, this high level of power is not encountered during the EPA driving cycle, and only rarely in the "real world".

Additional analysis from the combustor computer model revealed that a constant 60-40% fuel split at any engine speed beyond 60% engine speed would meet the NOx standard (using diesel fuel). The installation of two identical fuel atomizers, using a simple solenoid and restrictor on one of them, was deemed a low-cost and reliable method of achieving the necessary flame temperature control over a wide variation in power levels.

Design Program and Tradeoff Investigation - Numerous aspects of the computer code have been discussed in Section 5.1.6.1. A package consisting of a brief writeup covering input and output, a code listing (about 1,000 lines), a sample input deck and a program deck is part of the deliverable items for program close-out. This section summarizes some of the more important findings as input parameters were varied and perturbations of the final design were made.

Although the combustor could be designed for any operating state, it was found simplest to design at idle, where the most time is spent on a typical driving cycle. All other conditions, including 100% speed, are off-design.

A design air-fuel ratio of 65.0:1 at idle was found to be a good choice. It allows a wide range of operating conditions. Only at 60-70% speed (the cross-over to two-stage operation and slightly beyond) does the leaner stage fall slightly below the White or LeFebvre lean limits. However, the NASA combustion rig data indicates that more margin is available than these calculations indicate. Furthermore, the richer (and hotter) first stage should stabilize the "cool" one. Continued CO reaction will occur even in the volute after dilution air is added.

The velocity safety factor to avoid flashback into an atomizer is 1.4 at idle. It becomes 1.6, 2.2, 2.3, and 2.4 at 50%, 60%, 70%, and 80% speeds, respectively. Although greater margins of safety would be better, the resulting high entrance velocities would lengthen the combustor and increase the total pressure drop. Experimentation is essential. It might even be possible to lower the atomizer exit velocity and thereby reduce the combustor length.

The liner diameter was computed as a multiple of the atomizer exit area. A factor of eight allows a large residence time to be achieved in a fairly short length. Greater distance could not be easily used because of engine packaging and insulation requirements.

The annulus Mach number was selected to give minimum total pressure drop due to mixing. Substantial mixing penetration (and hence, losses) is not necessary since the disparity between primary and secondary temperatures is small compared to traditional combustors. Additionally, the turbine volute provides good mixing.

Blockage values (area reduction factors due to boundary layer displacement thicknesses) are difficult to obtain or estimate. Fortunately, they have little effect upon the final design if the blockage is small. Estimates of 1 to 10% were used for various regions of the combustor. With the exception of the recirculation zone, high blockages due to flow separation are not likely in this device.

Atomizer SMD values of 5, 8, 10, 12 and 15 microns were input for each run. The largest (15) appears to be marginal since the fraction of the fuel burning as droplets (at idle) ranged from 0.124 for ethanol to 0.412 for heptane. Other operating requirements provided similar values. An SMD of 10 microns shows better behavior:

0.202 (heptane), 0.029 (iso-octane), 0.090 (iso-dodecane) and 0.022 (ethanol). Thus once again the requirements of very fine atomization become evident.

Important characteristics of the final design are presented in Table 7.

Fuel Metering - Figure 71 presents the fuel metering system, which is similar to that of the Upgraded Engine. Check valves are used extensively to allow fuel to be blown back into the tank during shutdown. This approach prevents sooting and helps control hydrocarbon emissions, smoke and odor on restarts.

The startup nozzle is a new component. It runs only until engine temperature and pressure levels are suitable for stable operation of the airblast atomizer alone. This pressure-atomizing nozzle has a small orifice. Following its switchoff, it is continuously purged with a small quantity of compressor discharge air to provide cleaning and cooling.

The system includes a valve which opens at or above 60% engine speed to operate the second stage. A restrictor provides the 60-40% fuel split between stages. Although not shown, it may be necessary to also supply a small quantity of compressor discharge air to the second stage when it is not functioning in order to protect the atomizer.

Engine Startup - A ceramic glowbar ignitor was chosen instead of the traditional spark plug system. Ceramic ignitors are now capable of very high temperatures (close to 2500F) which insures ignition of a variety of fuels over a broad range of fuel/air ratios. Furthermore, glowbar warmup can be achieved within a few seconds, thus providing the quick starts expected by typical drivers. The glowbar is not prone to wet-fouling or carbon shorting as is the spark plug. Since only simple support electronics are needed and deterioration is not significant, the glowbar ignitor should allow reliable, long-life ignition while exhibiting little fuel sensitivity.

As mentioned, the startup nozzle is a simple pressure-atomizing type. DeLevan Corporation can supply an adequate design which flows the 6-15 lb/hr needed for startup. Since air is used for purging and cooling, problems are not expected.

Since the startup system is completely independent of LPP operation, it would be developed separately, beginning on existing engines.

Control - Although the control of the LPP combustor will be slightly more complex than the Upgraded Engine combustor, it is still fairly simple. There is only one metering valve. The second stage valve is either on or off depending upon engine speed. The startup scie-

noid can be controlled using functions of time, turbine exit temperature, and engine speed. An over-fueling schedule for engine acceleration can be handled as per past experience with the Upgraded Engine control system.

Final Design Geometry - Figure 72 is a design layout of the LPP combustor mounted in the AGT-102 engine. The combustor is shown with a 3mm ceramic liner wall thickness, but a detailed structural analysis had not been performed. Although not shown on the figure, it is likely that the combustor would need to be fabricated in several pieces to provide greater tolerance to temperature gradients.

The atomizing stages are shown mounted in a spherical cap of 93mm radius. The atomizers have an inlet hole area approximately equal to their exit area. They are canted with an included angle of 37° to provide mixing shortly after the initial reaction zone. Most of the heat of reaction is released within the first 4 cm of distance from the atomizer exit. A 38mm long septum divides the reaction region into two distinct zones to prevent interaction between the stages during the initial combustion process. This design feature allows the "hotter" stage to develop combustion events, unencumbered by events in the leaner stage. This hot wall section also serves to promote ignition.

Adequate ground clearance is available with this combustor design. A "skid plate" under the combustor dome is anticipated to provide protection of fuel lines and fittings from rocks, etc.

An insulation thickness of 25-50mm should limit heat losses to values close to the thermodynamic cycle estimates. There is room for some additional insulation if it is deemed necessary. The burner cap is a significant region for heat loss, and this factor influences fuel economy, especially under low power conditions.

The startup nozzle is not shown. It is mounted near the ceramic ignitor and is similar in size. Rig development will be needed to optimize the startup system.

Pressure Drop - The breakdown of total pressure losses over the entire engine operating range is presented in Figure 73. The maximum total pressure loss of 4% is higher than desired. No reduction in atomization losses is anticipated. Any reduction in fundamental pressure drop (due to atomizer hole size increase) would be modest. However, it is likely that a decrease in mixing losses could be achieved through development.

Heat Transfer - The combustor heat transfer program was used to investigate a variety of thermal assumptions. It was decided that the most realistic value of flame luminosity for LPP combustion would be 1.0. Using the measured conductivity of SiC and assuming an emissivity of 0.9, the inner and outer liner temperatures shown on Table 8 are obtained.

Although the program gives only one-dimensional answers, it does provide a useful overview. The low temperature gradient through the liner reflects its high conductivity, and it indicates that stresses will be low. Most of the stress will originate from interaction between the various segments of the combustor and its attachment to supporting engine parts.

The low liner temperature compared to the flame temperature reflects a major advantage of LPP combustion.

Emissions - Using the NASA high temperature rig data, the combustor program estimates an EPA urban cycle NOx emission of 0.09 gm/mi with diesel fuel. Recent data (Reference 20), however, indicates that NOx emissions could increase by a factor of approximately 3 if gasohol is burned. Although the emission (0.27 gm/mi) would still be under the 0.40 gram per mile standard, the two-fold safety factor would not be met. Other fuels should also be investigated.

The CO emission estimate of 1.07 gm/mi is well under the 3.4 gm/mi standard, and the conservative residence time calculation plus the additional reaction time in the radial turbine volute insure that values well under 1.0 gm/mi would be achieved. CO does not exhibit the fuel sensitivity that NOx does.

The Mellor characteristic time estimate predicts 1.3 gm/mi NOx if a diffusion flame using the unevaporated fuel develops. This estimate gives an upper bound on NOx emissions, and it underscores the importance of atomization (the 1.3 gm/mi is based upon an SMD of 15 microns using iso-octane).

In summary, the fuel-splitting design philosophy for the AGT-102 combustor provides a simple method to control flame temperature and no insurmountable difficulties are foreseen. Although rig development is certainly needed, it is anticipated that no major problems with the startup system should be present.

The major concern of this combustor (and any other LPP design including variable geometry or catalytic combustor) is uncertainty about the ability of the atomizer to achieve the necessary droplet size and fuel spatial distribution.

REFERENCES

Section 5.1.6

1. Spadaccini, L. J., "Autoignition of Fuels", United Technologies Research Corp., N79-250001.
2. Mullins, B. P., Fuel, London (1949), P. 205-207; (1953), P. 211-252, P. 327-379, P. 451-492.
3. Spalding, D. B., Some Fundamentals of Combustion, Academic Press Inc., New York, Butterworths Scientific Publications, London, 1955.
4. deBoer, P.C.T., "Droplet Burning and Evaporation Times for Distillate and Residual Fuel Oils", A.S.M.E. 80-GT-59.
5. Simmons, H. C., "The Correlation of Drop-Size Distributions in Fuel Nozzle Sprays", Parts I and II, J. of Eng. For Power, July, 1977.
- 5a. Simmons, H. C., "The Prediction of Sauter Mean Diameter for Gas Turbine Fuel Nozzles of Different Types", J. of Eng. for Power, July, 1980.
6. Borodin, V. A., Dityakin, Y. F., and Klyacho, L. A., "Atomization of Liquids", July 1968, AD 685151.
7. Bitron, M. D., "Atomization of Liquids by Supersonic Air Jets", Industrial and Engineering Chemistry, Vol. 47, No. 1, Jan. 1955.
8. LeFebvre, A. H., and El-Shawawany, M. S., "Airblast Atomization: The Effect of Linear Scale on Mean Drop Size", A.S.M.E. 80-GT-74.
9. Simmons, H. C., Conrad, R.R., and Mihkel, O., U.S. Patent 3,980,233, Sept. 14, 1976.
10. Anderson, D. N., "Ultra-Lean Combustion at High Inlet Temperatures", NASA TM-81640 (DOE/NASA/1011-33), March, 1981.
11. Mellor, A. M., and Washam, R. M., "Characteristic Time Correlations of Pollutant Emissions From an Annular Gas Turbine Combustor", A.S.M.E. 79-GT-194.
12. Bittker, D. A., and Scullin, V. J., "General Chemical Kinetics Computer Program for Static and Flow Reactions, With Application to Combustion and Shock-Tube Kinetics", NASA TN D-6586.
13. Koehl, D. K., "Laminar-Burning Velocities of Propane-Air Mixtures", 8th Symposium (International) on Combustion, P. 510-521.
14. Ballal, D. R., and LeFebvre, A. H., "The Structure and Propagation of Turbulent Flames", Proc. Royal Society of London, A. 344, P. 217-234 (1975).

REFERENCES (continued)

15. Khitrin, L. N., Moin, P. B., Smirnov, D. B., and Shevchuk, V. U., "Peculiarities of Laminar- and Turbulent-Flame Flashbacks". Tenth Symposium (International) on Combustion, pp. 1285-1291 (1965).
16. Ballal, D. R., and LeFebvre, A. H., "Weak Extinction Limits of Turbulent Flowing Mixtures (A.S.M.E. 78-GT-144)", J. of Eng. For Power, Vol. 101, P. 343-348, July 1979.
17. LeFebvre, A. H., and Norster, E. R., "The Design of Tubular Gas Turbine Combustion Chambers for Optimum Mixing Performance", Paper 15, Technical Advances In Gas Turbine Design (1969), Institute of Mechanical Engineers.
18. L'Ecuyer, M. R., "Heat Transfer in Gas Turbine Combustors", Purdue University (Unpublished).
19. Krieger, R. B., and Borman, G. L., "The Computation of Apparent Heat Release for Internal Combustion Engines", A.S.M.E. 66-WA/DGP-4, 1966.
20. Anderson, D. N., Personal Communication, February, 1981.

5.1.7 Regenerator and Seal System

Design and development strategy for the AGT regenerator and seal system was based on the successful approach proven on the Upgraded Engine and modified as needed for the higher temperatures. Dual regenerators were chosen to achieve a practical front-wheel drive package, but otherwise the matrix drive, support systems, and outer seals are directly evolved from the Upgraded Engine.

Figure 74 shows the regenerator and seal system, the regenerator cover, and ceramic inner housing. Following previous Chrysler practice, the core is driven through a ring gear and pinion and is supported at the center with a graphite bearing. A spring system connects the ring gear to the matrix through pads of silicone elastomer, bonded near the cold face of the core. The outer rubbing seal is a monolithic D-shaped piece of graphite/polyimide composite material, similar to the system successfully tested in an Upgraded Engine by NASA. The static seal bridging the gap between the rubbing seal and the cover is Chrysler's proprietary "L" seal, backed up by a rope spring of knitted metal mesh. In place of the typical inner seal system is a dry-lubricant wear surface applied directly to the ceramic inner housing.

Not shown in Figure 74 is the drive pinion that mates with the ring gear. Because the drive pinion and regenerator center bearing are both supported by the cover, gear center distance variations are minimized. This permits the elimination of the eccentric bearing sleeve, used for setting gear backlash on previous designs, allowing the graphite bearing to run directly on the center shaft. The ceramic disk, cemented into the core hub on the hot face, serves to seal the hub against leakage and to shield the bearing from the hot inner housing. The relatively large hub diameter results from manufacturing limitations in the wrapped ceramic matrix currently available. Future cores, which may be fabricated from extruded segments cemented together, may have smaller hubs.

Because of the large increase in cycle temperature over previous designs, an area of concern was the elastomeric bond between the ring gear and the matrix. This concern was heightened early in 1980 by a series of elastomer failures in an Upgraded Engine at NASA. While these failures were later traced to a loss of regenerator running clearance at high operating temperatures, they still served to focus attention on the design limitations of the Upgraded elastomeric mount, and they led to a major investigation of elastomer properties and alternative mount designs.

The following sub-sections describe in greater detail the design and development progress in elastomeric mount optimization, matrix sizing, gear selection, and rig design. In addition, major efforts in the analysis and development of such regenerator system materials as silicone elastomers and plasma-sprayed seal coatings are presented in Section 5.2.

5.1.7.1 Performance Considerations in Core Sizing

The aerothermodynamic analysis of the AGT-102 regenerator uses the E-N_{tu,o} method for counterflow heat exchangers developed by Copping and London (Reference 1). This heat transfer calculation results in the ideal regenerator effectiveness and pressure drop as a function of engine speed. This method is not a design tool, but a means of analysis.

The AGT-102 regenerators use the same ceramic matrix (Corning code 9461 material with T14-20 geometry), and same massflow per unit area, as the Upgraded core. An analysis of this initial sizing predicts satisfactory performance; see Table 9 and Figure 75. With engine volume limited by vehicle space it would be difficult to improve upon this design; see Figure 76 (note that lines of constant effectiveness approximate constant volume). These calculated effectiveness values have been reduced by two points in making engine performance predictions to account for the influence of axial conduction (1/2 point) and non-uniform matrix flow (1 1/2 points). Calculated carry-over leakage due to matrix rotation is about one tenth of predicted overall regenerator high to low pressure leakage.

Although a larger regenerator is more effective and reduces fuel consumption, a smaller regenerator requires less warm-up fuel. The impact of warm-up fuel upon combined fuel economy was quantified, and compared with the drop in SFC due to a corresponding drop in regenerator effectiveness. Despite the gains in warm-up fuel, the SFC loss was greater, resulting in a net loss in fuel economy as the regenerator was reduced in size.

5.1.7.2 Seal Pressure Balancing and Core Drive Requirements

Seal pressure balancing was completed using an approach similar to that utilized in the Upgraded and prior engines that has resulted in regenerator systems with good sealing characteristics and low drive torques. A significant difference however, is that the AGT uses no separate inner rubbing seal. The regenerator core runs directly on a coated seal platform surface of the ceramic inner housing. Therefore, the sealing force must be sufficient to hold the core in intimate contact with the inner seal platform under all conditions, including "g" loads resulting from vehicle operation. In line with the above the seals are pressure balanced to provide a full speed clamping load of 9 lb/in. on the crossarm and 3 lb/in. on the rim. The configuration of the pressure-balancing grooves is shown in Figure 77.

In addition, a 1 lb/in. preload from the "L" seal spring serves to hold the regenerator in intimate contact with the inner housing and prevent seal leakage during starting or fretting damage between the two ceramic surfaces during towing or transporting of the vehicle. The combined clamping load from air pressure and spring preload totals 177 lb at 100% speed and 52 lb at 50% speed. The latter load is equivalent to a core restraining force of 5g.

Core torque is 22 lb-ft at 100% speed and 7 lb-ft at 50% speed per core, after break-in, and assuming the coefficient of friction of ZrO_2/CaF_2 to be 0.3, and the coefficient of friction of polyimide/graphite to be 0.08. The drive power per core, as shown in Figure 78, is 0.08 HP at 100% speed (20 core RPM), and 0.02 HP at 50% speed (10 core RPM).

These torque and drive power requirements are a direct function of the seal friction coefficients which were estimated from preliminary tests. These values should be updated as friction coefficients are better defined, particularly during break-in when they are higher.

The hub loads due to gear driving forces, core weight, and seal friction are shown in Figure 79. The hub load with either direction of rotation is less than on previous engines, indicating that there should be no problems with the center bearing or matrix near the hub.

The drive forces from the ring gear and the center bearing are in different planes and therefore apply an overturning moment to the core. The flow pressure drops through the matrix also apply an overturning moment, and in a different direction. These overturning moments affect the clamping load distribution between the core and inner housing. With clockwise core rotation these two overturning moments tend to cancel, and therefore this is the preferred direction of rotation even though the hub reaction is somewhat larger.

The effect of the gear drive moment could, of course, be reduced by locating the center bearing closer to the plane of the gear. This, however, would cause the bearing to run warmer, add weight, and require a more substantial center shaft support.

5.1.7.3 Regenerator Drive Gears

The design of the regenerator drive gears was largely based on Chrysler's past experience with the Upgraded Engine regenerator drive, which demonstrated excellent performance and life. An additional factor was that gear tooling costs could thus be minimized. The AGT gear design is shown in Figure 80.

The AGT gears should outperform the Upgraded Engine gears for several reasons: a 50% reduction in tooth bending stress, a 28% reduction in Hertzian contact stresses (both primarily due to an 80% reduction in tooth load), and a 36% reduction in tooth sliding velocities (primarily due to lower pinion RPM). These improvements provide a greater safety margin for unexpected loads or temperatures. The gear design is also conservative in assuming a worst-case center distance variation of $\pm .040$ in. Since both gears will be assembled on the regenerator cover, the center distance variation due to thermal distortion and tolerance stack-up should be much less.

5.1.7.4 Elastomer Mount -- Thermal Model

Due to the elevated operating temperatures of the AGT-102 engine, an important consideration is the elastomer temperature during high speed operation and soakback. To evaluate the elastomer temperature a thermal analysis was necessary; however, several heat transfer coefficients in the regenerator system were difficult to determine analytically. To determine these coefficients, tests were performed on the Upgraded Engine which provided regenerator system temperature data during operation and soakback conditions at various steady-state operating speeds.

A regenerator thermal CINDA model of the Upgraded Engine was created, as shown in Figure 81. Also included in the figure are the locations of thermocouples used in the engine tests. The coefficients in question were adjusted in the model so that the calculated temperatures reasonably agreed with measured temperatures.

The model and experimental temperatures agreed reasonably well, with excellent agreement in the housing, ring gear and elastomer temperatures. The engine housing side seal platform temperatures compared well in steady-state operation, but exhibited different soakback cooling rates, due to the complex bridge seal and rubbing seal mechanism heat transfer, which was shown to have little effect on the elastomer area. As can be seen in Figure 82, the maximum elastomer temperature occurs at node #175, which was inaccessible to experimental verification due to the ring gear. The maximum elastomer temperature is predicted to occur in steady-state operation rather than during soakback. The elastomer temperature is expected to reach 423F at 80% gas generator speed and 508F at 100% speed.

When the AGT temperatures are inserted into the Upgraded Engine model, the maximum elastomer temperature, as shown in Figure 83, is predicted to reach 545F. The cycle temperature of compressor discharge air at 100% speed is 428F.

The excessive elastomer temperature was reduced by moving the elastomer outboard and extending matrix material radially to further isolate the elastomer from the core. In the thermal model, this configuration (shown in Figure 83) is predicted to reach a maximum elastomer temperature of 480F at 100% speed, a decrease of 65F. This temperature is within the manufacturer's specified operating temperature limit for the Upgraded Engine elastomer. If the temperature of the elastomer must be reduced further, alternatives should be considered: increase isolation of the elastomer from the core, increase cooling of the elastomer and rim projection, reposition the elastomer nearer the cold side of the core, or insert a low-conductivity insulating material between the core and the elastomer.

Additionally, the stresses imposed on the elastomer by the drive system should be evaluated. This work was just being initiated when the program was terminated.

5.1.7.5 Regenerator System Test Rigs

Three full-scale test rigs were planned for optimal development of the AGT-102 regenerator system components:

Flow Distribution Rig - This rig was designed for use in optimizing air flow distribution to the regenerator faces. It utilizes cold low-pressure, high-volume air flow, through ducting simulating the engine design, at Reynolds' numbers matching the hot engine conditions. Instrumentation at the regenerator exit faces measures local velocity at a number of points across each face. Flow contours can then be adjusted until uniform velocity is achieved. Provision was made for testing various turbine exhaust diffuser configurations and for imparting various degrees of positive and negative swirl at the diffuser exit. Figures 84 and 85 illustrate how the rig was to be used for testing the high and low pressure sides, respectively. At the end of the program the detail design was 95% complete, with the long lead-time items out for quotes.

Hot Regenerator Test Rig - This rig, shown schematically in Figure 86, was designed to test the regenerator matrix, elastomer, drive gears, and seals at engine temperature, pressure, and airflow. When the program ended the rig layout had only been completed in the area of the external burner loop. Layout of the housing structure had been delayed pending resolution of the ceramic inner housing design. Piping and metering orifices had been sized, and the drive system had been designed.

Ceramic Components Test Rig - This rig was to be the thermal shock device for screening the static ceramic components -- combustor, volute, nozzle, and inner housing -- under engine temperature, flow, and pressure conditions. It had not progressed beyond the conceptual stage, as shown on Figure 87.

REFERENCE

1. J. E. Coppage and A. L. London, "The Periodic-flow Regenerator - A Summary of Design Theory," Trans. ASME, Vol. 75, 779-787 (1953).

5.1.8 Inner Housing

This is one of the most critical parts in the engine. It contains the engine hot parts, it partitions the hot gas flow, and, most importantly in this design, it forms the turbine rotor outer shroud and is therefore a major control of turbine blade tip clearance. Its side flanges and their flatness vitally affect regenerator sealing. Consequently, it is essential that the inner housing have very low deflections and distortions. It is therefore made symmetrical except where the burner must pierce the front lower half. It is made of ceramic for low thermal expansion and high temperature strength.

The highest thermal stress and distortion occurs during warm-up. The housing is heated by convection from the regenerated air and turbine exhaust gas, by conduction from mating parts, and by radiation from the combustor, volute, turbine nozzle, and rotor. Emissivity and thermal conductivity of its material are important as well as coefficient of thermal expansion, modulus of elasticity, and modulus of rupture.

The design was not finished. In fact, it was to evolve as better materials and their fabrication were developed.

The initial modeling used alpha silicon carbide with a constant 0.15 in. wall thickness, suitable for a slip cast ceramic part. Design iterations to lower the thermal gradients and thermal stresses were made in the bulkhead, the regenerator flanges, and the front half where it is supported by the compressor housing. At the time work was stopped it appeared that alpha SiC could be made to work. However, fabrication problems with alpha SiC made it advisable to consider LAS (lithium aluminum silicate) to assure that initial deliveries of inner housings would be made on schedule. LAS has lower strength but it has very low thermal expansion. Design considerations are described in the following sections.

5.1.8.1 Modelling

A finite element model of the inner housing preliminary design was made using the ANSYS finite element computer program. Both thermal and structural analyses were made using this same model. This model was used to evaluate the basic concept of using ceramics for this type of structure and as a tool for optimizing the design. The analyses included both steady-state and transient temperatures and stresses due to pressure loads. The model is shown in Figure 88.

Based on the preliminary analyses, critical areas were identified and the model was revised to improve the design. This included:

- * Optimum location of the insulation to eliminate hot spots
- * Modification of regenerator seal flange to reduce thermal gradients

- * Establishing the need to control radiant heating from the combustor and volute.

5.1.8.2 Thermal Analysis

The thermal analysis included radiation, convection, and conduction. The primary source of heating and thermal gradients was radiant heat from the combustor and volute. In the preliminary design a local hot spot occurred at the center of the housing due to the close proximity of the volute, and cold areas occurred at the corners of the forward face of the housing. Large gradients also occurred between the housing body and the regenerator seal flanges. These resulted in unacceptably high stresses. Subsequent analysis showed that gradients could be reduced by changing the location of the insulation package that protects the compressor housing.

Emissivity values of .95 to .40 showed considerable effect on the transient gradients. An emissivity of .95 was considered the probable value. Coating the surfaces of the ceramic hardware to obtain lower emissivities was also considered. However, assumed values as low as .40 still did not adequately reduce stress levels in the regenerator seal flanges. The design was therefore changed to attach the housing wall to the outer edge of the regenerator seal flange instead of the inner edge. This change, shown in Figure 89, significantly lowered thermal gradients.

5.1.8.3 Stress Analysis

The stress analysis used a three dimensional shell type element which calculates stresses through the thickness at the bottom, middle, and top surfaces of the shell. Temperatures are input directly from the heat transfer analysis. The analysis includes both thermal and pressure stresses, steady-state and transient.

Stresses for the last iteration of the original design are shown in Figure 90. The maximum principal stresses shown include pressure as well as thermal stresses, both steady-state and transient values. It can be observed that the transient stresses are considerably higher. Figure 91 shows the corresponding out-of-flat displacement of the regenerator seal flange from ambient temperature to steady-state operating temperature. The out-of-flatness is about .003 in., more than is desirable for regenerator leakage.

5.1.8.4 Current Housing Configuration

Based on the above results a new design was initiated. This design consisted of two intersecting cylinders and incorporated the flared flange and improved insulation described in the preliminary analysis. A finite element model was constructed depicting this configuration but the AGT-102 program was terminated before any thermal calculations were obtained. Figure 92 shows the configuration.

5.1.8.5 Alternate Materials

Studies to date indicate a good potential for a successful inner housing of Carborundum alpha SiC. Considering that the thermal stresses could be adequately controlled through suitable design, shielding and/or coatings to reduce emissivity and minimize thermal gradients, the alpha SiC offers important weight and strength benefits. Unresolved near-term fabrication and processing problems, however, were seen to be a threat to regenerator system development and the program schedule. The regenerator hot test rig was designed for a ceramic inner housing, and with no guarantee in delivery of this component, a serious slippage in regenerator rig testing would result. Therefore, alternate materials and/or vendors were considered.

The Norton Company was found to have demonstrated satisfactory fabrication of large ceramic components in NC430, a reaction bonded SiC. The MOR strength of this material, however, is 35 to 40 ksi (3 point bend) which is much less than the 50 ksi MOR strength (4 point bend) of alpha SiC. Since stress analysis of the inner housing indicated stresses of 30,000 psi it was felt that the probability of survival of an NC430 inner housing would be inadequate. Therefore, work with Norton using this material was terminated.

The Carborundum Company is developing a fine-grain Super KT reaction bonded silicon carbide (RBSC) which has a much lower modulus of elasticity, 33×10^6 PSI as compared to 59×10^6 psi for alpha SiC. If the other properties such as, thermal expansion and conductivity, specific heat, density, and emissivity remain similar, then the thermal stresses would be significantly reduced. Carborundum is obtaining strength and reliability properties.

An alternative to SiC materials is lithium aluminum silicate (LAS) as developed by Corning Glass Works. Initial discussions with Corning revealed that high strength joining methods are not available with this material. Although it is felt that the required techniques could eventually be developed, the possibility of fabricating a large LAS structure by joining several smaller sections could not be considered in the near term. However, fabricating the housing in one piece by slip casting was proposed as an alternative. A flat bulkhead with some draft to the rear in the central area and increasing wall thickness to 0.375 in. would facilitate this approach.

Finite element stress analysis for pressure loading only was completed for both the flat and conical bulkhead variations. Thermal analysis had not been completed for LAS in this configuration, but thermal stresses had been found to be negligible for LAS in an earlier housing configuration.

A summary of the results is shown in Figures 93 and 94. As can be seen, the maximum stresses occur in the bulkhead. The maximum principal stresses are 4000 psi in the cone-shaped bulkhead and 5330 psi in the flat bulkhead.

The deformation of the seal platform is shown in Figure 95. Note that the rim section is only nominally out of plane, with the high pressure segment on the front being about .0007 in. inboard. The crossarm section however, does have a significant deflection of .0033 in. across its width, with the front section moving inboard on the high pressure side as expected. The Weibull statistical analysis program was completed, checked out, and ready to use to determine inner housing reliability when the program was terminated.

5.1.9 Rotor System

Emphasis in the preliminary design work was on the three bearing arrangement (Figure 96) with a single compliant foil air bearing between the turbine and compressor and ball bearings on either side of the helical pinion. During the study more than six variations on the rotor arrangement were considered in order to obtain the optimum configuration, including the influence of both a metal and ceramic turbine.

At the conclusion of the study, two primary rotor configurations had been selected. These were:

- a. Three bearing arrangement, Figure 96.
- b. Three bearing arrangement with a floating oil film damper, Figure 97.

In addition, a third configuration with a split shaft on four bearings was to be designed as a backup system, Figure 98.

The following technical work was performed in reaching these recommended rotor configurations.

5.1.9.1 Rotor Dynamic Analysis

The critical speeds for the rotor system were determined using MTI Computer Code CAD 20. Figure 99 shows critical speeds for the three bearing rotor arrangement. While it was possible to position the critical speeds out of the operating range of idle to overspeed, it was found that significant bending would occur while passing through the second critical speed with the assumed rotor unbalance. This precipitated investigation of rotor damping devices, including oil dampers and coulomb friction devices. The result of this study was to continue with the three bearing arrangement, leaving room for an oil film damper. Early development testing would be done with a precisely balanced rotor system. Rotors with greater unbalance would then be introduced as development progressed, to determine what levels could be tolerated. The oil film damper could be incorporated at any time engine testing showed the undamped design to be unacceptable. If, in further development, this design proved unacceptable, the four bearing design could be used as a fall-back position.

5.1.9.2 Unbalance Response Analysis

The primary designs and the four bearing backup system were analyzed to determine their response to unbalance in the turbine and compressor rotors. The details of this analysis are contained in Appendix C. It is evident from the analysis that oil film dampers would allow successful operation of highly unbalanced rotors, but the damper has to be functional at all operating speeds, not just when needed. This results in a significant power loss, Table 10, and balancing the rotor to the lowest level attainable becomes a priority objective.

5.1.9.3 Maneuver Load Analysis

Each rotor system was analyzed to determine its response to acceleration and precession loads. The details of these analyses are contained in Appendix C. The results showed that the worst combination of maneuvers did not create a pressure loading on the air bearing above the 22 psi maximum recommended value.

5.1.10 Recuperator

A non-rotating ceramic recuperator was studied as an alternative to the rotary regenerator for the AGT-102 powertrain. The annular configuration (Figure 100) selected provides a compact engine package by minimizing the manifolding and the annular flow passages would promote uniform flow distribution at all power levels. Hot exhaust gas flows axially through the recuperator while the relatively cold compressor discharge air flows in a "Z" pattern starting in one corner on the outside of the ring and ending on the opposite corner on the inside of the ring.

The recuperator would be assembled from ceramic plates that form alternate high pressure and low pressure flow passages as shown in Figure 101. These plates would be assembled into an annular package, allowing the constant-thickness plates to form spirally to fill the annular space. The ceramic assembly would then be fired to bond the plates structurally and to seal the edges of the plates.

The heat exchanger matrix configuration is composed of rectangular flow passages with an approximate four-to-one aspect ratio (Figure 102). The heat flow and pressure loss characteristics of this configuration are well defined by empirically-based data from established sources. The aspect ratio was determined by the bending and thermal stresses and the allowable stress of the material.

Compared with the regenerator, the recuperator is larger and heavier for the same effectiveness and pressure drop. But for the very high temperatures in the AGT-102 it does eliminate potential regenerator problems such as seal materials, ring gear drive, elastomer, and center bearing.

5.1.10.1 Recuperator Performance Analysis

A general heat transfer program was written to analyze a "Z" configuration counterflow heat exchanger. The purpose of the program is to predict the performance of the recuperator based on input geometry and operating performance parameters. The geometry can then be varied over a range to perform optimization studies.

The pressure losses and effectiveness are calculated along with the flow distribution patterns for both the hot and cold sides. The knowledge of the flow distribution patterns will allow the designer to modify the input geometry and evaluate the results regarding effectiveness and pressure loss.

In addition to allowing for non-uniform flow distribution patterns, the program calculates the material temperatures on the entire recuperator plate incorporating in-plane conduction methods for both the transient and steady-state modes of operation. The material temperature data can be used for micro and macro types of structural analysis programs to check stress levels during startup, running, and shutdown. Again, the interior geometry may be altered by the designer to redistribute the temperature gradients to relieve any resultant stress problems.

5.1.10.2 Recuperator Structural Analysis

A steady-state heat transfer analysis was completed by EDS Associates in support of a structural assessment of the ceramic recuperator and the material of construction. The thermal efficiency of the recuperator was determined and compared with Williams Research values. The temperature distribution was determined to establish the thermal loads for the stress analysis.

The overall effort consisted of the following tasks:

- a. Demonstration of the validity of the structural arrangements and material of construction.
- b. Study of the steady-state and transient structural responses under various power conditions.
- c. Thermal analysis to establish the thermal loads for the structural.

A steady-state heat transfer analysis of the recuperator at 100 and 50 percent engine speed conditions was completed using the general-purpose finite-element program ANSYS. The gross thermal model approximated the recuperator with a series of hot and cold fluid flow pipes separated by a plate. The plate simulated various regions of the recuperator by using equivalent thermal properties depending on location. The equivalent thermal properties were determined by using small preliminary models of various regions of the recuperator, crossflow or counterflow; the equivalent values

were then used in the gross thermal model. The general-purpose engineering program ANSYS was used because it has the capability of determining the heat transfer and pressure loss characteristics of the recuperator simultaneously. These two properties are dependent on each other, and, therefore, need to be determined simultaneously.

The relative size of the individual channels compared with the size of the recuperator indicate extremely large input and an extremely large solution requirement would be required for the computer model. To keep the model size and the computer costs small, the recuperator was modeled with equivalent flow channels and equivalent thermal properties for the separator plate.

The recuperator is represented by one separator plate out of the hundreds of plates that comprise the recuperator. The separator plate has cold flow channels on one side and hot flow channels on the other side. The hot flow channels represent flow that passes through the recuperator parallel to the axis of the annulus. Ten flow channels represent the hot flow. The cold flow which enters and exits the recuperator radially was represented by ten flow channels which vary in size depending on their locations in the recuperator.

The results of the analysis include the thermodynamic effectiveness and the steady-state temperature distribution of the recuperator. No further technical work on the recuperator as an alternative to the regenerator was planned for the program beyond this initial analysis.

5.2 MATERIALS

5.2.1 Ceramic Components

Preliminary design philosophy dictated that the following components were to be manufactured from ceramics:

- a. Turbine Rotor
- b. Nozzle
- c. Volute
- d. Combustor
- e. Inner Housing
- f. Regenerator Core

The first four components (a through d) need to withstand the maximum steady-state temperature of 2300F and also accept short-duration transients to higher temperatures. The housing and regenerator core (e and f) need be stable to 2000F and 1800F, respectively.

The extensive materials review for the automotive turbine engine has already been reported (DOE/NASA/2749-79/4 Vol. 4) under Contract No. EY-76-C-02-2749.A011. Ceramic selection was accomplished primarily based upon the above review, data compiled by IITRI under Contract No. F33615-79-C-5100, and analysis of data from potential suppliers.

Criteria used in the preliminary selections were:

- a. Mechanical Properties
- b. Stability of Mechanical and Chemical Properties, e.g., Subcritical Crack Growth, Oxidation.
- c. Fabricability
- d. Availability
- e. Potential Cost
- f. Current High-Performance Experience, e.g., Results of other AGT programs.

Using the above criteria, the ceramics offering the highest overall potential for the high-stress/high-temperature applications appeared to be those based upon alpha silicon carbide (SiC). For the inner housing, calculated temperatures were sufficiently low to permit the use initially of lithium aluminum silicate (LAS). The regenerator material which appeared to combine chemical stability

with thermal durability was the aluminum silicate structure formed by replacing the lithium ions of LAS with hydrogen (leached keatite structure). Materials properties are summarized in Table 11. Specific material for each component is discussed under the component heading.

5.2.1.1 Turbine Rotor

The preliminary selection for this element was injection-molded sintered alpha silicon carbide (alpha SiC). Carborundum Weibull data ($\sigma_{AVG} = 66.6$ ksi, $M = 6.7$) were used for preliminary analysis of the rotor stresses. Injection molding is a technique which has shown the capability of fabricating the intricate geometry of the radial rotor; however, the combination of high Weibull parameters with the specific rotor geometry has to be established.

Currently, Weibull parameters are limited by microflaws caused by processing variability, improved processing techniques would help to eliminate these flaws.

5.2.1.2 Turbine Inlet Volute

The complexity of the volute geometry dictates that slip casting be used for experimental engine parts. Sintered alpha silicon carbide was selected rather than the low-shrinkage reaction bonded material; free silicon, present in reaction bonded materials, could sweat from the pores during high thermal spikes.

5.2.1.3 Nozzle Assembly

Development toward the final design of the turbine nozzle assembly, made of alpha SiC, would normally mean several iterations, determined by rig testing, of the initial concept. The cost of tooling for injection molding monolithic nozzles, or of furnace fixtures for brazing assemblies, is inherently high and would become prohibitive in the normal development process requiring several successive dimensional changes. A proposed concept for fabricating nozzle assemblies by brazing individual vanes pinned to a base ring was being explored.

In this new technique, jig-located holes are ultrasonically drilled through a base ring into the vanes using a tubular drill. Pins made of suitable material are inserted into the holes to accurately locate the vanes during the brazing operation. This is shown in Figure 103.

Experimental Work - Several experiments on silicon brazing of simulated alpha SiC nozzle assemblies were performed using commercial steel roll pins and molybdenum tubular pins made by forming thin sheet around a cylindrical mandrel.

The progress of the work is shown in Figure 104 where a steel pin was used and in Figure 105 with a molybdenum pin. In both cases excess silicon was placed in contact with the pins. In the steel-pinned sample, complete alloying of the pin with silicon is noted as well as reaction of the resulting alloy with the silicon carbide. Also evident are the thin braze line and generous silicon fillet. A similar assembly was thermally cycled ten times to 2200F without suffering gross damage. The high silicon content of the alloy formed very effectively suppresses transformation on cycling through the critical range, lessening the differential expansion stresses. The high silicon content also serves to reduce oxidation damage. However, at brazing temperature, as the silicon content of the steel reaches about 4%, melting of the pin gradually occurs until all the metal is liquid. In the molybdenum-pinned assembly (Figure 105) wetting of the pin material by the molten silicon produced a solid surface layer of molybdenum disilicide continuously increasing in depth until either the molybdenum or the silicon was all consumed. The molybdenum disilicide is resistant to oxidation to very high temperatures and effectively protects any remaining pure metal against catastrophic oxidation during service. Similar samples were not thermally cycled, but it is expected that the close expansion match of the materials used would preclude the occurrence of gross damage.

Both techniques appear promising, but close dimensional control of vane location would appear to be more positive with the molybdenum pins, which remain solid at brazing temperature. Additional experimental work is required to fully develop the process.

5.2.1.4 Combustor

Sintered alpha silicon carbide was selected as the combustor material based on previous experience, both in turbine engine combustors and stationary combustion equipment, which has shown that silicon carbide is a suitable combustor material. As in the volute and the nozzle, the possible sweating of unreacted silicon from reaction bonded SiC advises against its use in the combustor.

5.2.1.5 Inner Housing

Slip-cast lithium aluminum silicate (LAS) has been selected for initial experimental engine units. Finite element stress analysis of the housing, using the properties of silicon carbide, showed that high local stresses were generated during thermal transients. Additionally, it was determined that, with silicon carbide, pressure stresses formed a relatively small component of the overall stress picture. As a consequence, emphasis was switched to the slip-cast LAS (Corning) material. The low thermal expansion coefficient of the LAS serves to reduce thermal stresses and also minimizes the deflection of the regenerator seal platforms.

The geometry of the LAS housing confines the fabrication technique to slip casting. Current state-of-the-art in LAS does not permit forming high strength joints; consequently, preliminary fabrication was to be aimed at a monolithic structure.

An advanced reaction bonded silicon carbide (Carborundum fine grain Super KT) was found to offer potential as a housing material. This silicon carbide, which is currently under development, would allow the housing to be fabricated segmentally. Segments could then be subsequently brazed to form the final housing geometry. However, emittance control coatings appear to be required on silicon carbide to decrease thermal stresses in the inner housing.

5.2.2 Metallic Components

5.2.2.1 Compressor

A cast aluminum alloy was selected as the preliminary compressor rotor material. This presumes that the final design will limit operating and soakback temperatures to a 400F maximum. A cost-effective, mass producible, and light weight material is necessary.

If stress levels exclude the traditional high-strength, easily cast, 300 series aluminum/silicon alloys, newer alloys such as Al-206 and Al-224 with zero to only very small amounts of silver could be considered. Higher strength alloys such as Al-201 could be considered, but the presence of 0.4/1.0 percent silver makes this material quite expensive.

Titanium alloys and steels were reviewed but these materials were not selected for several reasons. Titanium, relative to aluminum, is heavier, more expensive and limited in its availability for mass production. Titanium cannot be cast to extremely thin sections and cannot tolerate large cross-sectional changes. Steels incur a 3:1 weight and inertia penalty, affecting engine response characteristics.

5.2.2.2 Compressor Diffuser/Turbine Support

A molybdenum/silicon-containing ductile iron was selected as the compressor diffuser turbine support material. This part is the major component between the cold and hot section of the engine. Stress levels in this component are predicted as low, hence the moderate elevated temperature strengths of ductile iron will suffice. Sufficient oxidation resistance up to 1500F of the higher silicon (5-6%) ductile iron alloys, along with their cost-effective castability, promote their selection.

5.2.2.3 Inner Housing Support Spring

The inner housing support spring contacts the ceramic inner housing and metallic outer housing. It is designed to transmit a forward axial force to retain the inner housing against the turbine support. However, inner housing surface temperatures over 1800F are expected, far in excess of the capabilities of the wrought nickel-base alloys commonly used for high temperature springs. The current service temperature limit of about 1200F for these materials would require modification and/or relocation of the support spring concept.

5.2.2.4 Metallic Turbine Rotor

A metallic turbine rotor was to be used in early development work to eliminate the ceramic rotor variable permitting other structural ceramic hardware evaluation. A lower TIT 2100F and limited life was intended. A nickel-base superalloy MAR-M 247 was selected due to its high elevated temperature rupture strength, sufficient limited time oxidation resistance, and excellent castability.

Inertia welding was the selected method for joining the rotor to the gas generator shaft. Chrysler has in-depth experience in inertia welding both iron-base and nickel-base superalloys to carbon and stainless steels. Weld development for this application was to be in the area of tooling design to hold the rotor and shaft within the required runout tolerances during welding. Demonstration welds between MAR-M 247 and SAE 8640, and between MAR-M 247 and 17-4PH, have indicated that the process can be employed to create high quality joints.

5.2.2.5 Outer Housing

The outer housing was selected to be fabricated from low-alloy steel sheet. Due to the 300F surface temperatures and very low induced stresses during engine operation, the moderate strength, easily formed low-alloy sheet steels appear as solid cost-conscious selections.

5.2.3 Regenerator and Seal System

5.2.3.1 Cold Side Seal

Graphite has traditionally been used as seal material against the cold face of the regenerator matrix; it has a low coefficient of friction and easily withstands the core face temperature (600F). The seals are machined to shape from graphite plates using conventional shop procedures.

The proposed graphite/polyimide resin composite seals originated at NASA-Lewis where they were tested on the Upgraded Engine.

Limited test data showed performance at least equal to graphite and an apparent extremely low wear rate. The seals were pressure molded in a simple aluminum alloy die from T-300 (Union Carbide) graphite cloth impregnated with PRM-15 monomer and machined to size. Several seal blanks were supplied by NASA for Chrysler evaluation on an Upgraded Engine and for a bench-type seal test fixture, but program termination occurred before tests to measure friction characteristics were run.

The potential advantages of this type of seal are listed below:

1. Low coefficient of friction which tends to decrease with increasing temperatures.
2. High mechanical strength; could allow the use of a thinner seal and save space.
3. Moldable to net shape, particularly if change to powder graphite filler is possible; may result in cost savings in large quantities.

5.2.3.2 Hot Side Seal

The concept of a ceramic inner housing of low thermal expansion coefficient and the symmetry of the dual regenerator design should result in a housing with negligible thermal distortion. Consequently, the need for spring loaded, conforming crossarm and rim seals on the hot side of the regenerator (as in previous engines) is eliminated. It is therefore a matter of practical importance to develop a wear resistant, low friction coating for application onto the housing platforms. This would permit running the ceramic regenerators directly on the housing (via the solid-lubricant-containing coating), without the complexity and associated high parasitic leakage of the traditional hot side seal systems.

Two wear test machines, originally built by Corning Glass Works, and eventually purchased by Chrysler, were intended to serve as an integral part of the hot seal development program, yielding seal/matrix wear and dynamic friction vs. time data at elevated temperatures (Figure 106).

Plasma spraying has been the traditional method for applying solid lubricants such as NiO/CaF_2 or $\text{ZrO}_2/\text{CaF}_2$ to metal substrates. This method was used to develop a bond coat which is compatible with solid lubricants for the candidate ceramic housing materials, silicon carbide and lithium aluminum silicate.

A potential bond coat for sintered alpha silicon carbide was developed. It consisted of a plasma-sprayed Si bond coat with an intermediate layer of Y_2O_3 -stabilized ZrO_2 ($\text{ZrO}_2/8-12\% \text{Y}_2\text{O}_3$), top coated with Y_2O_3 -stabilized $\text{ZrO}_2/\text{CaF}_2$ ($(\text{ZrO}_2/20\% \text{Y}_2\text{O}_3)/20\% \text{CaF}_2$). Thermal cycle tests to 1800F have indicated excellent bonding without microcracking or spalling.

Development of a low friction seal surface applied to LAS presented greater challenges than experienced with SiC because of the unusual thermal expansion properties of the LAS. As can be seen in Figure 107, this material initially shrinks when heated, then begins expanding as the temperature increases above 700F. However, even at temperatures exceeding 1500F, the total expansion is quite low. To clarify the role of thermal expansion in attempts to bond other materials to LAS, the theoretical treatment discussed in Section 5.2.8 was applied. Families of curves were generated as shown in Figure 108, such that generally any material with modulus and coefficient of expansion falling between the origin and the limiting curve would at least have mechanical compatibility for a sound bond with LAS. This analysis confirmed that a match was most difficult in the low-temperature regimes and indicated that there were no obvious candidate materials for bonding to LAS.

The approach was therefore taken to create a suitable material by grading mixtures of LAS with other materials. Scrap LAS regenerator cores were crushed, ball milled and sieved to obtain the proper particle size and distribution for plasma spraying, and the experiments listed in Table 12 were conducted. A 50/50 (Vol.) mixture of LAS/ZrO₂ (sample 2-L) sprayed on a LAS substrate .012-.015 inch thick formed an intimate bond which withstood thermal cycling. However, sample 3-L and 4-L, which were duplicates of 2-L with the addition of an intermediate coating of ZrO₂ and a final coating of 80% ZrO₂/20% CaF₂, resulted in failure. A series of graduated coatings were being considered as a way to achieve success with this system. Sample 5-L represents another approach in which an 80 wt% LAS/20 wt% CaF₂ mixture was plasma sprayed on an LAS substrate (.037 inch) which had been heated to 500F. No cracking was observed after thermal cycling to 1800F for one hour and air cooling. However, because of the possibility of chemical reaction between these two materials a SEM analysis was made which indicated the following:

1. There was a good bond between the substrate and the coating. No cracks were observed at the interface, nor were there any large cracks in the coating layer. The coating itself was quite porous (Figure 109).
2. Two distinct phases were observed in the coating (Figure 110). The major area "A" exhibited no traces of CaF₂ (Figure 111). The other area, designated, "B", was high in Ca as well as Al and Si. (Li and F are below the limits of detection of the EDX). This would indicate that most of the CaF₂ has reacted with the LAS and that very little free or unreacted CaF₂ remains in the sprayed layer.

5.2.3.3 Ring Gear Elastomeric Mounting

Problems encountered with regenerator drive elastomer mounting in the Upgraded Engine at NASA-Lewis prompted a re-examination of the proposed ring gear mounting system for the AGT-102. Of parti-

cular concern were the hot strength of the material (Dow Corning Sylgard 186) and the effect of temperature on its chemical stability.

A shear strength test fixture, simulating service load and temperature conditions, was designed and fabricated. It is shown in Figure 112 mounted on the Instron test machine and schematically in Figure 113.

The specimens were prepared under conditions closely approximating actual ring gear mounting. The samples (shown in Figure 114) were approximately 0.27" thick with a nominal cross section of one square inch. Results are plotted in Figure 115 for tests run from room temperature to 600F with a soaking time of 5-10 minutes at temperature prior to testing. It was noted that all the room temperature samples failed by peeling. At higher temperatures they failed in a mixed mode, and at 500F and above the failure was in shear. Tests were also run to determine long term chemical stability of the elastomer by measuring weight loss with time at temperature. Initial tests were conducted on small cubes of elastomer (approximately 1 cm edge) heated in circulating air for periods of 3 and 15 hours. Results are plotted in Figure 116. Planned hot shear tests on thermally degraded samples were not run because of close-out of the AGT-102 program.

Design analysis indicated that if the thermal conductivity of the elastomer could be increased its operating temperature would be decreased. A "temperature drop" apparatus was designed and built to measure relative conductivity. This is shown in Figure 117, and some results, obtained on commercial materials, are shown in Figure 118.

A survey of commercial elastomers has shown that the silicone base systems are still the most practical for this application. While their maximum service temperature exceeds that of other systems, chemical degradation and loss of properties are fairly severe above 500F. The heat resistance of silicone elastomers is exceeded only by some of the fluorocarbon elastomers which are prohibitive in cost and would have to be pressure molded to shape instead of poured as in the conventional "potting" operations. It appears doubtful that significant modification of the elastomer by addition of high conductivity filler can be done effectively without serious strength degradation. Design efforts aimed at lowering the maximum regenerator rim and ring gear drive temperature appear to be the most potentially fruitful method of insuring elastomer survival.

5.2.4 Ceramic Wheel Shaft Attachment

The proposed method of shaft attachment requires that a metallic sleeve be joined to the ceramic stub shaft either by electromagnetic forming or brazing. This would be followed by inertia welding the sleeve to a metal shaft.

5.2.4.1 Sleeve Attachment

Electromagnetic Forming - Electromagnetic forming was selected as the most promising method for early demonstration and eventual high volume production attachment of a SiC ceramic rotor to the gas generator shaft. A proprietary adaptation of electromagnetic forming was successfully used by Chrysler to form sleeves of arc cast molybdenum around solid cylindrical sections of sintered alpha SiC (Figure 119). This process has the potential of generating and maintaining clamping forces on the ceramic rotor stub shaft limited only by the yield strength of the alloy sleeve when formed and the creep or relaxation rate of the alloy sleeve under engine operating conditions.

Figure 120 illustrates the development plan to apply existing electromagnetic technology for the shaft attachment requirements.

The nature of the forming process as well as the design properties of the completed joint dictate some rather stringent materials requirements for the intermediate sleeve. They are listed below:

- a. High electrical conductivity for maximum induced current and minimum resistive heating during EM forming.
- b. Low coefficient of expansion to minimize relaxation of the clamping force on heating the joint to service and soakback temperatures (1650F).
- c. High yield and creep strengths at temperature for minimum clamping force relaxation under centrifugal loading in service.
- d. Sufficient ductility and a low ductile-to-brittle transition temperature (DBTT) to insure adequate formability.
- e. Oxidation resistance at service and soakback temperatures (1650F).

Few metals or alloys will satisfy these requirements. Refractory metals as a class appear to provide most of the needed properties except for oxidation resistance. However, a comparison of electrical resistivity, tabulated below, shows that the choice is limited to molybdenum and tungsten.

Electrical Resistivity of Refractory Metals

Cb	13*	micro-ohm-cm
Mo	5.2*	
Mo (TZM)	5.2	
Ta	12.8*	
W	5.6*	

* Average of several sources

Poor fabricability and high cost rule out tungsten, leaving molybdenum and its alloys as prime candidates. Because of the undesirably high ductile-to-brittle transition temperature (DBTT) of the commonly available alloys, the choice is further restricted to either severely-deformed TZM or a grade of "doped" pure molybdenum used for heating elements and furnace fixtures (HT Molybdenum - Schwarzkopf Development Corporation). The latter features a high resistance to recrystallization and a low DBTT (-40 to -80F). High strength is attained through severe deformation and is retained to temperatures much in excess of that projected for the wheel/shaft joint.

However, the very rapid oxidation of molybdenum alloys at predicted operating temperature of 1300 to 1700F mandates the need for an oxidation-resistant coating on the sleeve. Due to the inaccessibility of the sleeve/rotor interface after forming, it is necessary to coat the molybdenum alloy sleeve prior to electromagnetic forming. Promising coatings would be the more ductile electroplated metallic coatings: gold, silver, platinum, palladium, nickel and chromium. Minor plating problems with molybdenum, due to its high oxidation potential, are contact point elimination, pre-cleaning, and post-plating diffusion cycles. Alternative less-ductile coatings would include flame-sprayed oxidation-resistant NiCr alloy coatings, sputtered or chemically-vapor-deposited metallic coatings, and the diffusion-bonded aluminides and silicides. With electromagnetic forming there is a very fast (10^{-6} second) release of energy and subsequently very fast metal movement. Since the strain rate sensitivity of most coatings to very fast strain rates is unknown, some investigation will be needed to assess the less ductile coatings.

Brazing - This proposed joining technique is a true brazing operation in that a filler alloy is used that has a melting point below that of either material being joined.

Joining of the alpha SiC wheel stub shaft would be done either directly to the gas generator shaft or, more likely, to an intermediate transition piece. In either case, wetting of both the ceramic material and the mating metal piece by the molten brazing alloy is necessary to affect a secure joint. Additional requirements for a viable joint are more restrictive; they are listed below:

- a. The brazing alloy must have a melting point above projected joint service temperature.
- b. The brazing alloy must be oxidation resistant at projected joint temperatures.
- c. The brazing alloy must have sufficient strength at projected service temperature.
- d. The brazing alloy reaction rate with either material being joined must be minimal at projected service temperature.

- e. The coefficient of expansion of the brazing alloy should match that of alpha SiC as closely as possible.
- f. The coefficient of expansion of the metal piece should match that of alpha SiC as closely as possible.

Some of those requirements can be partially circumvented by novel joint designs. Experimental work on candidate brazing and intermediate alloys is described in Section 5.2.8.

5.2.4.2 Shaft Attachment

Material Selection - The main criteria for selection of the shaft material are the operating and soakback temperatures experienced. If maximum temperatures are limited to predicted operating temperatures of 700 to 800F, a low-expansion, high-strength 400 series martensitic stainless steel is selected. Since it is speculated that a bonded interface will exist between the sleeve and shaft, the low-expansion 400 series stainless steel will limit stresses to acceptable levels of 70 to 80 ksi.

Inertia Welding - Inertia welding is the primary method for joining the ceramic rotor sleeve to the gas generator shaft. Advantages of this process include high volume potential, low piece cost, moderate capital requirements, and excellent quality potential. Demonstration welds have been made at Chrysler between a Mo-30Ni alloy and SAE 8640 steel.

Electron Beam Welding - Electron beam welding would be a less desirable approach. One problem with EB welding is the complex metallurgical interaction between the sleeve material and shaft material in the fusion zone. In addition, the thermal expansion differences between a low expansion sleeve material and relatively high expansion shaft material may require an intermediate material to avoid cracking on cool down from the welding temperature. Finally, electron beam welding is not as production oriented both from a cost and time standpoint.

Electromagnetic Forming - Electromagnetic forming of the sleeve around the gas generator shaft could be considered an alternative joining method to inertia welding, but more space would be required to accommodate the sleeve-shaft overlap.

5.2.5 Insulation

The requirements of high overall thermal efficiency of the engine, the limited temperature capabilities of some of the materials, and the necessity of avoiding extreme thermal stresses in the inner housing under start-up conditions, call for means of restricting and directing the flow of heat. Management of conductive and radiative heat transfer was to be achieved by the use of insulation and controlled-emittance coatings.

5.2.5.1 Insulating Materials

The insulating material used for the Upgraded Engine will be used for the AGT-102. The formulation, known as CR95C, consists of:

H ₂ O (distilled)	14,875 ml
Dispal	2,700 gm
HCl 6M	480 ml
Pluronic 31R2	225 ml
Natrosol 250LR	450 ml
10% Sol.	
NH ₄ OH 20% of Conc.	740 ml
Kaowool Bulk A	4,380 gms

CR95C is prepared as follows:

Mix the Dispal and water, add HCl, Pluronic and Natrosol, stir until thoroughly mixed, then add NH₄OH; the slurry will gel. Add the Kaowool in small quantities and stir until the Kaowool is completely wet. Store in an air-tight container to prevent moisture from escaping and the insulation from drying.

An abrasion-resistant coating is used to paint the surface of the insulation. It can resist hot gas erosion, has a low permeability, and can withstand 3000F. This coating is known as CR124 and it consists of:

50% by Vol. Dupont Ludox Colloidal Silica Rigidizer
50% by Vol. Johns-Manville Cera Kote

This coat, after being applied, can be fired at up to 1000F before use.

A "Delta T" rig was constructed with alumina insulation material and Kanthal 33 heating elements, Figure 121. This rig provides the versatility of high temperature and rapid cycling mode. Figure 122 shows the results of the first tests. The measured temperature difference for Fiberfrax was compared to Carborundum's reported values and found to be close, indicating that the Delta T Rig will produce acceptable results. Future tests were planned to evaluate multilayer insulation composites and coated insulations. Delta T measurements on commercial materials of known "K" values were to provide a basis for estimating "K" values of experimental materials based on their Delta T values.

5.2.5.2 Low-Emittance Coatings

In addition to thermal insulation, heat management must consider and utilize thermal radiative properties of surfaces.

Crude attempts at comparative estimation of the emittance of the ceramic materials of potential use in the engine showed that a) composition, surface finish, environment and surface coatings can make a significant difference in the measured emittance of a component, and b) sophisticated measuring techniques will be required to obtain dependable emittance values. The planned program in this area was to:

- a) Procure suitable samples of Carborundum's alpha SiC, fine grain Super KT and Corning LAS for emittance measurements by IRCON.
- b) Use suitable radiation pyrometry equipment, and the samples in a), to evaluate other materials and/or components.

5.2.6 Ceramic Development Testing

5.2.6.1 Spin Testing

A 13" I.D. by 14" deep instrumented vacuum spin pit has been modified by fitting a Lexan window in the bottom to permit strobe photography of failure events. The intent was to obtain multiple exposure photographic records of, for example, a ceramic rotor failure with the individual exposures timed such that examination of the photograph might reveal the portion of the tested part containing the fracture origin. The drive for this test system includes an air motor capable of speeds in excess of 100,000 RPM. In addition to developmental rotor testing and rotor proof testing, this facility was to be used to spin a "dog bone" shaped ceramic test bar designed for uniform tensile loading along a 0.75" gauge length. Design of this test bar features a continuously-decreasing gauge section area, following a parabolic function as the radial length increases, to compensate for proportional decreases in the rotating mass. Figure 123 illustrates this test bar. Stress at failure can be calculated as follows:

$$S = 0.000252 \times \text{Density (lb/in}^3) \times (\text{RPM})^2$$

For example, a specimen with a density of 0.1 lb/in³ which breaks at 20,000 RPM has a calculated tensile strength of 10,080 psi.

5.2.6.2 Flaw Characterization

The nature and character of failures occurring in the testing of ceramic components were to be investigated by the use of brittle materials fractographic techniques employing fracture surface observations as well as SEM analysis. Whenever possible, acoustic emissions techniques were to be used to detect the onset of the fracture and/or the location of the fracture-initiating flaws.

5.2.7 Ceramic Interfacing

Knowledge of the behavior of different materials in intimate contact in various hot areas of the AGT-102 is necessary to insure proper material selection and adequate service life. The chemical and structural stability of touching pairs of ceramic and metallic materials under various conditions of temperature, pressure, and atmosphere will determine material choice and/or surface treatment, assembly methods and joint configuration. Temperature limitations of single materials are well known but experience is lacking in predicting the high temperature interfacing behavior of high performance ceramics with metallic alloys (superalloys in particular) and other high-performance ceramics.

Experimental work on solid and liquid state interfacing was undertaken to a) screen materials pairs for non-seizing contact and b) characterize interfaces of potential use.

5.2.7.1 Interfacing Rig

A simple but effective apparatus was built to apply a constant load to a test couple in a semi-gas-tight enclosure contained in a fast heating furnace. A vertically-guided reaction-bonded silicon carbide (RBSC) rod served to load the sample through a self-aligning hemispherical stabilized-zirconia pad. A platen at the top end of the rod held deadweights. The sample area was contained in a chamber fabricated of an RBSC pipe section and plates with suitable access openings for loading rod and sample insertion, thermocouple, and gas inlet tube. The reaction chamber was installed in a high-temperature furnace. The loading rod rested on the sample through a hole in the top of the furnace. Oxygen could be excluded from the chamber by flooding with an inert gas.

A total of thirty-five runs, most of them of four hours' duration, were made in the apparatus. Additional long-term tests (500 hours) were run in the standard bench-type box furnace. The tests are summarized in Table 13.

5.2.7.2 Ceramic/Ceramic

Results in Table 13 show the apparent universal inertness of stabilized zirconia toward RBSC, alpha SiC and LAS; no reaction was observed at 2300F at high pressure (1000psi) against RBSC or SiC, or long times (576 and 632 hours) on alpha SiC. This absence of reaction was verified by EDX analysis of a ZrO₂/alpha SiC couple after 500 hours at temperature. As shown in Figure 124 and 125, no trace of zirconia could be found at the area of contact on the SiC plate. A short-time test (four hours) against LAS, under more realistic conditions (26 psi, 1800F), also showed no apparent reaction. Alumina did not react with LAS under the same conditions.

Silicon carbide, either alpha or RBSC, bonded to itself at 2300F and 60 psi, in air. In argon, RBSC bonded to itself, indicating a bonding mechanism other than the formation of a glassy SiO₂ layer.

5.2.7.3 Ceramic/Metal

Alpha silicon carbide-metal couples were the only ceramic/metal systems tested. In general, the alloys appeared to react with the ceramic somewhat proportionally to their nickel (or to a lesser extent cobalt or chromium) contents. This was shown by adhering residual oxide or discoloration of the SiC. Pure nickel, even about 1000F below its melting point, formed a liquid phase containing silicon and flake graphite, similar to cast iron. Aluminum-containing alloys showed a tendency to form an interfacial scale with enough alumina to inhibit, to varying extents, reaction with the ceramic.

5.2.8 Brazing to Ceramics

Information available on reactions of molten alloys with high performance ceramics is also very limited. Such data are of particular significance in potential brazing processes for metal/ceramic joining.

Experimental work was therefore undertaken to examine the reaction between ceramics and various metals and alloys heated to their liquid state.

The apparatus consisted merely of a high temperature tube furnace, with a gas train to provide pure and dry hydrogen and argon. The samples were placed in zircon (zirconium silicate) combustion boats for easy insertion into the hot zone of the furnace. Samples were placed in the cold furnace, which was then carefully purged with argon, and brought up to temperature at maximum furnace heating rate. Cooling was done in the furnace under the inert atmosphere.

Since the primary objective of this investigation was to explore alloys with potential for attaching the SiC rotor to a metal shaft, all the experiments were run against that material. A total of 97 experiments were performed. They are summarized in Table 14.

In general, it was found that alloys based on silicon, iron, nickel, and cobalt react with and wet alpha silicon carbide. As the amount of reacting metal decreased with increased alloying, the reactivity of the metal also decreased with an observed change in the apparent wetting angle. Manganese, copper, and silver, which themselves are inert to SiC, are useful as diluents; they can also serve as melting point depressants. Their reactivity or wetting ability can be enhanced by additions of active metals such as titanium and zirconium. However, with the exception of silicon, the reactive metals have a high coefficient of thermal expansion which results in high interfacial tensile stresses accompanied by peripheral cracking in the SiC. Low expansion fillers such as coarse molybdenum, columbium and alpha silicon carbide powders appear to partially alleviate the problem. Complex, multicomponent alloys containing low solubility phases and having a wide "mushy" range also perform better by allowing partial stress relieving during freezing of the alloy.

Assuming that a molten alloy wets the ceramic surface, it has been shown that lower interfacial stresses are developed with thinner alloy layers. Experimentally, lower stresses also appear to result from a reduced wetted area (smaller length and width). A commercial brazing "stop-off" material, consisting mainly of titanium dioxide, was found to be very effective in restricting the reaction area when using Ni or Co base alloys on alpha silicon carbide. This technique was successfully applied to attach molybdenum or niobium samples to silicon carbide bars as shown in experiments 90A and 92A (Table 14). The same brazing alloys were found to be too aggressive for joining high Ni or Ni-base alloys to alpha SiC. Thus far, minimal peripheral cracking has been obtained with a commercial Ni-Mn-Si-Cu brazing alloy (Exp. 96).

Desirable characteristics for joining metals to alpha silicon carbide appear to be:

- Low expansion brazing alloy (minimize expansion mismatch)
- Low liquidus brazing alloy (minimize total contraction on cooling)
- Wide solidus/liquidus range brazing alloys (allows stress relief in the brazing alloy)
- Low expansion mating metal piece (minimize expansion mismatch)

Theoretical Analysis - In an effort to gain an insight into the factors involved in joining alpha SiC to other materials, a theoretical treatment was attempted. In "Joining of Engineering Ceramics" by the British Ceramic Research Association, M. E. Twentyman quotes a version of Timoshenko's treatment of a two-layer composite lamina. Equations are given for the residual stresses at the surface of the two layers of the lamina as a function of their thickness, elastic modulus, and coefficient of thermal expansion for cooling from a given joining temperature. Substituting the properties of alpha SiC and solving for the coefficient of expansion of the unknown material over a range of modulus, at constant thickness, residual stress and/or temperature range, families of curves can be generated as shown in Figures 126, 127, and 128. Under the specified conditions any material with modulus and coefficient of expansion falling between the origin and the limiting curve will form a sound joint with alpha SiC. Some limitations of the model are evident: variations of modulus and coefficient of expansion with temperature are not taken into account, a realistic tensile stress in the ceramic material, chemical and physical compatibility (melting point, wettability, reactivity, etc.) have to be known. However, general conclusions can be drawn:

- a) Low-expansion, high modulus materials are suitable for joining to alpha SiC.
- b) High-expansion, low modulus materials are also suitable.

- c) As the acceptable residual tensile stress in the ceramic materials increases, a wider range of materials becomes usable.
- d) As the thickness of the unknown material decreases, a wider range of materials become usable.
- e) Increasing the temperature range moves the constant stress and constant thickness curves toward the origin.

5.2.9 Materials Status Summary

Materials together with means of fabrication and processing have been initially selected for all critical engine components. This includes all hot section ceramic components, means for metal to ceramic shaft attachment, a back-up metallic turbine wheel, housing insulation, regenerator core, drive, and seal system, and for the compressor impeller.

Areas requiring development such as: consistency of ceramic materials strength, metallic oxidation protection, practical ceramic processing methods, emissivity control, regenerator seal coatings and elastomer temperature and strength requirements have been identified and development efforts initiated.

With continuation of these efforts it would appear that all program goals related to material requirements could be met.

5.3 DRIVETRAIN AND CONTROL

5.3.1 Reduction Gear

5.3.1.1 Gear Train Description and Selection Criteria

Studies were conducted to evaluate configuration alternatives and design features for the gear box. Design targets and considerations for the 20:1 ratio two stage parallel axis helical gear set were as follows:

- * Provide support and drive requirements for the Response Assist Flywheel (RAF), regenerator, starter, and vehicle accessories. Location of above units to be compatible with vehicle components.
- * Low noise level.
- * Ease of serviceability.
- * Compatible directions of rotation between engine, transmission, and accessories.
- * Light weight.
- * Low cost.

A summary of speeds for the engine, auxiliaries and accessories is tabulated in Table 15.

The reduction gear system initially proposed with an idler gear is shown schematically on Figure 129. One system without an idler was studied and compared with the idler system. This is discussed in detail later in this section. Briefly, the study indicated that the idler should be retained to provide the center distance required for transmission to flywheel housing clearance. The design with the idler would allow the flywheel unit to be easily removed for service, an important factor for the EPD development engine. The idler shaft also supports a pinion for driving a gear on an ancillary shaft. This in turn drives the regenerators and vehicle accessories through a pulley and belt system. See Figure 129. Straddle mounting the high speed pinion minimizes its deflection and resulting gear noise. The spline and diametrical pilot connection between the rotor shaft assembly and pinion will also reduce noise transmission. The other high speed gears (except for the transmission input gear) are also straddle mounted, the front bearings mounted in the main reduction gear-air intake housing and the rear bearings mounted in a bridge supported from the main housing. This arrangement allows line boring the bearing bores and facilitates assembly of the gears prior to installing the transmission. All gear shafts are supported in ball bearings to minimize power loss; housings are aluminum for low weight.

The steel gears would be hobbled, shaved, and possibly honed to provide AGMA class 12 quality for minimum noise and cost. The hardness would be specified in line with these manufacturing process requirements. Design work was initiated on the EPD gears considering them to be manufactured using Upgraded Engine tooling. Diameters and center distances were determined. Upgraded Engine gearing was designed with a high pitch (36) and helix angle (39°) and has been demonstrated to operate well at high speeds and low noise levels. Use of this tooling would expedite procurement of gears for high speed performance testing in rig and early engines. It also would have allowed the time for an optimized gear design to be scheduled somewhat later in the program.

5.3.1.2 Gear and Bearing Deflection Study

Helical gears can operate more quietly at high speeds, but their thrust loads aggravate misalignment. Short bearing spans also increase gear misalignment from thrust loads. Bearing deflections were calculated for various load conditions. The results of this analysis, which is described below, were then to be used in calculating gear deflections and the gear crowning requirements to avoid edge loading and excessive noise.

Within the constraints of function and packaging, bearing deflections were calculated for variations of helix angle and hand, and angular location of the idler gear relative to the intermediate gears. Calculations were made assuming full drive torque, RAF assisted engine acceleration, and engine braking, the latter two torques being assumed equal to the maximum drive torque.

Figure 129 shows the gear train using the idler gear. The high speed shaft rotates clockwise in this case to match the transmission direction of rotation. If the idler gear were eliminated so that the intermediate gear connected directly to the transmission, then the high speed shaft would reverse its rotation. Also shown is Angle " ", the angular location of the idler or other gear meshing with the intermediate pinion. The variables were:

Helix Angle	10,20,30,39°
Hand	Right and Left high & low speeds pinions (4 combinations)
Angle	0, 30, 60, 90°

Figures 130, 131, and 132 represent the deflected bearings of the high speed pinion and intermediate gear in their plane of rotation as viewed from the left (driver's) side of the vehicle. The horizontal projections of the axis lines represent lead error and the vertical projections represent errors in and out of mesh, both of which will require crowning to avoid tooth edge loading.

The bearing spans used for the figures shown are 1.3 in. for the high speed pinion and 1.9 in. for the intermediate gear. Increasing the intermediate bearing span significantly reduces the angularity error. Some increase in span could be provided by supporting the outboard intermediate shaft bearing in a boss projecting beyond the plane of the bearing support bridge.

Figure 130 shows, as expected, that the smaller helix angles give lower thrust loads and less misalignment. The different character of deflections between 130a and 130b is because the RAF input is pure torque to the intermediate gear set, i.e., the low speed pinion is not loaded.

Figure 132 shows how the helix hands affect deflections when they are reversed to reduce bearing thrust loads on the intermediate gear set for the idler gear arrangement. Figure 132 also illustrates the effect of eliminating the idler gear with different helix hand combinations.

Comparing the results of a change in angle from 30° to 90° on Figure 130a and 132a indicates some advantage in alignment and bearing loads with the higher . An of about 60° could be obtained by eliminating the idler, Figure 133, but there are several reasons why this was not done, at least for the experimental engine. They are discussed below.

5.3.1.3 Comparison of Reduction Gears With and Without Idler

A proposed transmission-reduction gear configuration having fewer reduction gears (no idler) and the flywheel housing integrated

with the transmission housing was evaluated relative to the initial arrangement having an idler and a flywheel housing separate from the transmission housing. The initial arrangement has seven gears including a gear-driven ancillary shaft for the accessory and regenerator drive as described above (Figure 129). The proposed arrangement with four gears and a chain-driven ancillary shaft is shown in Figure 133. The latter arrangement is simpler, but there is less space for the flywheel and it would therefore be substantially heavier. Also, the flywheel section of the integral housing is larger, extending further outboard from the reduction gear, and the flywheel could not be serviced in the vehicle (removing the transmission assembly from the reduction gear box is required).

Weighing these considerations resulted in a decision to retain the initial reduction gear system with the idler gear. The advantages of fewer gears, however, are significant and further studies at a later date, i.e., for a production engine (final RPD), could result in a decision favoring the alternate approach.

5.3.1.4 Gear Development Test Rig Status and Planned Activity

The rotative speeds of the AGT-102 will result in a pinion pitch line velocity of 24,500 ft/min. This is considered to be within the state of the art for high speed gears; Chrysler-Williams have run gearing up to 27,000 ft/min. The Upgraded Engine gears were designed to have a relatively high oil film thickness at a design speed of 18,300 ft/min, and this characteristic is expected to be maintained up to the AGT-102 speeds. Nevertheless, rig testing of the Upgraded gears up to maximum AGT-102 speed was scheduled to verify performance in the higher speed ranges.

A rig was designed consisting of two Upgraded gear sets installed back-to-back (Figure 134) and locked-up through a coupling to apply load to the gears. In addition to gear performance and noise, the rig was designed to allow parasitic power, measured with the aid of a torquemeter, to be characterized for a wide range of oil temperatures. Viewing ports provided aid in determining the major sources of oil churning losses. A similar test fixture, that subjected gear sets to endurance and performance tests, was utilized in the past to evaluate gear designs. The knowledge gained from this fixture revealed that the gear mesh loss, except for extremely low speed, is independent of load and speed, and is generally less than 1%.

Type A automatic transmission oil would be the basic lubricant, but other oils that are suitable to the overall engine system will also be tested. Two candidate oils are Conoco DM-600 and Mobil 1 (RN-1635). Both are synthetic lubricants developed to be compatible with mineral oils and to provide improvements in fuel economy as well as wear and cold starting. Procurement of the rig with ball bearing supported pinions, Figure 135 (journal bearing optional) was in process when the program was terminated.

Upon completion of this initial test work, another rig was planned for the AGT reduction gears made with Upgraded tooling. This

work was to allow an evaluation of the gear system throughout the required speed and load range before engine installation. Following this, gears optimized for life and noise factors such as stress, scoring factor, sliding velocity, and EHD film thickness were to be evaluated. These gears would have a fine pitch similar to that of the Upgraded gears, and therefore gear finishing methods which are economically feasible may be limited. A subsequent redesign, with a compromise in pitch, for example, would allow alternate manufacturing processes such as honing to be considered. The impact of the alternative finishing method on tolerance control, noise, and cost was to be determined.

Following verification of gear noise levels, further noise reductions would be related to gear quality, alignment, surface finish and treatment, damping, and/or isolation.

Modifications for increased efficiency were to include bearing and lubrication variations. Cost and power loss of several bearing schemes would have been examined utilizing vendor input.

Performance of these tasks is well suited to rig testing, due to the controlled environment obtainable and easy access to the hardware involved.

5.3.2 Continuously Variable Transmission

5.3.2.1 Introduction

The transmission is a particularly crucial element of a single shaft gas turbine automotive powertrain. Stringent demands are placed on its design because of the engine's inherent characteristics, e.g., a small overall speed range, high rotating inertia, and a close coupling between load and operating temperature. This section describes the evolution of a transmission concept which effectively and practically meets these demands. The following subjects are discussed:

- * The transmission requirements for a single shaft gas turbine vehicle.
- * The performance characteristics and control requirements of the van Doorne variable ratio metal belt.
- * The relative merits of other possible CVT arrangements.
- * The selected dual-range CVT design.

5.3.2.2 Requirements

The fundamental requirement is that the transmission be able to provide a continuously variable ratio. There are two basic reasons for this:

- * The high effective rotating inertia and the limited operating

speed range of the AGT-102 powerplant make good vehicle response impossible with a fixed ratio transmission.

- * The range of engine speed which provides good fuel economy for any given output is extremely narrow.

The single shaft engine output characteristics are shown in Figure 136A. This engine was coupled with a five speed transmission to produce the steady-state output capability, which is shown in Figure 136B. As can be seen, this combination falls far short of providing full engine power over a reasonable range of vehicle speeds even under steady-state conditions. Moreover, under accelerating conditions the power available is considerably less; with the first gear shown in Figure 136B, only 46% of the steady-state power is available to accelerate the vehicle, the larger portion being required to accelerate the high inertia single-shaft drive-train. In contrast, Figure 136C shows the power available with a CVT, and, since the input speed is constant, it can all be used to accelerate the vehicle. Thus, a CVT is the only reasonable way to achieve acceptable vehicle response.

As to fuel economy, Figure 137A illustrates the specific fuel consumption for the single shaft engine with a fixed ratio transmission and a CVT; Figure 137B shows the fuel economy of the fixed ratio unit relative to the CVT. As illustrated, substantial fuel economy penalties result with the fixed ratio box because it requires reduced turbine inlet temperatures; this results in severely compromised thermal efficiency.

Another requirement is provision for a suitable engagement or launch device. A fluid element is certainly the most easily controlled device, but it typically requires doubling the input speed at stall to go from a tolerable creep torque level to even a modest acceleration of the vehicle. It is, therefore, not practical in this application since the single shaft engine only has a two-to-one speed range.

The launch device which has been selected is based on work done at Chrysler with electronically-controlled application of a friction element; this work developed techniques for maintaining a small amount of clutch torque at stall and then controlling torque during launch so that the performance was similar to that of a fluid coupling. Although development would be required, the controlled application of a friction element is within the realm of current technology and stands to be a cost-effective solution. This is especially true since other factors have already established the need for sophisticated electronic controls; therefore only part of their cost is chargeable to the launch clutch control.

A review of the engine characteristics quickly shows that the required ratio range of the CVT is about 30:1. This range will provide good performance with a maximum flywheel-assisted engine speed of 75,000 RPM. Any less ratio will either compromise performance or require greater assist speeds. Moreover, the 30:1 range permits full engagement of the launch clutch by 4 mph and thereby limits the speed range over which good launch control must be

maintained, and improves the probability of the successful development of such controls. The large ratio range is needed for speed reduction because of the limited engine speed range; the torque multiplication with these ratios, however, can place some severe demands on the powertrain. In order to limit the size and weight of the components, it is a requirement that the high ratios be used only at low power levels. The controls section describes techniques used to limit the applied power over a substantial portion of the ratio range. The speed ratio range of a single variable ratio metal belt (discussed in next section) is about 5:1 with a belt in the 100 lb-ft capacity range. The belt, therefore, must be augmented with gearing in order to provide the required ratio range.

To meet the requirement that the AGT be competitive with other power plants, the cost, weight, and size of its transmission cannot be significantly different than current production units. Furthermore, its design must be suitable for high volume production and any side effects, like gear noise, cannot be significantly worse than today's units.

The parasitic loss and efficiency requirements for the CVT cannot be separated from the complete vehicle since the real requirement is that the total package be attractive enough to justify the effort and cost required to produce a totally new powertrain. With small cars, it is especially essential that parasitic losses be minimized. Since the continuously variable feature is so essential for the single shaft engine, there is no alternative other than that the efficiency be high enough and parasitic losses low enough to make the total package attractive.

5.3.2.3 Variable Ratio Metal Belt

The selection of a variable element for the CVT began with a review of candidate concepts. The most promising fall into three general groups:

1. Variable ratio pulleys
 - a. compression belt
 - b. rubber V-belt
 - c. special chain
2. Hydromechanical
3. Traction drive

A comparison chart summarizing the results of a design concept study is presented in Figure 13^R. Major considerations of the study were the CVT state of development, adaptability to mass production with reasonable cost, and acceptable packaging. The traction drive CVT is attractive for noise and cost, but, to date, this concept has only proved to be successful at lower power levels. The hydro-mechanical units have the most field experience, but they are noisy, expensive, and only moderately efficient. Of the variable pulley types the rubber V-belt is widely used and efficient, but there are

problems caused by its reliance on organic materials, namely, limited life and awkward packaging due to the need for large pulleys. The two remaining types use metal elements to overcome these problems, and between these two, the van Doorne compression belt appears to be simpler, less highly loaded, free of chordal action, and more thoroughly developed than the GKN special chain. Therefore, the compression belt has been chosen as the variable element for the CVT.

The compression belt concept is patented by van Doorne Transmissie of Holland. It transmits torque through compression loading of metal struts which are restrained by two, 10-layer, thin metal bands (see Figure 139). The operating characteristics of this type of belt are described in detail in the NASA report "Design Study of Steel V-Belt CVT for Electric Vehicles" by Battelle Columbus Laboratories; a more in-depth analysis of the belt losses is presented in the Battelle report "Van Doorne Belt Analysis" which is included in Appendix D.

In order to develop data on the belt's operating characteristics, a van Doorne industrial CVT was purchased, and a test rig was built (see Figure 140). The data from this rig are presented in Figures 141 and 142. In addition, a dynamic slip test was run; slip occurred at 70 lb-ft, at maximum reduction (about 2.23:1), and 4,400 rpm input speed, with pressure of 240 psi in the output pulley and 70 psi in the input pulley. The calculated friction coefficient between the struts and the pulley was 0.083 at the slip condition.

Although the testing and analysis are incomplete, it appears that precise control of pulley pressure can provide much improved efficiencies from those observed in the industrial unit. This is due to the fact that most of the losses are caused by sliding that occurs between belt components that move at slightly different velocities, and since this unit does not compensate the pulley pressure for input load, the excess pulley clamping load (which is almost 100% even at rated load) results in unnecessary losses. Our estimate of achievable power transmitting efficiency is 97% through the underdrive range, decreasing linearly with ratio to 93% at maximum overdrive. This does not include pump, bearing, seal, and clutch losses. It also appears that these efficiencies will deteriorate somewhat at higher speeds (especially with overdrive ratios). This deterioration, however, is not of much consequence since, for fuel economy, little time is spent at high speed, and for performance, small changes in efficiency have little effect.

The plan for controlling pulley pressures is to set minimum values for each pulley as a function of ratio, load, and speed; the clamping load on one of the pulleys, then, would be raised above the minimum value in order to maintain ratio or to achieve a rate of ratio change. The clamping load may also be varied to compensate for temperature effects on friction coefficient and engine output.

5.3.2.4 CVT Arrangement Possibilities

The large required ratio range dictates that the variable belt

be augmented with some other gearing. A two speed gearset could be used in series with the belt, but that would require moving the belt through its full range at each shift. This would not only result in a prolonged shift, but would also mean that the inescapable torque drop during the shift (Reference 1) would be about 80%. Regenerative arrangements are attractive because they have a large ratio capability; they typically have two inputs to a simple planetary gearset, one to the sun and one to the carrier with the annulus being the output. Battelle studied regenerative arrangements and suggested an interesting and potentially attractive unit which used a variable belt for each input and the RAF geared directly to the sun gear shaft (see Figure 143). This unit allowed for full compensation of the engine inertia with the flywheel. Further work on the concept was dropped because of the cost, complexity, and risk associated with the two variable belts.

Orshansky Transmission Corporation also reviewed a number of regenerative CVT arrangements and presented a detailed analysis of each. Their recommendation was for an arrangement very similar to the final selected design; the clutch location and final drive were revised (see next section).

Chrysler studied two basically different arrangements: a single range CVT and a dual range unit (see Figure 144). Table 16 summarizes the relative merits of each; the dual range unit was selected because it would provide better fuel economy.

5.3.2.5 Selected Design

A schematic of the selected design is shown in Figure 145. Figure 146 is a cross-section of the complete transmission. With this arrangement the variable belt is rotating all of the time which, through engine speed and output pulley speed sensors, permits selecting and verifying pulley ratio prior to engagement of the launch clutch. This is essential, since a wrong pulley ratio could produce a reverse ratio instead of a forward breakaway ratio. Additional speed sensors are required on the RAF to report flywheel speed, and on the transmission output to verify clutch engagement conditions. Separate solenoid control circuits are required for the two variable pulleys, the two CVT clutches, the two RAF clutches, and the pump pressure control. A pressure transducer is also required for pump pressure control. Proper functioning of all of these controls, and the processor, must be verified before any clutches are applied.

The regenerative gearing is such that breakaway Reverse is provided with the low or launch clutch engaged and the belt at 1.8:1 overdrive ratio (See Figure 147); maximum Reverse speed (-10mph at engine idle) is achieved at a belt ratio of 2.2:1 overdrive. The engine speed in Reverse is limited to that required to back a loaded vehicle up a 32% grade, about 60,000 rpm. This is done to limit the belt torque, which is most heavily loaded in Reverse (see Figure 148).

C-2

Breakaway forward ratio is achieved with the low clutch engaged and the belt at 1.5:1 overdrive ratio (ref. Figure 147). As car speed increases the belt ratio is reduced until it matches the fixed chain ratio of 0.5:1; at that time the low clutch is released and high clutch is applied. When this shift occurs, no speed changes are made, and no change in belt ratio is required. The output is then driven directly from the belt output since the planetary is locked up; as car speed increases further, the belt ratio is increased to a maximum of 2.2:1. The belt torque requirement for low and high ranges are also shown on Figure 148.

The pump selected for this transmission is the one used in the THM 125 transmission (Reference 2). It is a variable displacement unit which will permit keeping the parasitic losses at a minimum. Since the minimum input speed is over 2000 rpm (the pump operates as low as 700 rpm in the THM 125), the unit should have more than adequate output and pressure capability to insure rapid transmission response. A solenoid will be used to control pump offset and therefore displacement.

The low and high clutches have been located where their relative speeds when released are low (to minimize drag losses) and where they eliminate planetary gear rotation in high range (to avoid a gear noise problem). Their location also allows the use of only one bulkhead in the transmission. The arrangement also permits the final drive components to be housed in the transmission case, thus saving the cost of a separate casting and attachment.

The final drive is a unique arrangement which provides the required differential action between driving wheels from the same two planetaries which are used to achieve the 5:1 final reduction ratio. This permits a length reduction of almost two inches and saves the cost and weight of the differential housing and gears.

In summary, it appears that a CVT can be built which meets the performance criteria for the single shaft gas turbine vehicle. Moreover, its size, weight, cost, efficiency, and manufacturability appear to be comparable to current three-speed automatic transmissions and to be simpler than conventional four-speed units. In other words, it is believed this work has demonstrated that the technology is available to provide the required AGT transmission characteristics at a cost which is competitive with current SI engine transmissions.

REFERENCES

1. Winchell, F. J., and Route, W. D., "Ratio Changing the Passenger Car Automatic Transmission" in SAE AE-1, Design Practices for Passenger Car Transmissions, pp 57-61.
2. Koivunen, Erkki A., and LeBar, Philip A., Jr., "A New Automatic Transmission for Improved Fuel Economy--General Motors THM 125", SAE 790725.

5.3.3 Response Assist Flywheel

5.3.3.1 The Need For a Flywheel

Unlike gasoline or diesel engines where torque can be quickly changed by throttling or changing the fuel injection rate, the torque changes of a single shaft automotive gas turbine rely principally on achievement of rapid speed changes. As discussed in Section 5.4.2.1, use of VIGVs to reduce overall speed range is ineffective. Reliance on extreme overfueling to achieve rapid speed changes is limited by permissible material temperatures and by choking or surging in the aerodynamic components. The energy required to change speed in a small high speed gas turbine is large relative to its power generation at low speeds, and normal accelerations from low speeds are therefore slow, requiring on the order of a second or two. During deceleration the rotor kinetic energy and heat stored in the engine hot parts continue to supply unwanted power for a short time after the fuel is shut off.

Therefore, the automotive gas turbine, which operates very much in transient modes, needs extraordinary means to improve its response and, hence, vehicle driveability. The concept of a response assist flywheel has been analyzed to the point where it appears that it can effectively and practically supply this need.

5.3.3.2 Selected Speed Relationship

Engine response should be repeatable. The driver should always obtain the same acceleration or deceleration from the same conditions at the same demand. Therefore, the RAF should maintain charge capability as a function of engine speed.

Figure 149A illustrates an example of the speed relationships. As the engine accelerates from 42,000 RPM idle to 75,000 RPM maximum flywheel assist speed, the flywheel would be sized to decelerate from 20,000 RPM to 15,000 RPM (there is a 5:1 gear ratio between the RAF and the engine). This acceleration would require perhaps $\frac{1}{4}$ second, limited only by clutch, gear, and bearing capacities. As the engine decelerates from 75,000 to 42,000 RPM it would accelerate the flywheel through a recharging gear back up to 20,000 RPM. This latter maneuver, as described below, requires more energy than is available from momentum exchange, and would require perhaps a second or two to occur.

5.3.3.3 Relationship of Speeds, Losses and Inertias

The size of the flywheel is determined from the conservation of system angular momentum during engine acceleration. The engine and flywheel are coupled to each other through the first gearset in the

reduction gearing and through a clutch. For the gear/flywheel system,

$$I_E \Delta \omega_E = I_F \Delta \omega_F$$

WHERE

- I_E = Equivalent engine inertia at gear ($R^2 I_{eng}$)
- I_F = Flywheel inertia
- $\Delta \omega$ = Change of rotational speed
- I_{eng} = Actual engine inertia
- R = Gear ratio

The flywheel inertia is therefore,

$$I_F = I_E \frac{\Delta \omega_E}{\Delta \omega_F} = I_{eng} R^2 \frac{\Delta \omega_E}{\Delta \omega_F}$$

The energy exchanges during accel and decel are illustrated in Figure 150. The system energies are obtained from the ordinate and abscissa values of the shaded areas.

$$\begin{aligned} \Delta KE &= \frac{1}{2} I (\omega_f^2 - \omega_i^2) & \omega_f &= \omega_i + \Delta \omega \\ &= \frac{1}{2} I (2 \omega_i \Delta \omega + \Delta \omega^2) \\ &= (I \Delta \omega) \left(\omega_i + \frac{\Delta \omega}{2} \right) = \text{BASE} \times \text{AVG. HEIGHT} \end{aligned}$$

The lower part of Figure 150 shows the detailed relationships.

Using these relationships, typical energy changes are illustrated in Figure 149B.

The engine in accelerating from 42,000 to 75,000 RPM (8400 to 15,000 RPM at the flywheel clutch) requires the addition of about 16 HP-sec of kinetic energy. This requires that the flywheel give up 24 HP-sec of kinetic energy with 8 HP-sec being dissipated in clutch loss due to speed differences.

To re-accelerate the flywheel from 15,000 to 20,000 RPM requires that it be recharged with 24 HP-sec of energy. A speed step-up of over 2:1 is required so that the engine side clutch is always at a higher speed than the flywheel side clutch throughout the recharging cycle. Resulting clutch losses as the engine decelerates from 75,000 to 42,000 RPM and the flywheel accelerates from 15,000 to 20,000 RPM would be about 15 HP-sec. Total work required from the engine during flywheel recharge would therefore be 24 plus 15 or about 39 HP-sec. Since only 16 HP-sec is available from engine rotor kinetic energy, and additional 23 HP-sec must come from engine-generated power. The engine can generate the energy in

about 1.5 to 2 seconds from stored engine heat while decelerating with fuel off as illustrated in Figure 149C. The area under the curve is 23 HP-sec.

5.3.3.4 RAF Control Logic Effects

When the accel clutch is applied to assist the engine to a higher speed, the RAF end speed would be somewhat greater than the level indicated in Figure 149A because the engine will provide a portion of the required energy. The control logic then must simply allow the flywheel to coast. The decel clutch should only be applied to maintain flywheel speed when the RAF speed falls below the levels indicated by Figure 149A. Since this is a negative torque on the engine, this clutch must be able to be applied at very low torques in order to avoid objectionable driveline disturbances.

5.3.3.5 RAF Design

The RAF gearing and clutching for various operational modes is shown in Figure 151. The gearset used employs a compound planet carrier with two sun gears. The clutches and connections are shown in 151A. The RPM relations between the parts are illustrated by the lever analogy 151B, the RPM being proportional to the length of the arrows. Two numbers are shown for engine speed, the lower one being the intermediate reduction gear shaft to which the RAF connects; it is 1/5 of the engine rotor RPM.

The latest design, shown in Figure 152, incorporates the following assumptions:

- Engine idle speed 42,000 RPM
- Maximum assisted speed 75,000 RPM
- Accel through this range in .6 sec. under flywheel energy alone
- Max. flywheel speed 20,000 RPM
- Engine rotor inertia 0.005 lb-in-sec²
- Flywheel inertia 0.165 lb-in-sec².

The gears, bearings, and clutches are as small as possible in order to minimize parasitic losses. The clutches have been sized to keep the BTU/in² of facing area within normal transmission practice. The lube circuit has been designed to provide for proper cooling of each disc. The lube circuit of the decel clutch can be used to maintain flywheel speed during cruise since viscous drag between clutch discs is more than adequate to accelerate the flywheel. The piston of the accel clutch applies a force through a bearing in order to avoid problems with centrifugal oil pressure; if those problems could be solved, however, it would be desirable to elimi-

nate that bearing and its parasitic losses. The grounded side of the decel clutch was located at the inside diameter so that centrifugal force would purge the clutch of oil and reduce clutch drag. The clutch packs are offset so that lube oil for one would not cause drag in the other. The small gear diameters should minimize pitch line velocities and noise. A diametral pitch of 36 was planned for the gears. No stress work has been done on the flywheel, but the peripheral speeds indicate that no problems exist.

5.3.3.6 Battelle Subcontract Work

Chrysler's early conception of the RAF was that it should have a size and speed range which could provide several engine accelerations between re-charges and also absorb vehicle braking. The clutch design and development under these missions was considered to be so large a task that specialized knowledge was required. Therefore, Chrysler turned to Battelle because of their special expertise in high speed clutches.

Battelle began an initial assessment based on the same mission assumptions Chrysler had proposed, while Chrysler continued studies of various mission demands and control strategies. It became increasingly apparent that less charge capacity should be used, that the flywheel-engine speed should be directly dependent, and that vehicle braking would not save much, if any, energy.

With this reduced mission demand, the clutch problems moved from one of pioneering to one of conventional engineering.

Battelle's independent confirmation of this direction was extremely valuable. They also considered other concepts for possible improvements: traction rollers to reduce gear noise and variable belt drive to eliminate slipping clutches. But these developments were considered too costly.

The Battelle Report is included in Appendix D.

5.3.4 Parasitic Losses

To accurately assess the performance of the AGT-102, it was necessary to estimate the power consumption of the accessories. Parasitic losses as a function of speed were calculated for the reduction gears, RAF, power steering, alternator, regenerator drive, transmission fluid pump, CVT, and air bearing, with special attention to the high speed shaft ball bearings. These estimates were made for prototype components, some of which were designed for the 10:1 speed range of a spark ignition engine. The AGT-102 experiences only a 2:1 speed range; thus accessory optimization would reduce parasitic losses. Details of individual component losses are shown on Figures 153 and 154.

High Speed Bearings - The air bearing parasitic loss was estimated at idle and at full speed, and it was assumed to vary with RPM squared. This loss is less than 10% of total high speed bearing loss. Characterization of high speed ball bearing power loss in Reference 1 was compared to Chrysler data, and then used to estimate the power consumption of the AGT pinion bearings shown on Figure 153A.

Reduction Gears - Mesh and bearing loss friction, not including high speed rotor bearings, consumes approximately 3% of the power transmitted through the 20:1, two-stage, helical, reduction gear set. The reduction gear parasitic losses are assumed to be a parabolic fit of the projected pinion HP vs. RPM, multiplied by .03.

RAF - Although sizing of the RAF was not completed, the parasitic power estimate includes windage, clutch drag, and the gear mesh. This is shown as a cubic curve on Figure 153D, with the high losses above 75% speed resulting from high relative velocity across the carrier to ground charge clutch.

Power Steering - Power steering pump HP requirements vs. speed, for various maneuvers, are shown on Figure 153C. The minimum pressure line is used for prediction of chassis rolls fuel economy.

Alternator - The AGT-102 alternator load was compiled and a 65-amp automotive alternator chosen. Typical drive cycle current draw would be 10 to 20 amps. Alternator speed range was set at 2500 to 5000 RPM with the power loss as shown on Figure 153D.

Regenerator Drive - The drive system includes the twin cores, two dry core bearings, two dry pinion bearings, two lubricated worm bearings with two lubricated worm wheel bearings, one pulley ball bearing, and a V-belt. Power was calculated from the mesh and belt efficiencies and the bearing friction, speeds and loads. This distribution of loads is shown on Figure 154.

Transmission Fluid Pump - The friction torque due to the pump, seals, bearings, and clutches was estimated both at idle and at design RPM, and was assumed to vary linearly with speed. Resultant horsepower (Figure 153D) varied from 1.1 at idle to 4.3 at full speed.

CVT Internal Parasitics - The equivalent power loss due to the CVT is computed from road load HP and transmission ratio. The CVT efficiency is a function of speed ratio only. The characteristic used is shown on Figure 153B.

In the Federal drive cycle air conditioning is not included, the alternator does not account for the headlight load, and the power steering is set for straight ahead driving.

At the time of program close-out, it remained to more accurately assess each production AGT parasitic loss, and to extend the analysis to the new idle speed of 44,000 RPM. At present, the total parasitic horsepower is broken down by component, and the cumulative affect of each loss is shown in Figure 155.

REFERENCE

1. Trippett, R. J.: "A High-Speed Rolling-Element Bearing Loss Investigation," Trans ASME Jour. Eng. Power, pp. 40-47, January, 1978.

5.3.5 Control System

5.3.5.1 Requirements

The control system for a single-shaft gas turbine engine must be reliable and failsafe. With this engine and its continuously-variable drivetrain, a properly functioning control system is essential to accomplish even the most minor maneuvers. Moreover, a number of functions must be performed properly in order to avoid hazardous overspeed operation. It has thus been concluded that the only failsafe mode is to shut off the engine and place the drivetrain in neutral. Since this action prevents any further powered motion of the car, it must not be allowed to occur except under very rare circumstances; therefore, the overall control system must be extremely reliable. Indeed, the control system of the single shaft engine powertrain is as essential to safe and proper car operation as the steering system, and the reliability must approach that standard. The failsafe requirement means that the control system must be able to verify the proper functioning of all subsystems; the reliability requirement probably means that some redundant components will be needed.

With standard SI reciprocating engines, the accelerator pedal controls the throttle valve which, by limiting air flow, controls engine torque. It seems appropriate, therefore, to attempt to provide a similar effect with the AGT-102. Since, with the single-shaft engine, the only way to significantly increase torque is to increase engine speed, the simplest approach would be to have a direct relationship between pedal travel and engine speed, Figure 156 (engine torque varies approximately linearly with engine speed). This approach, however, would have two undesirable effects. The first is that full pedal travel would impose excessive torque on the drive system and/or generate wheel slippage, from 0 mph to about 20 mph. To avoid this condition, engine speeds must be limited in the 0-20 mph range. The other undesirable effect is that if the pedal is depressed quickly, the response (with controls as indicated by Figure 156) would be somewhat delayed by the necessity to change engine speed, and the response would not provide feedback to the driver in a time frame that might allow him to select a smaller

pedal depression. It is believed that a more driveable control strategy would provide, say, 2/3 of commanded increase immediately and spread the last 1/3 increase over the next 2 to 3 seconds. Thus, it appears that the relationship shown in Figure 156 can be the basic response to accelerator pedal commands provided that modifications are incorporated to limit engine speeds in the 0-20 mph range and to incorporate a time-based response to pedal commands.

A study of vehicle acceleration reveals the need for a further modification of the engine speed limitation. Incorporating the engine speed limit in the 0-20 mph range, discussed above, gives curve #1 shown in Figure 157. Curves #2 and #3 show the modifications needed to overcome the engine's own inertia at a rate that does not compromise vehicle acceleration. This modification does not increase drive torque because the increased engine output is used to accelerate engine mass and not applied to the wheels.

In summary, the specific engine speed relationship which must be established by the CVT ratio control is a function of:

- * pedal position -- to provide the requested speed (torque).
- * car speed -- to limit torque to useable levels at low car speeds
- * time -- to allow driver feedback for better controllability
- * car acceleration rate -- to establish the level of power needed for engine acceleration.

The breakaway or launch event requires control logic for both the response assist flywheel (RAF) and the CVT launch clutch. The RAF accel clutch should be applied first to bring the engine speed up to the level commanded by pedal travel as indicated above. The launch clutch should then be applied at a torque level appropriate to pedal position.

The CVT has a variable displacement pump to minimize parasitic losses which the control system will complement by maintaining hydraulic pressure at a level no higher than required. This requirement will vary with engine speed (i.e., torque), variable belt ratio, and the commanded rate of change of belt ratio.

In addition to breakaway, the RAF accel clutch must have logic to allow it to assist during increase pedal travel events. The RAF decel clutch must maintain RAF speed during cruise and assist in reducing engine speed during reduced pedal events. These events also require fuel cut-off and compressor bleed with logic to control the actions as needed.

5.3.5.2 Torque-Sensor-Based Control Logic

The key to structuring a control logic which is inherently simple is to incorporate a torque sensor on the transmission input

gear. A concept for the torque sensor is described in the following section (5.3.5.3). A structure for such control logic in response to partial closing of the accelerator pedal is shown in Figure 158. Pedal position commands two values - one for input torque and one for engine speed. The transmission ratio control responds only to the commanded engine speed, and at a rate which is determined by the speed error. The RAF clutch is pressurized only in response to RAF speed so as to maintain the programmed speed levels which are required to accelerate the engine back to 75,000 rpm. The torque sensor is used to control both fuel cutoff and compressor bleed. The elegant feature of this control is that the torque sensor, by measuring transmission input torque, T_Q , sums the inertia torque effects of changing transmission ratio and the torque effects of applying the RAF clutch before exercising its control of fuel and bleed. Thus the CVT ratio control and RAF clutch control can operate on independent logic without their torque effects disrupting the drive torque. Furthermore, by deliberately biasing the accelerator pedal torque commands to values above the turbine exit temperature (TET) limited levels, a smooth transition is accomplished between TET control and fuel cut-off control.

The control logic sequence to respond to increased accelerator pedal commands also depends on the torque sensor. First it is necessary to establish a desired engine speed, N_{DE} ; this is done in the manner described in the requirements section and:

$$N_{DE} = f(\text{Pedal Position, time, instantaneous car speed, car acceleration}).$$

The CVT control logic compares N_E , actual engine speed, to N_{DE} and responds as follows:

$$N_E < N_{DE} = \text{Increase Transmission Ratio}$$

Again, as with reduced pedal logic, the rate of ratio change depends on the error; these rates are selected to give rapid response without overloading the RAF. The RAF, of course, must provide most of the energy required to accelerate the engine at the rapid rates dictated by the CVT control or else the energy will come from the vehicle's own inertia by slowing the car's speed. As indicated in the reduced pedal sequence, the processor has stored a torque value appropriate for all engine speeds. The RAF accel clutch control logic uses that value and the torque sensor as follows:

$$T_Q < K (T_{\text{appropriate}}) = \text{RAF accel clutch ON}$$

The constant K will be selected to allow some of the engine's torque to contribute to its own acceleration, but not so much as to cause an objectionable disturbance in drive torque; the probable value for K is between 0.3 and 0.7. As stated earlier, RAF operation is limited to engine speeds below 75,000 rpm. An additional RAF control statement is needed below four mph to accommodate break-away and the CVT ratio limit:

$$N_E < N_{DE} \text{ and (CVT ratio = max) = RAF accel clutch ON}$$

The value of (T desired) is the torque appropriate to the desired engine speed, N_{DE} , as shown by line 1 in Figure 157. It does not contain an increment of torque needed to accelerate the vehicle (lines 2 and 3) since such an increment is intended to increase engine speed rather than output torque to the transmission.

The advantage of this logic is that the CVT control can do its job of providing the pedal-commanded engine power almost without concern for the transient torque effects. The RAF, through the use of the torque sensor, maintains reasonable output torque levels which reflect the engine's ability to provide torque and minimizes the magnitude of torque changes during transient maneuvers. Acceleration fuel schedules can be added without logic modification; altitude and temperature effects can be accommodated. The logic development should be relatively easy because the logic statements are simple and independent. The primary task is to provide valid information to the processor and to develop CVT rates of response which allow time for RAF response.

5.3.5.3 Control Components

Torque Sensor - A concept for the torque sensor (see Figure 159) was developed which appears to be capable of providing the accurate, reliable torque information needed for good control. This sensor employs springs which deflect in response to torque being transmitted to the transmission input shaft. The deflection is measured as a change in location of every other tooth on the input speed sensor gear. The no-load condition can be observed during start-up, thus permitting automatic calibration of the no-load point. This point is crucial since control actions at no load can cause multiple crossings of drive train backlash and result in annoying "klunks". The torque indicated at higher levels will only be in error to the extent that the actual spring rate differs from the design value.

The processor planned for these controls must have very fast response and be capable of high resolution. Although the exact requirements have not been determined, a similar application required that the total control program be processed in 2½ milliseconds; a 16 bit machine was used so that eight bits of data could be handled in each operation. The processor could measure velocities every 2½ milliseconds which were accurate to within 0.0025%. Furthermore, the processor had the ability to verify the proper functioning of all control components, and if an error were found, it could in all cases achieve a failsafe operating mode. The AGT control system should have similar capabilities.

Electronic Control Unit (ECU) - It is planned that an electronic digital microprocessor would serve as the central controller for the powertrain system. This would contain logic for both the torque sensor based control and the engine start-safety system.

An initial controller input-output schematic is shown on Figure 160. Logic diagrams were not completed prior to program closeout.

Ambient temperature and pressure inputs are required for the controller to modify speed, torque, temperature and fuel schedules to maintain engine operation within safe limits. Driver inputs would be through the key switch, accelerator pedal, and transmission selector switch. The one and two low gear selector positions would not be appropriate to the basic CVT control, but consideration is being given to their retention for setting higher levels of idle speeds for downhill braking with compressor bleed.

Powertrain inputs to the controller would be speed, temperature, and pressure signals as indicated on the schematic. The torque sensor and transmission input speed signal would use a common transducer with the controller calculating the time between blips for torque and blips per unit time for speed. Control is based on turbine exit temperature (TET) which can be sensed by conventional Chromel-Alumel thermocouples. Turbine inlet temperature level is outside the range of conventional low-cost sensors. A regenerator outlet temperature (T9) signal is required for each regenerator as part of the safety system to indicate failure of the regenerator drive system.

Controller outputs as indicated on the Figure 160 schematic include a variable fuel metering valve signal and off-on signals to a series of solenoid valves for control of fuel, compressor bleed, the RAF, and the CVT.

Other Control Items - For initial experimental engines, satisfactory operation could be expected using a controlled flapper-type metering valve similar to that used by Chrysler on the Upgraded Engine. However, program efforts would include development of a simple and reliable fuel metering valve capable of accurately maintaining extremely low flows for future production use.

Other items such as temperature, pressure, and speed transducers, hydraulic and fuel system solenoids, and the compressor bleed valve would be selected based on automotive practice for the specific category of item.

5.4 VEHICLE PERFORMANCE

5.4.1 Fuel Economy Studies

5.4.1.1 Fuel Economy Estimates

As discussed in Sections 5.1.1.3 and 5.3.2, AGT-102 experimental engine development would initially rely on use of a metal superalloy turbine wheel. This option would require a cycle revision with maximum TIT reduced to 2100F compared with the 2300F ceramic wheel cycle. Details of the two cycles are tabulated in Appendix B. Although there is a significant reduction in maximum power (66 vs. 78 HP) at the lower temperature, part-load SFC characteristics are almost identical. Accordingly, calculations which

were made of drive cycle fuel economy (Table 17) show surprisingly little difference between the metal-turbine engine and the ceramic-turbine engine. The fuel economy is based on a warm-up fuel estimate of 0.81 lb (15,000 BTU) and a fuel heating value of 18,500 BTU/lb (gasoline).

As discussed in Section 4.3, a 10% improvement in currently projected RPD fuel economy is needed to achieve the 30% minimum program goal. Therefore, to guide program development efforts, a study was carried out to determine the sensitivity of drive cycle fuel economy to changes in powertrain parasitic power losses and warm-up fuel requirement. The results of this study are summarized on Figure 161.

Considered individually, to achieve a 10% improvement would require that warm-up fuel be reduced from a 15,000 BTU requirement to about 5,000 BTU's, or parasitic power be reduced by about 35%. A more realistic goal would be to work toward reducing warm-up fuel to 10,000 BTU's and parasitic losses 20%.

5.4.1.2 Warm-up Fuel Characterization Tests

Warm-up fuel requirement cannot be derived directly from engine mass and steady-state temperatures. Parts such as the compressor, regenerator cover, and regenerator cold side are heated by compressor air and some warm-up heat comes from engine exhaust which runs cooler during warm-up. These factors were roughly accounted for in establishing the original 15,000 BTU estimate, but the need for a better model was recognized.

As an aid to establishing a more accurate model for the AGT-102 system, an Upgraded Engine, Power Plant 3-13AB, was tested on a dynamometer to determine experimental reference values for starting and warm-up fuel requirements. The test consisted of starting the engine cold (after an overnight room-temperature soak), bringing it up to standard idle conditions (50% gas generator speed match point) and holding this match point until fuel flow reached an asymptotic minimum value.

Figure 162 shows the shape of the fuel flow versus time curve for the 30 minute test period required to establish an asymptotic minimum fuel flow value.

Transient temperatures during the start and warm-up are plotted on Figure 163. These show the relatively slow rise in exhaust gas temperature; corresponding exhaust heat rejection is shown in Figure 164.

5.4.1.3 Warm-up Fuel Analytical Model

The Upgraded Engine data were used in structuring a warm-up model based on the characterization approach illustrated in Figure

165. Here total heat stored in the engine is separated into two parts: (1) heat from warm-up fuel and (2) heat recovered from the exhaust.

Upgraded Engine total steady-state heat storage was calculated as the product of the: a) mass, b) specific heat, and c) temperature difference between the hot and cold state for each component of the engine. Calculations were performed from temperature data and estimates at 50% speed and 80% speed. The results were linearly interpolated to determine the heat storage at 65% speed which is the estimated average speed during the drive cycle. The heat storage was computed to be 20,100 BTU. The test value of exhaust heat contribution was determined from Figure 164, where the area between the T9 curve and the asymptotic exhaust temperature of 270F yielded a value of 4,100 BTU.

Subtracting 4,100 BTU due to exhaust heat gives 16,000 BTU or 0.9 lb of fuel for engine warm-up. This compares closely with the measured value of 1.0 lb of fuel measured on test (Upgraded Engine Final Report, Vol. 2 of 4, Table 25). This includes 0.8 lb during the 550-second time period and a residual 0.2 lb during the remaining 822 seconds.

Generalization of this modeling approach requires an analytical or empirical model for the exhaust temperature warm-up characteristic. Initial efforts in this regard are shown in Figure 166. A family of curves is presented in which the increase in exhaust temperature from 85F as a fraction of the final temperature increase is expressed as a function of the time according to the equation,

$$(T-85)/(T_f-85) = 1 - \text{EXP}(-t/K)$$

where

T = Temperature at time, t, deg. F.
T_f = Final Temperature
K = A Constant

The value of K has to be determined experimentally. If the warm-up time is known (warm-up time being the time required to reach 95% of the difference between initial and final temperatures), the heat storage can be corrected for exhaust heat contribution during warm-up. Comparison test results show an agreement in trend but the shape of the test curve has a sharper bend at 200 seconds. Curtailment of the program precluded further refinement efforts.

5.4.2 Performance Studies

The performance estimates at the time of program close-out are shown on Table 17. Included on the table are performance values for the ceramic-turbine engine and the metal-turbine engine. The differences in turbine materials are reflected in higher maximum turbine inlet temperature for the ceramic turbine which results in better vehicle response.

Acceleration is aided by the response assist flywheel for both engines; flywheel size for the ceramic-turbine engine is about one-half the size for the metal-turbine engine. As described in the following, VIGV's were dropped from the RPD. Therefore, these performance results were generated assuming no VIGV power augmentation at maximum speed. A road-load curve is shown in Figure 167. The final RPD cycle is tabulated in Appendix B at the end of the report. Information is presented along the engine operating line from 50% to 100% speed. Power reduction with idle speed reduction is shown on Page B-8. Idle speed as shown is 41,675 RPM.

5.4.2.1 VIGV Trade-off Study

A study was conducted to determine the minimum value of idle speed and to evaluate the effectiveness of VIGV for power augmentation at maximum speed and load reduction at 50% speed. This section summarizes this study and presents the results which led to selection of an idle speed and to the removal of the VIGV from the original engine concept.

Detailed performance studies on the original RPD concept showed that to achieve a reduction from drive to idle horsepower at 50% speed (3.5 HP to 1.1 HP) required almost a 600F reduction in turbine exit temperature in addition to a maximum deflection of the VIGV's in the positive preswirl direction. VIGV preswirl could achieve only 10 of the required 69 percent power reduction. Not enough power reduction was achieved by the VIGV because of conflicting results with flow reduction from preswirl for the backswept impeller. As preswirl increases, mass flow is reduced and compressor work should diminish because of the positive preswirl. However, at the rotor exit, as mass flow decreases, tangential velocity increases, thus countering the effect of preswirl.

Lowering TET was judged as impracticable because stored heat in the engine would result in a long overrun period before the lower TET level could be reached, the burner would not relight spontaneously as designed, and control of CO and HC emissions would be severely compromised. Lowering speed as an alternative to lowering temperature was considered because it could be accommodated without compromising driveability by resizing the response assist flywheel.

Additionally, concerns developed regarding the practicality of 10% VIGV power augmentation. Design studies indicated that the purely axial VIGV configuration would require actuation of the forward half of the vane as well as the rearward half. Such a configuration has a negative appeal because of hardware and control system cost and complexity. Alternatively, a radial-axial configuration was proposed. In this approach, only the rear flap has to be actuated. The fluid mechanic approach appeared plausible but objectively there was an element of risk since there existed no documented precedent for the proposed design.

Because of the small return on power reduction with VIGV and concern for the aerodynamic development needed to achieve power augmentation, a study was conducted to evaluate the overall importance of the VIGV toward achieving program goals. The vehicle fuel economy and performance were evaluated for:

1. An engine with VIGV; power reduced by VIGV and speed reduction,
2. An engine with VIGV; power reduced by VIGV and TET reduction,
3. The same engine as (1) and (2) above, but VIGV removed; power reduced by speed reduction, and
4. Engine (3) scaled to match the maximum augmented power of (1) and (2).

The fourth case was computed to compare the fuel economy relative to case (1). The reason for using VIGV's was to be able to design a smaller engine and thus achieve better fuel economy through smaller parasitic losses, with maximum power achieved through negative preswirl.

The results are shown on Table 18. The first two columns show the results of cases (1) and (2), respectively. The third column is for case (3), and the fourth column is for case (4).

The first two columns show an increase of 1 mpg in combined fuel economy if power reduction is accomplished with speed reduction instead of TET reduction. Columns 1 and 3 show little difference in city cycle fuel economy and a small gain in highway fuel economy for Column 3 due to the absence of the VIGV loss. Columns 1 and 4 show an improvement of 0.5 mpg on combined fuel economy for a smaller engine with augmentation than for a larger engine without VIGV. The table shows a slightly poorer performance without VIGV (Columns 1 and 3), but still comparable or better performance than the SI baseline (Table 17).

Overall the VIGV payoff seemed too small in comparison with the cost and complexity of its mechanical design and control. Accordingly, the VIGV's were removed from the RPD.

5.4.3 Accel Model

5.4.3.1 Background

To quantify the events taking place in the powertrain during vehicle acceleration and deceleration as described in Section 5.3.5, work was carried out to develop a mathematical simulation of control system logic and execution.

Sections 5.4.3 and 5.4.4 summarize the modeling work. Section 5.4.3 discusses the modeling for the interfacing of the flywheel with the transmission during vehicle acceleration. Section 5.4.4 discusses the modeling of flywheel charging and compressor bleed in simplified interfacing with the transmission. In both of these sections, the roles played by the various components may or may not be completely consistent with Section 5.3.5 since the final control logic was defined after the model development was completed. The interfacing among the components during model development did, however, provide valuable background for use in the final control system simulation.

5.4.3.2 Modeling

The wide open throttle (WOT) launch from a standing start was analyzed in four different modes:

1. Engine acceleration only.
2. Combined engine and vehicle acceleration during the slipping of the launch clutch at constant CVT ratio.
3. Combined engine and vehicle acceleration with a fully engaged clutch and a changing CVT ratio.
4. Engine at maximum speed with all power going to the vehicle.

These events and the interface with the flywheel unit were mathematically modeled, and the WOT performance of the AGT was computed.

The engine power was modeled as a function of speed only. Steady-state operating conditions were principally used in the analysis. Transient engine performance at TIT values slightly higher than steady-state were to be considered during the control system simulation work if needed for optimum matching between engine, flywheel and transmission. The shaft inertia, as sensed by the rest of the drivetrain, was increased by a factor of the reduction gear ratio squared. The flywheel discharged its energy to accelerate the engine; the efficiency of the energy transfer was determined by the ratio of the intermediate reduction gear speed to the flywheel speed. The flywheel stores enough energy for one launch.

The transmission launch clutch is modeled as a uniform-pressure clutch connecting two spinning discs. The disc size was determined by a loading requirement of 1 HP/in^2 . The clutch torque was a function of the coefficient of friction, the actuating force and the clutch geometry. Calculations were carried out in small time steps, and at each step the change in engine and vehicle speeds was computed as well as clutch temperature rise. If the clutch force was too strong, the model predicted engine stall. The time steps were 0.001 second up to 0.3 second, and then the steps were 0.1 second. Transmission efficiency was modeled as a function of CVT ratio only.

Figure 168 shows the events taking place during a WOT launch. The symbols show information every 0.1 second. Wheel slip limits the rate of vehicle acceleration to 15 ft/sec². The flywheel assists engine acceleration for 0.68 seconds. During this time period the transmission clutch engagement begins at 0.42 seconds. The clutch is fully engaged at 0.81 seconds. During this engagement period, the CVT ratio is held constant at 16:1; after this period, CVT ratio changes as the engine accelerates to maximum speed. Calculations were performed for engine configurations with ceramic and metal turbines. It was this model that was used to compute the performance values on Table 17. Table 19 shows the CVT efficiency values at two values of input torque; linear interpolation and extrapolation were used for other values. Table 20 is a complete listing of the accel events in 0.1 second intervals up to 18 seconds. It is based on use of the 44,000 RPM idle speed discussed in Section 5.4.4.2.

To model part-throttle acceleration during the model development period, a simple scheme was used in which CVT ratio was a function of pedal position and vehicle acceleration. (The torque sensor logic had not been conceived of at that time). An example for an acceleration from 40 mph to 70 mph is shown on Figure 169. As the pedal was changed to a new position, CVT ratio was increased, power was reduced to the vehicle, and the engine was allowed to accelerate. When the CVT ratio associated with the changed pedal position and the vehicle acceleration demand was obtained, CVT ratio was reduced, engine speed was held constant, and power was delivered for vehicle acceleration. When road-load speed associated with the changed pedal position was achieved, engine speed and CVT ratio were reduced to meet road-load conditions.

In this example there is an initial reduction in vehicle speed as shown in Figure 169C, because engine acceleration power comes only by increased engine speed and at the expense of road-load power. If provision is made for acceleration fuel flow, vehicle "coast down" can be avoided and vehicle speed maintained until the desired CVT ratio is acquired. In a real system some flywheel energy would be transmitted to the vehicle and no lag at all would be experienced. Examples of all three modes of operation are illustrated on Figure 170. Calculations were performed with engine configurations with ceramic and metal turbines.

In the early example, the kinematics of the system (CVT ratio) and the accel power requirement are combined. In the final control logic in Section 5.3.5, the logic for CVT ratio changing is independent of power demand logic due to the incorporation of the torque sensor.

5.4.4 Decel Model

In support of the decel control logic described in Section 5.3.5, simple models of the control events were studied to evaluate 1) the effectiveness of compressor bleed on power reduction, 2) the

transient operation during flywheel charging, and 3) the role of the CVT. These simple models were studied before the final logic described in Section 5.3.5 was conceived. They served to establish an appreciation for the level of bleed capacity needed and for the clutching rate for flywheel charging. The next step at the time of program close-out was to combine compressor bleed and flywheel charging into the logic discussed in Section 5.3.5.

5.4.4.1 Bleed Study

The effectiveness of compressor bleed on vehicle deceleration was evaluated by computing the time to stop the AGT vehicle from a steady-state speed of 60 mph and from a speed during launch when the engine reached maximum speed but accel is still in progress. The decel from 60 mph was compared to data available for the AGT vehicle using an SI engine and coasting with the automatic transmission left in gear. The evaluation of the launch interrupt was based on the judgment of a reasonable time to stop (2-3 seconds). In both cases, the decel event started with instantaneous fuel cut-off, followed by bleed. The results included contribution of stored heat.

The values of compressor bleed were obtained from compressor and turbine matching calculations. After fuel cut-off but prior to bleed, the engine operating line shifts to higher flows as shown in Figure 171 for the compressor and Figure 172 for the turbine. During bleed, the compressor operating line stays constant but the turbine operating line follows a constant-speed line as shown in Figure 172.

To compute the bleed flow, a match condition is selected along the bleed line. This determines turbine mass flow and work, which are used to compute engine output power. As turbine flow decreases, output power decreases and bleed flow increases. If turbine flow is low enough (or bleed high enough), the turbine power can be too low to even drive the compressor. This negative power was used as retarding power for vehicle deceleration. The bleed flow is the difference between compressor flow and turbine flow.

The results of these calculations at a number of selected match points at fixed engine speed are shown on Figure 173 for 80% speed. Included on the figure is a plot of the required bleed hole diameter corresponding to the bleed values shown on the plot for a discharge coefficient of unity.

A cross plot of output power versus percent engine speed is shown in Figure 174 for three values of bleed hole diameter. The vehicle deceleration calculations used the power characteristic for a bleed hole diameter of 0.5 inch.

The deceleration of the AGT vehicle from 60 mph to stop is shown on Figure 175. For this model, CVT ratio was held constant down to 50% engine speed. At this speed, CVT ratio was varied until vehicle stop. Included on this figure is the coastdown character-

istic of an AGT type of vehicle with automatic transmission in gear. The decel characteristics are very similar for about the first 30 seconds, then the turbine-powered vehicle comes to a quicker stop. The turbine-powered vehicle stops in 38 seconds; the SI vehicle stops in 57 seconds.

For the accel interrupt model, the launch model information at the time showed a vehicle speed of 15 mph when the engine reached maximum speed. The results are shown in Figure 176; the vehicle stops in 2.8 seconds. Again, CVT ratio was held constant down to 50% engine speed, which occurred at 1.2 seconds. Beyond this time, engine speed was held constant while CVT ratio was changed.

These two simple models showed that sufficient bleed could be called upon for probably any control logic. They showed that the driver could expect decel motion similar to that experienced with SI-engine powered vehicles. The calculations also suggested that CVT ratio could be used to refine the decel characteristics, if needed, rather than simply hold ratio constant during the initial speed reduction. This was to be examined in the final control logic.

5.4.4.2 Flywheel Charging Study

For steady-state conditions, a linear relation between flywheel speed and engine speed has been defined in Section 5.3.3. At 75,000 RPM engine speed, flywheel speed is 15,000 RPM; at idle engine speed, flywheel speed is 20,000 RPM. During charging, however, the linear relation cannot be maintained. Charging takes place during engine decel from 75,000 RPM to some lower speed; the linear relation simply defines the desired flywheel speed at the lower engine speed when steady-state conditions have been restored. A study was conducted to compute the actual transient speed relations and to estimate the clutch forces needed to insure the intended speed match-up at the end of the deceleration period. A weak clutch, or delayed clutching, results in excessive engine overspeed. The engine will not be brought down to 44,000 RPM, but to a higher speed which delivers unwanted excess power. If the clutch is too strong, or if clutching occurs too soon, the engine will drop below 44,000 RPM without bringing the flywheel up to 20,000 RPM.

In this study, a simple model was used in which fuel flow was instantly cut off and the engine was instantly declutched from the transmission. The power remaining after fuel cut-off was used to charge the flywheel and to overcome flywheel clutch losses. No bleed was used in this study, but the effect of power reduction with progressive cool-down of the regenerator was included. Speed changes were computed from unbalanced torques, and conservation of energy was used to calculate the heat rise in the clutch.

The flywheel was accelerated from 15,000 RPM to 20,000 RPM as the engine decelerated from 75,000 RPM to 44,000 RPM. Just before AGT program close-out, adjustment of the value of idle speed from

41,675 RPM to some slightly higher value was in progress. This adjustment was required in order to accommodate updates in accessory and auxiliary drive requirements as idle speed was reduced below the initial value of 50,000 RPM. A value of 44,000 RPM was projected to be the next likely selection for idle speed based on a match-up between engine power available and accessory and auxiliary power required.

The results of the study are shown in Figures 177 to 180. The variations of engine speed and flywheel speed with time are given in Figure 177. The transient relationship between flywheel speed and engine speed is shown in Figure 178. The figure shows the difference between the linear steady-state relationship and the transient variation. Figure 179 shows the miss in engine/flywheel match-up at the end of the deceleration period with clutch forces that are too strong and too weak. Figure 180 shows the temporal variation of engine torque, output clutch torque and torque delivered through a drop in engine kinetic energy. The total heat addition to the clutch was 12 BTU.

This simple model showed that a reasonable engine speed transient could be expected during the decel event. The clutch force was 110 lbs for a 3-disk configuration; this gives a reasonable clutch design.

The next task, which had just begun at the time of program close-out, was to combine the bleed and flywheel charging models into the control logic described in Section 5.3.5.

6.0 CONCLUDING COMMENTS

The fundamental soundness of the AGT-102 concept has been supported by these initial design and development efforts. Most significantly, it has been concluded that by using a small response assist flywheel and compressor bleed, competitive response and driveability can be achieved with a highly regenerative single shaft engine, even if equipped with a relatively high inertia metal radial turbine wheel. Design requirements of the transmission, flywheel, and control systems fall within the scope of conventional engineering practice.

The major development challenge of the concept relates to fuel economy, where it remains to be shown that warm-up fuel requirement can be limited to about 0.5 lb, and that compressor and turbine efficiency levels of 0.81 and 0.88, respectively, can be practically achieved in a 0.62 lb/sec size. Accordingly, turbomachinery aerodynamics and design, to minimize hot section warm-up mass, are areas dependent on "developing technology" where development and demonstration must be carried out before the fundamental soundness of the concept for practical automotive application can be judged.

Other areas of developing technology judged to be less critical but also requiring development and practical demonstration are the high speed bearing and shaft system, properties and processing of the ceramic components, design for practical control of shutdown soakback temperatures, performance of a fixed-geometry lean, premixed, prevaporized combustor system, and design of practical, quiet, high speed gearing.

Finally, cost, manufacturing and marketability studies on a developed design would be made to confirm the concept's suitability for high volume automotive use.

	<u>RPD</u>	<u>SI Base</u>
Vehicle	K Body, FWD	K Body, FWD
Transmission	A6T-102, CVT	3 Spd. Auto. Transaxle with Lock-Up. 2.78 Equiv. Axle Ratio
Weight, Curb, lbs.	2,250	2,325
Perf., Test, lbs.	2,950	3,025
(Inertia) Fuel Econ. Test, lbs.	2,750	2,875
Idle RPM	41,675	750
Fuel Econ., MPC Gas. City/Highway/Combined	26.1/47.1/32.6	23.2/36.7/27.8
1 sec., distance, ft.	3	2
2 sec. distance, ft.	18	16
4 sec. distance, ft.	89	72
5 sec. distance, ft.	138	110
0-60 MPH Time, sec.	12.5	14.7
Engine Maximum HP to Transmission	78	84
MPG, City	= 7.45 miles/(gal. fuel, hot cycle + 0.43 x gal. fuel, warm-up)	
MPG, Highway	= 10.2 miles/gal fuel, cycle	
MPG, Combined	= 1/(0.55/MPG, city + 0.45/MPG, highway)	
Fuel	= Gasoline, 6.2 lbs/gal, 18,500 BTU/lb	
Ambient Conditions	= 85°F, 14.43 PSIA	

**Comparison of Performance and Fuel Economy
Between RPD and Baseline SI Powertrain Systems**

Table 1

ADVANTAGES

- o More confident prediction of flow conditions at impeller leading edge
- o Difficult to control endwall clearance - especially at hub
- o Stronger wakes to excite inducer vibrations
- o Longer axial flowpath length
- o Actuation mechanism is more difficult at small radius
- o Higher leading edge Mach number and blade angles than for radial VIGV, therefore, less choke margin
- o Lower efficiencies
- o Less augmentation capability
- o Reduced surge margin

Table 2, 3

Axial VIGV Summary

Table 2

ADVANTAGES

- o Low Mach number region
- o Smooth flowpath into impeller
- o Less vane wake excitation for inducer vibratory stresses
- o Produces lower inducer blade angles, Mach number, therefore, more choke margin
- o Long chord VIGV airfoils to minimize manufacturing tolerance effects available without extending engine length
- o Swirl amplification due to radial in-flow flowpath achieves required inducer flow angles with less VIGV camber/flap angle and lower VIGV pressure loss coefficients, and therefore:
 - Better efficiency
 - Better surge margin
 - More augmentation capability

DISADVANTAGES

- o Endwall clearance requires spherical surfaces.
- o Less confidence in flow-field prediction capability around the bend than for axial VIGV.

Semi-Axial VIGV Summary

Table 3

ADVANTAGES

- o Low Mach region
- o Easier control of endwall clearance
- o Simpler design, actuation
- o Smooth flowpath
- o Less vane wake excitation for inducer vibratory stresses
- o Long chord airfoil to minimize manufacturing tolerance effects available without extending engine length
- o Constant VIGV airfoil cross section hub-to-shroud possible

DISADVANTAGES

- o Less confidence in flowfield prediction capability around bend than axial inlet or semi-axial designs.

Radial Inlet Guide Vane Summary

Inlet Total Temperature, °R	2760	Rotor Inlet Diameter, Inches	5.11
Inlet Total Pressure, psia	58.33	Rotor Exit Hub Diameter, Inches	1.134
Mass Flow Rate, lbm/sec	0.616	Rotor Exit Shroud Diameter, Inches	3.220
Mechanical Speed, rpm	99,500	Exit Hub-to-Tip Ratio	0.352
Total-to-Total Pressure Ratio	3.696	Rotor Axial Length, Inches	1.60
Specific Speed, N_s	68.9	Number of Rotor Blades	12
Work Coefficient	0.942	Nozzle Inlet Diameter, Inches	7.140
Blade-Jet Speed Ratio	0.665	Nozzle Exit Diameter, Inches	5.604
Tip Speed, U, ft/sec	2220	Nozzle Vane Height, Inch	0.275
Total-To-Total Efficiency, η_{t-t}	0.873	Number of Nozzle Vanes	19
Specific Work, BTU/lbm	186		
Corrected Flow, lbm/sec	0.358		
Corrected Speed, rpm	43,137		

Table 5, 6

Radial Inflow Turbine Design Requirements Radial Turbine Rotor and Nozzle Design Summary

Table 5

Table 6

OPERATING STATE:	STAGE 1		STAGE 2		WHITE LEAN LIMIT (AF)	LE FEBVRE LEAN LIMIT (AF)	AIRFLOW SPLIT TO A STAGE	PRIMARY RESIDENCE TIME (MSEC)	FLASHBACK SAFETY FACTOR
	AIR-FUEL RATIO	FLAME TEMP. (°R)	AIR-FUEL RATIO	FLAME TEMP. (°R)					
42% (IDLE)	65.0	2964	--	--	80.3	85.4	0.244	8.1	1.3
50%	58.5	3036	--	--	79.9	82.7	0.275	6.2	1.6
55%	51.9	3123	--	--	79.5	81.0	0.294	5.1	1.9
60%	80.5	2822	107.6	2672	79.0	79.9	0.303	5.2	2.2
65%	72.2	2885	96.1	2724	78.8	79.6	0.308	4.8	2.3
70%	65.5	2947	87.3	2772	78.6	79.5	0.311	4.6	2.3
75%	59.3	3016	79.7	2821	78.3	79.4	0.313	4.4	2.4
80%	52.2	3111	70.9	2891	77.9	79.7	0.313	4.2	2.4
90%	44.2	3195	60.5	2937	70.2	76.8	0.312	4.0	2.7
100%	39.3	3249	54.8	2950	63.9	74.2	0.308	4.0	2.9

Combustor Design Characterization

<u>ENGINE SPEED</u>	<u>T(°R), FLAME (STAGES 1 AND 2)</u>	<u>T(°R), ANNULUS AIR</u>	<u>T(°R), LINER INTERIOR</u>	<u>T(°R) LINER EXTERIOR</u>
IDLE	2964, ---	2205	2250	2248
60%	2822, 2672	2193	2244	2241
80%	3111, 2891	2182	2285	2278
100%	3249, 2950	2031	2211	2198

NOTE: HOTTER FLAME TEMPERATURE USED FOR LINER TEMPERATURE CALCULATIONS.

Combustor Liner Temperature Calculation

	50% SPEED		100% SPEED	
	HP SIDE	LP SIDE	HP SIDE	LP SIDE
INLET TEMPERATURE, DEG F	176.000	2082.500	427.000	1650.000
OUTLET TEMPERATURE, DEG F	2052.176	264.563	1551.579	577.437
BULK TEMPERATURE, DEG F	1114.088	1173.532	989.290	1113.719
VISCOSITY, LBM/(FT-HR)	.092	.094	.087	.092
PRANDTL NUMBER	.697	.698	.693	.697
SPECIFIC HEAT, BTU/(LBM-DEG F)	.270	.273	.265	.270
MASS FLOW RATE, LBM/HR	299.880	306.720	1097.640	1129.140
CAPACITY RATE, BTU/(HR-DEG F)	81.021	83.616	290.941	305.051
FREE FLOW AREA, SQ FT	.185	.185	.185	.185
MASS VELOCITY, LBM/(HR-SQ FT)	1623.999	1661.041	5944.264	6114.852
REYNOLDS' NUMBER	29.565	29.573	113.776	111.338
STANTON NUMBER	.114	.114	.030	.030
UNIT FILM CONDUCTANCE	50.048	51.558	46.852	50.038
HEAT TRANSFER AREA, SQ FT	110.931	110.931	110.931	110.931
MOD. NUMBER TRANSFER UNITS		34.771		9.226
CMIN/CMAX		.969		.954
MATRIX CAPACITY RATE		2250.000		4500.000
IDEAL EFFECTIVENESS		.984		.920

Regenerator Analysis at Idle and at Design Speed

ROTOR SYSTEM	FOIL BRG	AIR SEAL	OIL BRG/ DAMPER	BALL BRG 104	BALL BRG 202	SEAL (COLD END)	TOTAL POWER LOSS, HP
3 Brg	0.15	0.06 x 2	-	1.38 x 2	-	0.6	3.63
3 Brg With Damper	0.15	0.06 x 2	1.21	1.38 x 2	-	0.6	4.84
4 Brg	0.15	0.06 x 2	-	1.38	0.768 x 2	0.6	3.79

Rotor System Loss Estimates

Table 10

	CARBORUNDUM SINTERED ALPHA SiC	CARBORUNDUM FINE-GRAIN SUPER KT Si-SiC	CORNING CODE 9458 LAS
Density, G/CC	3.14 - 3.18	2.74 - 2.78	2.20 - 2.30
Young's Modulus, PSI x 10 ⁶	58.9	38	10
Flexural Strength (4-Point Bending) in air, KSI			
RT	66.6	60.8	12.6
600C			9.0
1000C	64.1		9.8
1100C		103.2	
1200C	65.3		
1400C	62.7	77.9	
Weibull Modulus	6.7 (RT)	4.6 (1100C)	11.5 (RT)
Thermal Expansion Coefficient, X 10 ⁻⁶ /C	4.02 (RT - 700C) 5.32 (700C - 2000C)		-0.25 (RT-400C) 0.27 (RT-900C) 0.40 (RT-1000C)

Materials Properties for Ceramic Components

SAMPLE No.	SPRAY MIXTURE			SUBSTRATE TEMP.	REMARKS
	1st COAT	2nd COAT	3rd COAT		
1-L	100% LAS			R.T.	- Surface friable - Few Bonded Areas
2-L	50% LAS/50% ZrO ₂ (20% Y ₂ O ₃)			500F	- Very Good Bond - Thermally Cycled 10 times to 1800F- OK
3-L	50% LAS/50% ZrO ₂ (20% Y ₂ O ₃)	ZrO ₂	80% ZrO ₂ /20% CaF ₂	500F	- 1 Cycle to 1800F (1 Hour) - Severe Buckling & Spalling of Coating
4-L	50% LAS/50% ZrO ₂ (20% Y ₂ O ₃)	80% ZrO ₂ /20% CaF ₂		500F	- As Above
5-L	80% LAS/20% CaF ₂			500F	- Very Good Bond - Thermally Cycled to 1800F - 1 Cycle - CaF ₂ reacted with LAS

Coating Samples on LAS Substrates

ORIGINAL PAGE IS
OF POOR QUALITY.

A	B	ATM	TEMP F	PRESS PSI	TIME MRS	REMARKS
RBSC	RBSC	AIR	2300	60	1	SEIZED
RBSC	RBSC	AIR	2300	60	1	SEIZED
AS1C11	AS1C11	AIR	2300	60	1	SEIZED
ZRO2E11	ZRO2E11	AIR	2300	1000	1	FREE
ZRO2E11	ZRO2E11	AIR	2300	1000	1	FREE
ZRO2E11	ZRO2E11	AIR	2300	1000	1	FREE
ZRO2E11	ZRO2E11	AIR	2300	1000	1	FREE
LAS	LAS	AIR	2300	100	4	SLIGHT REACTION, LAS DEFORMATION NO REACTION NECK. 30ND
AL2O3E11	AL2O3E11	AIR	2300	100	4	FREE
AL2O3E11	AL2O3E11	AIR	2300	25	4	SEIZED
RA339, FE	RA339, FE	AIR	1800	100	4	OX. ADHERING TO AS1C
430SS, FE	430SS, FE	AIR	1800	100	4	NO REACT. SL. DISCOL. AS1C
OHMALLOY, FE	OHMALLOY, FE	AIR	1800	100	4	SL. REACT. SPALLING AS1C
RENE41, NI	RENE41, NI	AIR	1800	100	4	ADHERING OXIDE
NI 1, FE	NI 1, FE	AIR	1800	100	4	VERY SL. REACT. NO SPALLING
MA5TX, NI	MA5TX, NI	AIR	1800	100	4	SL. REACTION
MS25, CO	MS25, CO	AIR	1800	100	4	VERY SL. REACTION. NO SPALLING
RA333, NI	RA333, NI	AIR	1800	100	4	REACTION & LOCAL SPALLING
INC0702, NI	INC0702, NI	AIR	1800	100	4	SEIZED. REACTION. MELTING
NI	NI	AIR	2300	800	.5	SEIZED. REACTION. MELTING
NI	NI	AIR	1700	110	.5	TOP SEIZED. LOCAL SPALLING. LOWER FREE
OHMALLOY, FOIL	OHMALLOY, FOIL	AIR	1800	100	4	FREE. ADHERING OXIDE
702, FOIL	702, FOIL	AIR	1800	100	4	FREE
MA-X, FOIL	MA-X, FOIL	AIR	1800	100	4	FREE. ADHERING OXIDE
MA-333, FOIL	MA-333, FOIL	AIR	1800	100	4	FREE. SL. SURF. RXN
NI-1, FOIL	NI-1, FOIL	AIR	1800	100	4	PARTS FREE SURF OF LAS PITTED
AS1C	AS1C	AIR	2300	25	4	PARTS FREE SURF OF LAS PITTED
RBSC	RBSC	AIR	2300	25	4	PARTS FREE NO SURFACE RXN
ZRO2	ZRO2	AIR	1800	25	4	PARTS FREE NO SURFACE RXN
AL2O3	AL2O3	AIR	1800	25	4	PARTS FREE NO SURFACE RXN
AS1C-T102	AS1C-T102	AIR	2300	25	4	COLORED GLASSY LAYER BONDING PARTS
AS1C-T102	AS1C-T102	AIR	2300	25	4	SEE LM489 + AS1C ADHERING TO LAS
MODULAR FE	MODULAR FE	AIR	1800	25	4	FREE. FE OXIDE ON LAS
AS1C	AS1C	AIR	2300	25	4	FREE. SURF OF LAS PITTED
AL ALLOY 365	AL ALLOY 365	AIR	700	25	60	PARTS FREE. NO RXN
LAS/AS1C	LAS/AS1C	AIR	2000	25	4	ALL PARTS FREE. NO RXN
ZRO2E11	ZRO2E11	AIR	2300	25	4	FREE. CUR. 3 RUNS. DISCOLORED UNDER ZRO2
ZRO2E11	ZRO2E11	AIR	2300	25	678	FREE. DISCOLORED UNDER ZRO2

1 TEST RUN IN BENCH TYPE FURNACE
21 ALUMINA SILICON CARBIDE
212 STABILIZED ZIRCONIA
2122 ALUMINA SLURRY COATING

Interfacing Tests

Table 13

EXP#	SUBS	BRAZE/ADD	SUPERS	ATH	TEMP F	REMARKS
1	ASIC	SI		AR	2875	COMMERCIAL SI, WETTING, POOR SPREADING, TEMP APPROX
2	ASIC	SI		AR	2885	COMMERCIAL SI, WETTING, POOR SPREADING, CAN'T USE PT IN H2 ATH.
3	ASIC	SI		H2	>2145	COM. SI, WETTING, POOR SPREADING, CAN'T USE PT IN H2 ATH.
4	ASIC	SI		H2	>2550	REPEAT EXP. 3 TO ELIMINATE H2 SHUTOFF WHICH OCCURRED IN EXP. 3
5	ASIC	SI		AR	2885	WETTING AND RXN U/SIC, BREAKAWAY IN SIC
6	ASIC	SI		AR	2890	NO WETTING, AL MELTED SELECTIVELY
7	ASIC	SI		AR	>2750	WETTING OF SIC, POOR SPREADING
8	ASIC	SI		AR	2890	COMMERCIAL SI, NO MELTING OF SI, SOME OXIDATION
9	ASIC	SI		AR	2890	COMMERCIAL SI, NO MELTING OF SI, SOME OXIDATION
10	ASIC	SI		AR	2890	COMMERCIAL SI, UNIFORM WETTING OF SIC, RXN WITH NO - NOSI2
11	ASIC	SI		AR	>1900	COMMERCIAL SI, UNIFORM WETTING OF SIC, RXN WITH NB - NBSI2?
12	ASIC	SI		AR	>1900	NO WETTING APPARENT
13	ASIC	SI	98CU3811RN	AR	>1900	NO MELTING
14	ASIC	SI	98CU3811RN	H2	>1900	NO WETTING
15	ASIC	SI	98CU3811RN	H2	>2000	NO WETTING
16	ASIC	SI	CU	H2	>2000	ABSOLUTELY NO WETTING
17	ASIC	SI	COLMG (NI-CR-FE-SI)	H2	>2000	LOOSE SCALE ON TOP
18	ASIC	SI	COLMG	H2	>2000	SMALL FLAKE BREAKAWAY IN SIC
19	ASIC	SI	56COLMG/5090	H2	>2000	WETTING AND BONDING TO SIC, REACTED U/SIC, LARGE PCE BREAKAWAY IN SIC
20	ASIC	SI	56COLMG/5090	H2	>2000	COLR ALLOWED U/SI, ONLY SLIGHT BOND
21	ASIC	SI	56COLMG/5051C	H2	>2000	WETTING OF SIC, BREAKAWAY IN SIC WHEN PIECE WAS DROPPED
22	ASIC	SI	56COLMG/5051C	H2	2025	COARSE SIC GRIT, WETG & BONDG TO ASIC, VERY LOOSE BOND TO NO
23	ASIC	SI	76CU30NI MIXTURE	H2	2034	ALL LAYERS BONDED, EXPANSION CRACKS IN SIC BELOW RXN ZONE
24	ASIC	SI	COLMG (NI-CR-FE-SI)	H2	2400	SLIGHT FLOW, HIGH WETTING ANGLE, CRACKS IN SIC
25	ASIC	SI	56COLMG/5051C	H2	2015	ALLOW LOCALIZED UNDER NO, WET BUT NO BOND TO NO, RXN U/SIC
26	ASIC	SI	56COLMG/5051C	H2	2033	600 FRESH SIC, TOO FINE FOR GOOD MIX, BOND: SIC-POOR, NO-LIGHT
27	ASIC	SI	56COLMG/5051C	H2	2042	ALSO PURE COLMG/NO CHIP, RESULTS DUPLICATE EXPS. 18 AND 23
28	ASIC	SI	56COLMG/5051C	H2	2042	100 FRESH SIC, WET ASIC, LOOSE BOND TO NO
29	ASIC	SI	56COLMG/5051C	H2	2042	100 FRESH SIC, WET ASIC, LOOSE BOND TO NO
30	ASIC	SI	COLMG (NI-CR-FE-SI)	H2	1502	ABSOLUTELY NO WETTING OF SIC, EXCELLENT WETTING OF NO
31	ASIC	SI	ULX50(CU+)	H2	2107	WETTING AND FLOW ON BOTH SIC AND NO, BREAKAWAY IN SIC
32	ASIC	SI	50ULX50/5090	H2	2110	WETTING AND FLOW, NO BONDED, BETTER BOND UNDER THINNER NO
33	ASIC	SI	ULX50(CO+)	H2	2110	WETTING AND FLOW, NO BONDED, BETTER BOND UNDER THINNER NO
34	ASIC	SI	50ULX50/4090	H2	>2000	WETTING AND FLOW, NO BONDED, BETTER BOND UNDER THINNER NO
35	ASIC	SI	50ULX50/2551C	H2	>2000	WETTING AND FLOW, NO BONDED, BETTER BOND UNDER THINNER NO
36	ASIC	SI	50ULX50/4090	H2	>2000	WETTING AND FLOW, NO BONDED, BETTER BOND UNDER THINNER NO
37	ASIC	SI	76CU30NI MIXTURE	H2	2400	P&S BINDER, BOND TO ASIC, NO BOND TO NO
38	ASIC	SI	76CU30NI FILINGS	H2	1800	100 FRESH SIC, BOND TO ASIC, NO BOND TO NO
39	ASIC	SI	LITHOBRAZERS (AG-CU-LI)	H2	1800	ASIC BURIED IN MIX TO STUDY REACTION OF EXP. 24, SLUG MELTED
40	ASIC	SI	50AG10RN WIRE	H2	1800	FILINGS, BEADED & ROLLED OFF, RXN & CRACKS AT CONTACTING ASIC
41	ASIC	SI	76CU30NI	H2	1801	NO WETG, SMALL BEADS ON ASIC, MOSTLY BEADED UP & FELL OFF
42	ASIC	SI	76CU30NI	H2	1801	P&S, MELTING NOT APPARENT (OXIDE DUE TO LATE SWITCH TO H2?)
43	ASIC	SI	76CU30NI MIXTURE	H2	1801	P&S, MELTING NOT APPARENT (OXIDE DUE TO LATE SWITCH TO H2?)
44	ASIC	SI	56COLMG/5051C	H2	22400	RXN U/SIC, U. HIGH WETG ANGLE, MOSTLY BEADED AND FELL OFF
45	ASIC	SI	76COLMG/5051C	H2	2805	POOR MIX, WETTING AND GOOD BOND TO ASIC, NO BOND TO NO
46	ASIC	SI	76COLMG/5051C	H2	2805	POOR MIX, WETTING AND GOOD BOND TO ASIC, NO BOND TO NO
47	ASIC	SI	98CU10TI	H2	28700	TEMP TOO HIGH, DARK SCALE OVER WELL MET AND BONDED AREA
48	ASIC	SI	98CU10TI	H2	28700	TEMP TOO HIGH, DARK SCALE OVER WELL MET AND BONDED AREA
49	ASIC	SI	98CU57R	AR	2895	NO BONDS, METAL LEFT ON ASIC, POSS. HYDRIDE FORMATION
50	ASIC	SI	98CU57R	AR	2895	NO BONDS, METAL LEFT ON ASIC, SELECT. MELTING LEFT TINY BEADS
51	ASIC	SI	98CU57R	AR	2895	BLACK/GOLD REMNANTS OVER GOLD METALLIZED AREA ON ASIC
52	ASIC	SI	98CU57R	AR	2895	MELTED AND FLOWED, WETTING ASIC, CRACKING NOT APPARENT
53	ASIC	SI	98CU57R	H2	2895	99.999% PURE, MELTED, WETTED, AND FLOWED

Ceramic Brazing

Table 14A

54	AS1C			H2	2158	MELTED, BEADED (POOR WETTING), BDN W/ASIC
55	AS1C			AR	2058	99.999% PURE, MELTED, FLOWED, AND WETTED
56	AS1C			H2	1003	LSE POUND. LAYER FLAKES OFF TO REUL WELL MET METAL LAYER
57	AS1C			AS (08)	2058	ELECTROLYTIC CO. SEVERE RBN W/ASIC
58	AS1C			AR	2057	WETTING, FLOW MODERATE
59	AS1C			AR	2057	WETTING, FLOW MODERATE
60	AS1C			AR	2054	WETTING AND FLOW EXCELLENT, EXCESSIVE AMT. OF METAL
61	AS1C			AR	2054	WETTING AND FLOW EXCELLENT, EXCESSIVE AMT. OF METAL
62	AS1C			H2	2100	MELTED, FLOWED, REACTED W/ASIC, EXCESSIVE AMT. OF METAL.
63	AS1C			H2	2230	MELTED, FLOWED, REACTED W/ASIC, EXCESSIVE AMT. OF METAL.
64	AS1C			H2	2100	REACTED W/ASIC, BREAKAWAY IN ASIC. EXCESSIVE AMT. OF METAL.
65	AS1C			H2	2102	LESS METAL THAN EXP. 62, MELTING NOT APPARENT, OXIDE APPARENT
66	AS1C			H2	2100	LESS METAL THAN EXP. 63, MELTING NOT APPARENT, OXIDE APPARENT
67	AS1C			H2	2100	MELTING NOT APPARENT, OXIDE APPARENT
68	AS1C			H2	2100	MELTING NOT APPARENT, OXIDE APPARENT
69	AS1C			AR	2055	REPEAT EXP. 69, LESS METAL, WETO & BONDG UNDER WHITE SCALE.
70	AS1C			AR	2055	REPEAT EXP. 61, LESS METAL, WETO & BONDG UNDER WHITE SCALE.
71	AS1C			AR	2055	99.999% COMPARISON W/91-2R ALLOYS, OXIDATION EVIDENT.
72	AS1C			AR	2057	INJECTION MOLDED V9. COLD PRESSED ASIC. INCONCLUSIVE.
73	AS1C			H2	2058	REPEAT EXP. 72 ON A BED OF ASIC POWDER. INCONCLUSIVE.
74	AS1C			H2	2057	REPEAT EXP. 72 ON A BED OF ASIC POWDER. INCONCLUSIVE.
75	AS1C (IM)			AR	2055	99.999% PURE SI, MET, FLOWED, BONDED, CHECK OUT NEU TUBE OK.
76	AS1C (CP)			AR	2055	99.999% PURE SI, MET, FLOWED, BONDED, CHECK OUT NEU TUBE OK.
77	AS1C			H2	2103	OXIDE SCALE EVIDENT, BONDING.
78	AS1C			H2	2100	OXIDE SCALE EVIDENT, BONDING.
79	AS1C			AR	2158	WETTING AND FLOW UNDER OXIDE SCALE
80	AS1C			AR	2158	WETTING AND FLOW UNDER OXIDE SCALE
81	AS1C			H2	2470	WETTING, POOR FLOW, SEPARATE, SICCRACKED.
82	AS1C			H2	2410	WETTING, POOR FLOW, SOME ATTACHED.
83	AS1C			H2	2410	WETTING, POOR FLOW, LOW WETTING ANGLE.
84	AS1C			H2	2058	NO WETTING APPARENT, NO RESIDUE, TRANSU. CRACK BAR.
85	AS1C			H2	2058	NO WETTING APPARENT, RESID. SKULL.
86	AS1C			H2	2058	POOR WETTING, NO BONDING.
87	AS1C			H2	2054	POOR WETTING, ONE LEG BONDED, POOR ATMOSP. (ALS086).
88	AS1C			H2	2100	GREEN STOPOFF, GOOD WETTING, FLOW RESTRICTED
89	AS1C			H2	2100	GREEN STOPOFF, GOOD WETTING, FLOW RESTRICTED
90	AS1C			H2	2100	GREEN STOPOFF, FLOW RESTRICTED, RA330 ATTACHED
91	AS1C			AR	2100	GREEN STOPOFF, FLOW RESTRICTED, RA330 ATTACHED
92	AS1C			AR	2100	GREEN STOPOFF, FLOW RESTRICTED, NB NOT BONDED
93	AS1C			AR	2100	GREEN STOPOFF, FLOW RESTRICTED, NB NOT BONDED
94	AS1C			AR	2100	GREEN STOPOFF, FLOW RESTRICTED, NB NOT BONDED
95	AS1C			AR	2100	GREEN STOPOFF, FLOW RESTRICTED, NB NOT BONDED
96	AS1C			AR	2100	GREEN STOPOFF, FLOW RESTRICTED, NB NOT BONDED
97	AS1C			H2	1000	GREEN STOPOFF, GOOD WETTING, FLOW RESTRICTED, CRACKED OFF
				H2	1000	GREEN STOPOFF, GOOD WETTING, FLOW RESTRICTED, CRACKED OFF
				H2	1700	GREEN STOPOFF, GOOD WETTING, FLOW RESTRICTED, GOOD BONDING
				H2	1700	GREEN STOPOFF, NO WETTING, NO FLOW, APPARENT OXIDATION

Ceramic Brazing

	<u>Idle Speed (RPM)</u>	<u>Maximum Speed (RPM)</u>
INPUT PINION (ENGINE ROTOR)	44,000	99,500
INTERMEDIATE GEAR	8,733	19,748
IDLER GEAR	3,821	8,640
OUTPUT GEAR (TRANSMISSION INPUT)	2,203	4,981
ACCESSORY DRIVE GEAR	1,075	2,430
AC COMPRESSOR	884	2,000
ALTERNATOR	2,211	5,000
POWER STEERING PUMP	1,106	2,500
REGENERATOR WORM	586	1,325
REGENERATOR CROSS SHAFT	73	166
REGENERATOR	8.84	20

Rotational Speeds

Table 15

DIFFERENCES

	<u>DUAL RANGE</u>	<u>SINGLE RANGE</u>
Reverse	Regenerated Ratio	Gearset Ratio
Final Drive Ratio	5:1	7:1
Components - Gearsets	2	2
- Clutches	2	2
- Belt	1	1
- Chain	1	1
Belt Torque Requirement (expressed as input torque at max. ratio)	125'#	130'#

TRADEOFFS

Shift Quality	Difficult	No problem
Cost	Baseline	Comparable
Package Size	Good	Acceptable
Fuel Economy	Baseline	Regeneration - 2%
		Final Drive - 1%
		Parasitic - 3%
	32.4 mpg	30.5 mph

Transmission Arrangement Comparison

	<u>RPD Engine</u>	<u>Exp. Eng.</u>	<u>SI Base</u>
Turbine Material	Ceramic	Metal	
Maximum TIT	2300F	2100F	
Idle RPM	41,675	41,675	750
Fuel Economy, MPG City/Hwy./Combined	26.1/47.1/32.6	25.6/46.3/32.0	23.2/36.7/27.8
1 sec. distance	3	2	2
2 sec. distance	18	18	16
4 sec. distance	89	84	72
5 sec. distance	138	129	110
0-60 MPH Time	12	15	15
Engine Maximum HP to Transmission	78	66	84

Performance Summary -- Ceramic vs. Metal Turbine

Method of Power Reduction at Idle	RPD WITH VIGV	Reduced Speed	RPD WITH VIGV	Reduced TET	RPD WITHOUT VIGV	Reduced Speed	SCALED 10% RPD w/o VIGV
Idle HP	1.0	1.0	1.1	1.1	1.1	1.1	1.1
Idle TET, Deg. F	1800	1800	1222	1222	1800	1800	1800
Idle Speed, RPM	42,410	42,410	50,000	50,000	41,675	41,675	40,167
Idle Fuel Flow, LBM/HR	1.70	1.70	2.07	2.07	1.70	1.80	1.80
Fuel Economy, MPG City/Highway / Combined	26.0/46.7/32.5	26.0/46.7/32.5	24.9/46.4/31.5	24.9/46.4/31.5	26.1/47.1/32.6	25.4/45.7/31.7	25.4/45.7/31.7
2-Sec. Distance, Ft.	19	19	21	21	18	18	18
4-Sec. Distance, Ft.	91	91	95	95	89	91	91
5-Sec. Distance, Ft.	141	141	146	146	138	142	142
0-60 MPH Time, Sec.	11.6	11.6	11.5	11.5	12.5	11.4	11.4
Engine Maximum HP	84	84	84	84	78	84	84

Gasoline Heating Value: 18500 BTU/LBM

Fuel Density: 6.2 LBM/Gal

Warm-Up Requirement: 15000 BTU

Effect of VIGVs on Fuel Economy and Performance

ORIGINAL PAGE IS
OF POOR QUALITY

CVT EFFICIENCY TABLE INPUT

NO/NI	25. FT-LBF	100. FT-LBF
0.00000	.59600	.59600
.06000	.59600	.59600
.08000	.65200	.65200
.10000	.69200	.69200
.15000	.76800	.76800
.20000	.81800	.81800
.25000	.85400	.85400
.30000	.88400	.88400
.35000	.90000	.90000
.40000	.91200	.91200
.45000	.92200	.92200
.50000	.93200	.93200
1.00000	.93200	.93200
2.00000	.93200	.93200
3.00000	.93200	.93200

THESE EFFICIENCIES INCLUDE THE FINAL DRIVE

CVT Efficiency vs. N_o/N_i

SINGLE SHAFT GAS TURBINE WITH CVT IN A K-HOBY 04/10/81

TIME SEC	RPM	HPH	DIST FEET	ACCEL FPS-SQ	RPM			HP			VEH KL	FLYWH MP	
					ENGINE	TRANS	IN	ENGINE	TRANS	IN			
0.0	0.0	0.0	0.0	0.0	0.0	0.0	0.0	0.0	0.0	0.0	0.0	0.0	0.0
START OF MODE 1, TIME=													
1.0	0.0	0.0	0.0	0.0	4600.	2200.	0.0	0.0	0.0	0.0	0.0	0.0	0.0
1.1	6.3	2.9	14.9	0.0	4375.	2188.	0.0	0.0	0.0	0.0	0.0	0.0	0.0
1.2	0.0	0.0	0.0	0.0	4151.	2208.	0.0	0.0	0.0	0.0	0.0	0.0	0.0
1.3	0.0	0.0	0.0	0.0	4173.	2459.	0.0	0.0	0.0	0.0	0.0	0.0	0.0
1.4	0.0	0.0	0.0	0.0	5612.	2806.	0.0	0.0	0.0	0.0	0.0	0.0	0.0
START OF MODE 2, TIME=													
1.5	3.3	0.12	15.0	0.0	6348.	3174.	0.0	0.0	0.0	0.0	0.0	0.0	0.0
1.6	2.4	0.15	15.0	0.0	7003.	3502.	0.0	0.0	0.0	0.0	0.0	0.0	0.0
1.7	2.4	0.15	15.0	0.0	7099.	3847.	0.0	0.0	0.0	0.0	0.0	0.0	0.0
START OF MODE 3, TIME=													
1.8	3.4	0.15	15.2	0.0	7912.	3956.	0.0	0.0	0.0	0.0	0.0	0.0	0.0
1.9	4.2	1.4	15.4	0.0	8206.	4103.	0.0	0.0	0.0	0.0	0.0	0.0	0.0
2.0	5.3	2.1	15.0	0.0	8427.	4214.	0.0	0.0	0.0	0.0	0.0	0.0	0.0
2.1	6.3	2.9	14.9	0.0	8644.	4322.	0.0	0.0	0.0	0.0	0.0	0.0	0.0
2.2	7.3	3.9	14.7	0.0	8856.	4428.	0.0	0.0	0.0	0.0	0.0	0.0	0.0
2.3	8.3	5.0	14.8	0.0	9064.	4532.	0.0	0.0	0.0	0.0	0.0	0.0	0.0
2.4	9.3	6.3	14.8	0.0	9269.	4635.	0.0	0.0	0.0	0.0	0.0	0.0	0.0
2.5	10.3	7.8	14.8	0.0	9472.	4736.	0.0	0.0	0.0	0.0	0.0	0.0	0.0
2.6	11.3	9.4	15.0	0.0	9671.	4834.	0.0	0.0	0.0	0.0	0.0	0.0	0.0
2.7	12.3	11.1	15.0	0.0	9869.	4935.	0.0	0.0	0.0	0.0	0.0	0.0	0.0
START OF MODE 4, TIME= 1.767 SECONDS													
2.8	13.4	13.0	17.7	0.0	10005.	5000.	0.0	0.0	0.0	0.0	0.0	0.0	0.0
2.9	14.4	15.0	16.7	0.0	10005.	5000.	0.0	0.0	0.0	0.0	0.0	0.0	0.0
3.0	15.4	17.2	15.7	0.0	10005.	5000.	0.0	0.0	0.0	0.0	0.0	0.0	0.0
3.1	16.4	19.5	14.9	0.0	10005.	5000.	0.0	0.0	0.0	0.0	0.0	0.0	0.0
3.2	17.4	22.0	14.2	0.0	10005.	5000.	0.0	0.0	0.0	0.0	0.0	0.0	0.0
3.3	18.4	24.6	13.4	0.0	10005.	5000.	0.0	0.0	0.0	0.0	0.0	0.0	0.0
3.4	19.3	27.4	13.0	0.0	10005.	5000.	0.0	0.0	0.0	0.0	0.0	0.0	0.0
3.5	20.1	30.3	12.5	0.0	10005.	5000.	0.0	0.0	0.0	0.0	0.0	0.0	0.0
3.6	21.0	33.3	12.1	0.0	10005.	5000.	0.0	0.0	0.0	0.0	0.0	0.0	0.0
3.7	21.8	36.4	11.7	0.0	10005.	5000.	0.0	0.0	0.0	0.0	0.0	0.0	0.0
3.8	22.6	39.7	11.3	0.0	10005.	5000.	0.0	0.0	0.0	0.0	0.0	0.0	0.0
3.9	23.3	43.0	10.9	0.0	10005.	5000.	0.0	0.0	0.0	0.0	0.0	0.0	0.0
4.0	24.1	46.5	10.6	0.0	10005.	5000.	0.0	0.0	0.0	0.0	0.0	0.0	0.0
4.1	24.8	50.1	10.3	0.0	10005.	5000.	0.0	0.0	0.0	0.0	0.0	0.0	0.0
4.2	25.5	53.8	10.0	0.0	10005.	5000.	0.0	0.0	0.0	0.0	0.0	0.0	0.0
4.3	26.1	57.6	9.8	0.0	10005.	5000.	0.0	0.0	0.0	0.0	0.0	0.0	0.0
4.4	26.8	61.5	9.5	0.0	10005.	5000.	0.0	0.0	0.0	0.0	0.0	0.0	0.0
4.5	27.4	65.4	9.3	0.0	10005.	5000.	0.0	0.0	0.0	0.0	0.0	0.0	0.0
4.6	28.1	69.5	9.1	0.0	10005.	5000.	0.0	0.0	0.0	0.0	0.0	0.0	0.0
4.7	28.7	73.7	8.9	0.0	10005.	5000.	0.0	0.0	0.0	0.0	0.0	0.0	0.0
4.8	29.3	77.9	8.7	0.0	10005.	5000.	0.0	0.0	0.0	0.0	0.0	0.0	0.0
4.9	29.9	82.2	8.5	0.0	10005.	5000.	0.0	0.0	0.0	0.0	0.0	0.0	0.0
5.0	30.4	86.7	8.4	0.0	10005.	5000.	0.0	0.0	0.0	0.0	0.0	0.0	0.0
5.1	31.0	91.2	8.2	0.0	10005.	5000.	0.0	0.0	0.0	0.0	0.0	0.0	0.0
5.2	31.6	95.8	8.1	0.0	10005.	5000.	0.0	0.0	0.0	0.0	0.0	0.0	0.0
5.3	32.1	100.4	7.9	0.0	10005.	5000.	0.0	0.0	0.0	0.0	0.0	0.0	0.0
5.4	32.6	105.2	7.8	0.0	10005.	5000.	0.0	0.0	0.0	0.0	0.0	0.0	0.0
5.5	33.2	110.0	7.7	0.0	10005.	5000.	0.0	0.0	0.0	0.0	0.0	0.0	0.0
5.6	33.7	114.9	7.5	0.0	10005.	5000.	0.0	0.0	0.0	0.0	0.0	0.0	0.0
5.7	34.2	119.9	7.4	0.0	10005.	5000.	0.0	0.0	0.0	0.0	0.0	0.0	0.0
5.8	34.7	124.9	7.3	0.0	10005.	5000.	0.0	0.0	0.0	0.0	0.0	0.0	0.0
5.9	35.2	130.1	7.2	0.0	10005.	5000.	0.0	0.0	0.0	0.0	0.0	0.0	0.0
6.0	35.7	135.3	7.1	0.0	10005.	5000.	0.0	0.0	0.0	0.0	0.0	0.0	0.0
6.1	36.2	140.5	7.0	0.0	10005.	5000.	0.0	0.0	0.0	0.0	0.0	0.0	0.0
6.2	36.6	145.9	6.8	0.0	10005.	5000.	0.0	0.0	0.0	0.0	0.0	0.0	0.0
6.3	37.1	151.3	6.7	0.0	10005.	5000.	0.0	0.0	0.0	0.0	0.0	0.0	0.0
6.4	37.5	156.8	6.5	0.0	10005.	5000.	0.0	0.0	0.0	0.0	0.0	0.0	0.0
6.5	38.0	162.3	6.5	0.0	10005.	5000.	0.0	0.0	0.0	0.0	0.0	0.0	0.0

Wide-Open-Throttle Launch

Table 20A

5.6	38.4	167.9	6.5	100005	5000	2775	575	1.40	.932	36.5	7840	73.6	0.0	73.6	68.6	60.0	2956	15357	0.0
5.7	38.9	173.6	6.4	100005	5000	2807	581	1.70	.932	36.5	7840	73.6	0.0	73.6	68.6	60.6	2956	15357	0.0
5.8	39.3	179.3	6.3	100005	5000	2838	588	1.76	.932	36.5	7840	73.6	0.0	73.6	68.6	60.6	2956	15357	0.0
5.9	39.7	185.1	6.2	100005	5000	2869	594	1.74	.932	36.5	7840	73.6	0.0	73.6	68.6	60.3	2956	15357	0.0
6.0	40.2	191.0	6.1	100005	5000	2899	600	1.72	.932	36.5	7840	73.6	0.0	73.6	68.6	60.1	2956	15357	0.0
6.2	41.0	202.9	6.0	100005	5000	2958	613	1.66	.932	36.5	7840	73.6	0.0	73.6	68.6	59.7	2956	15357	0.0
6.4	41.8	215.0	5.8	100005	5000	3016	625	1.66	.932	36.5	7840	73.6	0.0	73.6	68.6	59.4	2956	15357	0.0
6.6	42.9	227.4	5.7	100005	5000	3073	636	1.63	.932	36.5	7840	73.6	0.0	73.6	68.6	59.1	2956	15357	0.0
6.8	43.3	240.0	5.5	100005	5000	3128	648	1.60	.932	36.5	7840	73.6	0.0	73.6	68.6	58.7	2956	15357	0.0
7.0	44.1	252.8	5.4	100005	5000	3182	659	1.57	.932	36.5	7840	73.6	0.0	73.6	68.6	58.4	2956	15357	0.0
7.2	44.8	265.8	5.3	100005	5000	3234	670	1.55	.932	36.5	7840	73.6	0.0	73.6	68.6	58.0	2956	15357	0.0
7.4	45.5	279.1	5.2	100005	5000	3286	680	1.52	.932	36.5	7840	73.6	0.0	73.6	68.6	57.7	2956	15357	0.0
7.6	46.2	292.5	5.1	100005	5000	3336	691	1.50	.932	36.5	7840	73.6	0.0	73.6	68.6	57.3	2956	15357	0.0
7.8	46.9	306.2	5.0	100005	5000	3386	701	1.48	.932	36.5	7840	73.6	0.0	73.6	68.6	57.0	2956	15357	0.0
8.0	47.6	320.0	4.9	100005	5000	3434	711	1.46	.932	36.5	7840	73.6	0.0	73.6	68.6	56.7	2956	15357	0.0
8.2	48.2	334.1	4.8	100005	5000	3482	721	1.44	.932	36.5	7840	73.6	0.0	73.6	68.6	56.3	2956	15357	0.0
8.4	48.9	348.3	4.7	100005	5000	3528	730	1.42	.932	36.5	7840	73.6	0.0	73.6	68.6	56.0	2956	15357	0.0
8.6	49.5	362.7	4.6	100005	5000	3574	740	1.40	.932	36.5	7840	73.6	0.0	73.6	68.6	55.6	2956	15357	0.0
8.8	50.1	377.3	4.5	100005	5000	3618	749	1.38	.932	36.5	7840	73.6	0.0	73.6	68.6	55.3	2956	15357	0.0
9.0	50.7	392.1	4.4	100005	5000	3662	758	1.37	.932	36.5	7840	73.6	0.0	73.6	68.6	54.9	2956	15357	0.0
9.2	51.3	407.1	4.3	100005	5000	3705	767	1.35	.932	36.5	7840	73.6	0.0	73.6	68.6	54.5	2956	15357	0.0
9.4	51.9	422.2	4.3	100005	5000	3748	776	1.33	.932	36.5	7840	73.6	0.0	73.6	68.6	54.2	2956	15357	0.0
9.6	52.5	437.5	4.2	100005	5000	3789	785	1.32	.932	36.5	7840	73.6	0.0	73.6	68.6	53.8	2956	15357	0.0
9.8	53.0	453.0	4.1	100005	5000	3830	793	1.31	.932	36.5	7840	73.6	0.0	73.6	68.6	53.5	2956	15357	0.0
10.0	53.6	468.7	4.0	100005	5000	3870	801	1.29	.932	36.5	7840	73.6	0.0	73.6	68.6	53.1	2956	15357	0.0
10.2	54.1	484.5	4.0	100005	5000	3910	809	1.28	.932	36.5	7840	73.6	0.0	73.6	68.6	52.8	2956	15357	0.0
10.4	54.7	500.4	3.9	100005	5000	3949	818	1.27	.932	36.5	7840	73.6	0.0	73.6	68.6	52.4	2956	15357	0.0
10.6	55.2	516.6	3.8	100005	5000	3987	825	1.25	.932	36.5	7840	73.6	0.0	73.6	68.6	52.1	2956	15357	0.0
10.8	55.7	532.8	3.8	100005	5000	4025	833	1.24	.932	36.5	7840	73.6	0.0	73.6	68.6	51.7	2956	15357	0.0
11.0	56.2	549.3	3.7	100005	5000	4062	841	1.23	.932	36.5	7840	73.6	0.0	73.6	68.6	51.4	2956	15357	0.0
11.2	56.8	565.8	3.7	100005	5000	4098	848	1.22	.932	36.5	7840	73.6	0.0	73.6	68.6	51.0	2956	15357	0.0
11.4	57.3	582.5	3.6	100005	5000	4134	856	1.21	.932	36.5	7840	73.6	0.0	73.6	68.6	50.7	2956	15357	0.0
11.6	57.7	599.4	3.6	100005	5000	4169	863	1.20	.932	36.5	7840	73.6	0.0	73.6	68.6	50.3	2956	15357	0.0
11.8	58.2	616.4	3.5	100005	5000	4204	870	1.19	.932	36.5	7840	73.6	0.0	73.6	68.6	49.9	2956	15357	0.0
12.0	58.7	633.6	3.4	100005	5000	4238	877	1.18	.932	36.5	7840	73.6	0.0	73.6	68.6	49.6	2956	15357	0.0
12.2	59.2	650.9	3.4	100005	5000	4272	884	1.17	.932	36.5	7840	73.6	0.0	73.6	68.6	49.2	2956	15357	0.0
12.4	59.6	668.3	3.3	100005	5000	4305	891	1.16	.932	36.5	7840	73.6	0.0	73.6	68.6	48.9	2956	15357	0.0
12.6	60.1	685.8	3.3	100005	5000	4338	898	1.15	.932	36.5	7840	73.6	0.0	73.6	68.6	48.5	2956	15357	0.0
12.8	60.5	703.5	3.3	100005	5000	4370	905	1.14	.932	36.5	7840	73.6	0.0	73.6	68.6	48.2	2956	15357	0.0
13.0	61.0	721.3	3.2	100005	5000	4402	911	1.14	.932	36.5	7840	73.6	0.0	73.6	68.6	47.8	2956	15357	0.0
13.2	61.4	739.3	3.2	100005	5000	4433	918	1.13	.932	36.5	7840	73.6	0.0	73.6	68.6	47.5	2956	15357	0.0
13.4	61.8	757.4	3.1	100005	5000	4464	924	1.12	.932	36.5	7840	73.6	0.0	73.6	68.6	47.1	2956	15357	0.0
13.6	62.2	775.5	3.1	100005	5000	4494	930	1.11	.932	36.5	7840	73.6	0.0	73.6	68.6	46.8	2956	15357	0.0
13.8	62.7	793.9	3.0	100005	5000	4524	937	1.11	.932	36.5	7840	73.6	0.0	73.6	68.6	46.4	2956	15357	0.0
14.0	63.1	812.3	3.0	100005	5000	4554	943	1.10	.932	36.5	7840	73.6	0.0	73.6	68.6	46.1	2956	15357	0.0
14.2	63.5	830.9	2.9	100005	5000	4583	949	1.09	.932	36.5	7840	73.6	0.0	73.6	68.6	45.8	2956	15357	0.0
14.4	63.9	849.5	2.9	100005	5000	4612	955	1.08	.932	36.5	7840	73.6	0.0	73.6	68.6	45.4	2956	15357	0.0
14.6	64.3	868.3	2.9	100005	5000	4640	961	1.08	.932	36.5	7840	73.6	0.0	73.6	68.6	45.1	2956	15357	0.0
14.8	64.7	887.2	2.8	100005	5000	4668	966	1.07	.932	36.5	7840	73.6	0.0	73.6	68.6	44.7	2956	15357	0.0
15.0	65.0	906.3	2.8	100005	5000	4696	972	1.06	.932	36.5	7840	73.6	0.0	73.6	68.6	44.4	2956	15357	0.0
15.2	65.4	925.5	2.7	100005	5000	4723	978	1.06	.932	36.5	7840	73.6	0.0	73.6	68.6	44.1	2956	15357	0.0
15.4	65.8	944.6	2.7	100005	5000	4750	983	1.05	.932	36.5	7840	73.6	0.0	73.6	68.6	43.7	2956	15357	0.0
15.6	66.1	964.0	2.7	100005	5000	4776	989	1.05	.932	36.5	7840	73.6	0.0	73.6	68.6	43.4	2956	15357	0.0
15.8	66.5	983.4	2.6	100005	5000	4803	994	1.04	.932	36.5	7840	73.6	0.0	73.6	68.6	43.1	2956	15357	0.0
16.0	66.9	1003.0	2.6	100005	5000	4828	1000	1.04	.932	36.5	7840	73.6	0.0	73.6	68.6	42.7	2956	15357	0.0
16.2	67.2	1022.7	2.6	100005	5000	4854	1005	1.03	.932	36.5	7840	73.6	0.0	73.6	68.6	42.3	2956	15357	0.0
16.4	67.6	1042.3	2.5	100005	5000	4879	1010	1.02	.932	36.5	7840	73.6	0.0	73.6	68.6	42.0	2956	15357	0.0
16.6	67.9	1062.3	2.5	100005	5000	4904	1015	1.02	.932	36.5	7840	73.6	0.0	73.6	68.6	41.7	2956	15357	0.0
16.8	68.3	1082.3	2.5	100005	5000	4928	1020	1.01	.932	36.5	7840	73.6	0.0	73.6	68.6	41.3	2956	15357	0.0
17.0	68.6	1102.4	2.4	100005	5000	4953	1025	1.01	.932	36.5	7840	73.6	0.0	73.6	68.6	41.0	2956	15357	0.0
17.2	68.9	1122.5	2.4	100005	5000	4976	1030	1.00	.932	36.5	7840	73.6	0.0	73.6	68.6	40.7	2956	15357	0.0
17.4	69.2	1142.8	2.4	100005	5000	5000	1035	1.00	.932	36.5	7840	73.6	0.0	73.6	68.6	40.4	2956	15357	0.0
17.6	69.6	1163.1	2.3	100005	5000	5023	1040	1.00	.932	36.5	7840	73.6	0.0	73.6	68.6	40.0	2956	15357	0.0
17.8	69.9	1183.6	2.3	100005	5000	5046	1045	.99	.932	36.5	7840	73.6	0.0	73.6	68.6	39.7	2956	15357	0.0
18.0	70.2	1204.1	2.3	100005	5000	5069	1049	.99	.932	36.5	7840	73.6	0.0	73.6	68.6	39.4	2956	15357	0.0

Wide-Open-Throttle Launch

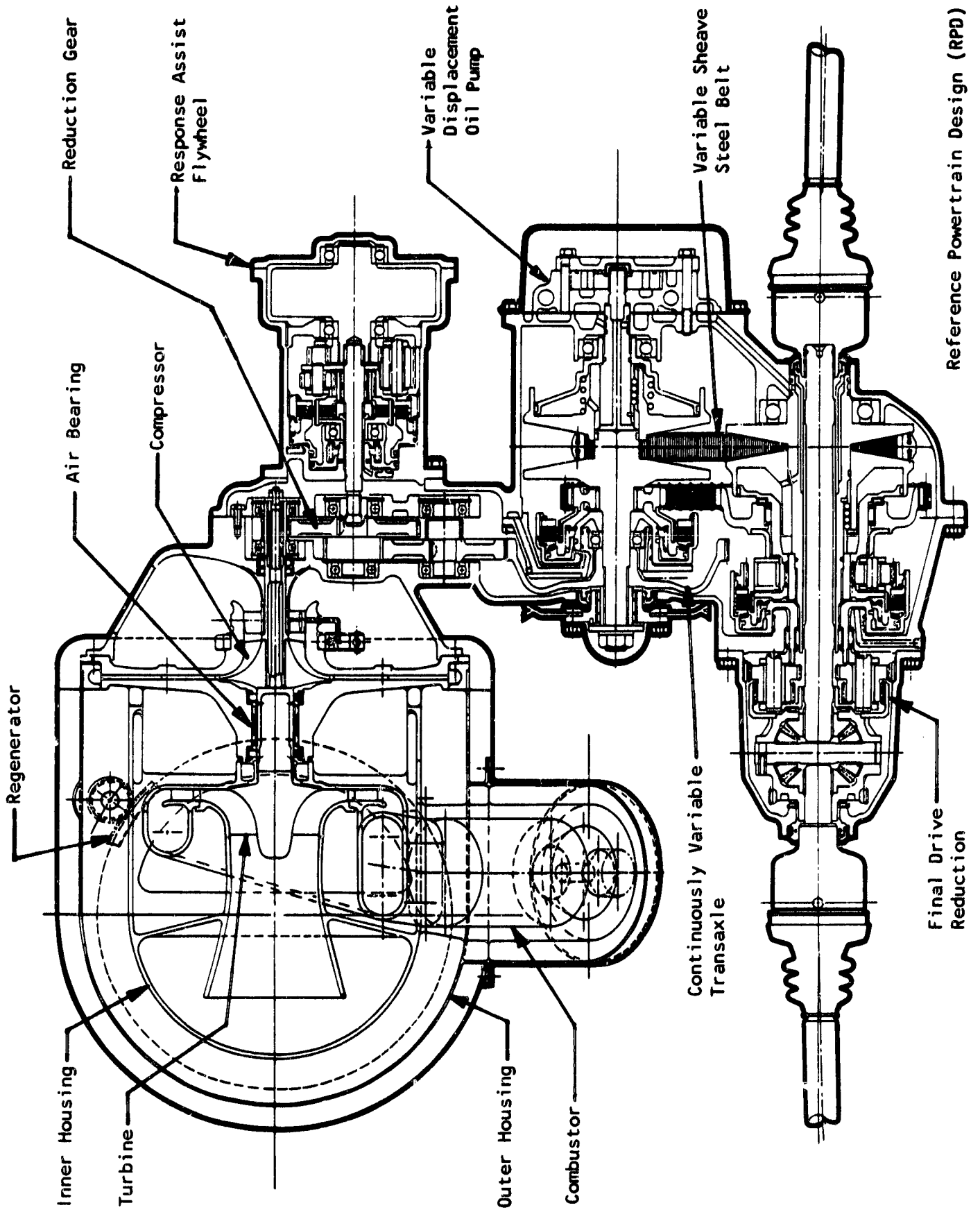


Figure 1

Reference Powertrain Design (RPD)

Final Drive Reduction

- 1. Air Inlet
- 2. Air Filter
- 3. Engine Intake
- 5. By-Pass Valve
- 6. Starter
- 7. Response Assist Flywheel
- 8. Transmission
- 10. Air Conditioner Compress
- 13. Battery

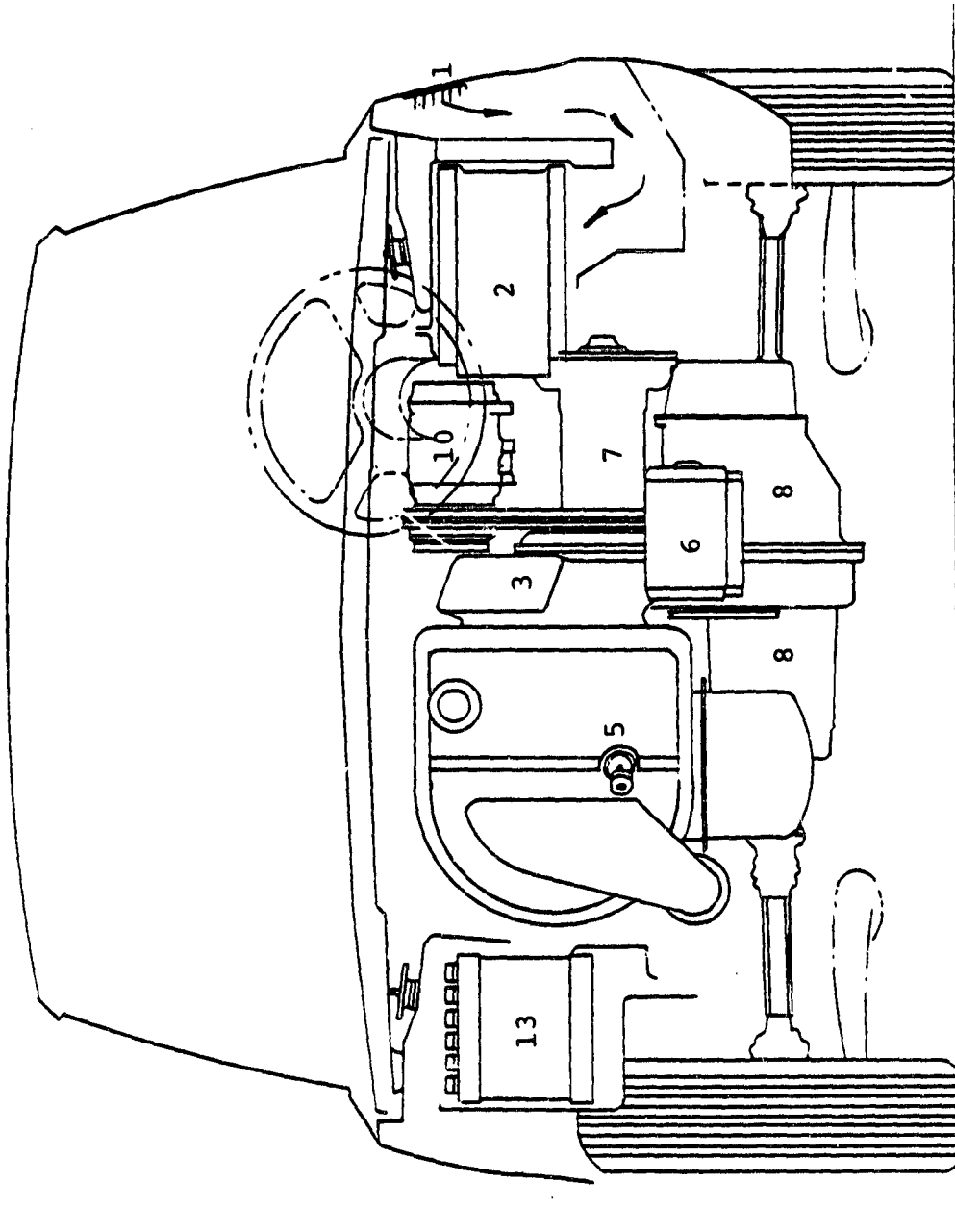


Figure 2

AGT-102 Vehicle Layout - Front View

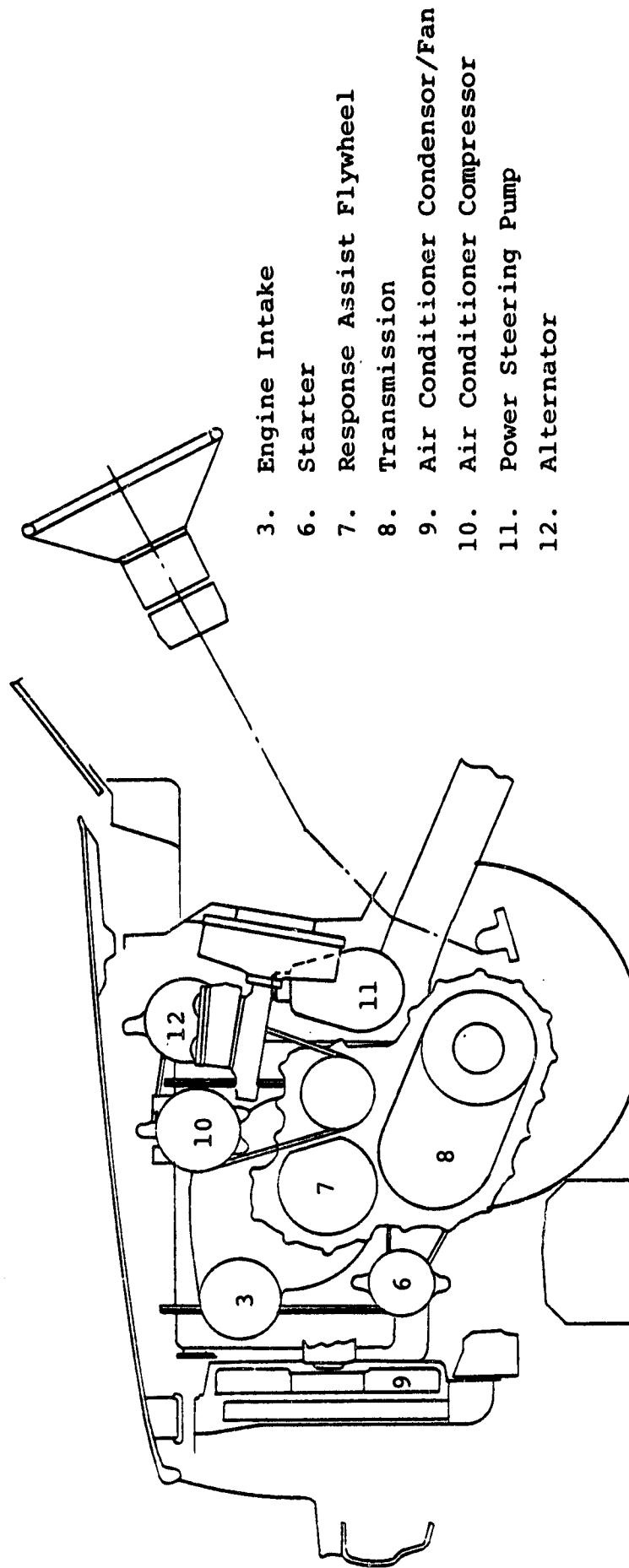
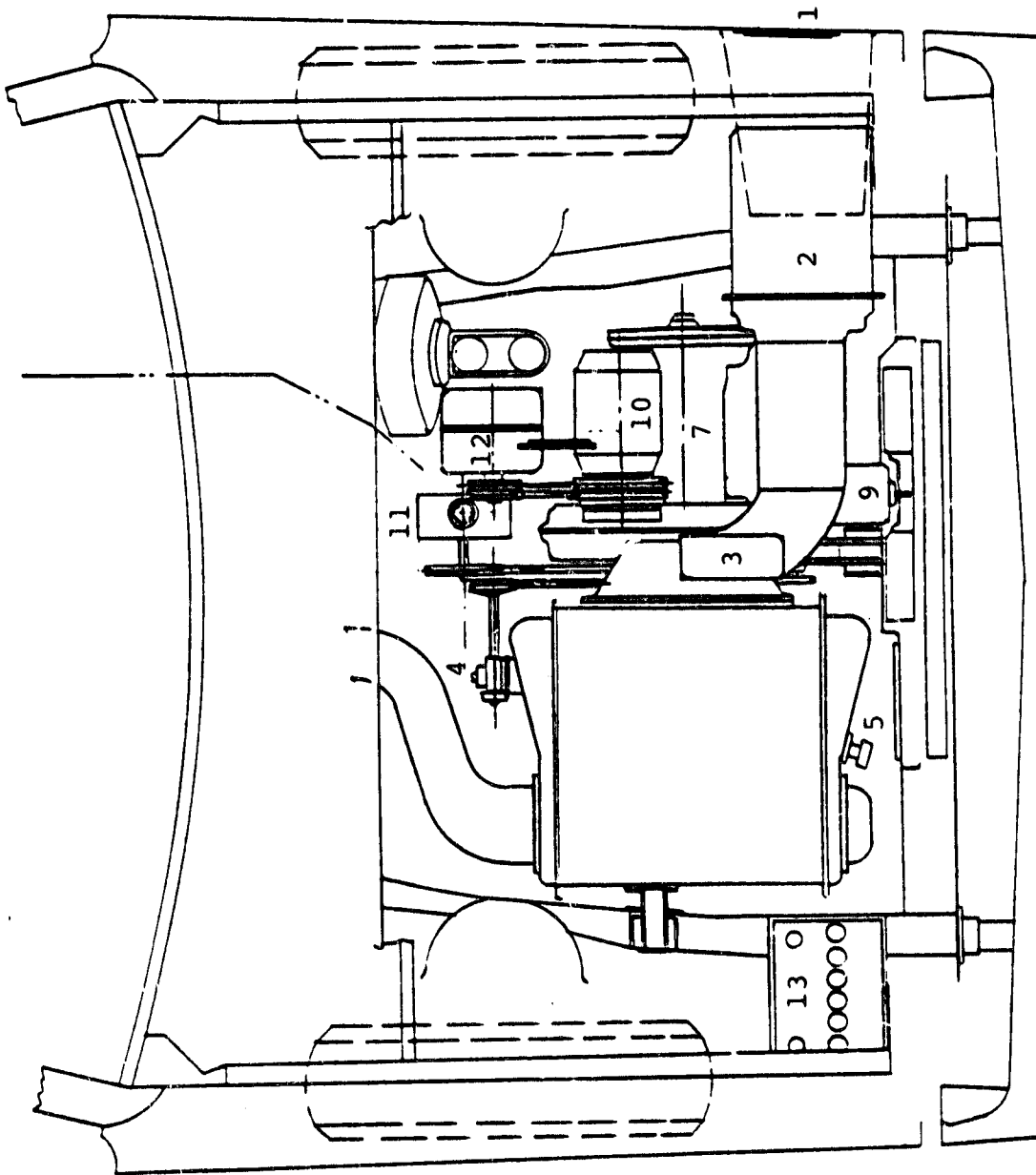


Figure 3

AGT-102 Vehicle Layout - Left Side View

- 1. Air Inlet
- 2. Air Filter
- 3. Engine Intake
- 4. Regenerator Drive Worm
- 5. By-Pass Valve
- 7. Response Assist Flywheel
- 9. Air Conditioner Condensor/
Fan
- 10. Air Conditioner Compressor
- 11. Power Steering Pump
- 12. Alternator
- 13. Battery



AGT-102 Vehicle Layout - Plan View

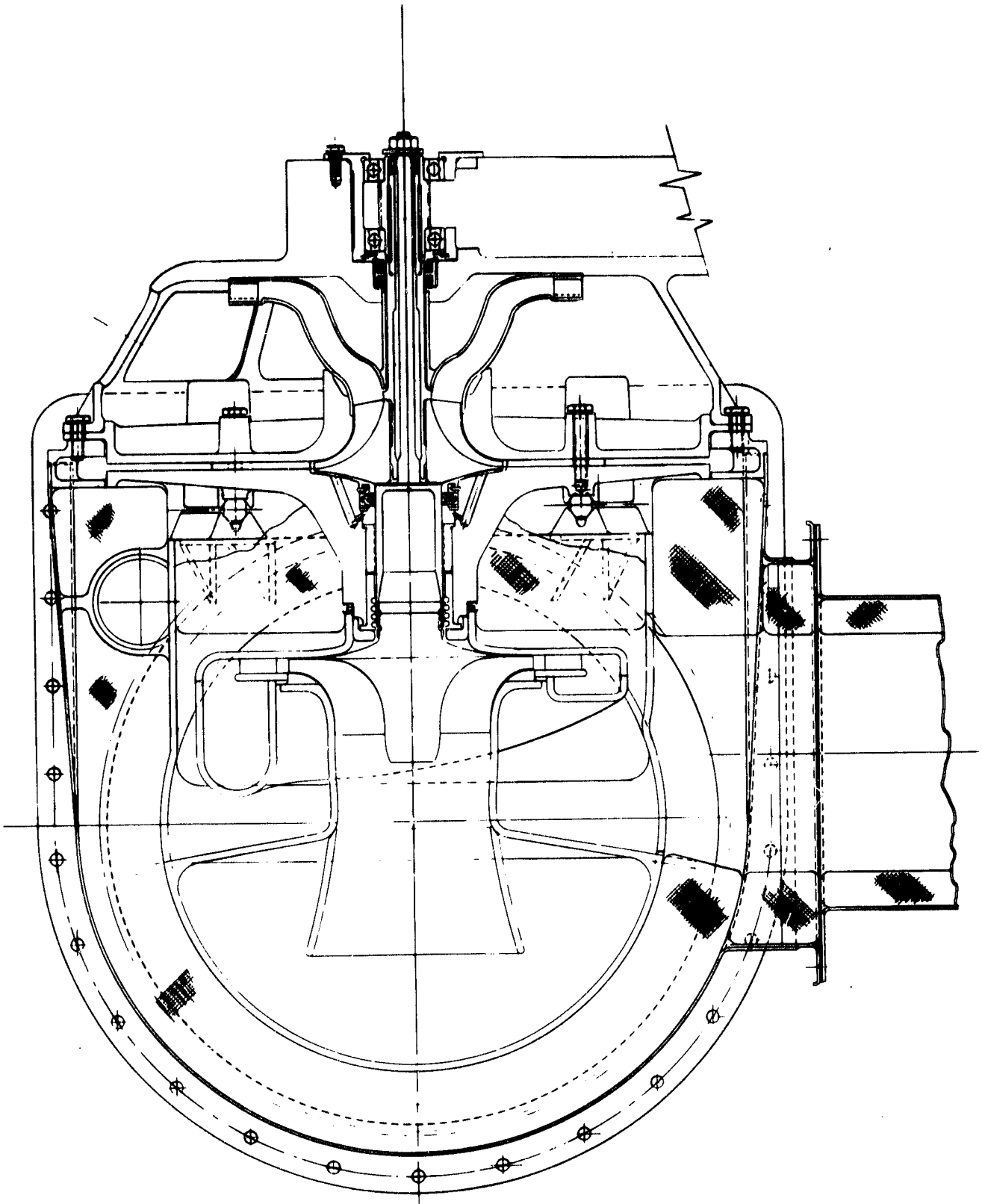
Figure 4

ORIGINAL PAGE IS
OF POOR QUALITY



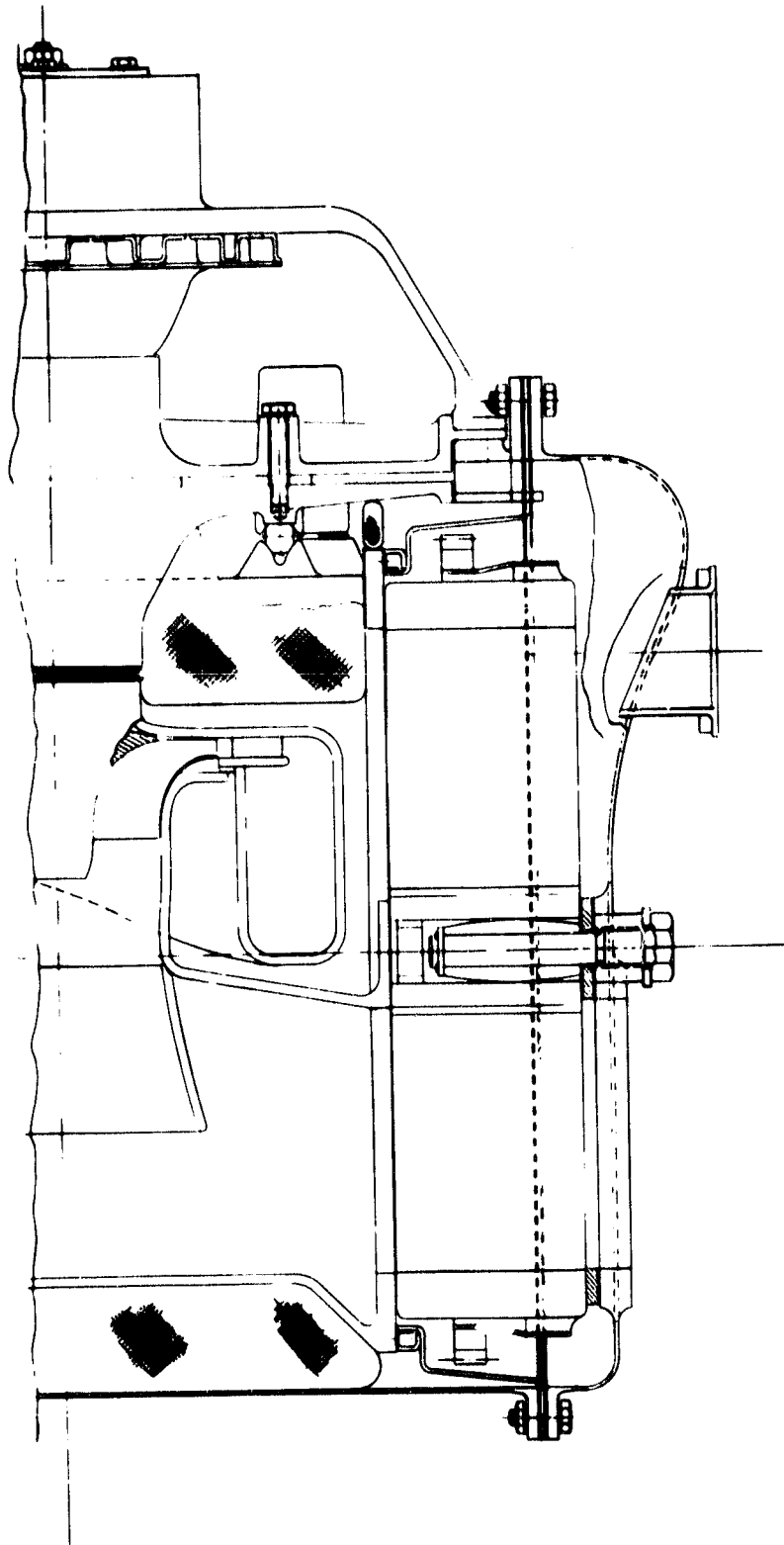
AGT-102 Powertrain Mock-up
Left Front Quarter View

Figure 5



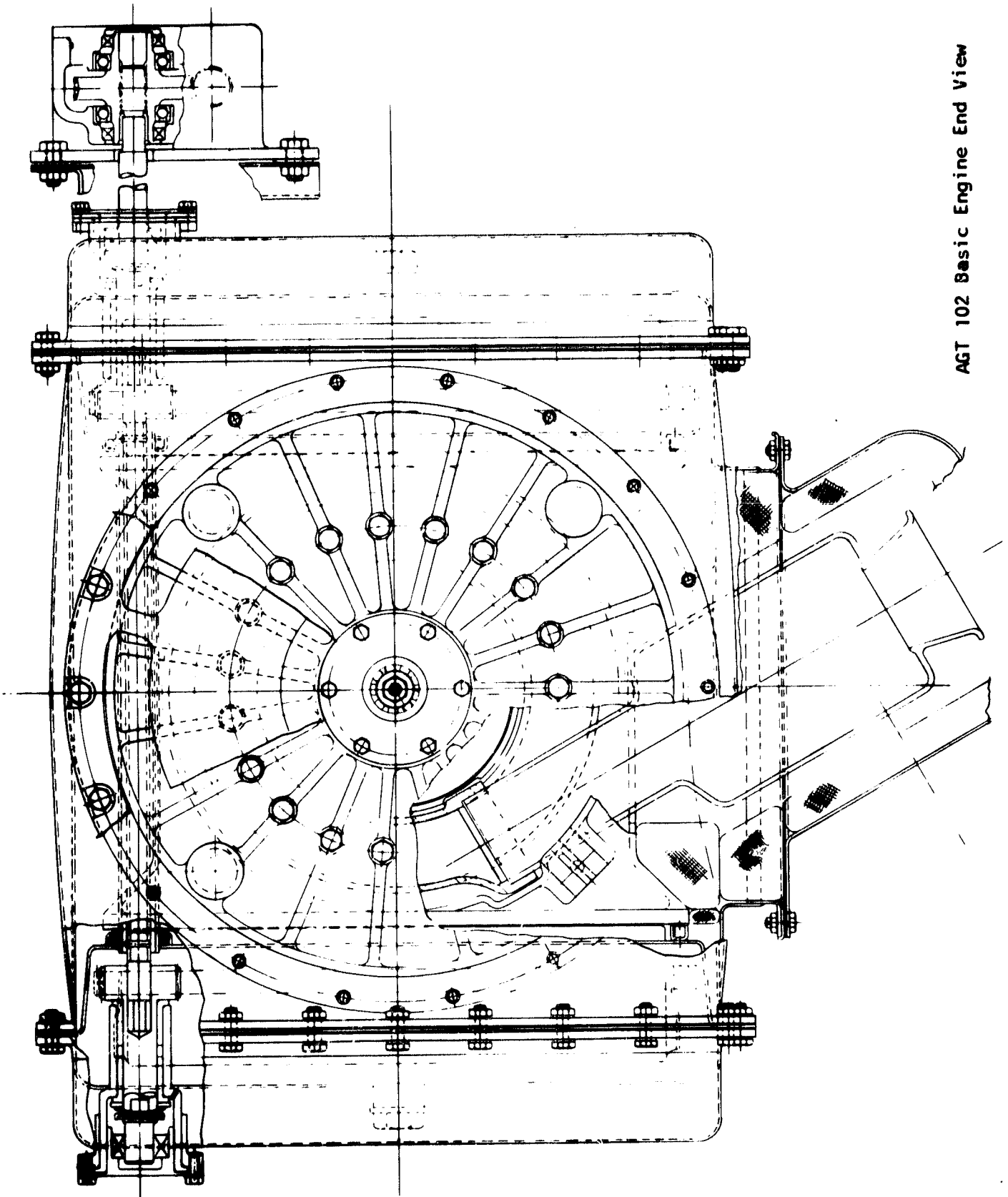
AGT 102 Basic Engine Cross Section

Figure 6



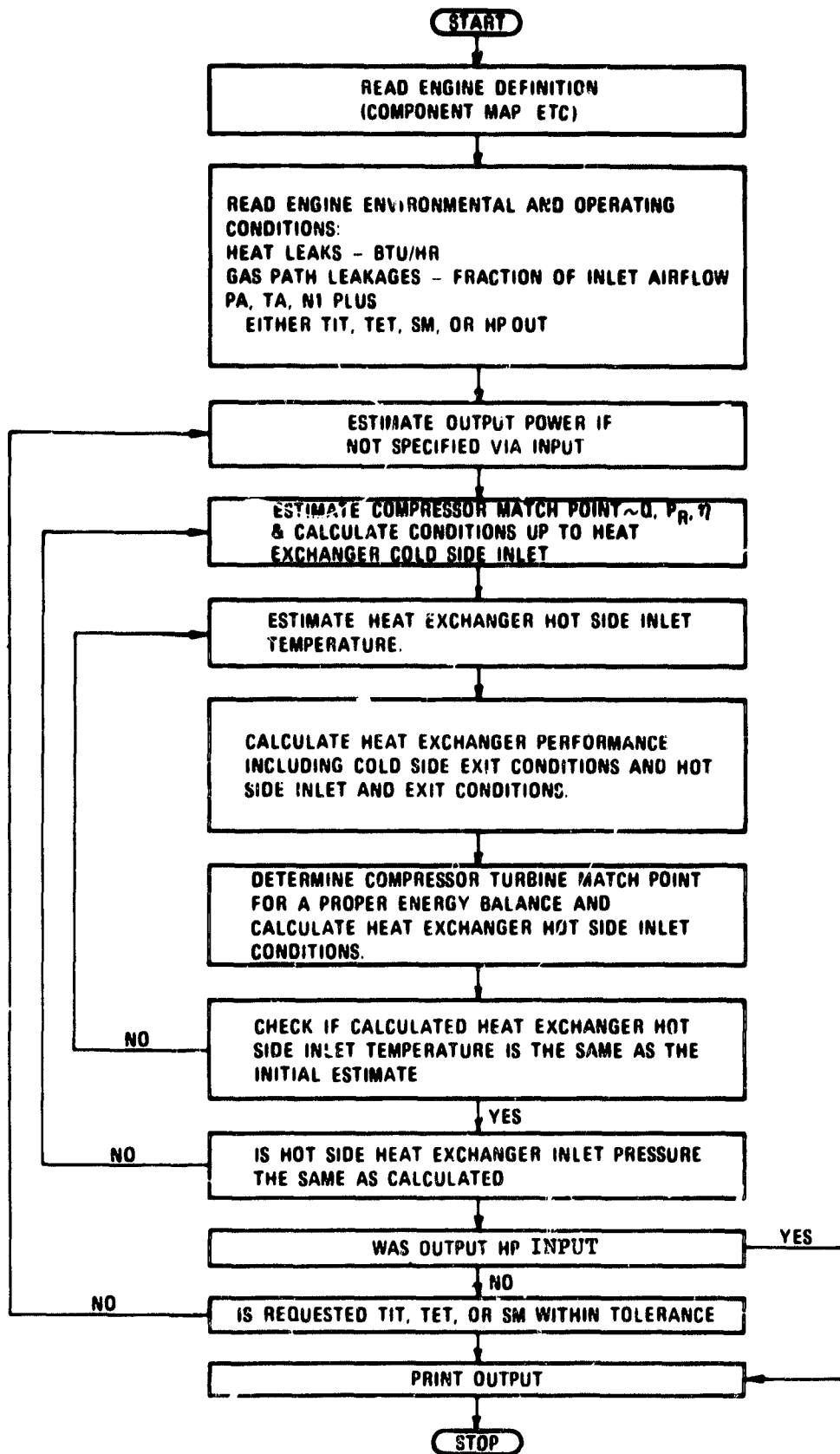
AGT 102 Basic Engine Horizontal Section

Figure 7



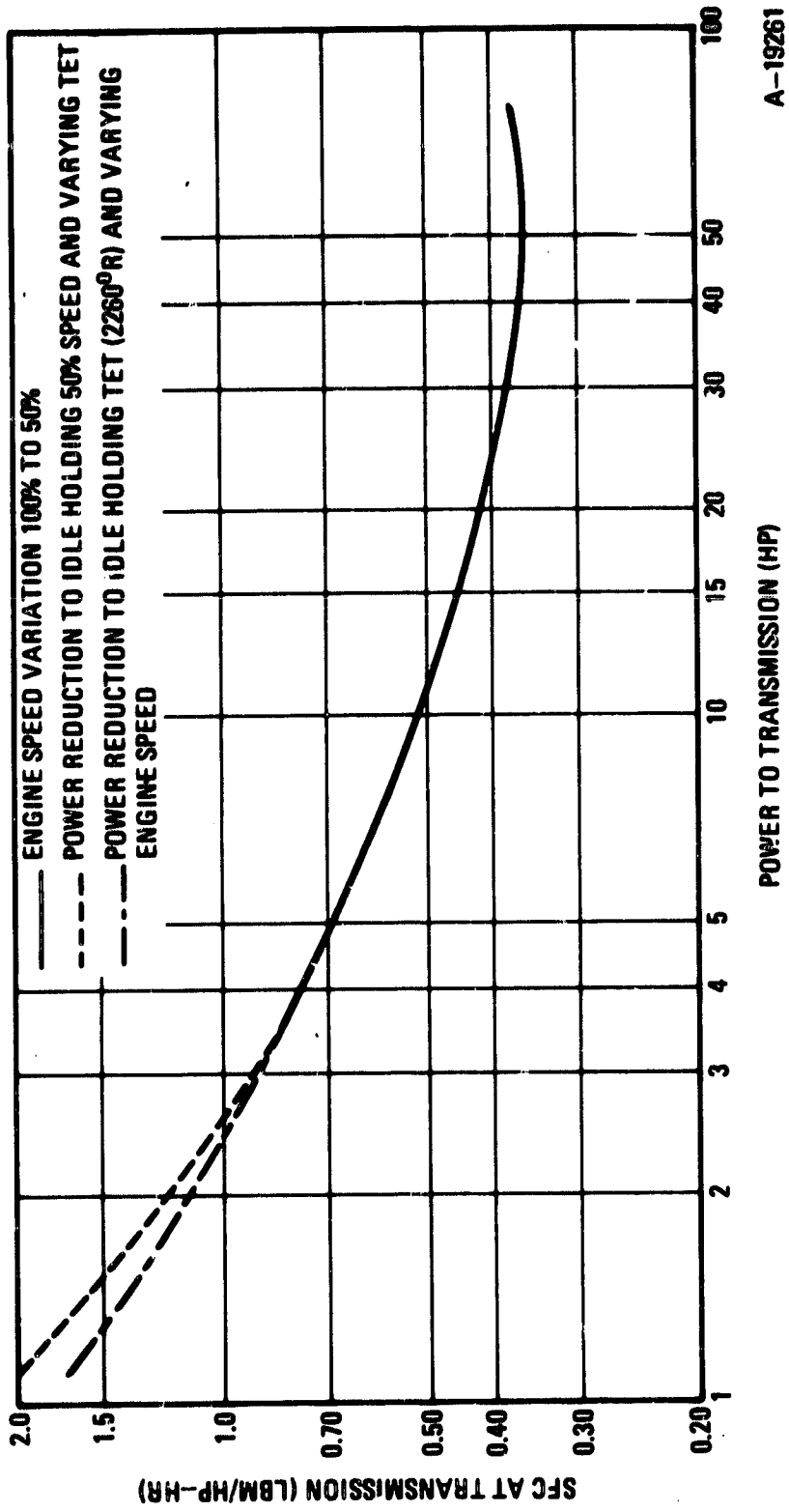
AGT 102 Basic Engine End View

Figure 8



Engine Simulation Model Logic Diagram

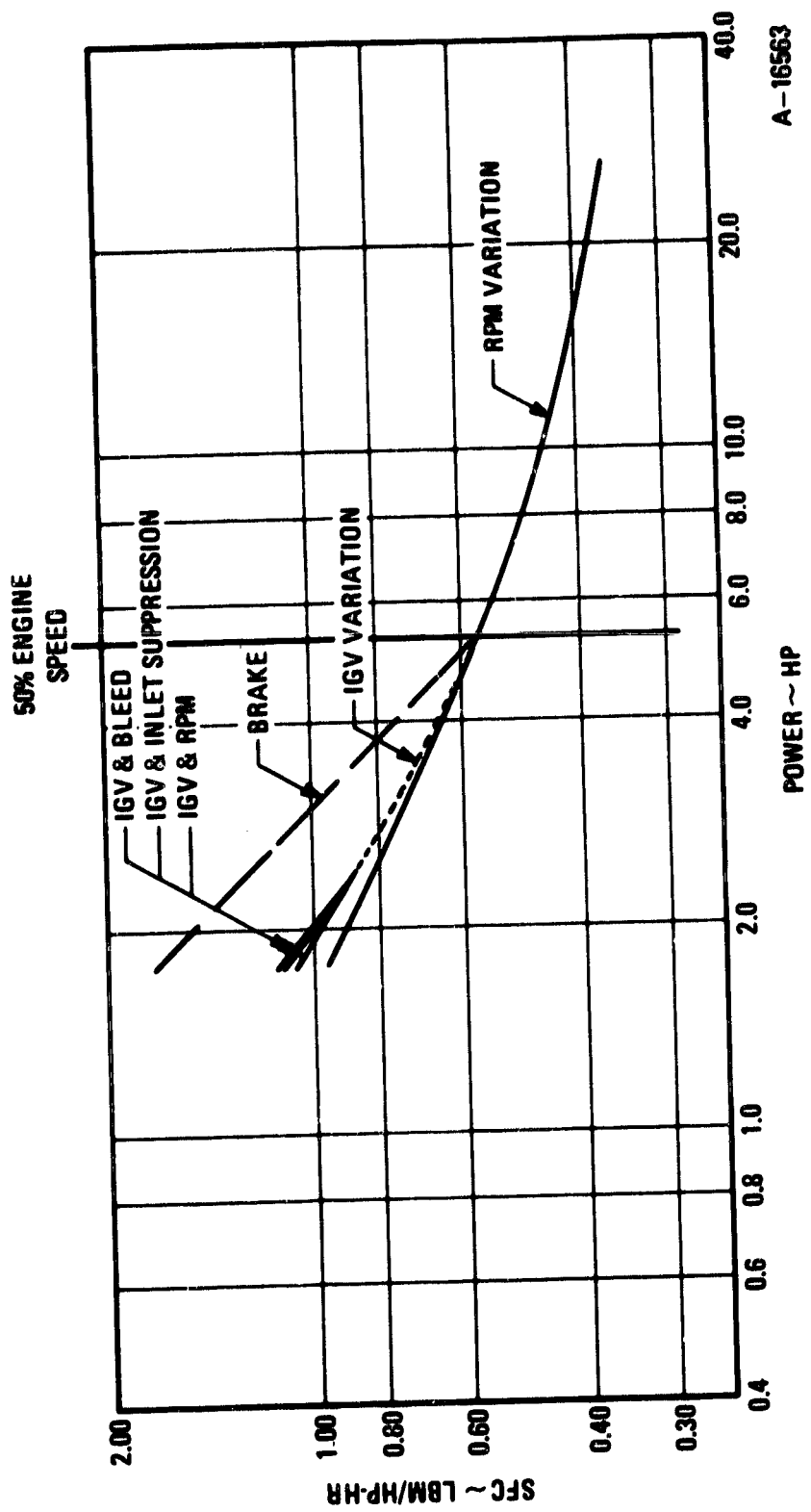
Figure 9



A-19261

Advanced Gas Turbine RPD Engine No. 1
No Inlet Guide Vanes

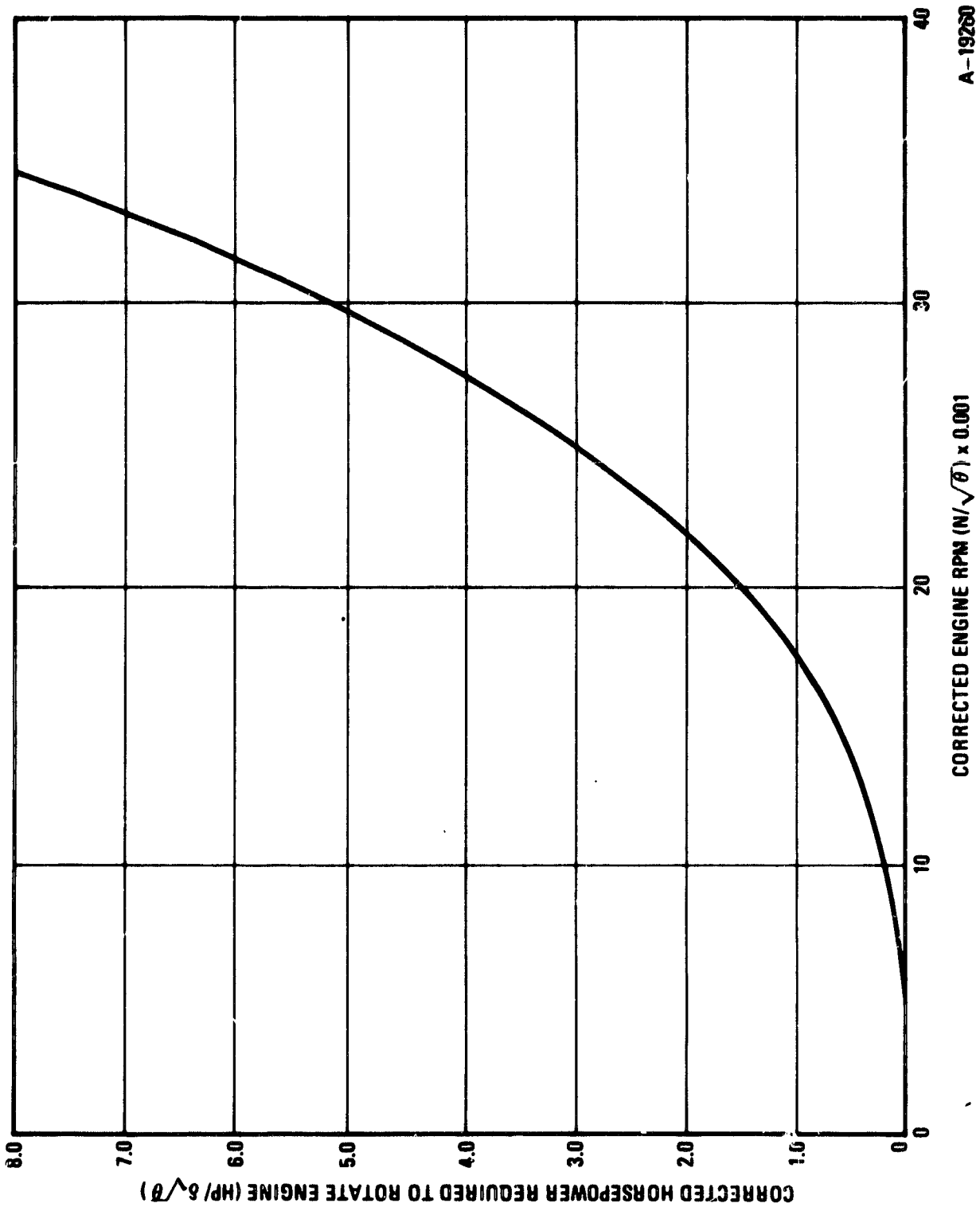
Figure 10



A-16563

Figure 11

Comparison of Various Methods of Achieving Idle Power



A-19280

Estimated RPD Starter Power Requirements
(Without Light-off)

Figure 12

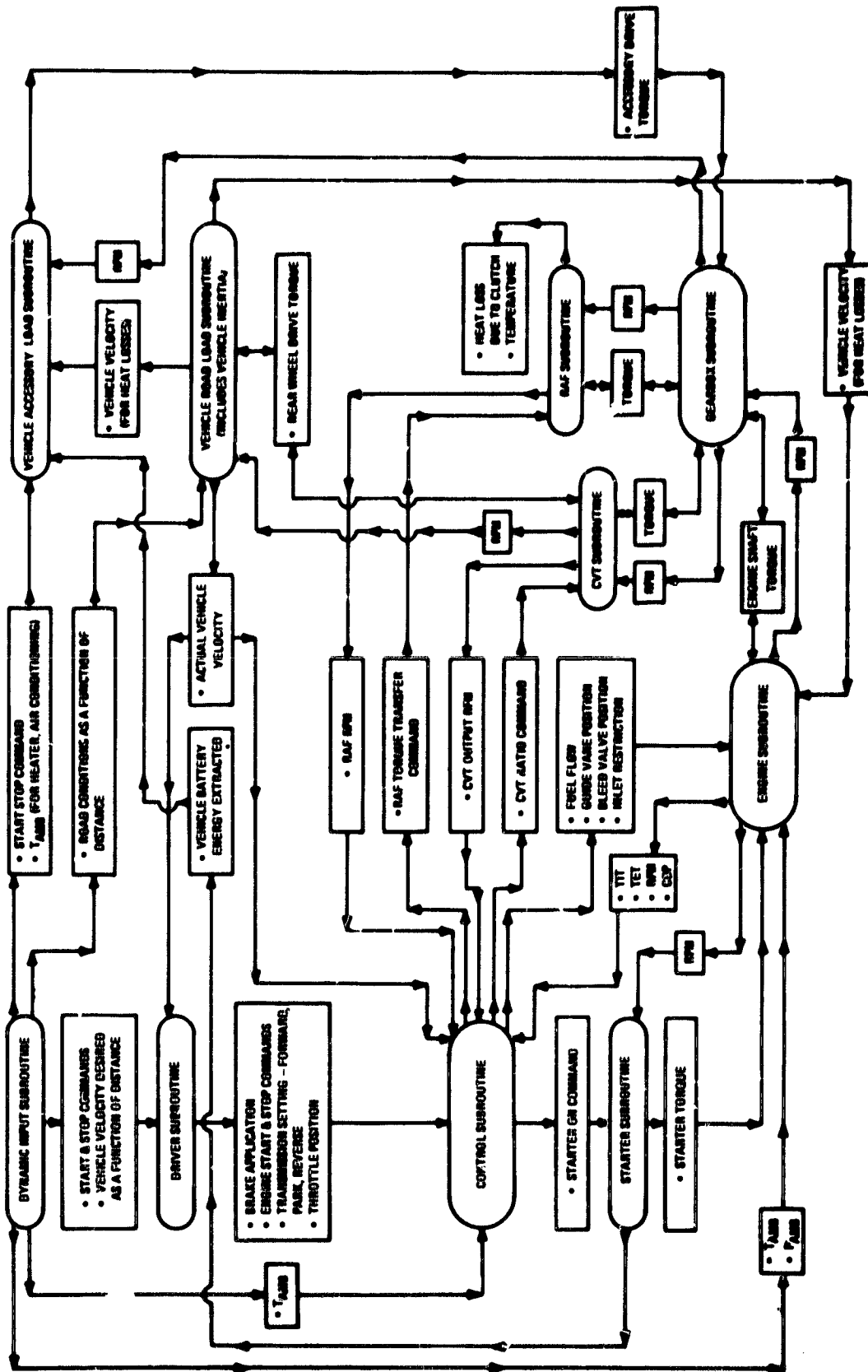
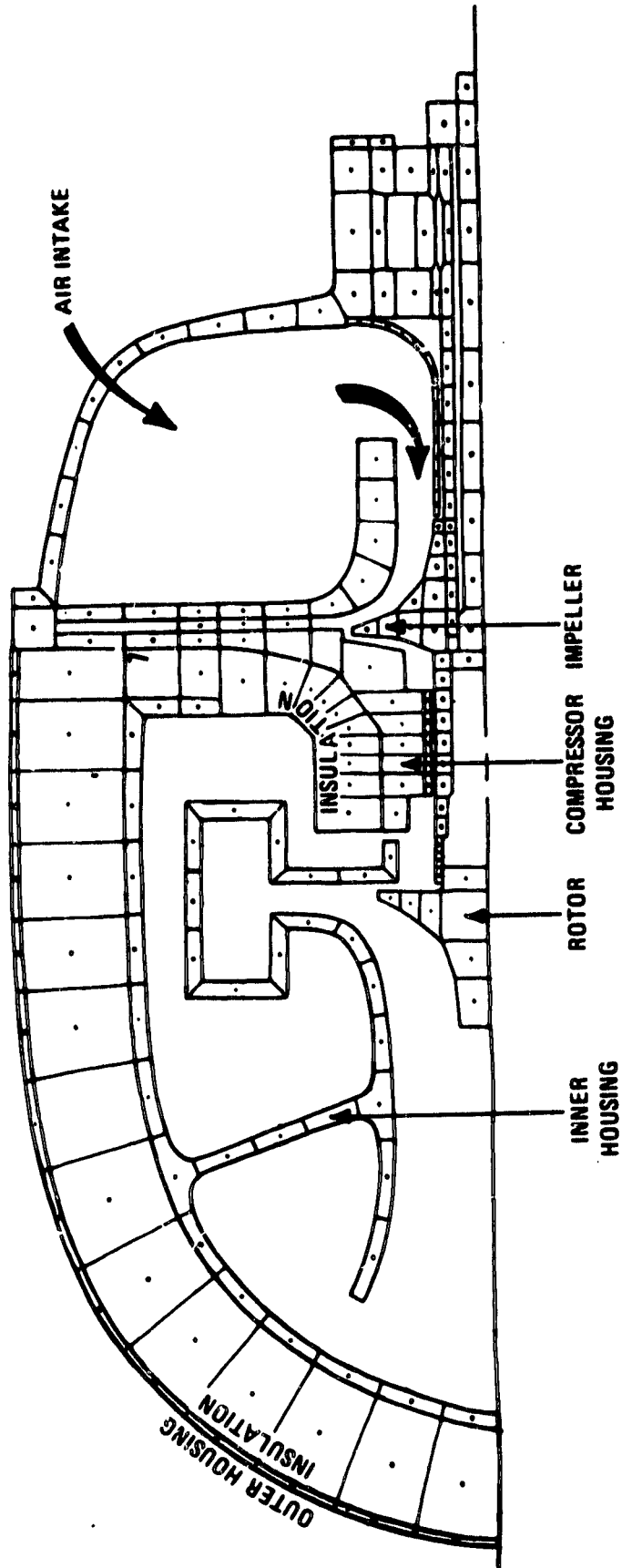
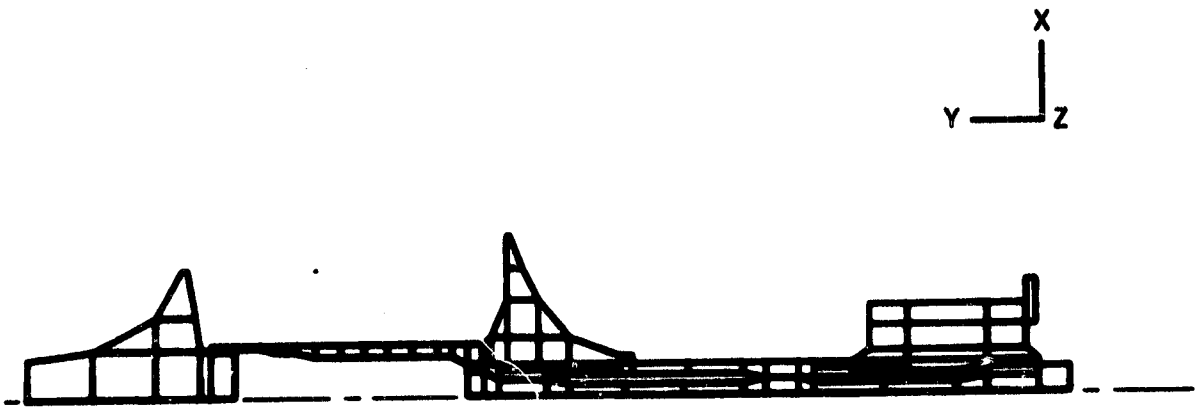


Figure 13



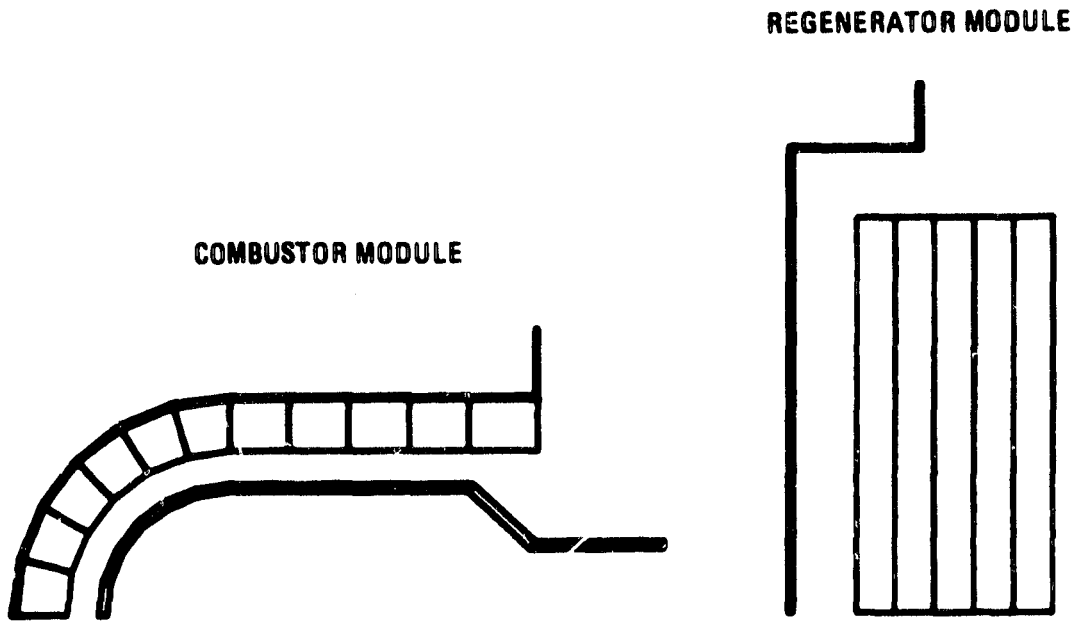
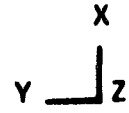
Basic Engine Thermal Model Geometry

Figure 14



Thermal Model Rotor System Elements

Figure 15

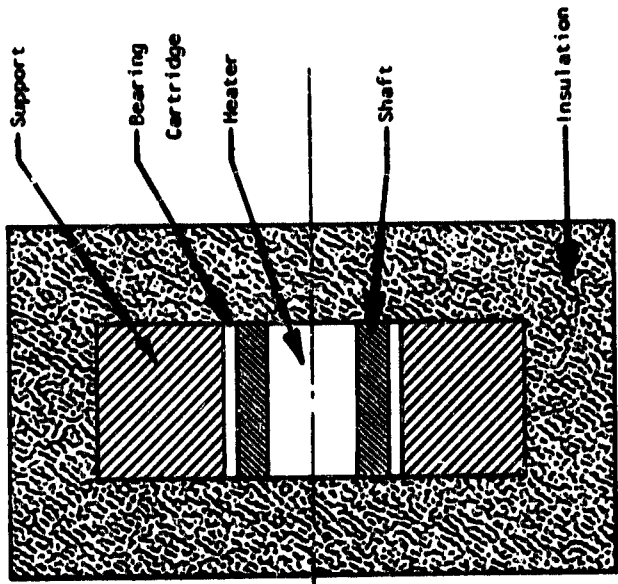
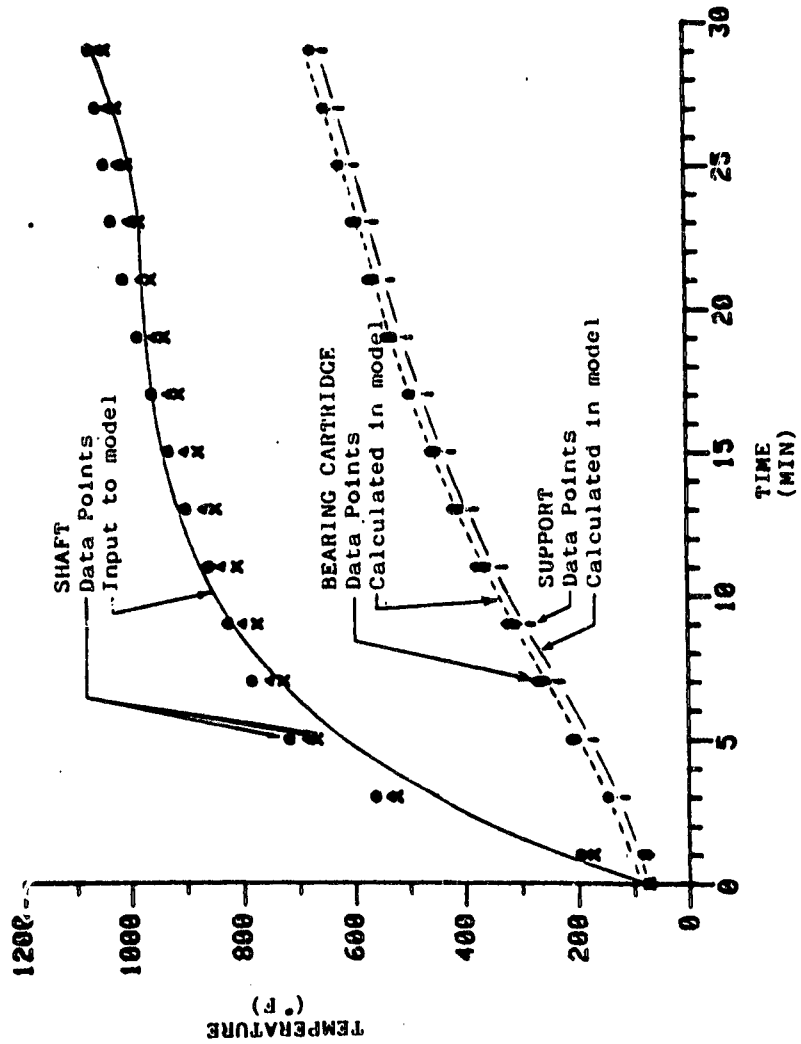


Thermal Model (Combustor and Regenerator Modules)

Figure 16

AIR BEARING HEAT TRANSFER COEFFICIENT

Heat Transfer Coefficient across
Air Bearing Foil = $43 \text{ Btu/hr/ft}^2/\text{f}$ in Model



Air Bearing Test Fixture Schematic

Air Bearing Heat Transfer Coefficient Test

Figure 17

ORIGINAL PAGE IS
OF POOR QUALITY

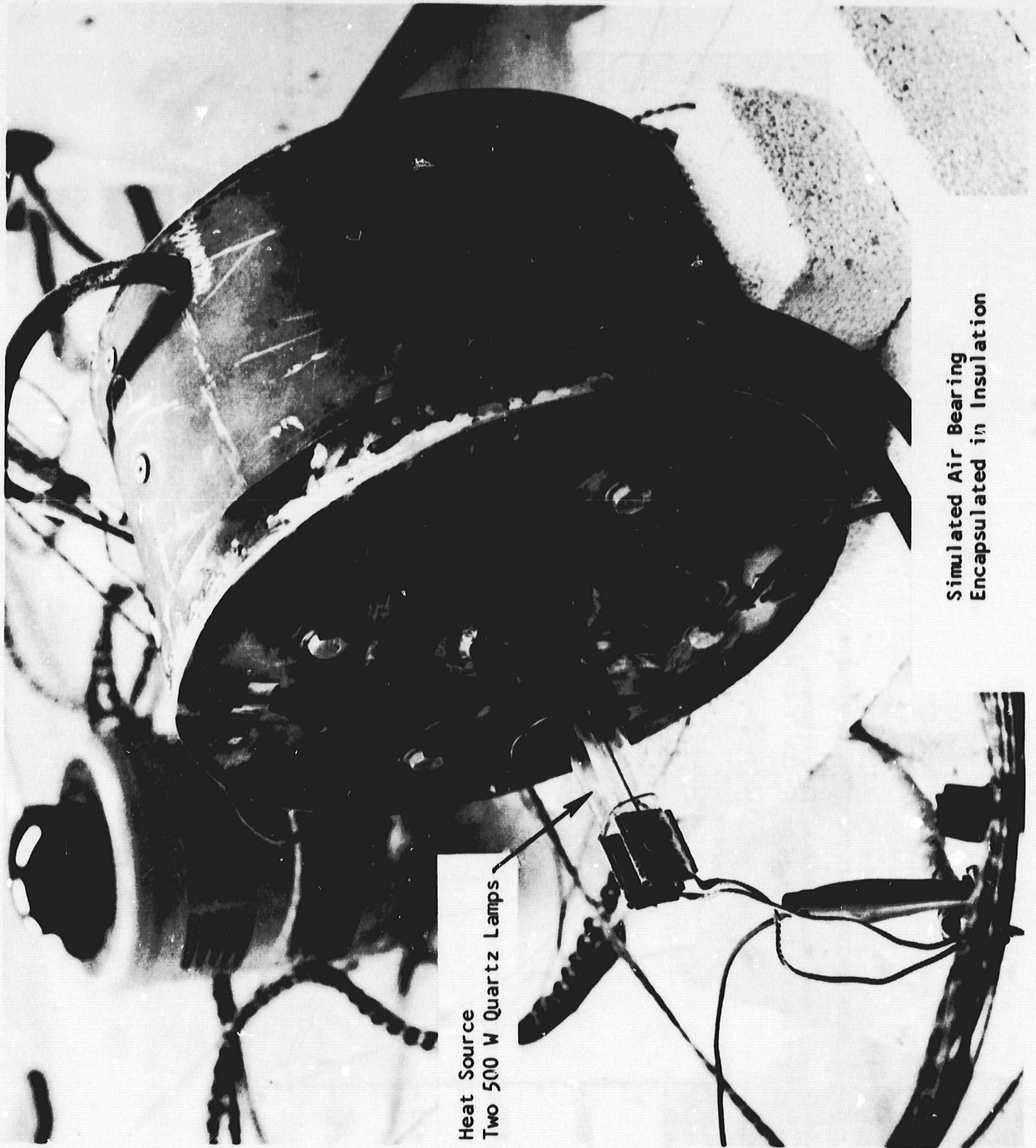
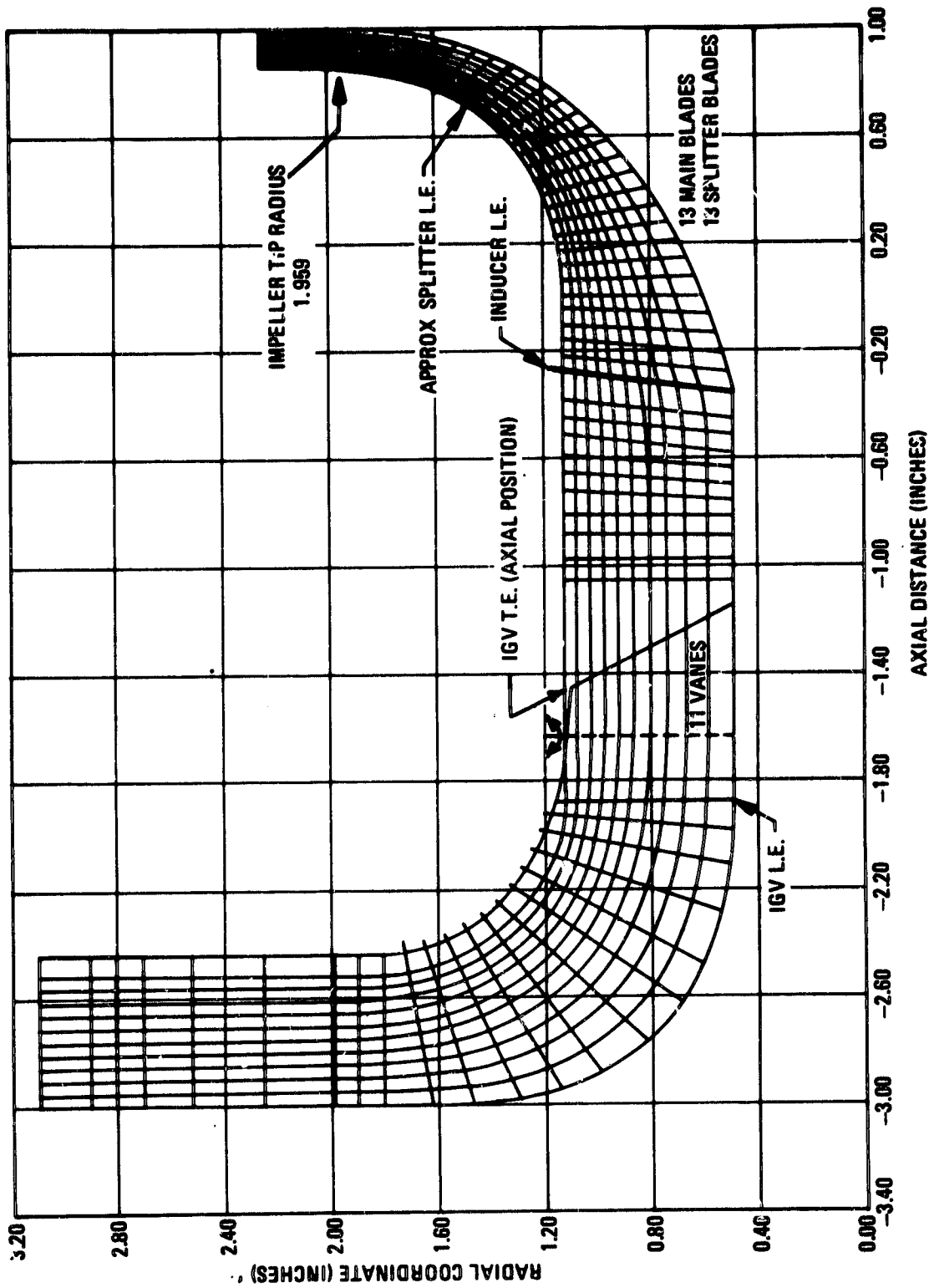
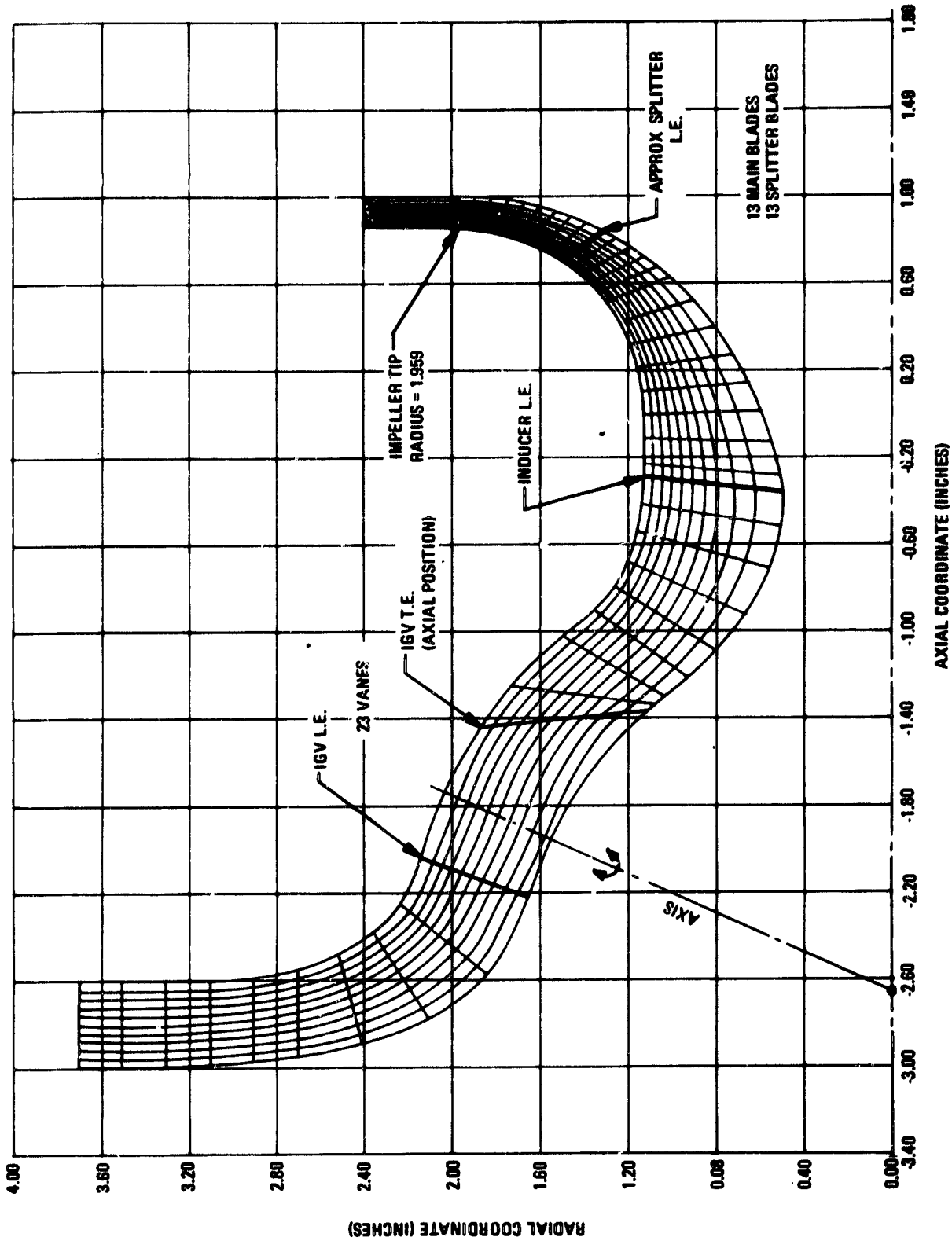


Figure 18



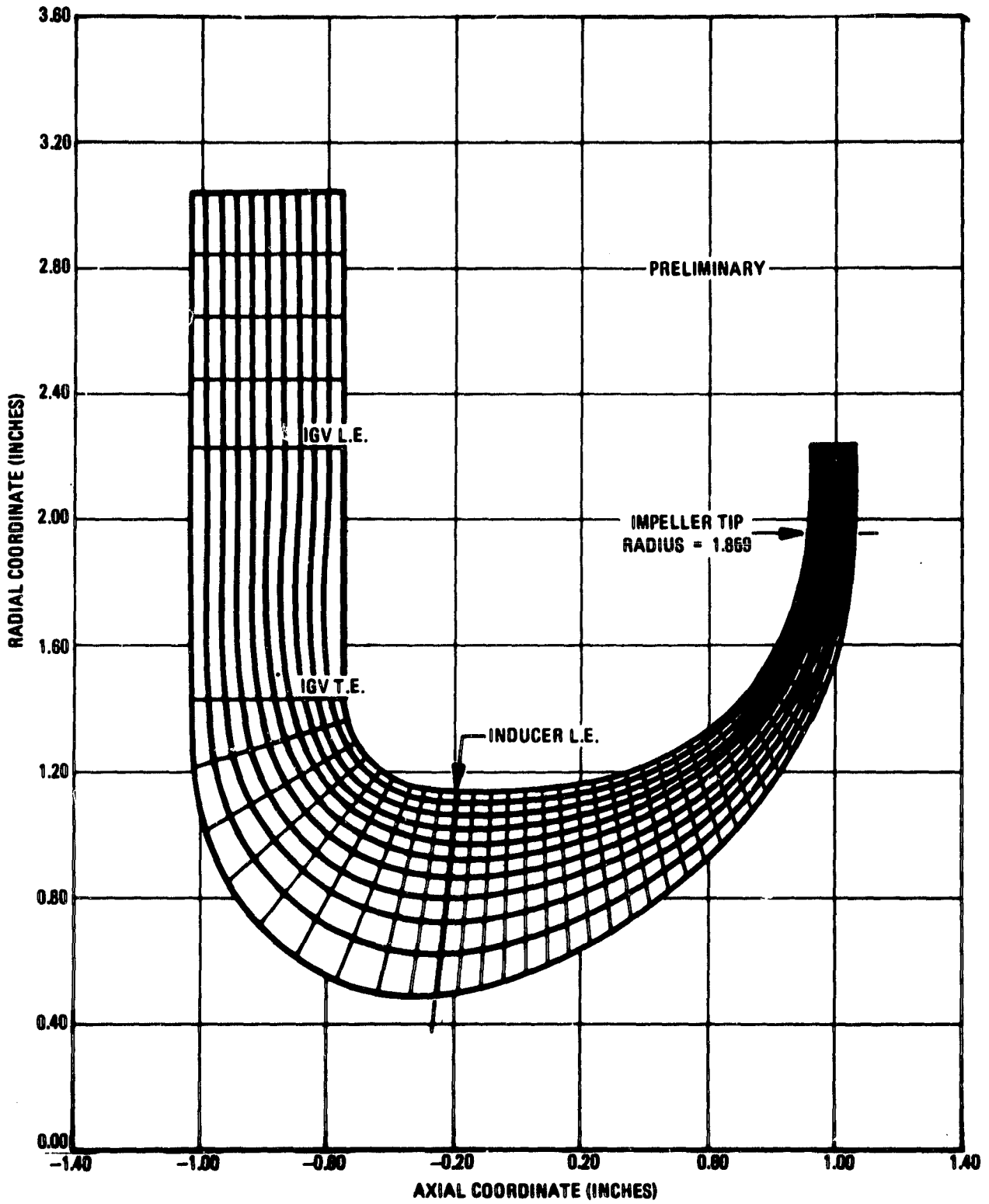
Compressor Axial Inlet Flowpath

Figure 19



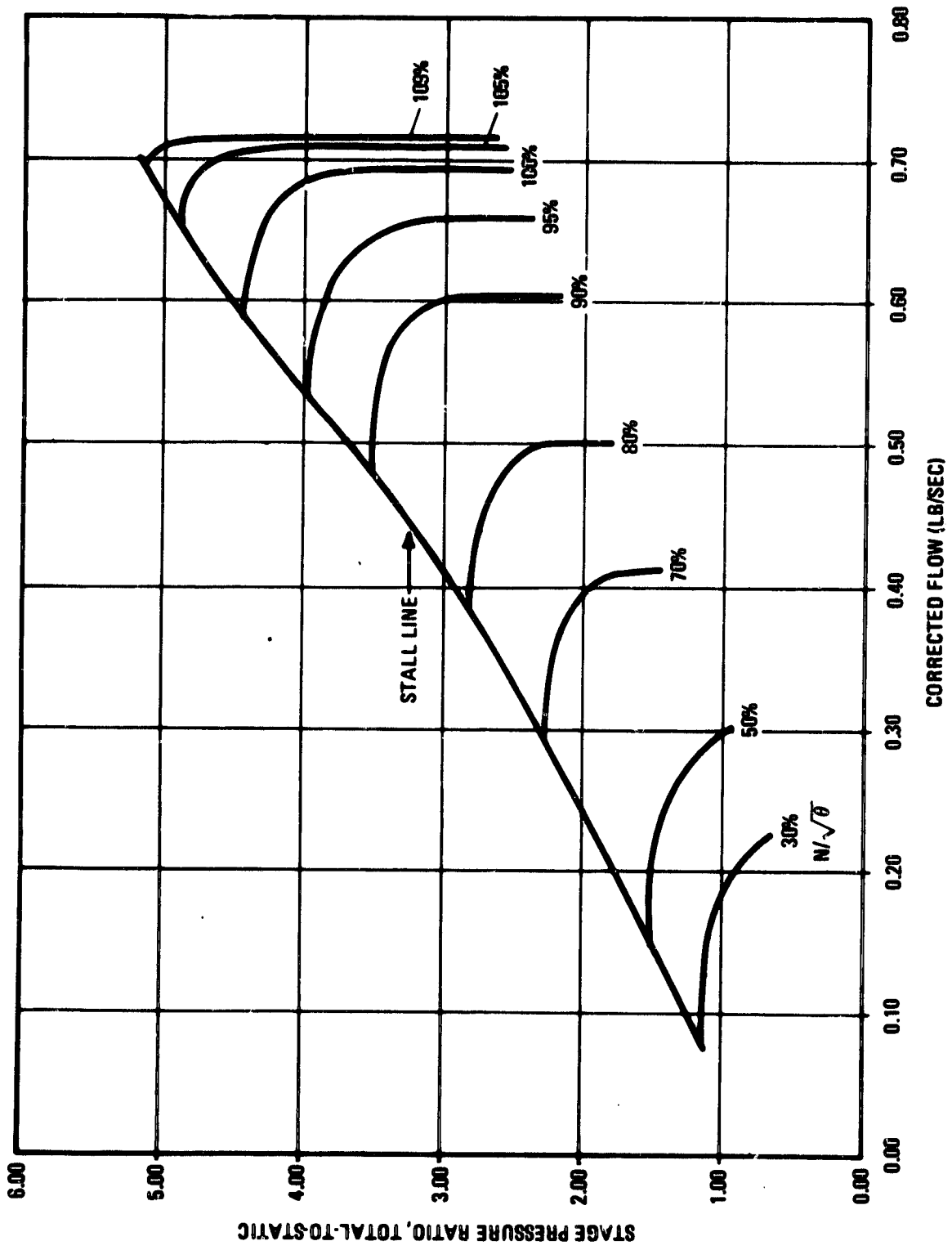
Compressor Semi-Axial Inlet Flowpath

Figure 20



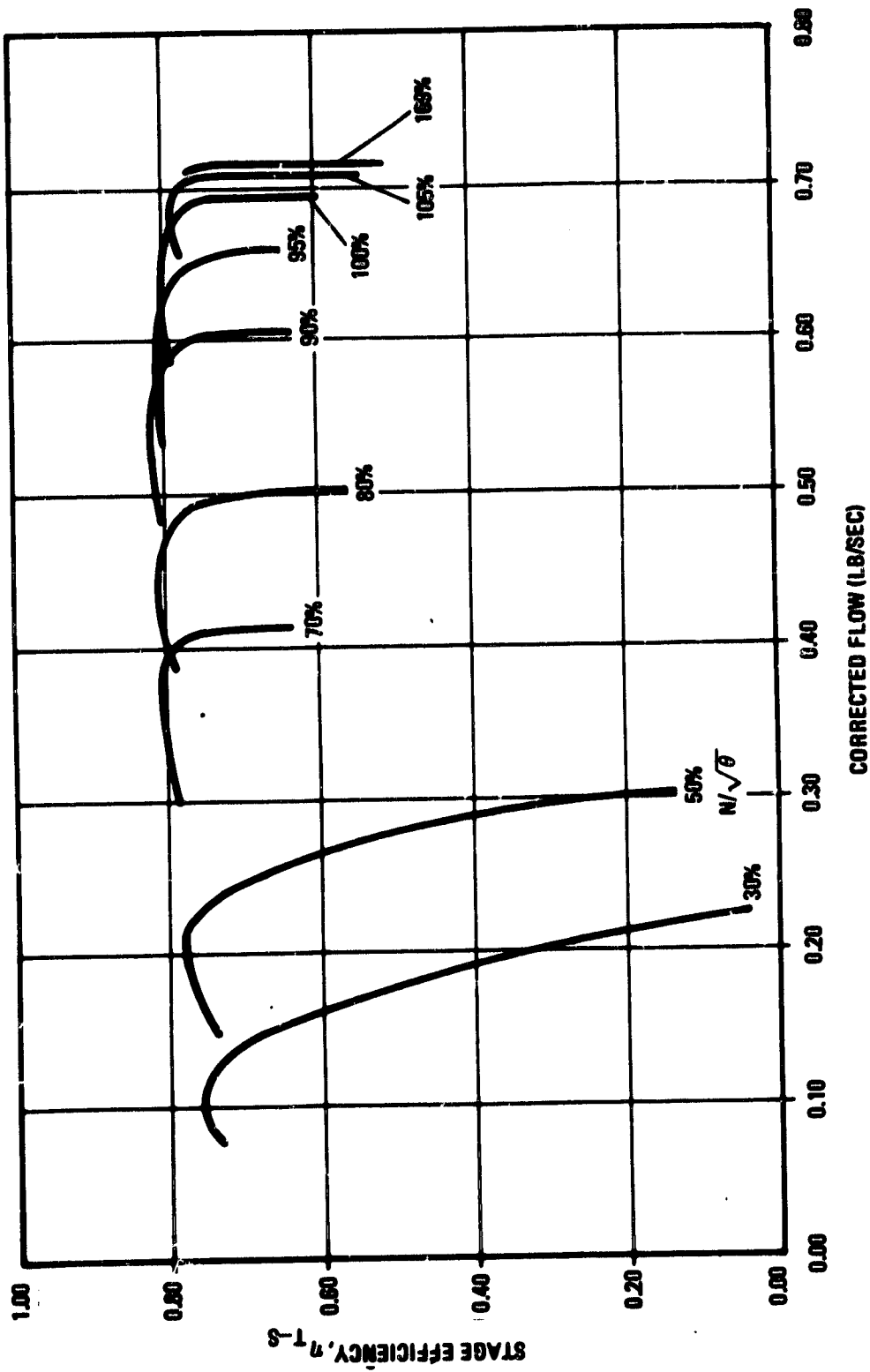
Compressor Radial VIGV Flowpath

Figure 21



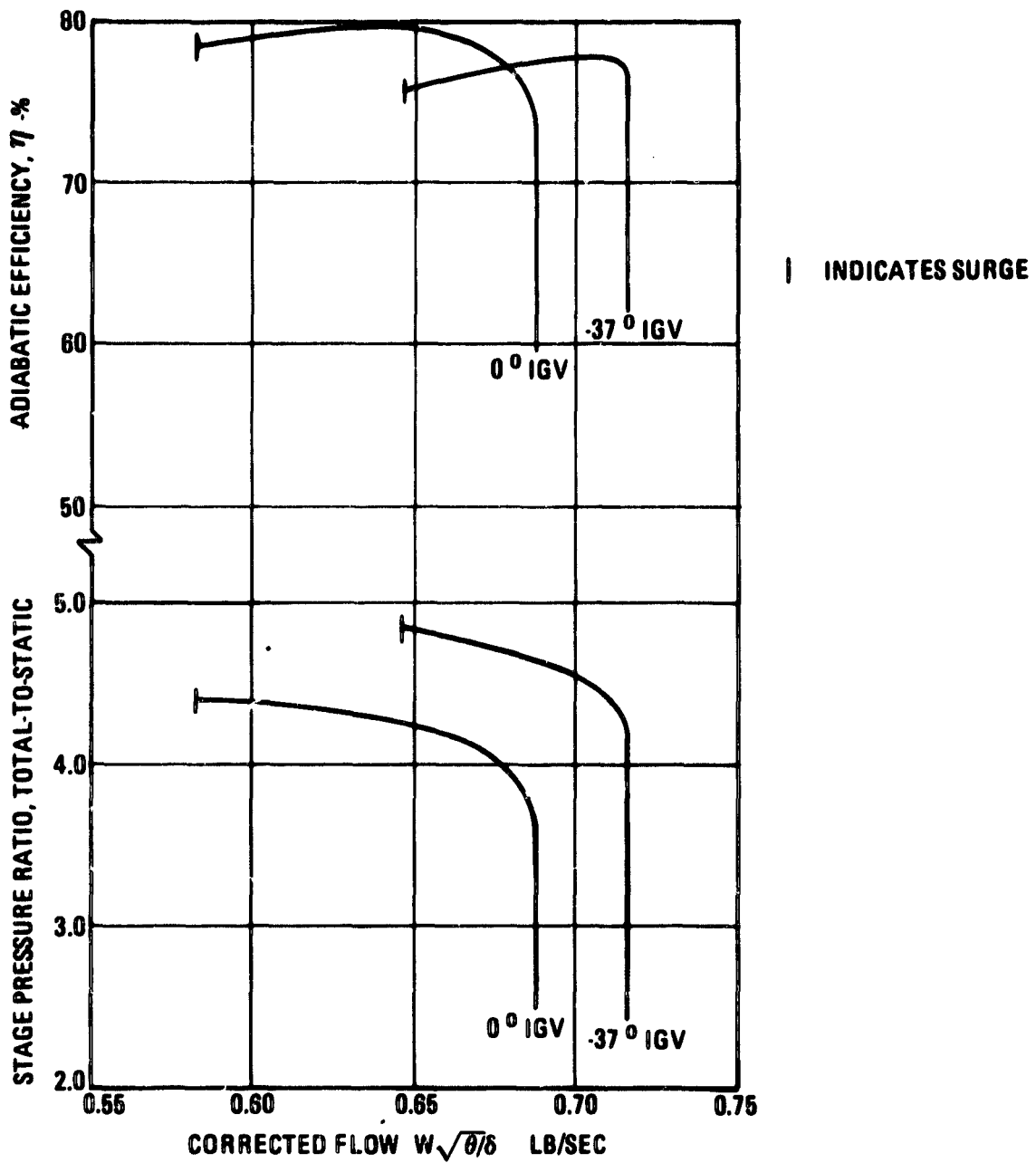
Compressor Performance with no VIGV

Figure 22



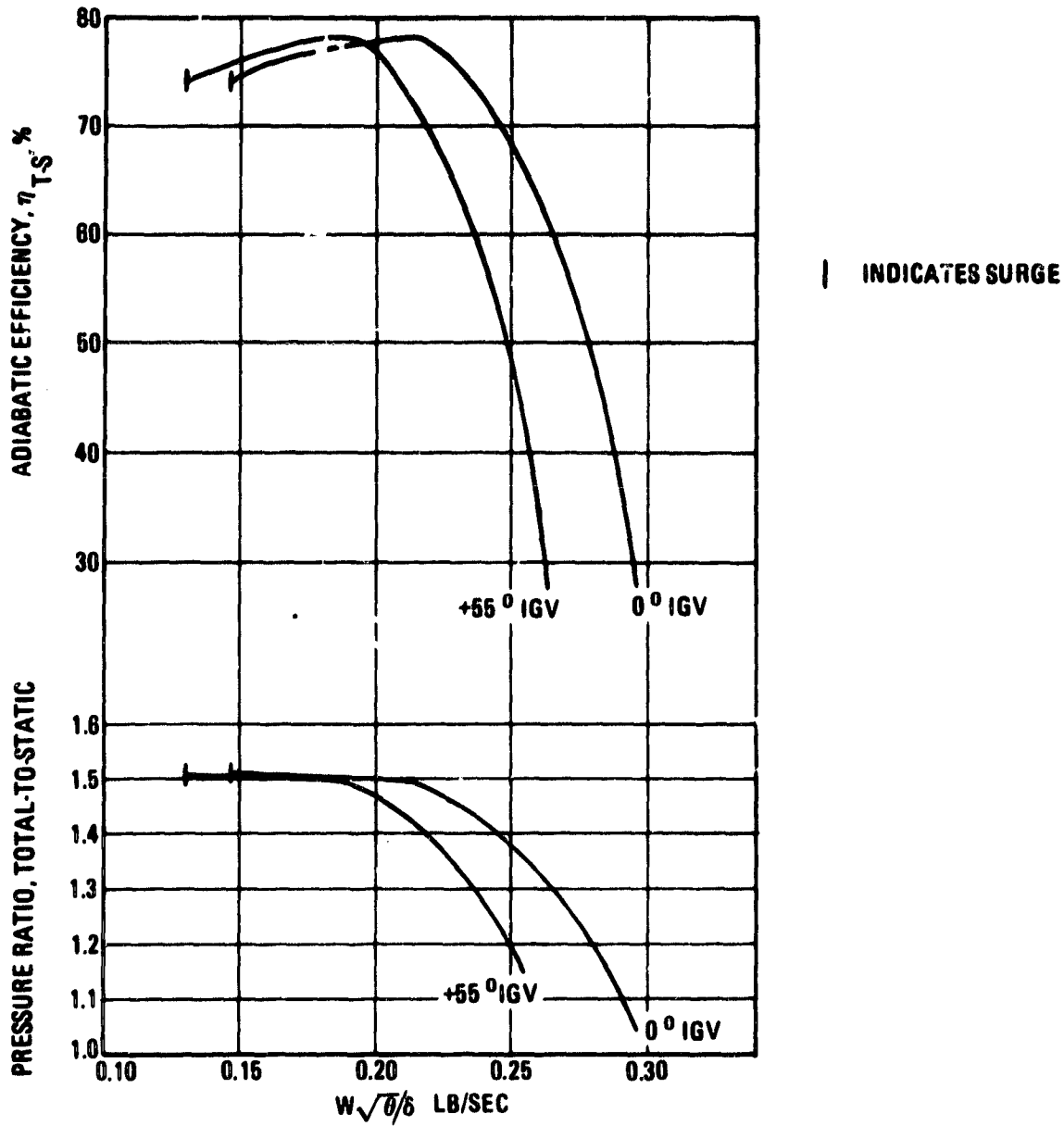
Compressor Performance with no VIGV

Figure 23



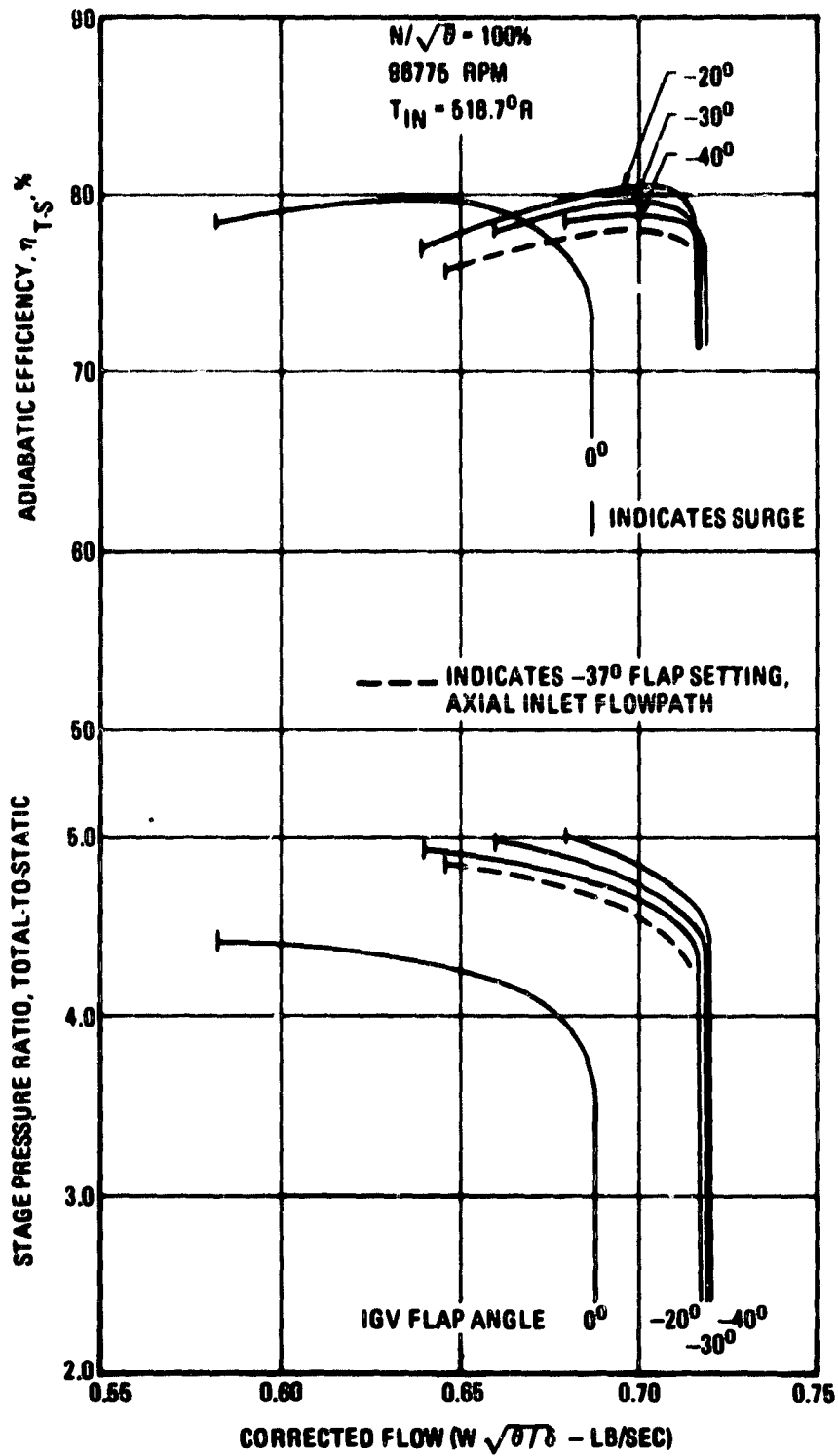
Compressor Performance with Axial VIGV
at 100 Percent Speed

Figure 24



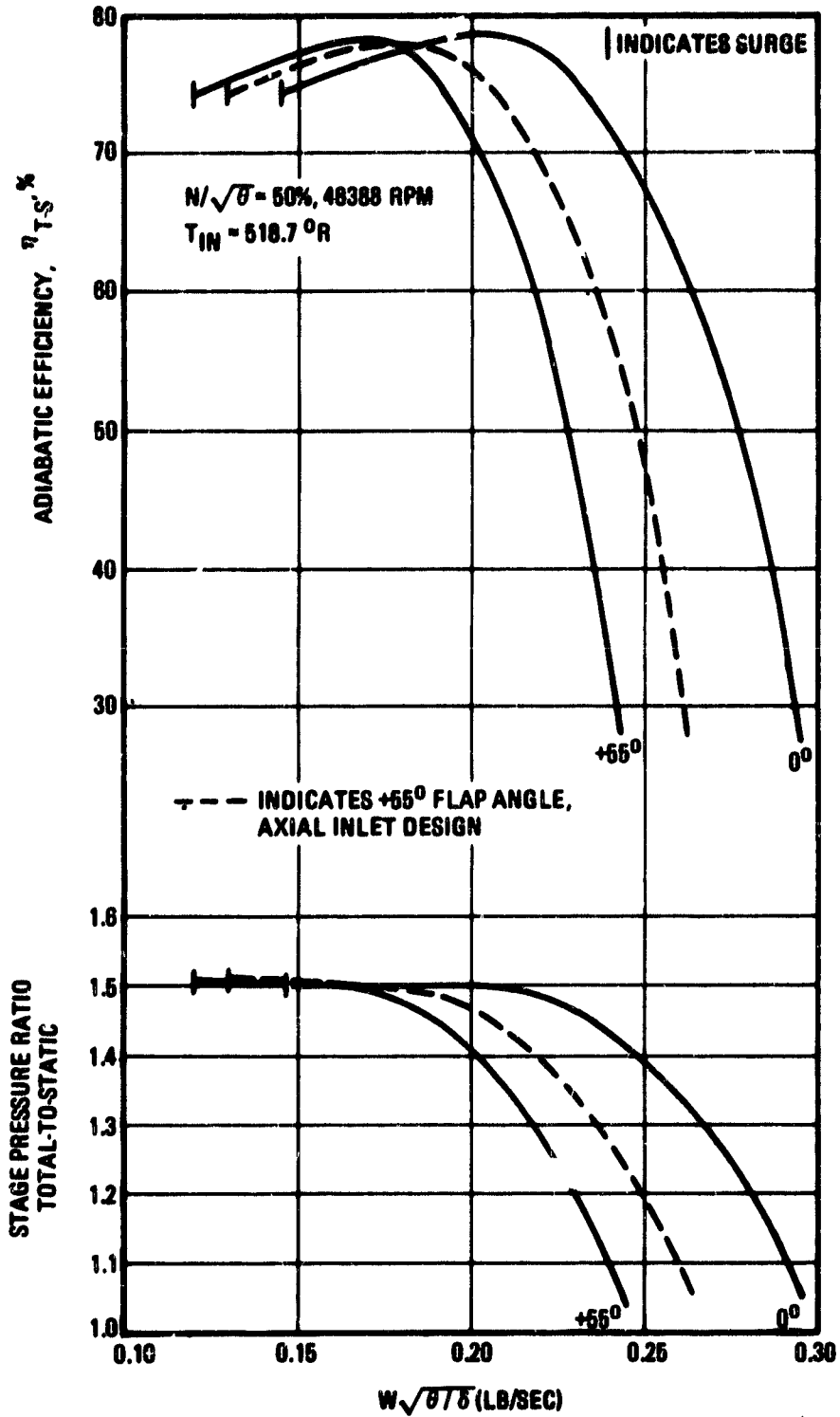
Compressor Performance with Axial VIGV
at 50 Percent Speed

Figure 25



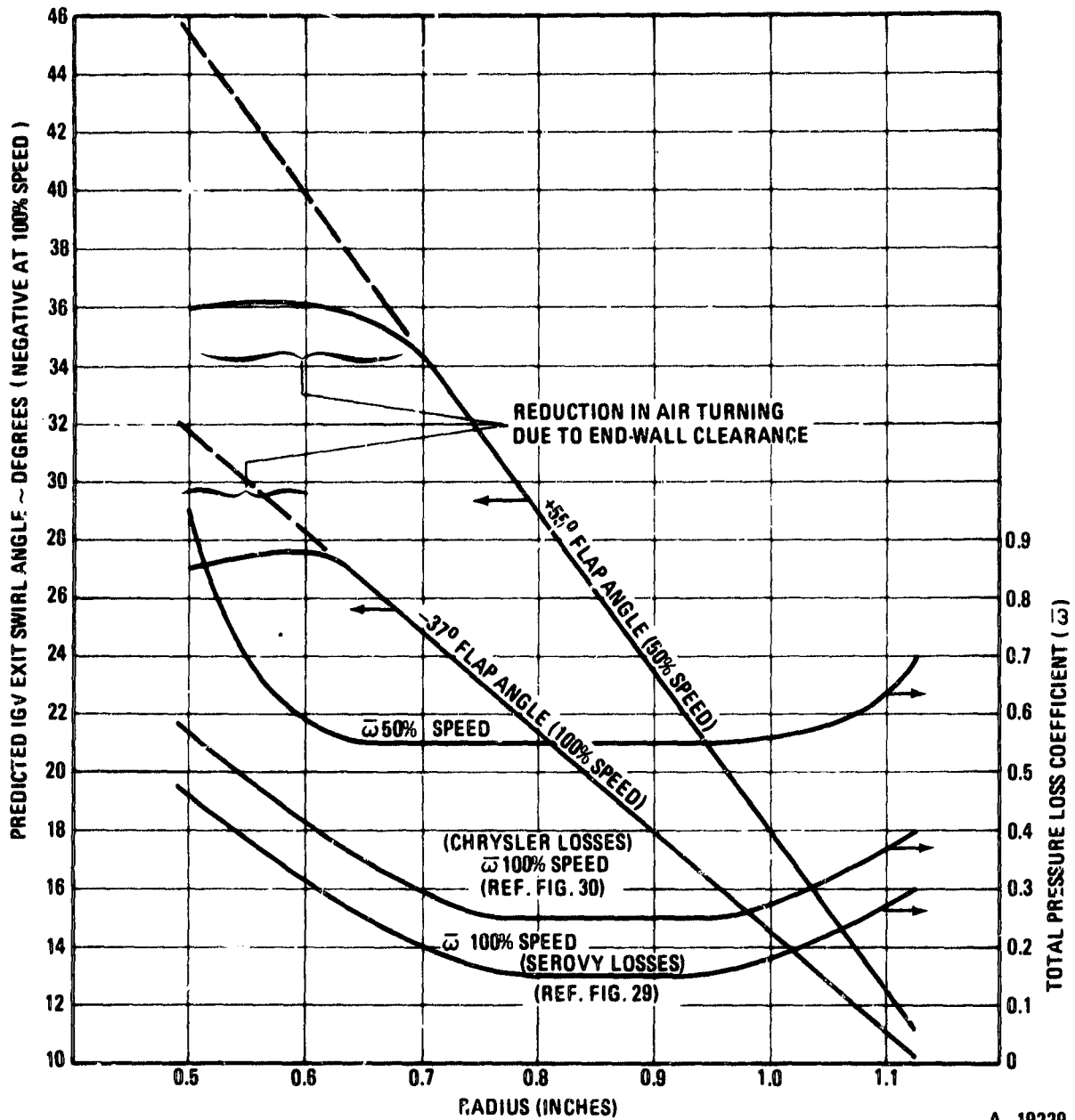
Compressor Performance with Semi-Axial VIGV at 100 Percent Speed

Figure 26



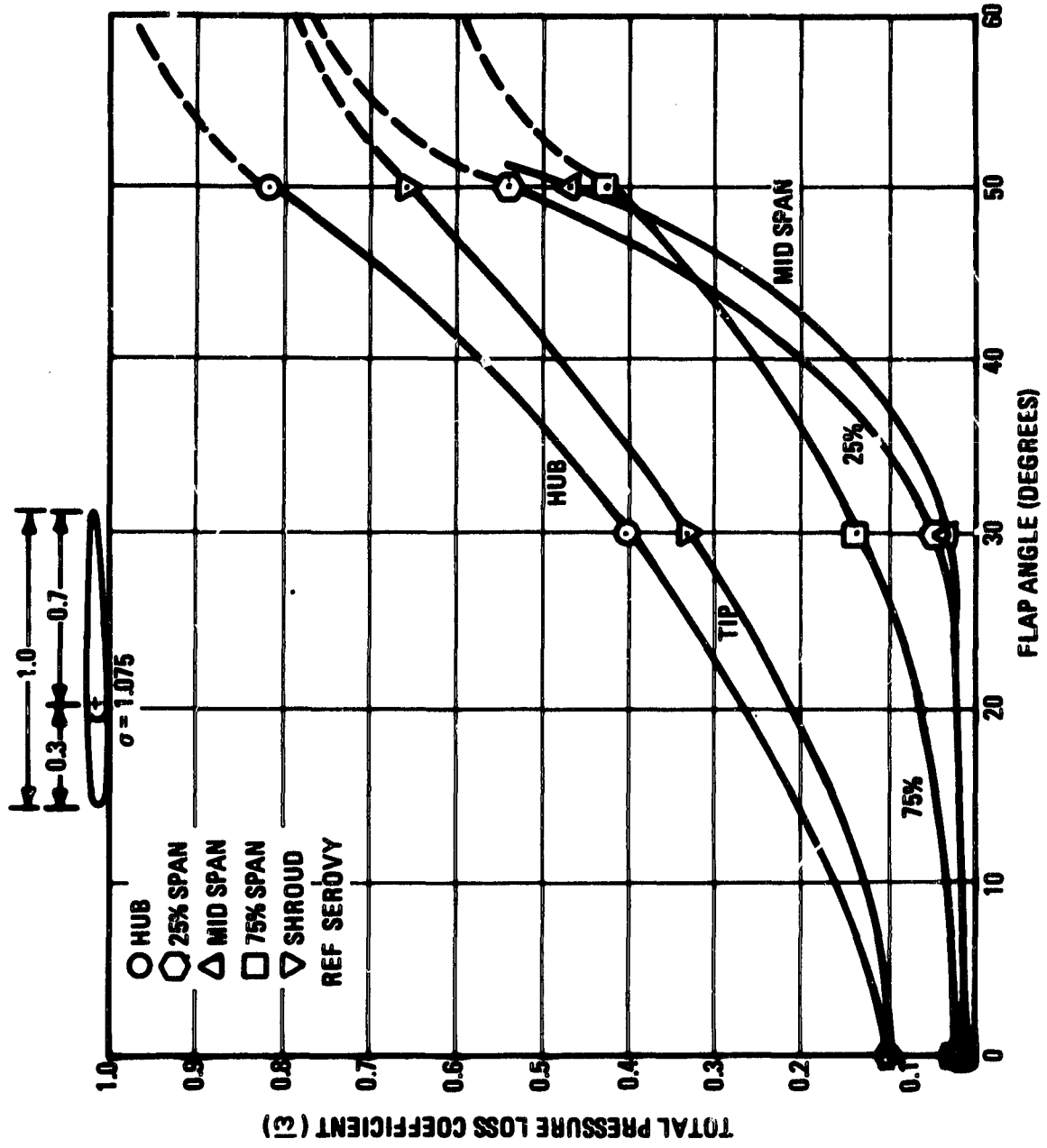
Compressor Performance with Semi-Axial VIGV at 50 Percent Speed

Figure 27



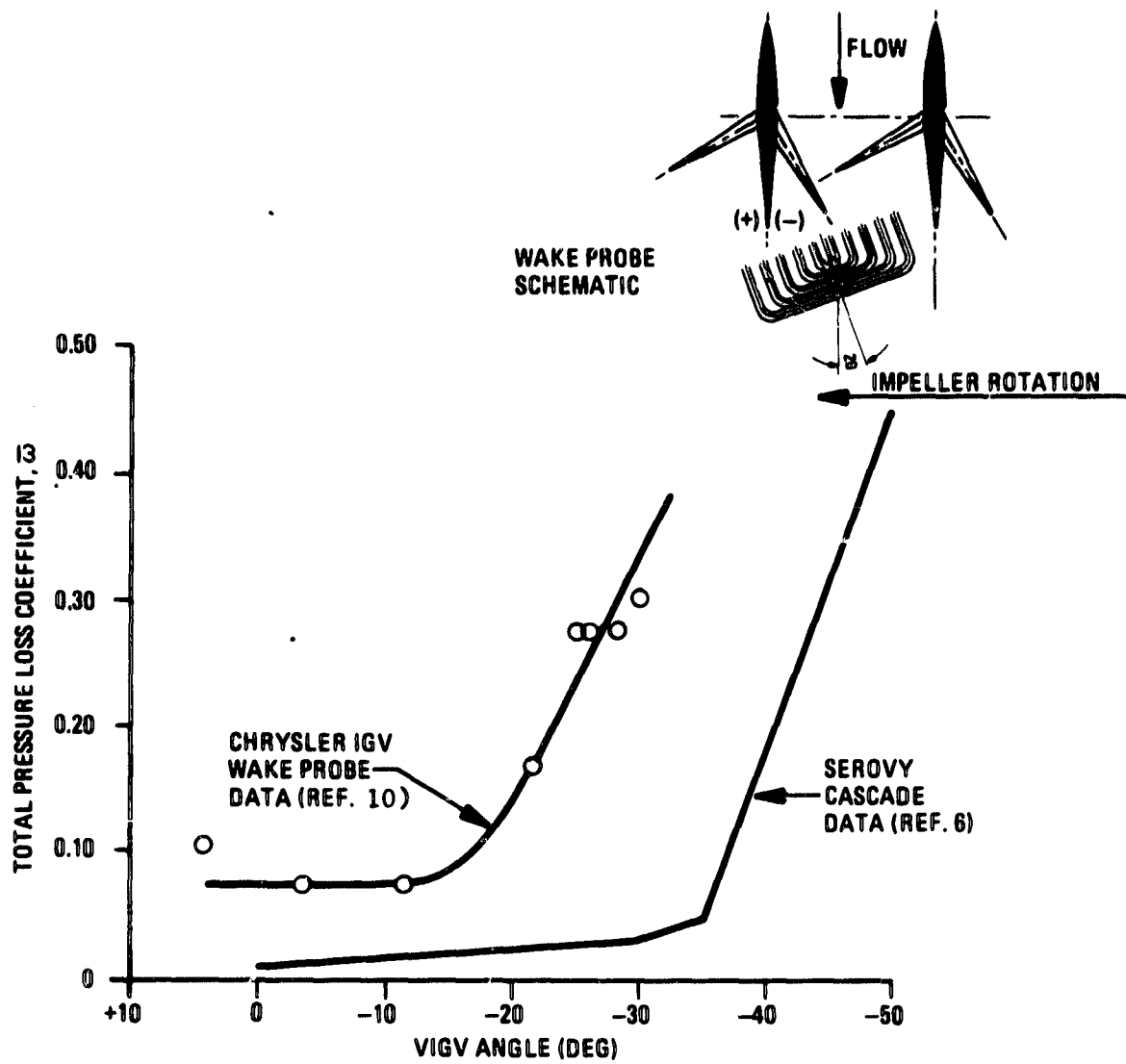
Compressor Axial Inlet VIGV Turning and Pressure Loss Model

FIGURE 28



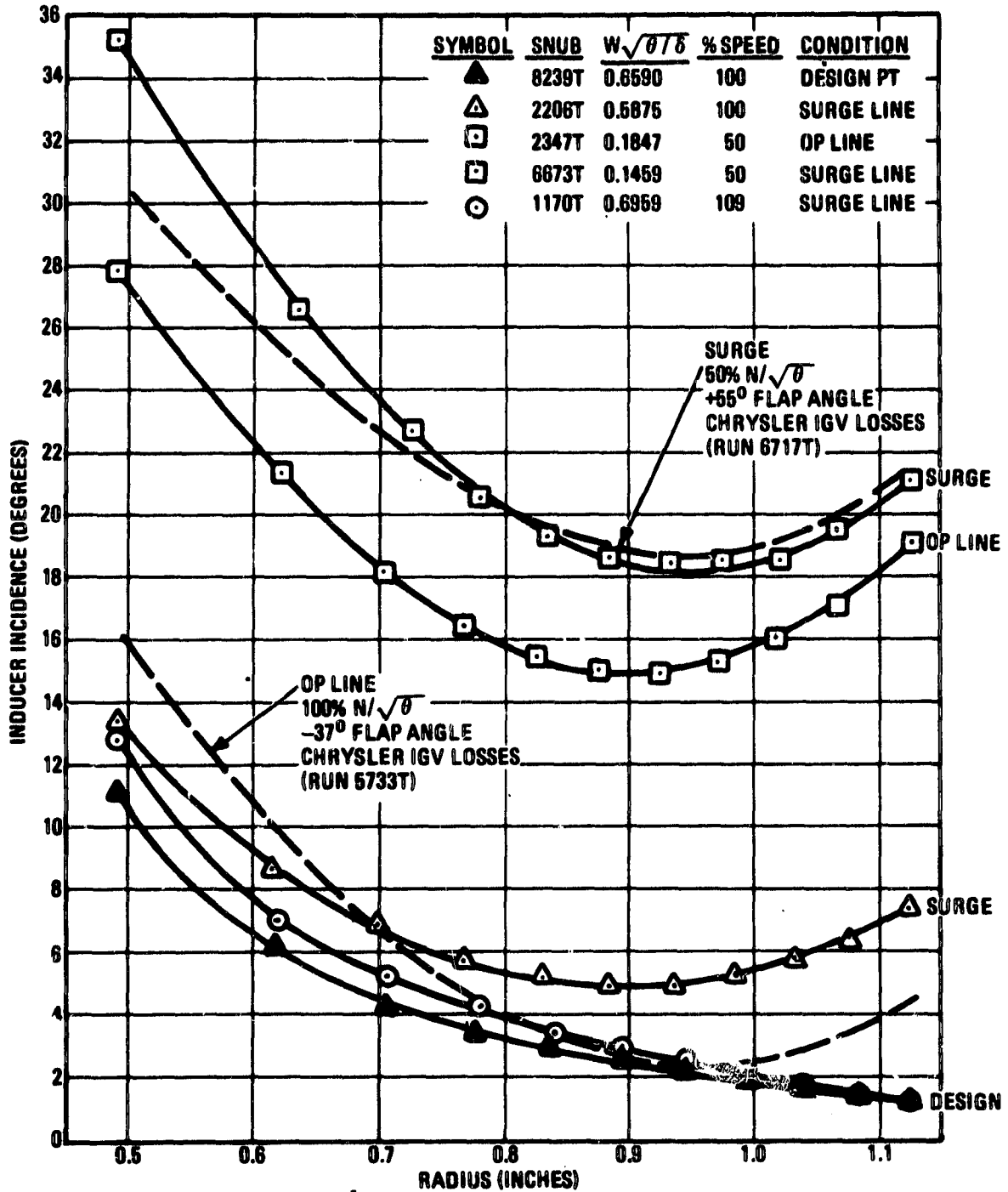
Flapped VIGV Total Pressure Loss Coefficient

Figure 29



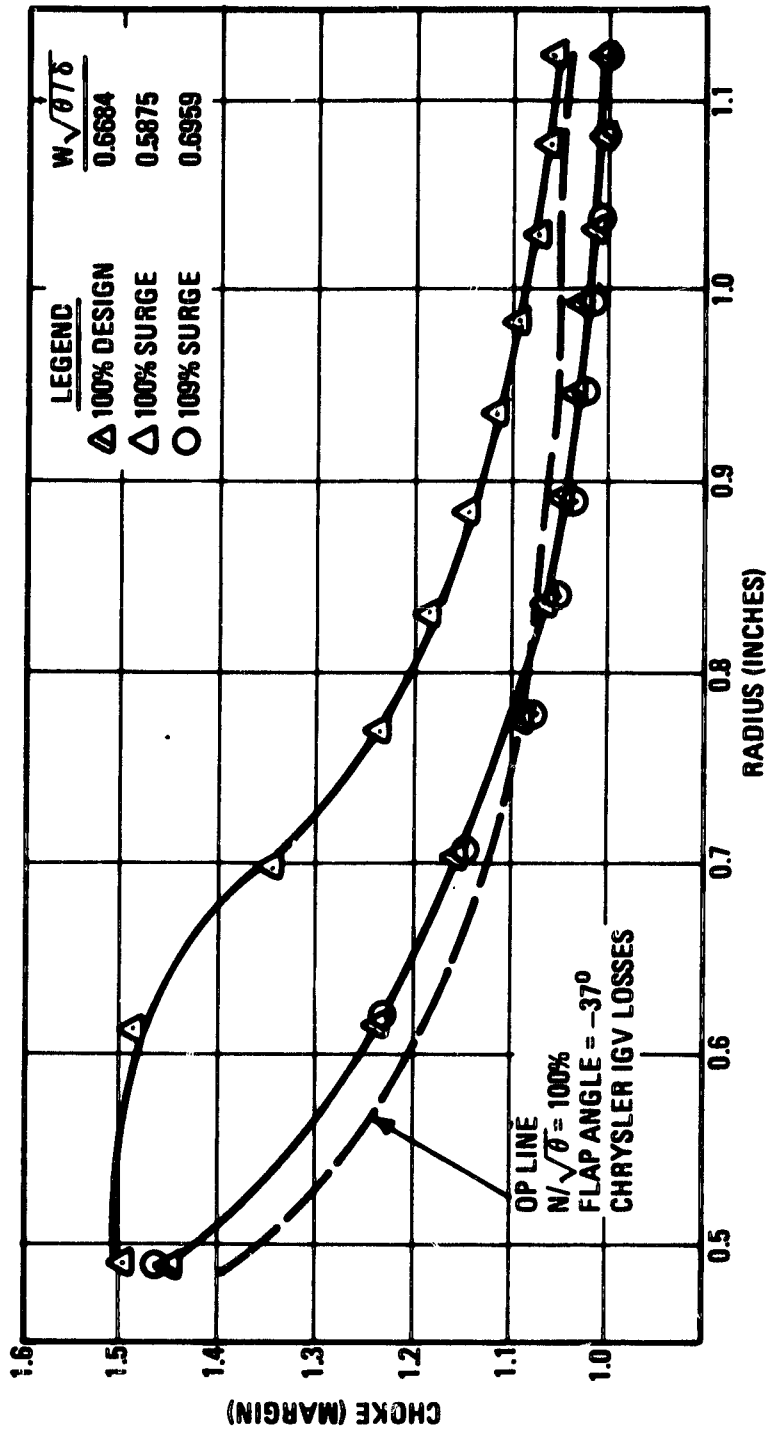
Variable Inlet Guide Vane Meanline Pressure Loss Characteristics

Figure 30



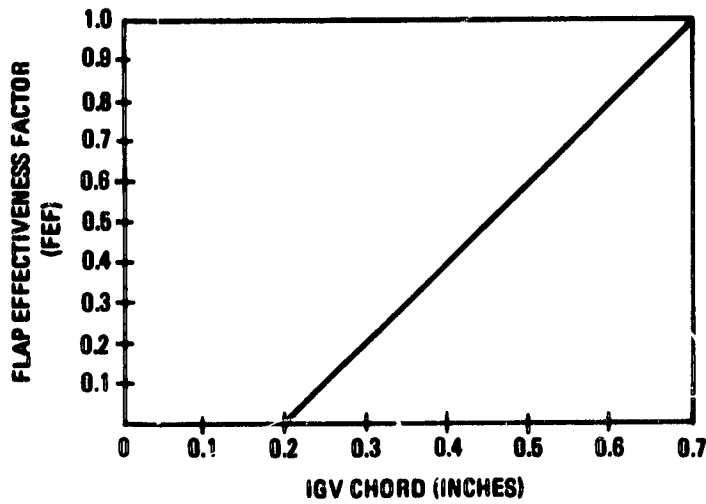
Compressor Inducer Incidence - Axial Inlet Design
Zero Inlet Swirl Angle

Figure 31



Compressor Inducer Choke Margin - Axial Inlet Flowpath
 Zero Swirl Angle

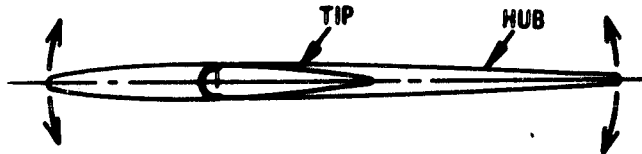
Figure 32



$$\delta = \frac{M_c \phi^\circ}{\sqrt{\sigma} \cdot \text{FEF}}$$

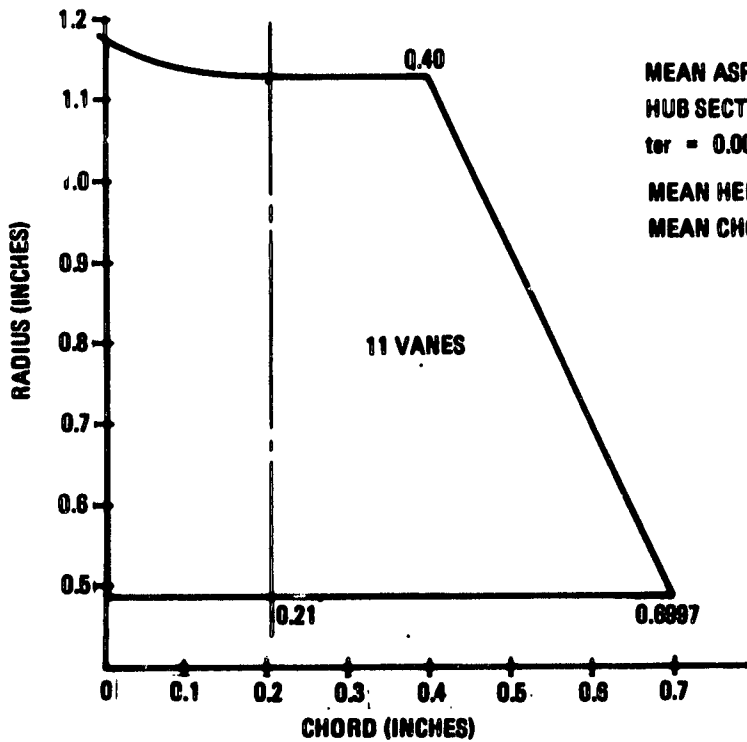
- δ = DEVIATION ANGLE
- M_c = FACTOR IN CARTER CORRELATION (FIG. 5.1.4.3.3-1)
- ϕ° = FLAP ANGLE
- σ = CASCADE STREAMLINE SOLIDITY (CHORD/SPACING)
- FEF = FLAP EFFECTIVENESS FACTOR

$t_{\text{MAX}} = 0.0632$ INCHES



MAX. THICKNESS/
CHORD RATIO

	t_{MAX}/C (%)	% FLAP CHORD
TIP	16.8	57.1
HUB	9.0	70.0



MEAN ASPECT RATIO = 1.16
 HUB SECTION IS NACA 63 SERIES
 $t_{\text{er}} = 0.0035$ IN.
 MEAN HEIGHT = 0.635 IN.
 MEAN CHORD = 0.55 IN.

Compressor Axial Inlet VIGV Design

BASIC CENTERS
EXPERIMENTAL RULE (REF. 4):
APPARATUS $\delta = \frac{M_c \phi^*}{\sqrt{\sigma}}$
2-D CASCADE
RIG
RIG
RIG
RIG

δ = EXIT DEVIATION ANGLE
 M_c = CORRELATION FACTOR
 ϕ^* = CAMBER OR FLAP ANGLE
 σ = CASCADE SOLIDITY

REF. **SYMBOL** **SOURCE**

5 ○ WHEELER - CAMBERED 65 SERIES, 10% THICK. $M < 0.25$ (MUST BE CA MEANLINE)
6 □ SEROVY - FLAPPED 0° CAMBER NACA 0005, 5% THICK. $M < 0.38$
7 △ JONES (P&W) FLAPPED NACA 63 SERIES - CAMBERED, 9% THICK, $M < 0.4$
8 ○ SAWYER (P&W) CAMBERED NACA 63 SERIES, 8% THICK (MEANLINE).
9 □ DOYLE, SHAW - 10 CA/30 C50 CAMBERED

OPEN SYMBOLS: CIRCULAR ARC MEANLINE
SOLID SYMBOLS: PARABOLIC ARC MEANLINE
FLAG ON SYMBOL: STALLED CONDITION

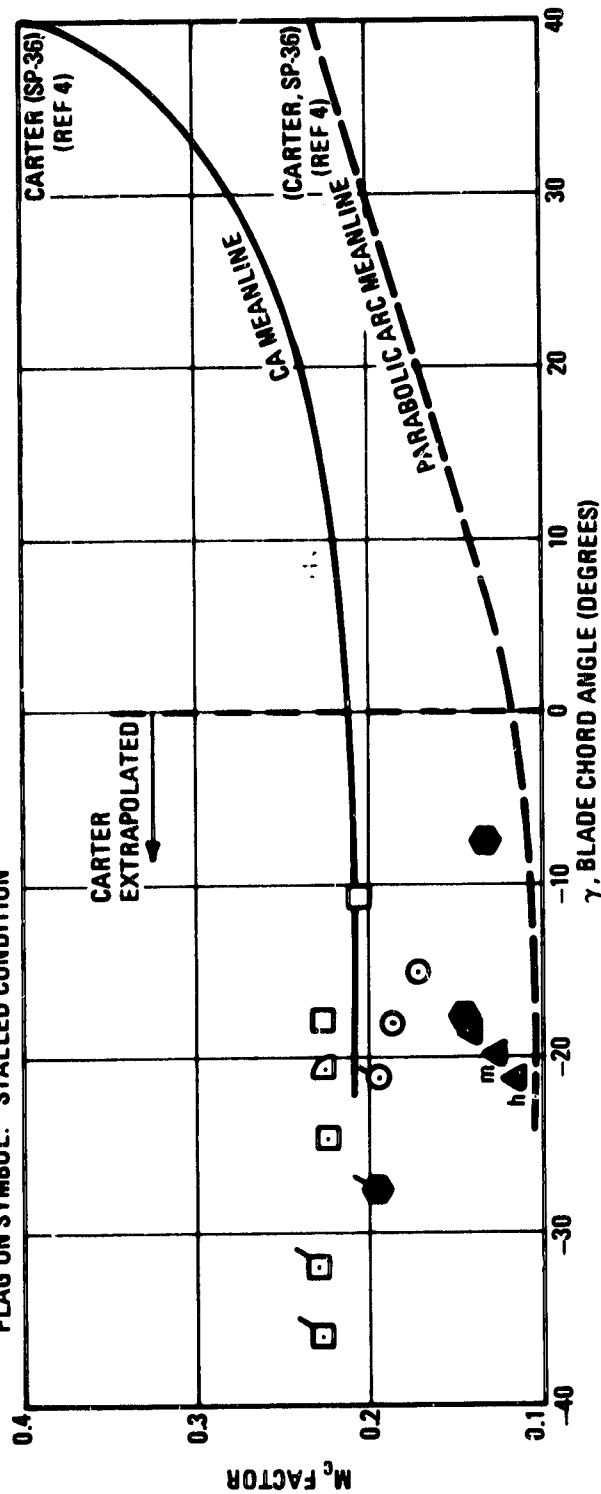
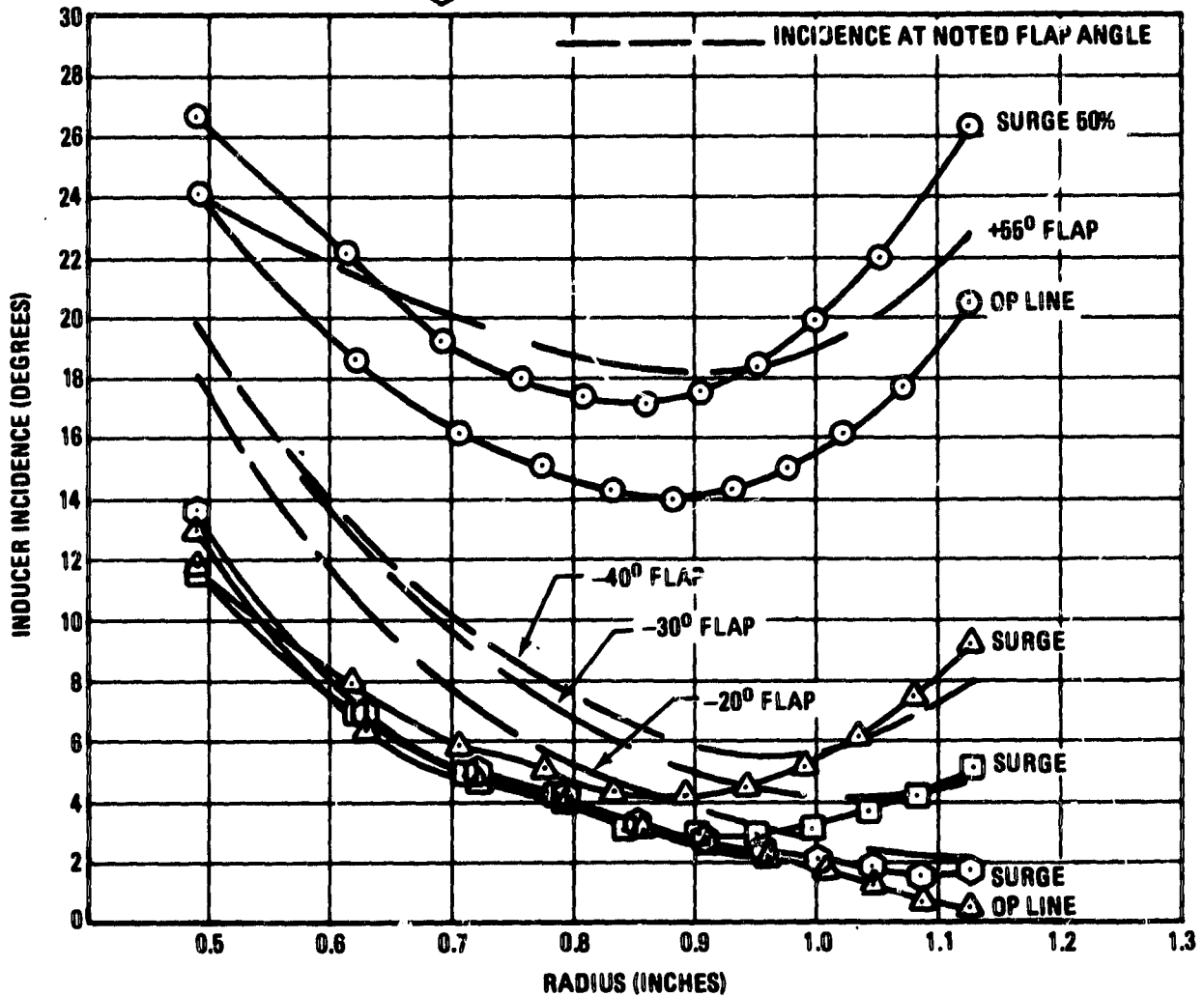


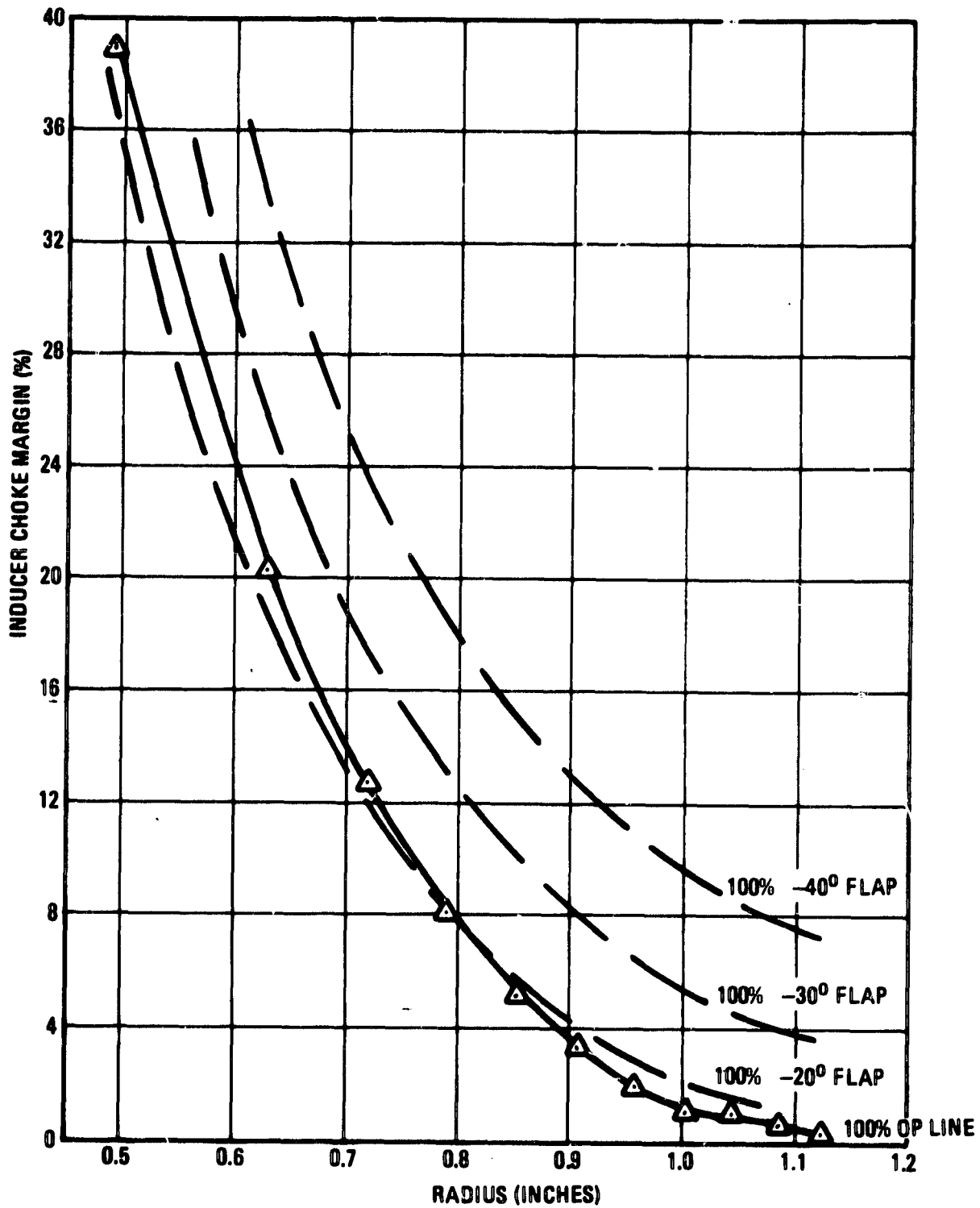
Figure 34

LEGEND			
SYMBOL	% SPEED	FLOW	CONDITION
○	50	0.1469	SURGE
○	50	0.1875	OP LINE
△	100	0.8690	OP LINE
△	100	0.6875	SURGE
□	106	0.6543	SURGE
⊙	109	0.6959	SURGE



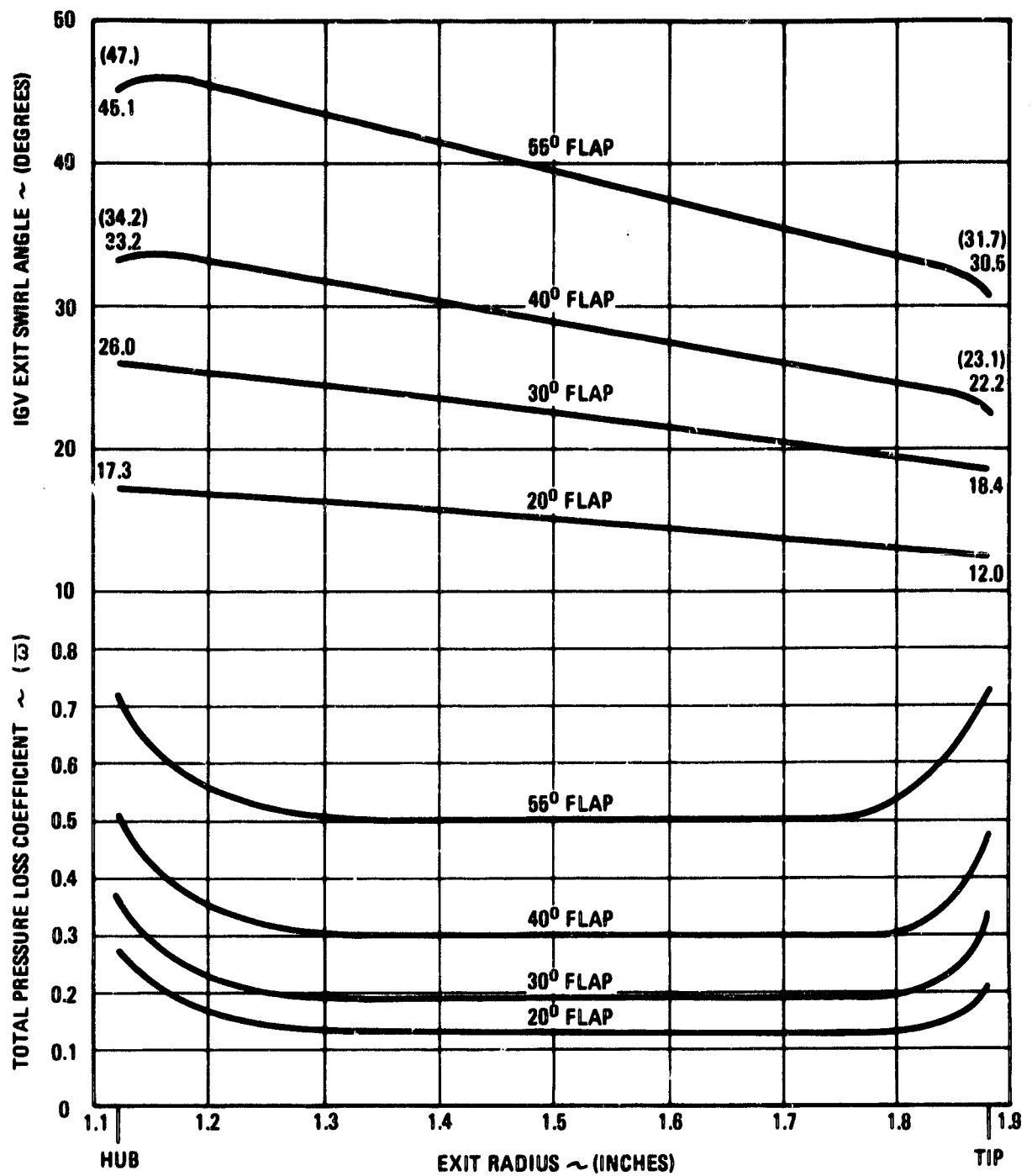
Compressor Inducer Incidence - Semi-Axial Inlet Design
Zero Inlet Swirl Angle

Figure 35



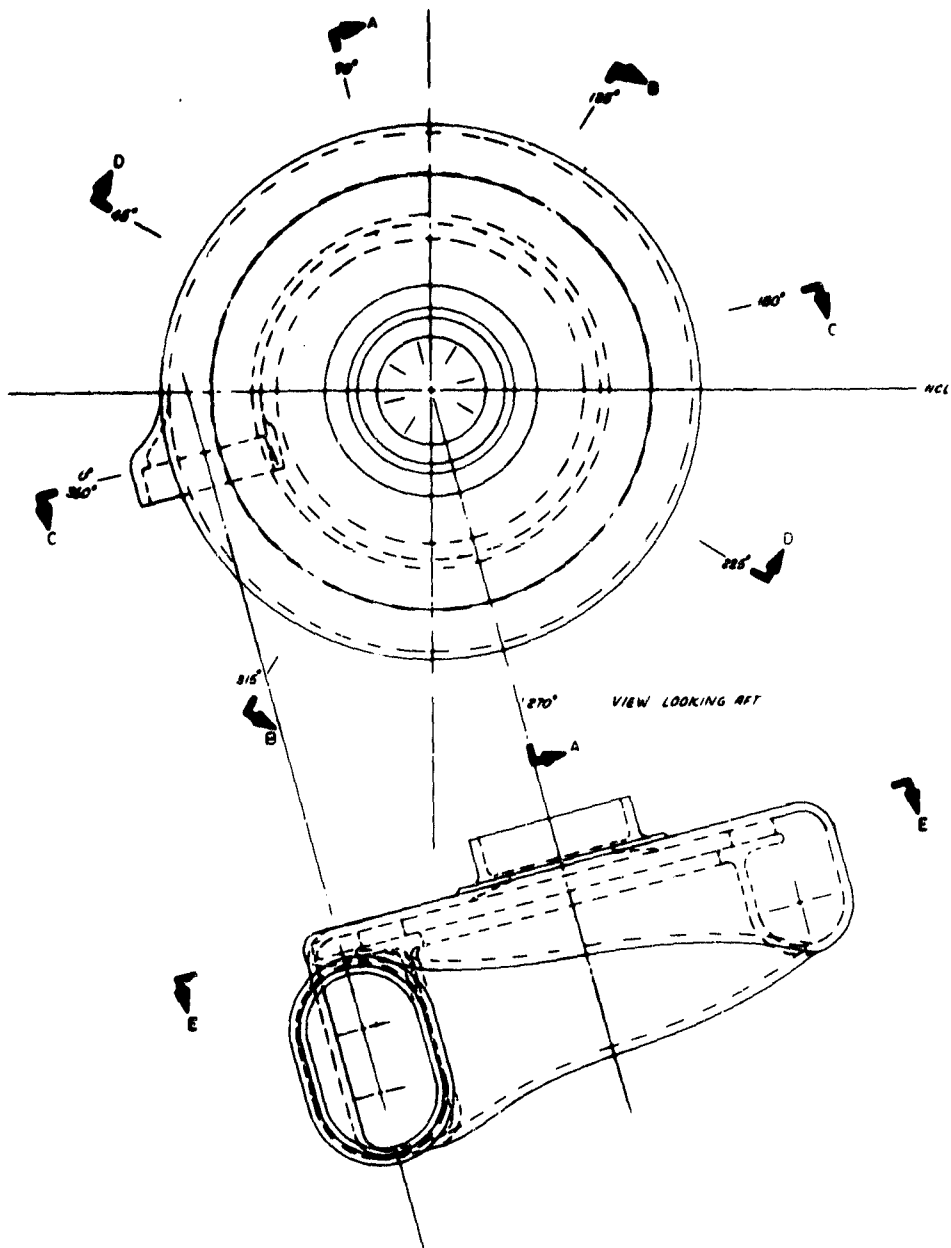
Compressor Inducer Choke Margin - Semi-Axial Inlet Design
Zero Swirl Angle

Figure 36



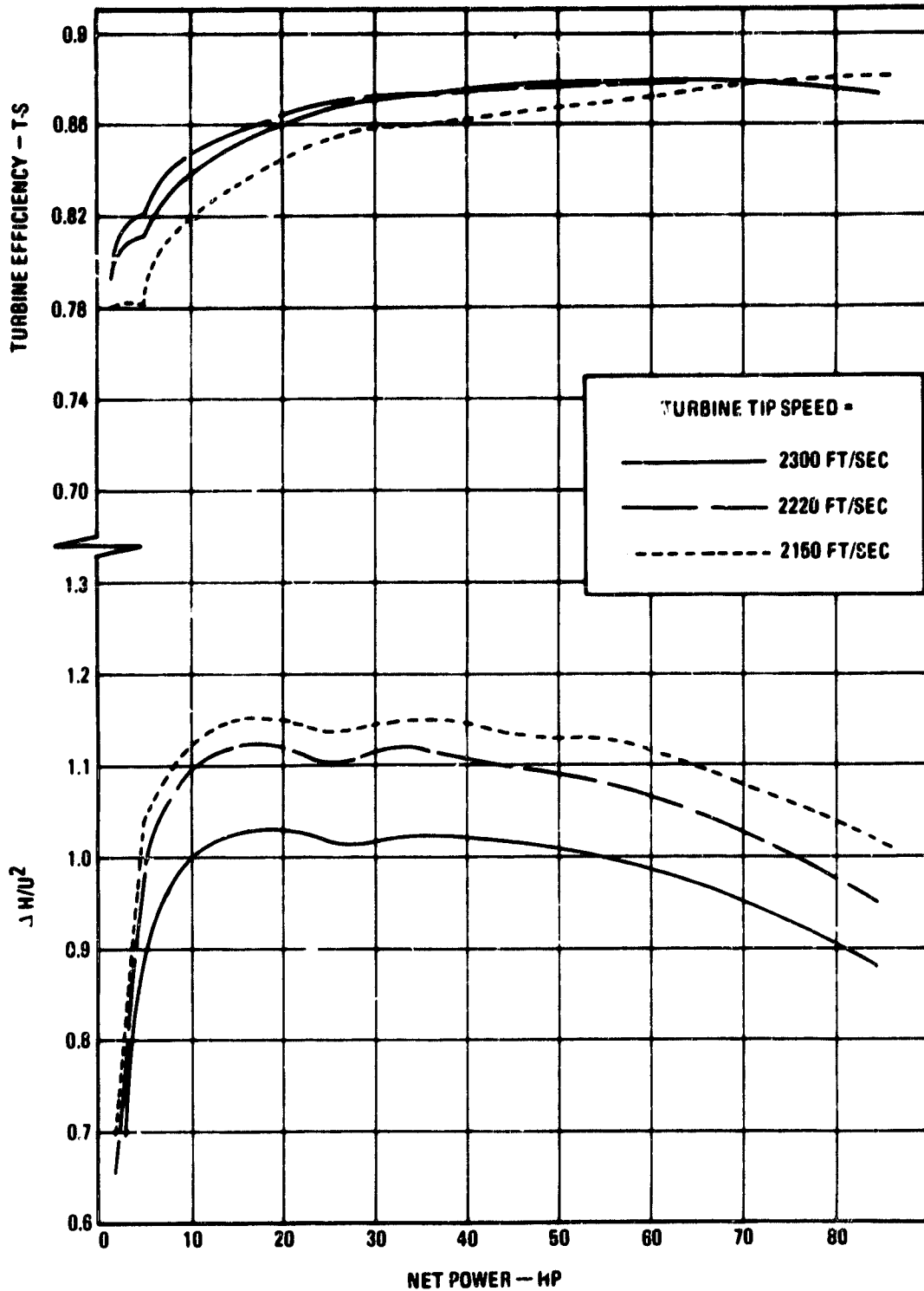
Compressor Semi-Axial VIGV Performance

Figure 37



Radial Turbine Inlet Scroll

Figure 38



Radial Turbine Tip Speed Comparison

Figure 39

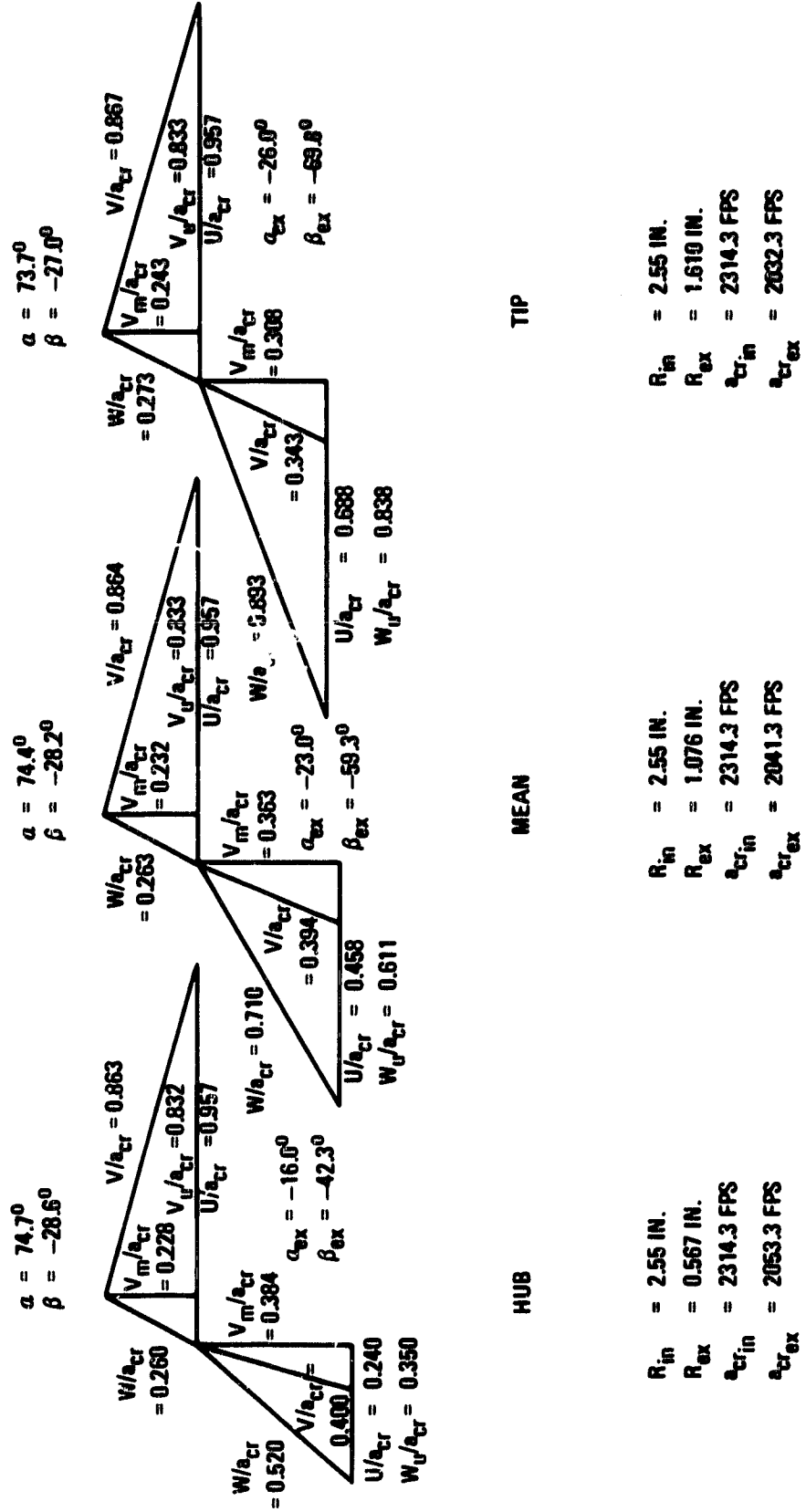
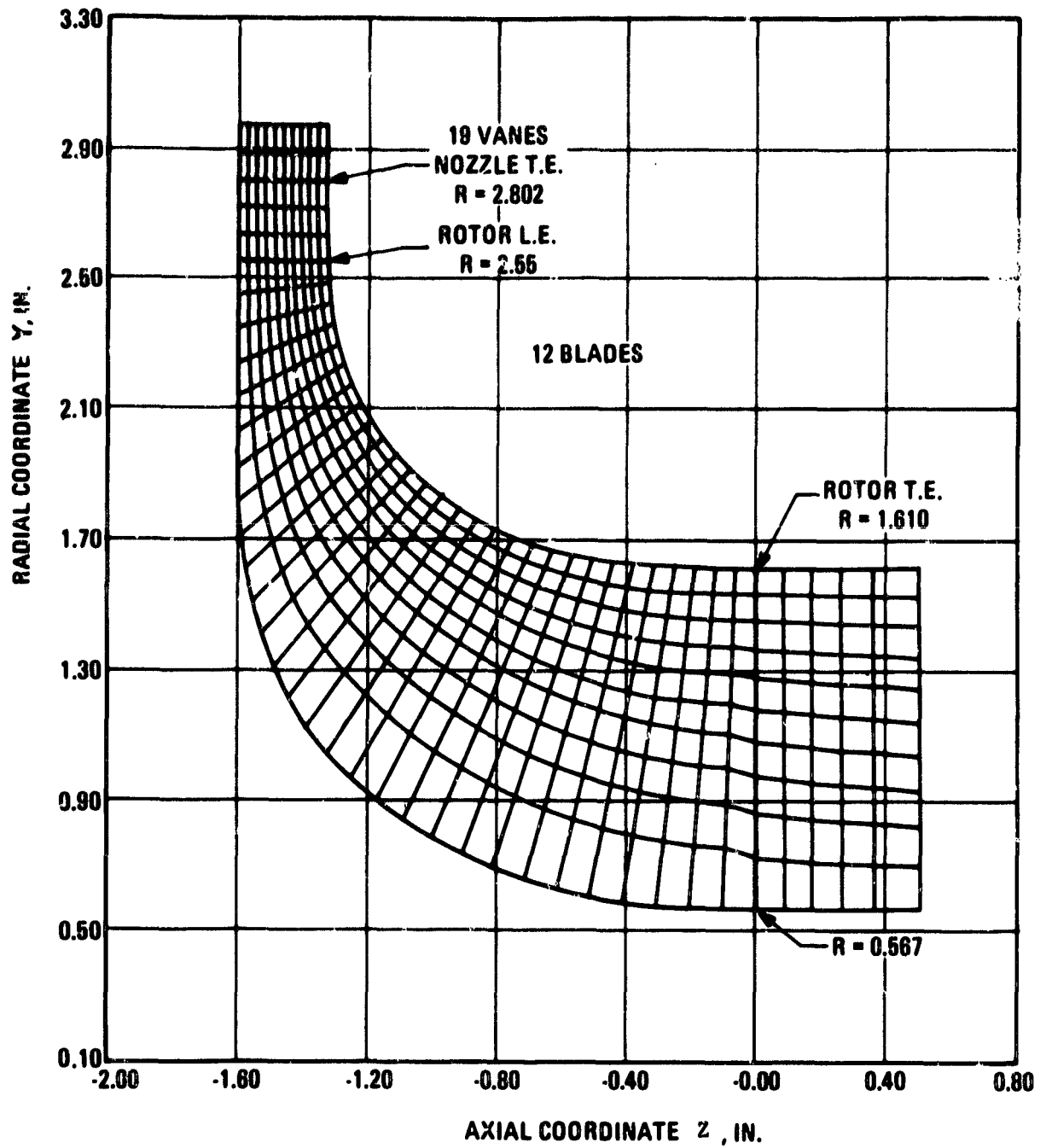


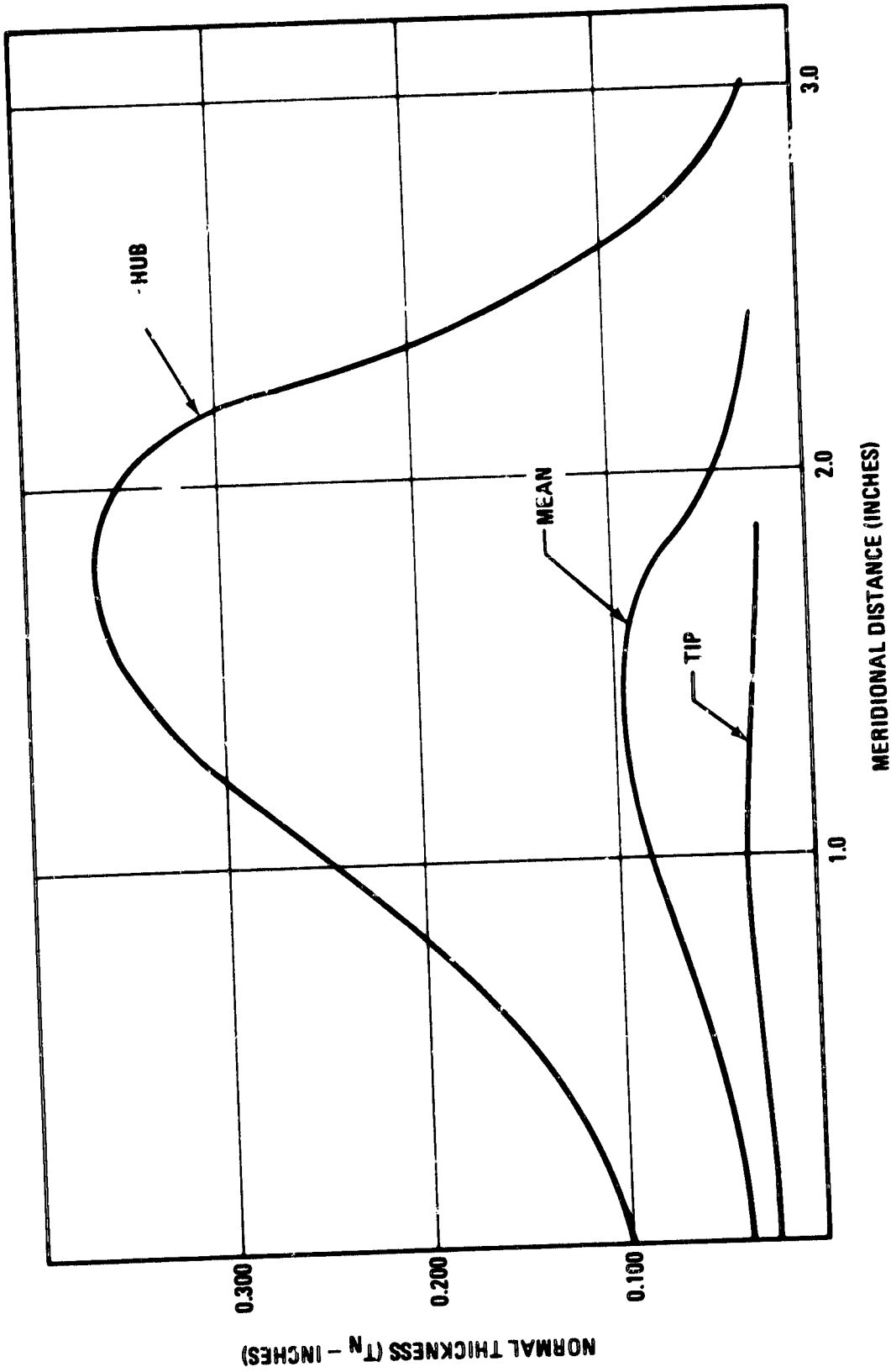
Figure 40

Radial Turbine Velocity Triangles at 100 Percent Speed



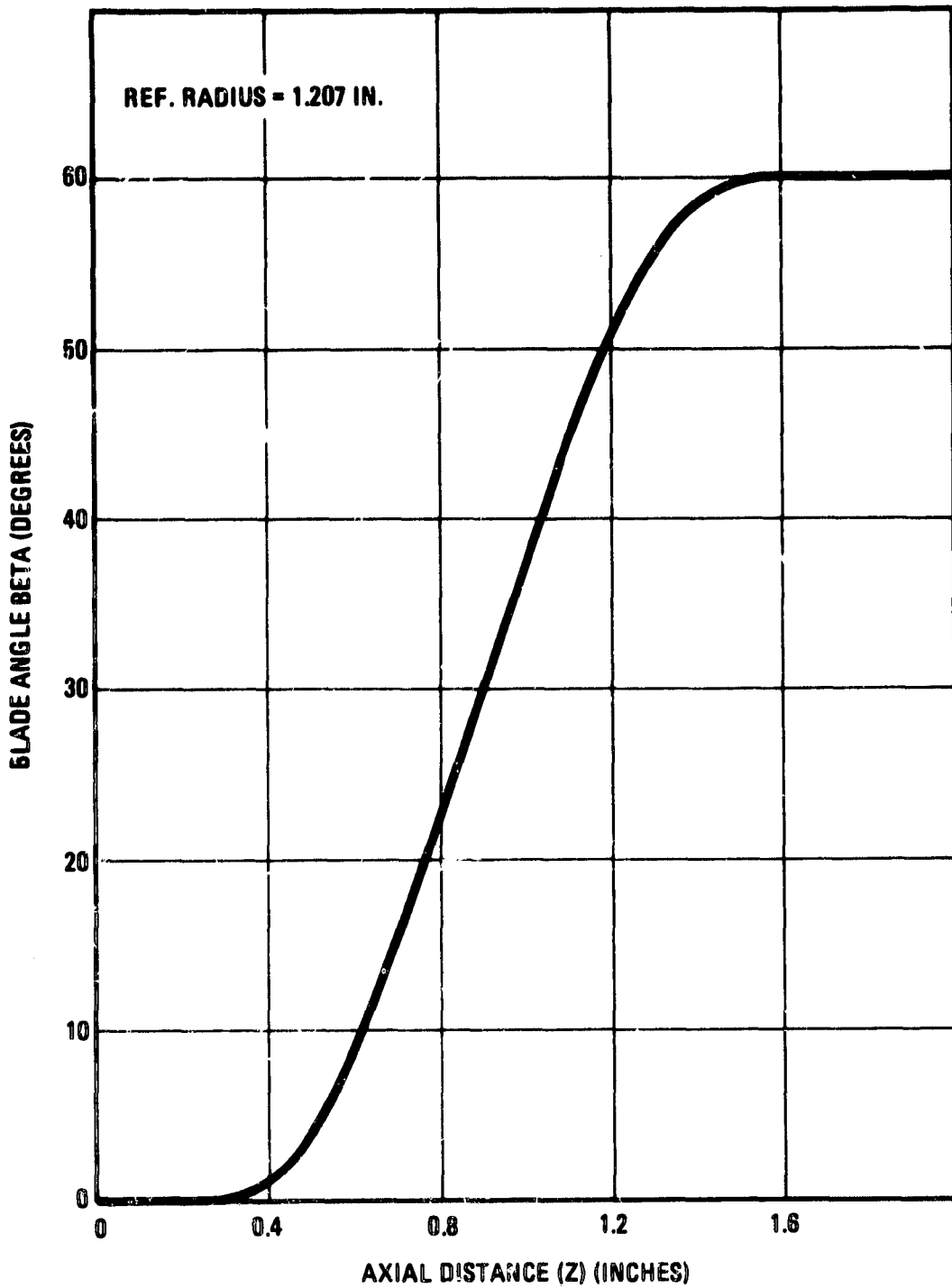
Radial Turbine Rotor Flowpath

Figure 41



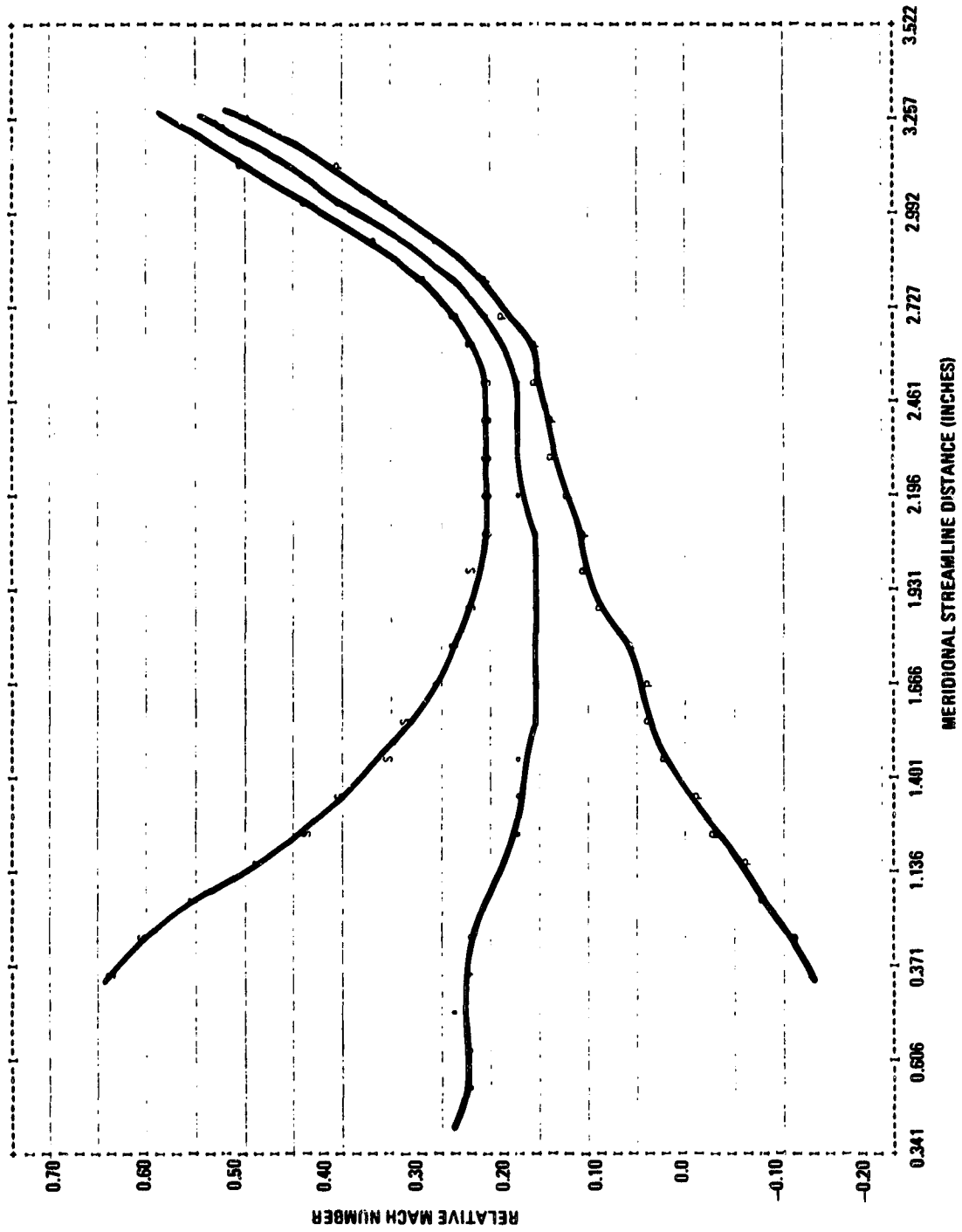
Radial Turbine Blade Normal Thickness Distribution

Figure 42



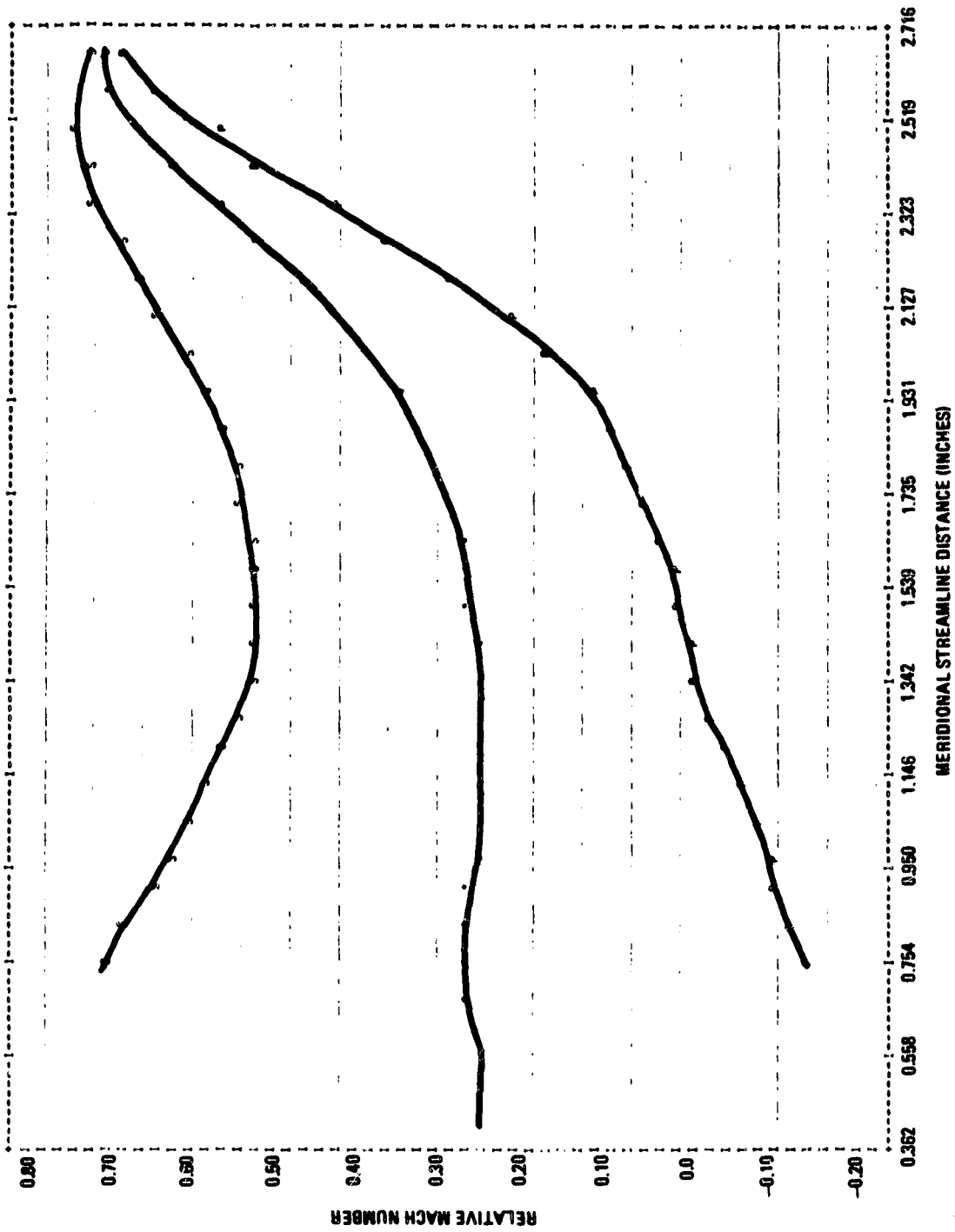
Radial Turbine Blade Angle Distribution
at Constant Radius

Figure 43



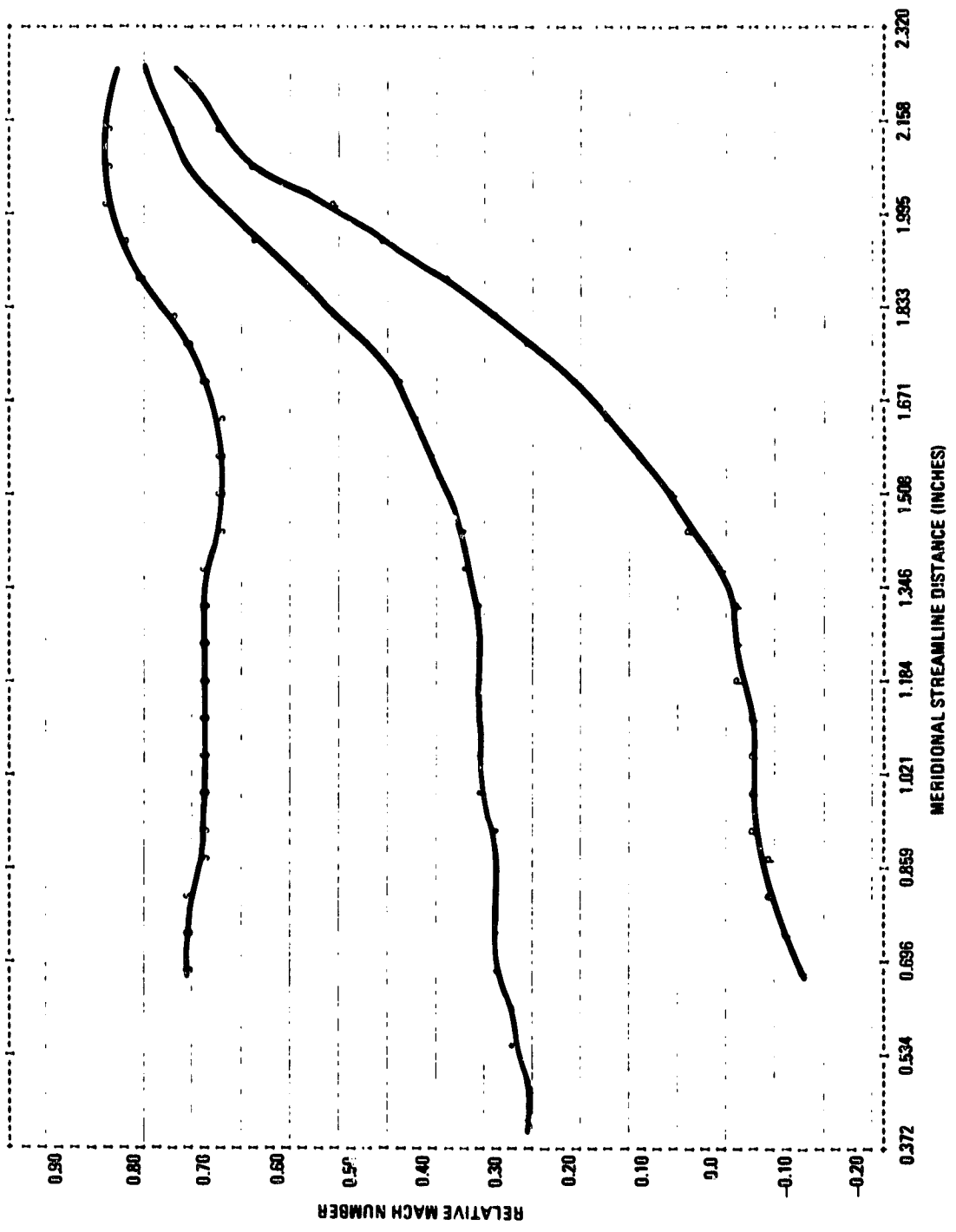
Radial Turbine Hub Streamline Loading

Figure 44



Radial Turbine Mean Streamline Loading

Figure 45



Radial Turbine Shroud Streamline Loading

Figure 46

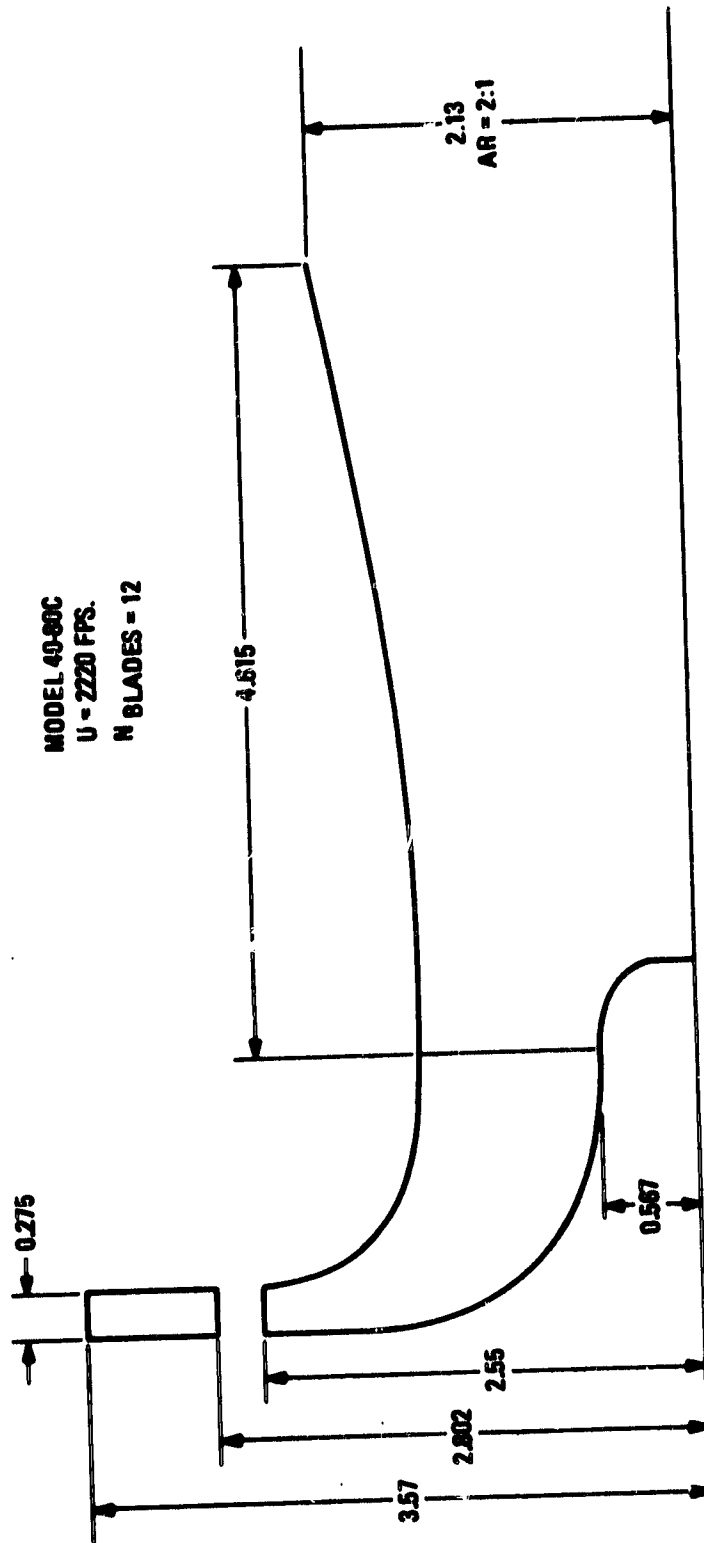
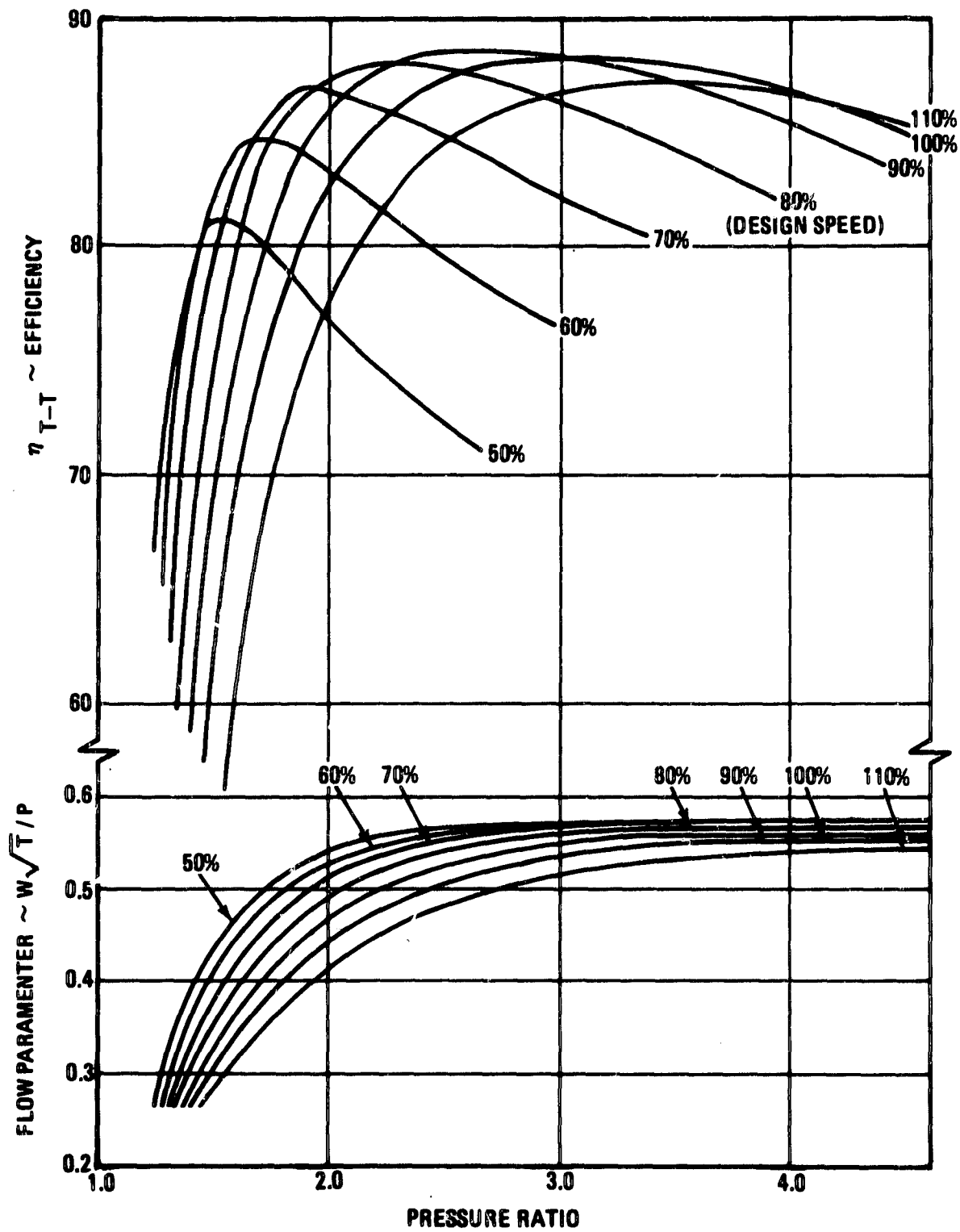


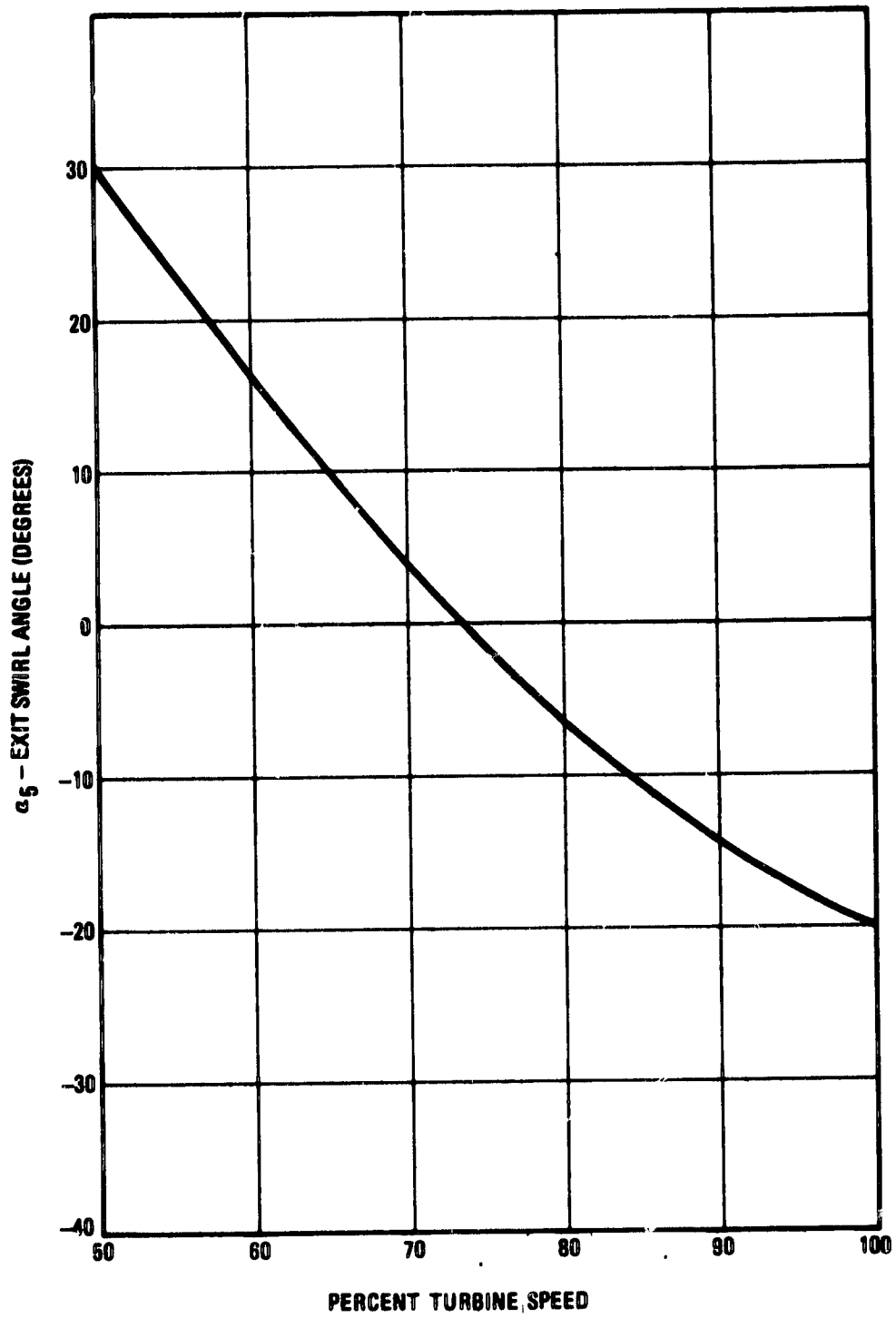
Figure 47

Radial Turbine Exhaust Diffuser



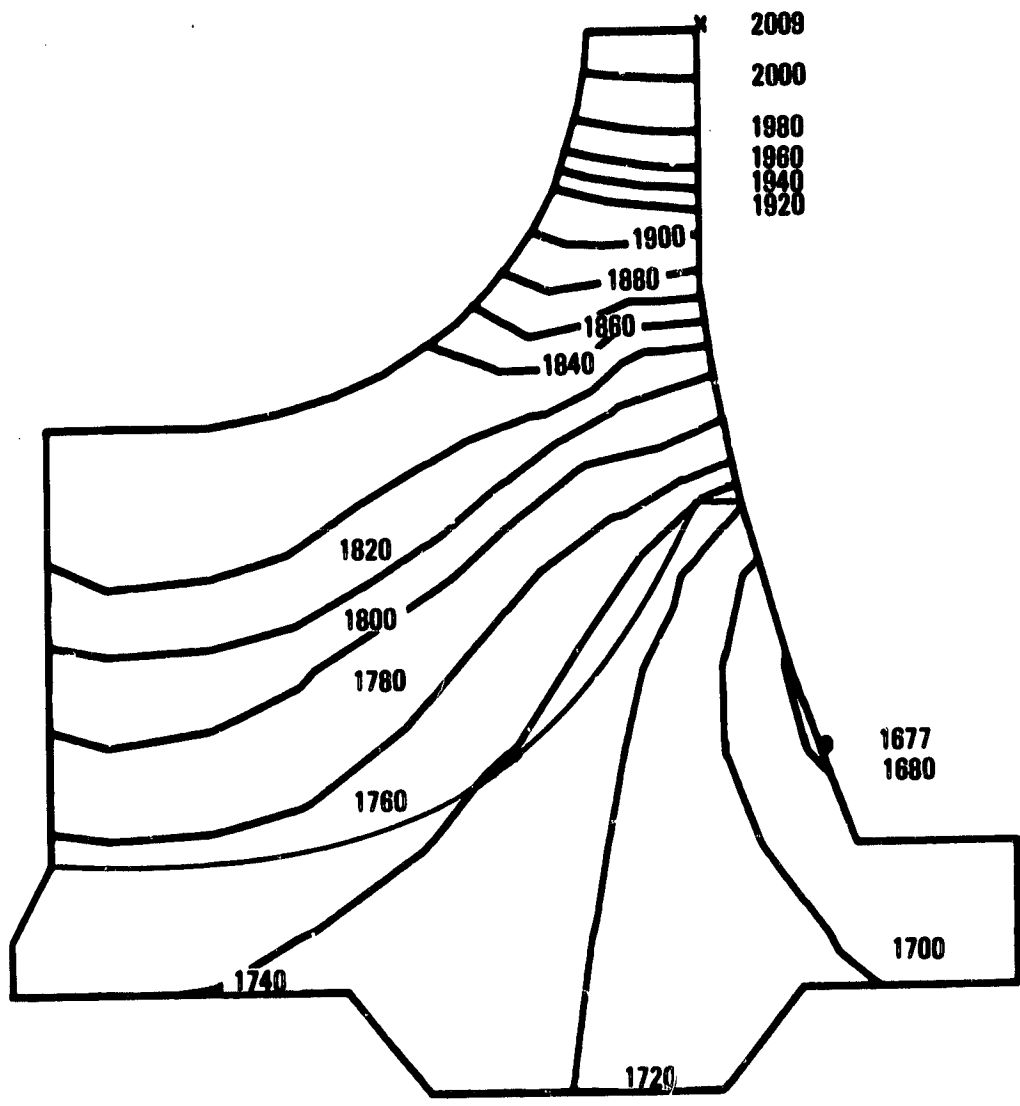
Radial Turbine Performance

Figure 48



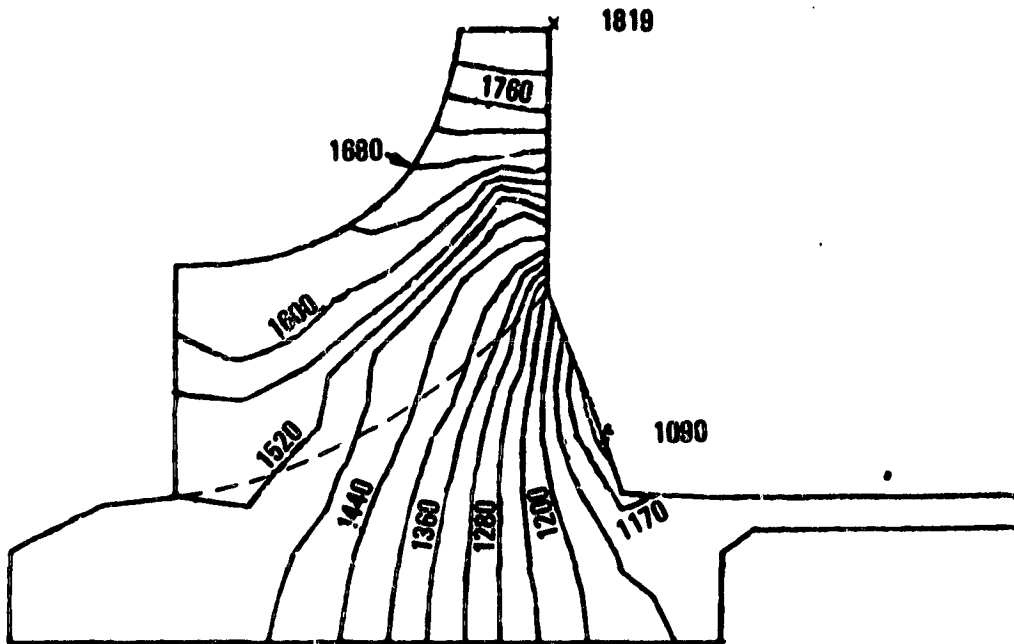
Radial Turbine Exit Swirl Angle

Figure 49



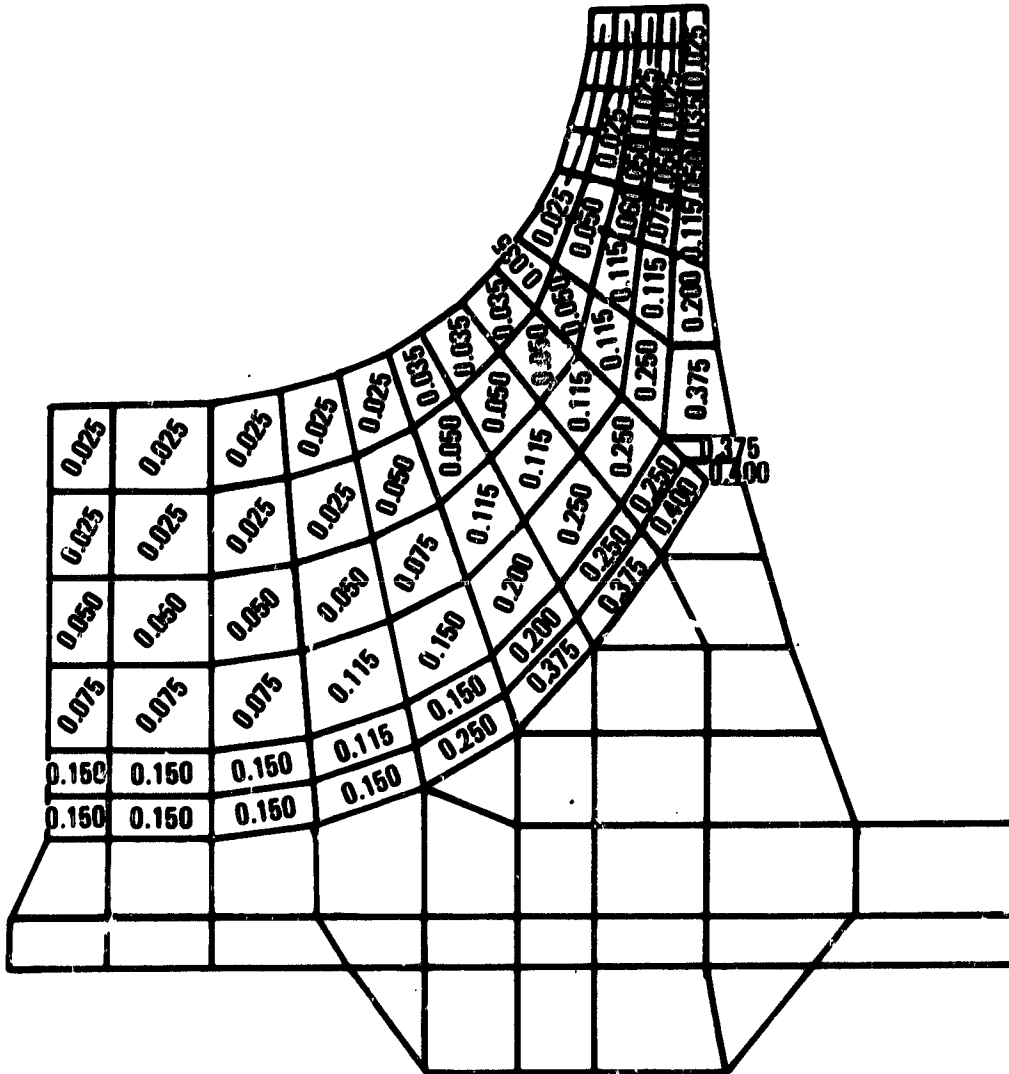
Ceramic Turbine Rotor Temperature (°F)

Figure 50



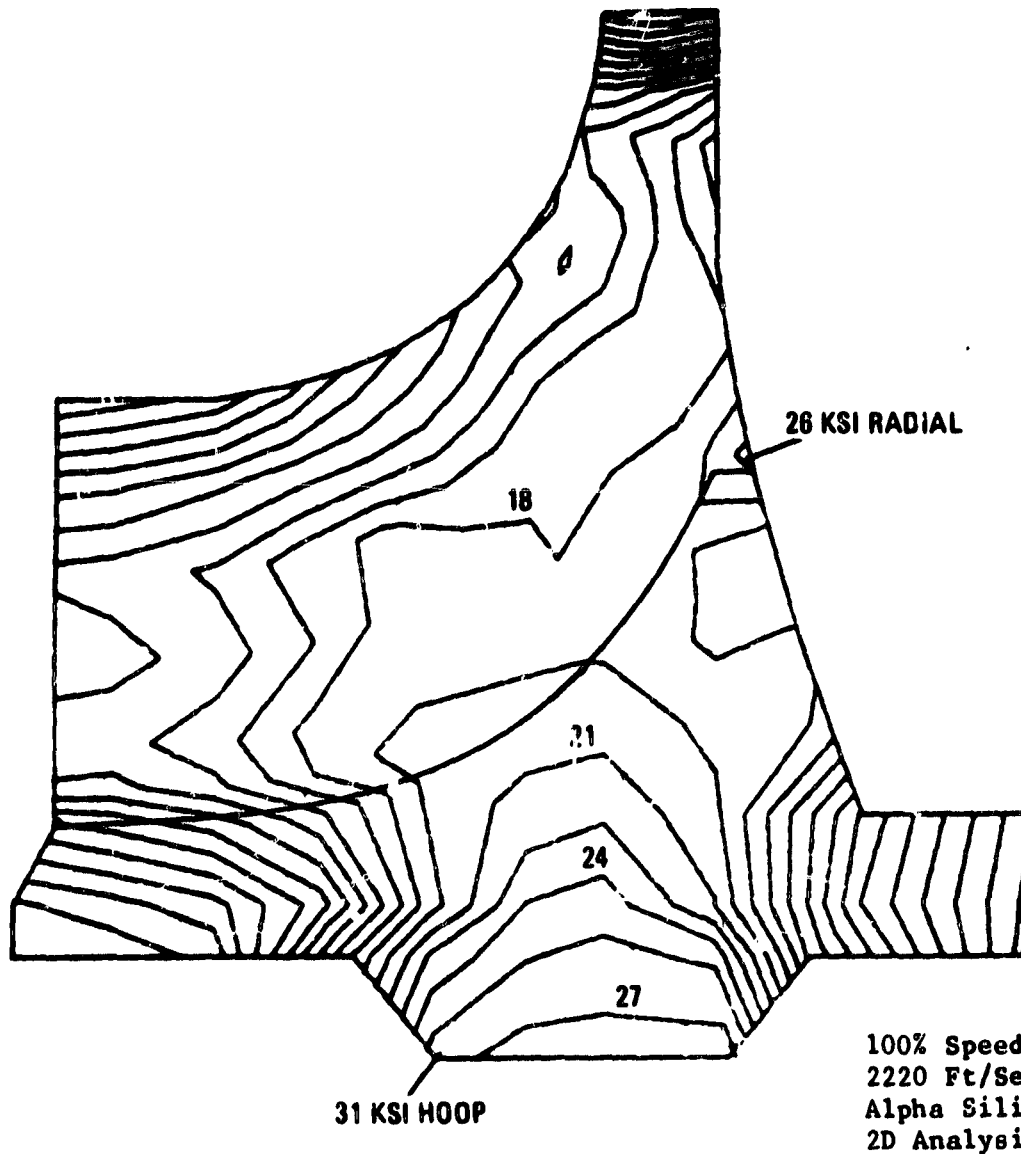
Metal Turbine Rotor Temperature (°F)

Figure 51



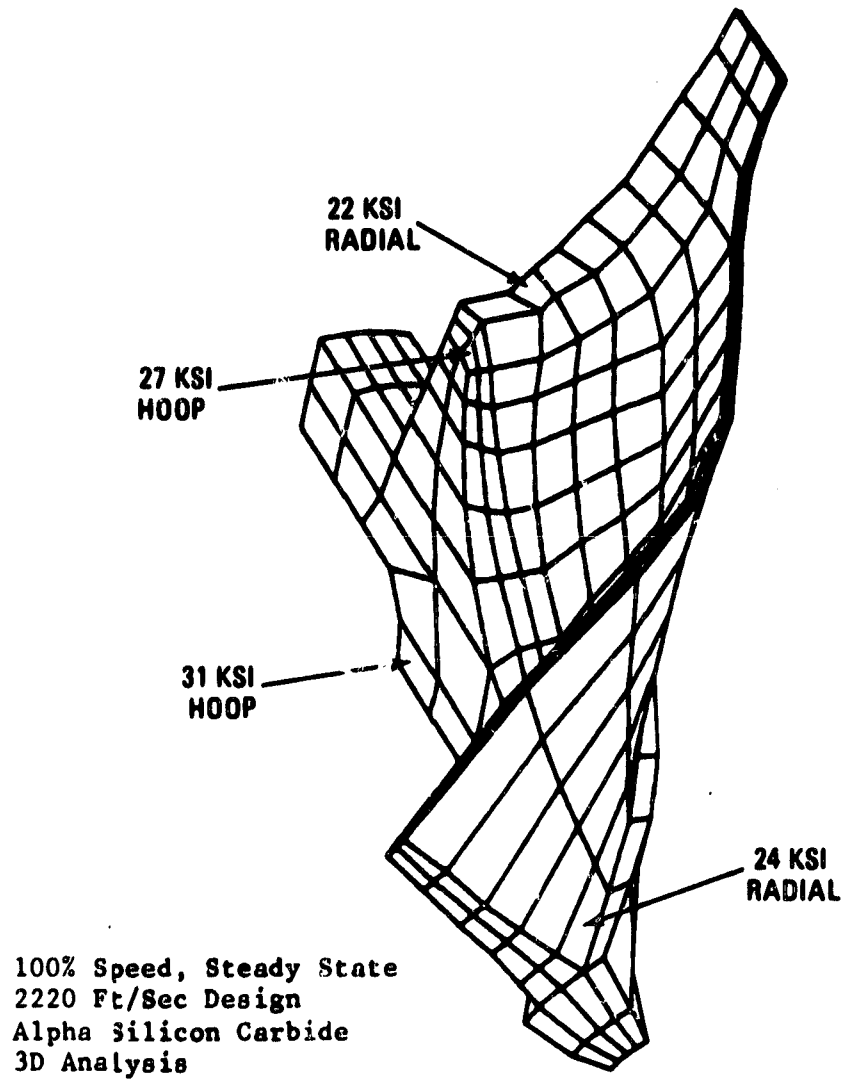
Ceramic Turbine Rotor Blade Thickness Distribution

Figure 52



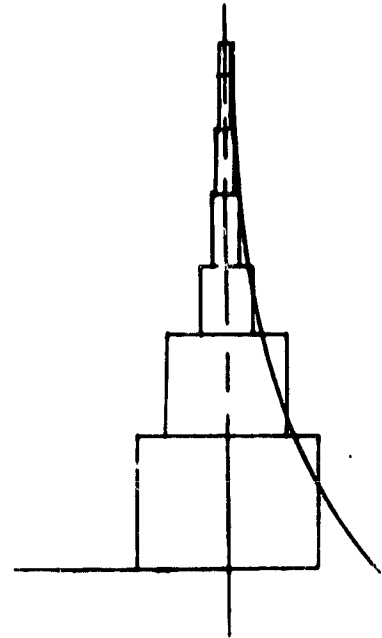
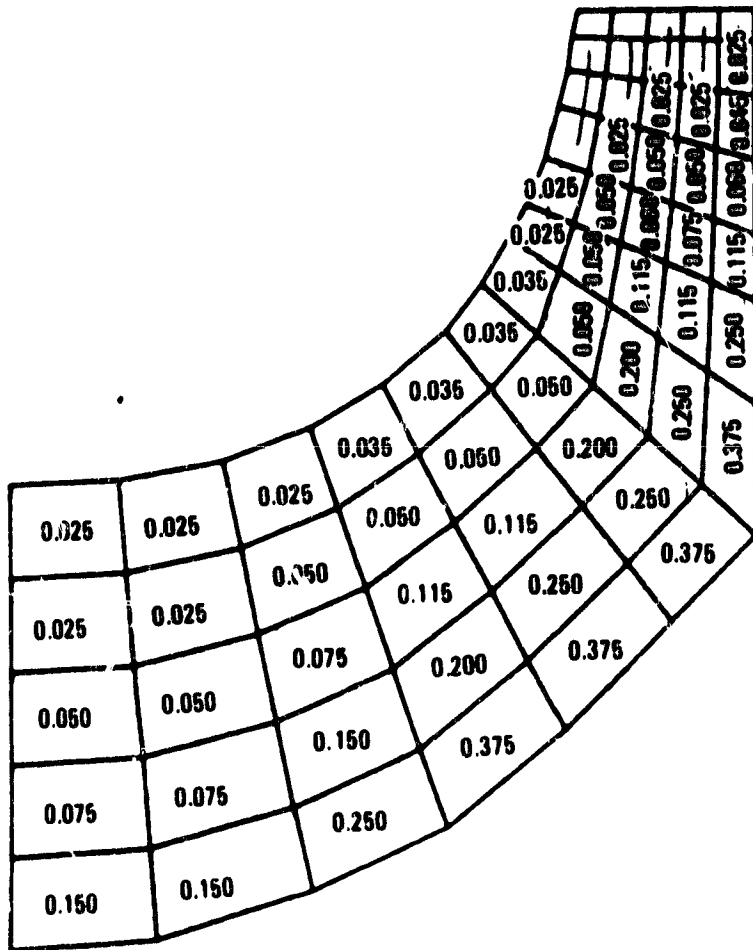
Ceramic Turbine Rotor Stress

Figure 53



Ceramic Turbine Rotor Centrifugal Stress

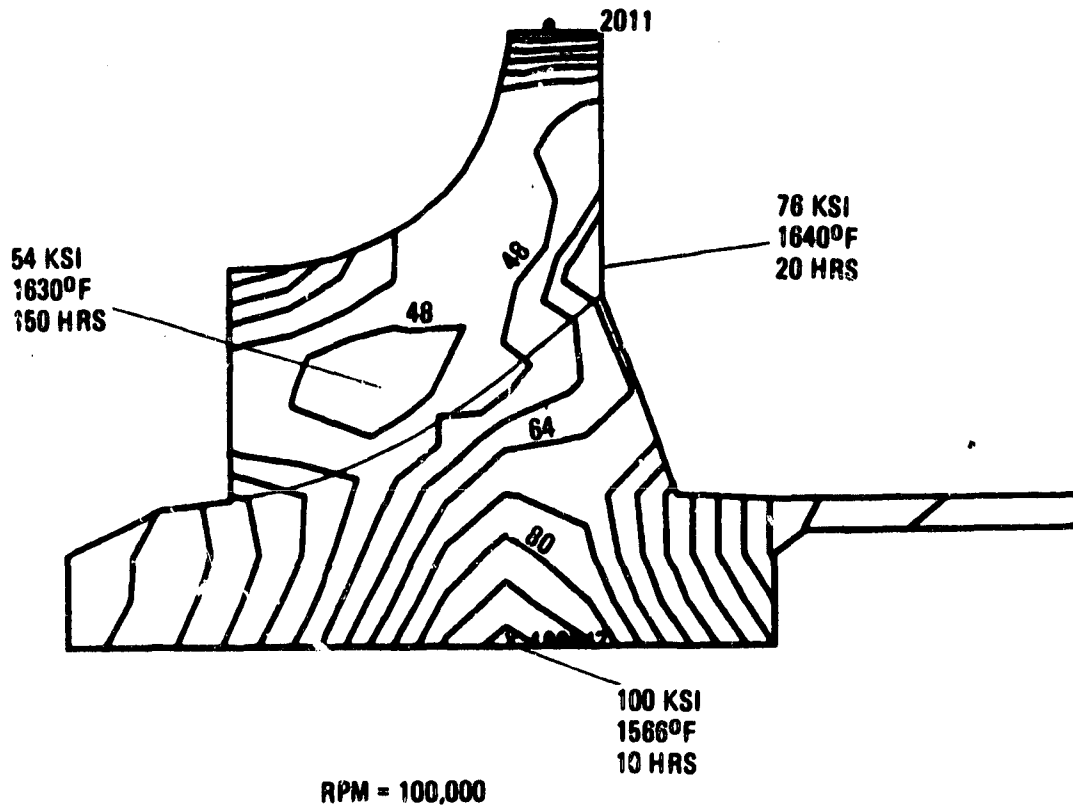
Figure 54



Metal Turbine Rotor Blade Thickness

Figure 55

ORIGINAL PAGE IS
OF POOR QUALITY

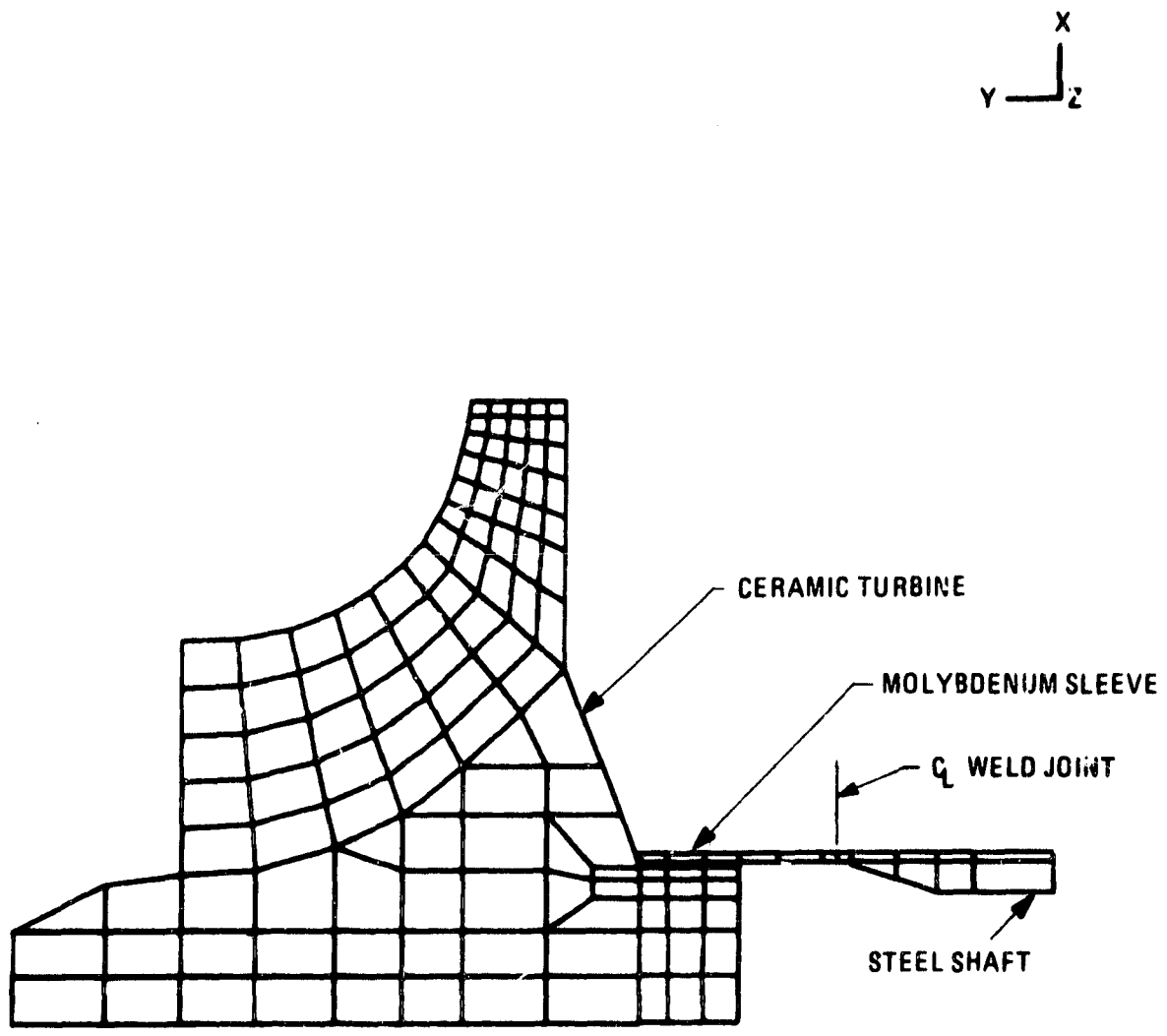


100% Speed, Steady State
2150 Ft/Sec Design
Mar-M 247
2D Analysis

Metal Turbine Rotor Stress

Figure 56

C-3



Ceramic Turbine Rotor Shaft Attachment
Finite Element Model

Figure 57

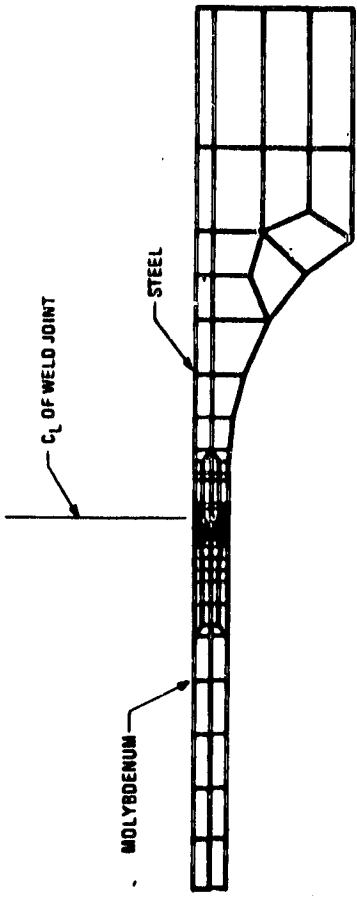


Figure 58 - Micro-Model

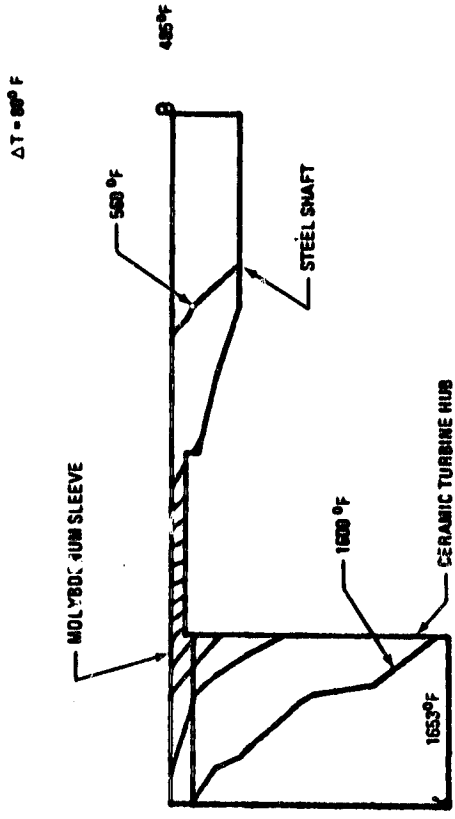


Figure 59 - Temperatures at Design Point

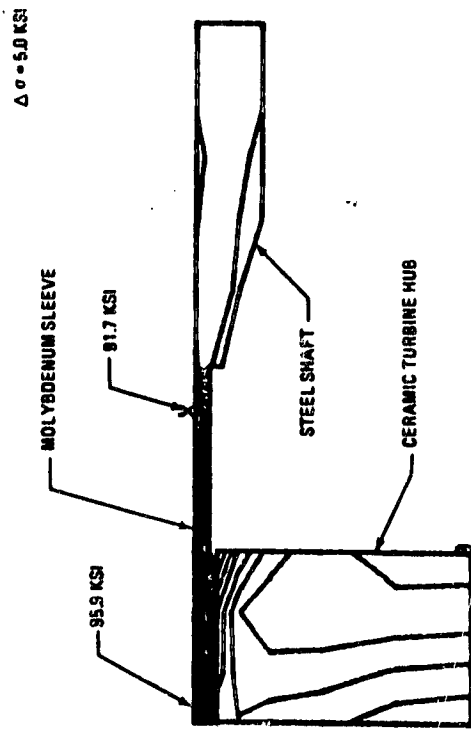


Figure 60 - Equivalent Stresses at Design Point

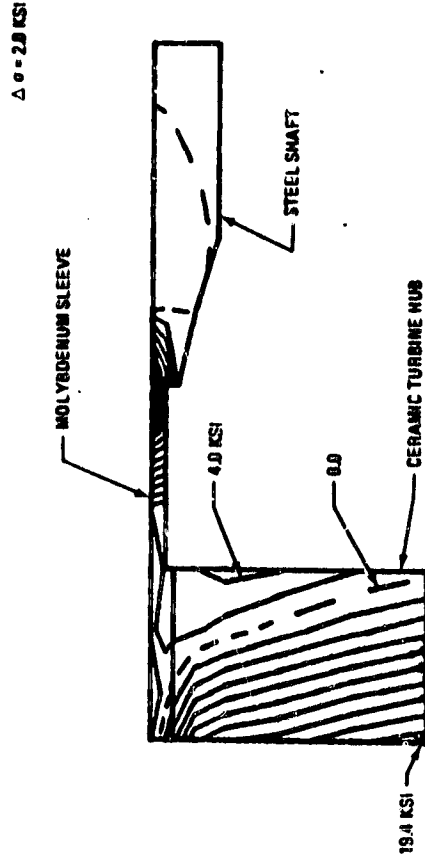


Figure 61 - Radial Stresses at Design Point

Figures 58,59,60,61

$\Delta T = 500^{\circ}F$

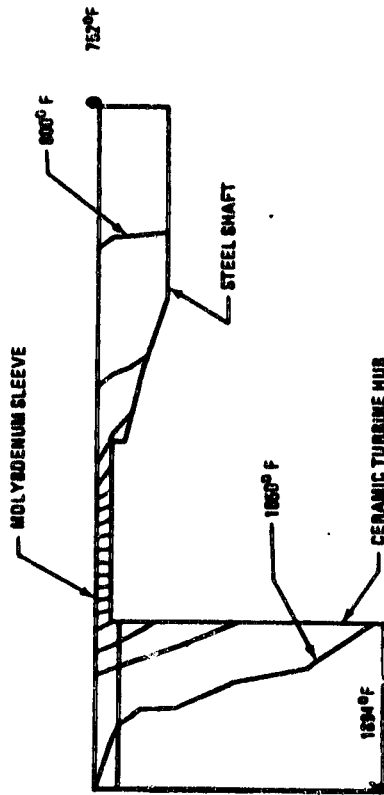


Figure 62 - Soak-back Temperature 100 Seconds after Shutdown

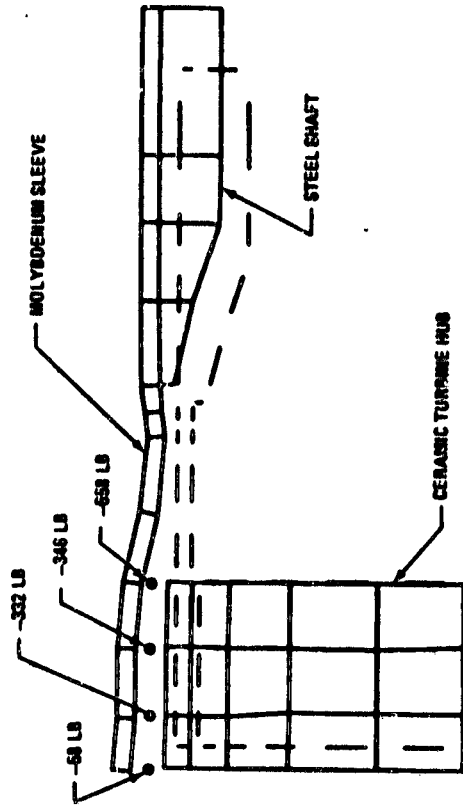


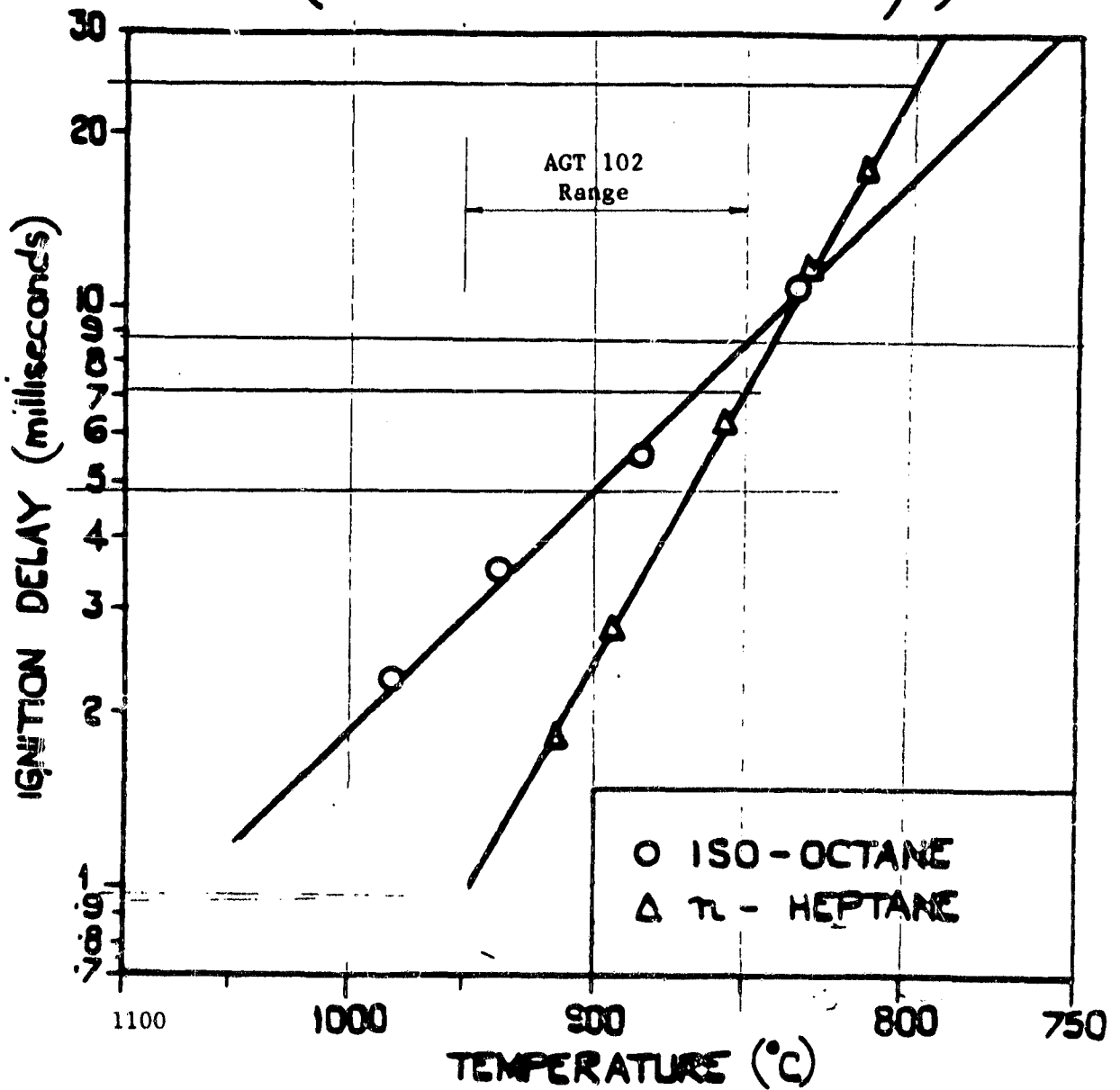
Figure 63 - Interference Fit 100 Seconds after Shutdown

Figures 62,63

CERAMIC TURBINE ROTOR SHAFT ATTACHMENT

ISO-OCTANE & n-HEPTANE

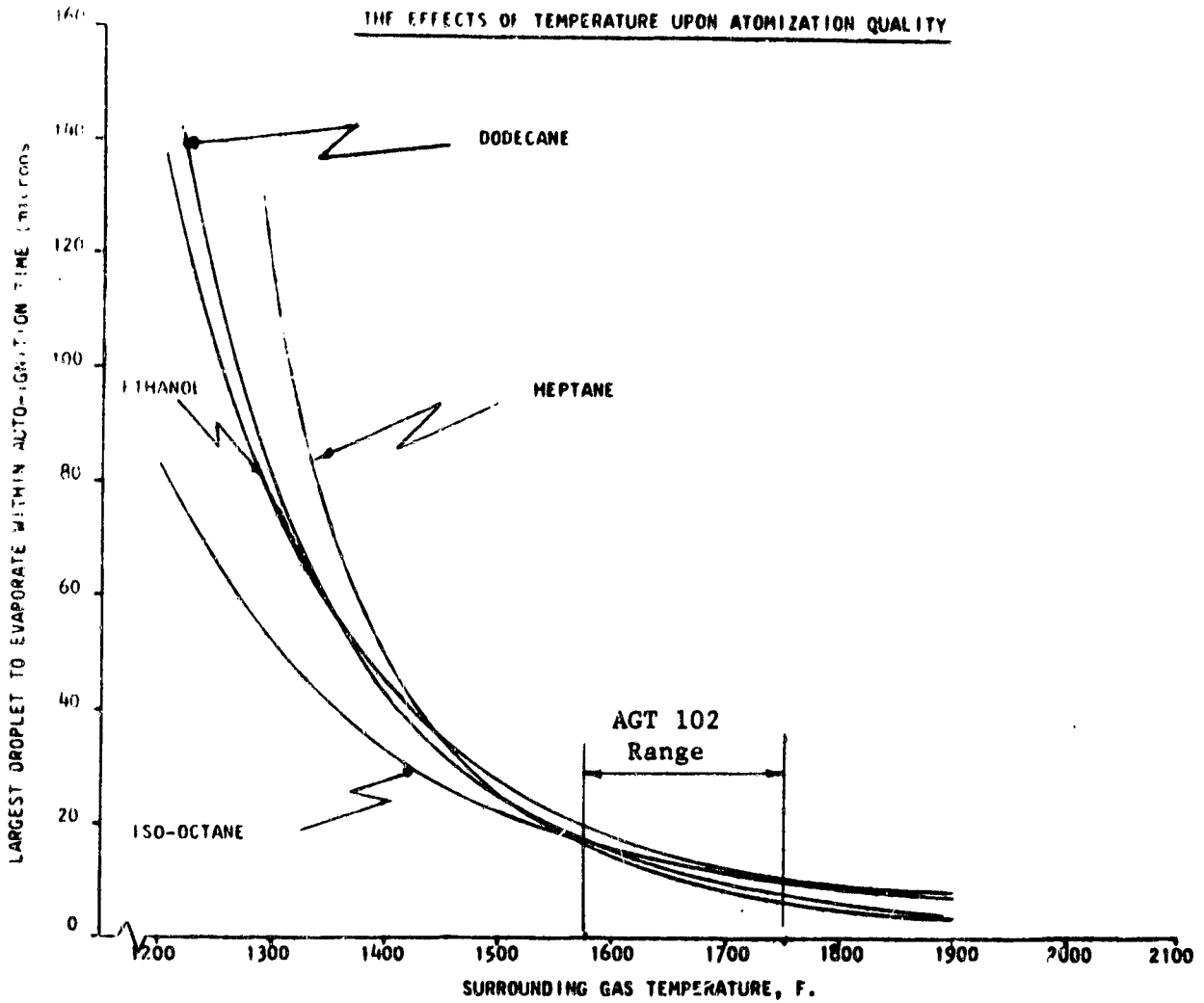
(SPRAY S.M.D. APPROX 80 μ)



EXAMPLE OF B. P. MULLINS' DATA

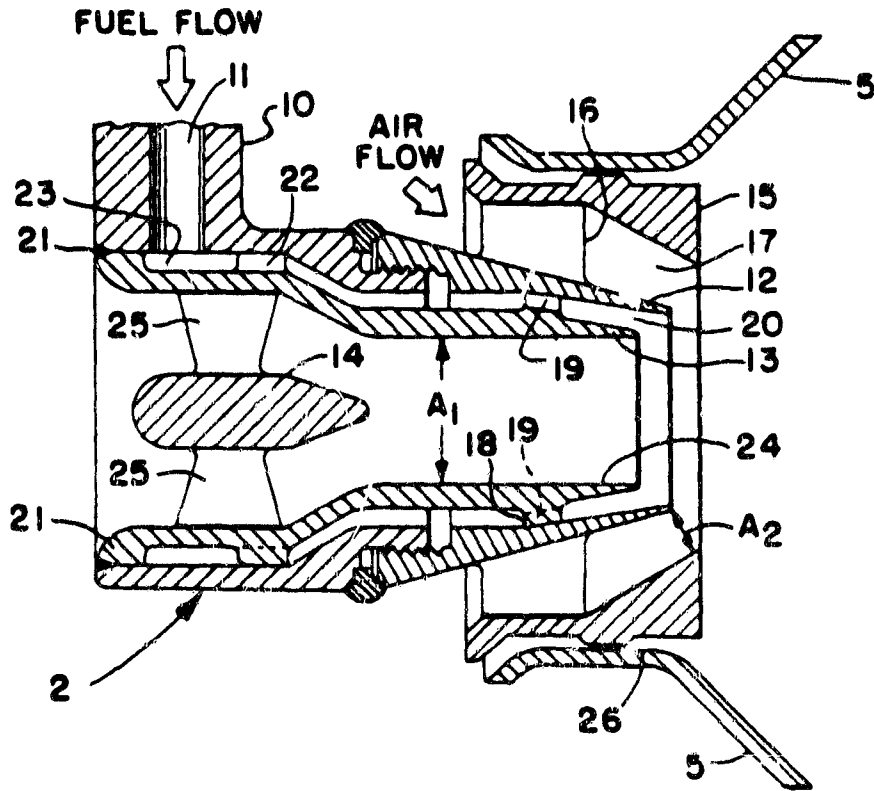
Figure 64

ORIGINAL PAGE IS
OF POOR QUALITY



MAXIMUM DROPLET SIZE TO AVOID AUTOIGNITION
FOR A GIVEN TEMPERATURE AND FUEL

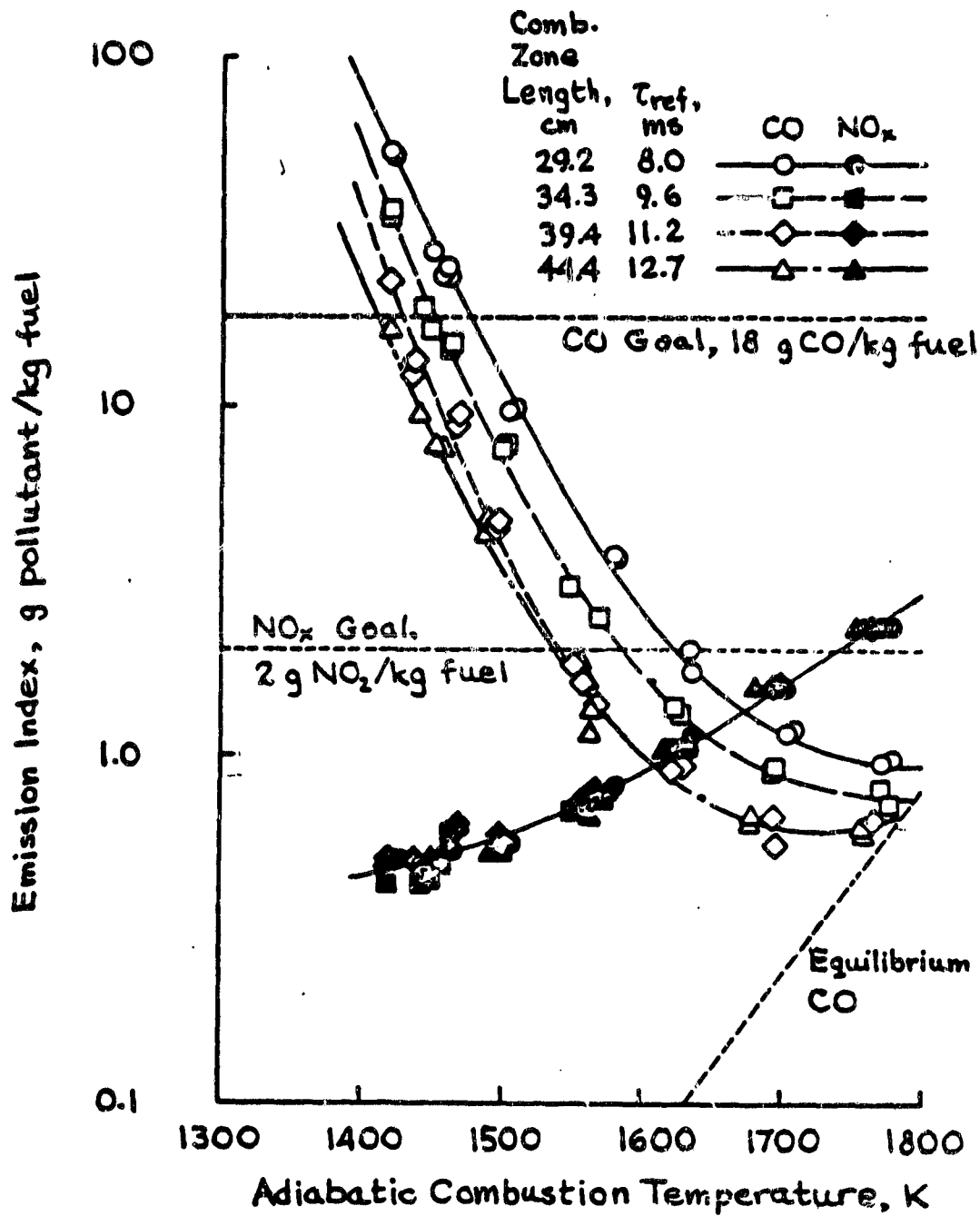
Figure 65



- | | |
|----------------------------------|---------------------------------------|
| A_1 - Inner Air Flow Area | 17 - Accelerating Outer Air Exit |
| A_2 - Outer Air Discharge Area | 18 - Fuel Manifold Exit |
| 2 - Airblast Atomizer | 19 - Fuel Swirler Vanes |
| 5 - Combustor Liner | 20 - Fuel Film Discharge |
| 10 - Fuel Support Structure | 21 - Sealing Weld |
| 11 - Fuel Inlet Tube | 22 - Spacers to Center Fuel Flow |
| 12 - Fuel/Air Mixing Structure | 23 - Fuel Manifold |
| 13 - Inner Air Flow Structure | 24 - Inner Air Discharge |
| 14 - Inner Air Centerbody | 25 - Inner Air Swirler Vanes |
| 16 - Outer Air Swirler Vanes | 26 - Alternative Attachment Technique |

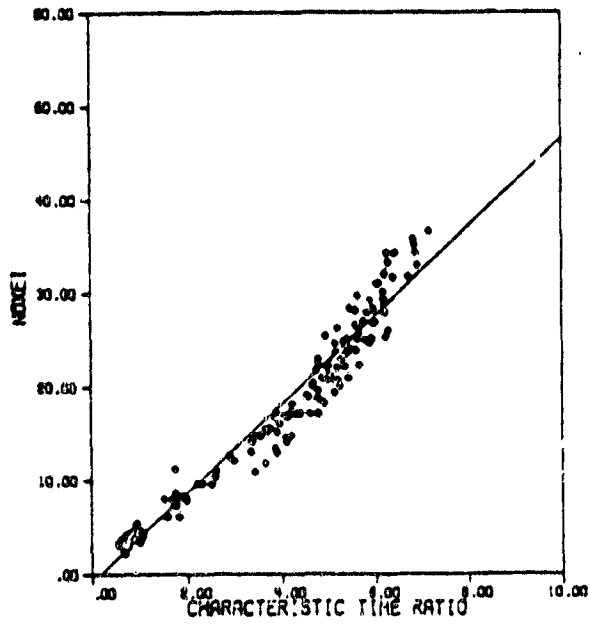
AIRBLAST ATOMIZER FROM U.S. PATENT NO. 3,980,233

Figure 66

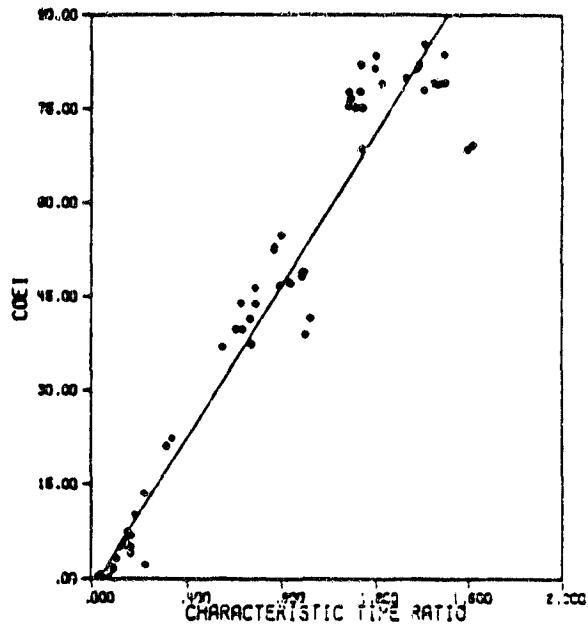


EMISSIONS DATA FROM NASA HIGH TEMPERATURE
ULTRA-LEAN COMBUSTION RIG

Figure 67



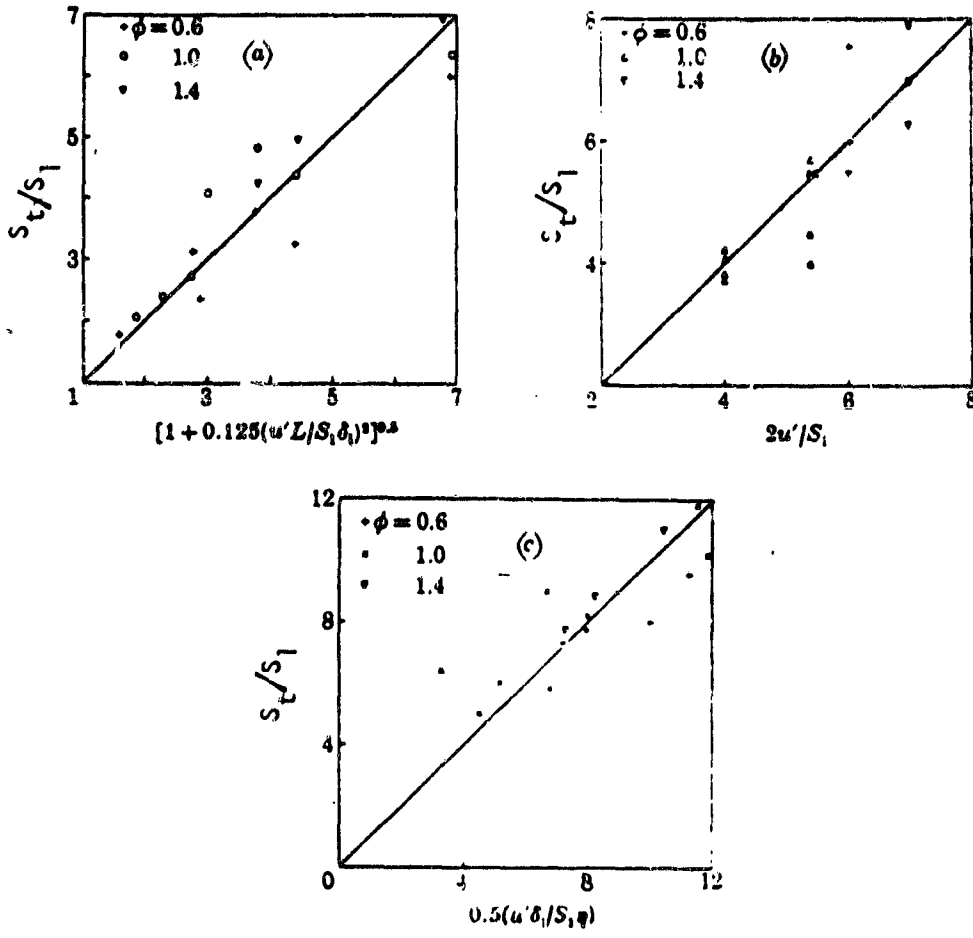
JT9D NO_x EI correlation



JT9D CO EI correlation

EXAMPLE OF MELLOR CHARACTERISTIC TIME METHOD

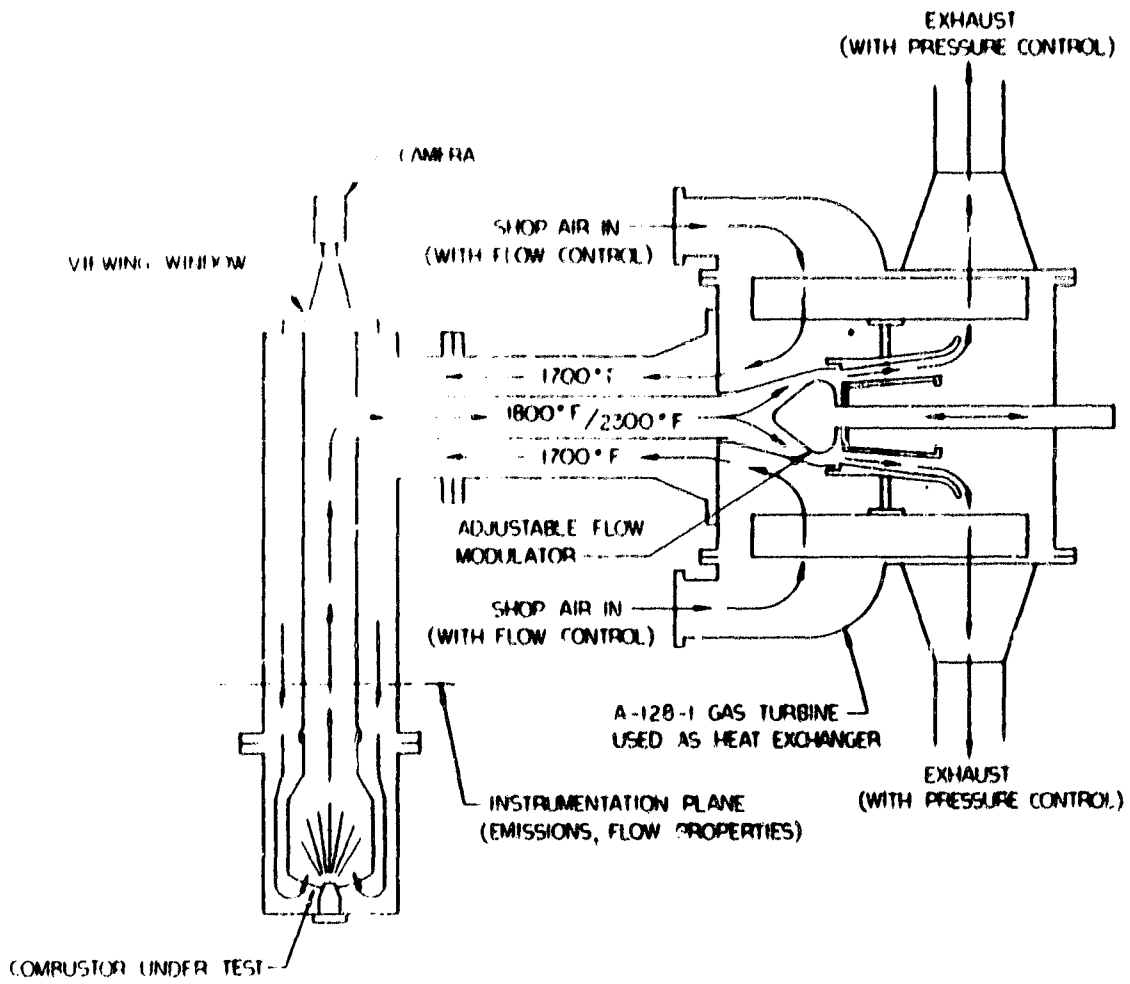
Figure 68



Comparison of experimental data with predictions based on the 3-region model of turbulent flames.

BALLAL AND LEFEBVRE THREE-REGION
TURBULENT FLAME MODEL

Figure 69



LPP COMBUSTOR RIG

Figure 70

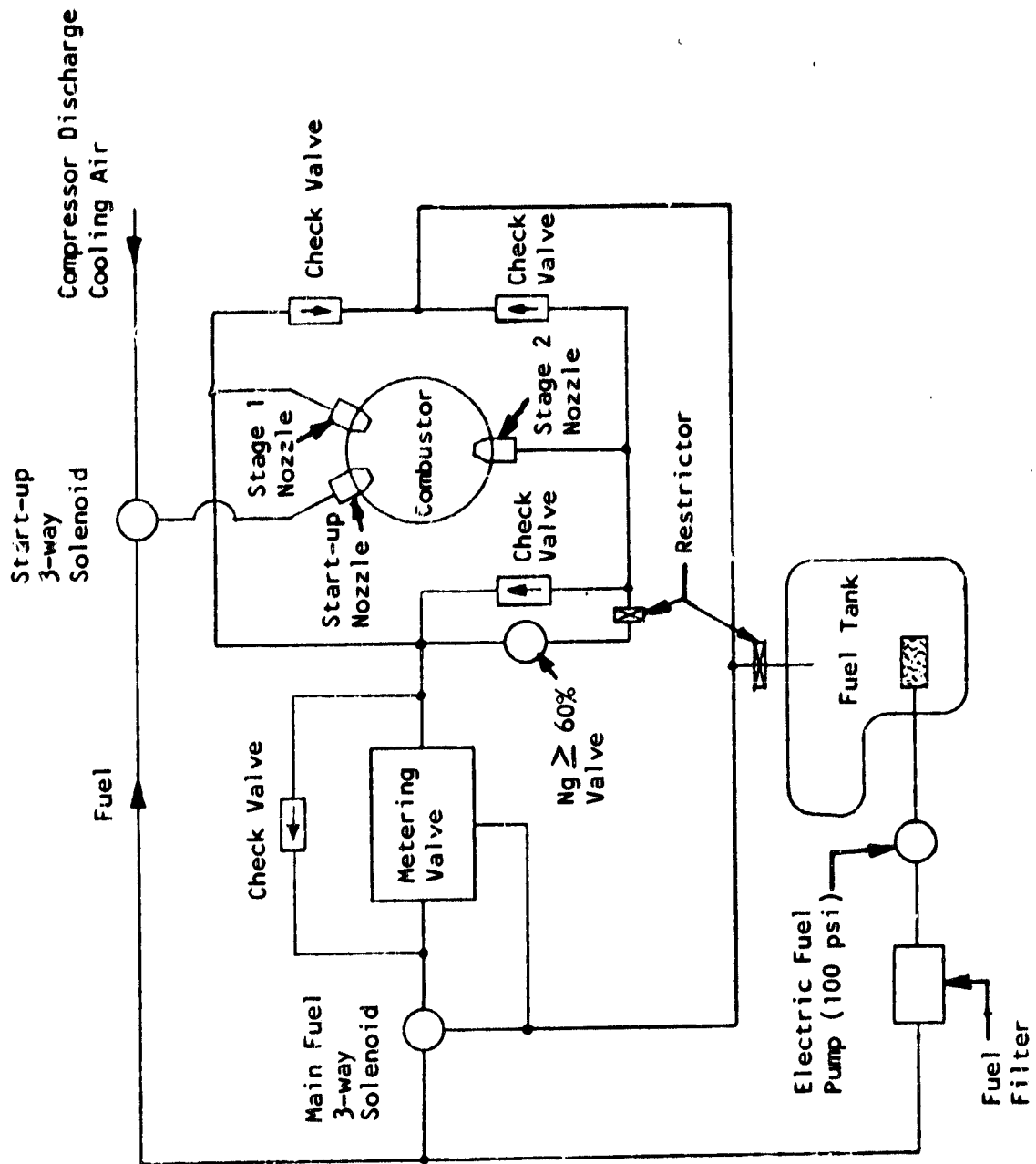
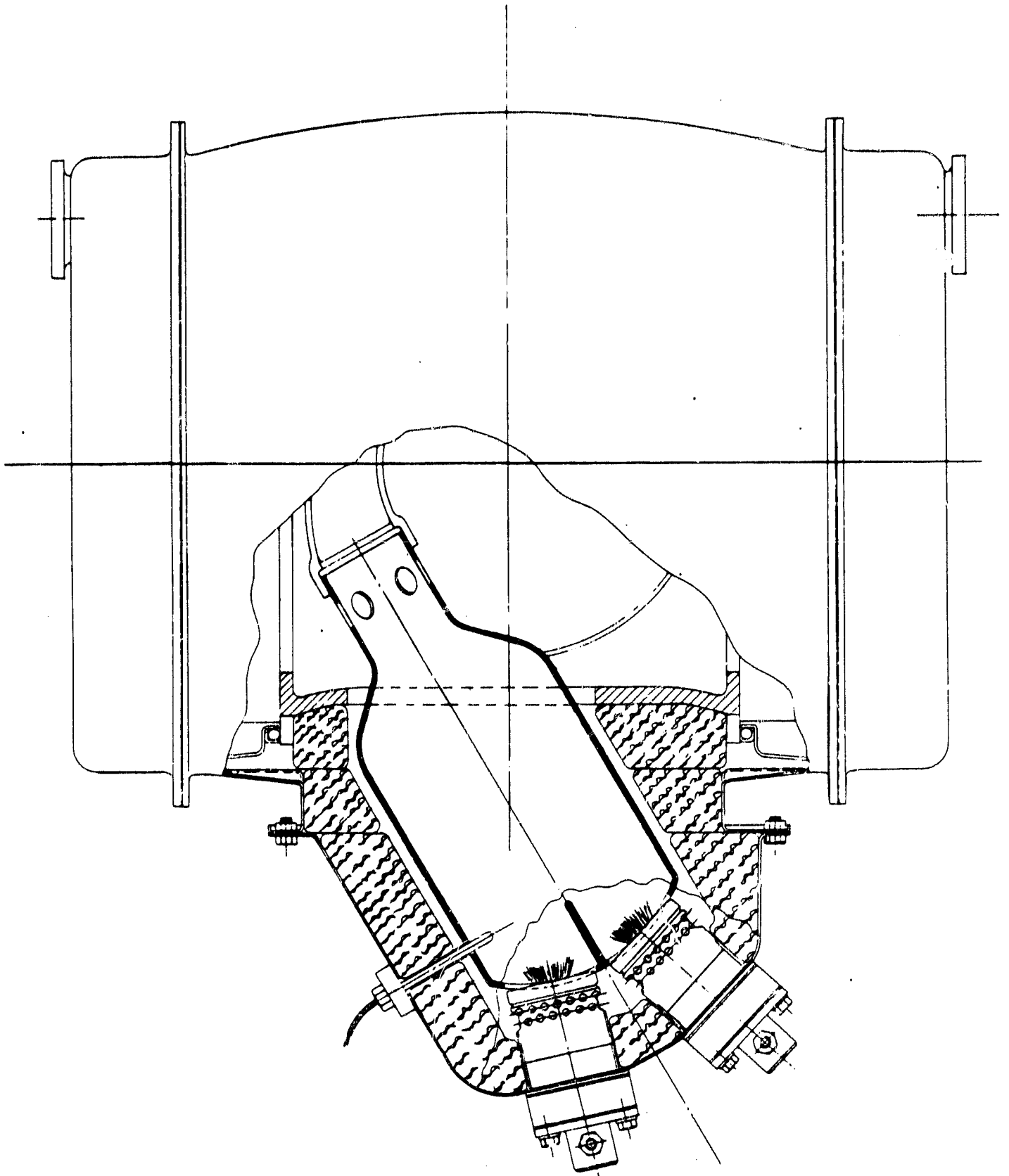


Figure 71

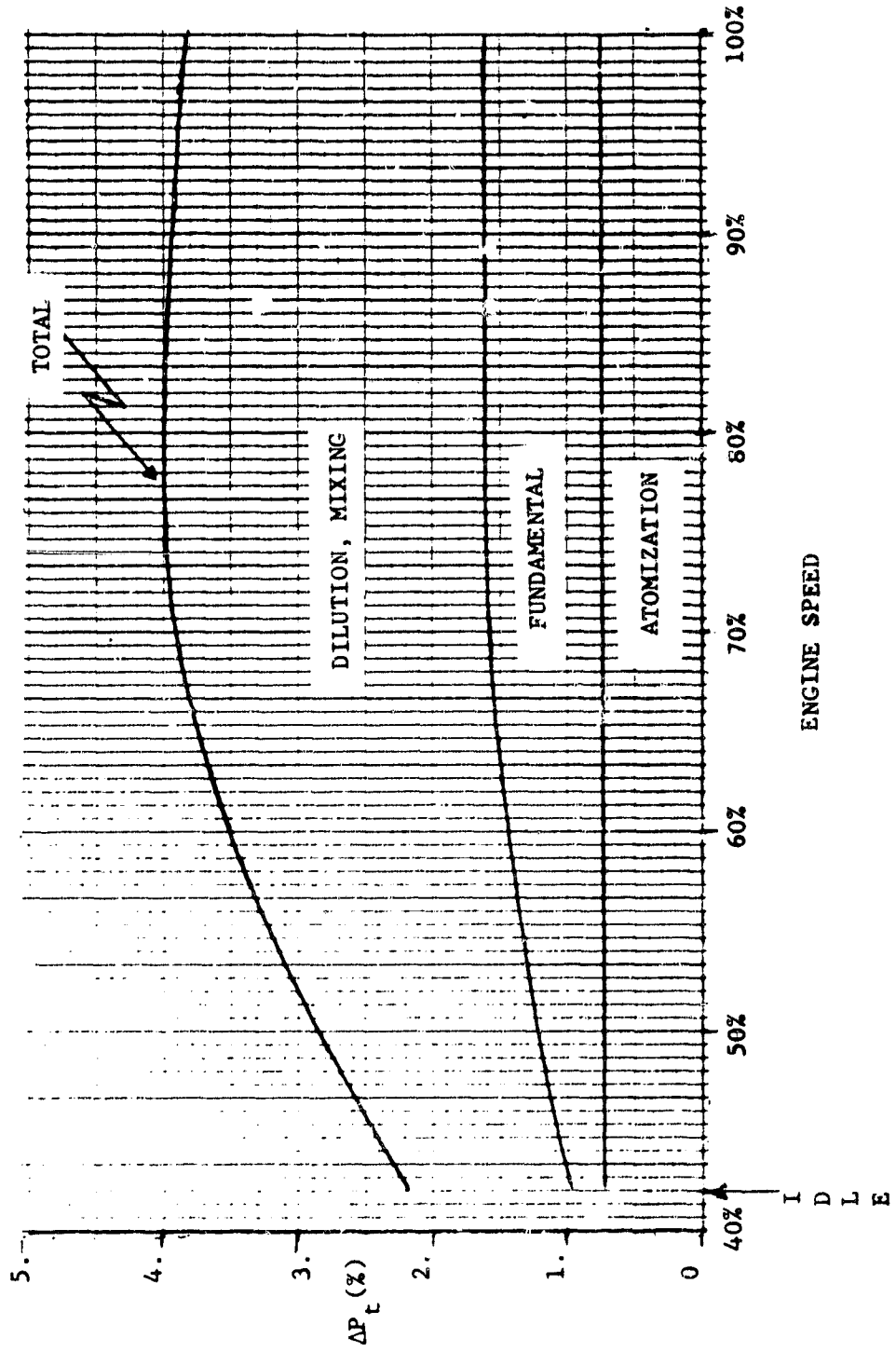
AGT-102 Fuel Metering Schematic



LPP Combustor in AGT-102 Engine

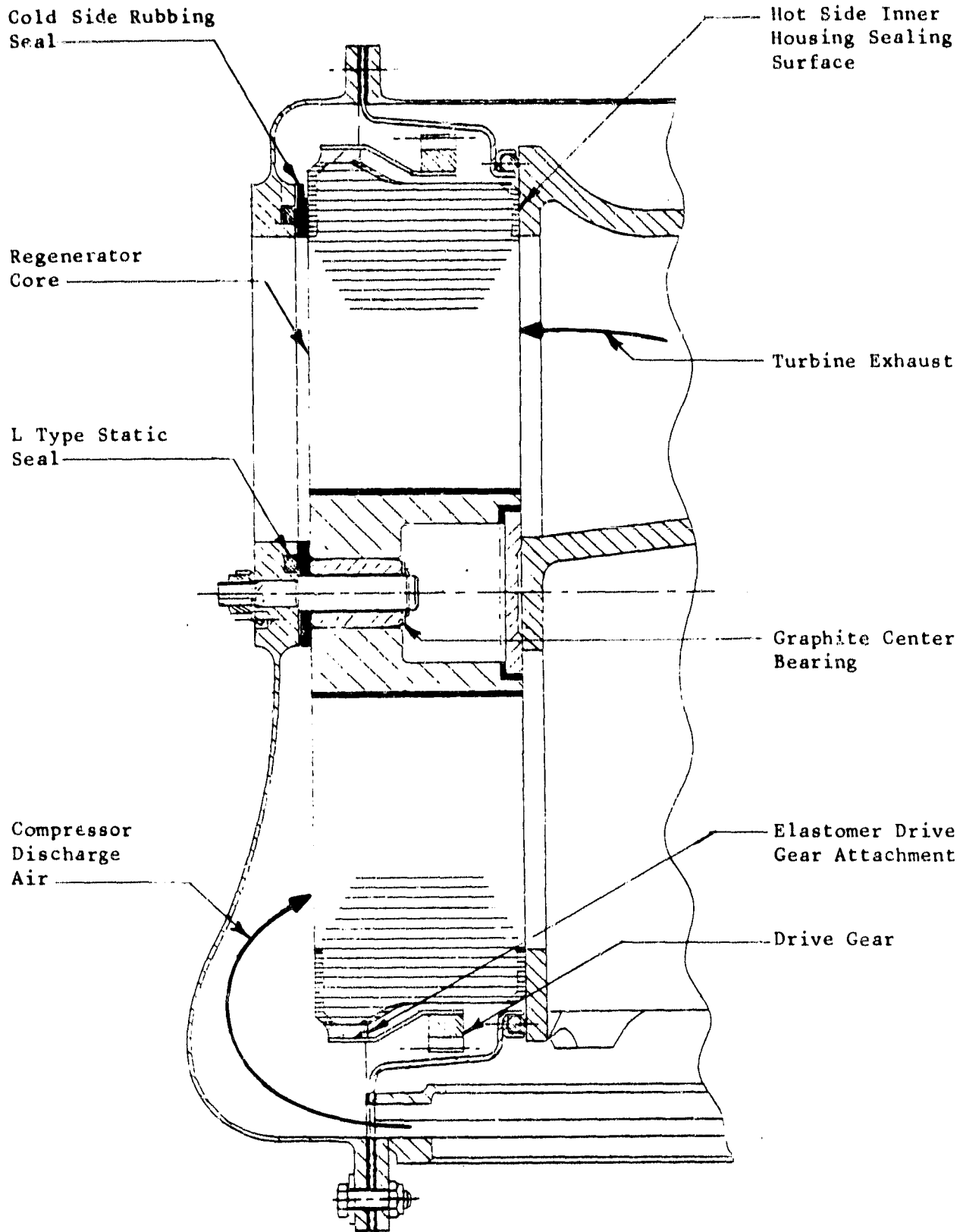
Figure 72

ORIGINAL PAGE IS
OF POOR QUALITY



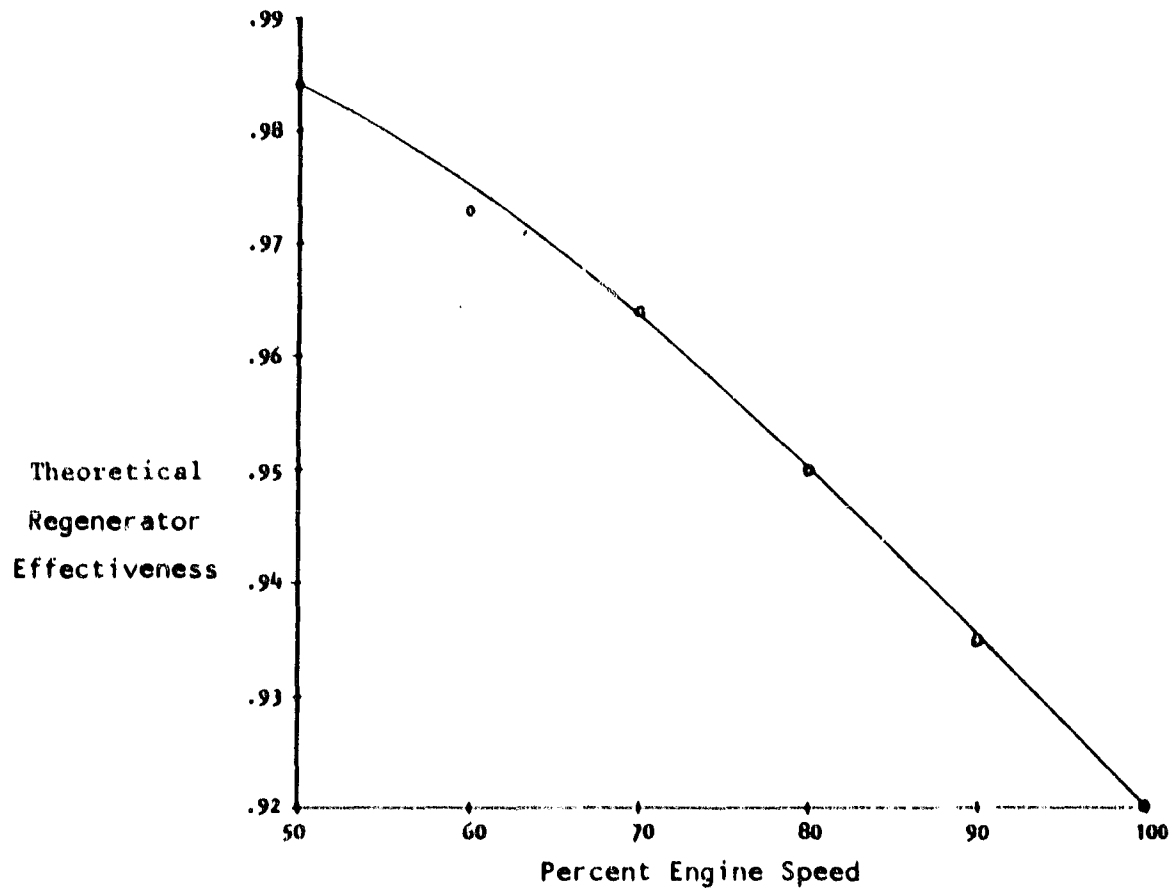
TOTAL PRESSURE LOSS IN LPP COMBUSTOR

Figure 73



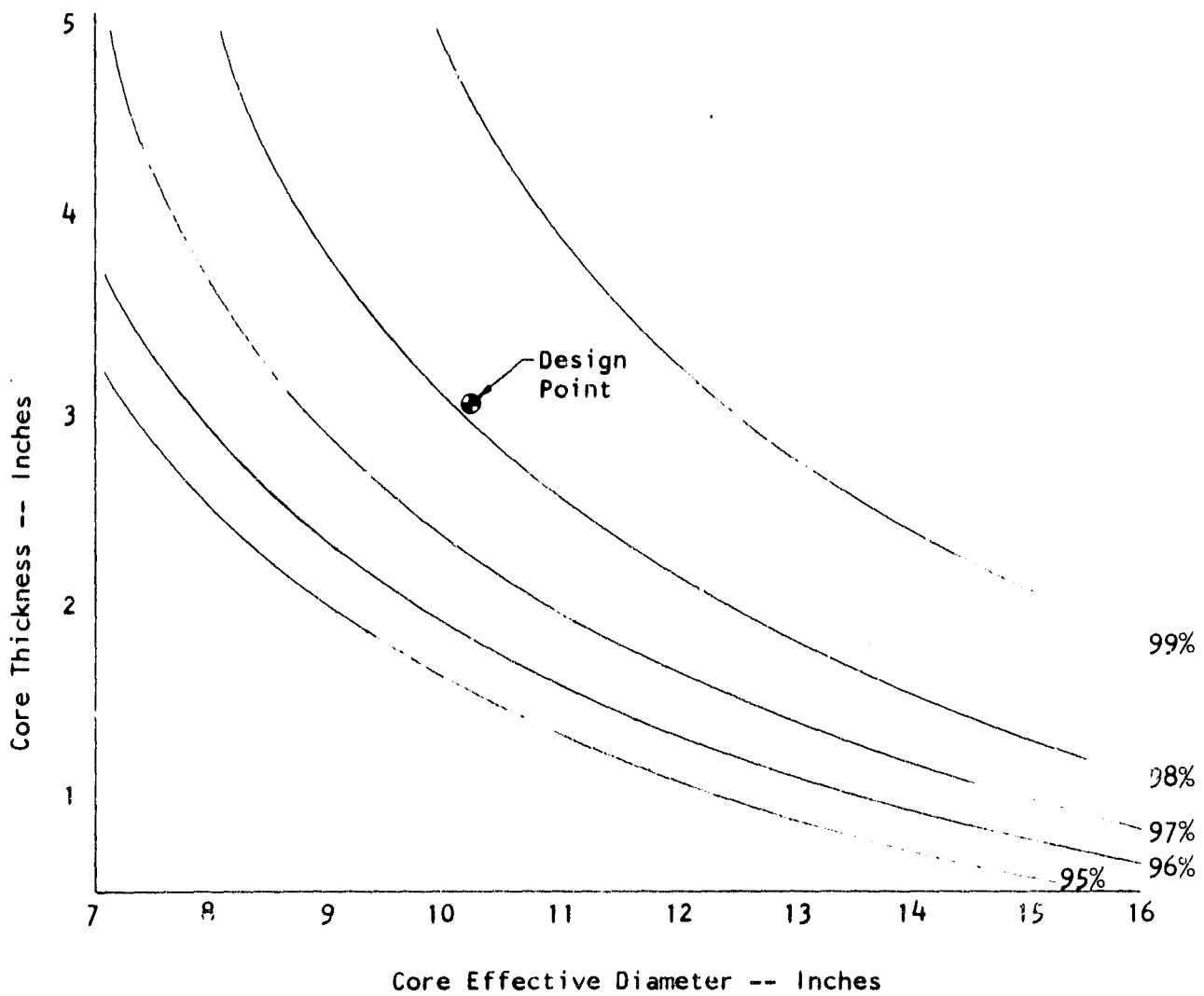
AGT Regenerator System

Figure 74



Regenerator Effectiveness vs. Percent Engine Speed

Figure 75

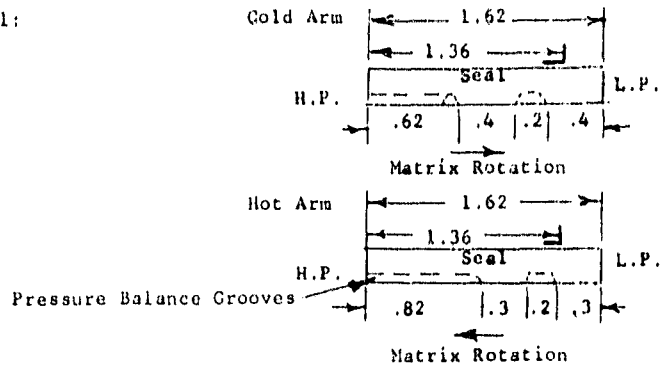


Lines of Constant Regenerator Effectiveness

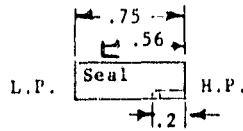
Figure 76

Outer "D" Seal:

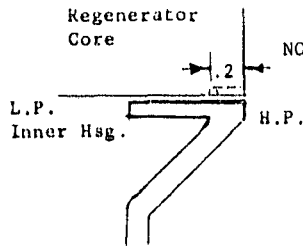
Crossarm Outer "D" Seal:



Rim Outer "D" Seal



Inner Seal:



NOTE: This pressure balancing groove can be either a) in the core b) in the inner hsg. c) in the plasma sprayed lubricant.

Speed (%)	Total Clamping Load (lbs)	Rim Load (lb/in)	Crossarm Load (lb/in)
100%	179 lbs 14g*	3 lb/in + 1 lb/in**	9 lb/in + 1 lb/in**
50%	56 lbs 5g*	0.6 lb/in + 1 lb/in**	1.6 lb/in + 1 lb/in**

Moment about Hub (ft-lbs)	Core Torque (ft-lbs)
13 ft-lbs	22 ft-lbs
	7 ft-lbs

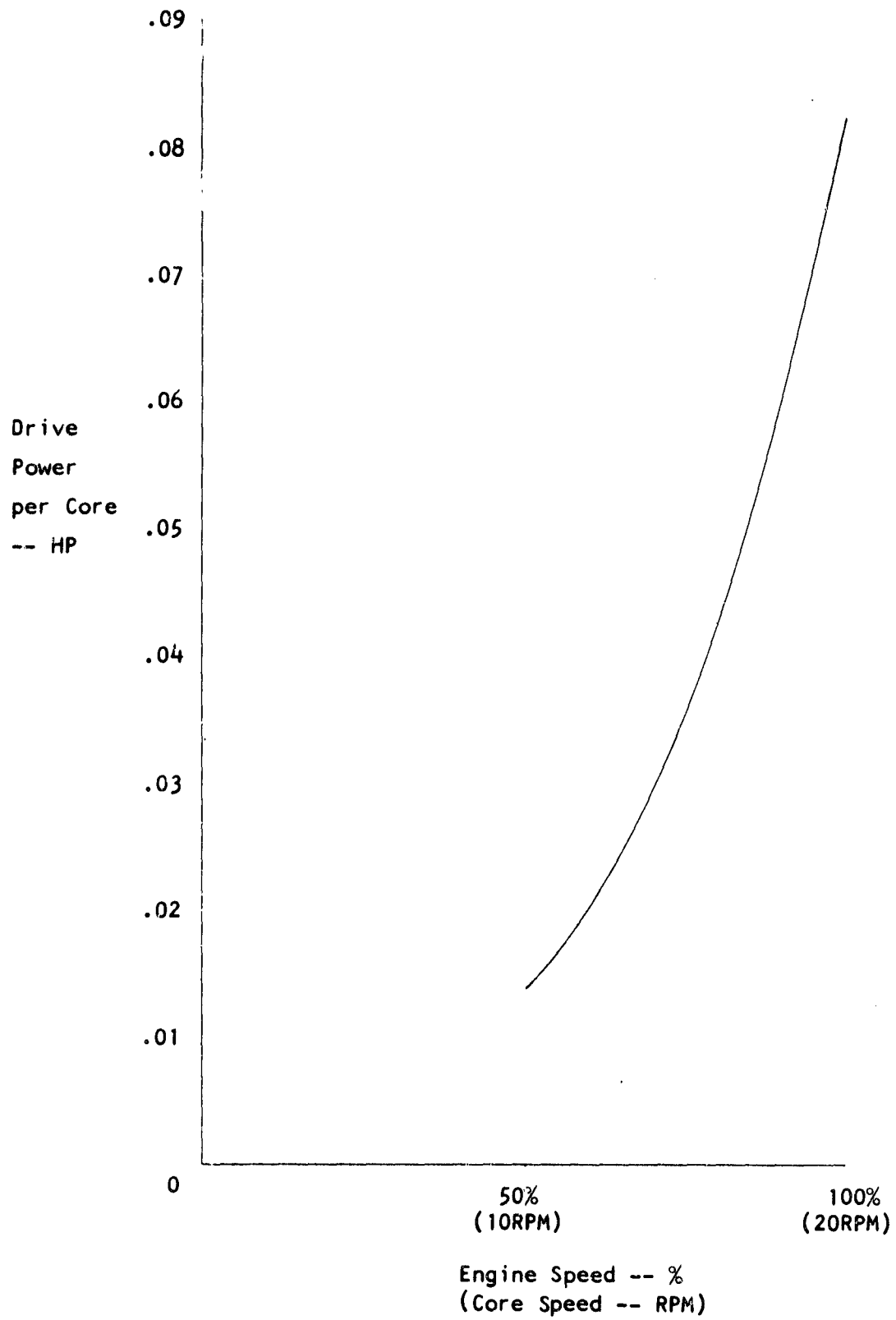
*Core Weight $\hat{=}$ 11.25 lbs.

**1 lb/in load due to "L" seal spring

$$\mu(\text{ZrO}_2/\text{CaF}_2) = .3$$

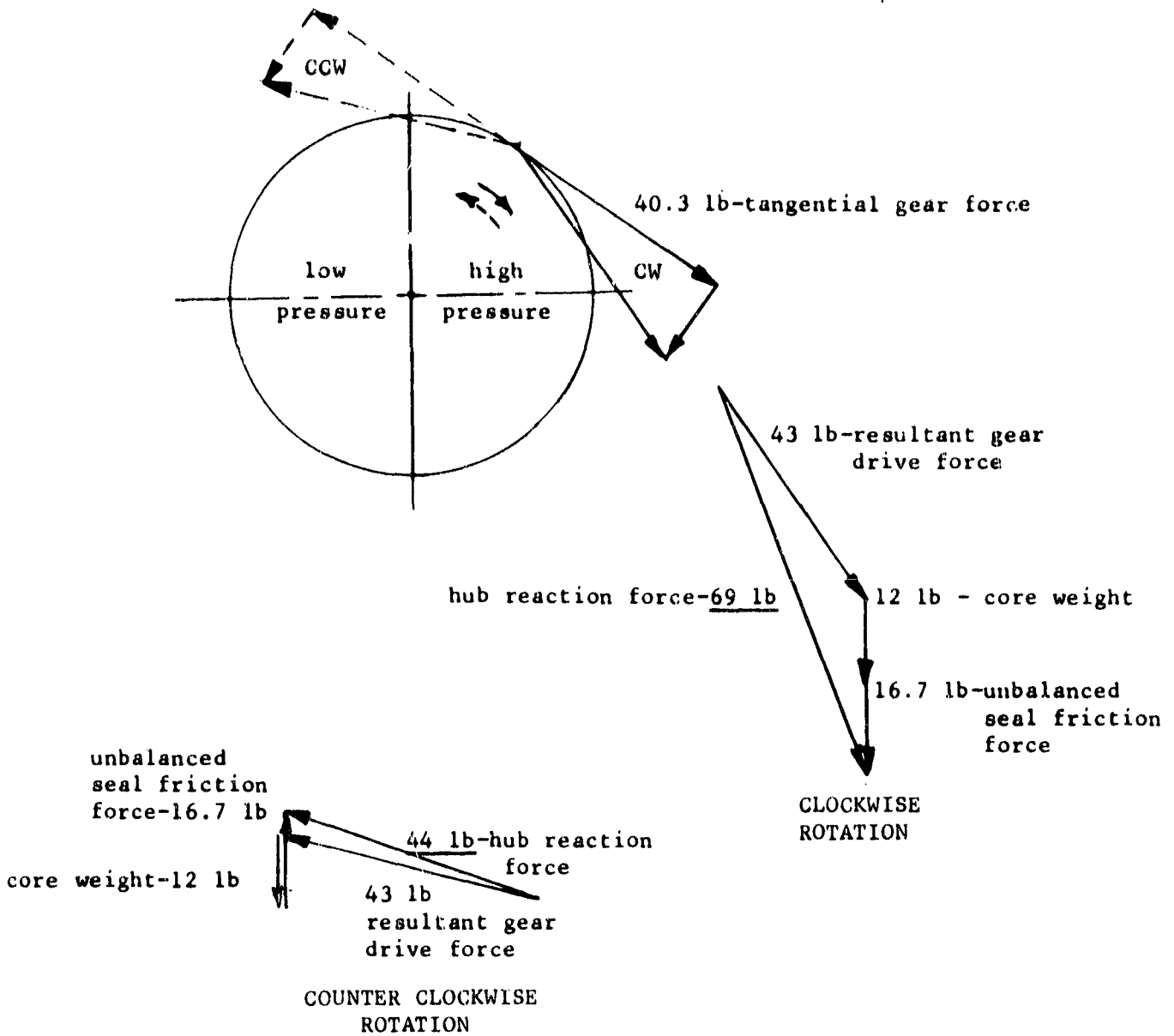
AGT-102 REGENERATOR SEAL SYSTEM
DESIGN STUDY

Figure 77



Regenerator Drive Power Requirement

Figure 78

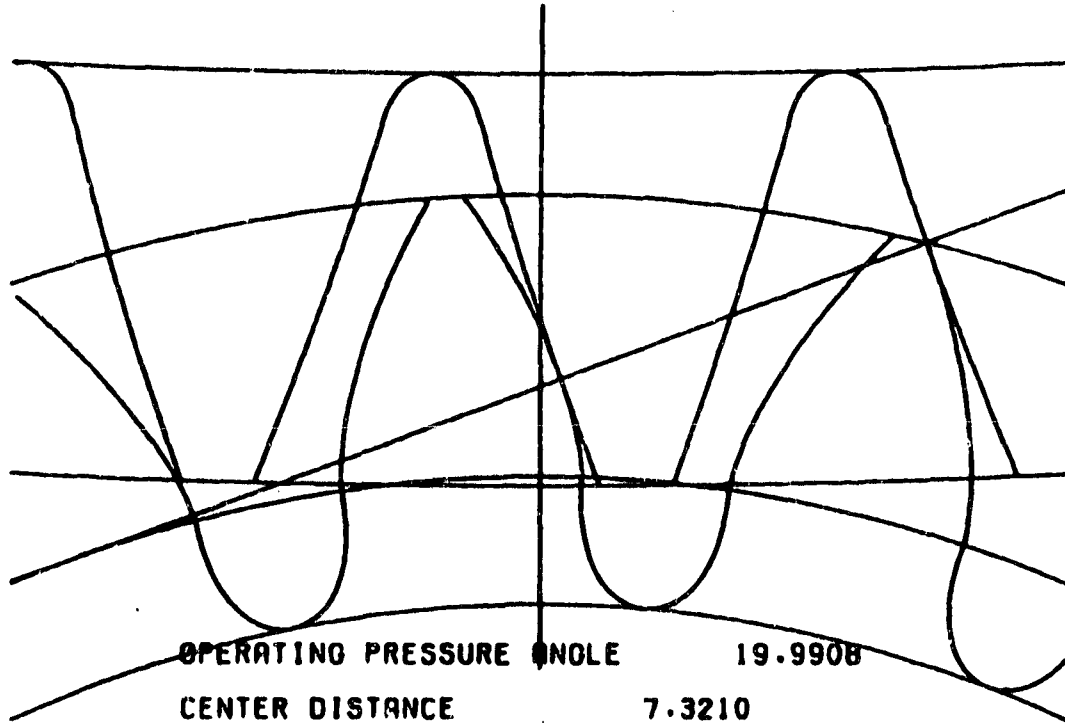


REGENERATOR CORE HUB LOAD
 100% SPEED, 22 LB-FT CORE DRIVE TORQUE

Figure 79

DESIGN MESH (MEAN DIMENSIONS)

**14.0 X SIZE = 1 D.P.
09/15/80**

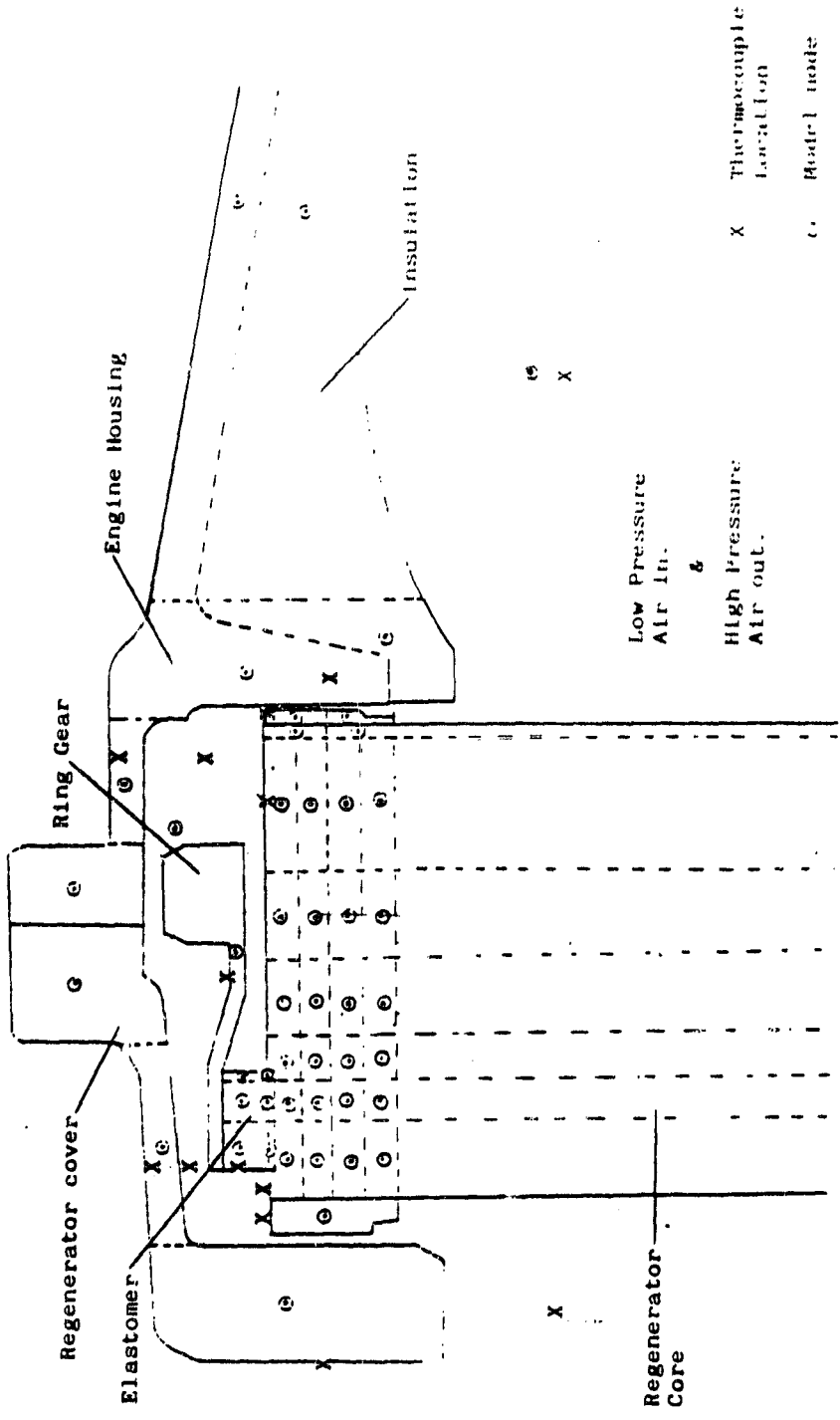


OPERATING PRESSURE ANGLE 19.9908

CENTER DISTANCE	7.3210	
PRESSURE ANGLE	20.0000	
DIAMETRAL PITCH	14.0000	
NUMBER OF TEETH	22.0000	183.0000
OUTSIDE DIAMETER	1.7735	13.1756
ROOT DIAMETER	1.3404	12.7417
HOB TIP RADIUS	0.0182	0.0182
ARC TOOTH THICKNESS	0.1152	0.0783

Regenerator Drive Gear Design

Figure 80



UPGRADED ENGINE REGENERATOR DRIVE
THERMAL MODEL AND TEST THERMOCOUPLE LOCATIONS

Figure 81

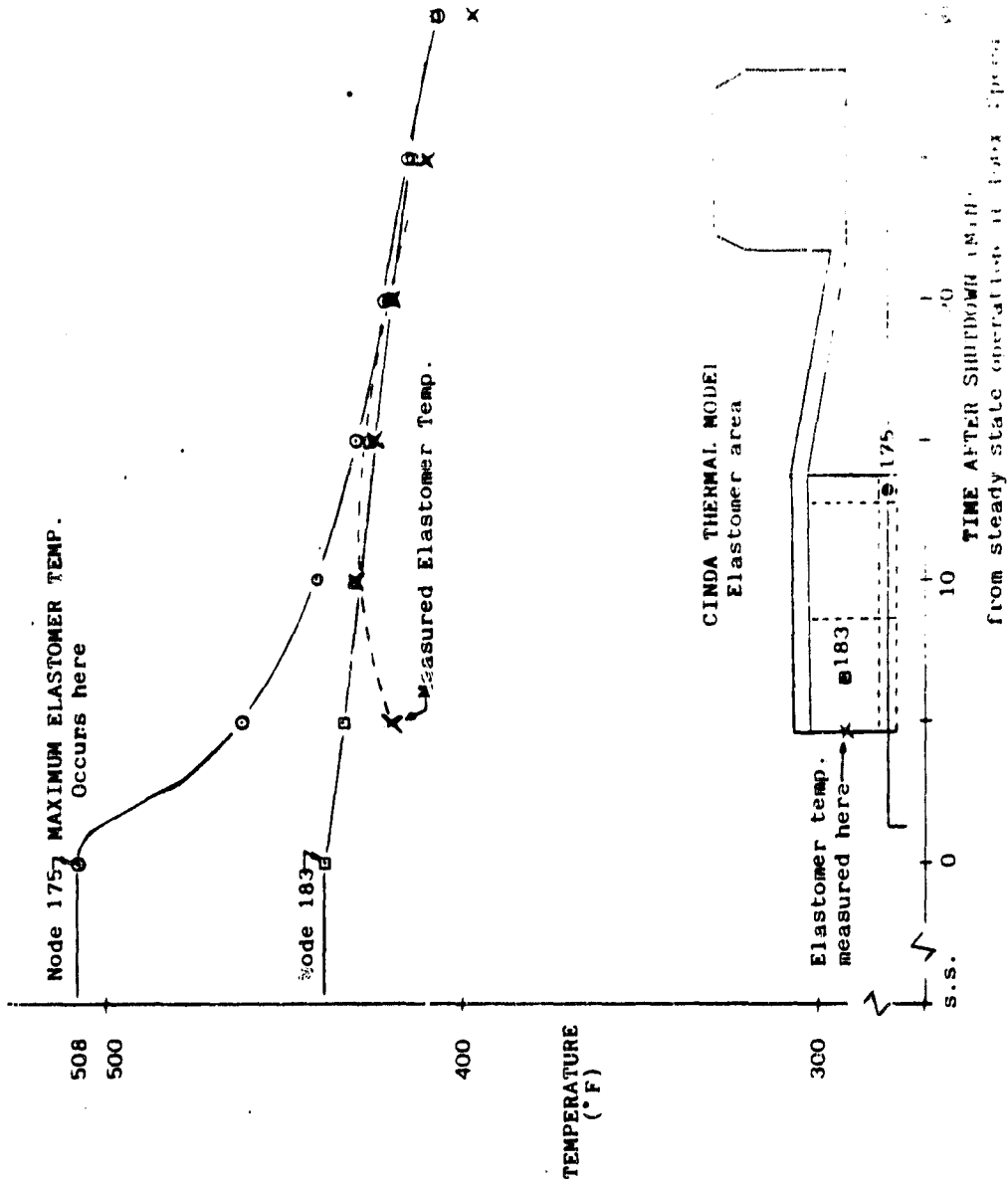


Figure 82

UPGRADED ENGINE REGENERATOR DRIVE
ELASTOMER SOAKBACK TEMPERATURE FROM 100% SPEED

AGT
 MAXIMUM ELASTOMER TEMPERATURE
 as predicted by AGT temperatures in UPGRADED ENGINE THERMAL MODEL.
 with & without a projection of the core under the elastomer:
 at 100% Steady State + Soakback

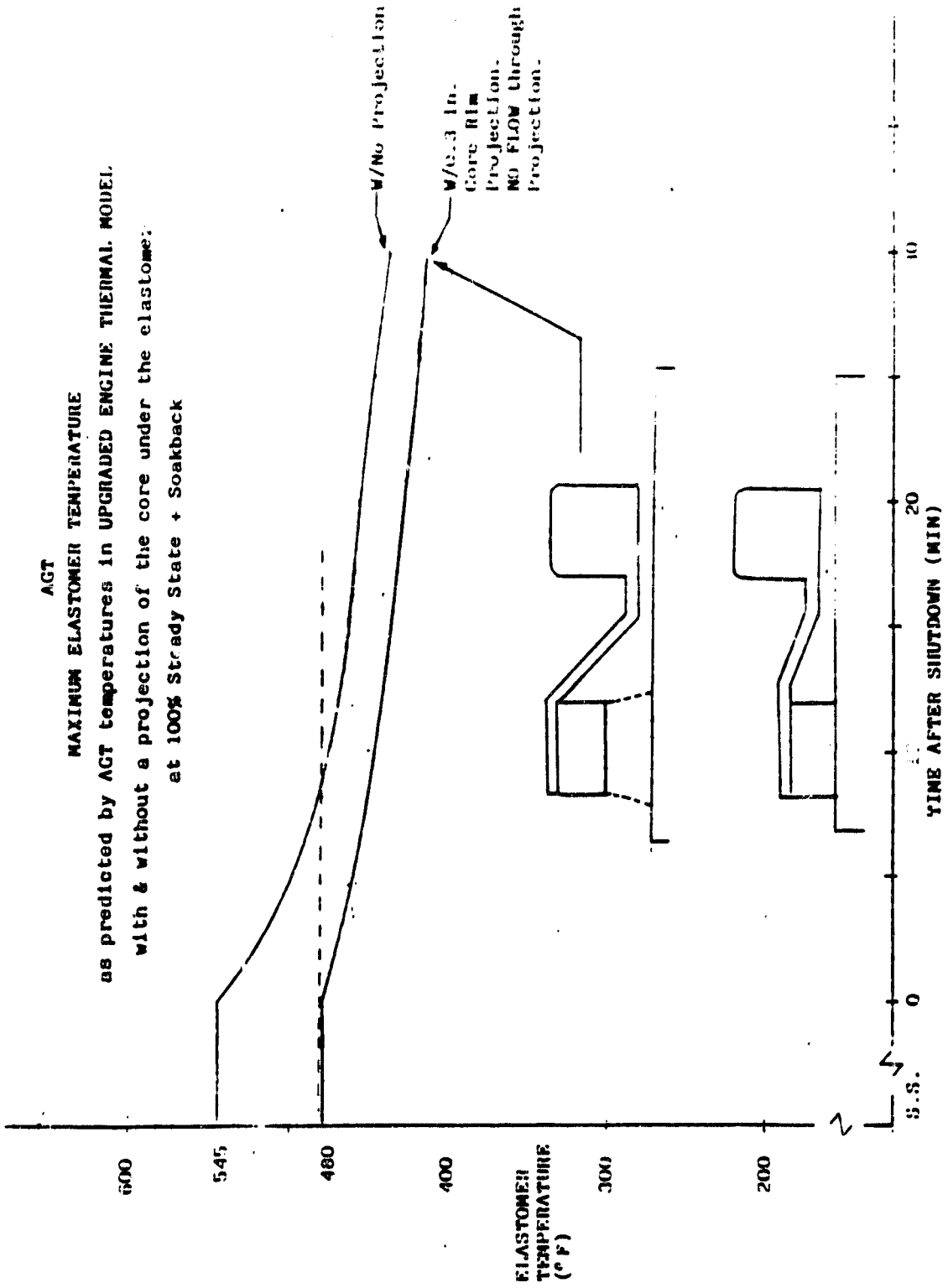


Figure 83

AGT-102 MAXIMUM ELASTOMER TEMPERATURE

REGENERATOR COLD FLOW RIG
TESTING HIGH PRESSURE SIDE

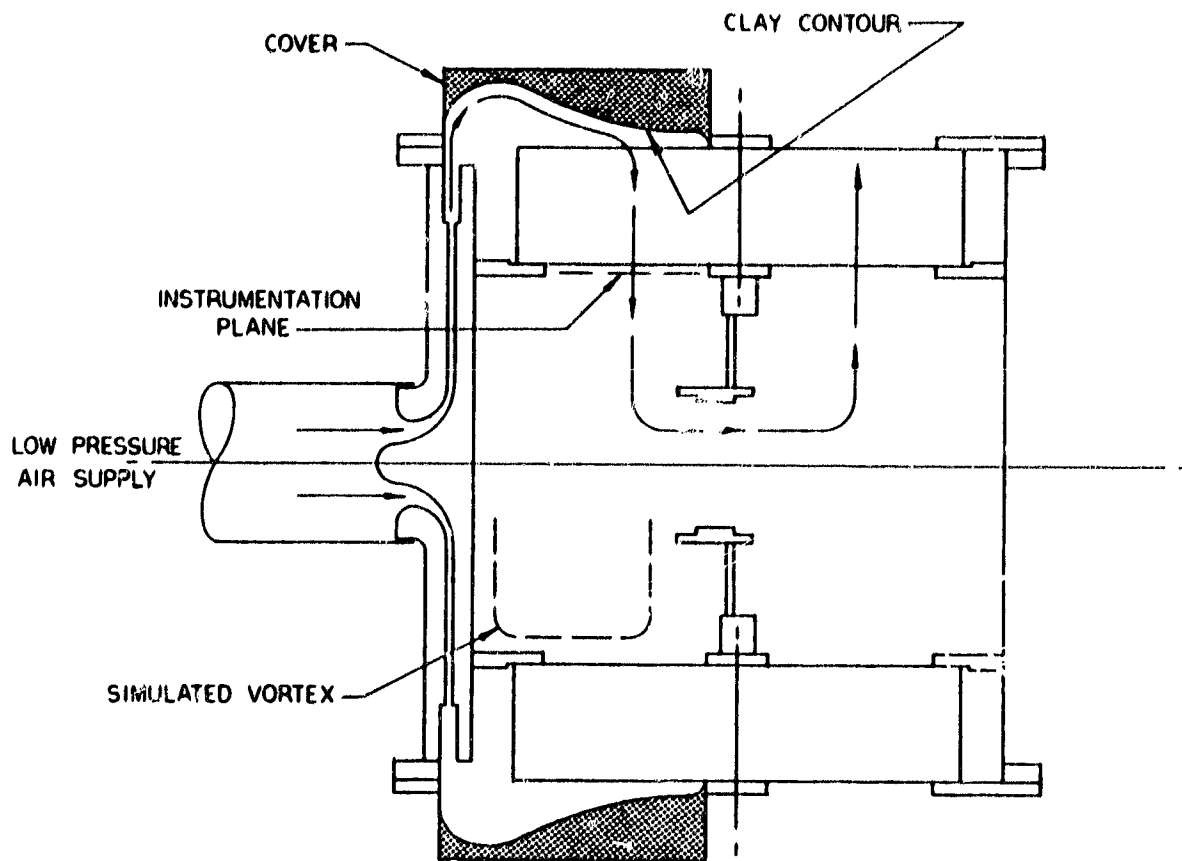


Figure 84

REGENERATOR COLD FLOW RIG
TESTING LOW PRESSURE SIDE

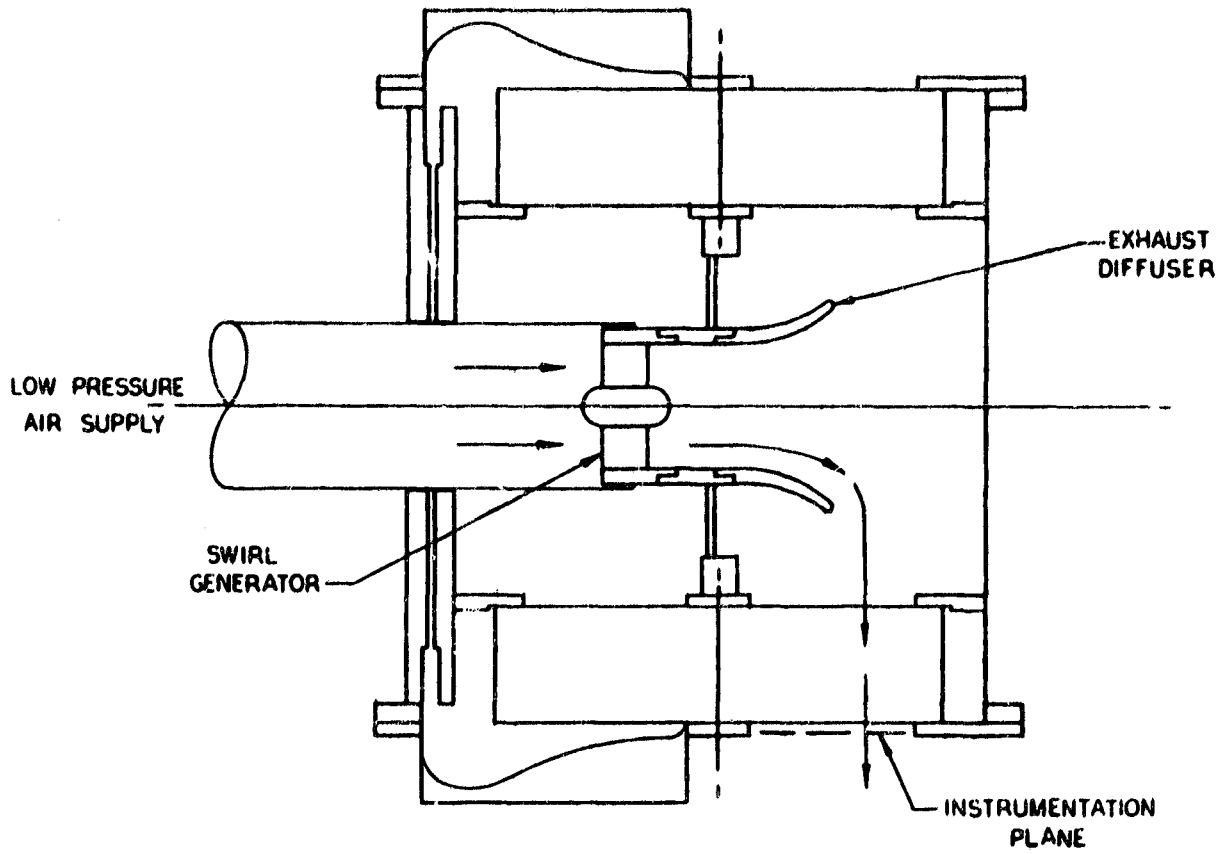
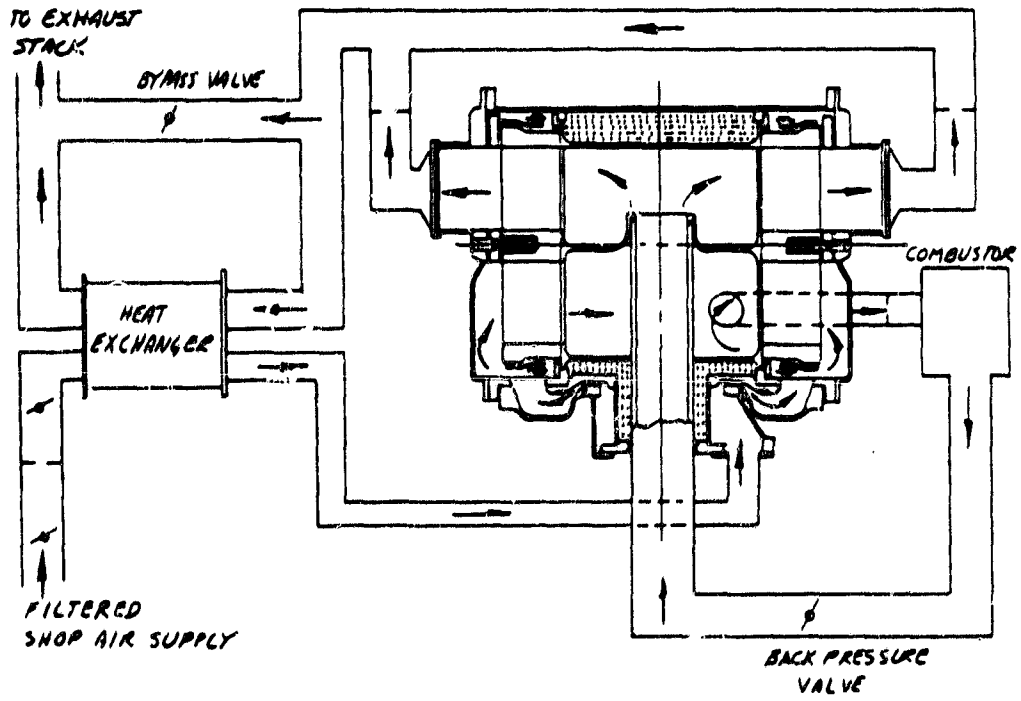
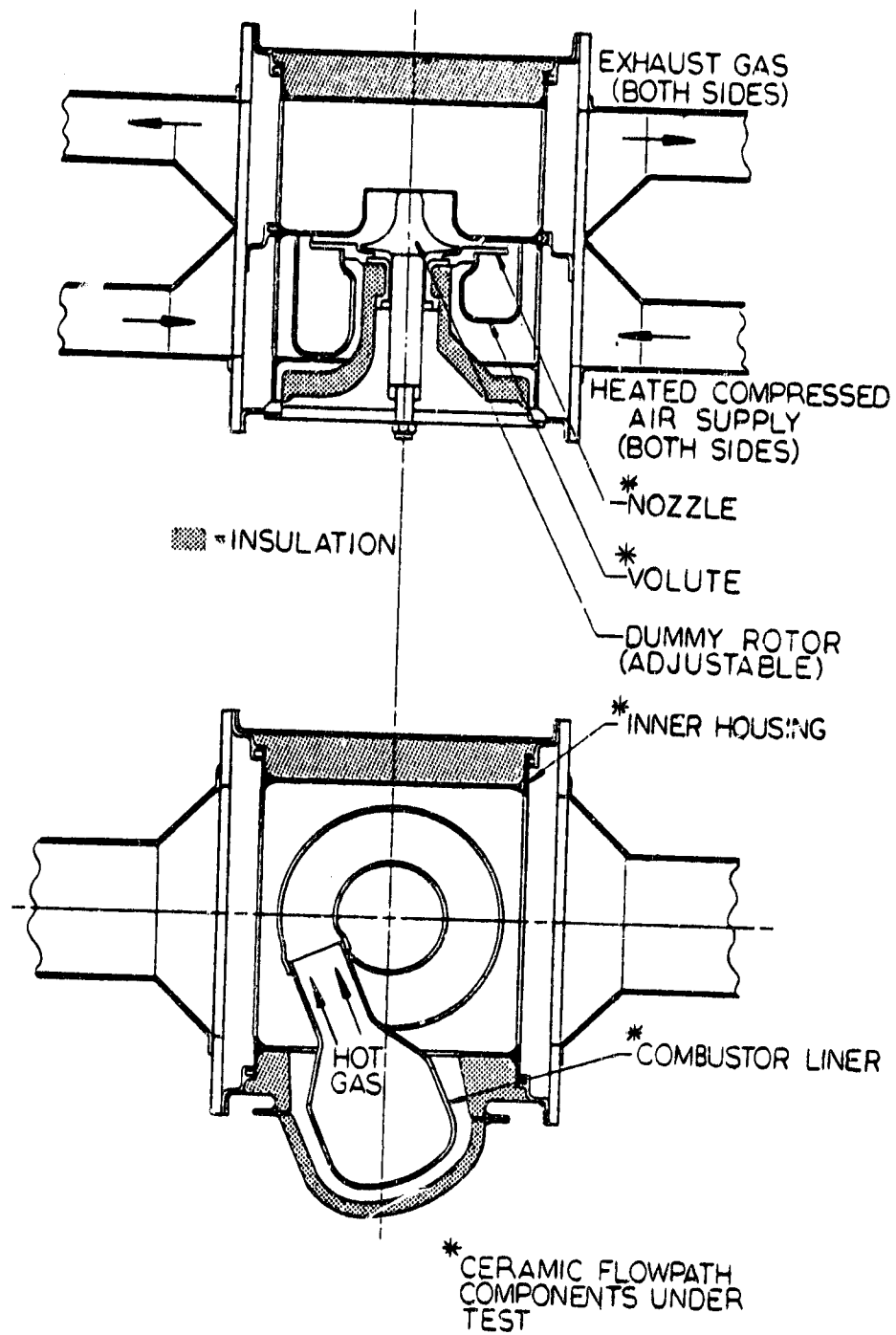


Figure 85



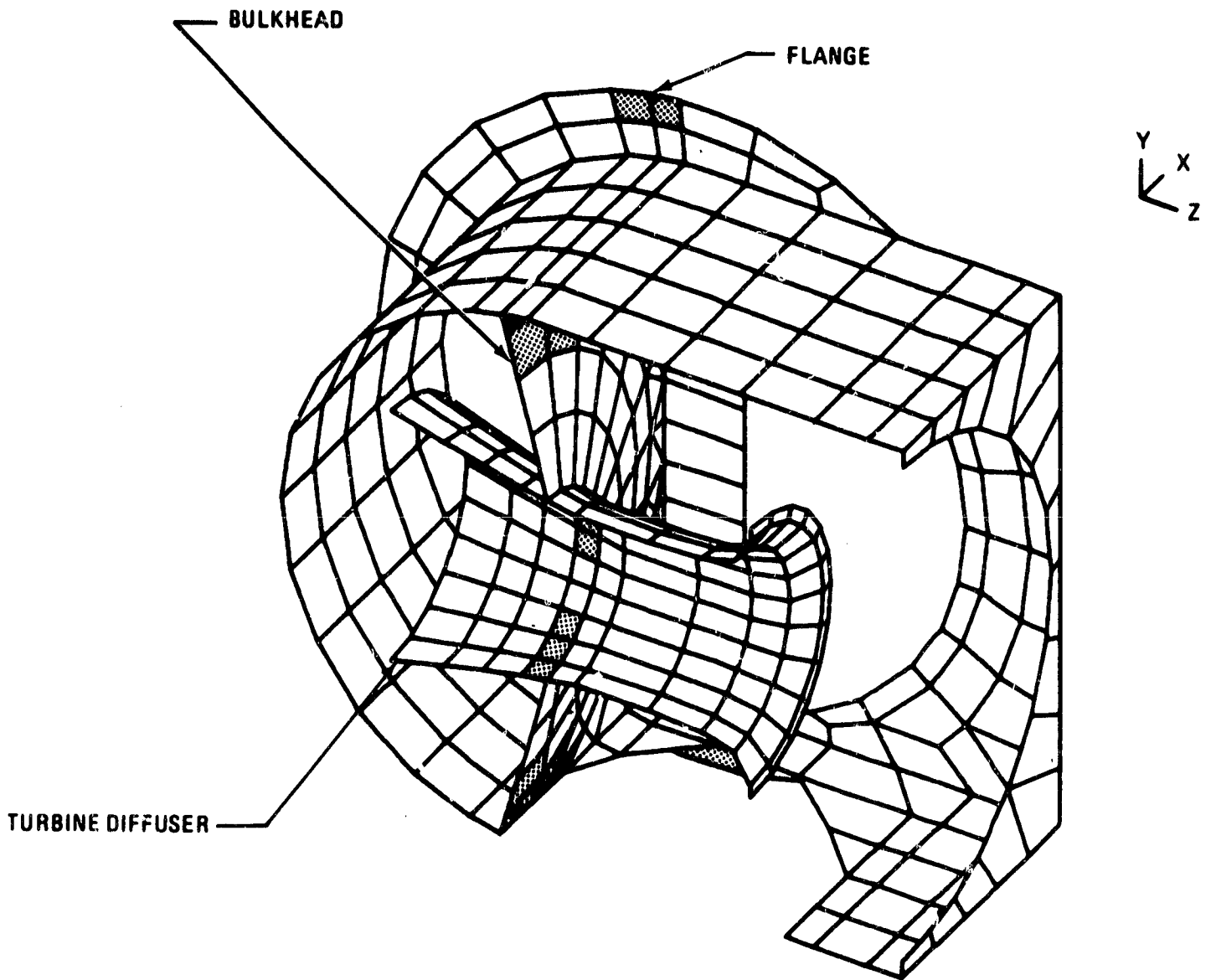
Hot Regenerator Test Rig
and Flow Schematic

Figure 86



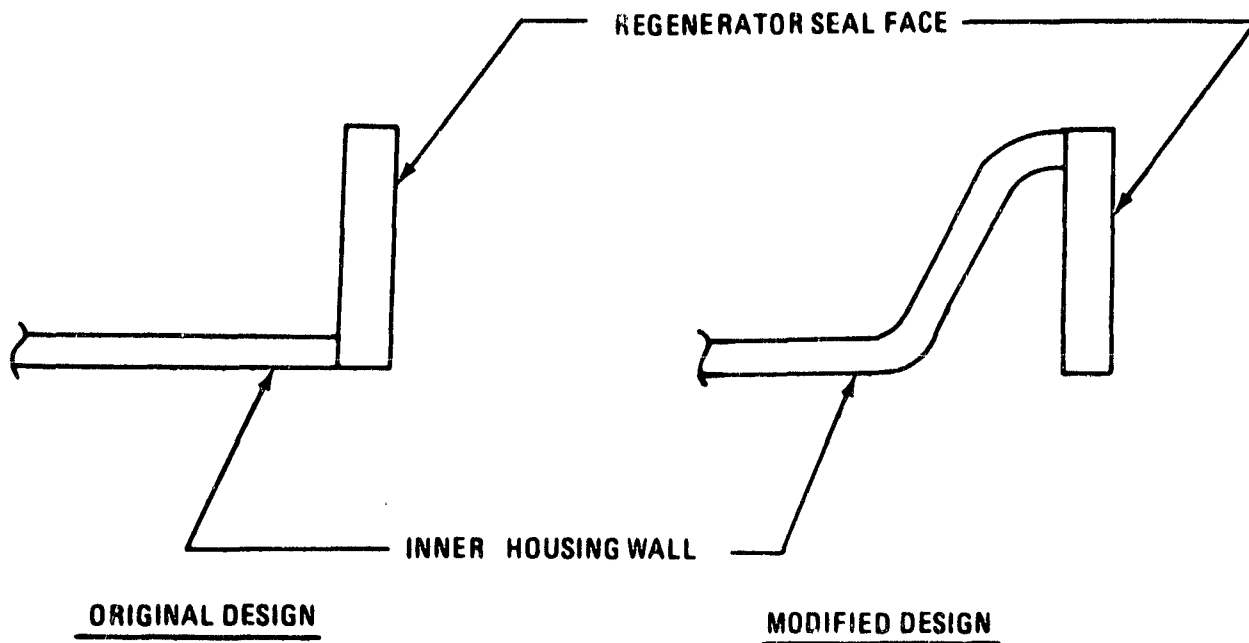
CERAMIC COMPONENT TEST RIG

Figure 87



Inner Housing Preliminary Design
Finite Element Model

Figure 88



Inner Housing Regenerator Seal Face Modification

Figure 89

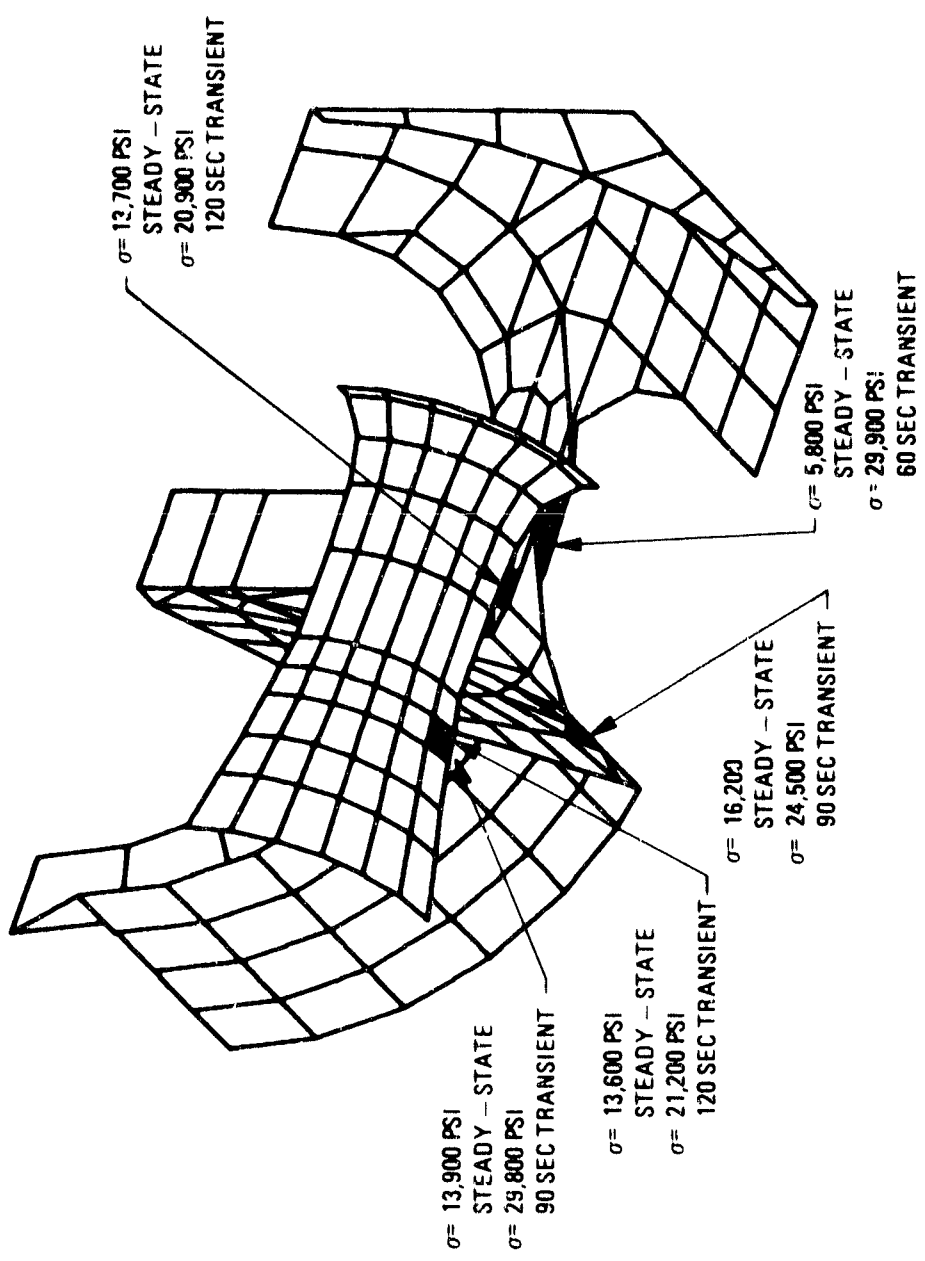


Figure 90

Alpha SiC Inner Housing Lower Quadrant Stresses Using Flared Flanges, $\nu = 0.95$

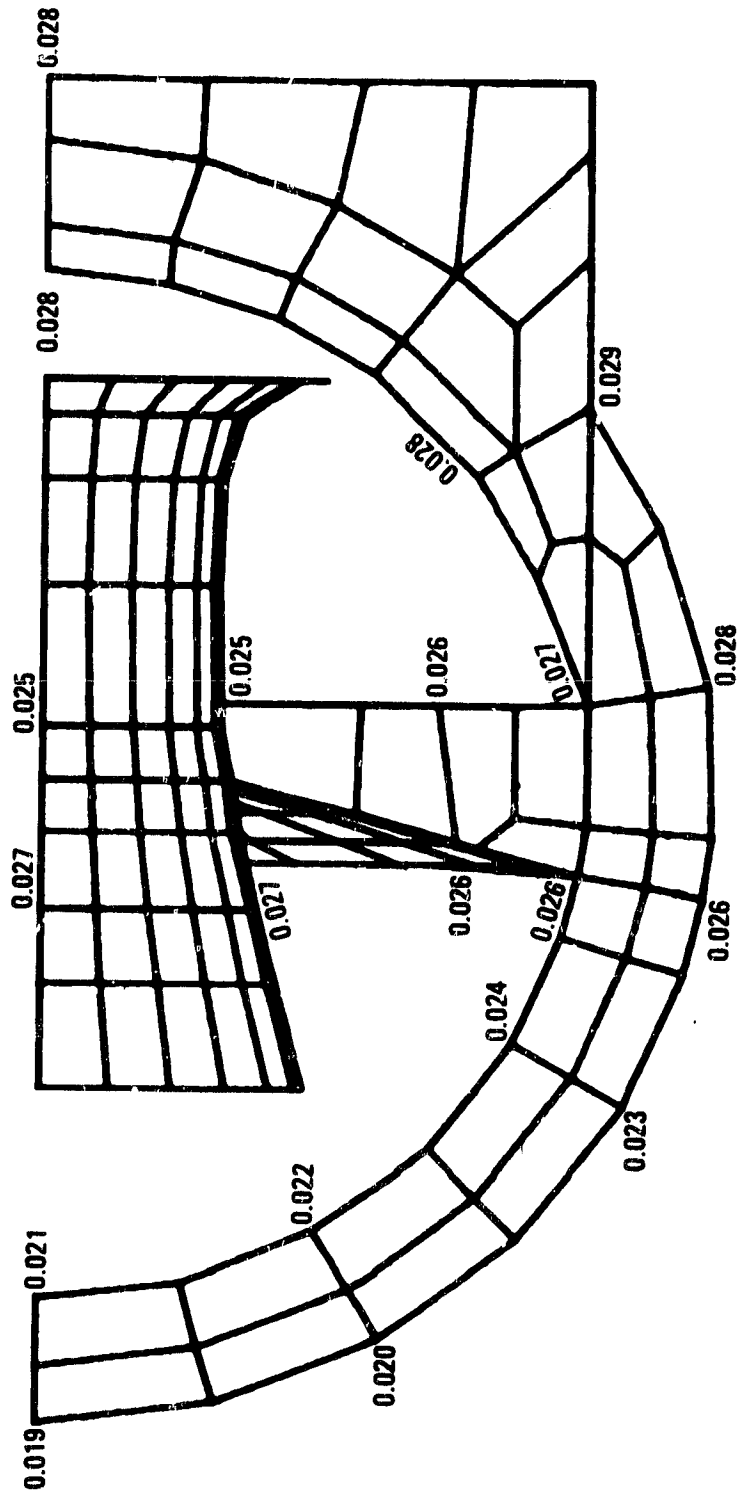
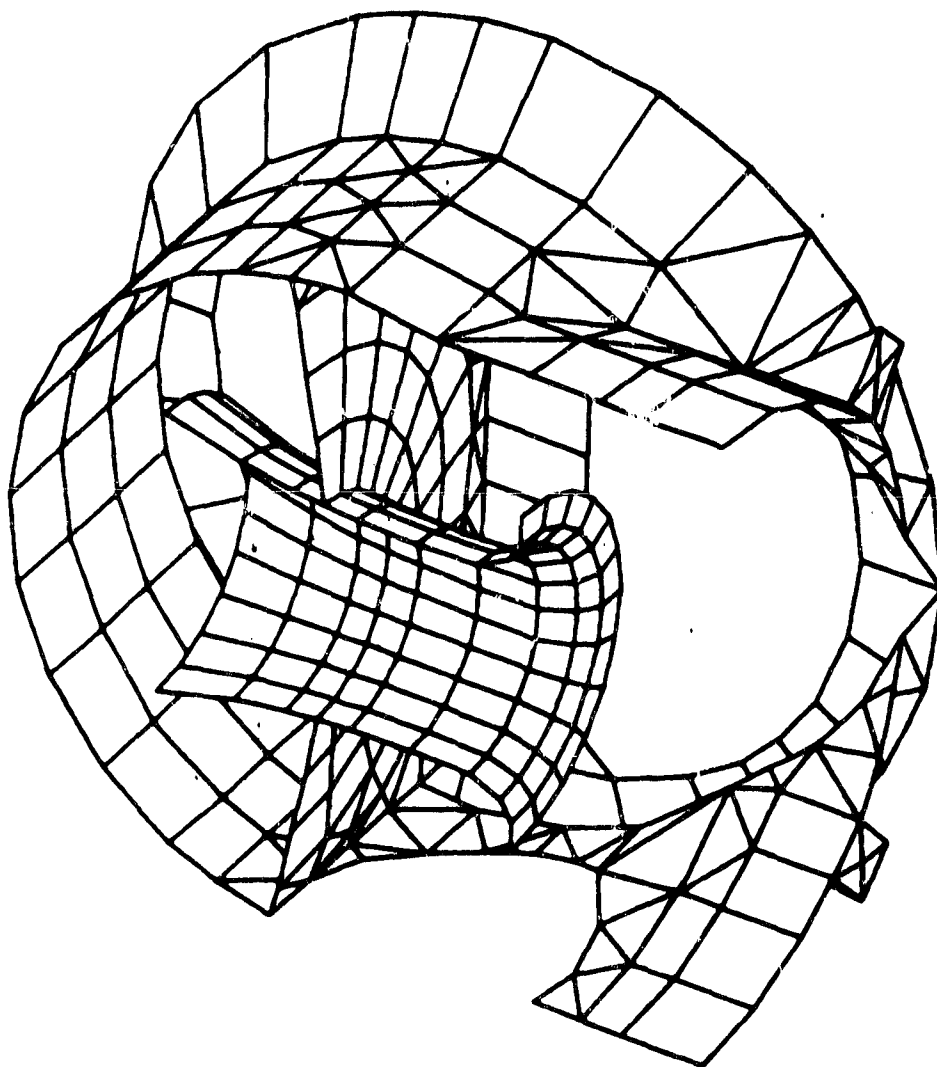


Figure 91

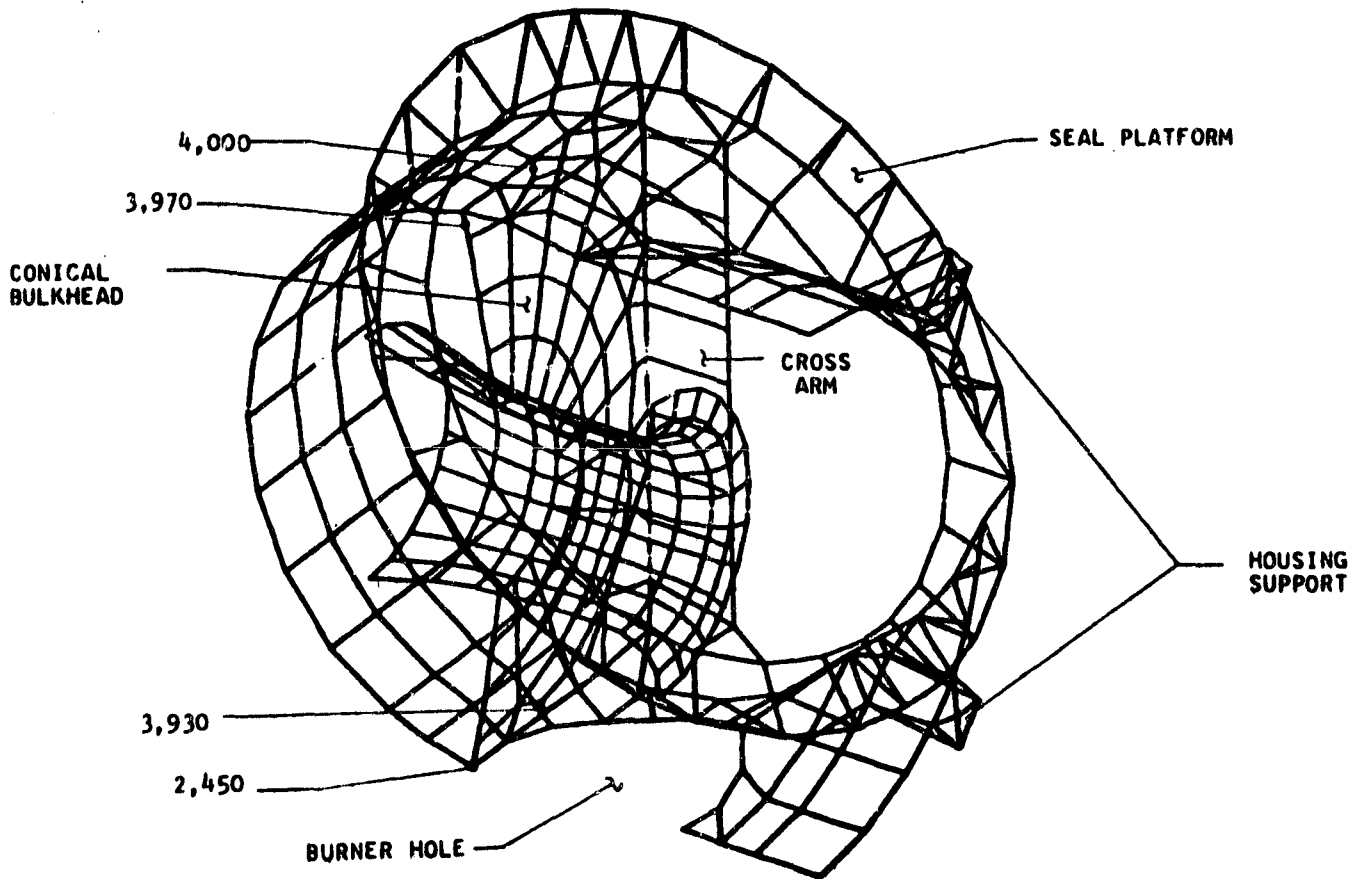
Alpha SiC Inner Housing Flange Displacement at Steady State Temperature
(Normal to Surface shown)



Inner Housing Current Design Finite Element Model

Figure 92

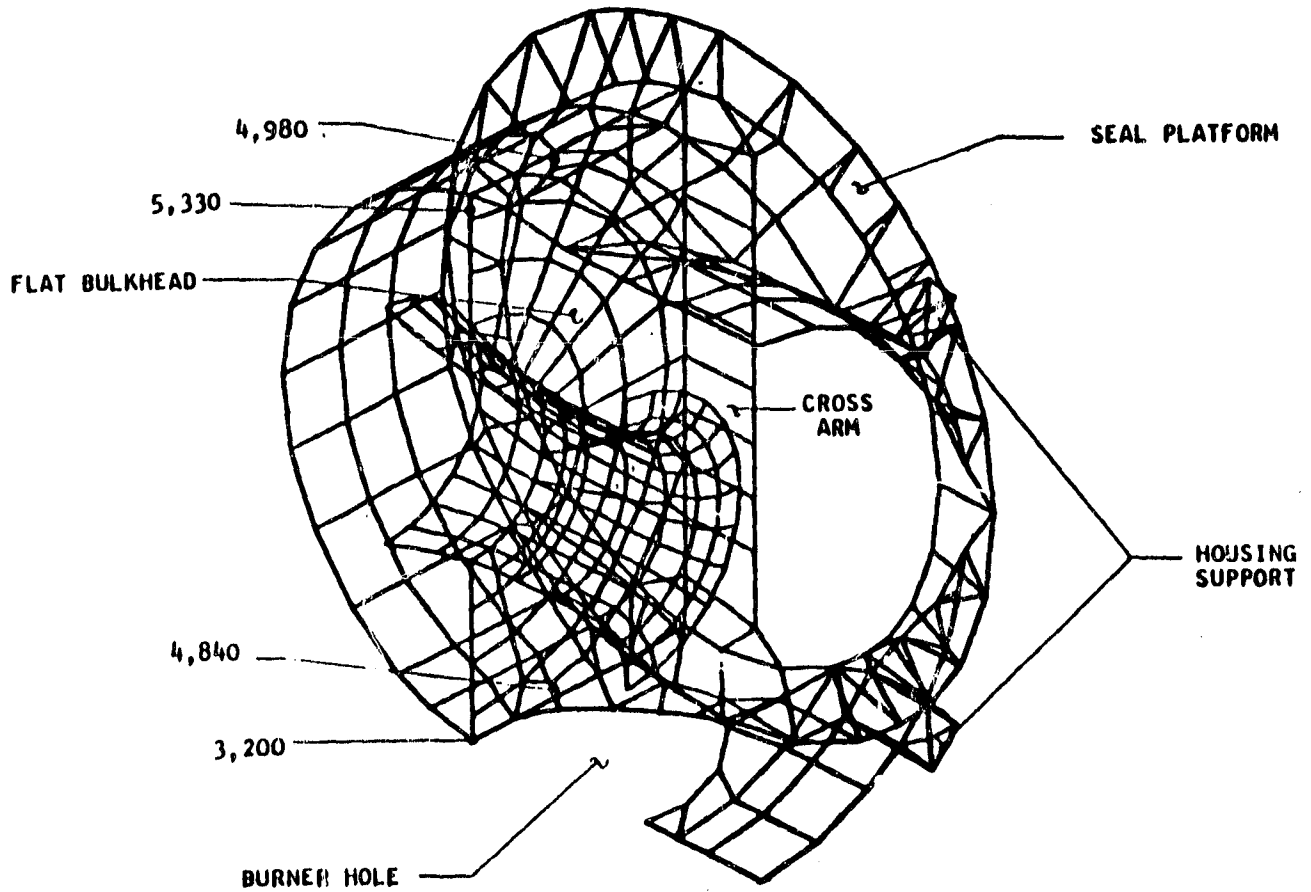
Maximum Principal Stresses -- psi
Pressure Load Only
Lithium Aluminum-Silicate (LAS) Material - .38 inch Thick



LAS Inner Housing - Finite Element Model
Conical Bulkhead

Figure 93

Maximum Principal Stresses -- psi
Pressure Load Only
Lithium Aluminum-Silicate (LAS) Material - .38 inch Thick

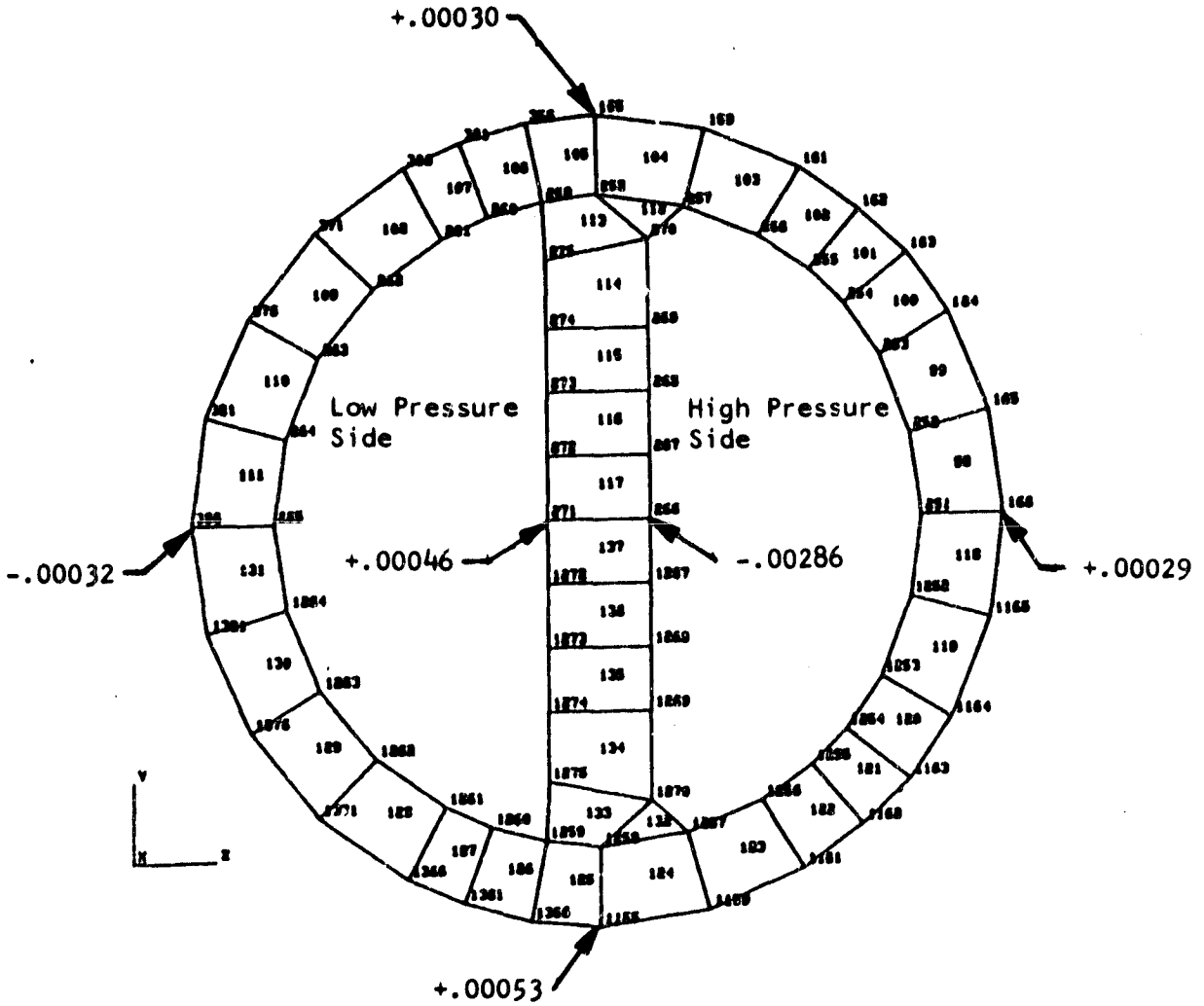


LAS Inner Housing - Finite Element Model

Flat Bulkhead

Figure 94

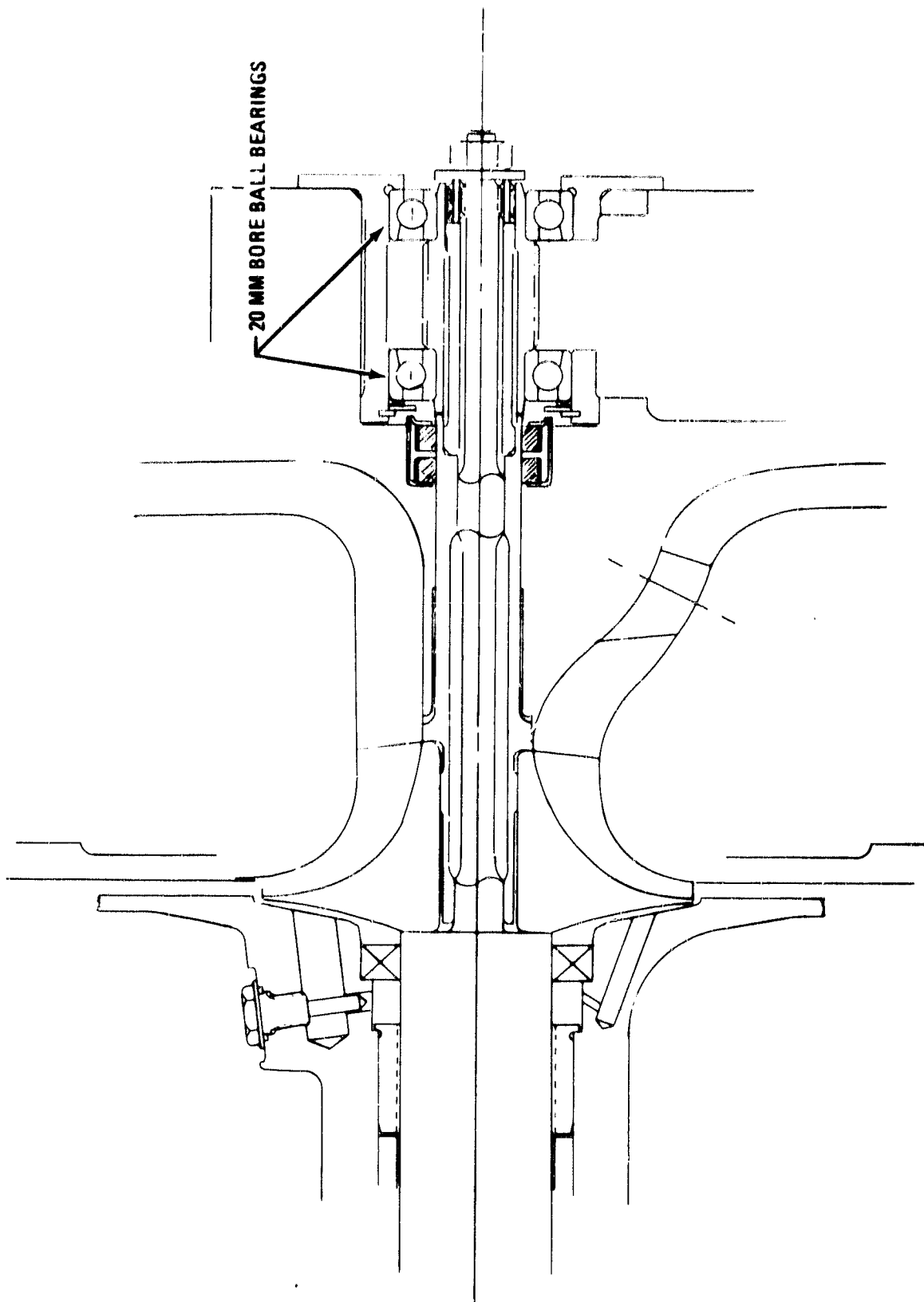
Deflection in 'X' Direction - inches



View From Inboard of Platform

LAS Inner Housing Seal Platform Deflection
Flat Bulkhead

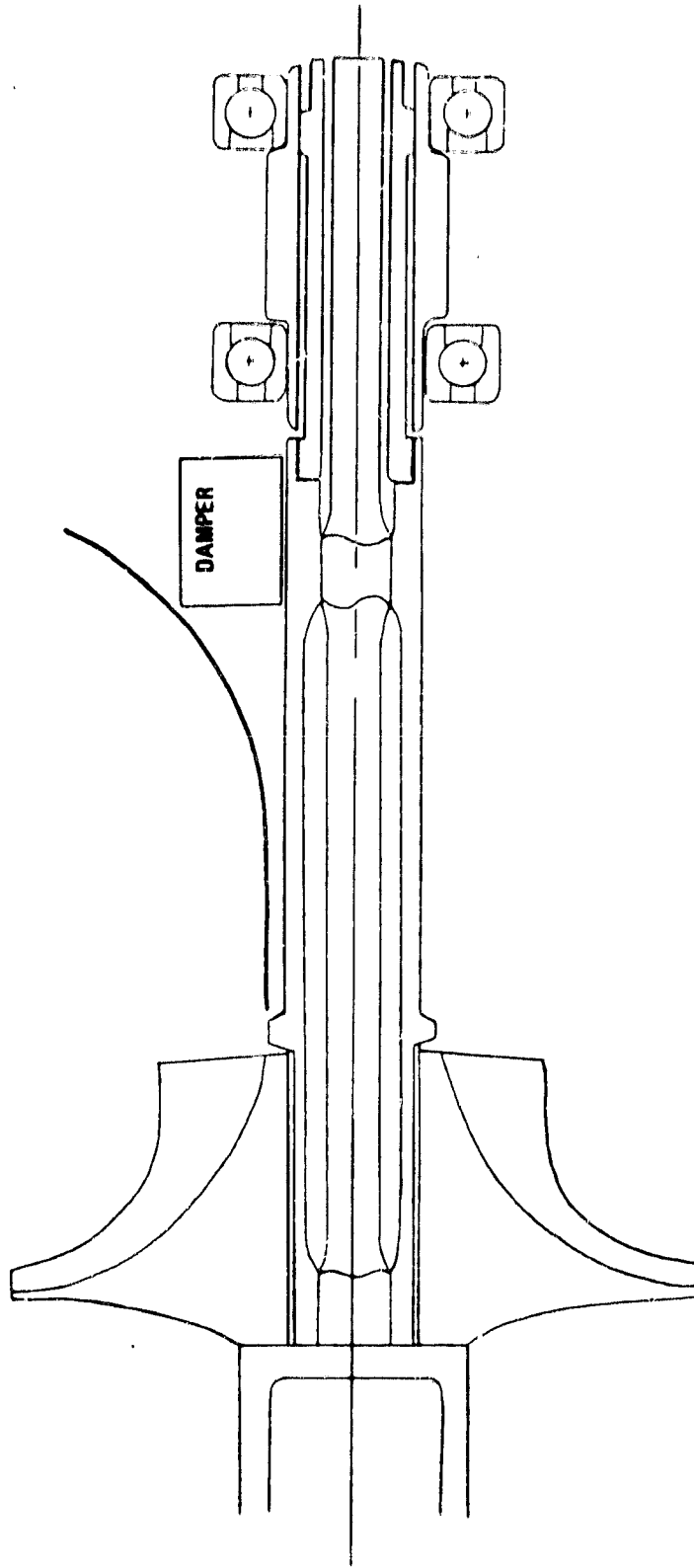
Figure 95



20 MM BORE BALL BEARINGS

Three Bearing Rotor System

Figure 96



Three Bearing Rotor System with Damper

Figure 97

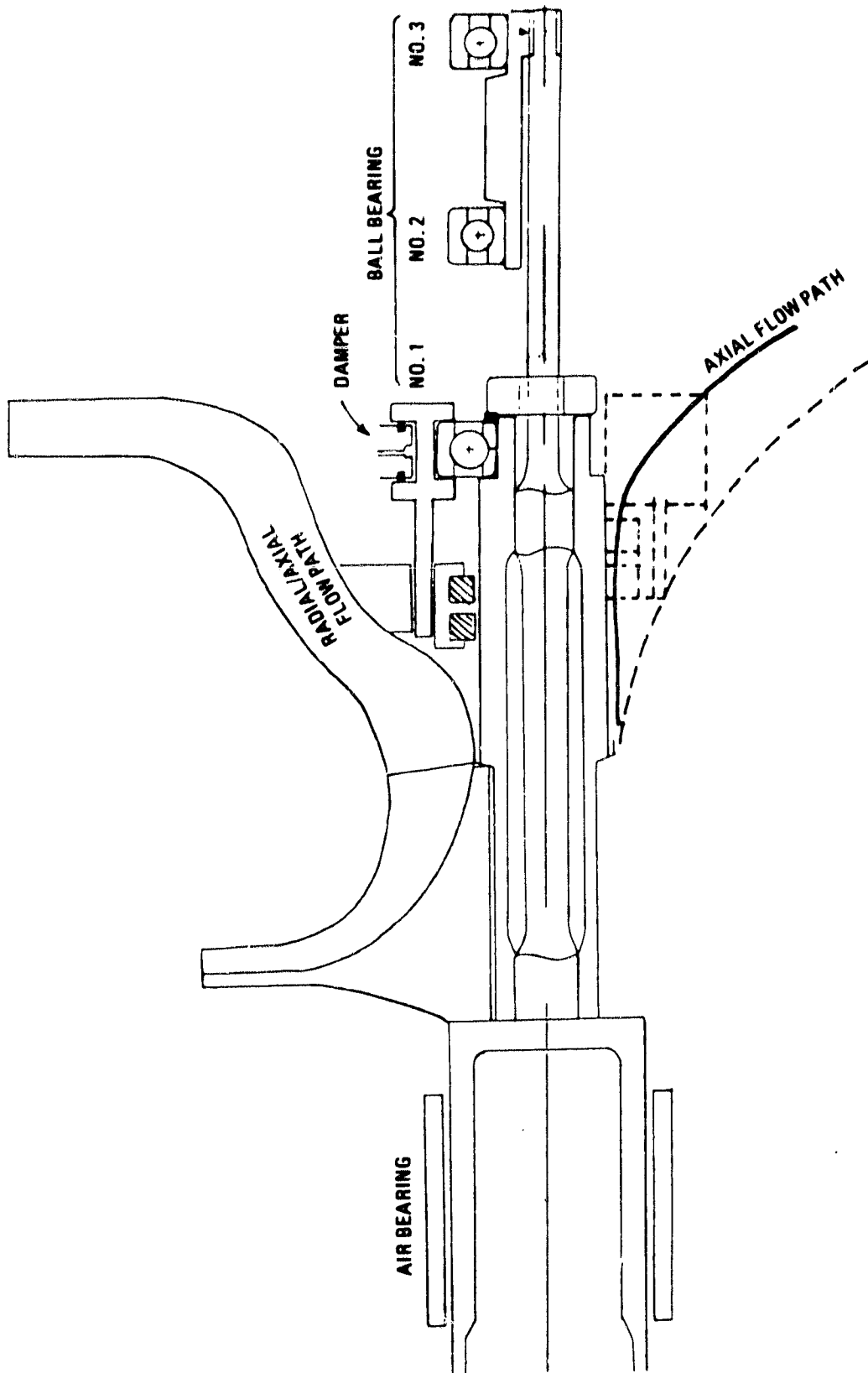
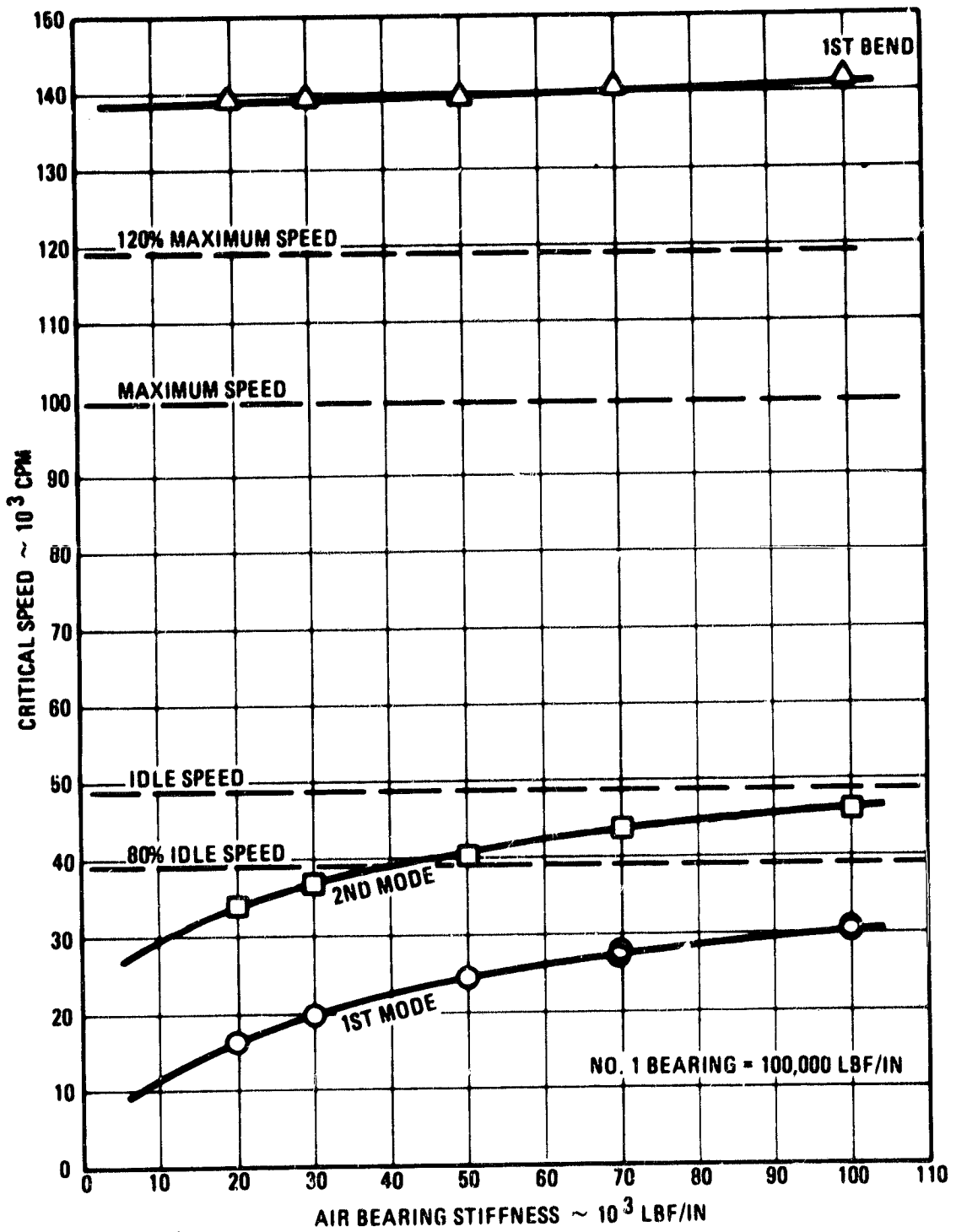


Figure 98



A-19389A

Three Bearing Rotor System Critical Speeds

Figure 99

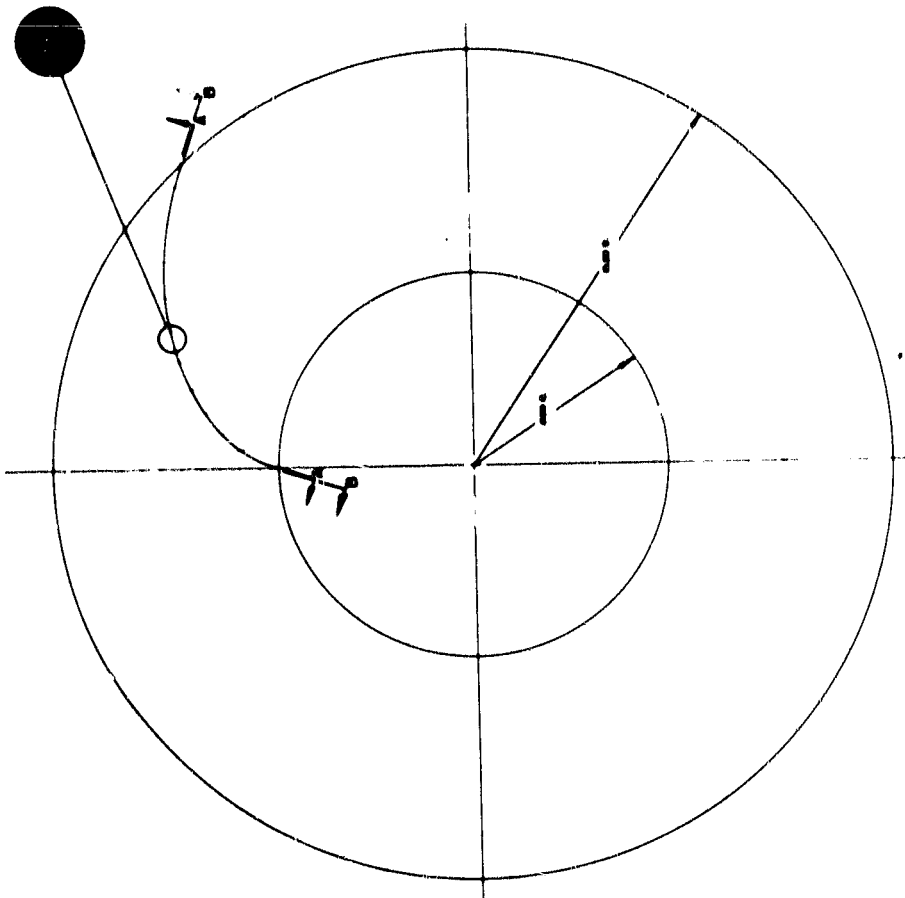
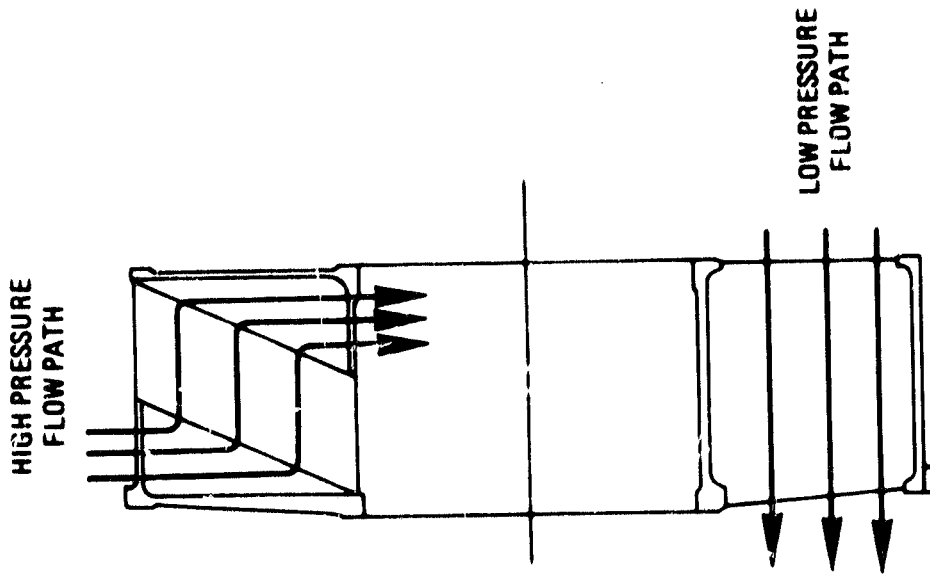
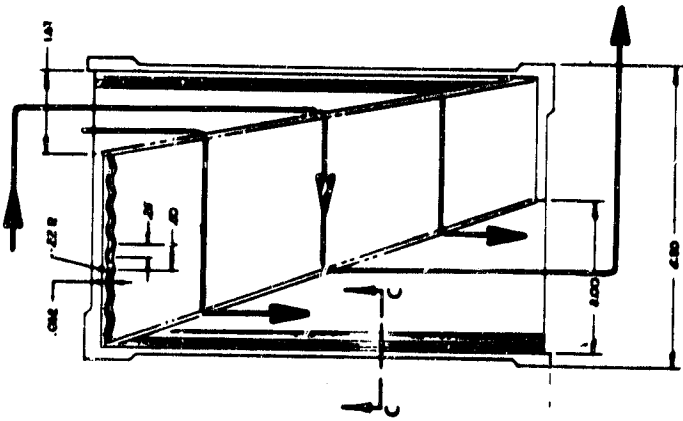


Figure 100

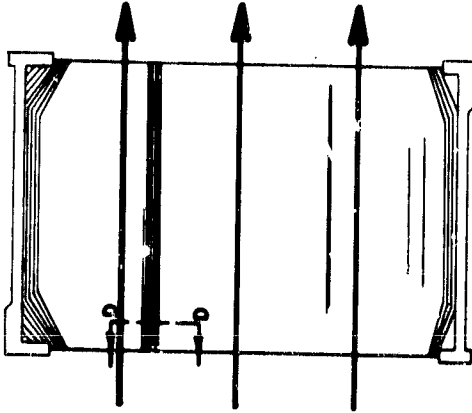
Annular Recuperator

HP PASSAGE

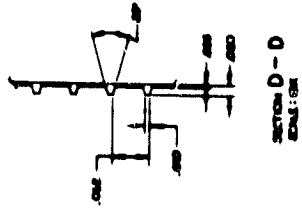


SECTION A - A
(COLD AND PRESSURE AIR)
APPROX. 1/8 SECTION 6550.

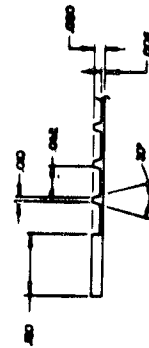
LP PASSAGE



SECTION B - B
(COLD LOW PRESSURE AIR)
APPROX. 1/8 SECTION 6550.



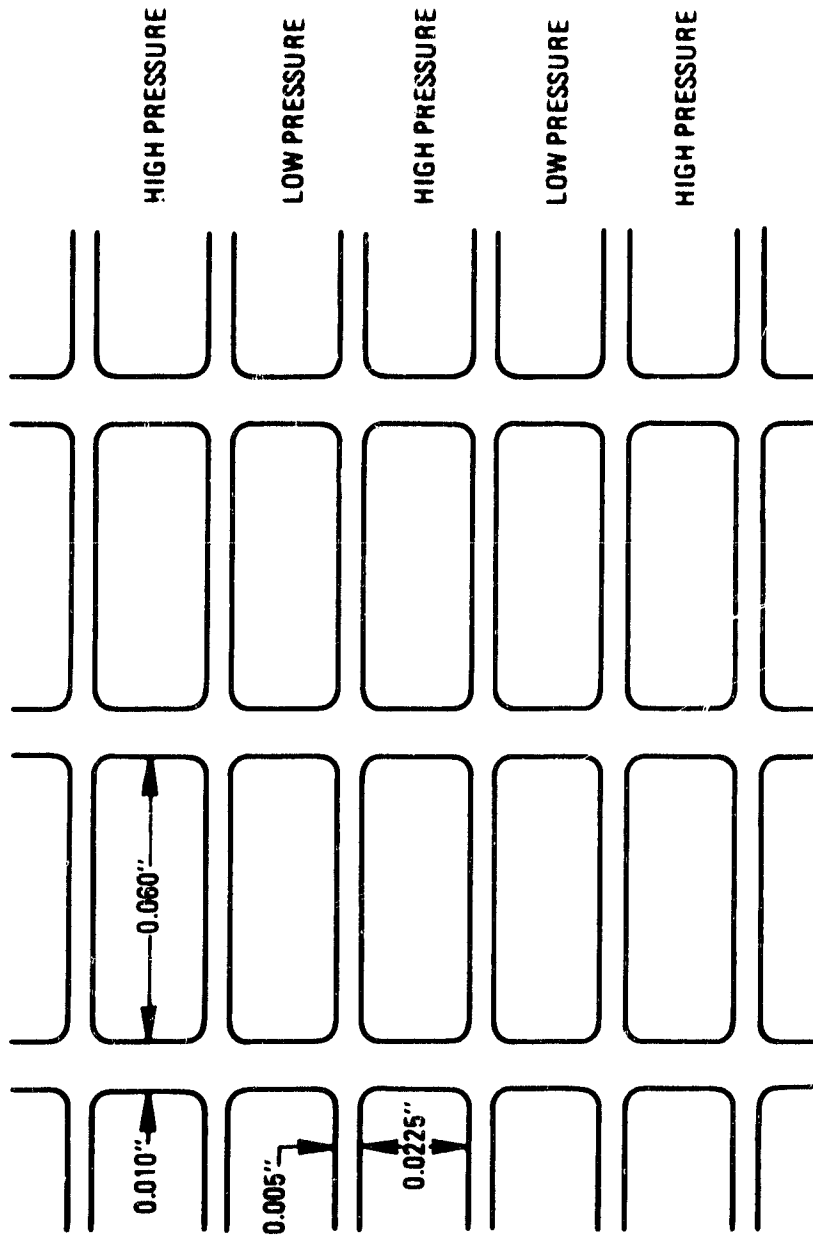
SECTION D - D
SCALE: 1/8"



SECTION C - C
SCALE: 1/8"

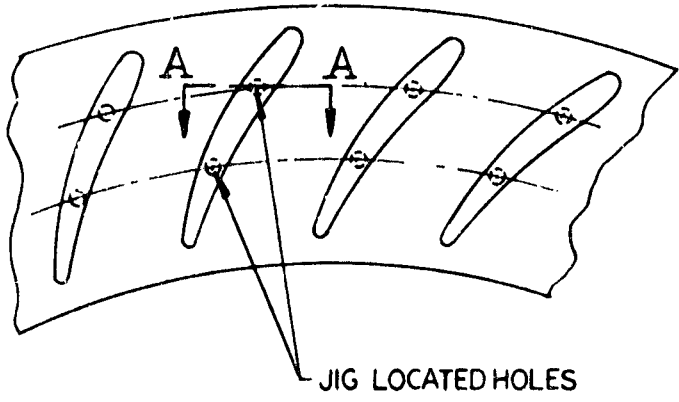
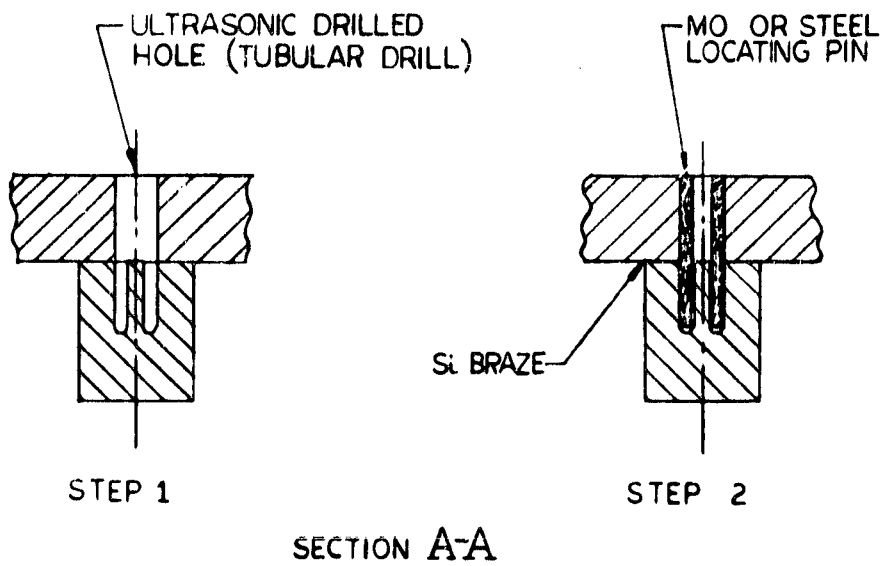
Recuperator Plates

Figure 101



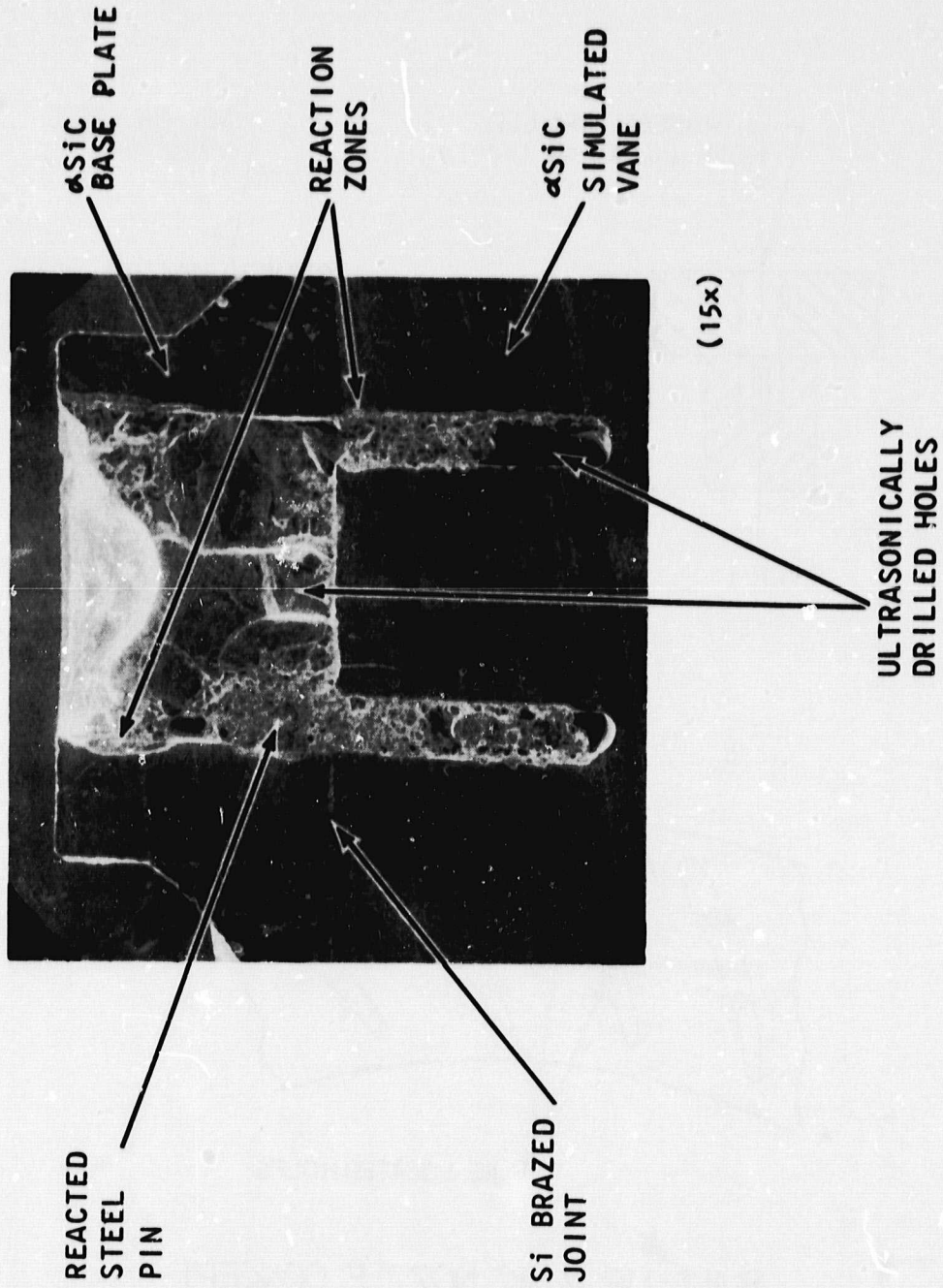
Recuperator Flow Passages

Figure 102



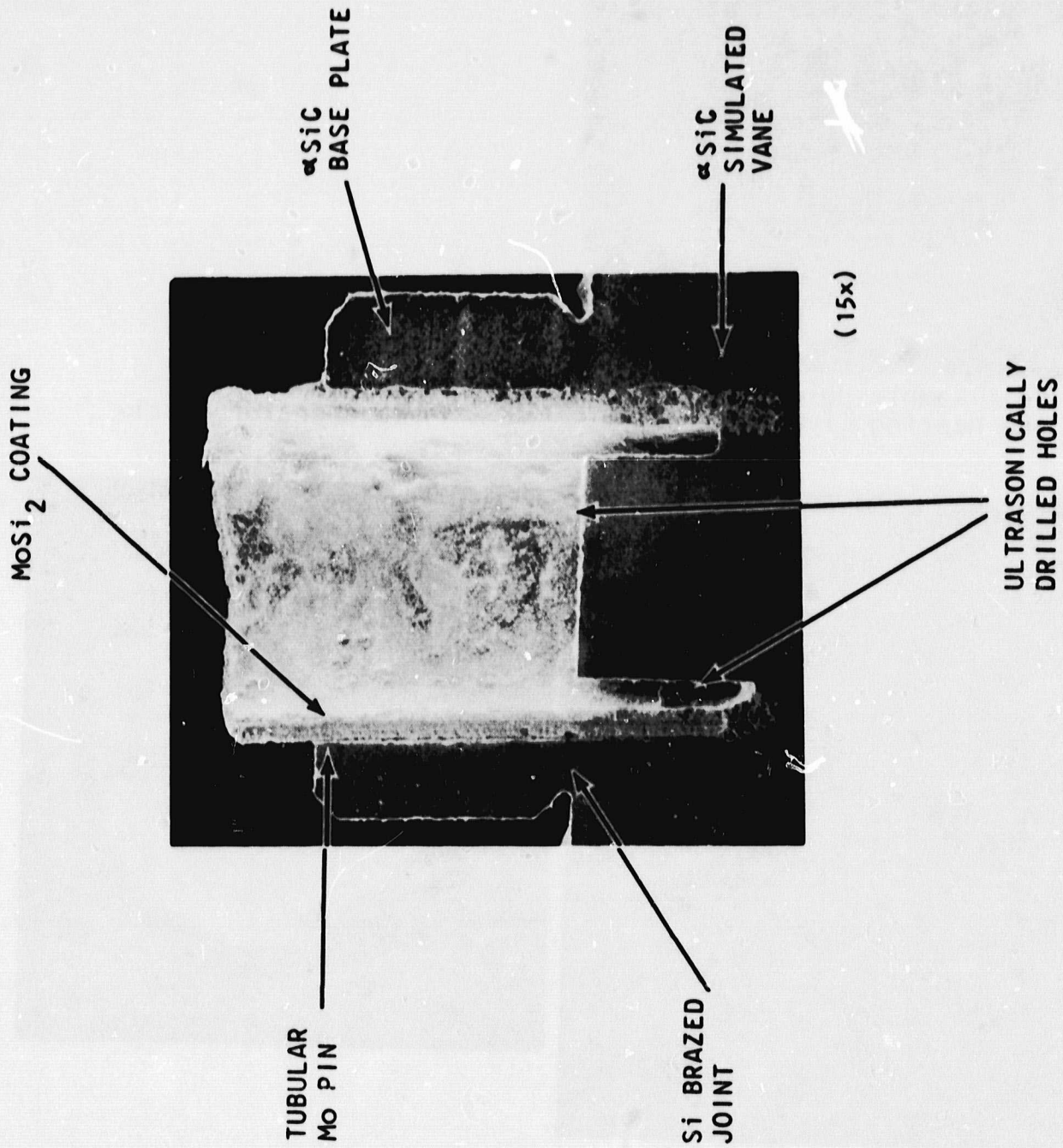
BUILT-UP α SiC NOZZLE CONCEPT

Figure 103



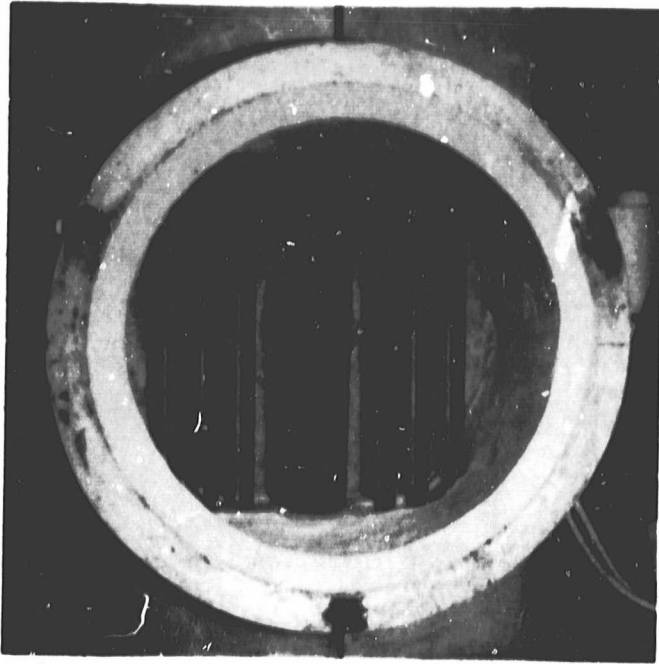
SECTION OF STEEL PINNED AND BRAZED NOZZLE SAMPLE

Figure 104



SECTION OF MOLYBDENUM PINNED AND BRAZED
NOZZLE SAMPLE

Figure 105



(a) Seal Sample Holder and Heating Elements

ORIGINAL PAGE IS
OF POOR QUALITY

(b) 9 Inch Sample
Regenerator Matrix



(c) Control Panel



Regenerator Seal Wear Test Machine

THERMAL EXPANSION - CORNING 9458 - LAS

01/16/81
13.18.58.

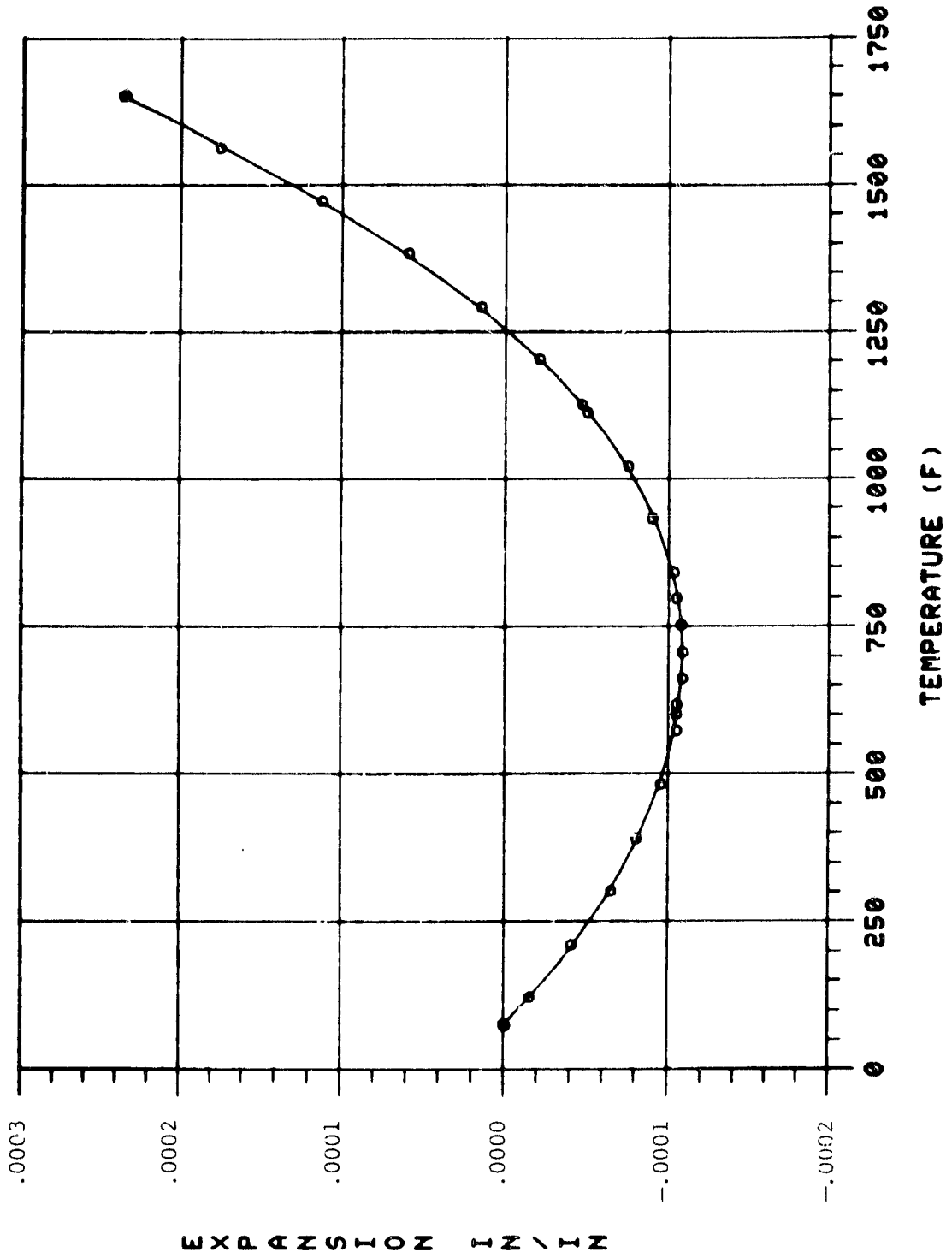


Figure 107

EXPANSION MATCHING - LAS HOT SEAL

01/16/81
09.03.24.

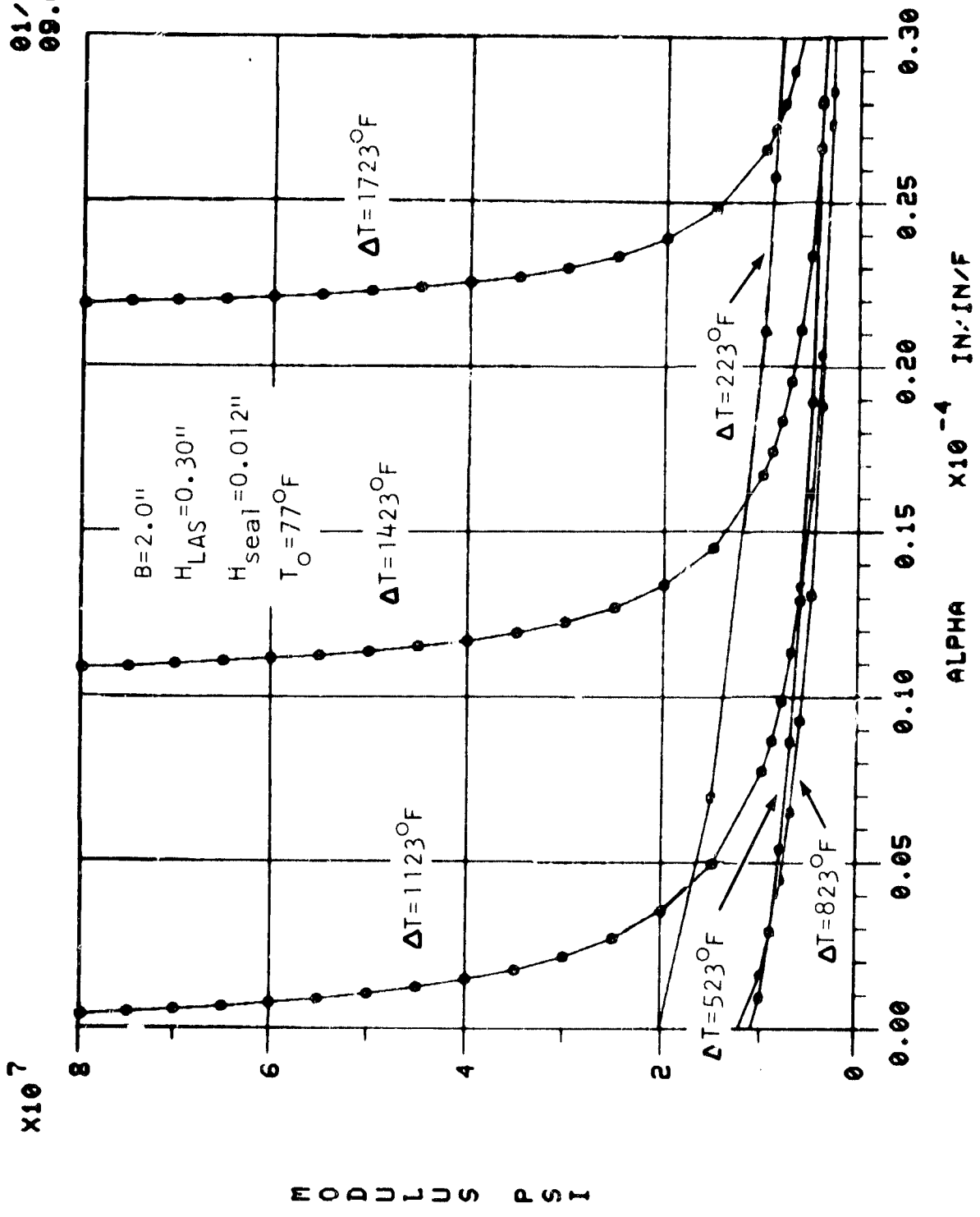
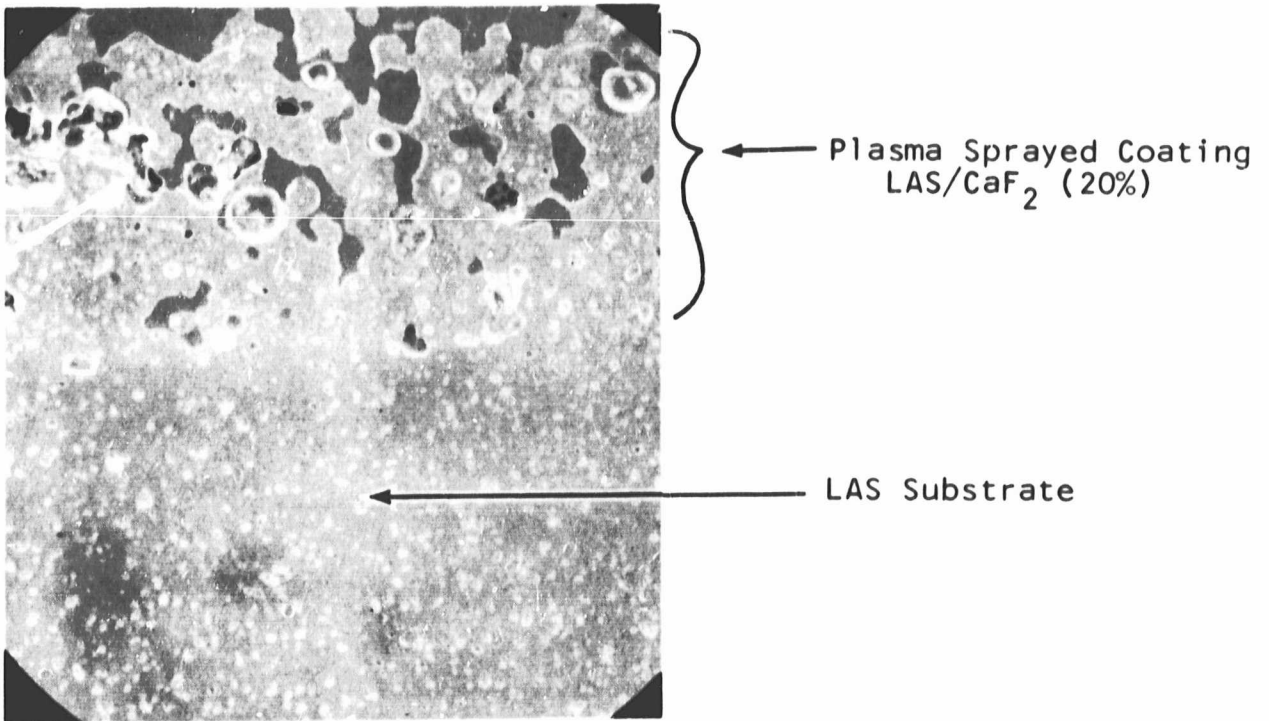


Figure 108

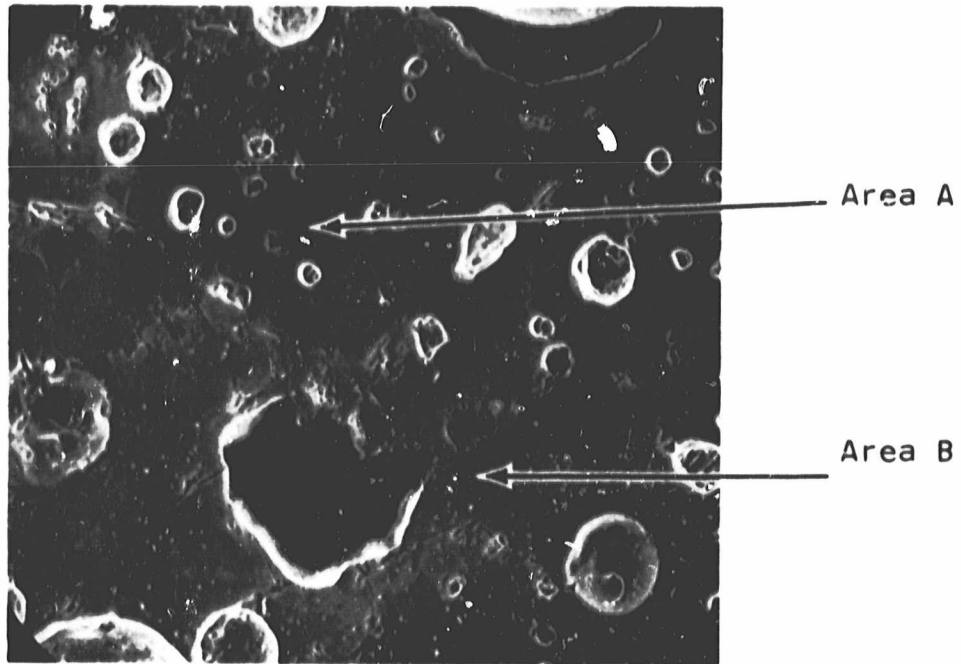
PLASMA SPRAYED LAS



(50x)

PLASMA SPRAYED LAS/CaF₂ MIXTURE ON LAS

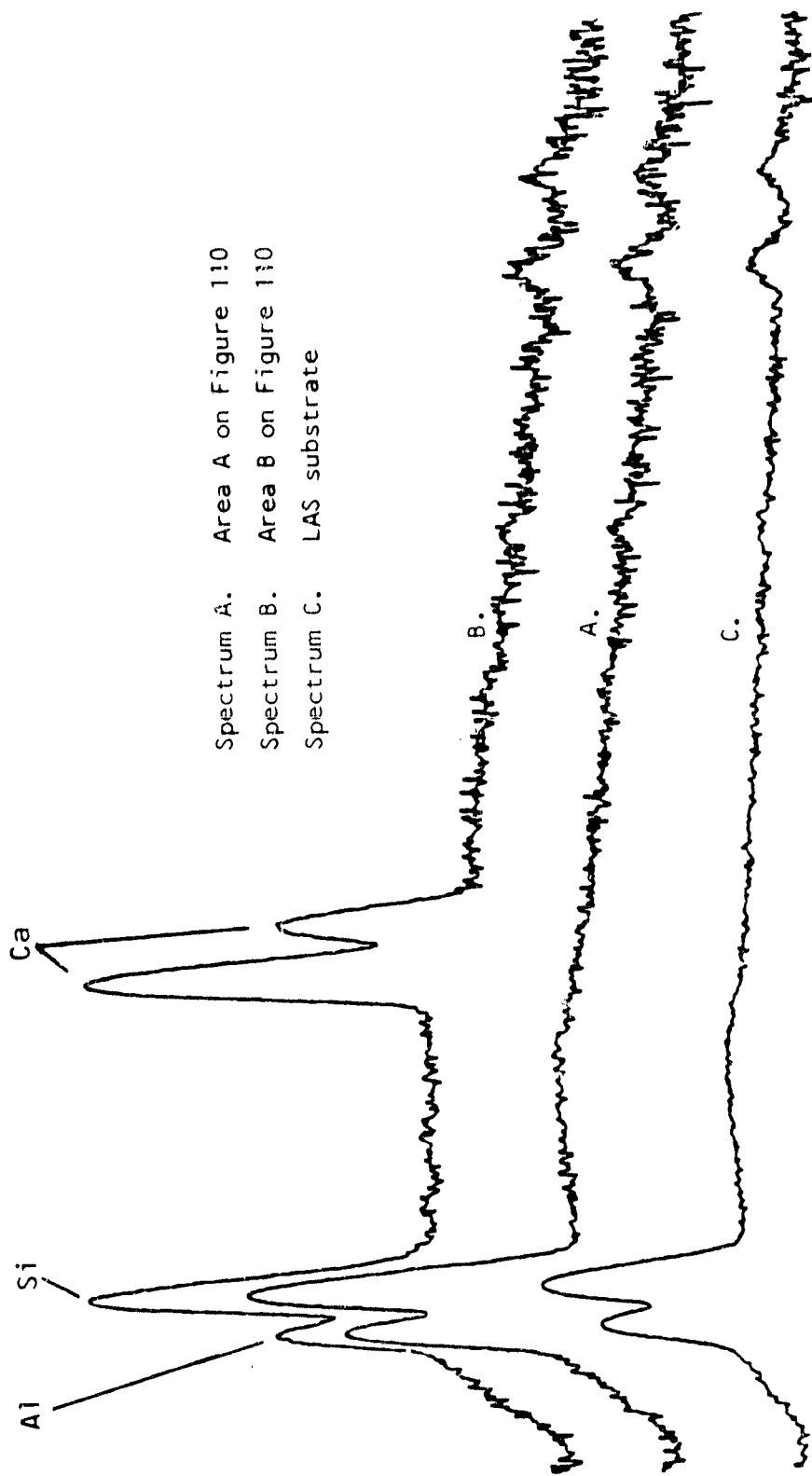
DETAIL OF COATING LAYER



(500x)

PLASMA SPRAYED LAS/ CaF_2 MIXTURE ON LAS

Figure 110

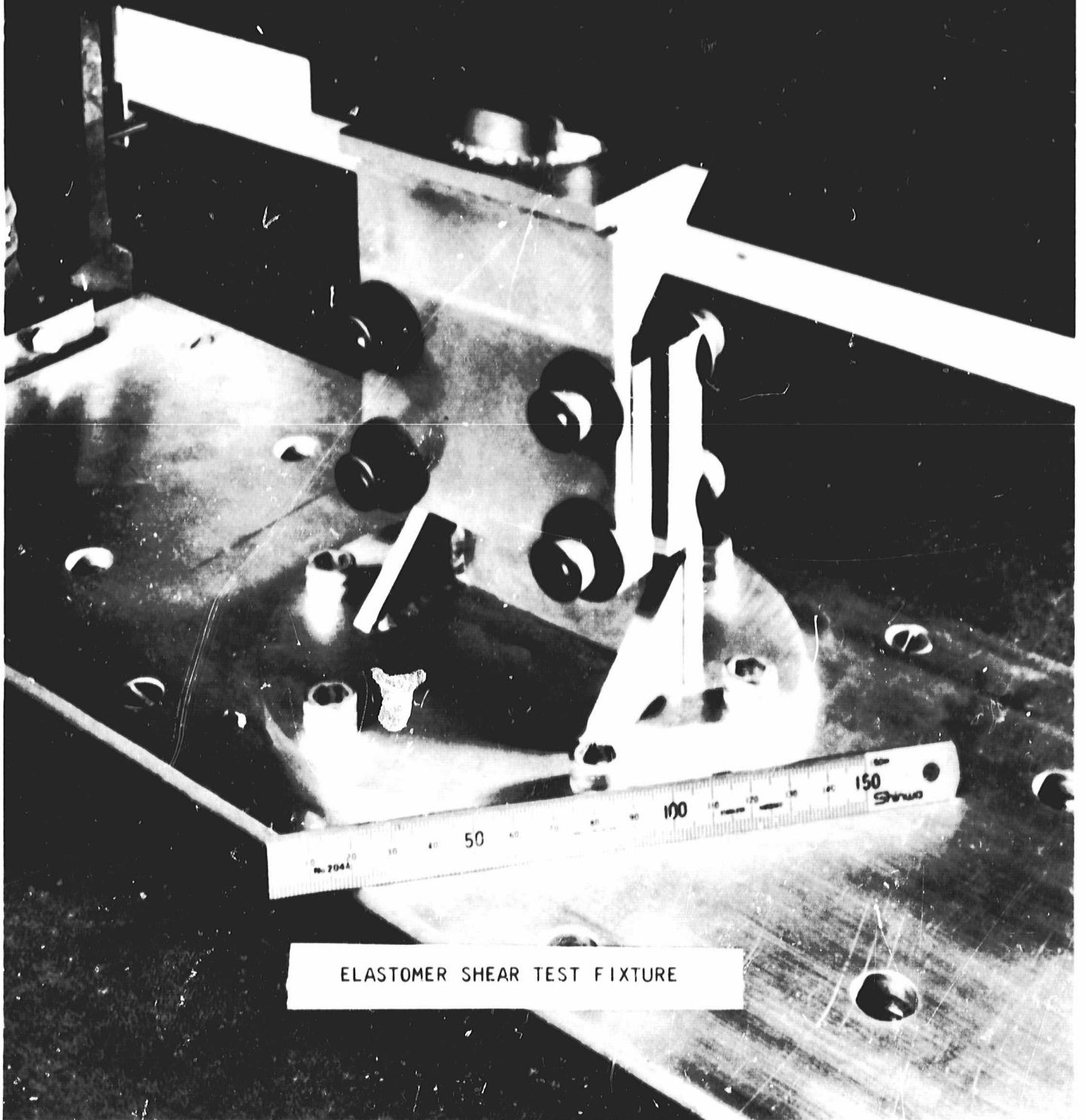


Spectrum A. Area A on Figure 110
 Spectrum B. Area B on Figure 110
 Spectrum C. LAS substrate

EDX SPECTRA OF LAS/CaF₂ LAYER

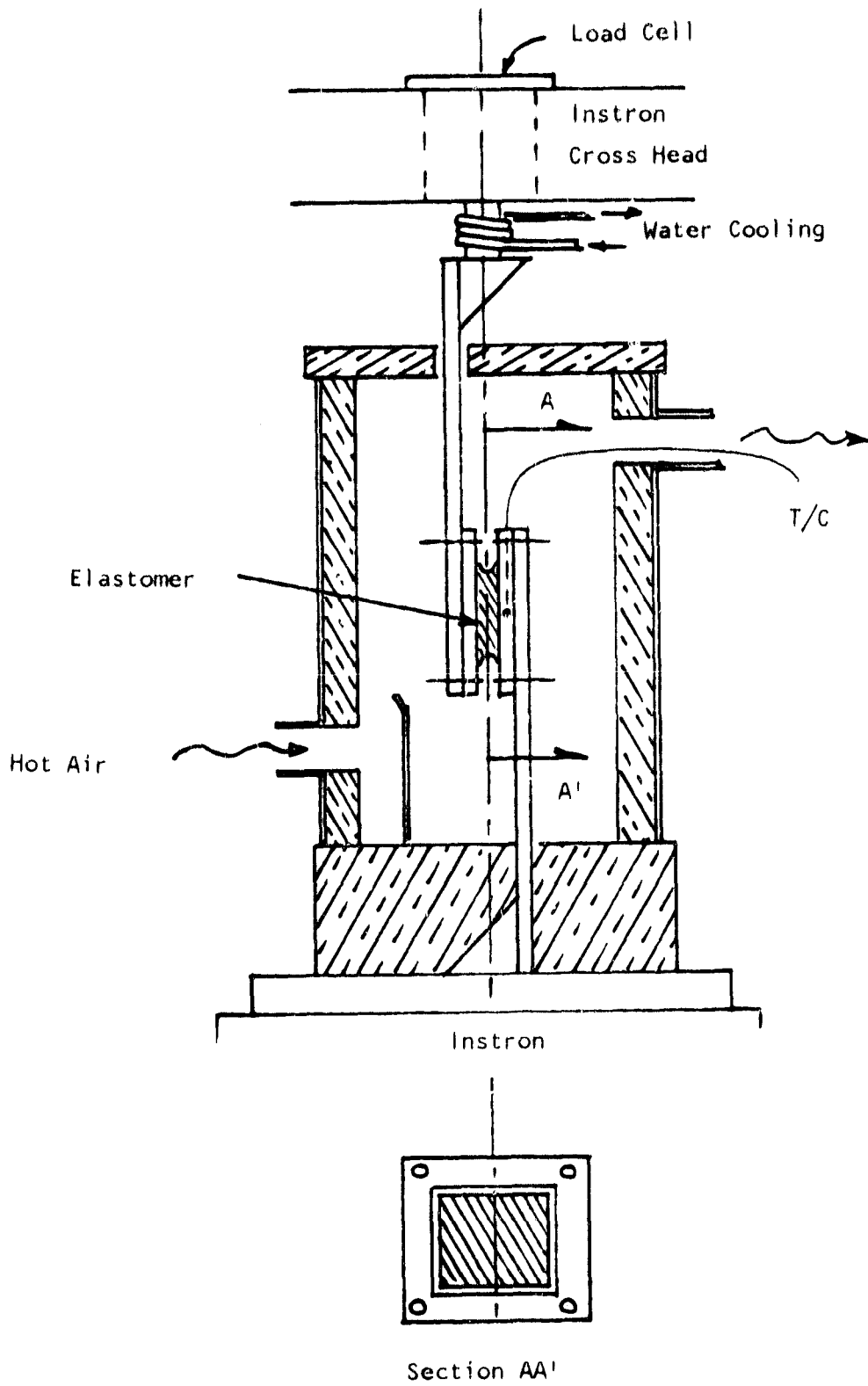
Figure 111

 **INSTRON**



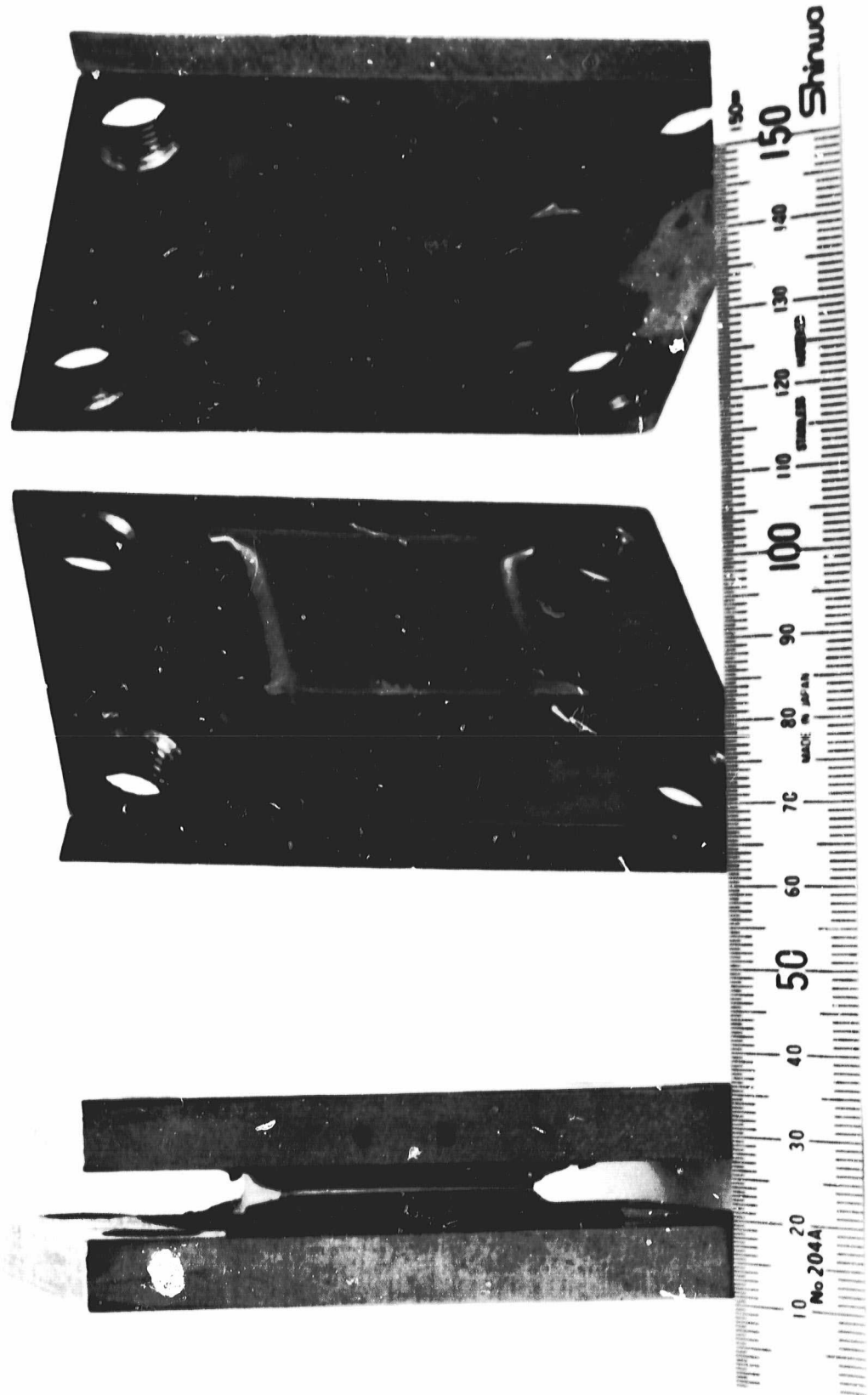
ELASTOMER SHEAR TEST FIXTURE

Figure 112



ELEVATED TEMPERATURE ELASTOMER SHEAR TEST FIXTURE

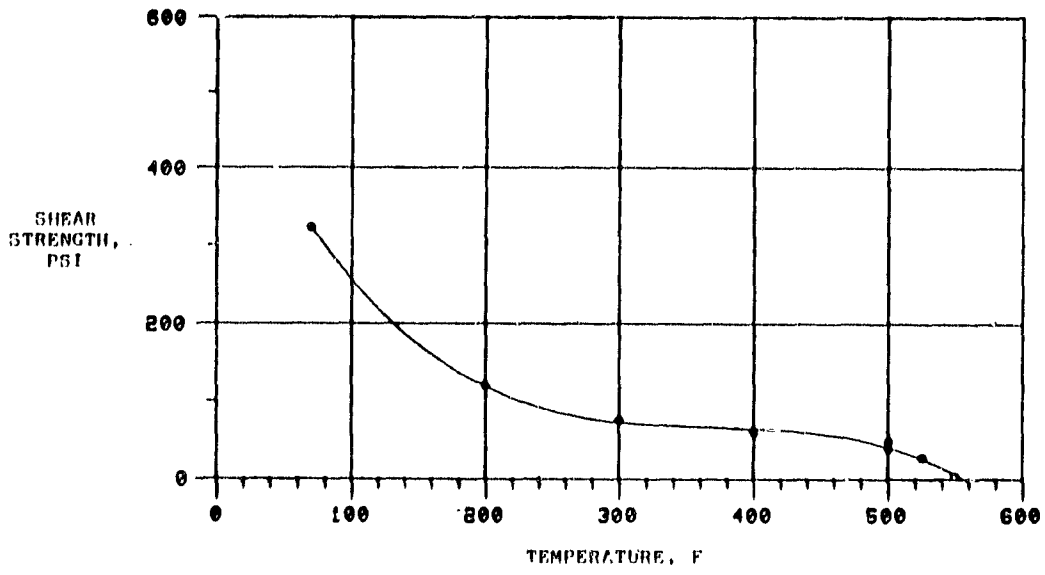
Figure 113



ELASTOMER SHEAR TEST SAMPLES

Figure 114

03/09/81
14.44.39.



ELASTOMER TEST RESULTS, ELEVATED TEMPERATURES

Figure 115

THermal STABILITY OF BYLOAD 100

18/05/80
13.04.10.

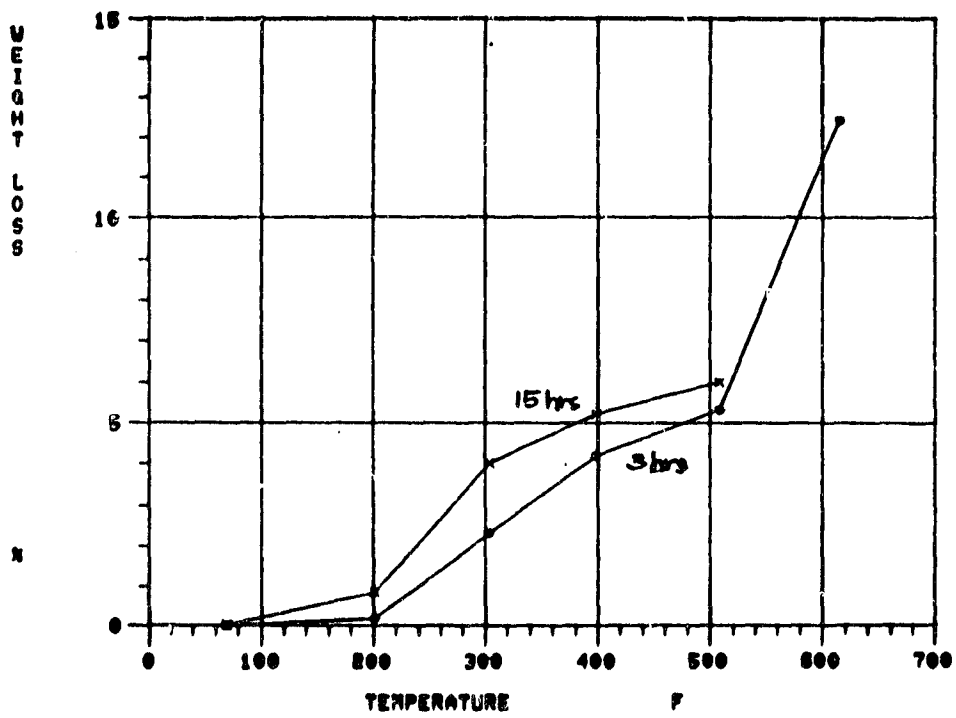
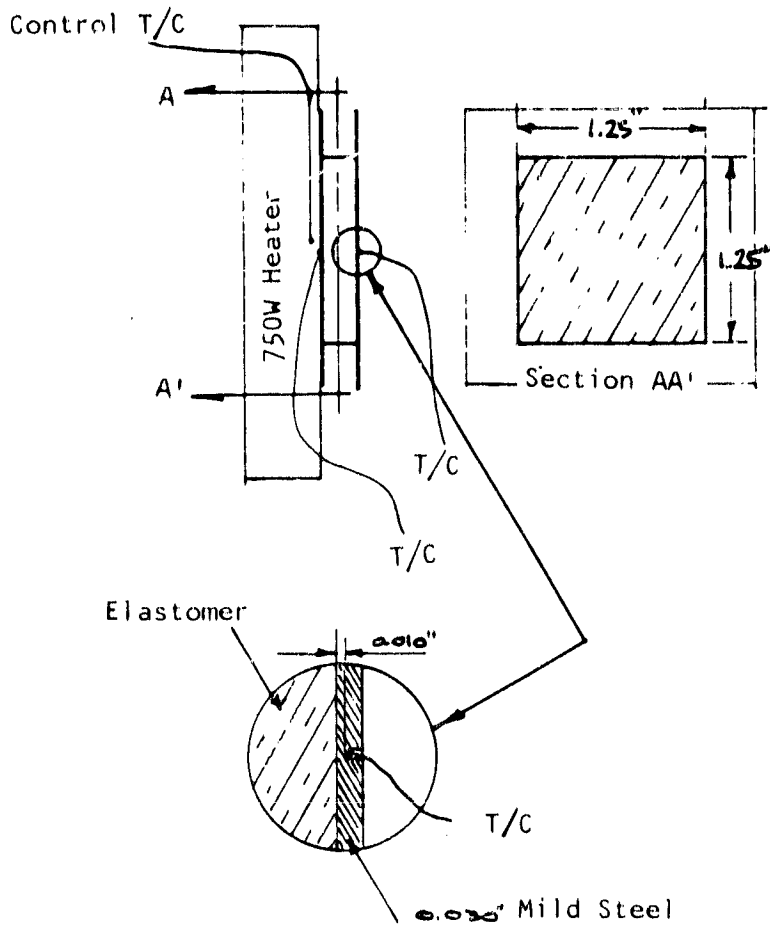


Figure 116



ELASTOMER
"CONDUCTIVITY"
RIG

Figure 117

'DELTA' T VS TEMPERATURE FOR THREE ELASTOMERS

02/02/71
08.13.42

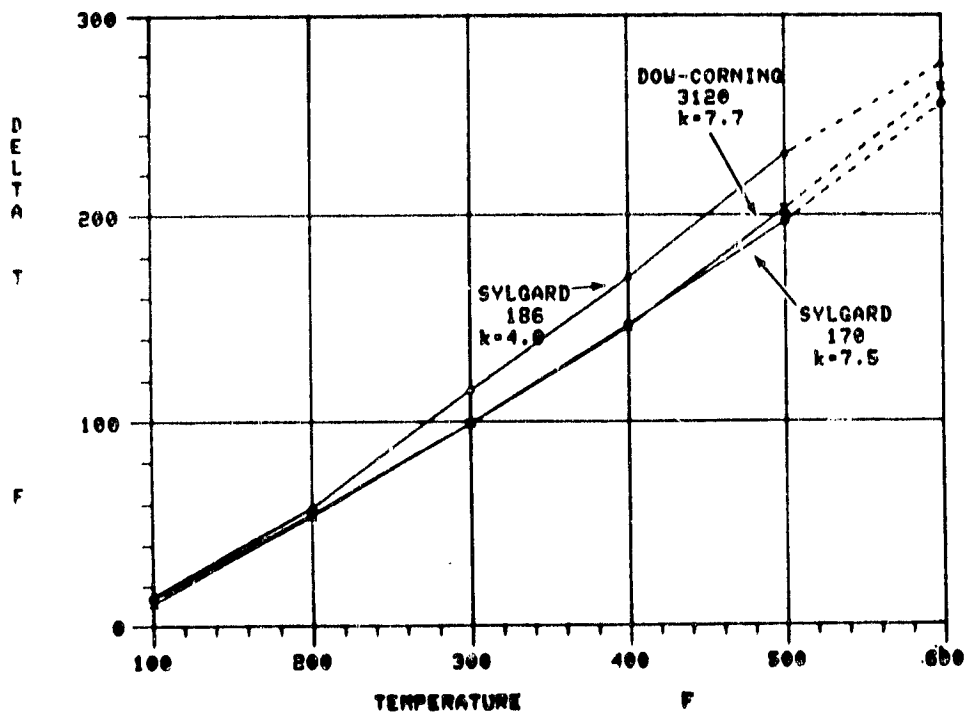
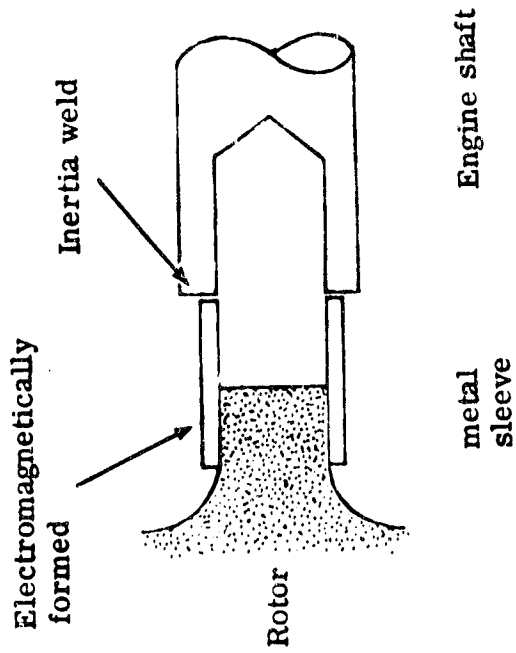
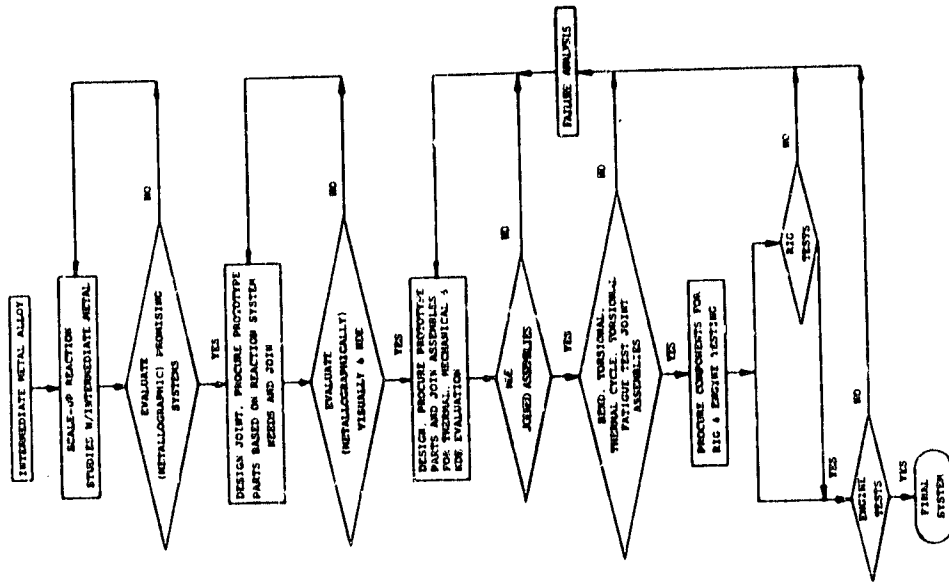


Figure 118



RPD ROTOR-SHAFT ATTACHMENT

Figure 119



DECISION PATH FOR ROTOR-SHAFT JOINING
ELECTROMAGNETIC FORMING

Figure 120

INSULATION ΔT RIG

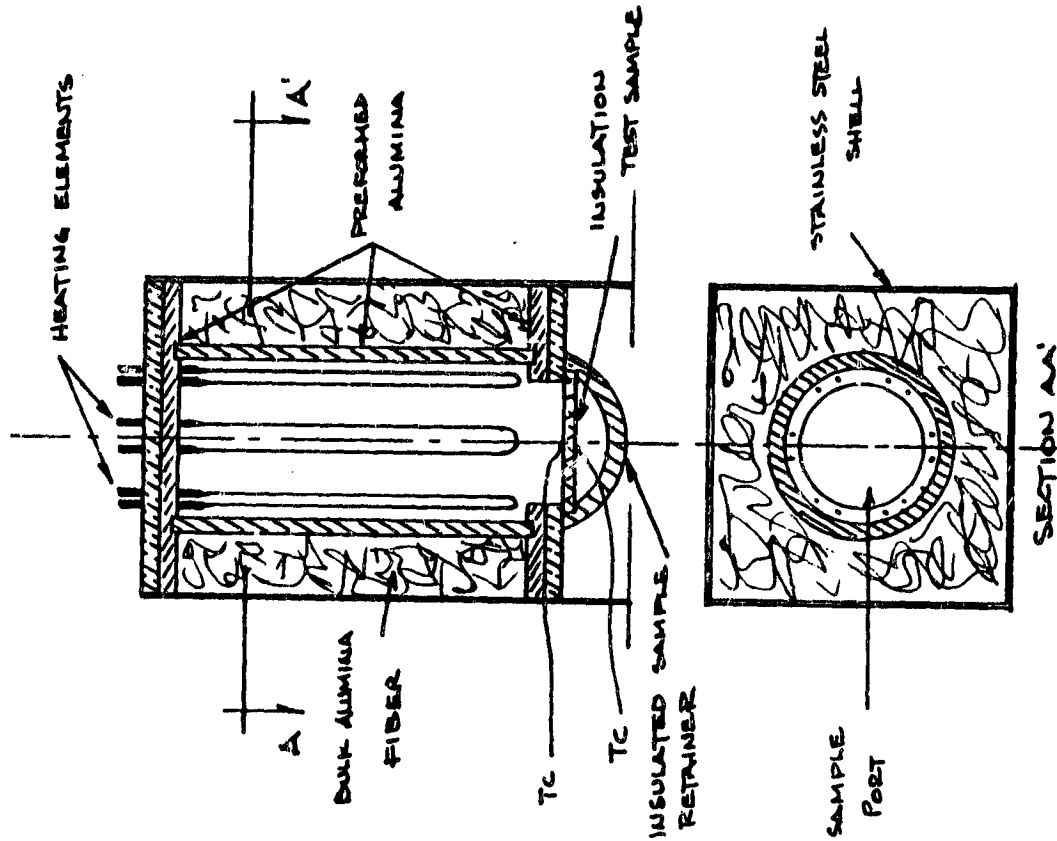
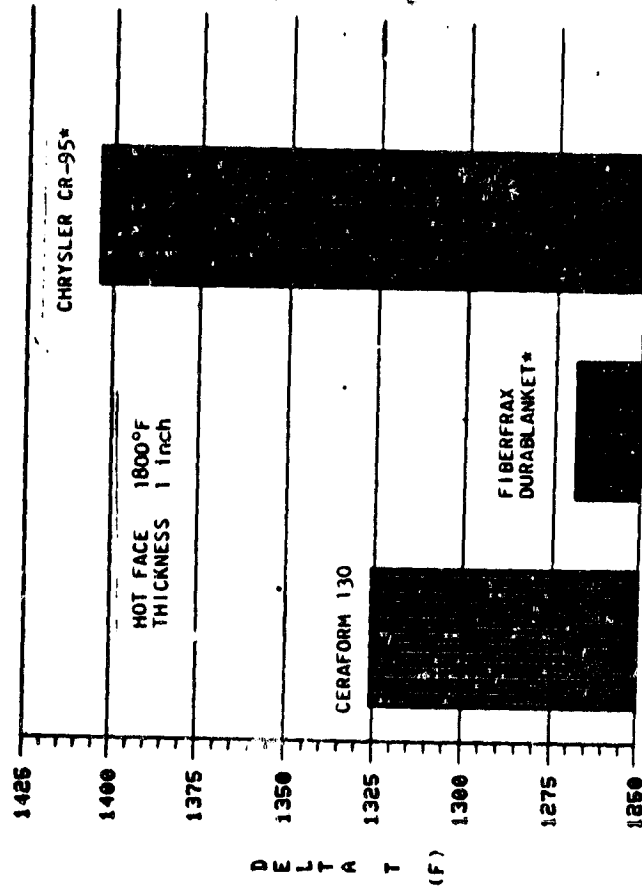


Figure 121

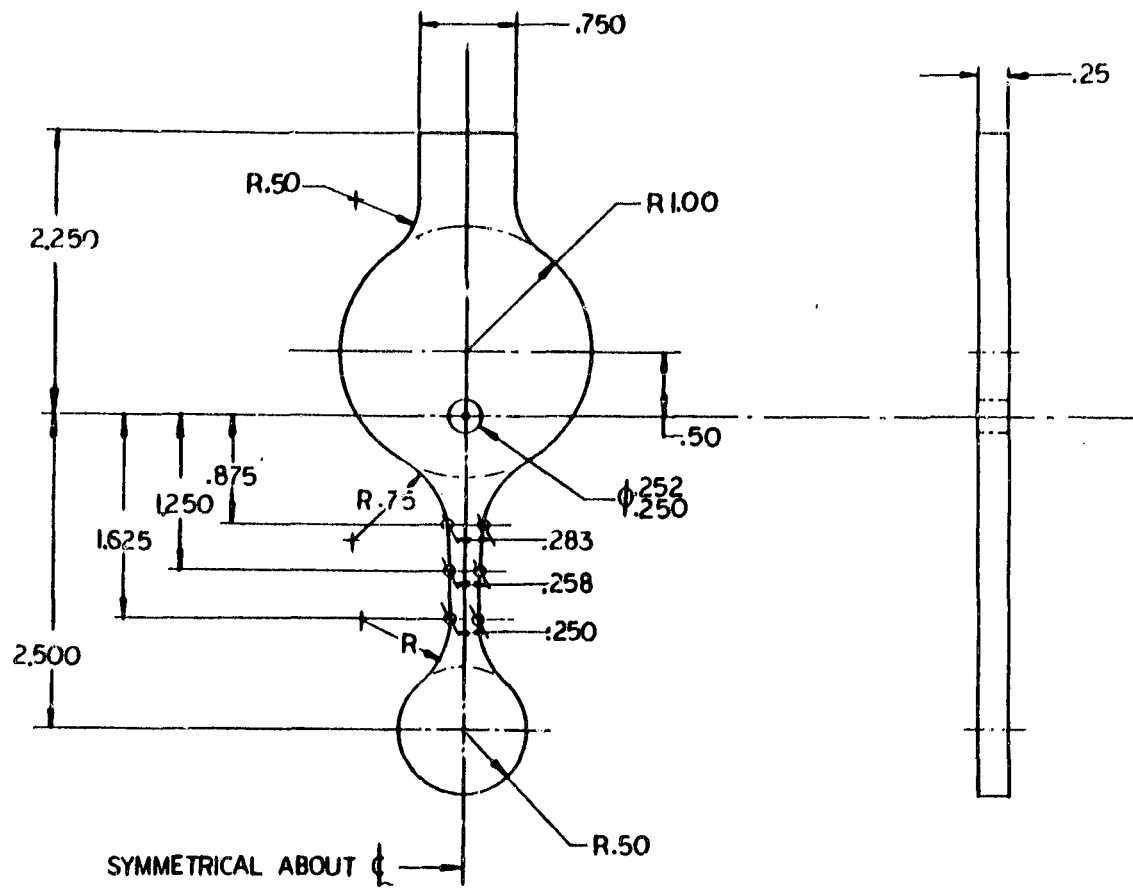
COMPARATIVE ΔT 's FOR INSULATION CANDIDATES



*Data has been corrected for thermocouple location

Figure 122

ORIGINAL PAGE IS OF POOR QUALITY

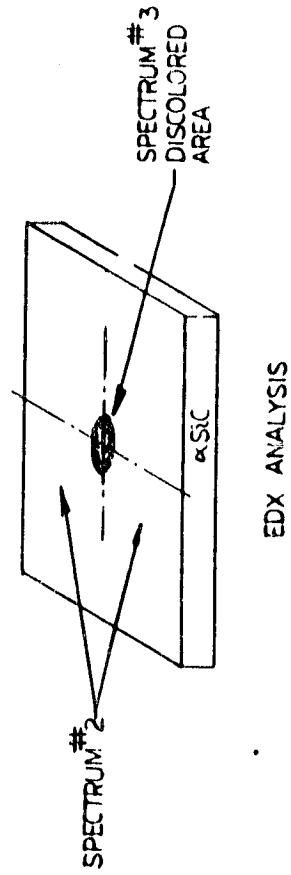
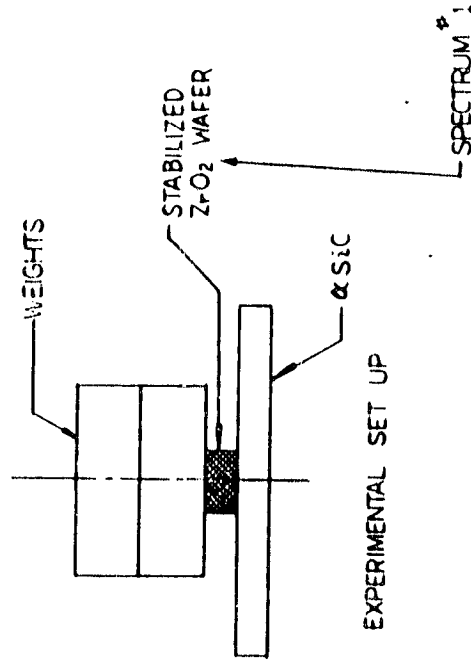


CERAMIC TEST BAR - SPIN TEST

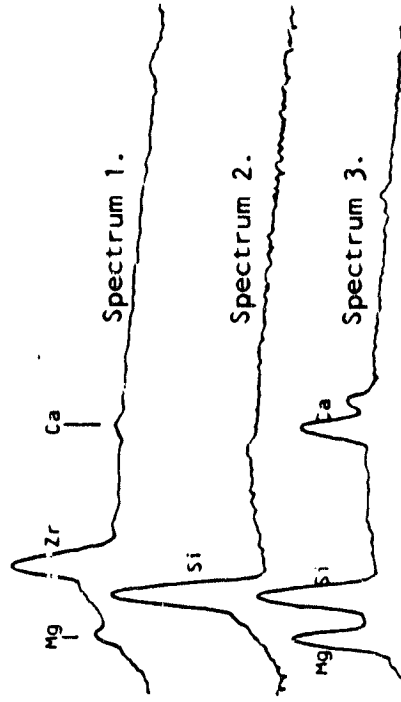
Figure 123

LONG TERM INTERFACING TEST
 $ZrO_2 / \alpha SiC$

> 500 HOURS AT 2300°F / 25 PSI



S i C / Z r O ₂ L O N G T E R M T E S T *



- Spectrum 1. ZrO_2 wafer (new)
- Spectrum 2. SiC bar outside white area.
- Spectrum 3. White area on SiC bar.

*Test Conditions: Temperature - 2300°F
 Load - 25 psi
 Time - 500+ hours

Figure 124

Figure 125

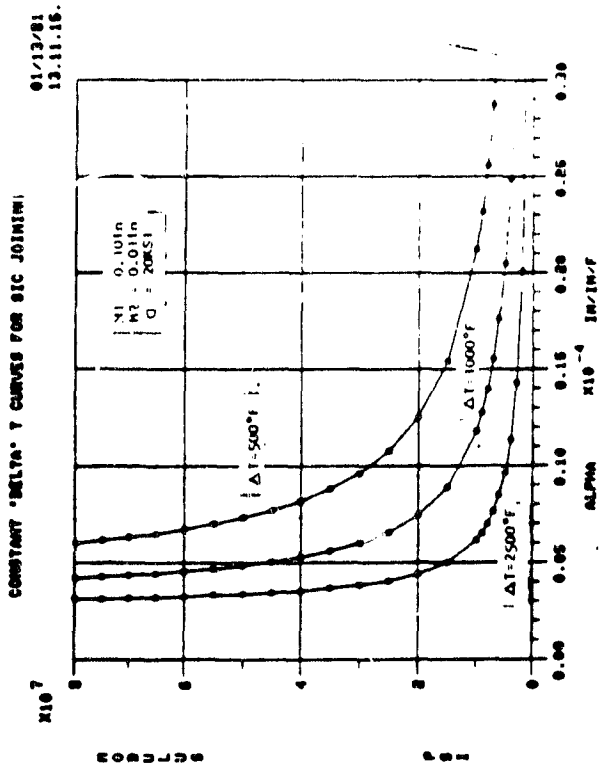


Figure 126

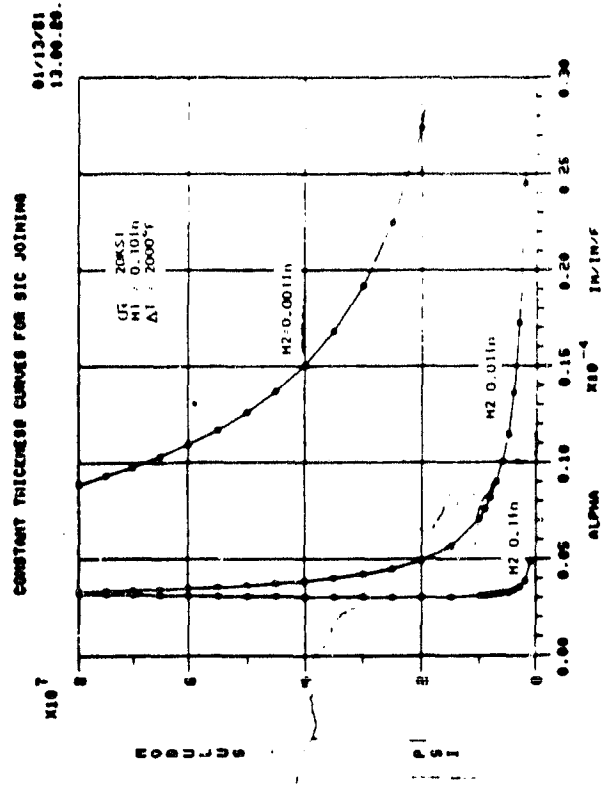


Figure 127

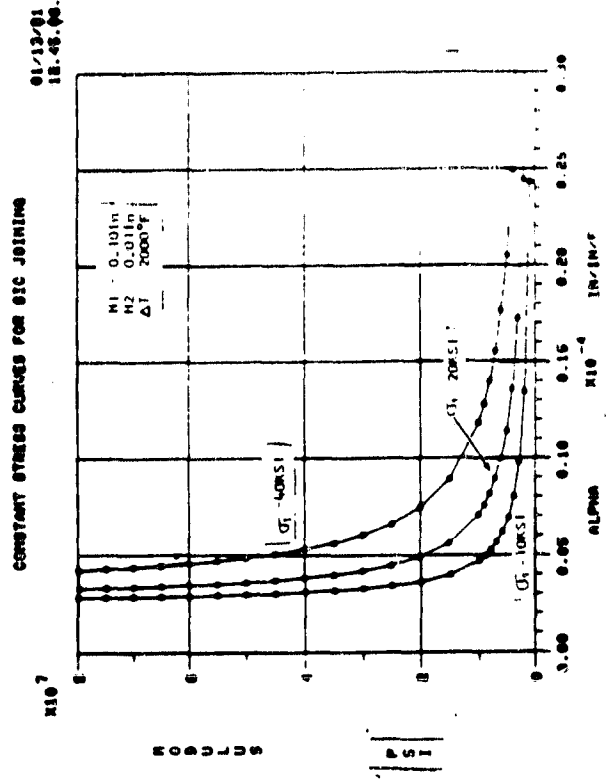
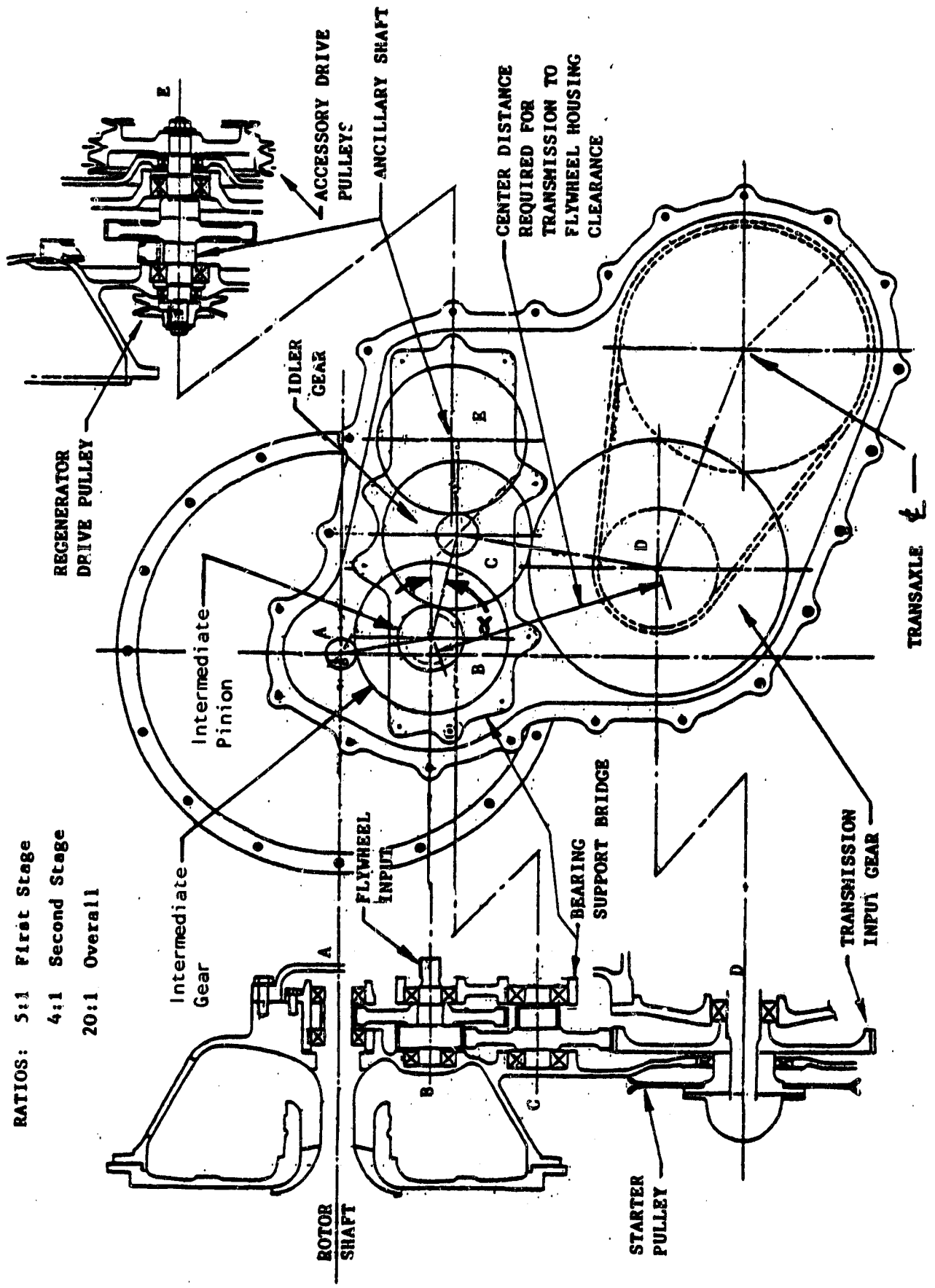


Figure 128

NOTE: Equations used to generate these curves were adapted from:
Brubaker, B.D. & Russel, R., Jr:
Residual Stress Development in
Laminar Ceramics.
Ceramic Bulletin V. 46,
No. 12 (1967).

RATIOS: 5:1 First Stage
 4:1 Second Stage
 20:1 Overall



AGT Reduction Gear

Figure 129

**TWO STAGE REDUCTION GEAR ANALYSIS
HIGH SPEED PINION-GEAR DEFLECTION**

Effect of Helix Angle and Load

○ Front Bearing | — 20° Helix
● Rear Bearing | - - - 39° Helix

← .001 in. Deflection Scale

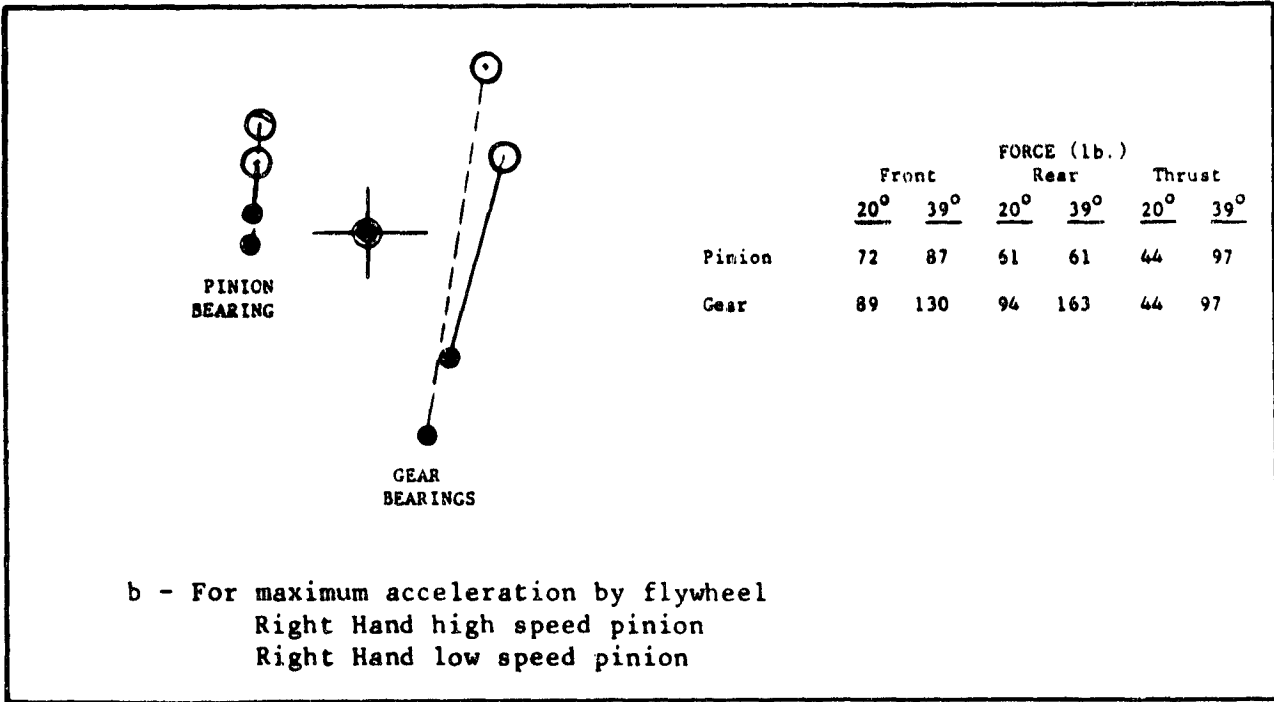
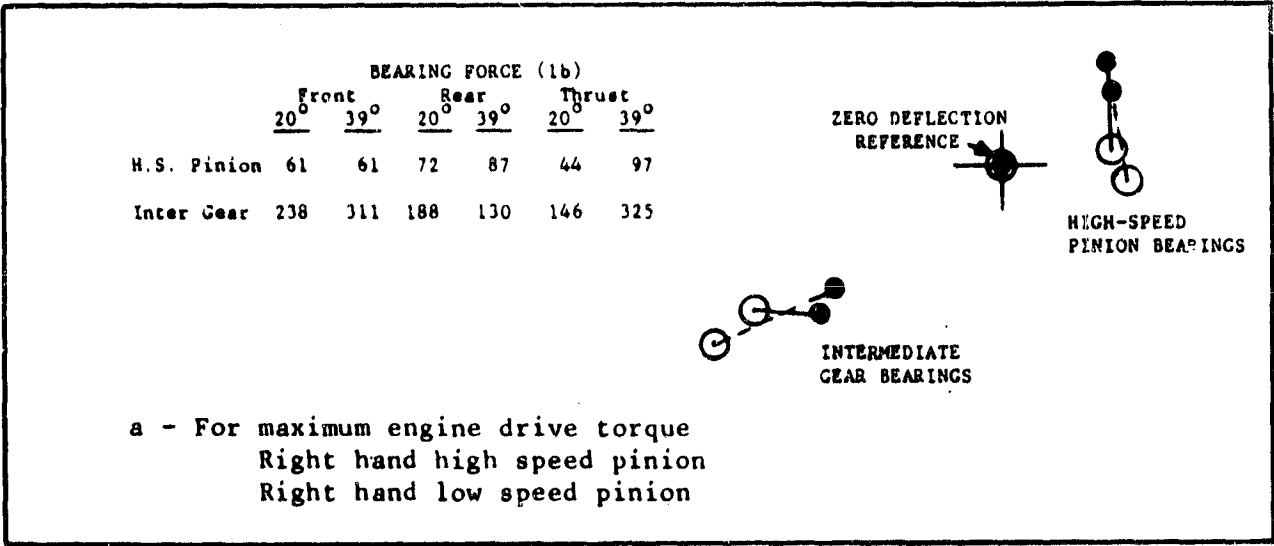
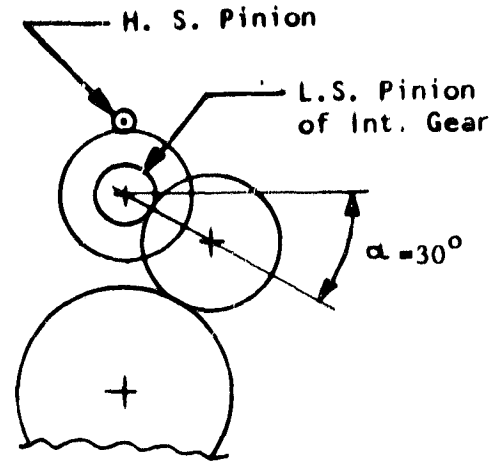


Figure 130

**TWO STAGE REDUCTION GEAR ANALYSIS
HIGH SPEED PINION-GEAR DEFLECTION**

Effect of Helix Angle and Hand

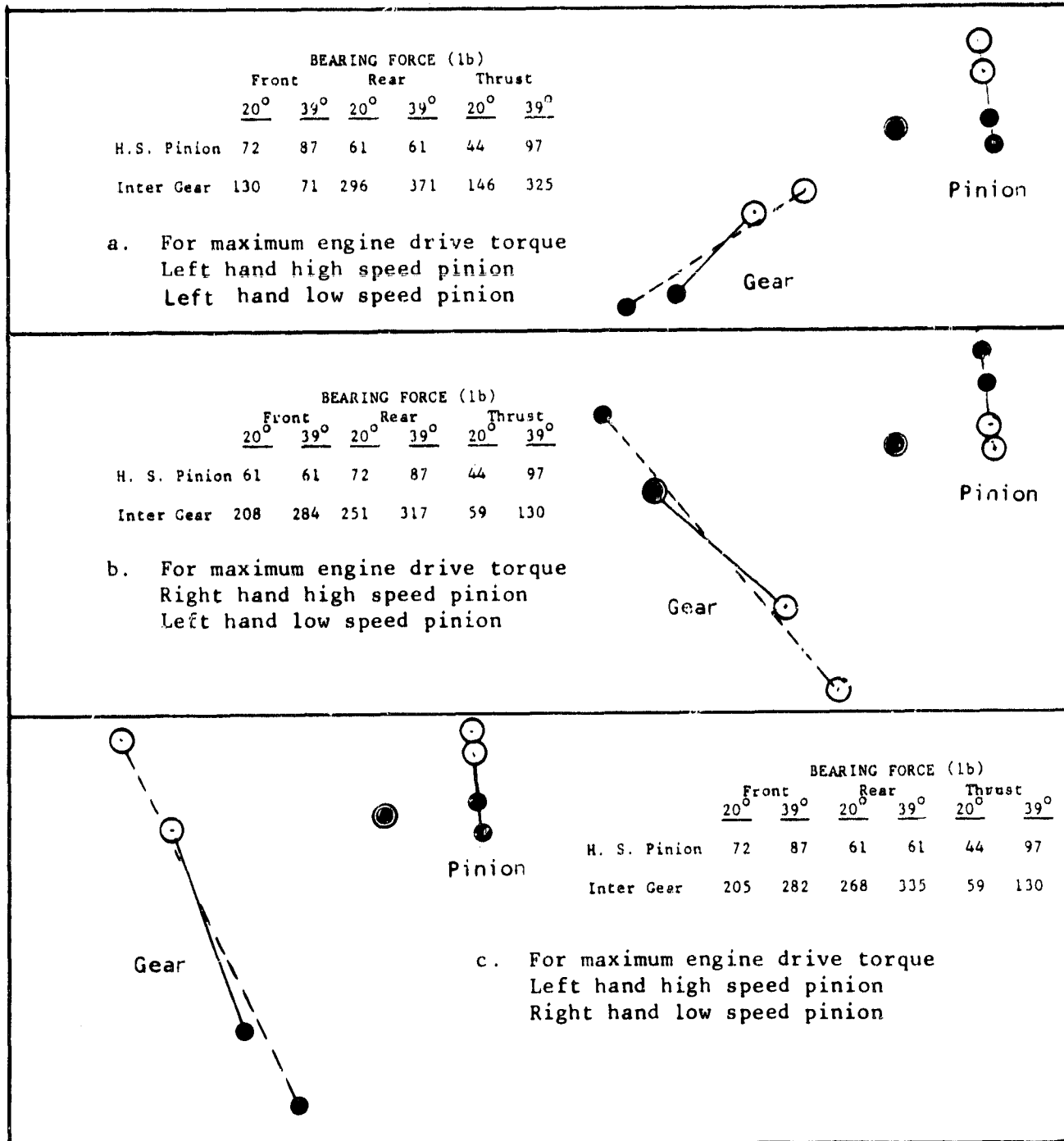
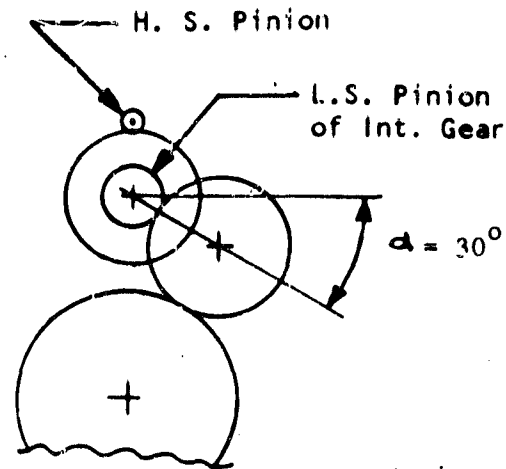
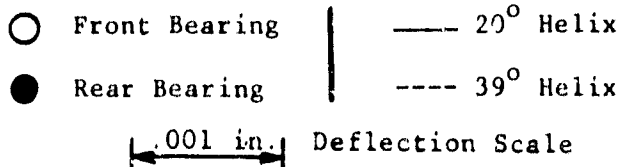
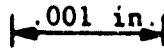


Figure 131

**TWO STAGE REDUCTION GEAR ANALYSIS
HIGH SPEED PINION-GEAR DEFLECTION**

Effect of Helix Angle and Hand
with no Idler Gear

- Front Bearing | ——— 20° Helix
- Rear Bearing | - - - 39° helix

 .001 in. Deflection Scale

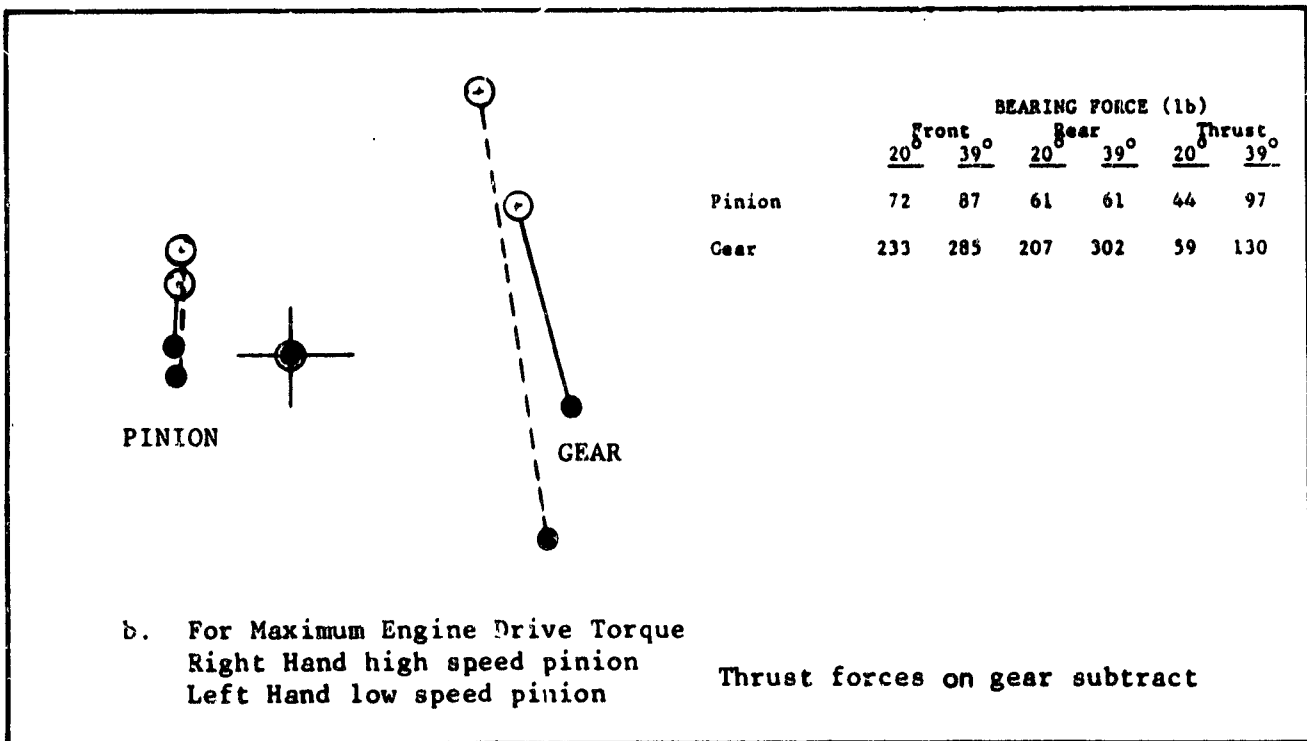
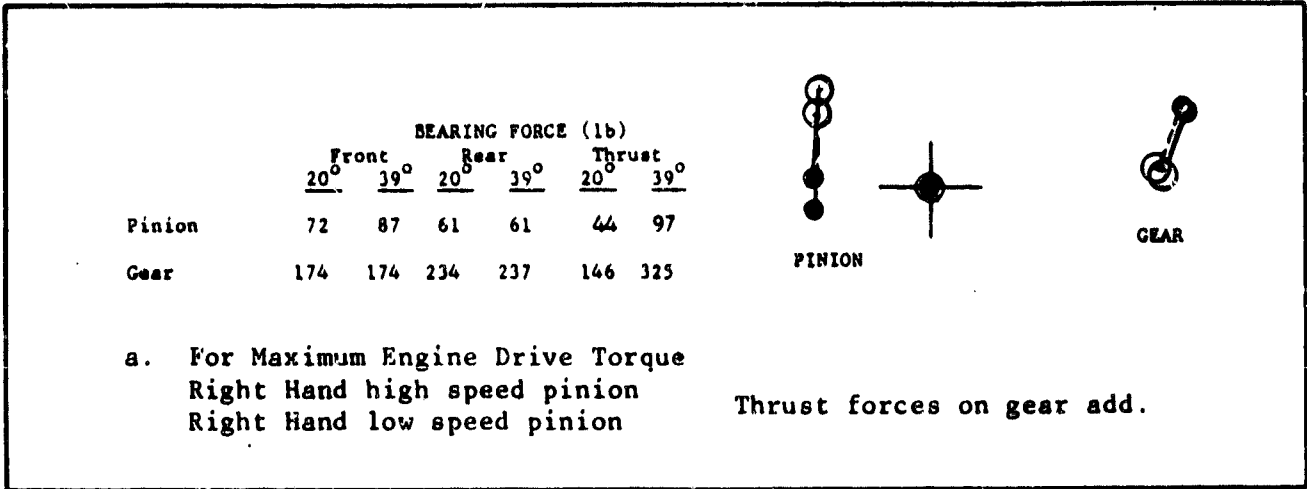
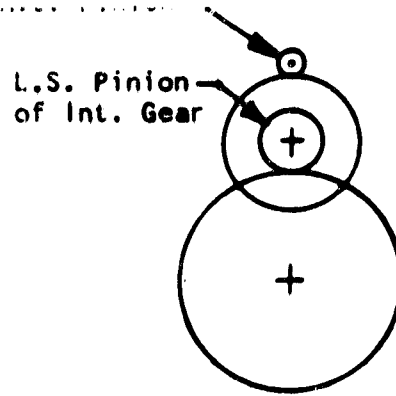


Figure 132

ACT REDUCTION GEAR

NO IDLER

CHAIN DRIVEN ANCILLARY SHAFT

RATIOS: 7:1 1st Stage
 2.86:1 2nd Stage
 20:1 Overall

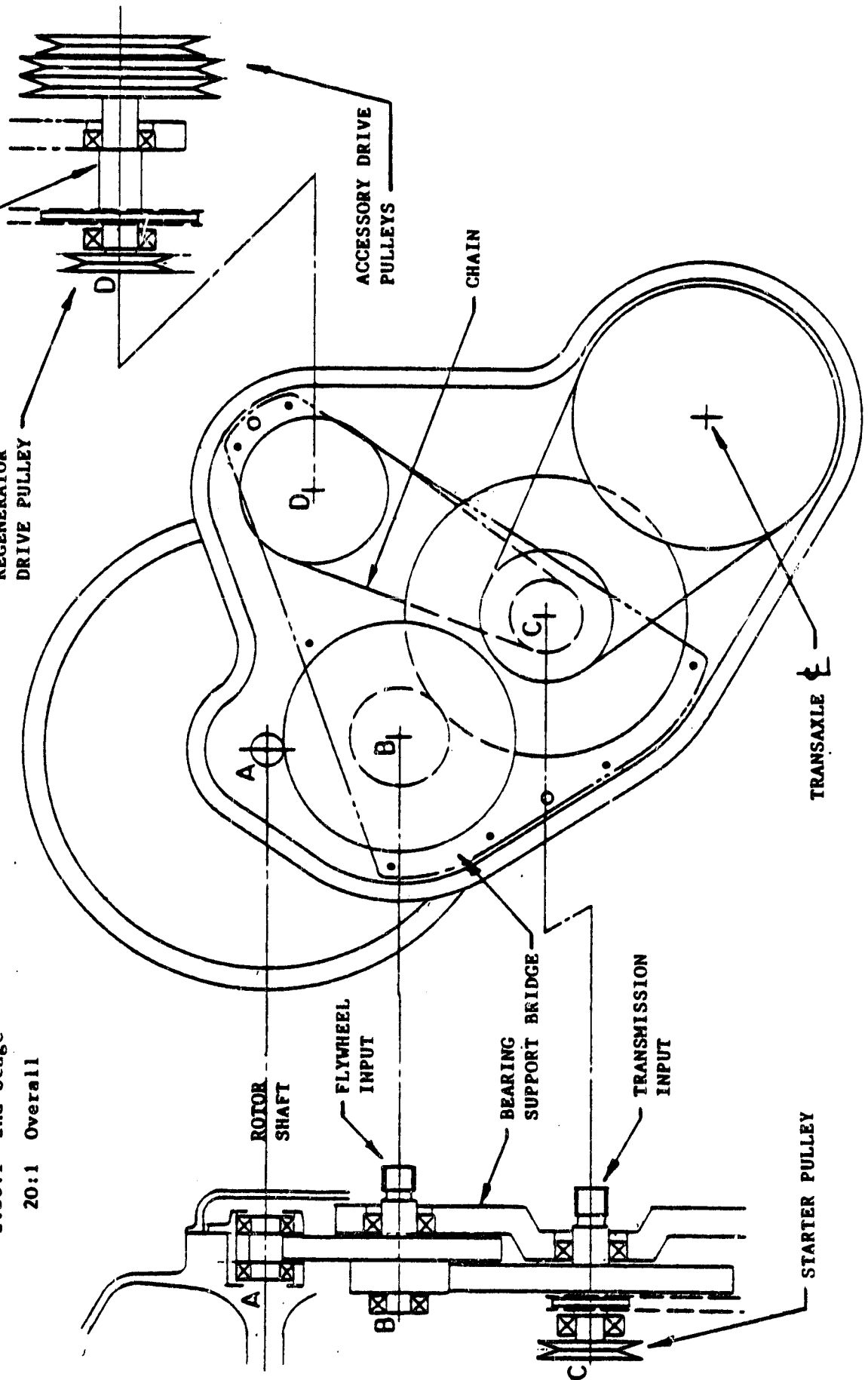
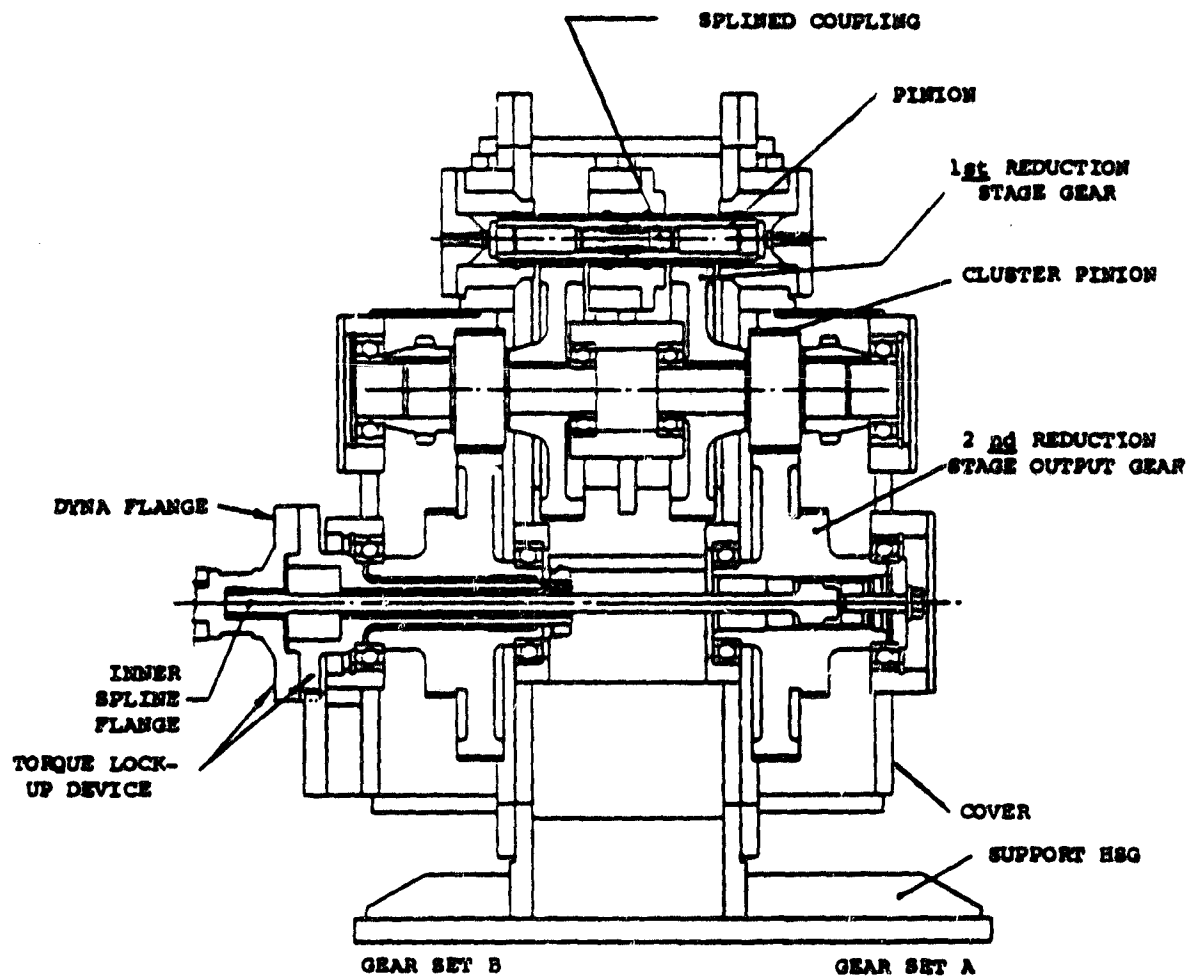
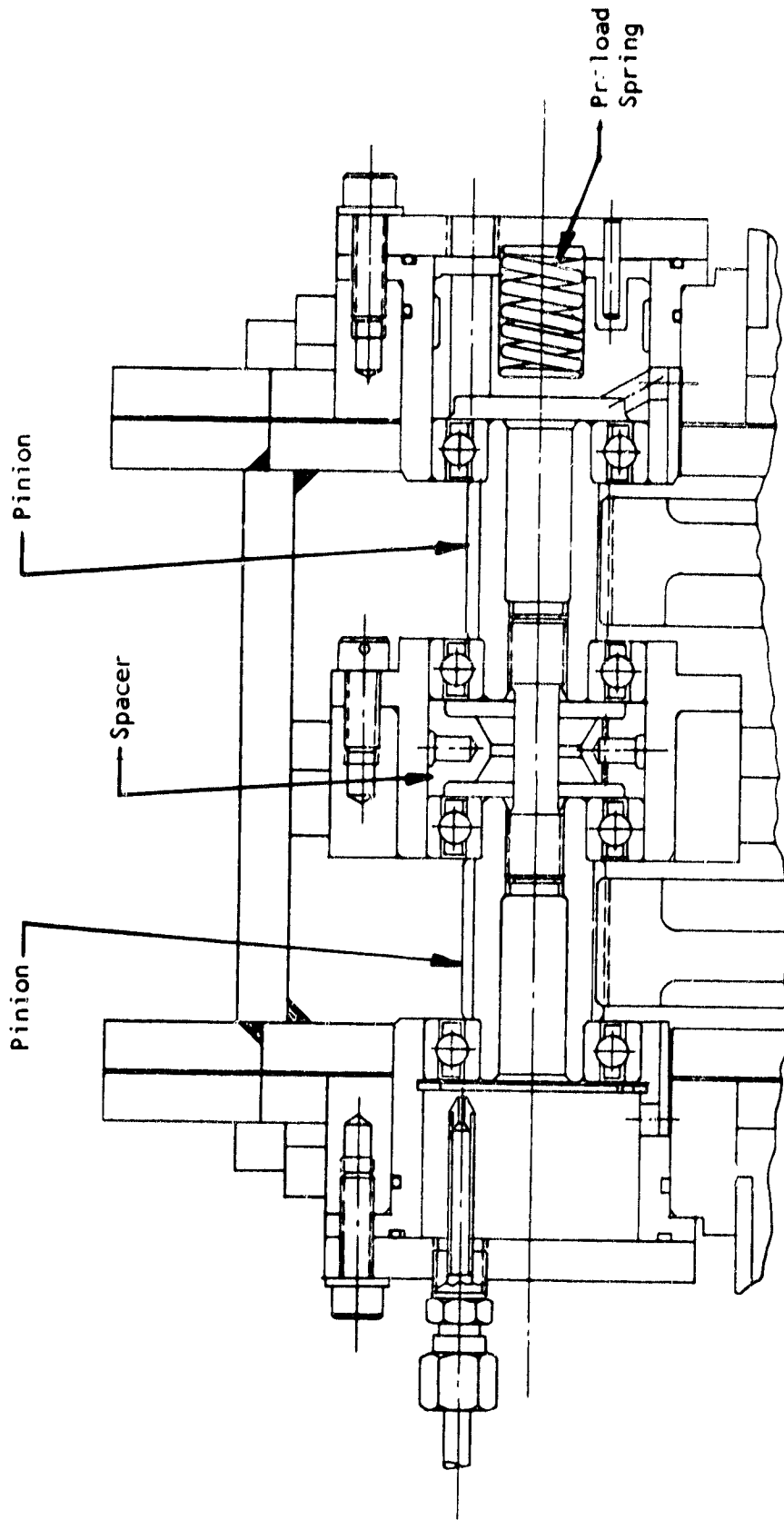


Figure 133

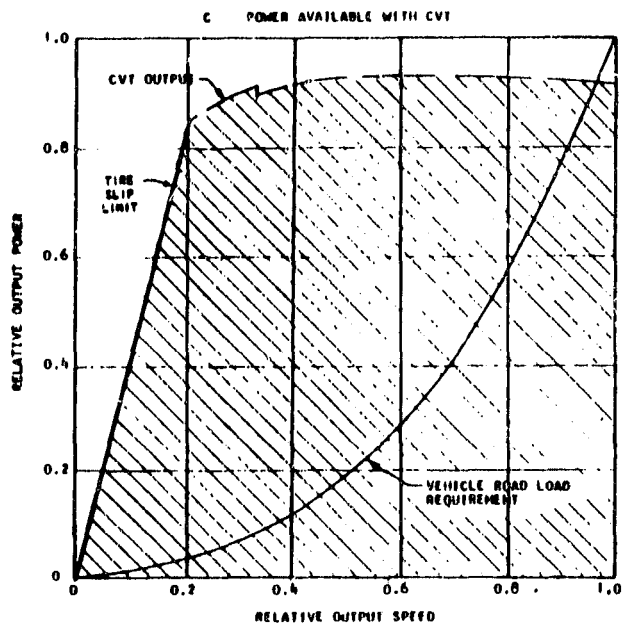
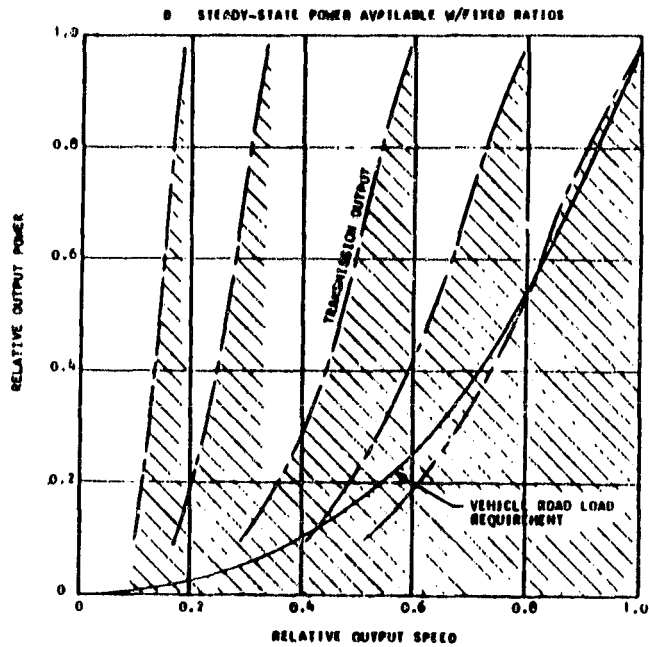
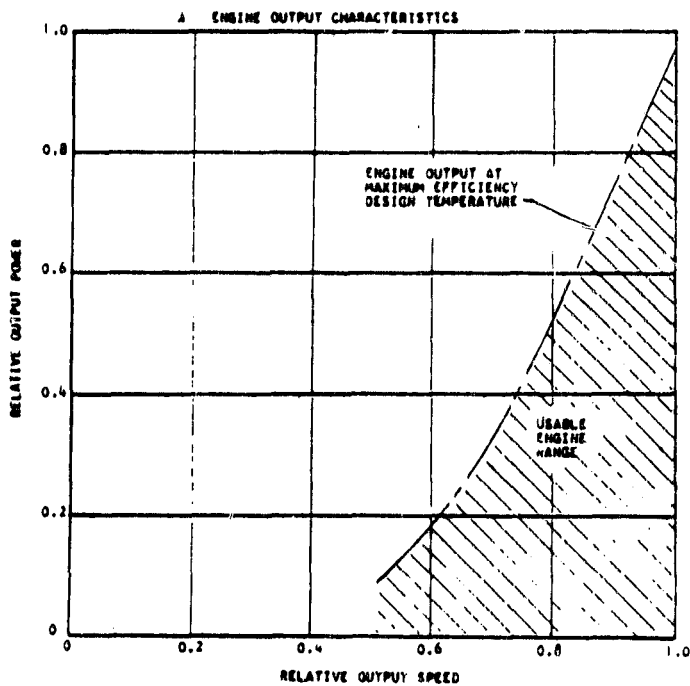


Back-To-Back Gear Test Rig



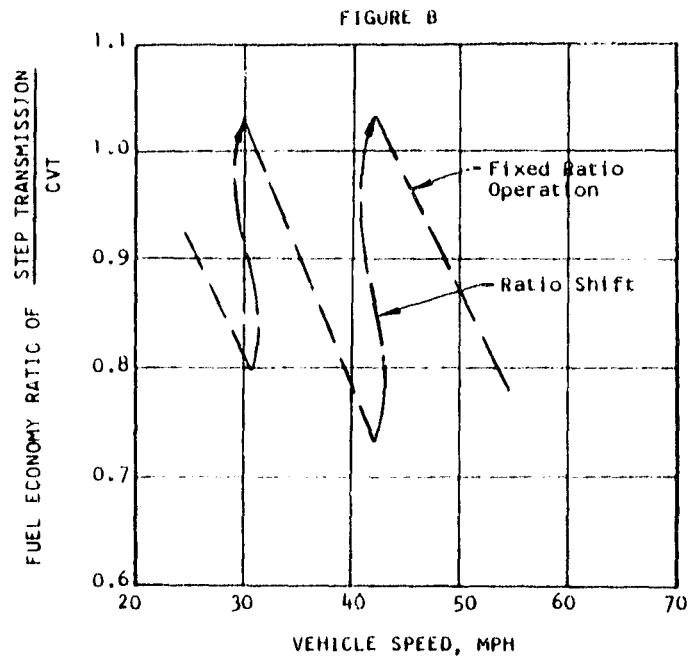
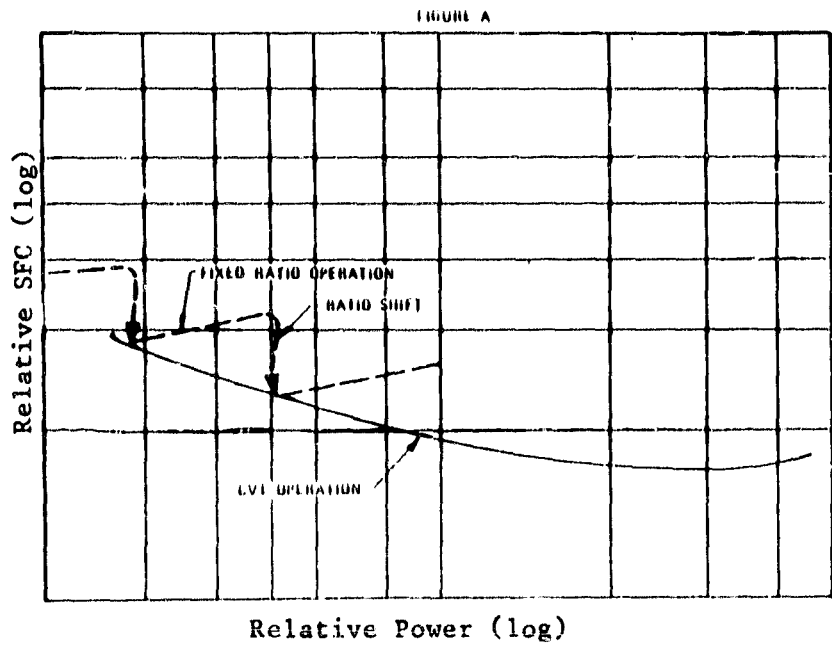
Ball Bearing Adaptation of Back to Back Rig

Figure 135



Effect of Transmission Concept on Output Power

Figure 136

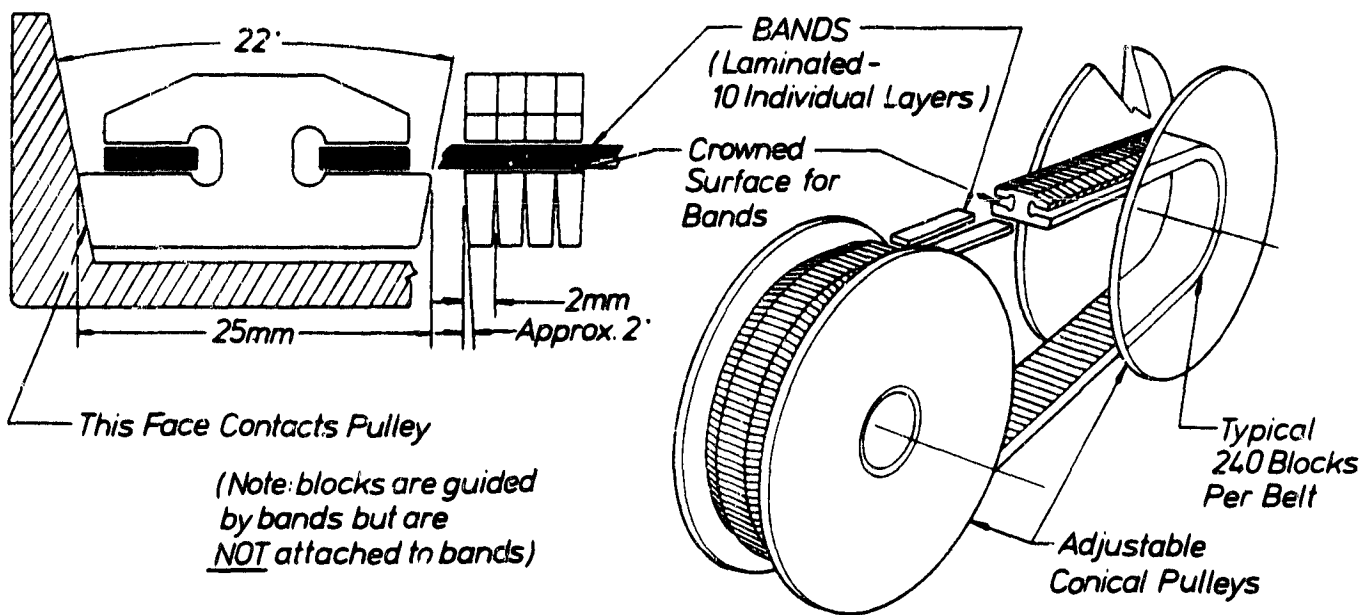


Effect of Transmission Concept on Vehicle Fuel Economy

Figure 137

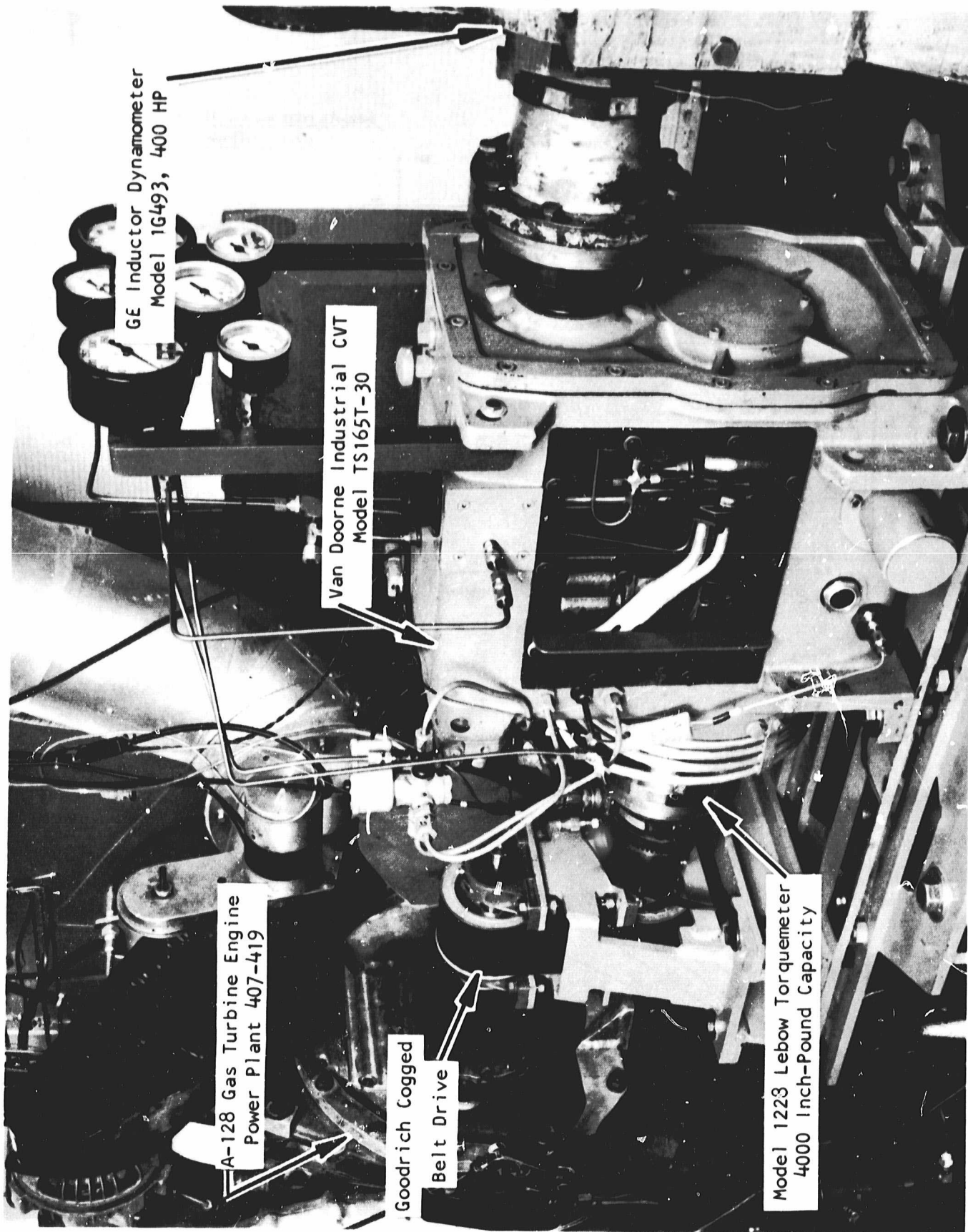
CVT POWER TRANSMISSION	TYPE	GOOD FEATURES	STATE OF DEV.	DISADVANTAGES
	COMPRESSION BELT	<ul style="list-style-type: none"> Compact Efficient Adaptable to Mass Prod. Fast Response Low Noise 	<ul style="list-style-type: none"> Industrial Units in Production Prototype Automotive Transmissions Being Demonstrated 	<ul style="list-style-type: none"> High Control Forces (Hydraulic) Limited Ratio Range
VARIABLE RATIO PULLEY	RUBBER V-BELT (Fabric Reinforced)	<ul style="list-style-type: none"> Low Cost Efficient Well Established Technology 	<ul style="list-style-type: none"> Used in 70 HP Automobile (Volvo 343) Used for Snowmobile Drives in Industrial Applications Several Automotive Prototype Drives Being Built and Tested 	<ul style="list-style-type: none"> Limited Belt Life Large Diameter Pulleys Required Awkward Packaging Limited Ratio Range
	Modified Chain (GRN Pin Variator)	<ul style="list-style-type: none"> Adaptable to Mass Production Efficient Compact 	<ul style="list-style-type: none"> Automotive Prototypes Being Developed 	<ul style="list-style-type: none"> Limited Ratio Range High Control Forces (Hydraulic) High Pin End Contact Stress Chordal Action
HYDROMECHANICAL	Variable Displacement Pump and Motor Plus Planetary Gearing	<ul style="list-style-type: none"> Reliable Well Established Technology Large Ratio Range 	<ul style="list-style-type: none"> Commercially Available Units for Large Trucks 100 HP Demonstration Unit for Automobiles 	<ul style="list-style-type: none"> Expensive Moisy
TRACTION DRIVE	Rolling Contact	<ul style="list-style-type: none"> Quiet Potential for Moderate Cost 	<ul style="list-style-type: none"> Prototypes Being Built and Tested for Automotive Use 	<ul style="list-style-type: none"> Limited Ratio Range Low Power Density High Surface Stresses High Control Forces

CVT Concept Comparison

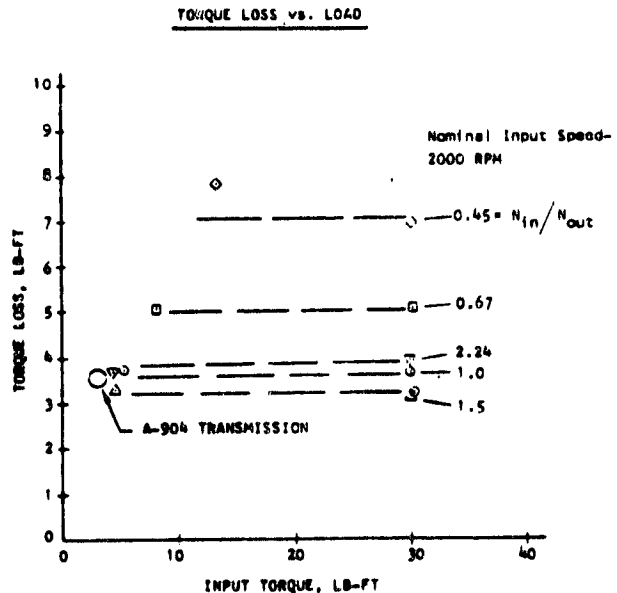
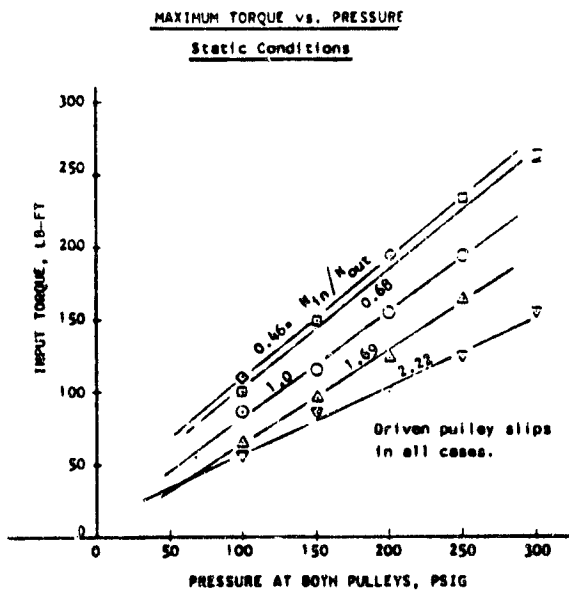
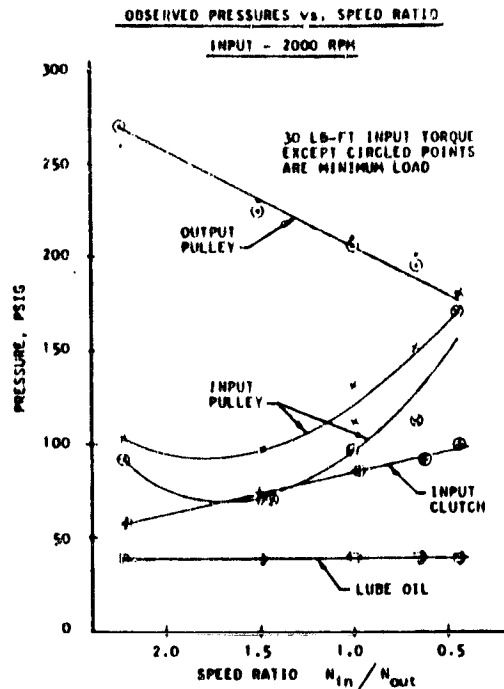
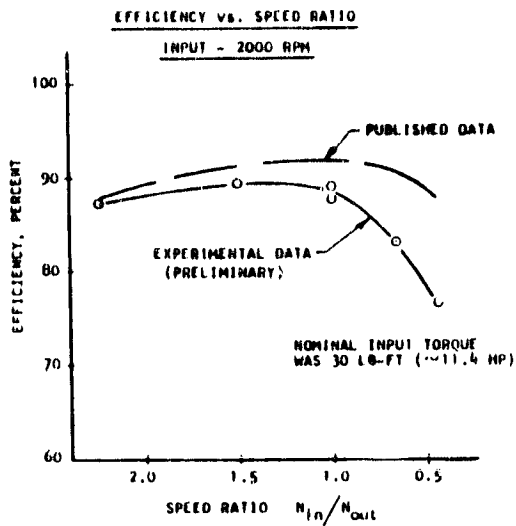


Metal Belt Drive

Figure 139

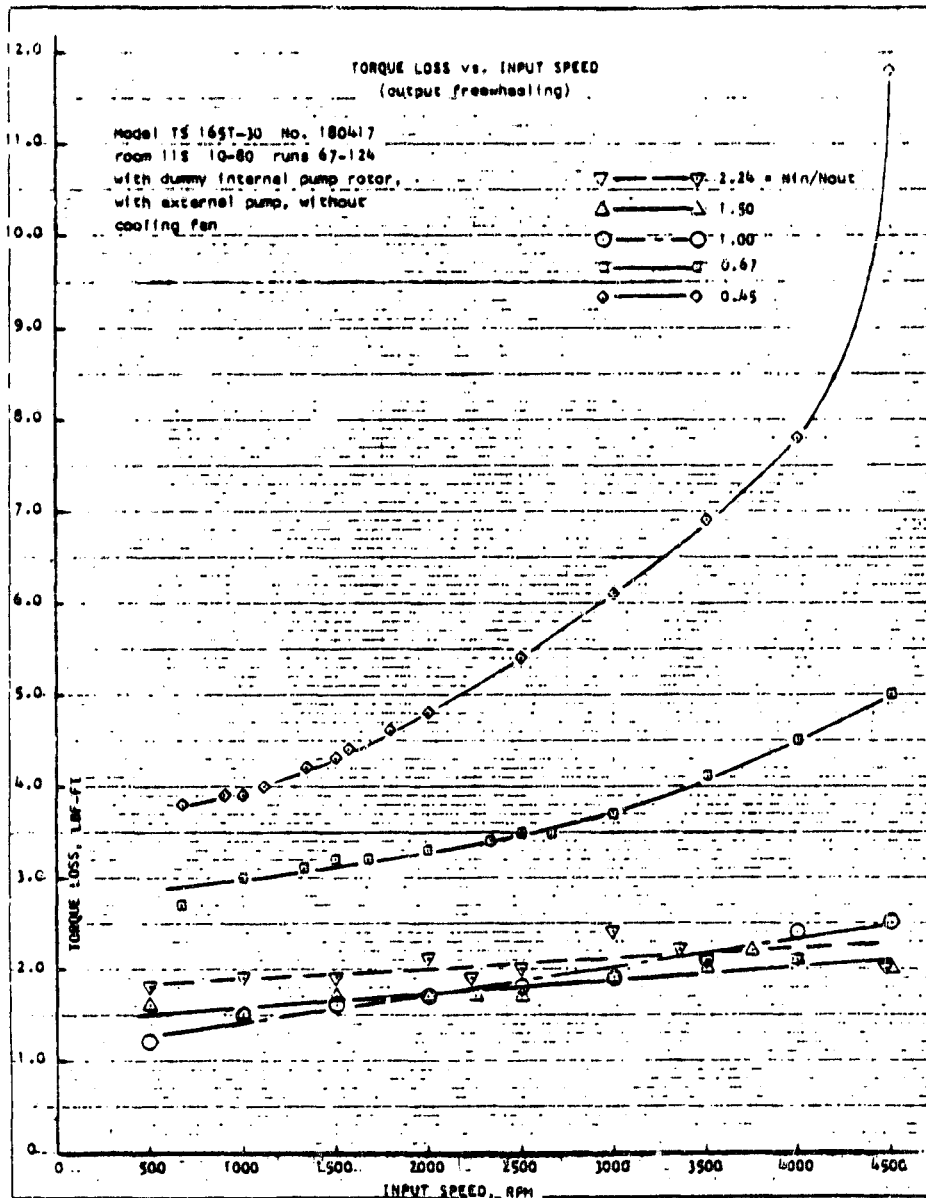


CVT Test Rig

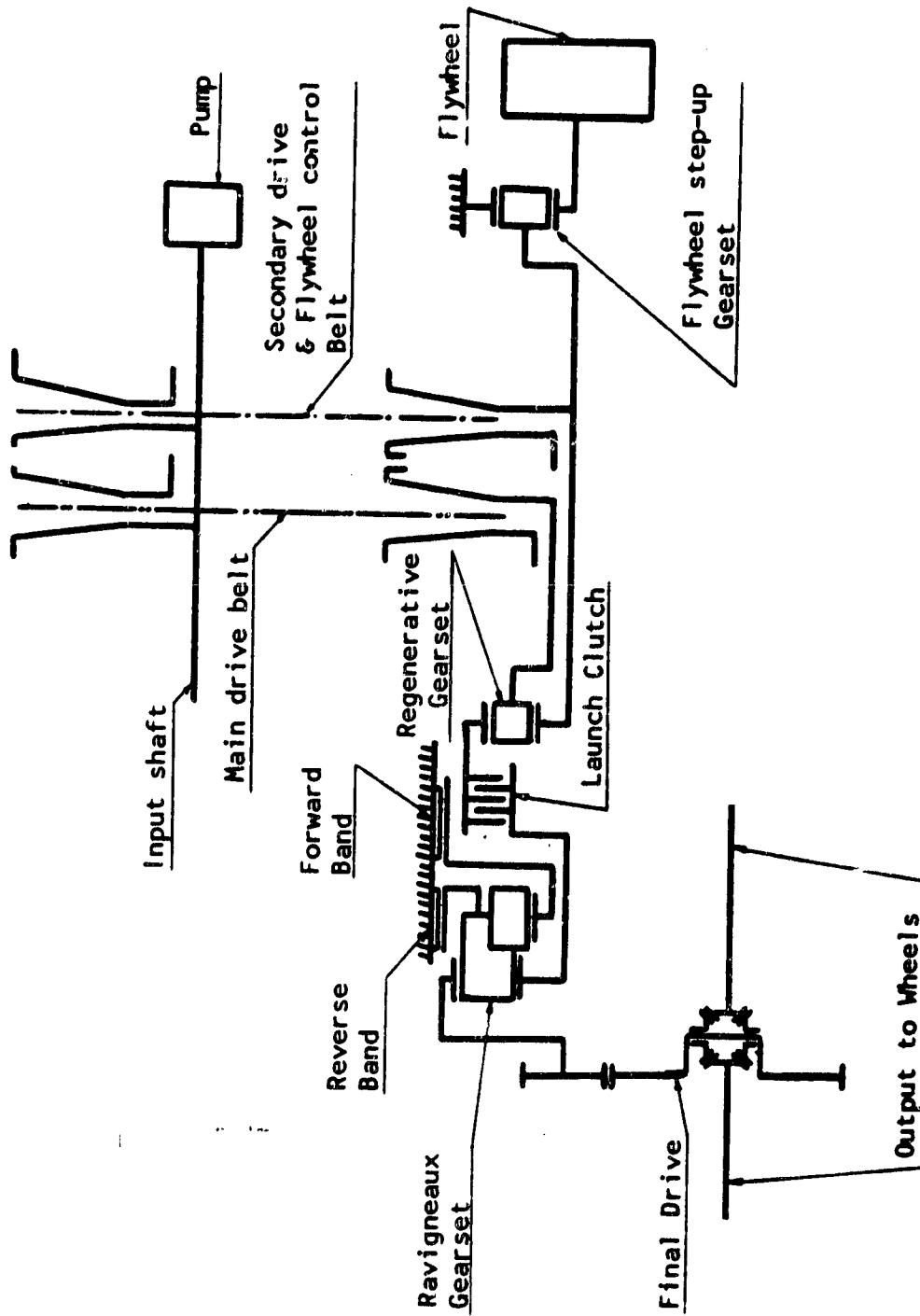


Van Doorne Industrial CVT Performance

Figure 14!



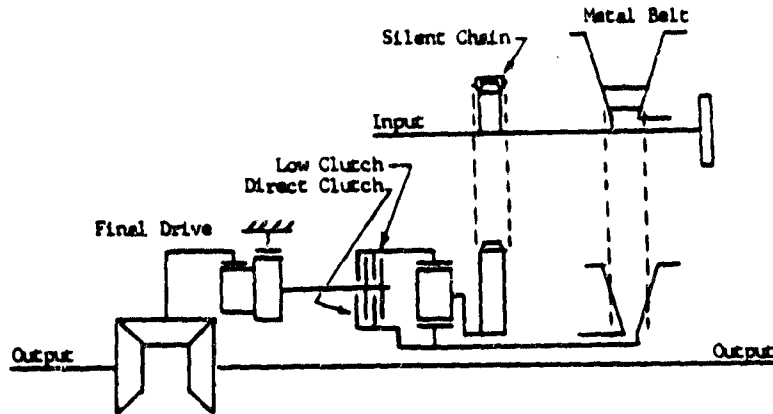
Van Doorne Industrial CVT Performance



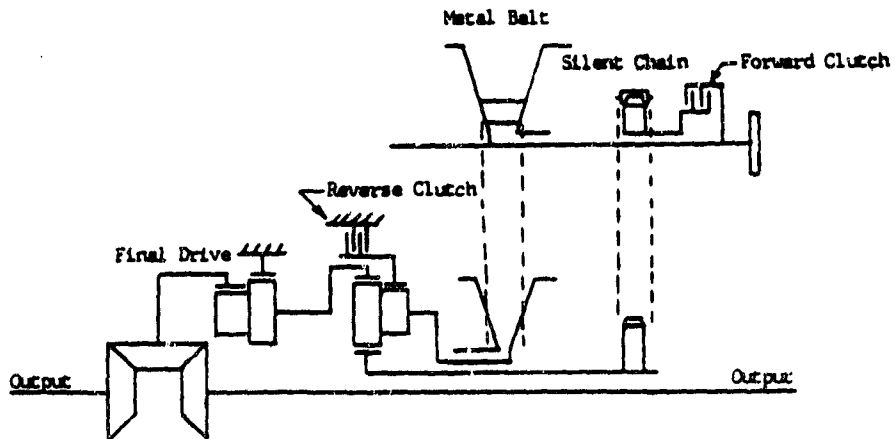
Battelle Integral Flywheel Dual Belt CVT Proposal

Figure 143

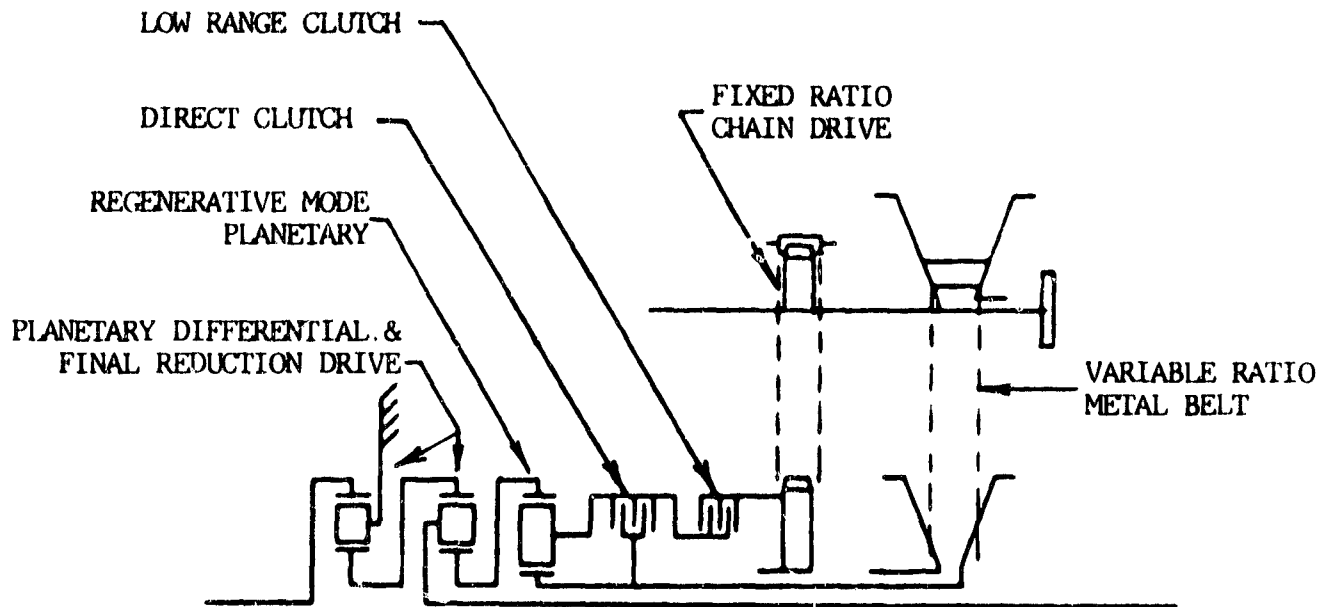
DUAL RANGE CVT



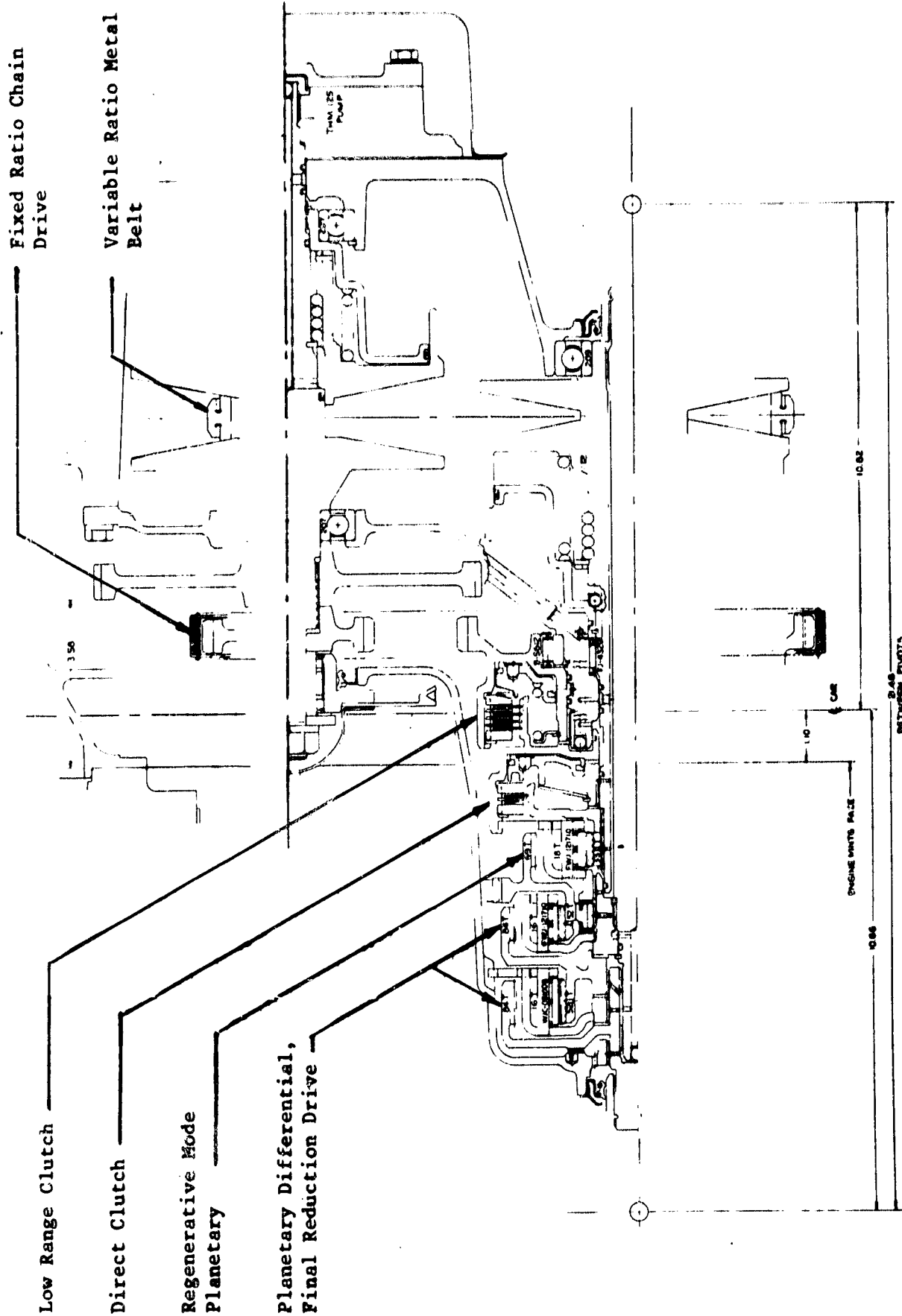
SINGLE RANGE CVT



Single and Dual Range CVT Comparison

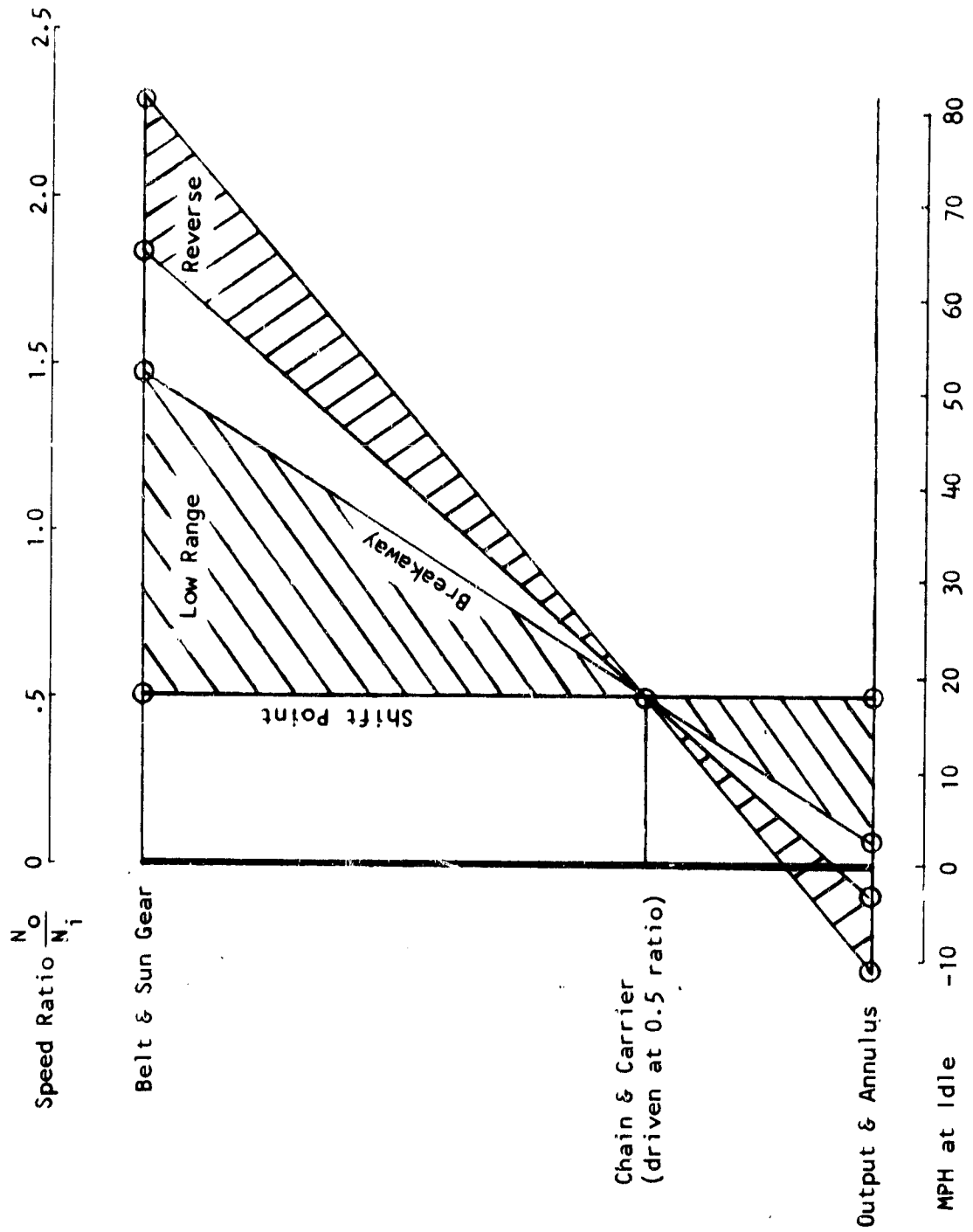


Selected Dual-Range CVT Arrangement



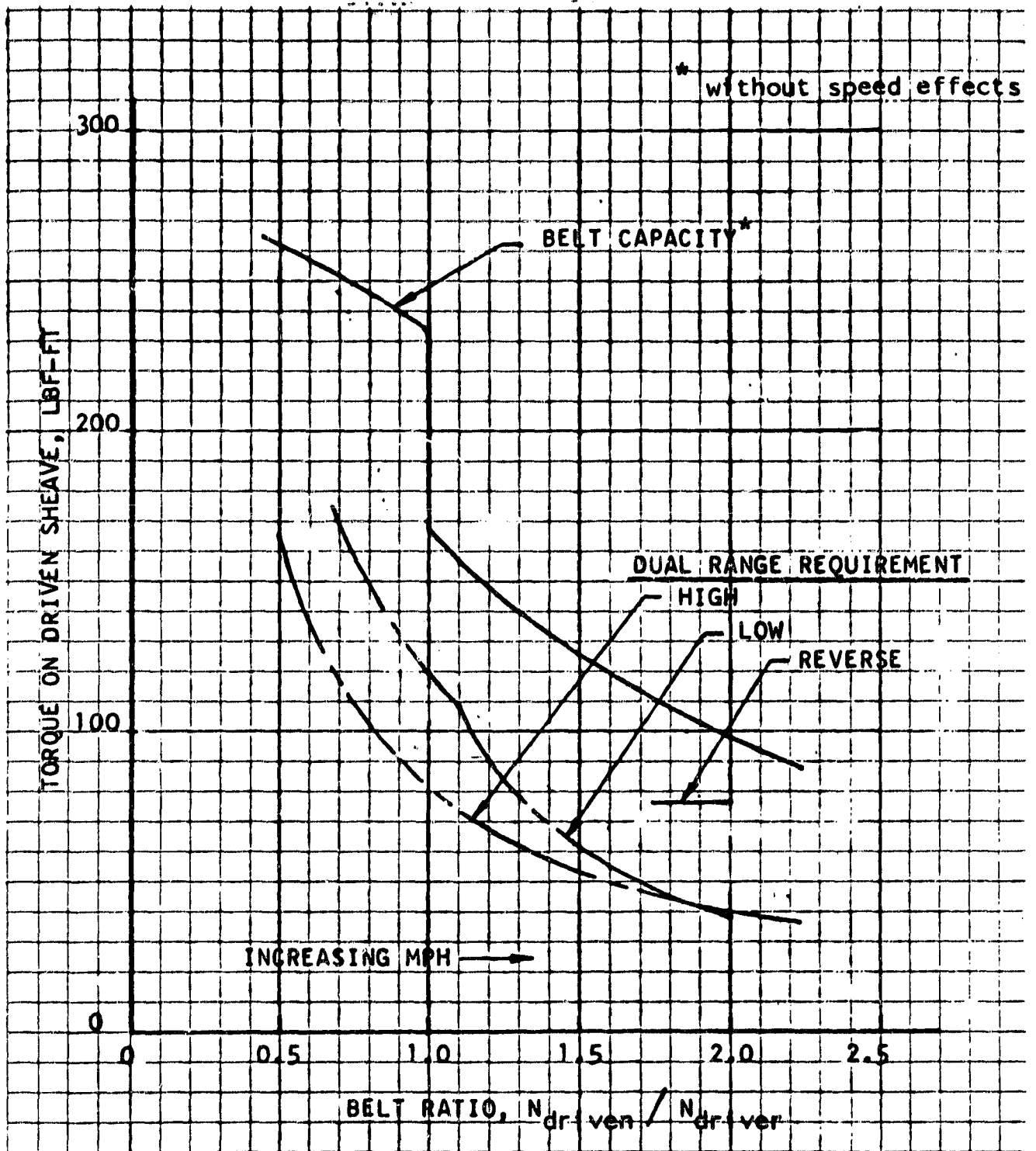
CVT Selected Arrangement Cross-Section

Figure 146



Dual-Range CVT --- Speed Relationships

Figure 147



Belt Torque Comparison

Figure 148

Figure A
Engine - RAF Speed Relation

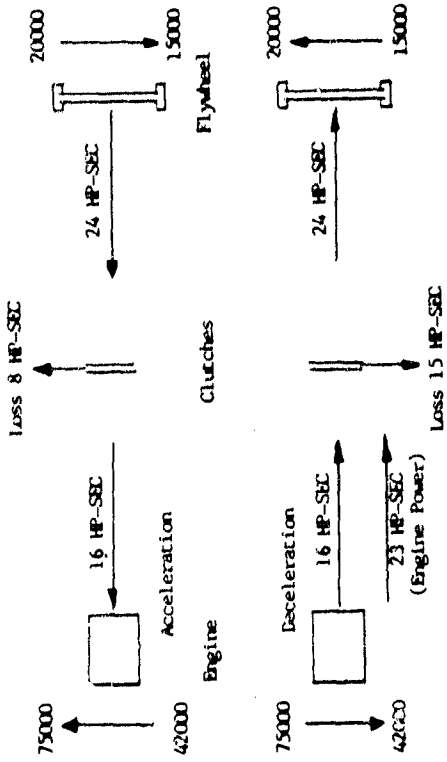
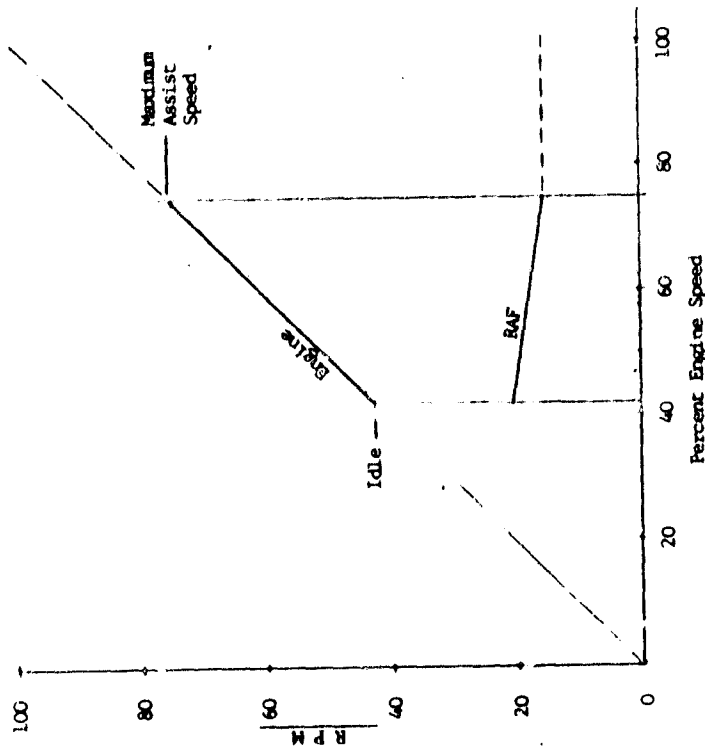


Figure B
Energy Exchanges and Clutch Losses

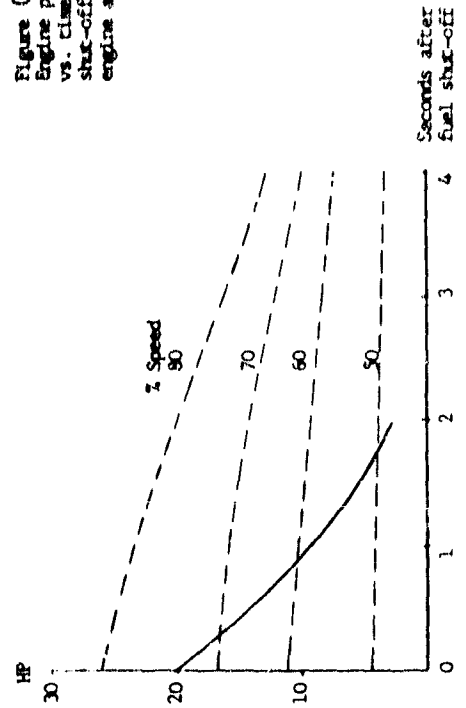
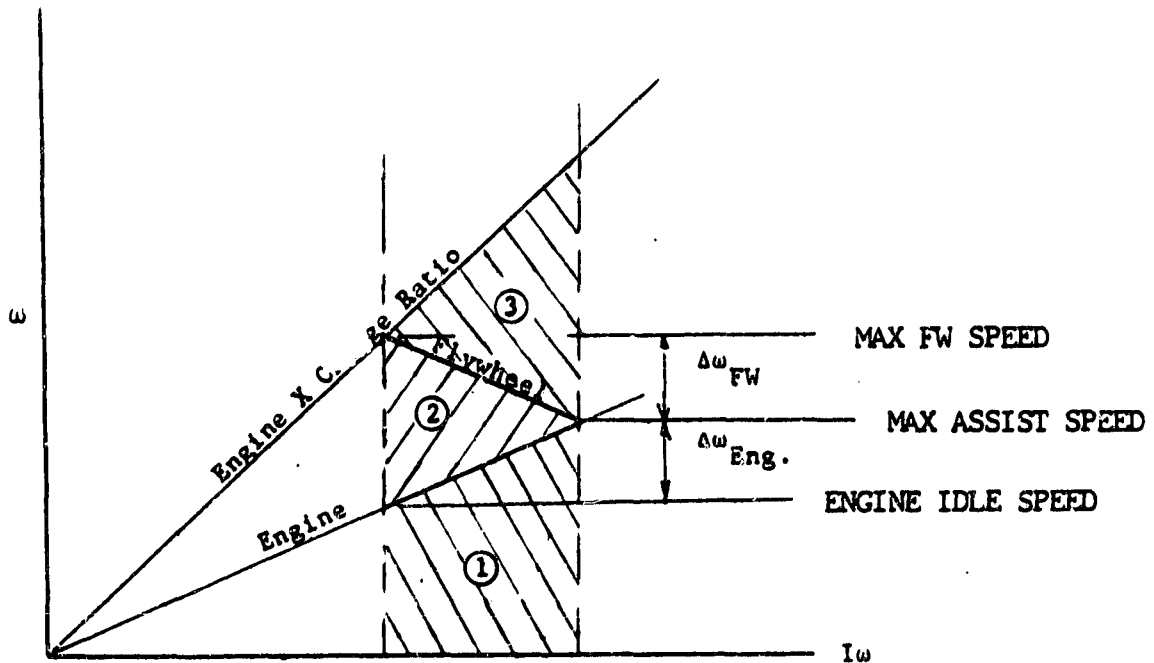


Figure C
Engine power and speed vs. time after fuel shut-off. Decelerating engine and recharging RAF.

RESPONSE ASSIST FLYWHEEL (RAF)
CHARACTERISTICS

RAF SIZE AND ENERGY EXCHANGE



Energy Exchange and Clutch Losses

. Engine Accel - FW Discharge

FW Loses Areas ① + ②

Engine Gains Area ① Clutch Loss = ②

. Engine Decel - FW Recharge

FW Gains Areas ① + ②

Engine Supplies Areas ① + ② + ③

① From Shaft KE

② & ③ From Power x Time

③ = Clutch Loss

. Overall Energy Eff. = ① / (① + ② + ③) = 1/Charge Ratio

Figure 150

RAF GEAR AND CLUTCH SCHEME

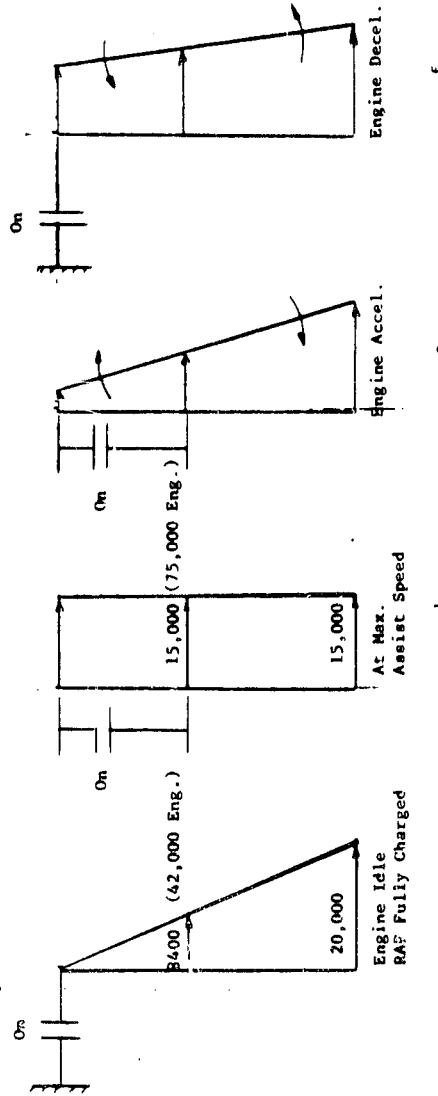
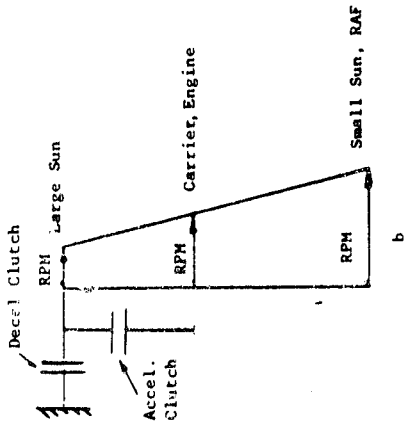
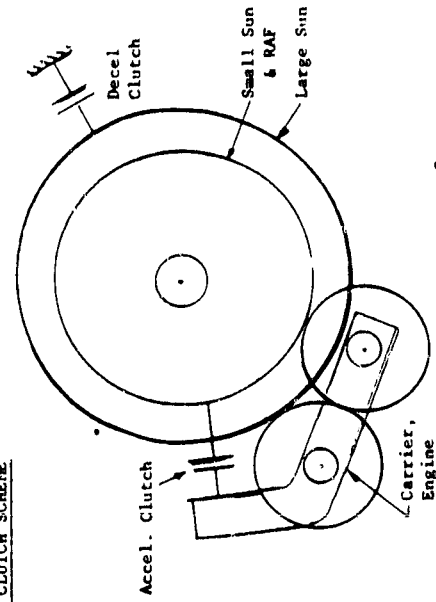


Figure 151

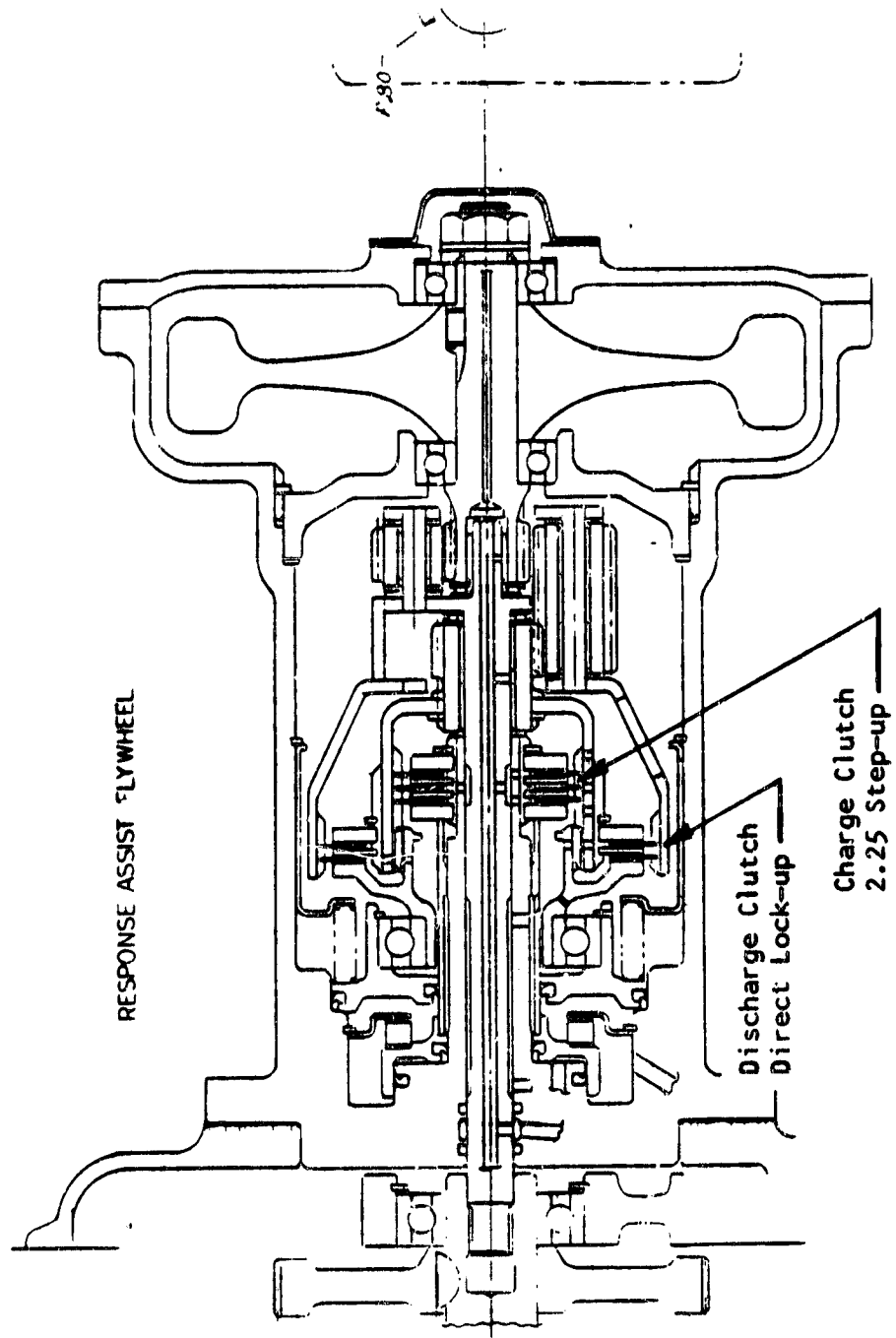


Figure 152

AGT-102 PARASITIC LOSS DETAILS

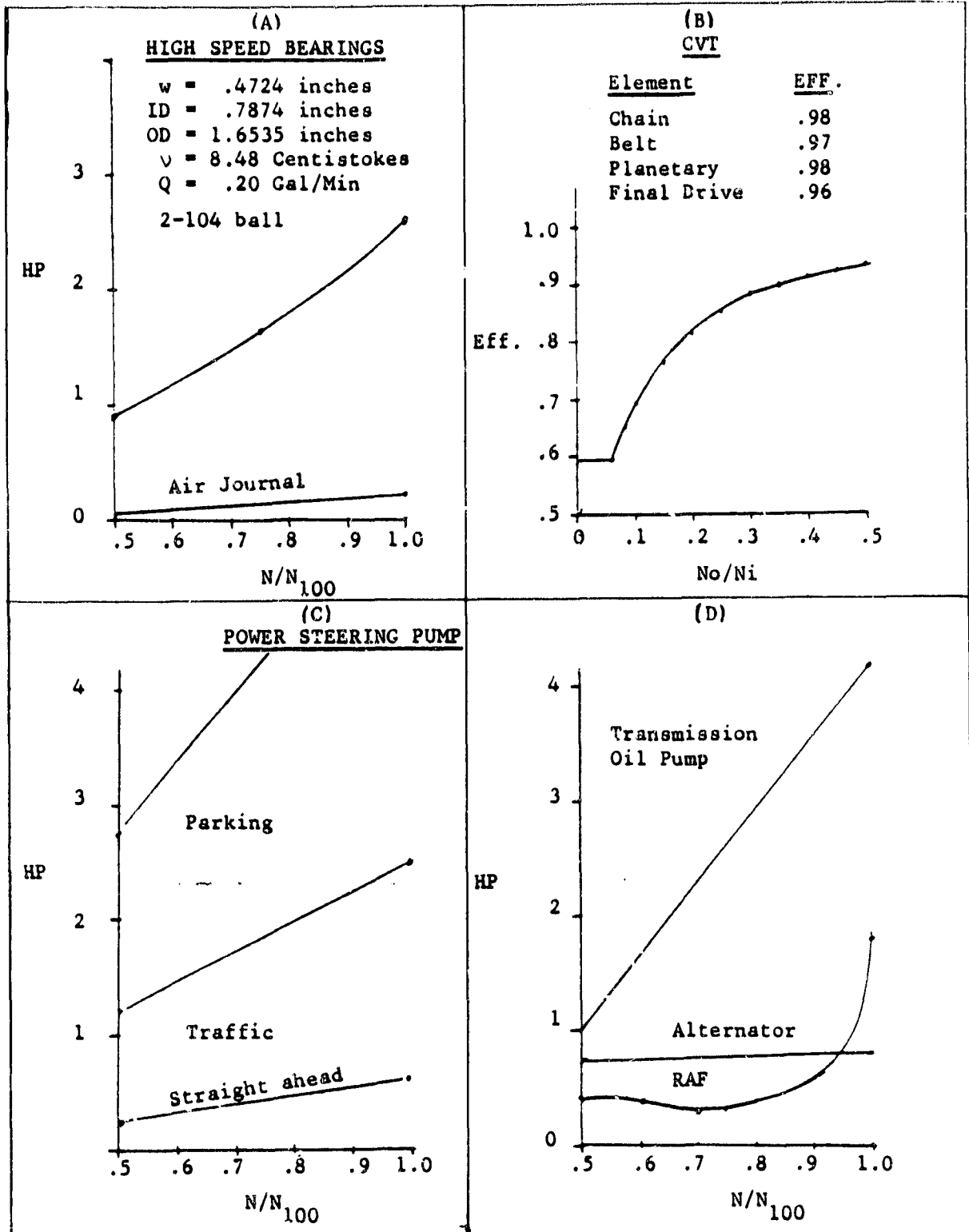
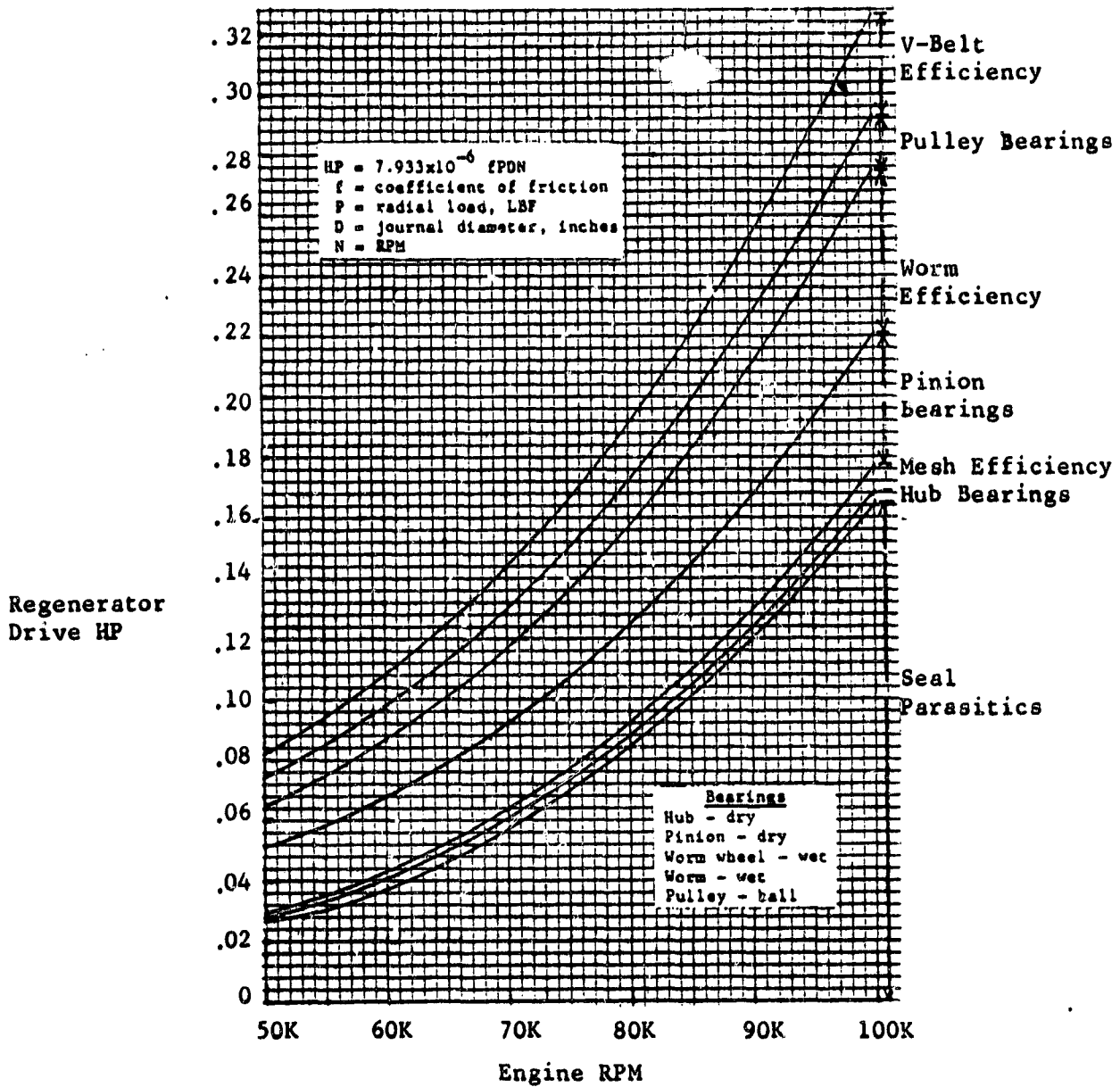
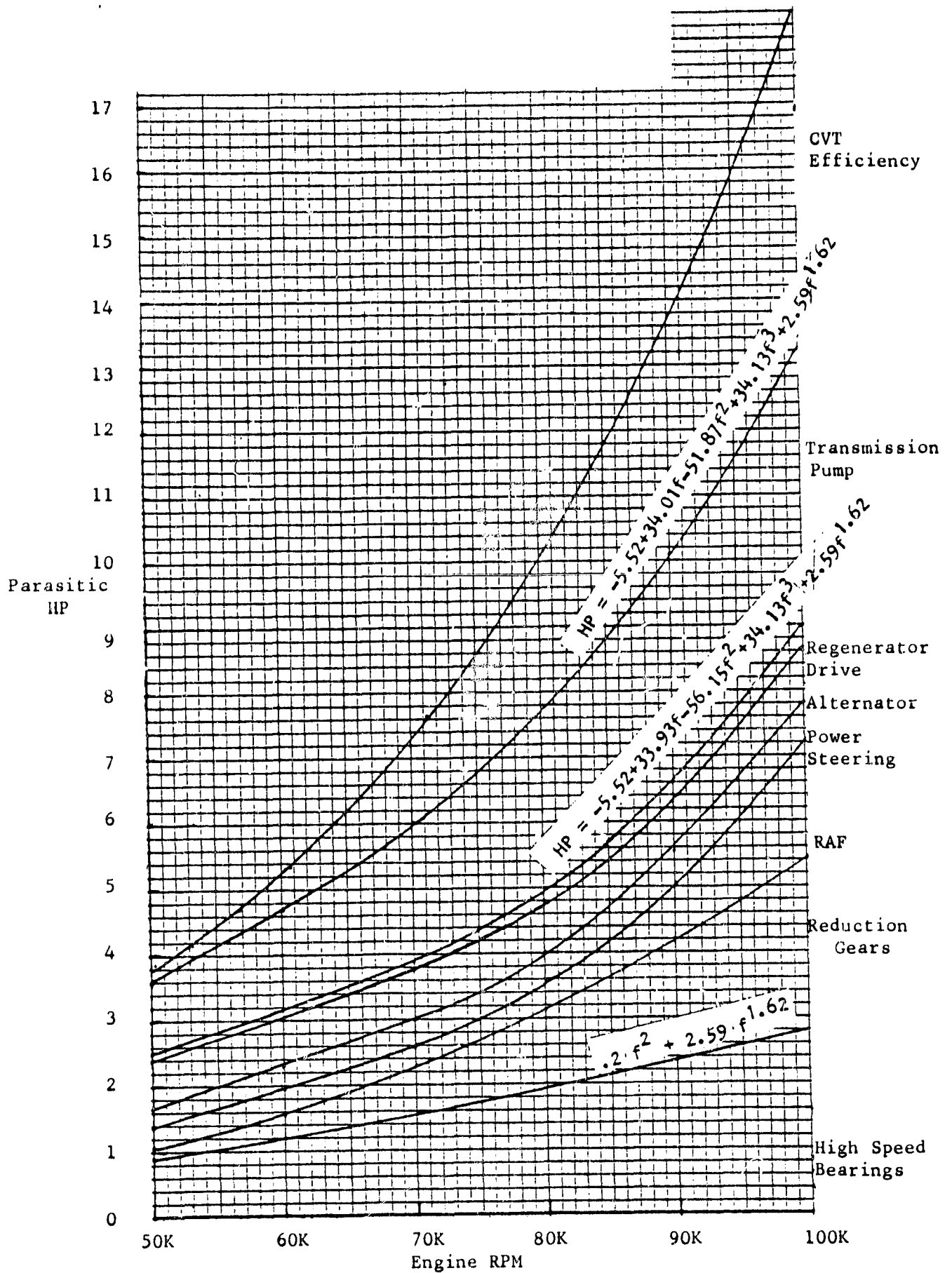


Figure 153



REGENERATOR DRIVE PARASITICS - BREAKDOWN BY COMPONENT

Figure 154



TOTAL PARASITIC HORSEPOWER - BREAKDOWN BY COMPONENT

Figure 155

Figure 156
Engine RPM vs. Pedal Angle

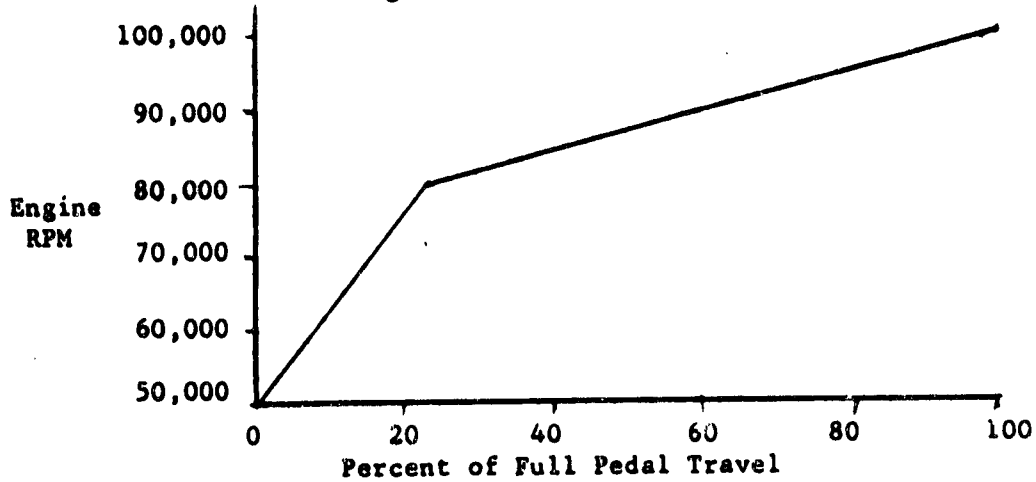
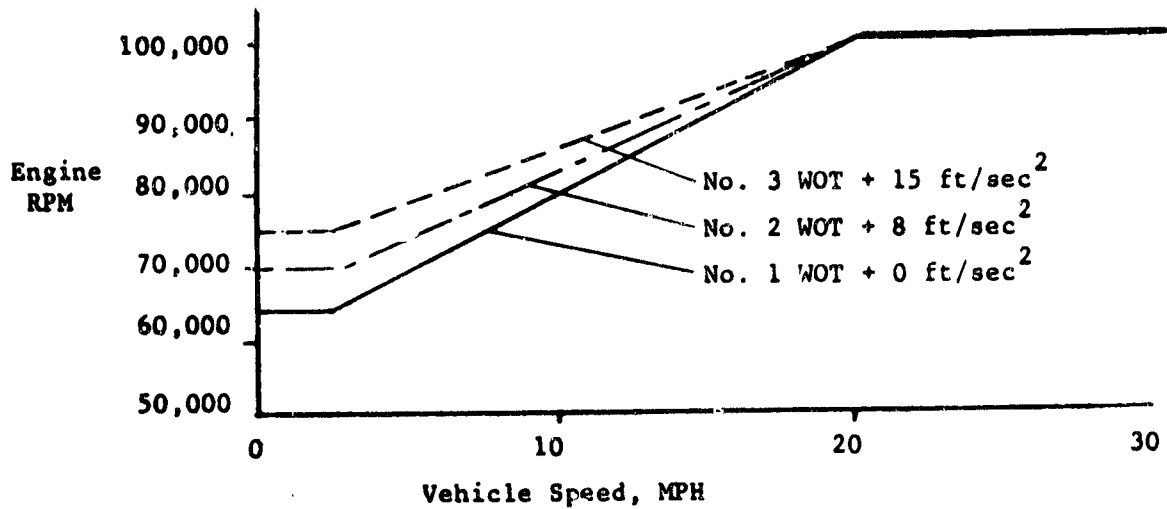
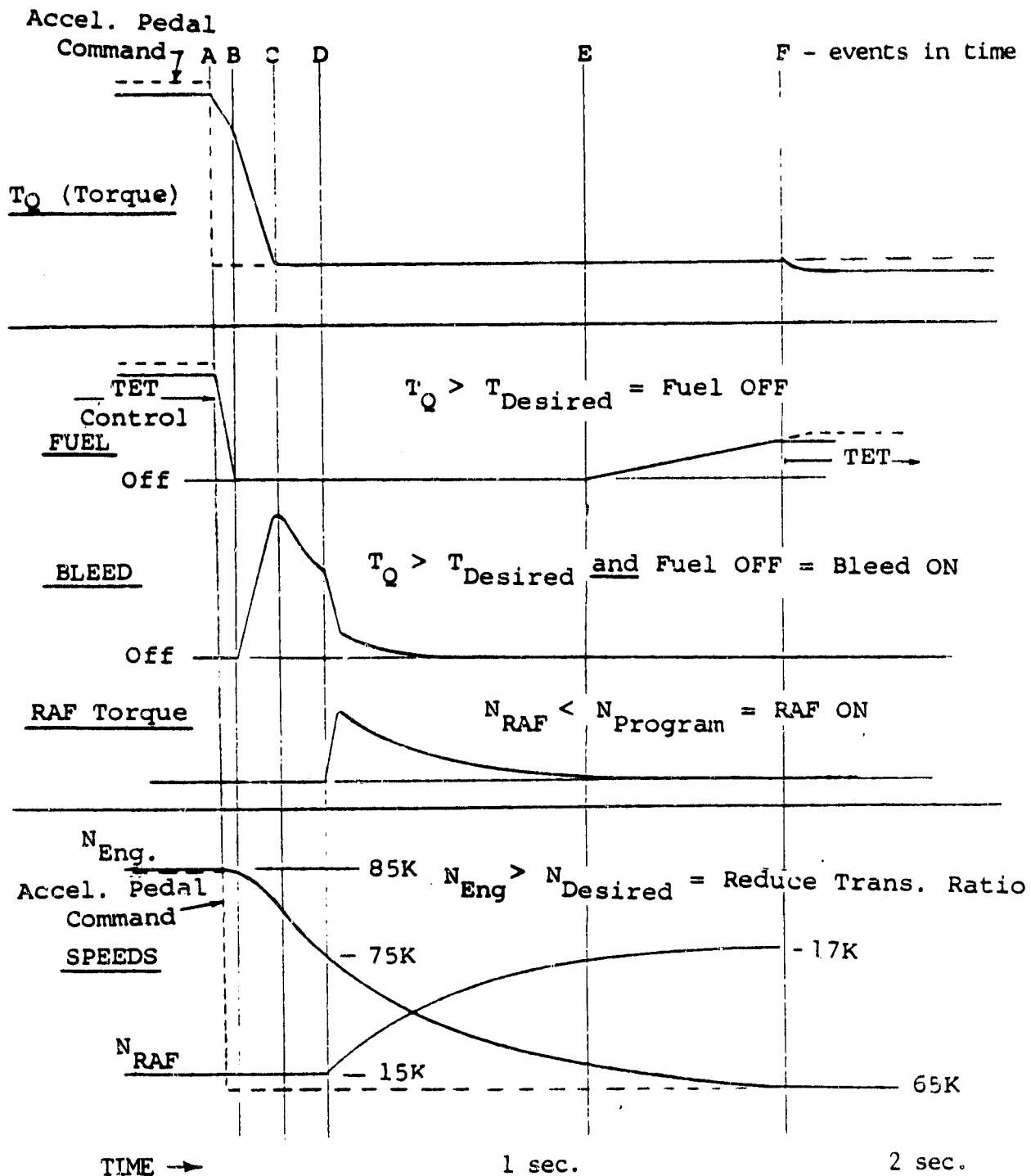


Figure 157
Engine Speed vs. Vehicle Speed for Various Vehicle Acceleration Rates



AGT REDUCED POWER LOGIC*



*scale for all parameters are indicative of direction only;
no quantitative calculations have been made.

TORQUE SENSOR

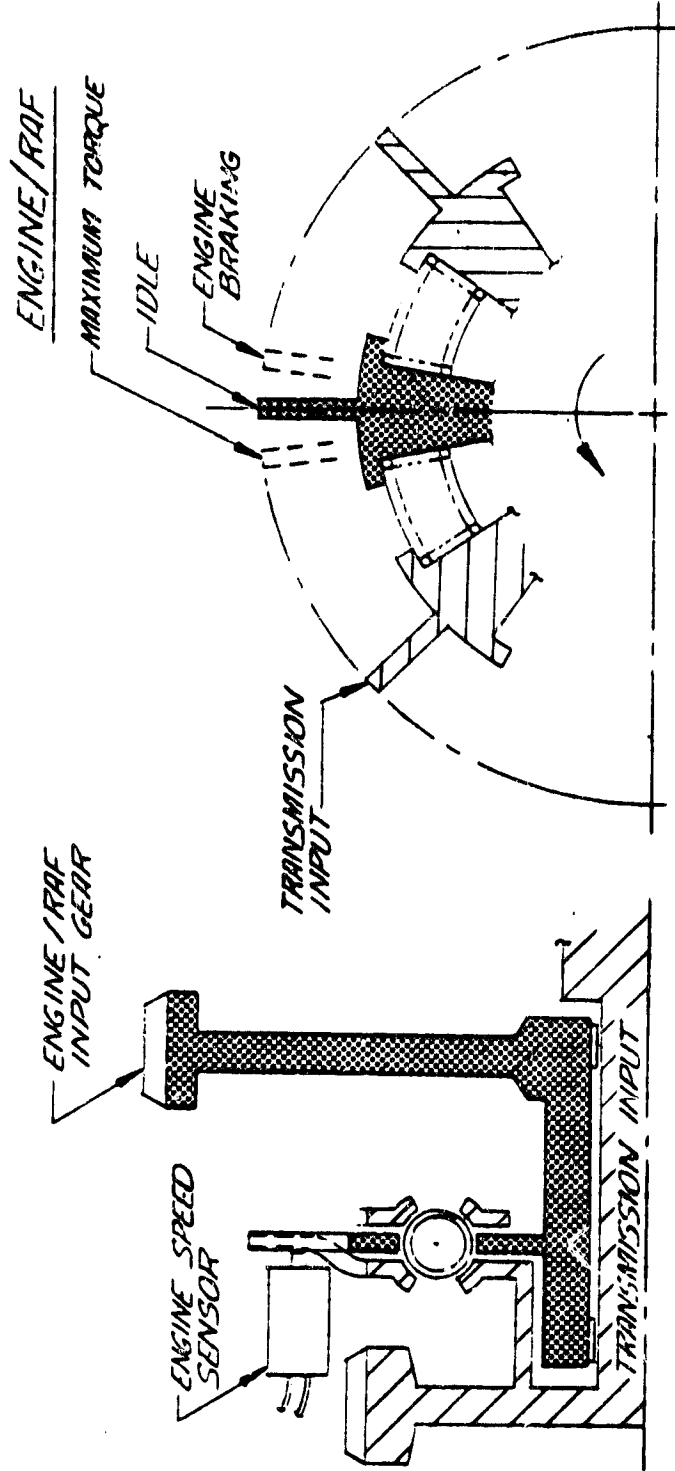


Figure 159

INPUTS

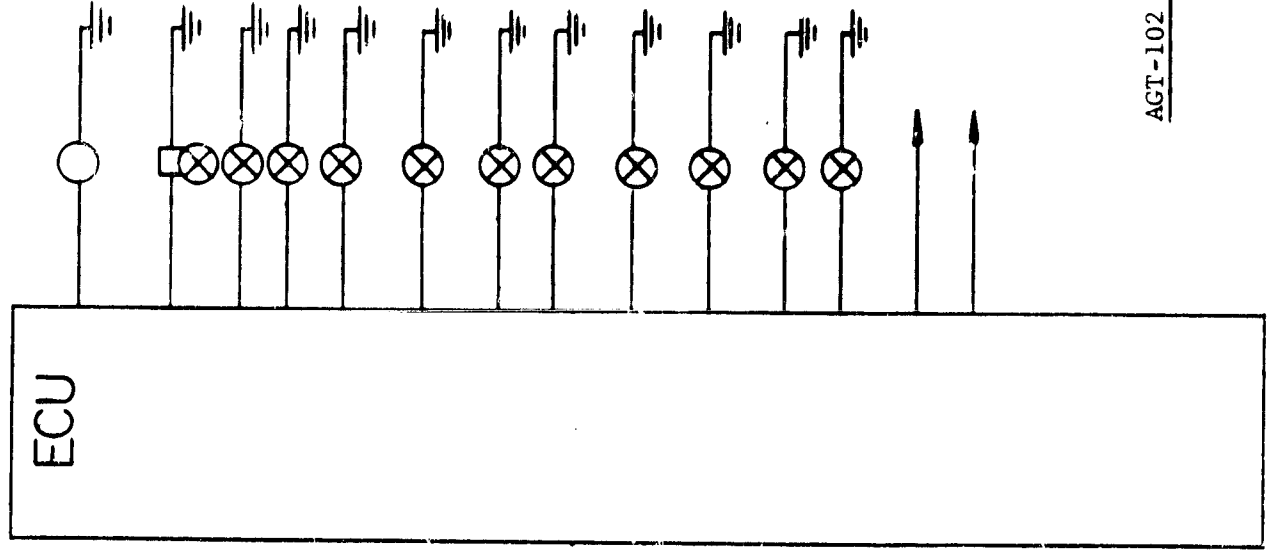
Ambient
 { Temperature
 Pressure

Driver
 { Key Switch
 Pedal Pot.
 Trans. Selector Switch

Speeds
 Engine/Trans. Input sp. & Torque Sensor

Driven Pulley
 Flywheel
 Vehicle
Power Train
 Temperatures Turbine Cut
 T9 Safety (2)
 Pressures Drive Pulley
 Driven Pulley

OUTPUTS



Starter Relay

Fuel Metering Valve
 Start Nozzle
 Stage 1 Nozzle
 Stage 2 Nozzle

Comp. Bleed

Charge Clutch
 Discharge Clutch

Drive Pulley
 Driven Pulley
 Regen. Clutch
 Direct Clutch

Driver Displays
 Diagnostics

AGT-102 CONTROL SYSTEM

Figure 160

AGT-102 Fuel Economy vs Parasitics
 Combined City-Highway Cycle, Gasoline

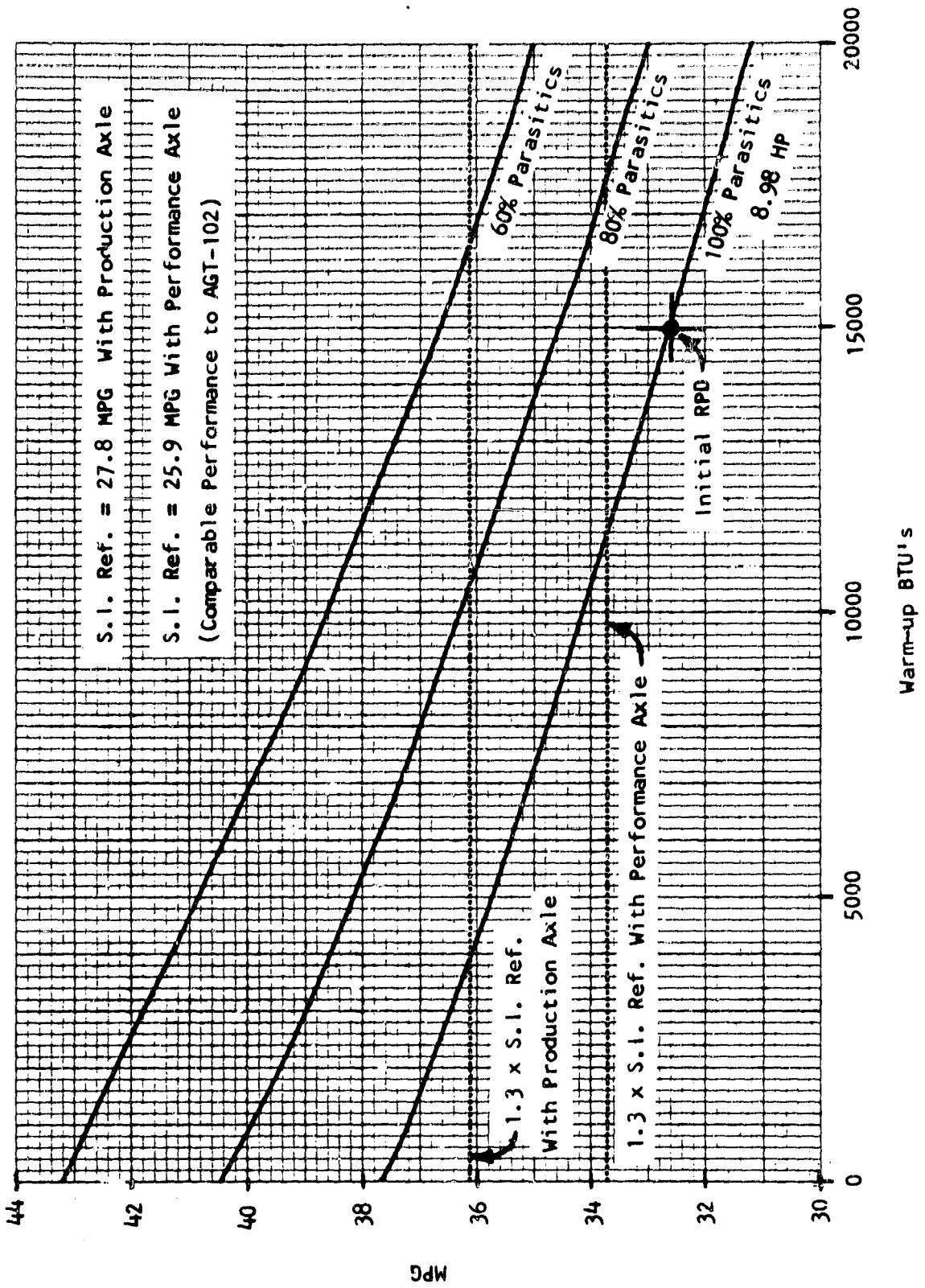


Figure 161

A-926-1 ENGINE

Start/Warmup Fuel Requirement Test

PP 3-13 AB room 12 S 01-29-81

- no oil cooling (final ~180°F.)
- exhaust fan on
- steady state idle fuel flow 6.48 PPH
- total 30-min. fuel 3.84 lb.
- less 30 min. idle fuel -3.24 lb.
- net start fuel 0.60 lb.

cell ambient 60°F.

T₁ avg 55°F.

T_{7.5} avg 1272°F.

dyno speed 1000 rpm

corr. N gg 50%

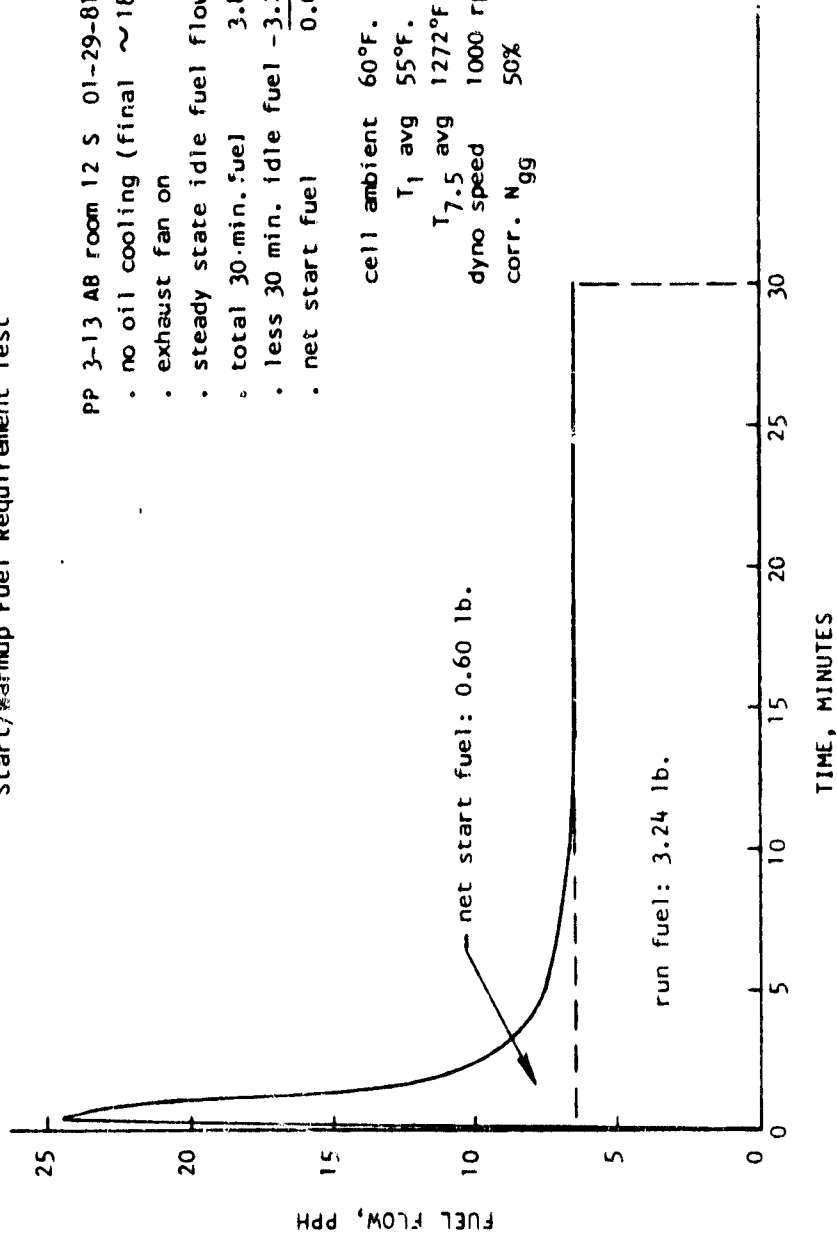


Figure 162

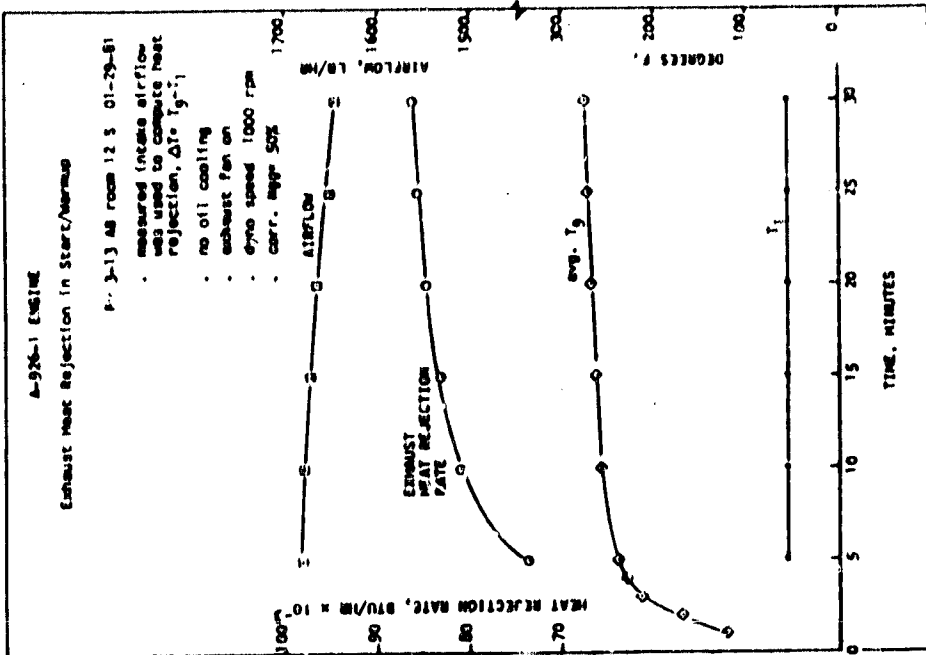


Figure 164

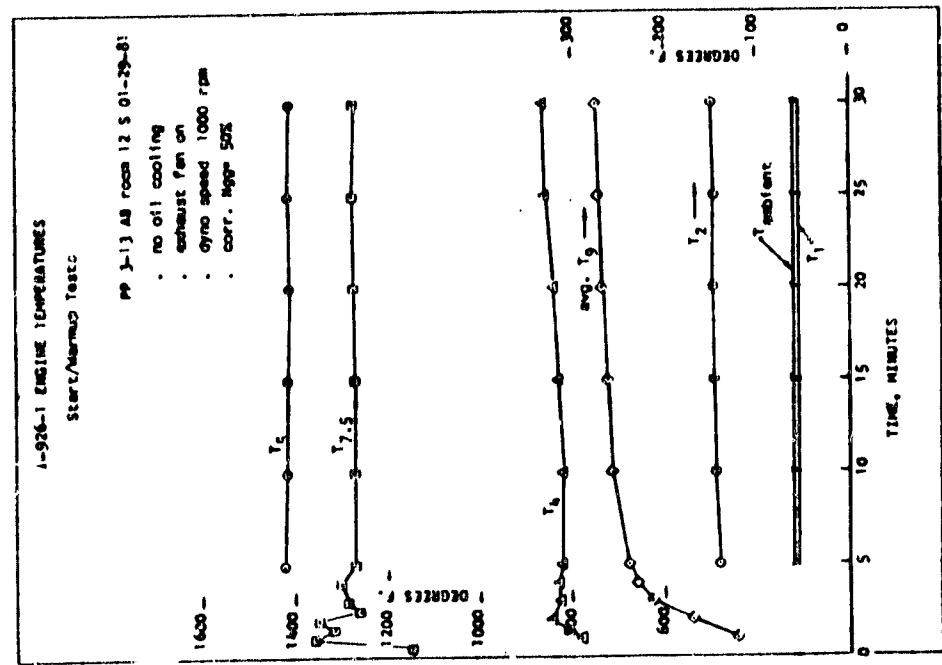
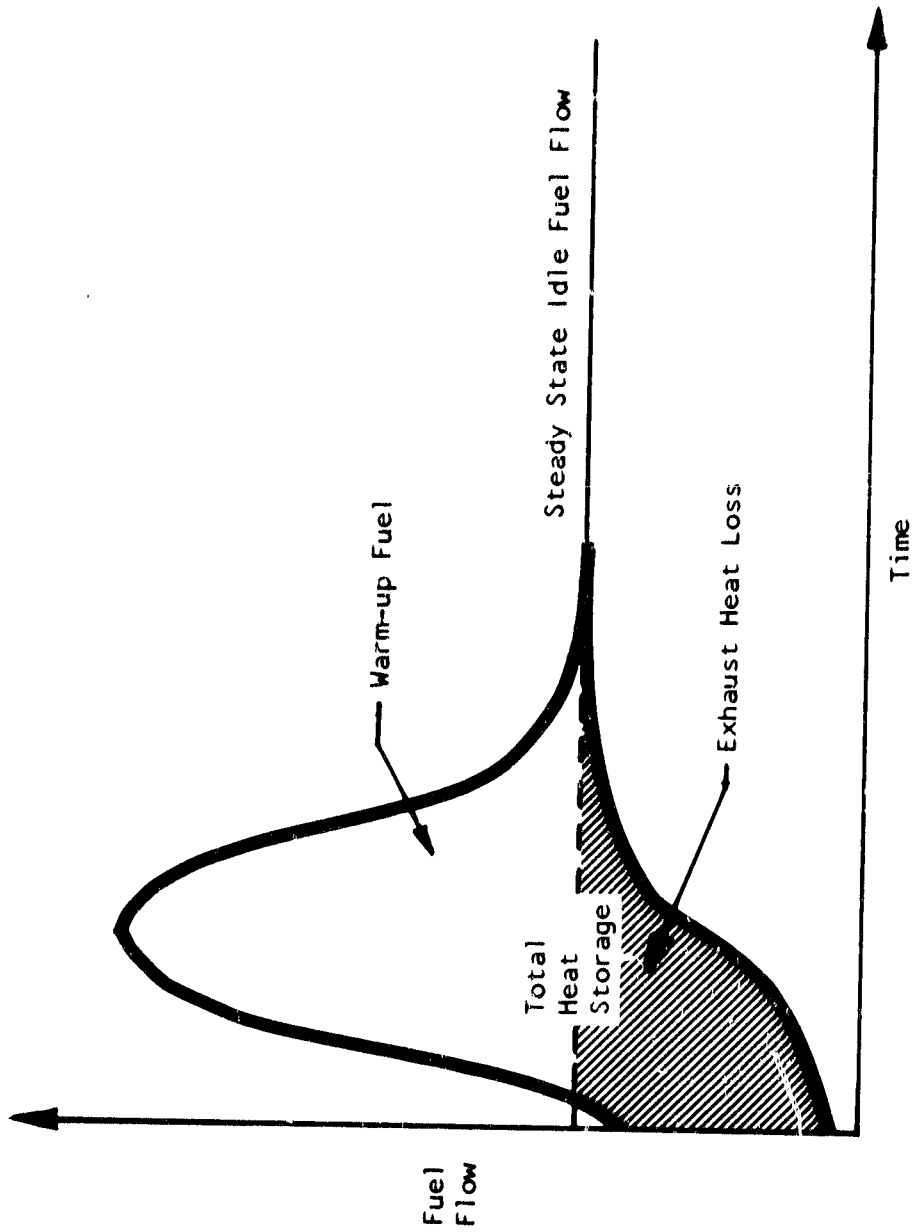
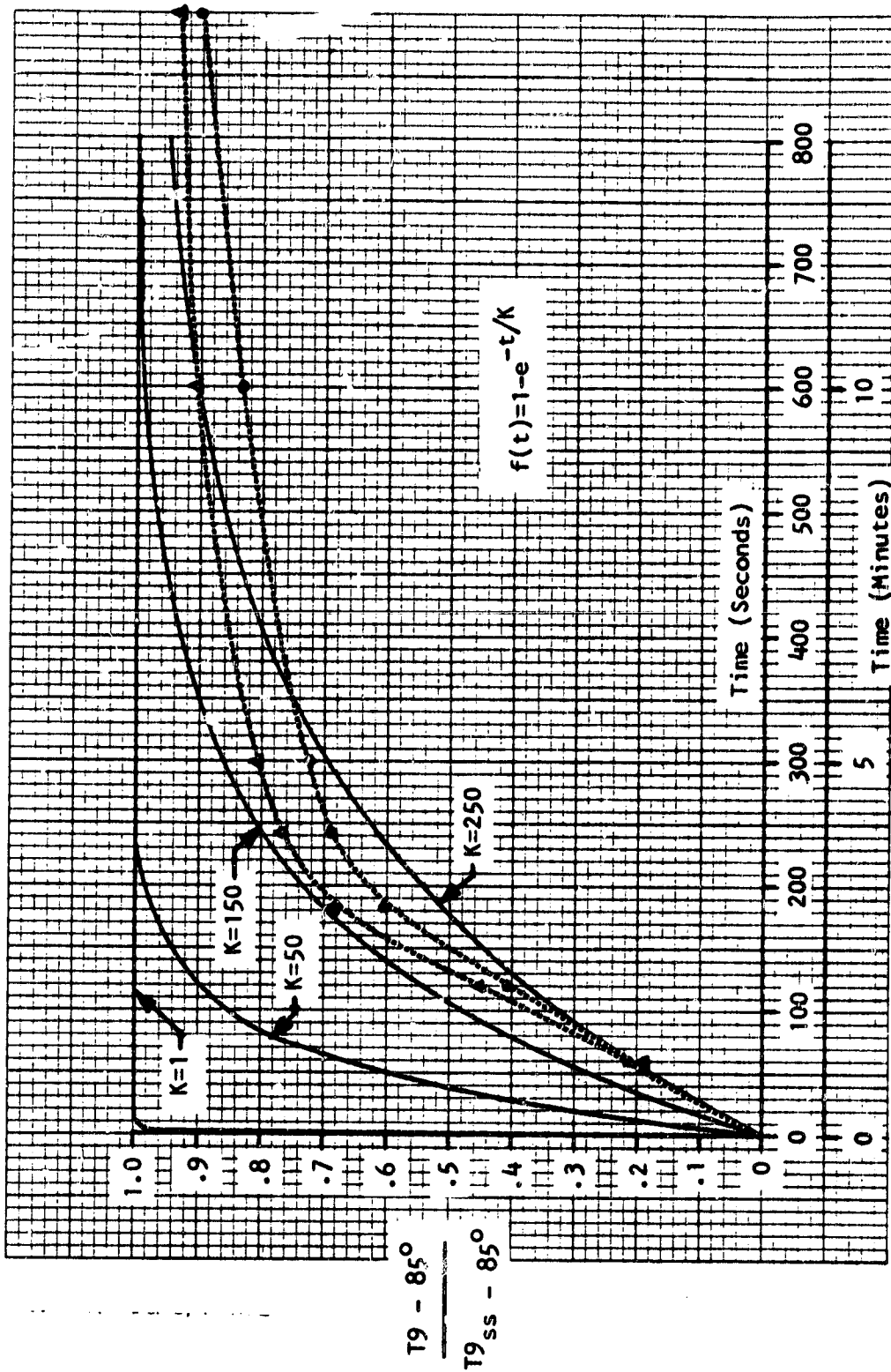


Figure 163



Warm-up Fuel Flow Model
 Upgraded Engine Reference Characterization

Figure 165



Engine Warm-up Model
 Exhaust Temperature Ratio Functions vs Data

Figure 166

C-4

AGT-102 POWERTRAIN
 VEHICLE ROAD LOAD CHARACTERISTICS

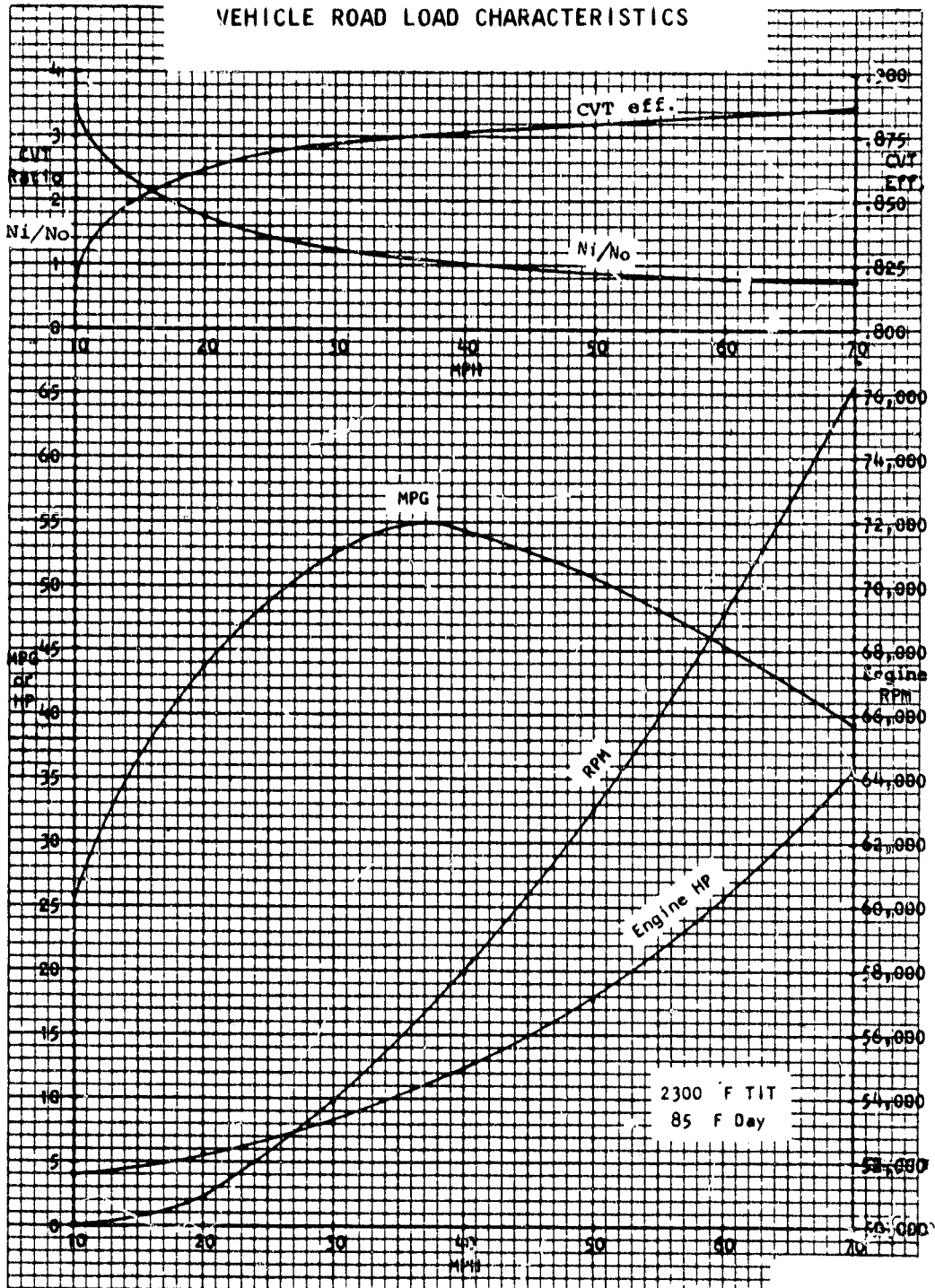


Figure 167

AGT-102 Vehicle Launch With 15 ft/sec² Acceleration

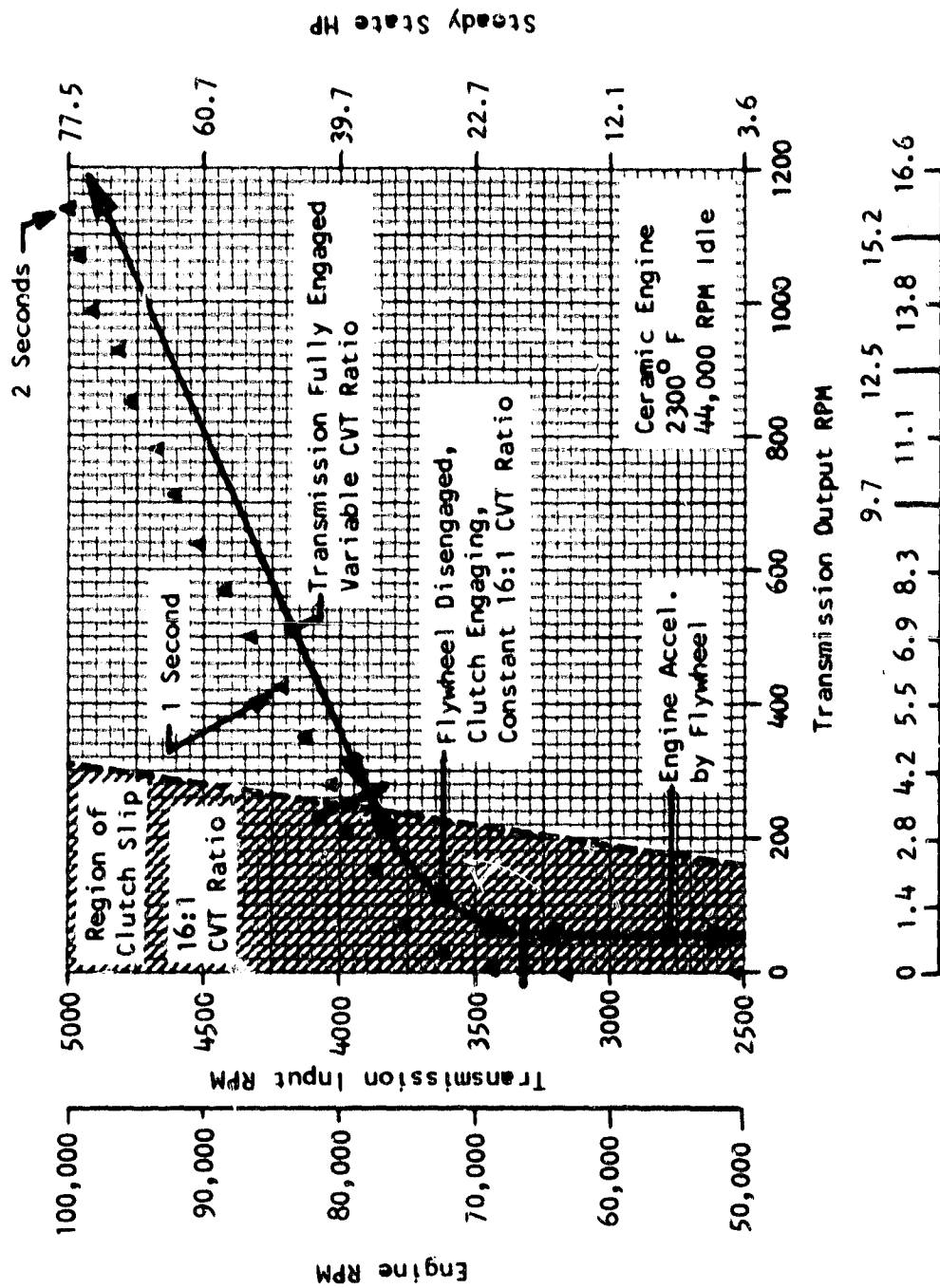


Figure 168

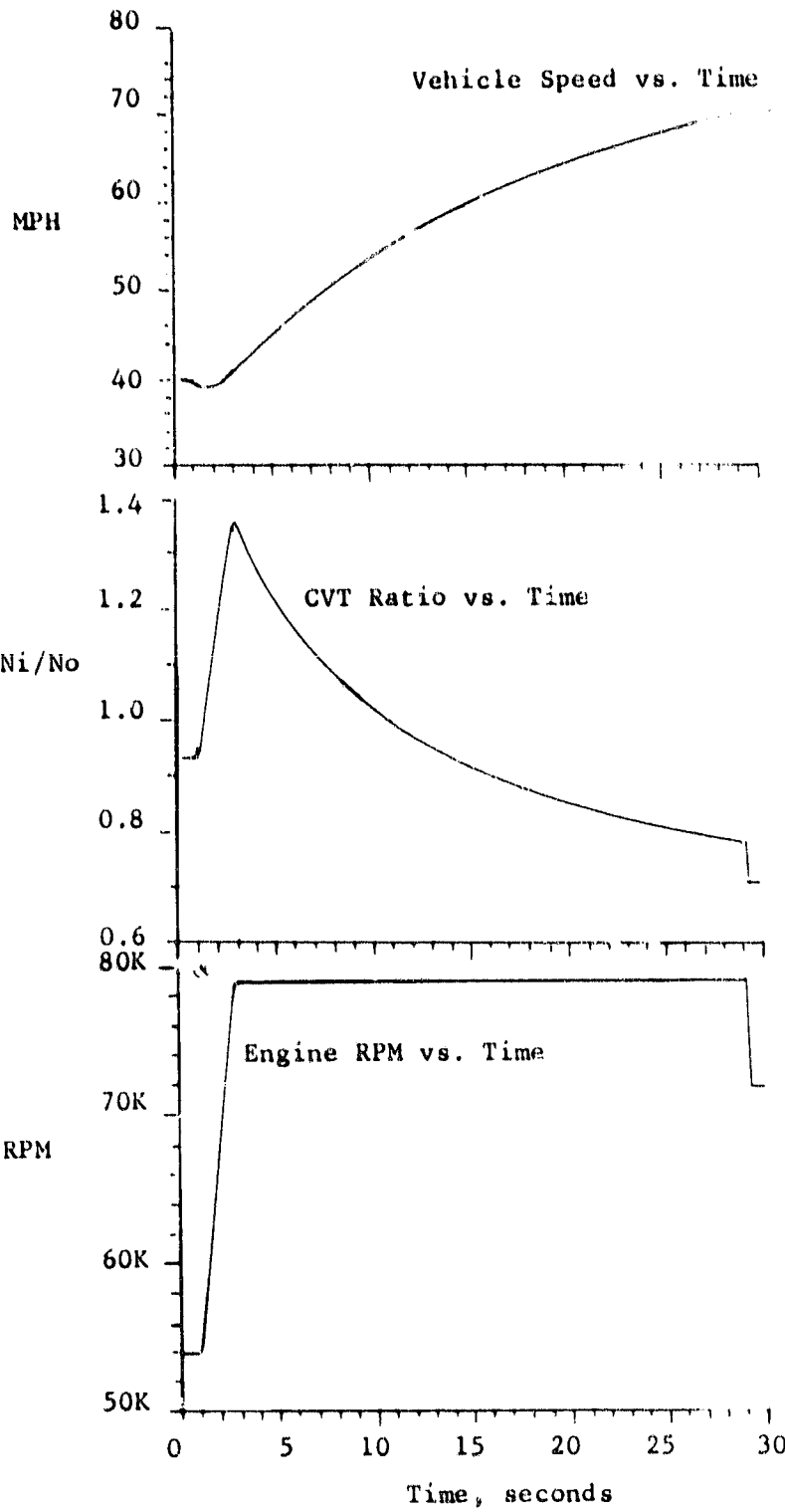


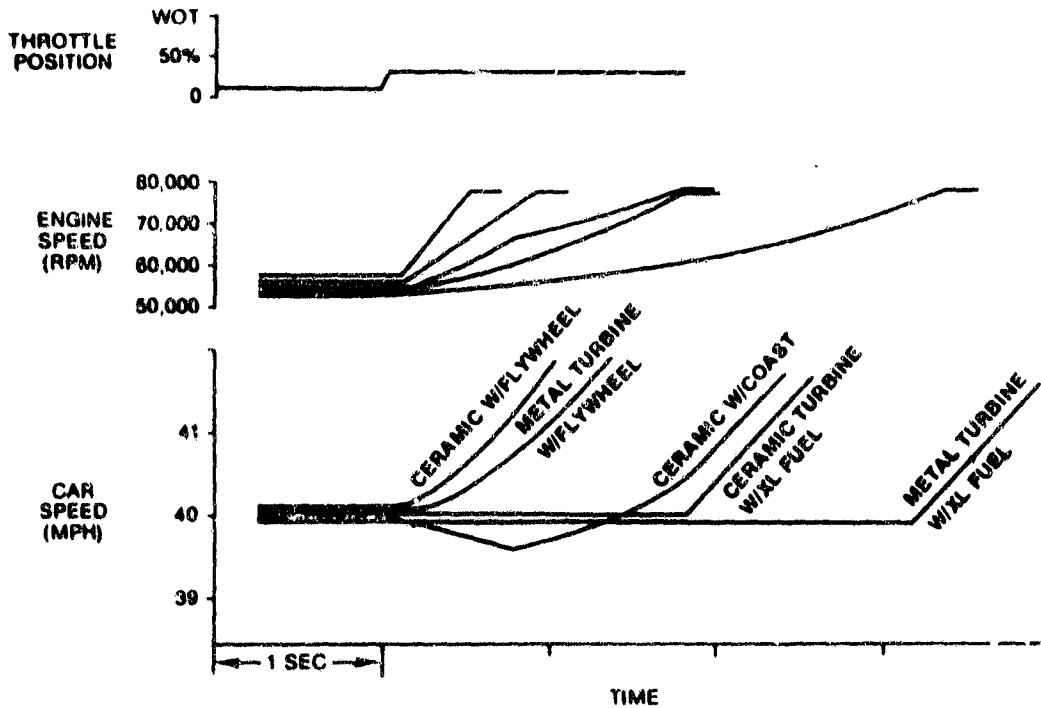
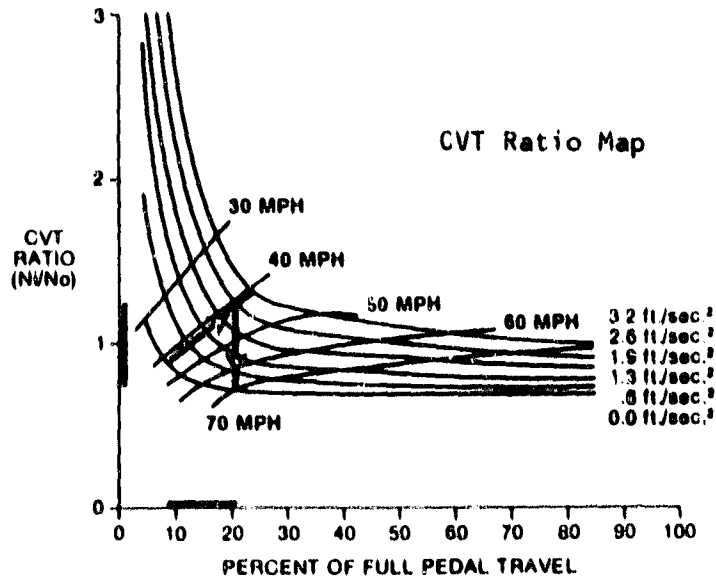
Figure 169C

Figure 169B

Figure 169A

AGT-102 Vehicle Performance Model - (Initial)
40 to 70 MPH Acceleration

Figure 169



Part Throttle Acceleration
From 40 MPH Cruise

Figure 170

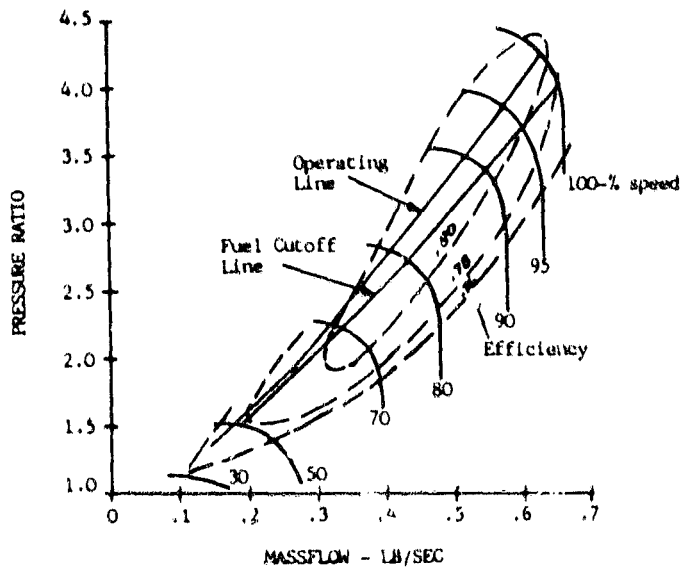


Figure 171, AGT-102 Estimated Compressor Performance

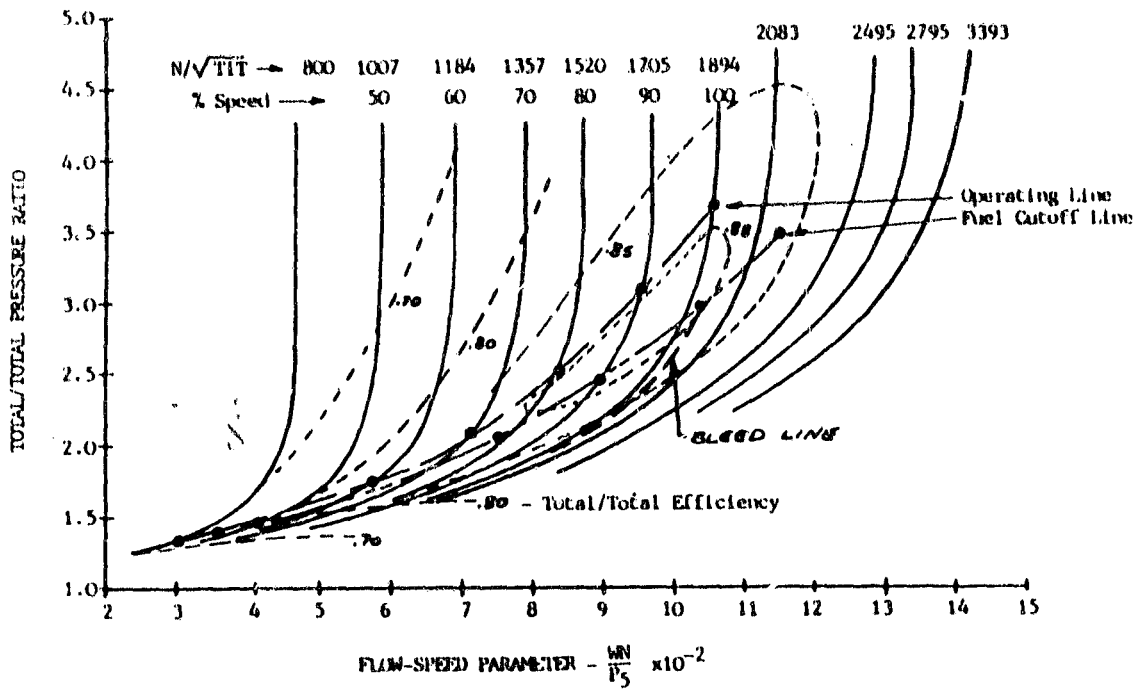


Figure 172, AGT-102 Estimated Turbine Performance

VARIATION OF REDUCTION GEAR
 OUTPUT POWER WITH PERCENT
 ENGINE SPEED FOR THREE BLEED
 HOLE DIAMETERS AND FOR FUEL
 CUT-OFF CONDITION

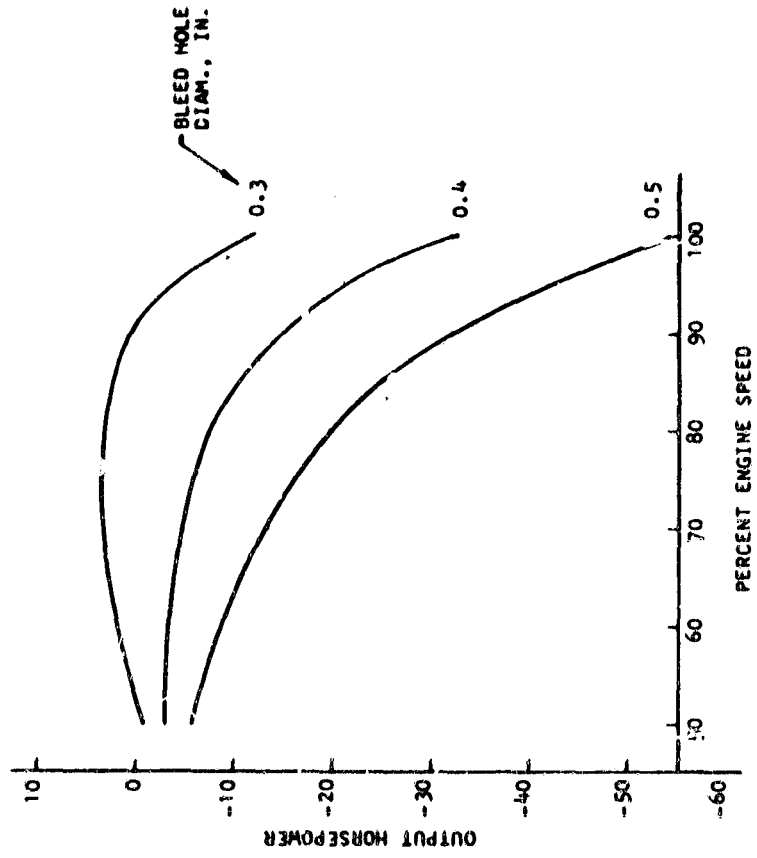
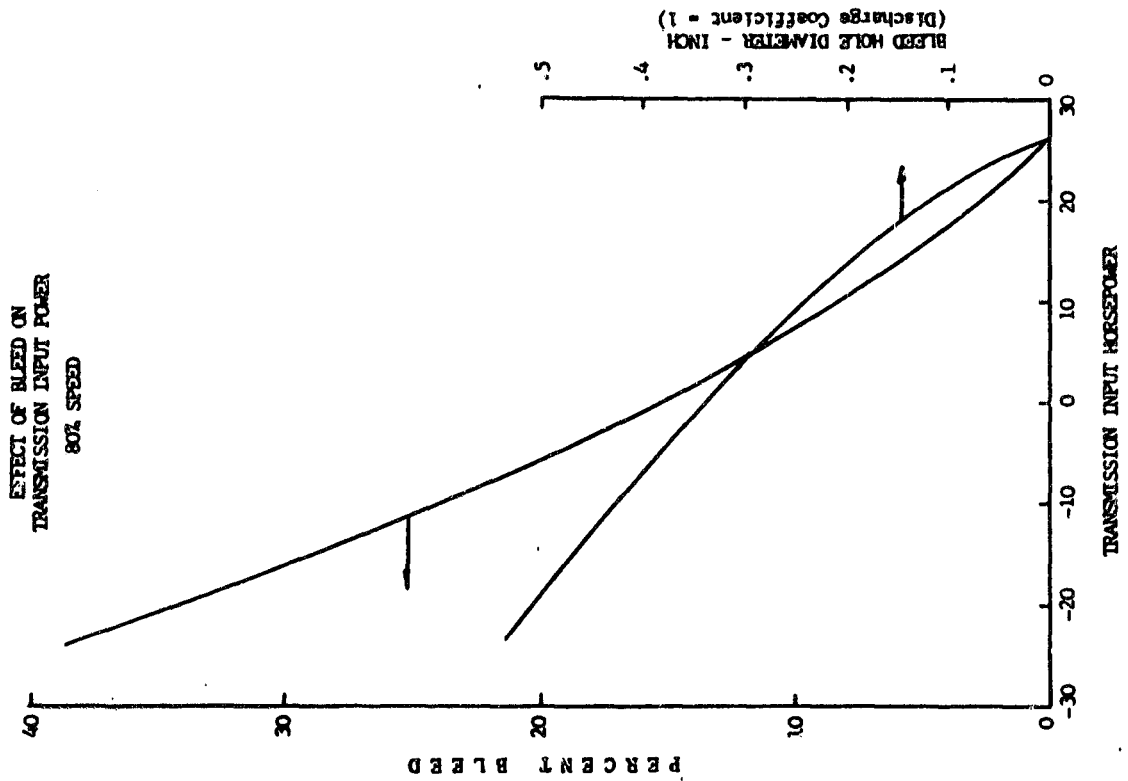


Figure 174



EFFECT OF BLEED ON
 TRANSMISSION INPUT POWER
 80% SPEED

Figure 173

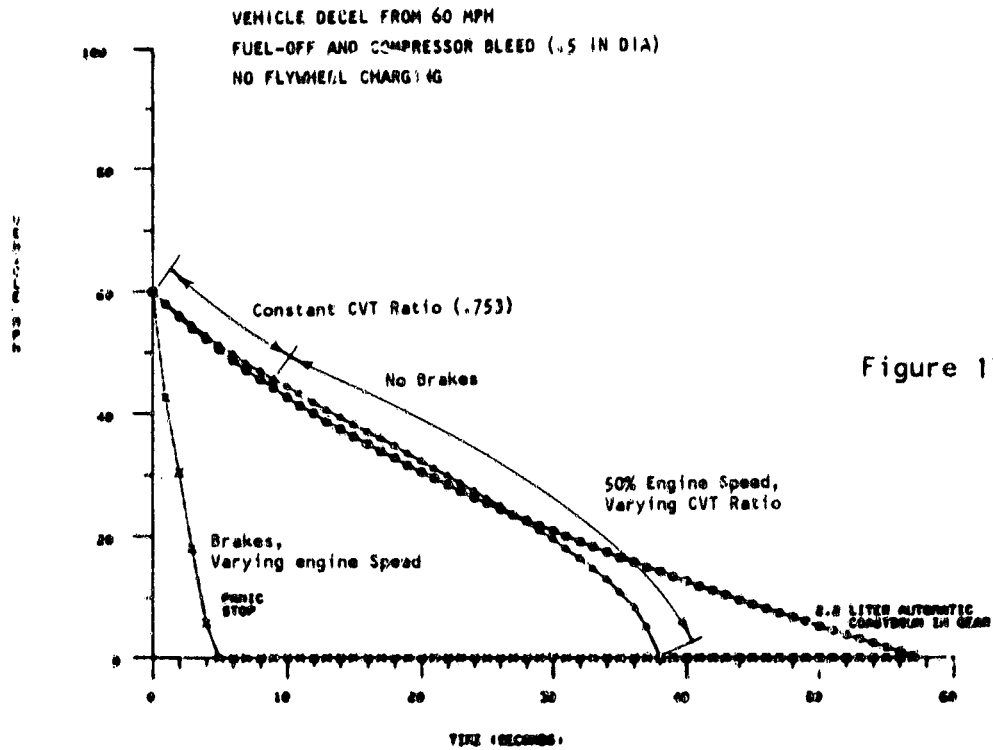


Figure 175

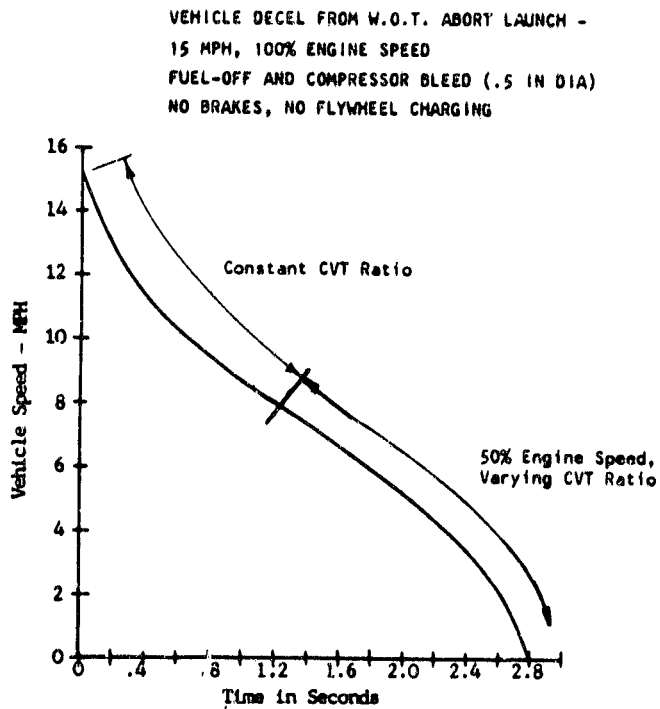
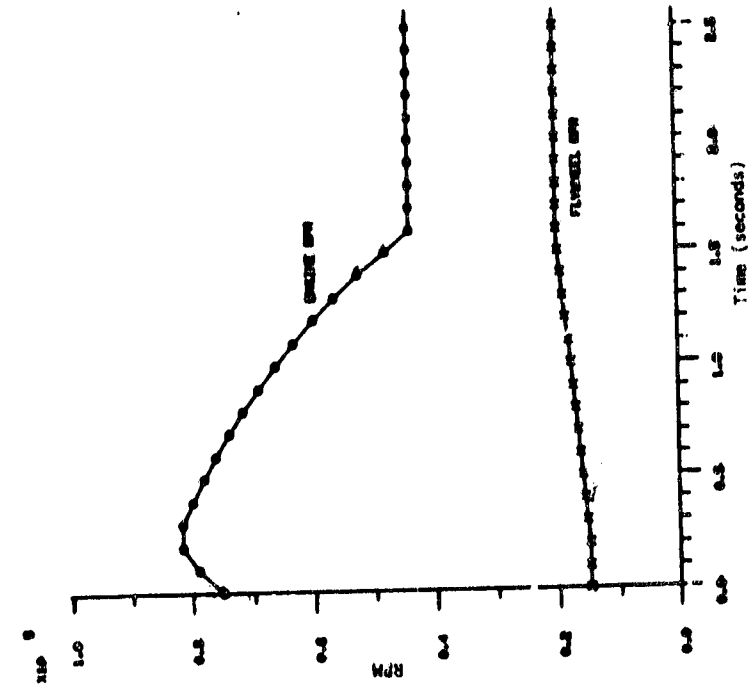


Figure 176

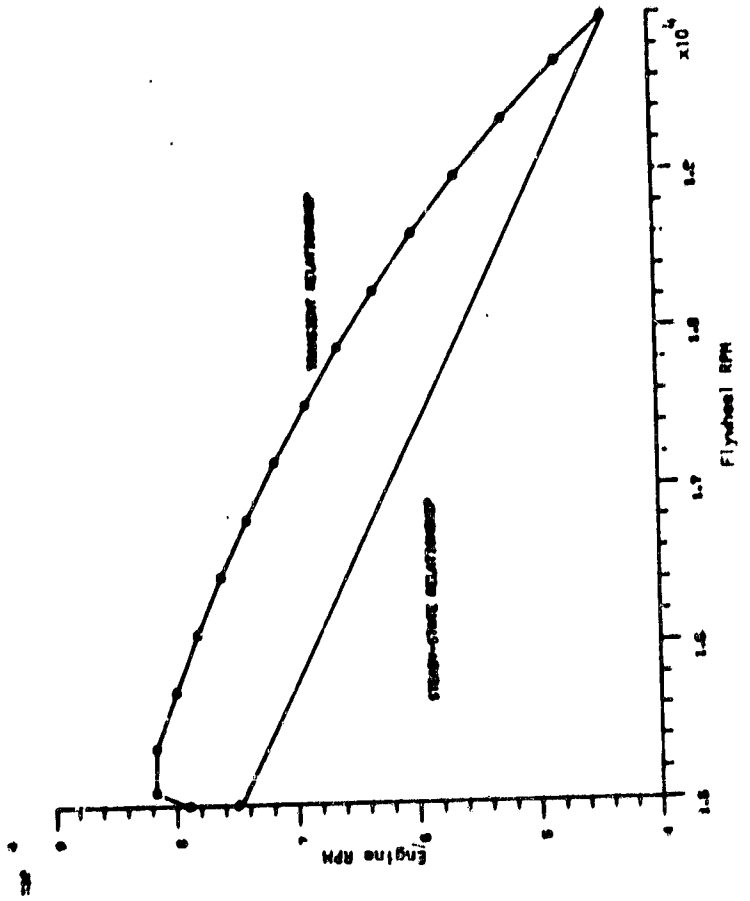
ENGINE DECEL/FLYWHEEL CHARGING CHARACTERISTICS

**Fuel Off, No Power To Vehicle, No Compressor Bleed,
Transient Engine Power From Regenerator Stored Heat**



ENGINE AND FLYWHEEL RPM VS. TIME

Figure 177

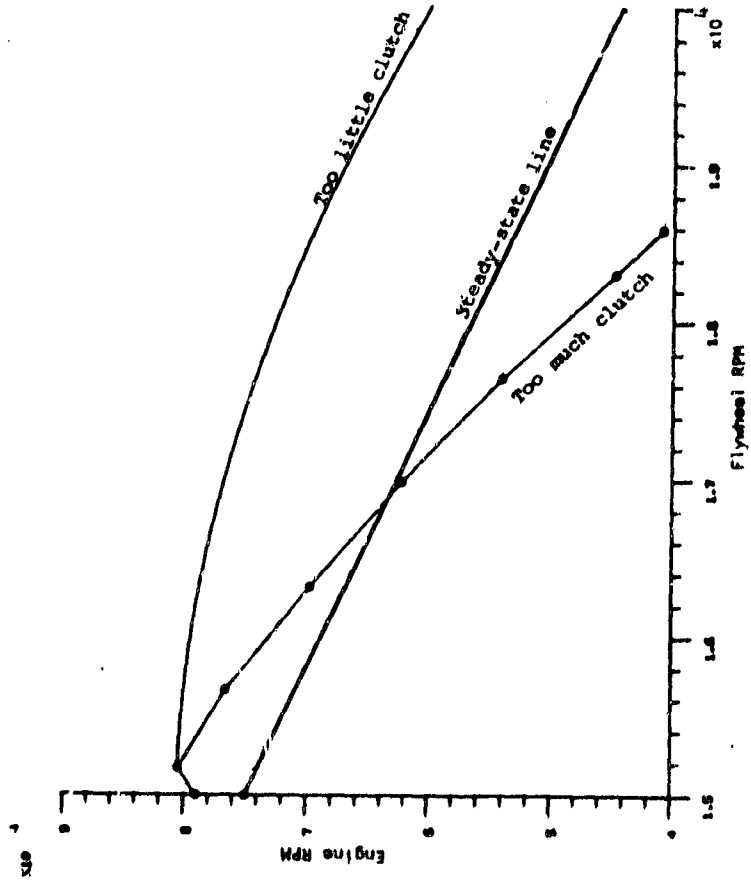


ENGINE RPM VS. FLYWHEEL RPM

Figure 178

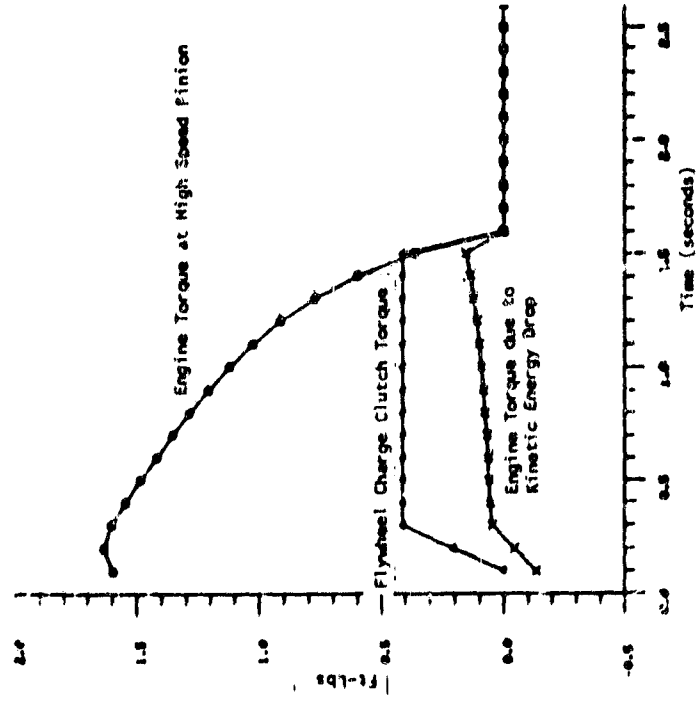
ENGINE DECEL/FLYWHEEL CHARGING CHARACTERISTICS

Fuel Off, No Power To Vehicle, No Compressor Bleed,
Transient Engine Power From Regenerator Stored Heat



**ENGINE RPM VS. FLYWHEEL RPM WITH
MISMATCHED FLYWHEEL CHARGE CLUTCH**

Figure 179



SYSTEM TORQUES VS. TIME

Figure 180

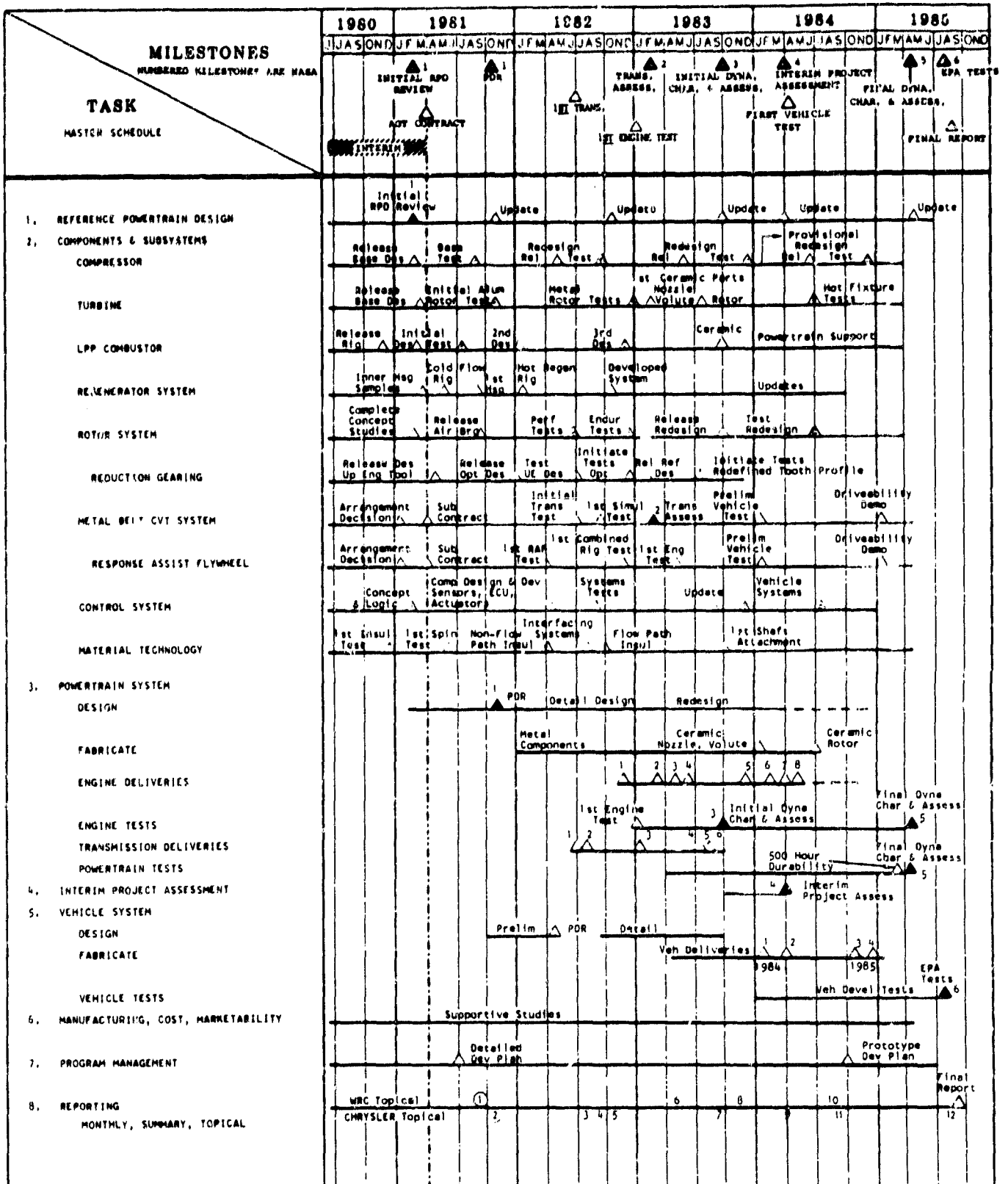
APPENDIX A

Program Goals, Master Schedule, and Program Tasks

The objective of the AGT-102 program was to develop and demonstrate, by July 31, 1985, an advanced automotive gas turbine powertrain system which, when installed in a 1985 vehicle, would meet the following goals:

- * At least a 30% improvement in combined cycle fuel economy (mpg) based on EPA test procedures over that presently predicted for a comparable 1985 production vehicle. The reference 1985 production vehicle was to be powered by a conventional spark-ignition powertrain system (Baseline System). Both the gas turbine and spark-ignition powertrain systems were to be installed in identical model vehicles and were to give substantially the same overall vehicle driveability and performance. The percentage improvement in fuel economy was to be based on fuel of the same energy content (BTU/gal), and at ambient temperature and pressure of 85F and 14.43 PSIA respectively. An absolute fuel economy goal for this project was to be determined by the contractor and concurred with by the Government during negotiations. It was recommended that this fuel economy goal be established based on diesel No. 2 fuel (130,650 BTU/gal) on a 59F day at sea level. The absolute fuel economy goal was not to vary over the life of the contract.
- * Gaseous emissions and particulate levels less than the following: 0.41 HC, 3.4 CO, 0.4 NOx gm/mile and a total particulate level of 0.2 gm/mile using the same fuel as used for fuel economy measurements.
- * Ability to use a variety of alternate fuels.
- * Reliability and life comparable with powertrains currently on the market.
- * A competitive initial cost and a life-cycle cost no greater than that of a comparable conventionally-powered automotive vehicle.
- * Vehicle response suitable for safety and consumer considerations.
- * Noise and safety characteristics that meet the current legislated or projected Federal Standards for 1985.

Master Schedule



AGT-102 Program Tasks

The following paragraphs describe the work which Chrysler Corporation and Williams Research Corporation planned in order to accomplish the program tasks listed in the preceding Master Schedule.

1.0 AGT REFERENCE POWERTRAIN DESIGN (RPD)

1.1 INITIAL REFERENCE POWERTRAIN DESIGN

The Contractor shall prepare a Reference Powertrain Design (RPD) based on a single-shaft engine, a speed reduction gearset, a continuously variable transmission (CVT) and a flywheel to assist engine response. This will be a preliminary engineering design of the powertrain system, vehicle layout, and integration. The powertrain will be installed in a six-passenger, front-wheel-drive vehicle with an inertia weight of 2750 pounds. Evolving technologies will be utilized to the extent that they can reasonably be expected to become available in time to support the accomplishment of the objectives of this project.

1.1.1 Basic Engine. The Contractor shall prepare the basic engine design for the RPD. This design will be based on the single-stage centrifugal compressor, single-stage radial turbine with ceramic rotor and nozzle, lean, premixed, prevaporized (LPP) combustor, and dual ceramic regenerators. The design will consider the requirements for the RPD, with interface dimensions and specifications as defined in Task 1.3 of this proposal.

1.1.2 Powertrain. The Contractor shall prepare the powertrain design for the RPD. This design will be based on a speed reduction gearset which is integrated with a response assist flywheel, engine auxiliaries, vehicle accessories, and a CVT. The flywheel will be used to assist engine response. The CVT will be a metal belt drive configuration. The design will consider the requirements for the RPD, with interface dimensions and specifications as defined in Task 1.3 of this proposal.

1.2 UPDATED REFERENCE POWERTRAIN DESIGN (RPD)

The Contractor shall update the RPD and maintain it current through the remainder of the contract, as information from Tasks 2 and 3 becomes available. The update of the RPD shall incorporate information gained from component and engine testing and shall be based on the latest system and component analyses, design, and cost study results. The RPD shall be modified as required to reasonably reflect significant improvements or changes in component and subsystem designs throughout the contract. The Updated RPD shall serve as a basis for development of follow-on evolutionary versions of the experimental system to be used for dynamometer and vehicle testing. The Contractor shall document and present at the yearly project reviews as stated in Task 7.3 the traceability of the current experimental powertrain to the Updated RPD.

All RPD modifications, including drawings, supporting information, and analyses, shall be submitted to the NASA Project Manager for review and concurrence. A complete set of microfilmed drawings of the final RPD shall be provided to the NASA Project Manager.

1.2.1 Basic Engine. As information from Tasks 2 and 3 becomes available, the Contractor shall update the basic engine design and maintain it current through the remainder of the contract. Specific updates shall occur to support program milestones as noted on the schedule. The updates shall incorporate information from component and engine testing and shall be based on system and component analyses, design, and cost study results.

The Contractor will submit basic engine modifications for review and concurrence with the RPD, including drawings, supporting information, and analyses.

1.2.2 Powertrain. As information from Tasks 2 and 3 becomes available, the Contractor shall update the powertrain and maintain it current through the remainder of the contract. Specific updates shall occur to support program

milestones as noted on the schedule. The updates shall incorporate information from component and engine testing and shall be based on system and component analyses, design and cost study results.

1.3 DESIGN REQUIREMENTS AND CRITERIA

The RPD shall be based on unleaded gasoline, pending concurrence by the NASA Project Manager. Taken into consideration shall be the compatibility (i.e., material compatibility, etc.) of the RPD with alternative fuels. As part of the supporting analysis, the Contractor will characterize the RPD performance with alternative fuels (as many as five) to be specified at a later date by the NASA Project Manager. The alternative fuels analysis shall assume no major modification of the RPD and shall include assessment of the impact of each fuel type on fuel economy, performance, and emissions.

The RPD shall include sufficient system and subsystem layouts, component layouts and vehicle installation drawings, showing key features and dimensions in compliance with the Schedule Article entitled "Conceptual and Developmental Design Drawings (level 1)". These RPD drawings shall serve as a basis for the component and engine detail design. Sufficient system and component design and analysis shall be performed to (1) assure that the potential exists for meeting the final project goal and objectives, (2) identify required supporting component, subsystem, and material technology activities, and (3) allow preliminary production and/or material cost assessments to be carried out. The recommended Initial RPD, appropriate drawings, and supporting information and analyses shall be formally reviewed at Lewis Research Center (LeRC) prior to concurrence by the NASA Project Manager. Formal review of the initial RPD will complete the first of two requirements for Milestone 1.

2.0 COMPONENT AND SUBSYSTEM DEVELOPMENT

2.1 COMPRESSOR

2.1.1 Design. Using aluminum as the compressor rotor material, the Contractor

will complete the basic design of the centrifugal compressor and make variant designs and revisions to explore methods of improving performance. The Contractor will revise and update the design to incorporate results from component and engine testing.

2.1.2 Fabrication. The Contractor will fabricate and procure aluminum hardware, including design variants, for component development and testing, both in rigs and in engines. Hardware will be modified as determined by test results or design changes.

2.1.3 Test. The Contractor will provide a test rig, including all equipment modifications and instrumentation, to test the aluminum compressor component with its variants and associated hardware in an existing compressor test facility. Performance tests will be conducted on the compressor hardware to evaluate the basic design and variant designs in order to determine methods of improving performance. The Contractor will explore, evaluate, and solve any mechanical problems that may be found during the component testing. Strain gage testing will be carried out on the aluminum compressor disk and blades. The Contractor will evaluate compressor inlet and outlet flow passages using flow-test models and/or simulated engine ducts on the compressor test rig.

2.2 TURBINE

2.2.1 Ceramic Stage (2300F Static and Cold Spin Rigs; Development Variants)

2.2.1.1. Design. The Contractor will design a radial turbine with ceramic rotor and nozzle, and conduct mechanical analyses, layout, and detailing as required. The Contractor will incorporate design changes based on fabrication experience and test results.

The Contractor will design a high temperature turbine test rig, including air heater, power absorber, and instrumentation to conduct and perform mechanical tests on the ceramic radial turbine stage. Rig design will accommodate engine hardware so that it may be used for non-regenerative engines.

2.2.1.2 Fabrication. Ceramic turbine components, including design variants, will be procured or fabricated in sufficient quantity to carry out the test program in cold and hot rigs. Reworking of the hardware to incorporate design changes will be carried out where feasible.

The Contractor will fabricate or procure a high temperature test rig with adequate power absorption capacity and instrumentation.

2.2.1.3 Test. The Contractor will perform ambient temperature spin testing of the ceramic rotor and variants thereof. Pressure and flow test rigs will be provided for testing the ceramic components with respect to individual and correlative mechanical integrity. Such tests will be carried out as required.

The Contractor will test the initial design concepts of ceramic components in a static rig.

The Contractor will perform hot flow tests on ceramic turbine components to evaluate mechanical and performance characteristics, and conduct operational tests on the ceramic turbine stage, including simulated starts and transients, to evaluate mechanical and thermal behavior and define problem areas requiring additional analysis and redesign. Performance tests will be conducted up to engine operating temperatures to confirm aerodynamic and mechanical capability prior to engine test.

2.2.2 Aero Development (Cold Rigs; Stage Variants)

2.2.2.1 Design. The Contractor will perform aerothermodynamic analyses to optimize the performance of the ceramic turbine stage. Layout, design, fabrication, and test activities will be monitored to assure maintenance of optimized design configurations, and designs revised as necessitated by feedback from fabrication and testing.

2.2.2.2. Fabrication. The Contractor will provide aluminum (or equivalent) models of the ceramic turbine rotor and static components, including design variants, for low temperature performance test of the ceramic turbine stage.

The Contractor will fabricate wood or plastic models of turbine components, including inlet and outlet flow passages, for flow test.

2.2.2.3 Test. The Contractor will provide a low temperature test rig with the required instrumentation and conduct performance tests on the model of the ceramic turbine and associated static components, including ductwork. The Contractor will perform flow tests on turbine components including inlet and outlet flow paths.

2.2.3 Metallic Stage

2.2.3.1 Design. The Contractor will design a metallic radial turbine stage, using a conventional superalloy rotor, for use in early rig and engine testing while the ceramic turbine stage is under development. The design will be compatible with the complementary ceramic parts (see paragraphs 2.2.1 and 2.2.2) except for reduced temperature and life. The metallic turbine rotor will be interchangeable with the ceramic turbine rotor as far as practical. Metallic static components will duplicate the ceramic flowpaths.

2.2.3.2 Fabrication. Metallic radial turbine rotors and static components will be procured/fabricated, to permit the required turbine component testing. An aluminum (or equivalent) rotor will be provided for low temperature performance test if the metallic rotor aerodynamic design is significantly different from the ceramic rotor.

2.2.3.3 Test. Testing will be performed on the metallic turbine stage to assure that it is capable of fulfilling the role of interim test hardware during the development of the ceramic rotors. This will include low temperature performance test if required, ambient temperature spin test of the metallic rotor, and hot performance and mechanical test of the turbine stage. This testing will utilize the test equipment provided for 2.2.1 and 2.2.2.

2.3 LPP COMBUSTOR

2.3.1 Design. The contractor will design a combustor to meet the grams/mile

standards of 0.41 HC, 3.4 CO and 0.4 NOx while simultaneously meeting the requirements of operating range, life, odor, noise, efficiency, and multifuel capability.

The basic direction of the design will be provided by a mathematical model of the physical phenomena involved in lean, premixed, prevaporized (LPP) combustion. The model will include: autoignition, droplet vaporization rates, pollutant formation and destruction, lean limits, turbulent flame speeds, the origin of total pressure losses, and other processes. All engine operating conditions will be described and a projection of EPA cycle emissions will be made using several different techniques.

A hot test rig will be designed to allow combustor tests under actual AGT engine massflows and temperatures. Startup and warmup modes will be investigated using an additional test rig designed to provide diffusion flame combustion.

The response assist flywheel, in tandem with parallel fuel staging, will permit a fixed geometry combustor. The durability and low-cost requirements of the automotive marketplace will thereby be assured.

2.3.2 Fabrication. Most of the combustor designs will employ metal construction to allow rapid modification during development. After the proper geometry is determined, ceramic parts will be introduced.

The hot test rig will incorporate a quartz viewing window since experience indicates observation of the flow-flame pattern is highly advantageous.

An existing gas turbine will be modified to provide the hot gas stream needed for the combustor inlet.

The hot test rig will use insulated metal components whenever possible with the necessary ceramic parts employing simple geometrical configurations such as cylinders. This approach allows rapid procurement and minimum operational risk.

The diffusion flame device will be constructed to provide great flexibility regarding ignitor and spray nozzle location so that multifuel startup and low emissions warmup can be accomplished.

2.3.3 Test. It is anticipated that three different combustor designs will be tested before a final design is achieved. With both the hot rig and the start-up rig, it is likely that a design satisfactory for AGT engine operation will be essentially complete when the engine first becomes available. After minor adjustments on the engine, EPA cycle vehicle tests will be run.

With proper design and verification, it should be possible to avoid a large number of the time-consuming and expensive vehicle-combustor iterations.

2.4 REGENERATOR

2.4.1 Core Assembly and Performance Rigs.

2.4.1.1 Design. Thermal, stress, and performance analyses will be conducted to assure a reliable and efficient final design. Performance estimates will be applied to the basic engine performance model. Components to be designed under this subtask include the regenerator matrix, elastomeric gear mount, ring gear and pinion, outer static "L" seals, center bearing and its related support structure, and the flowpath contours of the regenerator cover. Design efforts will also include both cold flow distribution and hot regenerator system test rigs.

2.4.1.2 Fabrication. The Contractor will work closely with ceramic and elastomer vendors in procurement of the best available matrix and mounting systems. As improved materials become available, they will be phased into the program. Facilities will be updated and test rigs fabricated and installed.

2.4.1.3 Test. Regenerator system components will be tested in appropriate cold and hot rigs, and improved designs developed based on test results. Corrections based on test results will also be made to the engine performance

model. Improved components will be evaluated in the rigs as they become available.

2.4.2 Seal System, Seal Rigs. Based on literature searches and previous development experience with high temperature dry lubricant seals and seal coatings, candidate materials will be selected for both the inner and outer regenerator rubbing seal locations. Selected coating materials for the coated inner seal surface will be applied to 9-inch samples of candidate inner housing materials. Samples of promising outer seal materials will also be procured in 9-inch test specimens. The two 9-inch seal test machines will be refurbished and updated for 1800 F operation. Seal samples will be wear tested against 9-inch diameter matrix samples in the seal test machines. Friction coefficients and wear rates will be determined for each material over a range of temperature and load conditions matching predicted AGT conditions. Friction data from the selected inner and outer seal materials will be used to update the engine performance model.

2.4.3 Ceramic Support (Inner) Housing

2.4.3.1 Design. The ceramic inner housing will be designed in close cooperation with one or more ceramic material/fabrication vendors. The design activity will include structural and thermal analyses, layout, and detailing. The design will be assessed and modified based on fabrication experience and test results. Concurrent with housing design, a ceramic components test rig will be designed for cold proof testing and hot thermal shock testing of the housing and related ceramic static components.

2.4.3.2 Fabrication. The Contractor will work in close cooperation with the selected ceramics vendors in development of the ceramic inner housing, including tooling qualification, part fabrication, machining, and application of seal coatings. The ceramic components test rig will be fabricated and installed in an appropriate facility.

2.4.3.3 Test. Completed housings will be cold proof tested and finally hot thermal shock tested in the test rig. Design and fabrication processes will be altered based on test results, in an iterative development program.

2.5 ROTOR AND REDUCTION GEARING

2.5.1 Rotor/Bearing System Design

2.5.1.1 Design. The Contractor will direct and support the design of the rotor/bearing system with applicable shaft dynamics analyses, interface studies, and incorporation of the design into the engine layouts. Computer-aided design techniques will be used, and redesigns will be based on analyses of experimental data from both engine and simulator rig tests.

2.5.1.2 Fabrication. The Contractor will fabricate or procure test hardware from vendors to simulate engine rotor systems for development test and evaluation.

2.5.1.3 Test. The Contractor will provide a test rig for simulated engine hardware, with instrumentation to measure bearing, shaft, and rotor system characteristics. The Contractor will test simulated engine rotor/bearing systems over a range of operating conditions, and evaluate bearing performance and rotor dynamics characteristics.

2.5.2 Reduction Gearing and Back-to-Back Rigs

2.5.2.1 Design. A reduction gear system will be designed to provide the required ratios for driving the transmission, response assist flywheel, engine auxiliaries, and vehicle accessories. Factors such as package size, cost, weight, gear noise, and gear manufacturing will be included in the design considerations.

The system will be integrated into the powertrain to meet the interface requirements of the vehicle, engine, and transmission.

2.5.2.2 Fabrication. The Contractor will procure and fabricate hardware necessary for rig and engine testing.

2.5.2.3 Test. Back-to-back rigs will be used to evaluate gear box performance with initial AGT gears from Upgraded tooling and optimized AGT gears with new tooling. A gear set utilizing a refined tooth profile will also be tested.

2.6 TRANSMISSION

2.6.1 Response Assist Flywheel

2.6.1.1 Design. The Contractor will effect the design of an engine response assist flywheel. The RAF system will be selected for performance, fuel economy, cost, and feasibility along with the capacities needed for engine acceleration and deceleration. The components will be designed to give adequate life and safety based on the selected mission.

2.6.1.2 Fabrication. The flywheel, gears and clutches will be procured for component and system testing and development.

2.6.1.3 Test. The Contractor will run tests for capacity, efficiency, durability, noise, and performance to improve the RAF and its control before installing it on the AGT.

2.6.2 Variable Ratio Metal Compression Belt

2.6.2.1 Design. The Contractor will effect the design of a metal compression belt and variable ratio pulleys for the RPD continuously-variable transmission. These components will be designed to give adequate life, based on vendor experience, with the projected torques and speeds of the RPD engine.

2.6.2.2 Fabrication. Variable ratio pulleys and metal compression belts will be procured for component and system testing and development.

2.6.2.3 Test. The Contractor will run capacity, efficiency, and performance tests on an industrial version of the metal compression belt in order to obtain operational data and confirm its acceptability for the RPD transmission. The designed components will be tested as part of the complete transmission, and developed toward the goal of meeting all of the normal requirements of an

automotive transmission, including low manufacturing cost, good efficiency, adequate component life, and good response and smoothness.

2.6.3 CVT System

2.6.3.1 Design. The Contractor will prepare a design of a complete continuously-variable transmission including all control elements needed to interface with the integrated electronic system. The design will use the metal compression belt as the variable ratio element, and will augment the ratio range with additional gearing as required to meet the project goals with projected engine performance. The design will use known workable and low-cost component constructions. Detailed design analyses will be completed and detailed design fabrication and assembly drawings will be made. These will be updated to reflect development changes throughout the contract period. The Contractor will supply a complete set of microfilm drawings of the final experimental transmission.

2.6.3.2 Fabrication. Complete CVT transmissions will be built by the Contractor in sufficient quantity to support the transmission, engine, and vehicle development programs. The transmissions will be updated to reflect development for the final vehicle evaluation.

2.6.3.3 Test. The Contractor will test and develop complete CVT transmissions on a dynamometer and in vehicles and run such supporting components tests as are deemed necessary. The goal of this development will be to demonstrate that the R&D transmission provides adequate life, good response and smoothness, and good efficiency at a reasonable manufacturing cost.

2.7 POWERTRAIN CONTROL

2.7.1 Engine Control (Sensors, FMV, Actuators, Dev. ECU).

2.7.1.1 Design. The control requirements for the projected engine operation will be defined. A microprocessor-based ECU and associated software will be designed. Sensors, actuators and fuel metering valve will be designed and

interfaced with the control unit. Hardware and software will be revised as determined by test results.

2.7.1.2 Fabrication. Hardware will be fabricated or procured from vendors for testing and evaluation. This hardware will be modified based on test results

2.7.1.3 Test. Component hardware will be bench tested prior to engine operation. The control system will be tested on the engine for starting, steady state, and transient operation. Performance, response, stability and integrity will be evaluated.

2.7.2 Integrated System (Vehicle, Transmission, Flywheel, Engine).

2.7.2.1 Design. The control requirements for the engine, flywheel, and transmission will be determined. The microprocessor control unit and software will be designed. Special vehicle requirements such as wiring harness and instrumentation will be designed. Modifications will be made during system integration testing.

2.7.2.2 Fabrication. Transmission and flywheel control hardware will be fabricated. The ECU and associated software will be fabricated. Modifications will be made to hardware and software as determined during system testing.

2.7.2.3 Test. Control logic for the flywheel and transmission will be integrated and tested on this assembly. The integrated system will then be tested and evaluated on complete powertrains as installed on test stands and in vehicles.

2.8 MATERIALS

2.8.1 Ceramic Characterization and Generic Machining. Working with selected suppliers, the Contractor shall engage in the development and characterization of high temperature ceramics for the engine by defining operating conditions, creating preliminary layouts of suggested design concepts, and analyzing

temperature gradients and stresses at steady-state and transient conditions, including start, acceleration, deceleration, and shutdown. Iterative design work will be based on the results of fabrication studies and testing of samples.

Working with material suppliers, the Contractor will develop fabrication processes necessary for the attainment of the AGT engine goals. Evaluation and analysis of the properties of the various ceramic materials used in the AGT engine will be conducted. In addition, machined test specimens and sample parts will be tested as necessary to determine the effects of candidate machining processes on the materials and select the optimum process for a given application. Evaluation will include flaw characterization and failure analysis when appropriate.

2.8.2 Shaft Attachment. The Contractor will develop design concepts based on functional requirements for ceramic turbine rotor/metal shaft attachment. The preferred design will be incorporated into basic engine layouts and detail designs. The Contractor will fabricate test samples representing ceramic rotor/metal shaft joints. Torsion, bending, thermal shock, and spin testing of samples will be used in the development and qualification of preferred designs.

2.8.3 Ceramic Interfacing. Working with material suppliers, the Contractor will design or coordinate the design of various types of ceramic-to-ceramic joints. Conceptual designs will be generated and applied to the actual construction of the AGT engine. Structural and aerothermodynamic analyses will be conducted on the various joint designs and the information will be used to guide layouts and detail drawings. Redesigns will be based on results of bench, rig, and engine testing.

Non-seize ceramic/ceramic and ceramic/metal interfacing systems will be identified and/or developed and these systems will be incorporated as needed in the design and construction of the AGT. The most promising joint designs

will be duplicated in sample hardware pieces for testing; actual engine parts using the developed joints will also be procured. Techniques for fabrication of non-seize surfaces will be developed as necessary, and complete interfacing will be provided for laboratory, rig, and engine testing. Testing of the candidate interface constructions will be conducted using basic bench tests or rig tests, as applicable. Successful designs will progress to full engine testing. Data obtained from the testing will be fed back into the design function.

2.8.4 Insulation (Flowpath, Non-flowpath, Emissivity-Control Coatings). The Contractor will identify requirements and develop design concepts for insulation in the basic engine, select and/or develop appropriate materials and coatings, and analyze temperature effects and heat loss. Selected concepts will be incorporated into the basic engine layouts and detail design. Insulation will be fabricated for both flowpath and non-flowpath applications, and will be installed as necessary in test rigs and engine assemblies. Fabrication of flow path insulation will include application of abrasion-resistant coatings as required. Components of high emissivity will be coated where appropriate with low-emissivity coatings developed for that purpose. Insulation and coating candidates will be characterized and evaluated in laboratory tests, including tests for heat transfer and abrasion resistance. The preferred materials will be tested further for performance in both rigs and engine assemblies.

3.0 EXPERIMENTAL POWERTRAIN DEVELOPMENT AND EVALUATION

3.1 PRELIMINARY DESIGN

3.1.1 Powertrain System. Preliminary iterative layouts will be made of the planned engine, reduction gear, transmission, final drive, intake and exhaust systems, response assist flywheel, and auxiliaries to assist the logical integration of elements into a package meeting the requirements for satisfactory operation and accessibility.

3.1.2 Engine System. Preliminary design layouts will be made of the basic engine, based on the single-stage centrifugal compressor, single-stage radial turbine, LPP combustor, and ceramic regenerators, with an engine housing and staged helical reduction gear for power output and accessory and auxiliary drive. These layouts will be based on the component designs revised as indicated by the component development programs and follow the requirements and constraints of Task 1.3 of this proposal. Metal components will be considered as substitutes for ceramic components as required to support the engine test and development schedule.

The Contractor will conduct thermal, structural, and dynamics analyses for the basic engine design to demonstrate design adequacy.

3.1.3 Preliminary Design Review. Basic engine and powertrain system performance objectives will be defined, and drawings, material selections, critical fabrication techniques, analytical results, and preliminary component development results will be provided with supportive information to assist in a meaningful Preliminary Design Review.

3.2 DETAIL DESIGN

3.2.1 Powertrain System. The Contractor will prepare detail drawings of parts and assemblies, along with appropriate specifications and procedures to integrate the various components (basic engine, response assist flywheel, reduction gear, transmission, and final drive) with necessary auxiliaries such as intake and exhaust systems, actuators, brackets, mounts, couplings, plumbing, and wiring. Structural, thermal, and aerodynamic analyses will be applied as required. Iterative design revisions will be conducted, as required, throughout the development period.

3.2.2 Engine System. Detail part and assembly drawings will be prepared, along with specifications and procedures to complete the basic engine package. Appropriate structural, aerodynamic, and thermal analyses will be conducted to

insure adequacy of each part and subassembly. Iterative revisions will be conducted throughout the development period, as required.

3.3 FABRICATION

3.3.1 Powertrain System. Powertrain components, subsystems, and parts will be fabricated/procured for incorporation into the basic engine for powertrain testing. Design changes, modifications, and updates will be incorporated to support an orderly development program and satisfy Milestones 4 (Interim Project Assessment) and 6 (EPA Vehicle Tests). The Contractor will specify a common powertrain/engine nomenclature which will carry over into vehicle application.

A sufficient number of spare parts, components, and subsystems will be stocked to support the program needs.

The Contractor will generate a common parts list for the AGT, and maintain it current throughout the program.

3.3.2 Engine System. The basic engine hardware will be fabricated and/or procured in accordance with the engine hardware plan. This will define quantity and schedule requirements by part number, and will provide for variant designs and modifications based on results of the component and engine development programs. Sufficient spare hardware will be ordered to support the engine development program.

3.4 POWERTRAIN DYNAMOMETER TEST AND EVALUATION

3.4.1 Powertrain System. Two test cells will be made available for powertrain development. The Contractor will submit a test plan to the NASA Project Manager for approval prior to initiation of testing.

Development tests shall include, but not be limited to, the following: steady-state and transient performance; transmission efficiency and shift control; regenerator system performance; LPP combustor evaluation; multifuel capabilities; emissions; control interaction, response, stability, and reliability;

noise; and hot and cold starting. Formal durability tests accumulating 500 hours on one powertrain will be run.

The powertrain will be constantly updated with components of improved performance and durability. The powertrain will be fully characterized as a total system supported by component data as required to meet Milestone 5 (Final Dynamometer Characterization and Assessment).

3.4.2 Engine System. The Contractor will assemble, check run, and perform development tests on the basic engine assemblies.

These tests shall include, but not be limited to, performance evaluation, subsystem development, operational and mechanical evaluation, control system development, emissions and alternate fuel evaluation, heat rejection, noise measurement, safety assessment, and durability testing.

The Contractor will disassemble the basic engine assemblies after test for evaluation of part condition and the determination of failures or impending failures. An individual failure report will be prepared for each functional failure. Parts and subassemblies will be modified based on component and engine development test results, and retested for verification of the corrective modification.

3.4.3 Non-Regenerative Engine. The Contractor will design a non-regenerative engine test rig to be used for characterizing the combined compressor and turbine stages without the use of the regenerators. Data on such tests shall be analyzed and the results presented.

The non-regenerative test rig shall be fabricated from engine parts wherever possible. A laboratory combustor will be procured which will provide the desired heat rise between the compressor discharge temperature and the turbine inlet temperature.

The Contractor will perform tests on the non-regenerative test rig, using engine parts and variants thereof, for the primary purpose of early

identification of problem areas in engine parts performance or durability. Parts shall be tested over the range of engine operating conditions.

4.0 INTERIM PROJECT ASSESSMENT

An objective assessment of progress made toward achieving the project goal and objectives will be prepared and included as part of the Reference Powertrain Design Topical Report. Specifically, this will include a detailed assessment of component tests, engine tests, drivetrain and transmission tests, control system development, and steady-state tests of the AGT powertrain. It will also include a report of progress being made on development of critical technology components, and a resulting updated projection of the RPD's performance potential. Both steady-state test data and proper analytical modeling of the powertrain under transient vehicle operation will be used in projecting RPD performance.

Additionally, an updated plan-to-completion for the RPD development program and a report on the RPD's marketability outlook will be made and included in the report as part of this assessment.

5.0 AGT POWERTRAIN SYSTEM/VEHICLE INTEGRATION, DEVELOPMENT, AND EVALUATION

5.1 PRELIMINARY POWERTRAIN SYSTEM/VEHICLE INTEGRATION

The Contractor will make layouts of the vehicle assembly with the complete powertrain system and all accessories to insure adequate space, proper function, and accessibility. Structural modifications will be kept to a minimum. Prior to initiating detail design, a formal preliminary design review of the powertrain system/vehicle integration will be presented to the NASA Project Manager.

5.2 DETAIL DESIGN

Detailed drawings and/or specifications will be prepared for all parts, assemblies, or modifications necessary to complete the conversion of a standard production vehicle to the RPD powertrain system. Normal engineering

practice will be utilized regarding loads, clearances, temperatures, noise control, etc. for anticipated vehicle static and dynamic conditions. Design revisions will be made throughout the program as needed to resolve problems or otherwise improve the vehicle package.

5.3 VEHICLE BUILDUP AND DEVELOPMENT

5.3.1 Vehicle Buildup. The Contractor will procure, modify, and assemble two 1984 and two 1985 front-wheel-drive vehicles (Chrysler K-Car). These vehicles will incorporate power steering, power brakes, and air conditioning. Production vehicle accessories and subassemblies will be used exclusively except where the uniqueness of the powertrain system dictates otherwise. A vehicle designation and/or identification system will be established which clearly identifies the vehicles.

5.3.2 Support Testing. The Contractor's various engineering departments will supply expertise during the vehicle development and contractors tests. Comparison tests, where required, between the Baseline (S.I.) and AGT will be conducted simultaneously to minimize ambient environmental effects.

5.3.3 Development Tests. The Contractor will conduct various tests to gauge the development progress and potential of the AGT vehicle. Tests will include, but not be limited to, the following: driveability, performance, fuel economy, noise, braking, emissions, hot and cold tests, and limited durability on alternate fuels. The performance model will be constantly updated with new data for use in predicting RPD performance.

5.4 VEHICLE TEST AND EVALUATION

5.4.1 Contractor. A vehicle test plan will be submitted to the NASA Project Manager thirty days prior to initiation of tests. These tests will be the final characterization of the AGT vehicle and a data base for subsequent EPA tests. These tests will include, but not be limited to, the following: power,

fuel economy, emissions, cold and hot starting, alternate fuel capability, and performance (0-60 MPH time, distance traveled during each second).

5.4.2 EPA. The Contractor will provide technical support and assistance to EPA during their tests and will have cognizant personnel on site when the vehicles are tested.

6.0 SUPPORTIVE MANUFACTURING, COST, AND MARKETABILITY STUDIES

The Contractor will conduct a continuing series of manufacturing feasibility, cost analysis, and marketability studies to support the development program. These studies shall begin with the Initial RPD and shall be prepared and maintained current as the RPD is updated. These study results, supporting information, and analyses for the pertinent RPD and preliminary engine design shall be included with the design review presentations.

6.1 MANUFACTURING FEASIBILITY

Manufacturing feasibility studies for each RPD shall be carried out to assess various mass production manufacturing and/or processing approaches that could be used for the production of all critical system components and of the complete system. These studies will be closely coordinated with, and provide major input to, the system design activities for each system, but especially for each Updated RPD.

6.1.1 Producibility Analyses. Producibility analyses shall be conducted with design studies, layouts, and detailed drawings of suggested design changes or concepts. This will include consideration of a stationary ceramic recuperator as a cost-effective replacement for the rotating ceramic regenerator. Design analyses shall be performed on parts and assemblies as required to guide the detail design and insure that the proposed design is functionally adequate.

6.1.2 Producibility Tests. Producibility studies shall include limited hardware fabrication, such as recuperator matrix samples, when it is required to

develop and/or demonstrate new manufacturing and/or processing approaches that are required for a key design feature.

6.2 COST ANALYSES

6.2.1 Production Costs. The Contractor will perform cost analyses on the initial RPD and on each major update of the RPD. Costs will be based on 500,000, 1,000,000, and 2,000,000 units per year, and will include realistic assessments of the cost of manufacture, including tooling, relative to the equivalent Baseline vehicle. For the initial cost analysis, manufacturing costs will be assessed primarily on the basis of material costs and a first order estimate of fabrication costs until adequate manufacturing information can be generated.

6.2.2 Life-Cycle Costs. Total life-cycle costs for the initial and updated RPD will be estimated and compared to the Baseline vehicle, including manufacturing costs, tooling, maintenance, and operation.

6.3 MARKETABILITY STUDIES

The potential marketability of the RPD system will be assessed utilizing the cost and manufacturing feasibility study results, along with projections of fuel economy, emissions, performance, noise, driveability, and startup characteristics, and maintenance and service requirements. A marketability study will be conducted as part of the Interim Project Assessment and again at the end of the program to verify the most desirable vehicle class and engine power level for introducing the AGT powertrain system into the market.

7.0 PROJECT MANAGEMENT

7.1 PROJECT PLANNING

7.1.1 Experimental Powertrain System Development Plan. The Contractor will establish a Work Breakdown Structure (WBS) based on the eight contract tasks. Within 90 days of the contract award, a detailed plan covering all phases of

the AGT Powertrain System Development Project will be submitted to the NASA Project Manager.

The plan will include the detailed design and test activity, division of work between the Contractor and its subcontractors, technical approach to be pursued, hardware to be fabricated, test efforts planned, and definition of test rigs and instrumentation.

Once each year, recommendations for revisions to the initial plan shall be made to the NASA Project Manager.

7.1.2 Prototype Powertrain System Development Plan. The Contractor will prepare and submit ten copies of a proposed Prototype Powertrain System Development Plan covering the period from May 1985 to the start of production engineering. It will be submitted to the NASA Project Manager by July 31, 1984.

The Prototype Powertrain System Development Plan will incorporate results of the previous development effort, and will be designed for proper life, operating conditions, weight, in-service maintenance requirements, and vehicle-imposed loads and constraints. The plan will also include the efforts of Task 6, including producibility, manufacturing, and cost information.

7.2 PROJECT DIRECTION

The Contractor's technical, administrative, financial, and contractual staffs will continuously assess project technical accomplishment and project funding, compare them to the planned program parameters, and establish a system of program management based on the agreed-upon WBS.

7.3 GOVERNMENT/INDUSTRY TECHNICAL MEETINGS

7.3.1 Monthly Planning and Coordination. The Contractor will plan and coordinate monthly meetings with NASA Project and DOE Program personnel.

7.3.2 Project Reviews. The Contractor will schedule and conduct project reviews, as specified in the Statement of Work, at least once a year. Ten days

prior to the review meeting, the NASA Project Manager will be notified as to the date, location and material to be presented.

7.3.3 Technical Meetings. The Contractor will participate in the Government-sponsored coordination meetings generally held at six month intervals. Participation shall include presentation of technical papers, and exhibits such as mock-ups, displays, and actual hardware.

The Contractor will also participate in meetings sponsored by the major technical societies where the project technical data will contribute to the industry's knowledge of applying advanced technologies to gas turbine engines.

8.0 REPORTING

8.1 MONTHLY AND QUARTERLY TECHNICAL AND FINANCIAL REPORTS

The Contractor will submit a Monthly Technical Progress Narrative (a maximum of 25 copies) and a Contractor Financial Management Performance Analysis Report (NASA Form 533P, a maximum of six copies) within ten working days after the closing date of the accounting month. The Contractor will also submit a Quarterly Contractor Financial Management Report (a maximum of six copies, NASA Form 533Q) no later than the fifteenth calendar day of the months of March, June, September and December.

8.2 RPD DESIGN INFORMATION AND TECHNICAL DATA

The Contractor will submit copies of analytical and design data, a micro-filmed set of all modified engine and component drawings, including layouts of any modifications required in the engine/vehicle installation, and modifications to the parts and material lists for each Reference Powertrain Design modification. Drawings shall be prepared according to the Schedule Article entitled "Conceptual and Developmental Design Drawings (level 1)". Also to be submitted are component and engine test data relative to each major modification, including performance maps, power levels, temperature schedules, control schedules, and emission and noise summaries if applicable.

8.3 SEMI-ANNUAL TECHNICAL SUMMARY REPORTS

The Contractor will prepare, publish, and distribute 150 copies of semi-annual technical summary reports. Each report shall include a section with information characterizing and modeling the current RPD. Eight such reports will be published and cover work accomplished from January 1 to June 30 and July 1 to December 31.

Four copies of the proposed semi-annual report will be submitted to the NASA Project Manager for approval, with publication targeted for August 30 and February 28. The reports will be distributed in accordance with a list furnished by the NASA Project Manager prior to publication of the first report.

8.4 TOPICAL REPORTS

8.4.1 Component and Subsystem Technology Reports. The Contractor shall submit to the NASA Project Manager for review and concurrence, 30 days after completion of each major component and/or subsystem test evaluation, a draft topical report. 150 copies of each of the approved topical reports will be distributed in accordance with a list provided by the NASA Project Manager. Ten such reports are planned, as listed in the Development Plan.

8.4.2 Reference Powertrain Design (RPD) Report. The Contractor shall prepare and submit in March 1984 an RPD Topical Report based on the results of the experimental powertrain tests completed before March 1984.

8.4.3 EPA Test Report. The Contractor will prepare a Topical Report of the results of the vehicle system EPA tests, and submit a review draft to the NASA Project Manager by August 1985.

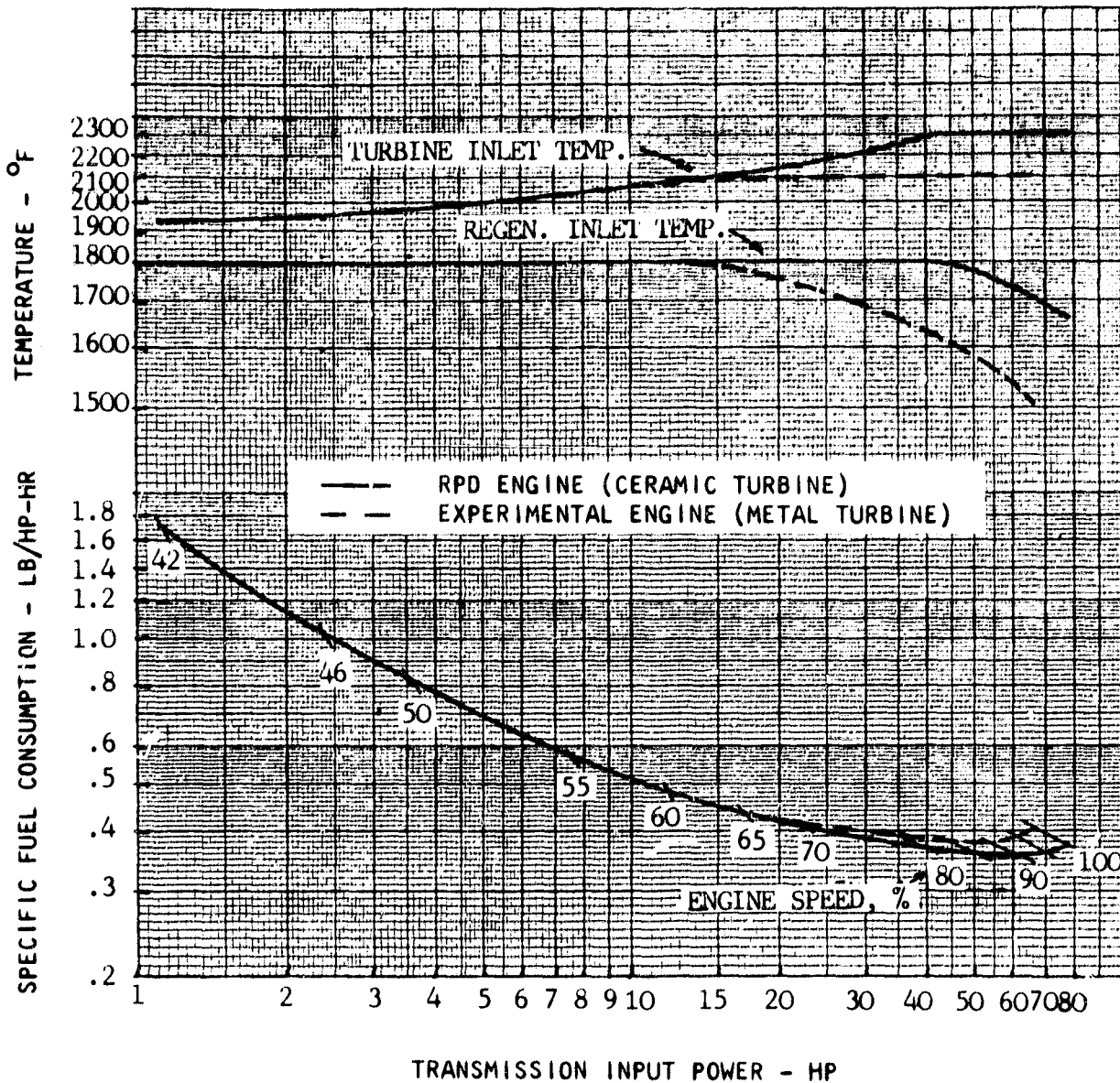
8.5 FINAL REPORT

The Contractor shall submit for review four copies of the proposed final report to the NASA Project Manager within 30 days following completion of the technical effort specified by the contract. The final report will be in accordance with the Reports of Work, paragraphs C through F, of the RFP.

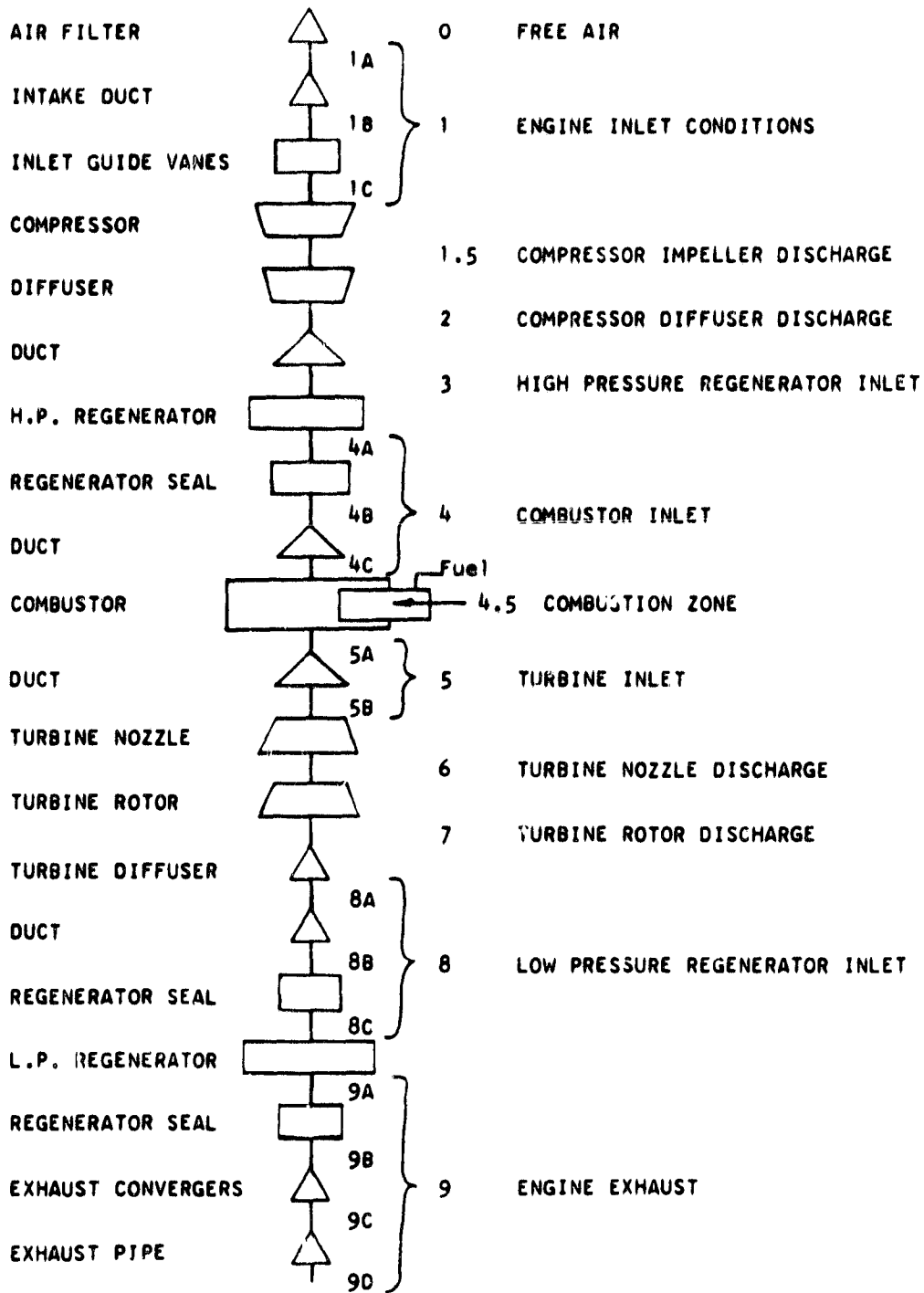
Within 30 calendar days after notification of approval of the proposed final report, the Contractor will distribute a maximum of 150 copies of the approved final report and shall furnish one set of glossy continuous tone prints of photographs included in the final report.

APPENDIX B

AGT-102 ENGINE PERFORMANCE CHARACTERISTICS



AGT-102 Station Notation



AGT-102 Basic Engine Characterization
 RPD (2300°F, Ceramic Turbine)

100% Through 50% Speed Points

TEMPERATURE (RANKINE)	545.0	545.0	545.0	545.0	545.0	545.0	545.0	545.0	545.0	545.0	545.0	545.0	545.0
STATION#0	545.0	545.0	545.0	545.0	545.0	545.0	545.0	545.0	545.0	545.0	545.0	545.0	545.0
STATION#1B	550.6	550.2	549.9	549.7	549.4	548.8	548.4	548.4	548.4	548.1	547.8	547.8	547.8
STATION#2	897.0	864.7	834.0	807.3	778.0	725.4	705.2	683.7	660.5	635.3	635.3	635.3	635.3
STATION#3	888.2	856.7	826.8	800.8	772.4	721.6	702.2	681.7	658.8	636.5	636.5	636.5	636.5
STATION#4A	1995.0	2031.3	2074.0	2122.9	2155.5	2169.2	2175.0	2180.5	2188.2	2197.0	2197.0	2197.0	2197.0
STATION#4B	1995.0	2031.3	2074.0	2122.9	2155.5	2169.2	2175.0	2180.5	2188.2	2197.0	2197.0	2197.0	2197.0
STATION#4C	2031.3	2065.6	2106.0	2152.1	2187.5	2190.3	2190.3	2192.9	2198.2	2201.6	2201.6	2201.6	2201.6
STATION#5A	2813.1	2811.9	2811.0	2805.8	2780.3	2667.9	2622.7	2574.0	2525.1	2470.8	2470.8	2470.8	2470.8
STATION#5B	2760.1	2759.8	2759.9	2760.1	2732.6	2625.1	2581.8	2535.2	2487.3	2435.6	2435.6	2435.6	2435.6
STATION#7	2126.5	2125.9	2126.3	2126.3	2108.7	2009.9	1971.5	1927.3	1878.3	1825.2	1825.2	1825.2	1825.2
STATION#8A	2127.8	2126.8	2126.9	2126.3	2108.7	2009.9	1971.5	1927.3	1878.3	1825.2	1825.2	1825.2	1825.2
STATION#8B	2126.6	2123.2	2121.0	2123.2	2108.7	2009.9	1971.5	1927.3	1878.3	1825.2	1825.2	1825.2	1825.2
STATION#9B	1655.1	1652.6	1620.1	1620.1	1620.1	1620.1	1620.1	1620.1	1620.1	1620.1	1620.1	1620.1	1620.1
STATION#9D	1082.2	1049.6	1017.3	987.4	951.5	881.8	855.2	825.7	793.7	758.5	758.5	758.5	758.5
FLOW (LB/SEC)													
STATION#0	0.6179	0.5642	0.5092	0.4553	0.4020	0.3172	0.2854	0.2518	0.2154	0.1749	0.1749	0.1749	0.1749
STATION#1B	0.6179	0.5642	0.5092	0.4553	0.4020	0.3172	0.2854	0.2518	0.2154	0.1749	0.1749	0.1749	0.1749
STATION#2	0.6179	0.5642	0.5092	0.4553	0.4020	0.3172	0.2854	0.2518	0.2154	0.1749	0.1749	0.1749	0.1749
STATION#3	0.5988	0.5468	0.4938	0.4418	0.3904	0.3081	0.2774	0.2450	0.2097	0.1703	0.1703	0.1703	0.1703
STATION#4A	0.5988	0.5468	0.4938	0.4418	0.3904	0.3081	0.2774	0.2450	0.2097	0.1703	0.1703	0.1703	0.1703
STATION#4B	0.5988	0.5468	0.4938	0.4418	0.3904	0.3081	0.2774	0.2450	0.2097	0.1703	0.1703	0.1703	0.1703
STATION#4C	0.5988	0.5468	0.4938	0.4418	0.3904	0.3081	0.2774	0.2450	0.2097	0.1703	0.1703	0.1703	0.1703
STATION#5A	0.6068	0.5542	0.5003	0.4475	0.3953	0.3117	0.2806	0.2476	0.2118	0.1720	0.1720	0.1720	0.1720
STATION#7	0.6106	0.5575	0.5034	0.4503	0.3977	0.3136	0.2824	0.2491	0.2131	0.1731	0.1731	0.1731	0.1731
STATION#8A	0.6106	0.5575	0.5034	0.4503	0.3977	0.3136	0.2824	0.2491	0.2131	0.1731	0.1731	0.1731	0.1731
STATION#8B	0.6161	0.5625	0.5077	0.4540	0.4009	0.3159	0.2844	0.2508	0.2145	0.1742	0.1742	0.1742	0.1742
STATION#9B	0.6260	0.5713	0.5153	0.4603	0.4061	0.3196	0.2875	0.2534	0.2166	0.1757	0.1757	0.1757	0.1757
FLOW FUNCTION													
STATION#1B	1.0142	0.9242	0.8327	0.7433	0.6554	0.5157	0.4641	0.4092	0.3490	0.2839	0.2839	0.2839	0.2839
STATION#2	0.3089	0.3027	0.2963	0.2893	0.2816	0.2658	0.2572	0.2452	0.2284	0.2036	0.2036	0.2036	0.2036
STATION#4A	0.452	0.4513	0.4549	0.4570	0.4570	0.4485	0.4406	0.4275	0.4057	0.3694	0.3694	0.3694	0.3694
STATION#5B	0.5571	0.5612	0.5591	0.5553	0.5480	0.5241	0.5092	0.4873	0.4553	0.4069	0.4069	0.4069	0.4069
STATION#7	1.7852	1.6597	1.5288	1.3920	1.2482	0.9990	0.9041	0.8071	0.6895	0.5630	0.5630	0.5630	0.5630
STATION#8B	1.8632	1.7234	1.5773	1.4310	1.2773	1.0149	0.9163	0.8106	0.6955	0.5665	0.5665	0.5665	0.5665
STATION#9B	1.3920	1.2541	1.1163	0.9847	0.8545	0.6491	0.5757	0.4902	0.4187	0.3323	0.3323	0.3323	0.3323
STATION#9D	1.4266	1.2822	1.1388	1.0021	0.8678	0.6574	0.5824	0.5045	0.4220	0.3353	0.3353	0.3353	0.3353
LEAKAGE FLOWS (LB/SEC)													
STATION#2-4B	0.0031	0.0030	0.0028	0.0026	0.0024	0.0022	0.0021	0.0019	0.0017	0.0015	0.0015	0.0015	0.0015
STATION#2-5B	0.0025	0.0023	0.0020	0.0018	0.0016	0.0013	0.0011	0.0010	0.0009	0.0007	0.0007	0.0007	0.0007
STATION#3-8B	0.0099	0.0087	0.0075	0.0063	0.0052	0.0037	0.0031	0.0026	0.0021	0.0016	0.0016	0.0016	0.0016
STATION#4B-5B	0.0037	0.0034	0.0031	0.0027	0.0023	0.0017	0.0016	0.0014	0.0011	0.0009	0.0009	0.0009	0.0009
STATION#4B-5B	0.0012	0.0011	0.0010	0.0009	0.0008	0.0007	0.0006	0.0006	0.0005	0.0004	0.0004	0.0004	0.0004
STATION#4B-8B	0.0019	0.0016	0.0013	0.0010	0.0008	0.0005	0.0004	0.0003	0.0002	0.0002	0.0002	0.0002	0.0002
HEAT LEAKS (BTU/HR)													
STATION#GEAR BCR-1B	554.6	516.8	477.0	436.9	396.3	328.9	302.9	274.4	242.6	205.8	205.8	205.8	205.8
STATION#2-0	3092.6	2884.3	2305.3	1978.2	1651.4	1135.0	956.5	777.0	599.0	422.0	422.0	422.0	422.0
STATION#5A-4C	24911.6	22061.4	19146.2	16276.8	13356.6	8759.4	7214.3	5705.1	4270.4	2914.6	2914.6	2914.6	2914.6
STATION#4.5-0	2391.1	2413.1	2439.2	2469.1	2470.4	2405.1	2378.6	2350.2	2321.9	2291.5	2291.5	2291.5	2291.5
STATION#8A-0	1264.5	1311.6	1342.9	1378.5	1408.0	1431.0	1402.3	1402.3	1402.3	1402.3	1402.3	1402.3	1402.3
STATION#5A-0	1113.0	1123.2	1135.4	1149.3	1149.3	1119.5	1107.2	1094.8	1080.8	1065.7	1065.7	1065.7	1065.7
STATION#5A-9A	2108.1	1871.3	1629.3	1385.5	1129.9	707.0	558.6	415.3	280.6	159.4	159.4	159.4	159.4
STATION#5A-2	732.0	756.0	786.9	805.3	821.0	821.1	820.9	820.7	821.3	822.4	822.4	822.4	822.4
STATION#2-1B	2418.0	2041.0	1698.6	1408.3	1131.4	722.3	589.1	460.5	337.5	222.4	222.4	222.4	222.4

AGT-102 Basic Engine Characterization
 RPD (2300°F, Ceramic Turbine)
 Various Idle Speed Points

TEMPERATURE (RANKINE)	545.0	545.0	545.0	545.0	545.0
STATION 0	547.8	547.7	547.6	547.6	547.6
STATION 1B	635.3	624.7	611.9	611.9	611.9
STATION 2	636.5	626.8	615.4	615.4	615.4
STATION 3	2196.4	2200.5	2205.2	2205.2	2205.2
STATION 4A	2200.9	2203.5	2206.4	2206.4	2206.4
STATION 4C	2470.1	2448.4	2423.2	2423.2	2423.2
STATION 5A	2278.6	2278.4	2278.5	2278.5	2278.5
STATION 7	2267.5	2268.3	2269.0	2269.0	2269.0
STATION 8A	2259.6	2260.4	2261.0	2261.0	2261.0
STATION 8B	758.5	746.8	727.3	727.3	727.3
STATION 9B	758.4	743.8	726.3	726.3	726.3

PLCW (LB./SEC)	0.1749	0.1581	0.1385	0.1385	0.1385
STATION 0	0.1749	0.1581	0.1385	0.1385	0.1385
STATION 1B	0.1749	0.1581	0.1385	0.1385	0.1385
STATION 2	0.1703	0.1539	0.1348	0.1348	0.1348
STATION 3	0.1703	0.1539	0.1348	0.1348	0.1348
STATION 4A	0.1703	0.1539	0.1348	0.1348	0.1348
STATION 4C	0.1712	0.1547	0.1355	0.1355	0.1355
STATION 5A	0.1720	0.1554	0.1360	0.1360	0.1360
STATION 7	0.1731	0.1564	0.1369	0.1369	0.1369
STATION 8A	0.1731	0.1564	0.1369	0.1369	0.1369
STATION 8B	0.1742	0.1574	0.1378	0.1378	0.1378
STATION 9B	0.1757	0.1588	0.1390	0.1390	0.1390

FLW FUNCTION	0.2539	0.2565	0.2246	0.2246	0.2246
STATION 1B	0.2539	0.2565	0.2246	0.2246	0.2246
STATION 2	0.2539	0.2565	0.2246	0.2246	0.2246
STATION 4A	0.3694	0.3502	0.3252	0.3252	0.3252
STATION 5B	0.4069	0.3824	0.3514	0.3514	0.3514
STATION 7	0.5629	0.5097	0.4475	0.4475	0.4475
STATION 8A	0.5665	0.5125	0.4495	0.4495	0.4495
STATION 9B	0.3324	0.2974	0.2573	0.2573	0.2573
STATION 9D	0.3353	0.3066	0.2596	0.2596	0.2596

LEAKAGE FLOWS (LB./SEC)	0.0015	0.0013	0.0011	0.0011	0.0011
STATION 2-4B	0.0015	0.0013	0.0011	0.0011	0.0011
STATION 2-5B	0.0007	0.0006	0.0006	0.0006	0.0006
STATION 3-9B	0.0016	0.0014	0.0012	0.0012	0.0012
STATION 3-8B	0.0009	0.0008	0.0007	0.0007	0.0007
STATION 4B-5B	0.0004	0.0004	0.0003	0.0003	0.0003
STATION 4B-8B	0.0002	0.0001	0.0001	0.0001	0.0001

HEAT LEAKS (BTU/HR)	205.8	189.9	171.0	171.0	171.0
STATION 6EAR BCX-1B	205.8	189.9	171.0	171.0	171.0
STATION 2-0	242.0	236.3	228.3	228.3	228.3
STATION 5A-4C	2414.2	2415.1	1804.3	1804.3	1804.3
STATION 4-5-0	2290.6	2278.6	2264.4	2264.4	2264.4
STATION 6A-0	1404.7	1408.3	1407.9	1407.9	1407.9
STATION 5A-0	1066.2	1069.7	1054.0	1054.0	1054.0
STATION 5A-8A	155.3	108.4	59.3	59.3	59.3
STATION 5A-2	821.8	821.8	823.3	823.3	823.3
STATION 2-1B	222.4	180.6	135.8	135.8	135.8

AMBIENT TEMPERATURE (RANKINE)	545.0	545.0	545.0	545.0	545.0
AMBIENT PRESSURE (PSIA)	14.434	14.434	14.434	14.434	14.434
GASIFIER SHAFT SPEED (MPH)	49750.	46000.	41675.	41675.	41675.
FRACTION OF DESIGN SPEED	0.5000	0.4623	0.4188	0.4188	0.4188
POWER AT PINION (HP)	6.07	4.64	3.09	3.09	3.09
POWER TO REDUCTION GEARS (MPT)	3.17	3.86	2.42	2.42	2.42
POWER TO TRANSMISSION (MP)	3.55	2.36	1.11	1.11	1.11
GROSS POWER (HP)	11.24	8.69	6.10	6.10	6.10
FUEL FLOW (LB/HR)	2.8997	2.4013	1.8839	1.8839	1.8839
SFC AT PINION (LB/HP-HR)	0.5606	0.6225	0.7776	0.7776	0.7776
SFC AT TRANSMISSION	0.8170	1.0163	1.6986	1.6986	1.6986
FUEL-AIR RATIO	0.00471	0.00431	0.00386	0.00386	0.00386
COMPONENT EFFICIENCY					
COMPRESSOR 1B-2	0.7705	0.7678	0.7653	0.7653	0.7653
TURBINE 5B-7	0.7998	0.7783	0.7481	0.7481	0.7481
BURNER 5C-5A	0.9982	0.9982	0.9982	0.9982	0.9982

REGENERATOR					
EFFECTIVENESS	0.9581	0.9605	0.9635	0.9635	0.9635
NTU	31.3355	34.5910	39.3766	39.3766	39.3766
CMIN/CMAX	0.9710	0.9719	0.9730	0.9730	0.9730
CR/CHIN	6.6211	6.7766	7.0123	7.0123	7.0123
FRACTION OF DELTA T FROM COMP. DISCHARGE TO CUMB EXIT	0.8674	0.8808	0.8967	0.8967	0.8967
COMPRESSOR SURGE MARGIN	21.072	20.391	19.276	19.276	19.276

PRESSURE RATIO					
STATION 1B/0	0.9992	0.9994	0.9995	0.9995	0.9995
STATION 2/1B	1.5016	1.4321	1.3521	1.3521	1.3521
STATION 4B/2	0.9976	0.9979	0.9982	0.9982	0.9982
STATION 5B/4A	0.9716	0.9745	0.9780	0.9780	0.9780
STATION 5B/7	1.4316	1.3725	1.3039	1.3039	1.3039
STATION 8B/7	0.9966	0.9971	0.9978	0.9978	0.9978
STATION 9B/8B	0.9882	0.9894	0.9908	0.9908	0.9908
STATION 9D/9B	0.9994	0.9996	0.9997	0.9997	0.9997

AGT-102 Basic Engine Characterization
 EPD (2100°F, Metal Turbine)
 Various Idle Speed Points

TEMPERATURE (RANKINE)	
STATION 0	545.0
STATION 18	547.6
STATION 2	635.4
STATION 3	636.6
STATION 4A	2197.6
STATION 4B	2197.6
STATION 4C	2202.2
STATION 5A	2419.1
STATION 5B	2436.4
STATION 7	2275.4
STATION 8A	2268.3
STATION 8B	2260.4
STATION 9B	759.3
STATION 9D	758.2

FLOW (LB./SEC)	
STATION 0	0.1734
STATION 18	0.1734
STATION 2	0.1734
STATION 3	0.1688
STATION 4A	0.1688
STATION 4B	0.1692
STATION 4C	0.1705
STATION 5A	0.1718
STATION 5B	0.1716
STATION 7	0.1726
STATION 8A	0.1726
STATION 8B	0.1742

LEAKAGE FLOWS (LB./SEC)	
STATION 2-9B	0.0074
STATION 2-5B	0.0007
STATION 3-9B	0.0016
STATION 3-8B	0.0009
STATION 4B-5B	0.0004
STATION 4B-8B	0.0002

HEAT LEAKS (BTU/HR)	
STATION GEAR BCX-1B	204.3
STATION 2-9	420.8
STATION 5A-4C	2896.5
STATION 4.5-0	2292.4
STATION 8A-0	1405.4
STATION 5A-0	1067.0
STATION 5A-8A	156.2
STATION 2-1B	221.2

AMBIENT TEMPERATURE (RANKINE)	545.0	545.0	545.0
AMBIENT PRESSURE (PSIA)	14.434	14.434	14.434
GASIFIER SHAFT SPEED (RPM)	49750.	46000.	41675.
FRACTION OF DESIGN SPEED	0.5000	0.4623	0.4188
POWER AT PINION (HP)	6.04	4.63	3.08
POWER TO REDUCTION GEARS (HP)	5.15	3.84	2.42
POWER TO TRANSMISSION (HP)	3.53	2.35	1.10
GROSS POWER (HP)	11.19	8.65	6.07
FUEL FLOW (LB/HR)	2.8799	2.3848	1.8725
SFC AT PINION (LB/M/HP-HR)	0.5591	0.6206	0.7747
SFC AT TRANSMISSION	0.8105	1.0158	1.5971
FUEL-AIR RATIO	0.00472	0.00432	0.00387
COMPONENT EFFICIENCY			
COMPRESSOR 1B-2	0.7699	0.7675	0.7648
TURBINE 5B-7	0.8003	0.7786	0.7445
BURNER 4C-5A	0.9982	0.9982	0.9982

REGENERATOR	
EFFECTIVENESS	0.9584
NTU	31.6202
CMIN/CMAX	0.9709
CR/CRMIN	6.6793
FRACTION OF DELTA T FROM COMP. DISCHARGE TO CUMB EXIT	0.8674
COMPRESSOR SURGE MARGIN	20.328

PRESSURE RATIO	
STATION 1B/0	0.9993
STATION 2/1B	1.5021
STATION 4A/2	0.9977
STATION 5B/4A	0.9721
STATION 5B/7	1.4330
STATION 8B/7	0.9966
STATION 9A/8B	0.9883
STATION 9D/9B	0.9995

APPENDIX C

MTI 81TR46

PRELIMINARY DESIGN AND SELECTION OF
BEARING-ROTOR SYSTEM FOR
THE AGT 102 ADVANCED AUTOMOTIVE GAS TURBINE

Prepared for:

Williams Research Corporation
Prepared Under P.O. No. 131235

April 1981

MECHANICAL TECHNOLOGY INCORPORATED
968 Albany-Shaker Road
Latham, New York 12110

TECHNICAL REPORT
PRELIMINARY DESIGN AND SELECTION OF
BEARING-ROTOR SYSTEM FOR
THE AGT 102 ADVANCED AUTOMOTIVE GAS TURBINE

Chester Lee *S. Gray*

Author (s) Chester Lee, Stanley Gray

S. Gray

Approved Stanley Gray

Jeffrey A. Asher

Approved Dr. Jeffrey Asher

Prepared for
Williams Research Corporation

Prepared under
P.O. No. 131235



MECHANICAL TECHNOLOGY INCORPORATED

968 ALBANY - SHAKER ROAD - LATHAM, NEW YORK -- PHONE 785-0922

TABLE OF CONTENTS

<u>SECTION</u>	<u>PAGE</u>
LIST OF FIGURES	C-4
LIST OF TABLES	C-5
LIST OF SYMBOLS	C-6
1. SUMMARY	C-7
2. INTRODUCTION	C-12
3. ROTOR DYNAMICS AND STABILITY EVALUATIONS OF VARIOUS ROTOR SYSTEMS	C-13
3.1 INITIAL DESIGN - WRC LAYOUT L-924	C-13
3.2 TECHNIQUE FOR IMPROVING ROTOR DYNAMIC PERFORMANCE	C-14
3.2.1 ALTERNATE ROTOR CONFIGURATIONS	C-14
3.2.2 OIL FILM BEARING AT COLD PINION END OF ROTOR	C-14
3.2.3 SQUEEZE FILM OR ELASTOMER DAMPER IN THE SYSTEM	C-15
3.2.4 SPLIT ROTOR - FOUR BEARING ARRANGEMENT	C-17
3.3 ROTOR STABILITY	C-18
4. DETERMINATION OF LOAD REGIME	C-37
5. FOIL JOURNAL BEARING ANALYSIS	C-42
6. BALL BEARING ANALYSIS	C-46
7. ROTOR FRICTIONAL POWER LOSSES	C-49
8. CONCLUSIONS WITH RECOMMENDED CONCEPTS AND RELATED DEVELOPMENTAL RISKS	C-51
REFERENCES	C-52

LIST OF FIGURES

	<u>PAGE</u>	
Figure 3.1	WRC L-924 Rotor-Bearing System	C-20
Figure 3.2	Critical Speed Analysis of WRC L-924	C-21
Figure 3.3	Out-of-phase Unbalance Response of L-924 Arrangement	C-22
Figure 3.4	Out-of-phase Unbalance Response of L-924 Arrangement	C-23
Figure 3.5	Rotor-Bearing System with Bearing/Damper for L-924	C-24
Figure 3.6	Oil Film Damper Cartridge - L-924 Arrangement	C-25
Figure 3.7	In-phase Unbalance Response of L-924 + Oil Film Damper at Position 21	C-26
Figure 3.8	Out-of-phase Unbalance Response of L-924 + Oil Film Damper at Position 21	C-27
Figure 3.9	Damping Generated by the Oil Film at Different Radial Clearances	C-28
Figure 3.10	Out-of-phase Unbalance Response at $U_B = 0.005$ oz.in.	C-29
Figure 3.11	Schematic Drawing of a Four-Bearing Design	C-30
Figure 3.12	Critical Speeds of a Four-Bearing Design	C-31
Figure 3.13	In-phase Response of Four-Bearing Rotor	C-32
Figure 3.14	Out-of-phase Response of Four-Bearing Rotor	C-33
Figure 3.15	Effect of Foil Bearing Damping on Rotor Stability	C-34
Figure 4.1	Bearing Loads at $U_B = 0.01$ oz.in. L-924 Rotor	C-38
Figure 4.2	Bearing Loads Due to Unbalance at 0.01 oz.in. Split Shaft - Four-Bearing Rotor	C-39
Figure 5.1	Typical Details of Hydresil Foil Air Bearing	C-44
Figure 5.2	Hydresil Journal Bearing Performance (Uncorrected)	C-45

LIST OF TABLES

	<u>PAGE</u>
Table 3.1 Listing of Modified Bearing-Rotor Concepts Studied	C-35
Table 3.2 Critical Speed Changes Due to Different Effective Stiffness at Cold End	C-36
Table 4.1 Comparison of Maneuvering Loads for the Two Different Designs (Ceramic Turbine)	C-40
Table 4.2 Bearing Load Summary at 100% Full Speed (Ceramic Turbine)	C-41
Table 5.1 Summary of Foil Air Bearing Characteristics	C-43
Table 7.1 Power Loss at 100% Speed (100,000 RPM)	C-50

LIST OF SYMBOLS

R	Radius	in.
L	Length	in.
C	Clearance	in.
ν	Absolute Viscosity	lb-s/in ²
ρ	Density	lb-s ² /in ⁴
U_B	Unbalance	oz.-in.
B	Damping Coefficient	lb-s/in.
K	Stiffness Coefficient	lb./in.

1. SUMMARY

This report details the results of the preliminary work completed for Williams Research Corporation (WRC) on the design and selection of a bearing-rotor system for the AGT 102 advanced automotive gas turbine. The work was done under Purchase Order No. 131235.

Rotor Arrangements

Emphasis in the preliminary design work was on WRC rotor layout L-924 with a single compliant foil air bearing between the turbine and compressor and ball bearings on either side of the helical pinion. During the study more than six variations on the rotor arrangement were considered in order to obtain the optimum configuration and the study included the influence of both a metal and ceramic turbine.

At the conclusion of the study, two rotor configurations had been selected. These were:

- (a) The L-924 three bearing arrangement with the addition of a floating oil film damper near the compressor inlet.
- (b) A split shaft arrangement with four bearings and a static oil film damper on the ball bearing outer race at the compressor inlet.

Conceptual Layouts and Determination of Bearing Loadings

Conceptual layouts were prepared for each configuration in enough detail to enable bearing loadings and rotor dynamic behavior to be predicted.

The vehicle and engine operating requirements were used as inputs to MTI Computer Code CAD 21, Unbalance Response of a Flexible Rotor, and MVLD, Maneuver Load, which can handle six degrees of freedom at each station and the resulting bearing loadings were determined.

Foil Bearings

The analysis of the HydresilTM compliant foil journal air bearing selected for the engine was based on a size of 1.375" dia. x 1.5" long. Designs were made at stiffness levels of 11,000 lbs./in. and 30,000 lbs./in. which would give design flexibility in developing the best rotor dynamic models. MTI Computer Codes JSTAT and HYDRE used in the analysis showed that a comfortable load performance margin would exist and that the size of the bearing could be reduced during detailed design. The selected bearing foil materials are Inconel X-750 or Inconel-718, and CdO+ graphite bonded high temperature coating was recommended for the start-stop contact wear resistance of the foil. Recommendations were made on rotor configurations in the region of the foil bearing which would minimize heat flow along the shaft and axial temperature gradients.

A three pad as opposed to a single pad foil journal bearing was selected because it provides an inherently greater stability margin for a high speed rotor. The design would be optimized to provide the highest possible internal coulomb frictional damping.

Oil Bearings

Within the scope of the completed work, oil film bearings at the cold end of the rotor did not appear to offer an attractive solution. This was because of the journal sizes dictated by the rotor configuration and the need for oil film thrust bearings which together gave unacceptably high frictional power losses.

Rolling Element Bearings

Two basic sizes of ball bearings were studied to suit the various rotor arrangements at the cold end positions. These were 202 (15 mm bore) and 104 (20 mm bore) sizes of either angular contact or split inner race designs. At normal max. speeds, the DN values of these bearings are 1.5×10^6 and 2.0×10^6 (RPM x mm) respectively. The MTI DREB, Dynamics of Rolling Element Bearings, computer code was used to analyze the bearings and to determine fatigue life, contact stresses and power losses. While it was not possible to optimize the designs, the following information was determined:

- (a) Based on the predicted speed-load regime, the 3500 hour life target with the ceramic rotor design should be achievable.
- (b) Adequate axial loading must be applied to the bearings at all times to insure all balls are loaded and ball skidding can be avoided.
- (c) Every effort should be made to minimize the bearing sizes in order to reduce bearing related power losses. The WRC integral inner race rotor concept would be attractive in the developed engine.
- (d) Careful design of the oil supply and drainage system at the bearings, recognizing the close proximity of the gear pinion to some bearings, is essential to minimize oil churning and heating.

Rotor Dynamic Review

The critical speeds for the rotor system were determined using MTI Computer Code CAD 20. While it was possible to position the critical speeds out of the operating range of idle to overspeed, it was found that significant bending occurred particularly in the L-924 arrangement with consequently large forces and amplitudes of the rotor due to unbalance when passing through the lower critical speeds and also in the operating range. This situation made the use of a rotor damper necessary and oil dampers and devices built into air seals to generate coulomb friction were reviewed.

The oil damper mechanism for the L-924 rotor design had to be applied to the rotating shaft. This necessitated, in effect, an additional journal bearing surface.

With the split rotor design, which had less rotor deflection problems and lower amplitudes, the oil damper could be positioned at the compressor end of the main rotor as part of the static mounting for the ball bearing.

It was evident from the analysis that oil film dampers are necessary for the successful operation of the rotor designs and must be functional at all times. Balancing the rotor to the lowest level of unbalance should always be a primary objective.

Sensitivity of Rotor-Bearing System to Subsynchronous Excitations

The stability analysis performed using MTI Computer Code CAD 25 indicated that adequate damping must be available in the system to control possible foil bearing and floating seal related subsynchronous excitations. From prior experience, the excitation is very often the first rigid body critical speed appearing at the operating speed.

As indicated previously a three pad design of foil air bearing was selected because of its greater stability margin and the design would be optimized to have the highest possible internal damping. These features combined with the damping provided by the oil film damper will ensure that no unacceptably high amplitude subsynchronous excitations will occur in the operating range.

Power System Losses

Careful estimates were prepared of the power losses of the various rotor configurations allowing for the effects of the air bearing, ball bearings, air seals and oil film dampers. The results of these estimates are tabulated in the report. It is evident that every effort must be maintained to minimize these losses, particularly at high rotor speeds, by the use of the optimum combination and sizes of these components.

Conclusions and Recommendations

The preliminary design work which has been completed has shown that practical bearing-rotor systems for this high speed gas turbine can be achieved with both metal and ceramic turbine wheels. Two designs are recommended for continued engineering into rotor-simulator evaluation.

These are:

- (a) The basic L-924 three bearing rotor with a floating oil film damper.
- (b) The split rotor, four bearing arrangement with a static oil damper at the outer race of the compressor inlet end ball bearing.

Of the two concepts, the split-rotor arrangement is considered to present the lower developmental risk because of the rigid nature of the rotor and

conventional damper techniques.

2. INTRODUCTION

In accordance with the requirements of Williams Research Corporation (WRC) Purchase Order No. 131235, this report details the analytical work performed by Mechanical Technology Inc. (MTI) on the preliminary design and selection of a bearing-rotor system for the AGT 102, advanced automotive gas turbine. This report covers work completed from September 15, 1980 until the project termination on February 17, 1981. The studies for the single rotor gas turbine design included the analysis of several different rotor configurations, bearing loads, rotor unbalance response, critical speeds, stability of the rotor and system power losses were determined.

Based on the preliminary study, two rotor/bearing systems were selected and recommended for further development.

3. ROTORDYNAMIC AND STABILITY EVALUATIONS OF VARIOUS ROTOR SYSTEMS

3.1 Initial Design WRC Layout L-924

The initial bearing support system L-924 of the AGT engine is a three bearing arrangement, as shown in Figure 3.1, consisting of a foil bearing between the turbine and compressor in combination with two ball bearings at the cold end that straddle the power take-off pinion. Only the outboard ball bearing is active in supporting the main rotor. Based on an assumed effective cold end ball bearing and support stiffness of 100,000 lb./in. and a foil bearing stiffness of 20,000 lb./in., the critical speeds of this L-924 layout were calculated as follows:

<u>Critical Speeds</u>	<u>Ceramic Turbine RPM</u>	<u>Metal Turbine RPM</u>
1	15,841	12,270
2	37,815	36,400
3	147,200	144,000

These can be related to the following engine operating speeds:

Idle	50,000 rpm
Normal Max.	100,000 rpm
Overspeed	120,000 rpm

This study revealed that this rotor, as shown by the mode shapes in Figure 3.2, will traverse one rigid body and one flexible mode before reaching idle speed. While critical speeds are shifted due to different materials used for the turbine, mode shapes of the shaft still remained essentially the same. Furthermore, shaft response and bearing forces were also calculated assuming both turbine and compressor had built-in mass unbalance. The worst case of unbalance was specified to be 0.01 oz.in. in each wheel plane. Calculations were made when both unbalances were in the same direction (in-phase) and 180° apart (out-of-phase). The results at both in-phase and out-of-phase unbalance showed large rotor amplitudes and resultant bearing forces when the rotor traverses the second criti-

cal speed. Figures 3.3 and 3.4 are two typical out-of-phase response plots at different shaft locations.

3.2 Techniques for Improving Rotor Dynamic Performance

To improve the rotor dynamic performance of the rotor, there are several possible different approaches which can be explored to modify the design. These include:

- (1) Change the rotor configuration such as making the shaft more rigid or moving bearing positions so that only one rigid body mode will be traversed.
- (2) Using an oil film bearing at the cold end to make the support stiffer and to provide damping.
- (3) Employing a squeeze film or elastomer damper in the system.

3.2.1 Alternate Rotor Configurations

Six different rotor/bearing arrangements were studied to see if any improvements could be made; their characteristics are listed in Table 3.1. Many of these configurations required major changes and only a few demonstrated some superiority. Within the critical limitation of a maximum shaft O.D. of 0.9 inch at the compressor inlet due to the air flow path requirement, minor changes of the original layout such as changing shaft diameter to increase shaft stiffness, or changing bearing locations, were also studied but no significant improvement was found. One alternate rotor arrangement selected for further study is discussed in Section 3.2.4.

3.2.2 Oil Film Bearing At Cold Pinion End of Rotor

The feasibility of an oil bearing at the cold end was studied. Two major reasons lead to the conclusion that oil bearings could not be recommended in this particular application. First, when the oil journal bearing is mounted at the cold end, a thrust bearing has to be provided to take the axial loading. Overall power loss will make this combination unacceptable.

Second, the large stiffness generated by the oil bearing will alter the natural frequencies of the system. Unless a major change is made in the rotor configuration, this type of bearing is not suitable for this system from a rotor dynamics point of view.

3.2.3 Squeeze Film or Elastomer Damper in the System

The L-924 model was next studied with a damper. Damping can be generated from either oil squeeze film action or by elastomers. A damper can not only reduce the shaft response and amplitude due to unbalance, but also make the system more stable against subsynchronous excitations.

One important factor in this approach is to select a proper location for a damper device. It was first mounted outside the ball bearing outer race, but little improvement was found. This is understandable since the ball bearing at the cold end is very close to a nodal point so that the amplitude there is not large enough to make the damper effective. The mode shape plot shown in Figure 3.2 clearly demonstrated this problem. For this reason, a damper was then placed at a more effective position at Station 21 of the rotor, or 10.8 inches from the turbine nose cone. Since this is not an active bearing location in the system, the damper must be connected to the shaft through either an additional oil-film bearing or possibly a ball bearing. The overall stiffness generated by this damper/bearing combination must be small such that no significant change of critical speed will occur. A schematic drawing of this arrangement is shown in Figure 3.5 and Figure 3.6 shows the damper details. The oil film bearing/oil damper combination was studied with a three-pad bearing being used to transmit the force from shaft to damper. Selected bearing dimensions were:

D = 0.82 in.
L = 0.40 in.
C = 0.0012 in.

and with lubricant properties for the Automatic Transmission Fluid:

$$\nu = 0.5 \times 10^{-6} \text{ lb-s/in.}^2$$

$$\rho = 0.9 \times 10^{-4} \text{ lb-s}^2/\text{in.}^4$$

$$T = 300^\circ \text{ F}$$

Load capacity and power losses were evaluated at different speeds. The following listings give the characteristics of this bearing:

RPM	Load Capacity (Lb.)	
	$\epsilon = 0.4$	$\epsilon = 0.6$
35,000	9.26	26.18
75,000	21.30	59.06
100,000	30.10	81.97

RPM	Power Loss (HP)	
	$\epsilon = 0.4$	$\epsilon = 0.6$
35,000	0.11	0.12
75,000	0.50	0.57
100,000	1.08	1.21

Assuming in the initial analysis 10 lb-s/in. damping and 10,000 lb./in. stiffness values for the oil film damper, shaft response due to unbalance of 0.01 oz.in. was significantly improved as shown in Figures 3.7 and 3.8. The out-of-phase amplitudes, however, is still not low enough to be acceptable. If the amount of damping is doubled, no drastic reduction in amplitudes was found, and as expected, the response became worse when the damping was reduced. For a dry elastomeric damper, 10 lb-s/in. damping is quite difficult to achieve and in addition the elastomer would probably suffer from temperature limitations. The oil film damper with very soft support is probably the only choice for this application. With the maximum reaction force at the damper of about 95 lb. the aforementioned three-pad bearing is potentially capable of carrying the load, assuming an adequate oil flow is available.

A damper with dimensions of $R = 0.6$ in. and $L = 0.6$ in. was analyzed at several different radial clearances. When $C = .0015$ in. as shown

in Figure 3.9, 8 lb-s/in. damping can be obtained. The analysis made here is based on the assumption that the oil film will be cavitating. When the damper is fully pressurized, i.e. no cavitation occurs in the oil film, the amount of damping will be doubled. Therefore, damper clearance at about .0018 in. will provide adequate damping to the system. If the amount of unbalance is controlled and reduced by 50%, the rotor amplitude due to unbalance will also be reduced accordingly. The out-of-phase unbalance response at unbalance of 0.005 oz.in. is shown in Figure 3.10.

It is very difficult to fit a damper/bearing package and an oil seal underneath the air flow path of the L-924 design. With 0.75 inch shaft extension between compressor and the cold end ball bearing, or the WRC radial/axial flow path enough room can be provided. A critical speed analysis of this extended shaft model was performed and the results are quite similar to that of the original shaft length.

It should also be noted here that in the analysis the stiffness of the cold end ball bearing is assumed to be 100,000 lb./in. Should the effective stiffness at this location be greatly reduced by the spline connection, the natural frequencies of this rotor system will be changed and one of the critical speeds may be shifted into the operating range. This effect is shown in Table 3.2.

3.2.4 Split Rotor - Four Bearing Arrangement

Among these different configurations studied in Table 3.1, the split-rotor four bearing shaft (No. 6) seems to be the most attractive and also the most practical design which fitted well with the WRC No. 2 flow path. As shown in Figure 3.11, the main portion of the shaft including turbine and compressor is supported on the foil bearing and a ball bearing in combination with a simple damper on the ball bearing outer race. Power is transmitted through a quill to the pinion shaft which is supported on two smaller ball bearings. A critical speed analysis of this model was made as shown in Figure 3.12. It can be seen clearly that

the rotor will traverse two critical speeds before reaching the idle speed at 50,000 RPM. The mode shape of the second critical speed, however, is fairly rigid between the two main shaft bearings. This is a more favorable design since no bending will occur around the air bearing. With an unbalance level of 0.01 oz.in. at each wheel, the responses were calculated as shown in Figures 3.13 and 3.14 and found to be acceptable. It is felt that less development risk will be involved with this type of rotor arrangements. Previous experiences with many rotors having similar characteristics showed that they performed satisfactorily.

3.3 Rotor Stability

Important requirements in the design are that the rotor system be inherently stable and that the rotor return to smooth operation following any excitations, such as caused by the bearings, seal rubs, aerodynamic forces, combustor or rotor unbalance, etc. As a design guide, stability analysis of this rotor was studied on a limited basis at 100% speed. The MTI CAD 25 Computer Code outputs are log decrement values which will show if the excitation will decay. Negative values indicate the probability of an inherently unstable condition and experience has shown positive values greater than about 0.2 are required for a stable system. One of the present design difficulties is that absolute values of principal and cross-coupled stiffness and damping coefficients for foil type air bearings have yet to be determined. Consequently, the analysis was done using the best estimate of bearing characteristics to obtain a design guide. Assuming (a) a set of stiffness coefficients for a typical single pad bearing of the characteristics which would match the engine as follows:

$$\begin{aligned}K_{xx} &= 16,000 \text{ lb./in.} \\K_{xy} &= 3,750 \text{ lb./in.} \\K_{yx} &= -3,400 \text{ lb./in.} \\K_{yy} &= 14,300 \text{ lb./in.}\end{aligned}$$

and (b), the combination of air film damping and internal coulomb frictional damping at the foil air bearing to be over the range of 2.5 and 7.5 lb.-s/in. Then the stability of the rotor was studied

with 5 lb.-s/in. damping (a conservative value) assumed to be provided by the oil squeeze film damper.

Figure 3.15 details the results of this analysis and shows the level of damping required from the foil bearing to achieve the necessary positive log decrement values for the L-924 design and the four-bearing rotor configurations. The achievement of adequate levels of damping are considered to be quite feasible. One method of improving the damping of a foil bearing is to increase the coulomb frictional damping within the foil members. A second approach for achieving a more stable system is to use a multi-pad foil bearing which will break up the destabilizing whirl component by reducing the cross-coupled stiffness and give a more favorable pressure profile at each pad.

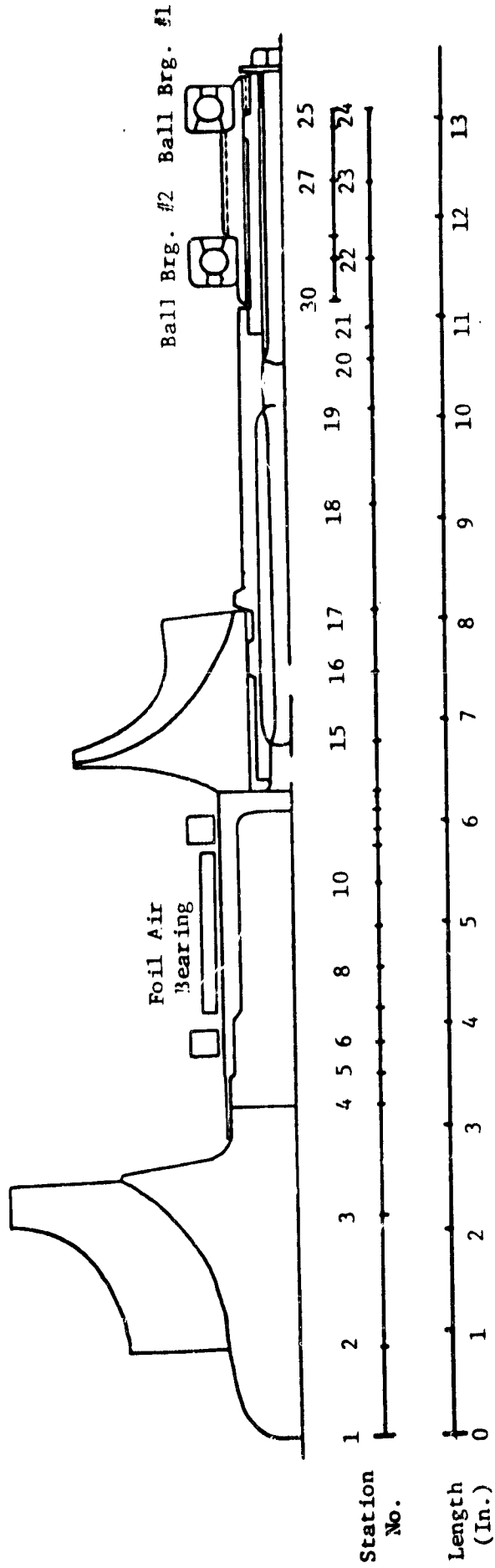


Figure 3.1 WRC L-924 Rotor-Bearing System

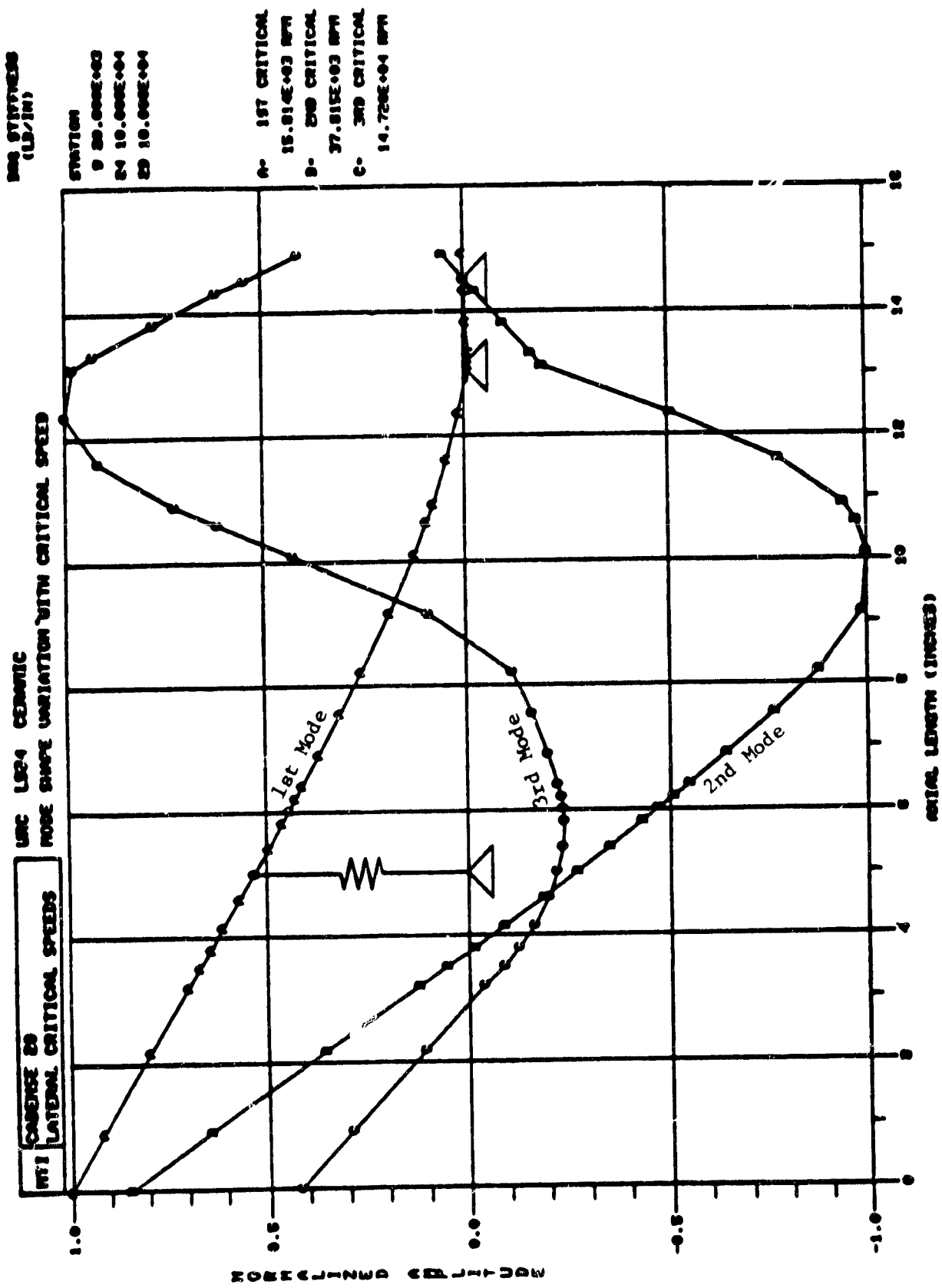


Figure 3.2 Critical Speed Analysis of WRC L-924

STATIONS

A - 3 TURBINE
B - 15 COMPRESSOR

URC 2060 OUT OF PHASE
HALF AMPLITUDE VS SPEED AT SELECTED STATIONS

CADENSE 21
RTI
UNBALANCE RESPONSE

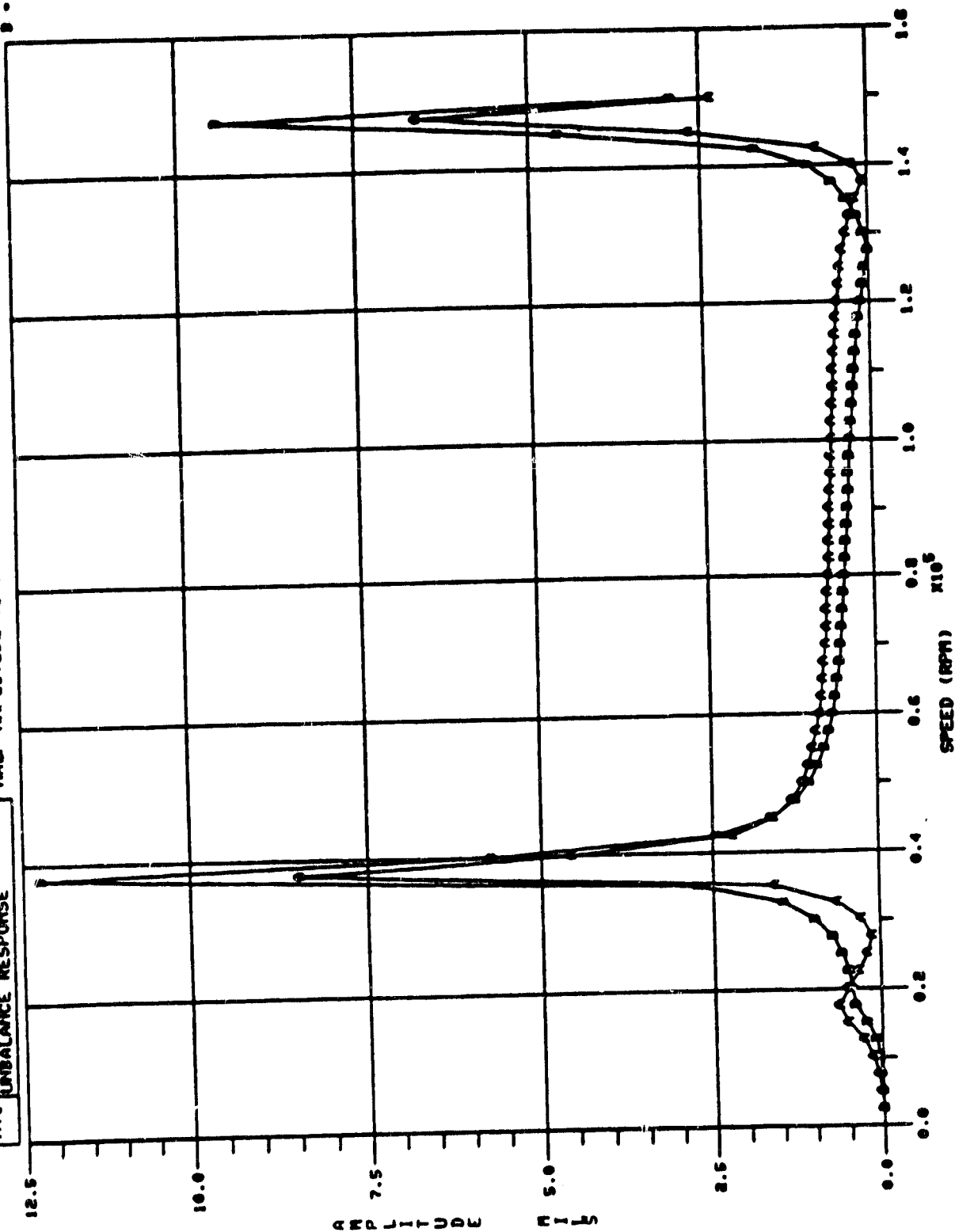


Figure 3.3 Out-of-phase Unbalance Response of L-924 Arrangement

STATIONS
 A - 0 AIR BRG.
 B - 81
 C - 84 BALL BRG.

URC 2060 OUT OF PHASE
 HALF AMPLITUDE VS SPEED AT SELECTED STATIONS

CADENSE 81
 UNBALANCE RESPONSE

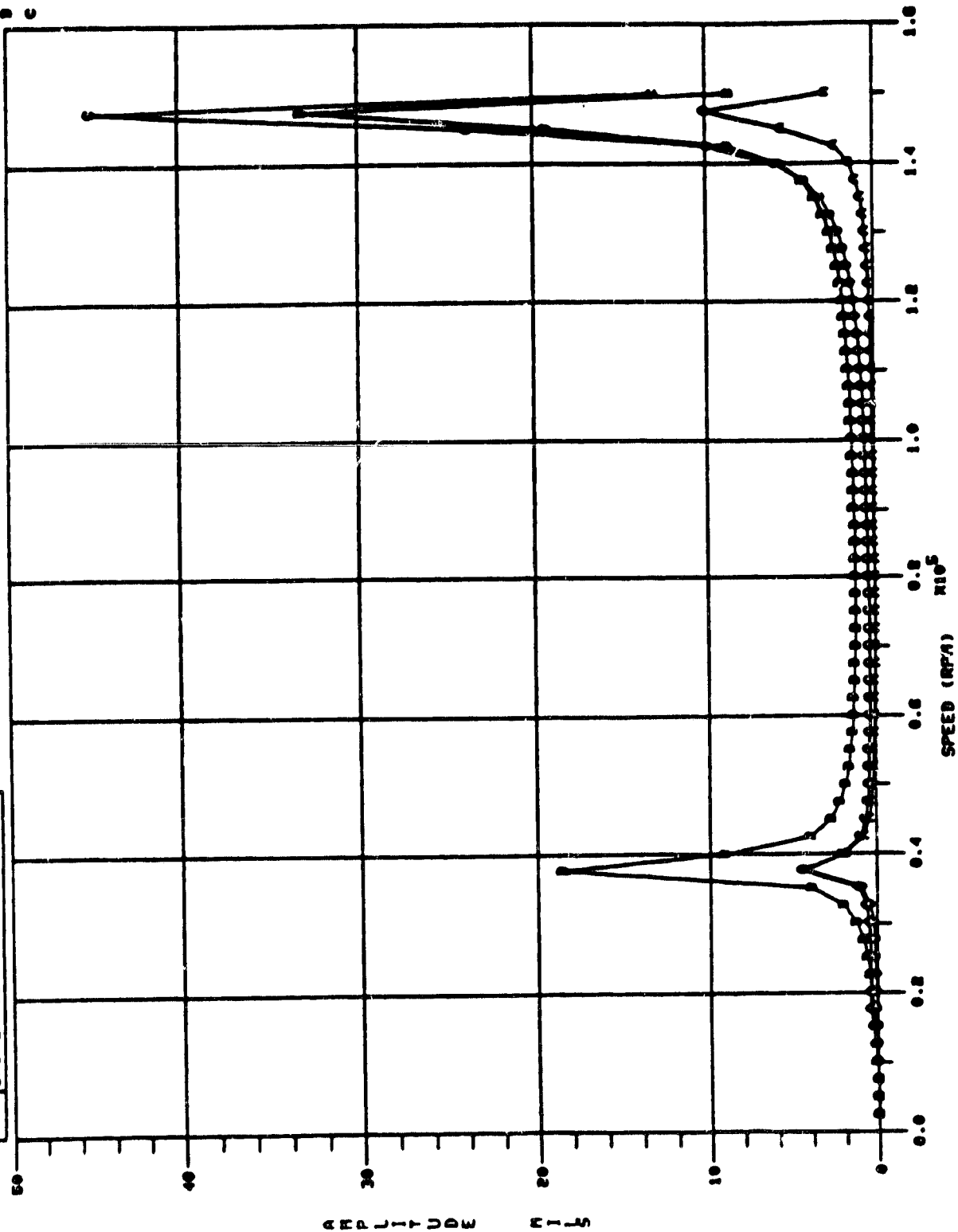


Figure 3.4 Out-of-phase Unbalance Response of L-924 Arrangement

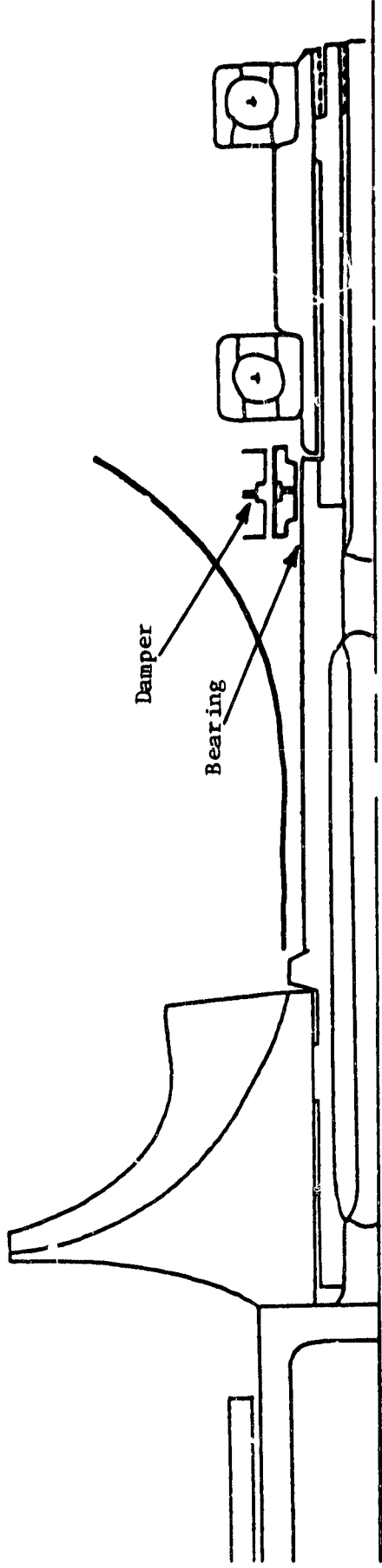
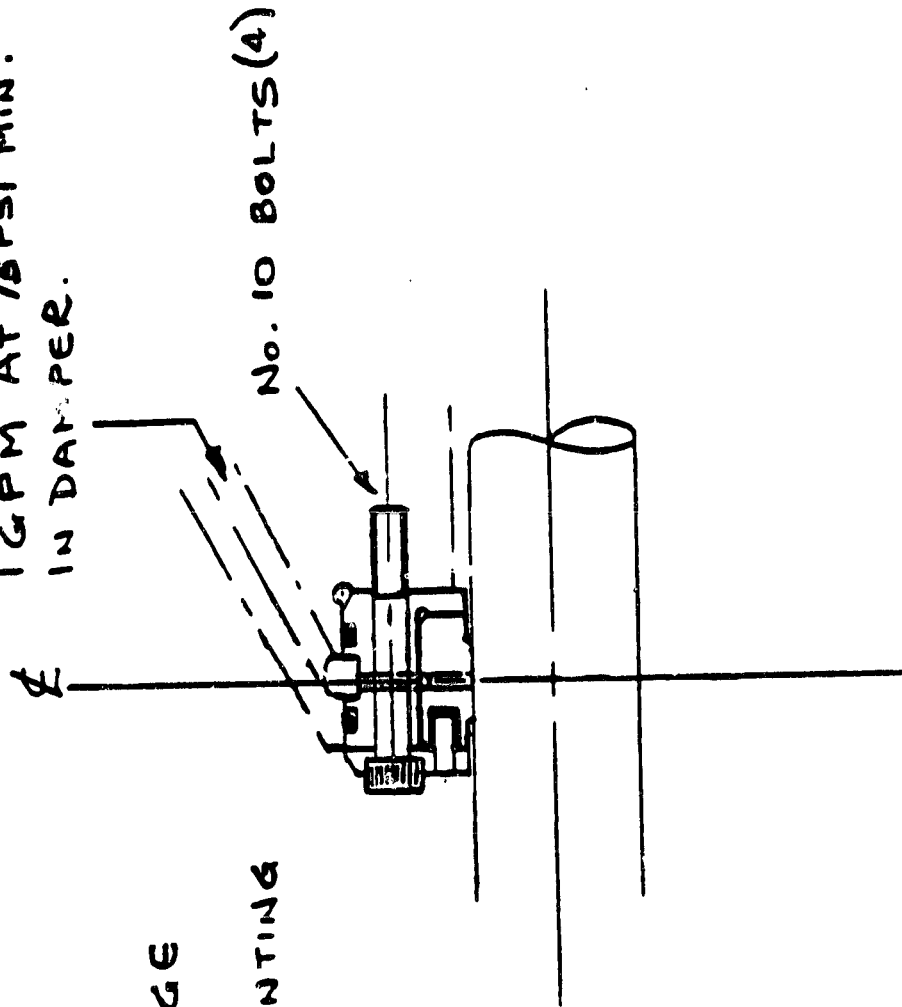


Figure 3.5 Rotor-Bearing System with Bearing/Damper for L-924

OIL REQUIREMENTS
1 GPM AT 75PSI MIN.
IN DAMPER.



DAMPER CARTRIDGE
CONCENTRICITY TO
BALL BEARING MOUNTING
IS IMPORTANT.

No. 10 BOLTS (4)

Figure 3.6 Oil Film Damper Cartridge - L-924 Arrangement

STATIONS

- A - 3 TURBINE
- B - 9 AIR BR'S.
- C - 15 COMP.
- D - 21 DAMPER

Damper

$$B = 10 \text{ lb-s/in}$$

$$K = 10,000 \text{ lb./in.}$$

URC 2063 IN PHASE .01 OZ-IN
 HALF AMPLITUDE VS SPEED AT SELECTED STATIONS

CADENSE 21
 MT1 UNBALANCE RESPONSE

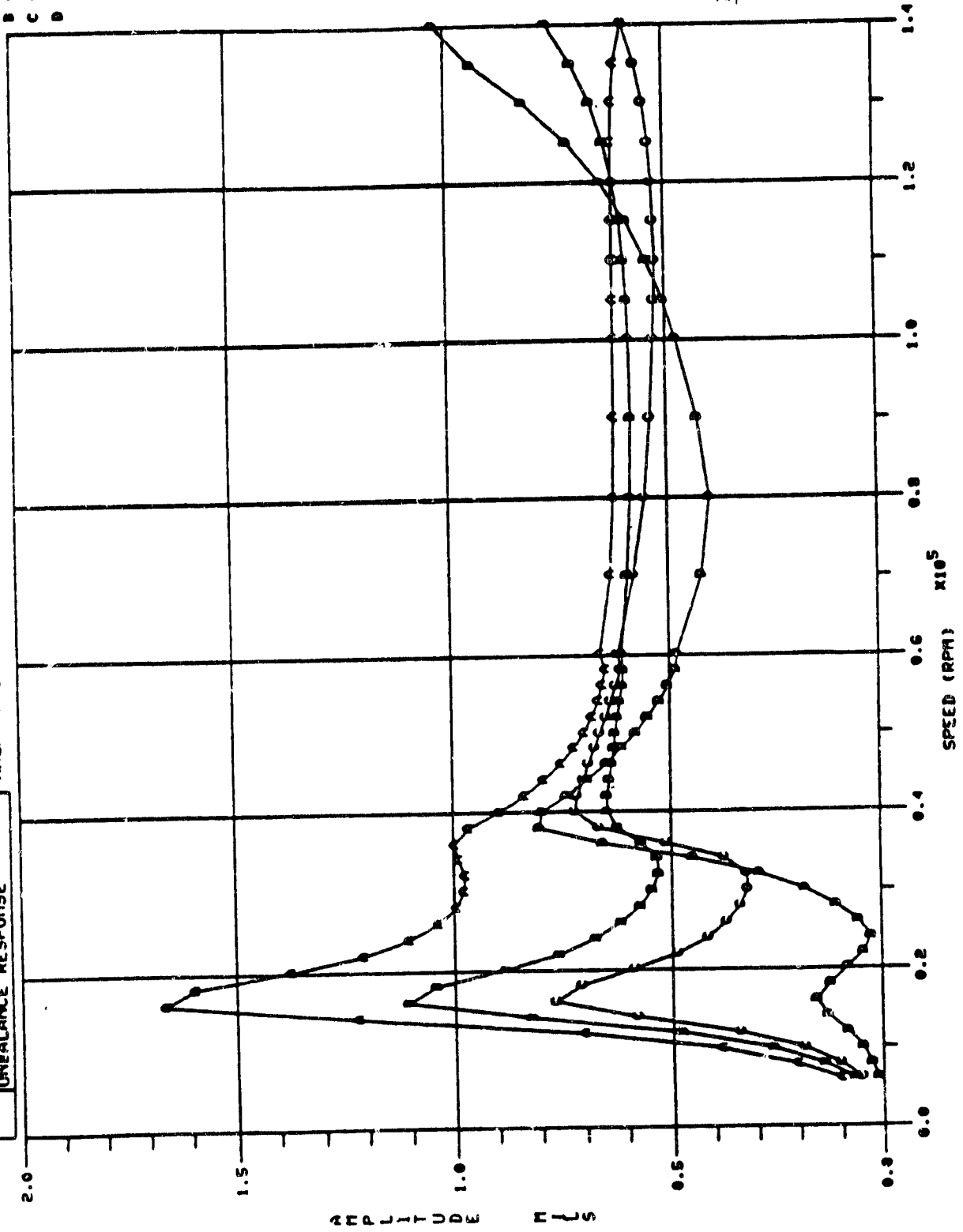
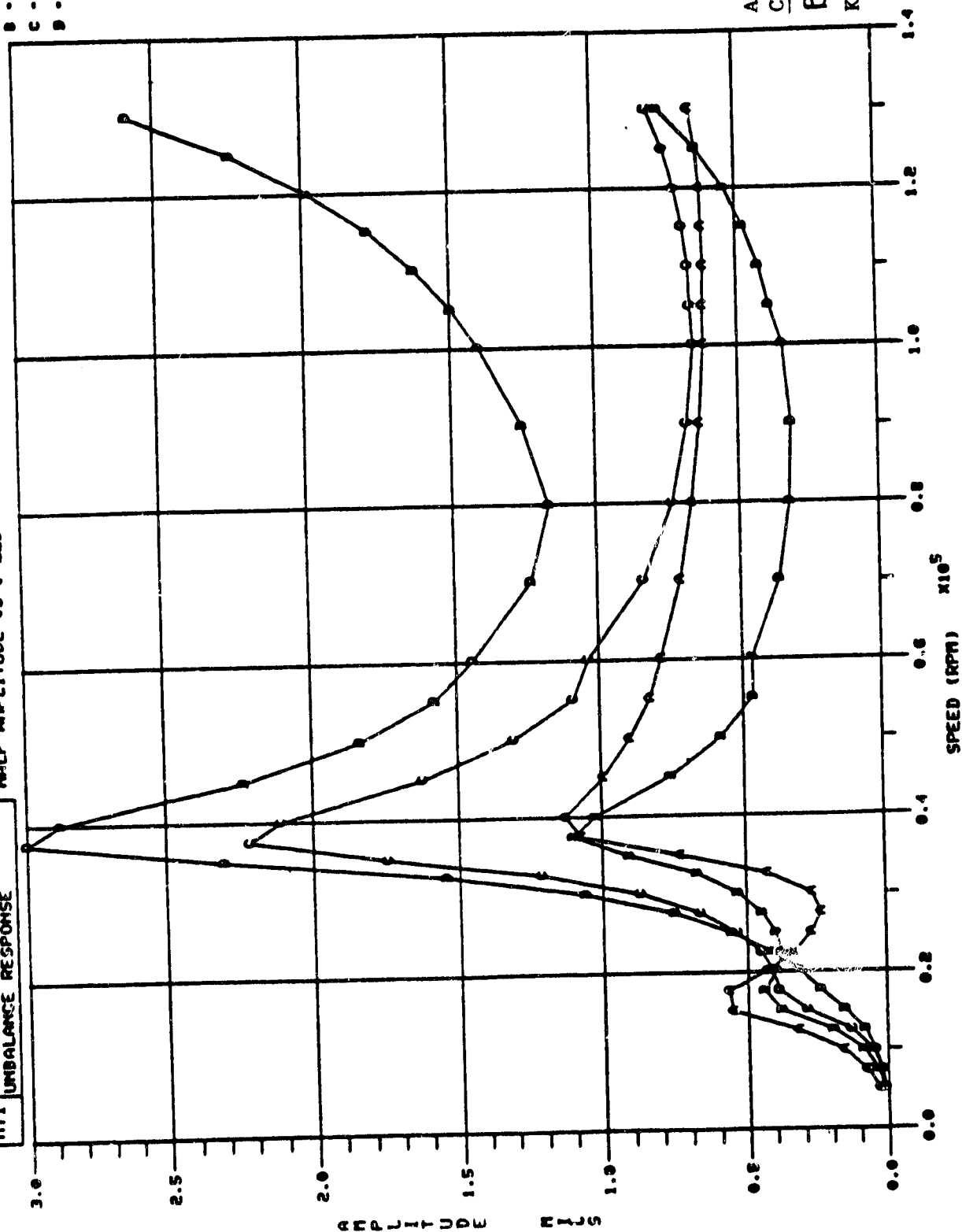


Figure 3.7 In-phase Unbalance Response of L-924 + Oil Film Damper at Position 21

STATIONS
 A - 3 TURBINE
 B - 9 AIR BRG.
 C - 15 COMP.
 D - 21 DAMPER.

URC 2063 OUT OF PHASE UNBALANCE .01 oz.in.
 HALF AMPLITUDE US SPEED AT SELECTED STATIONS

MTI UNBALANCE RESPONSE
 CADENSE 21



Assumed Damper Characteristics
 $B = 10 \text{ lb}\cdot\text{s}/\text{in}$
 $K = 10,000 \text{ lb./in.}$

Figure 3.8 Out-of-phase Unbalance Response of L-924 + Oil Film Damper at Position 21

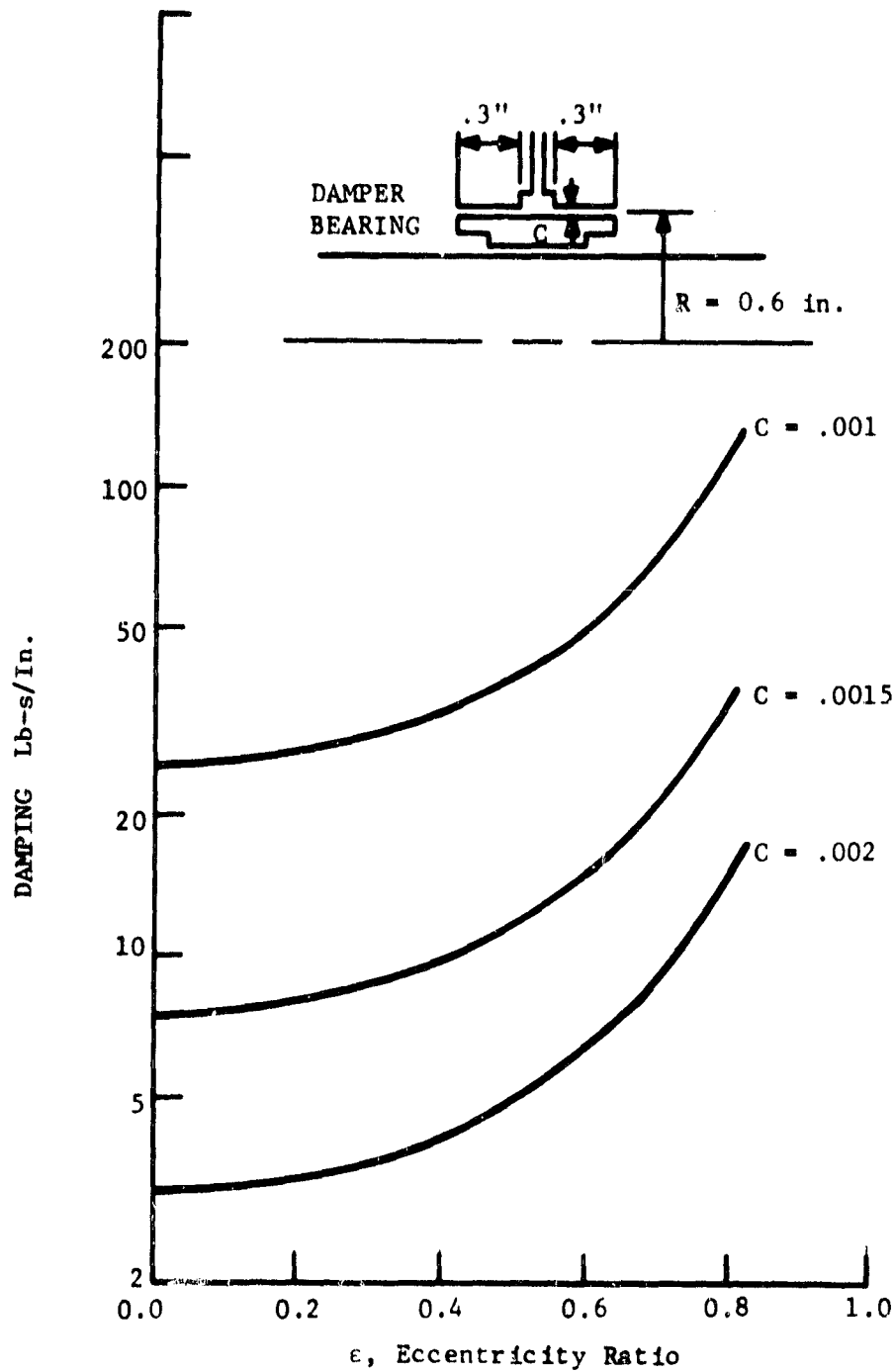


Figure 3.9 Damping Generated by the Oil Film at Different Radial Clearances

- STATIONS
 A - 3 TURB
 B - 9 AIR BRG
 C - 15 COMP
 D - 21 DAMPER

$U_b = 0.005 \text{ oz-in}$
 $B = 10 \text{ lb-} \frac{1}{2} \text{ in}$

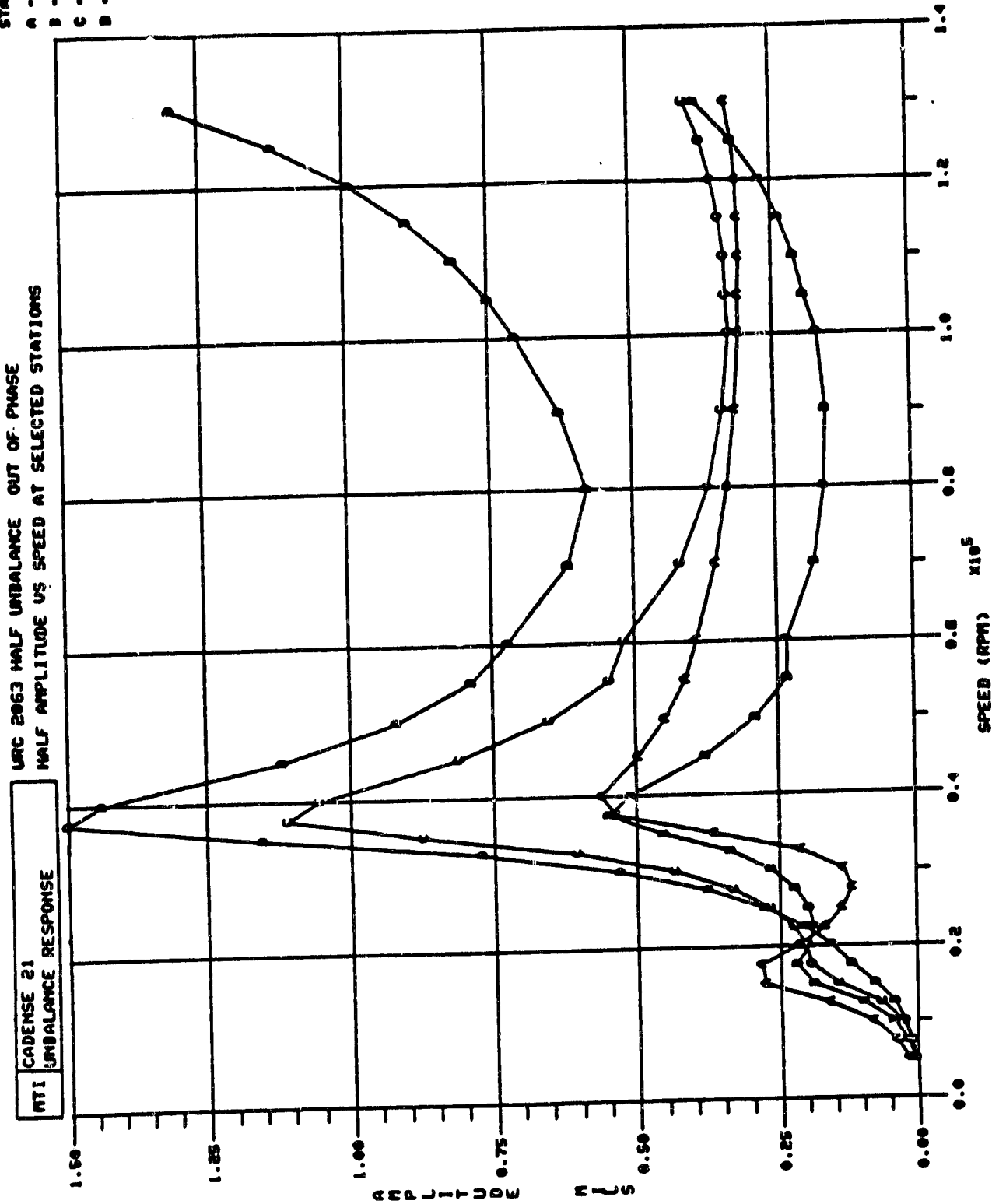


Figure 3.10 Out-of-phase Unbalance Response at $U_b = 0.005 \text{ oz-in}$.

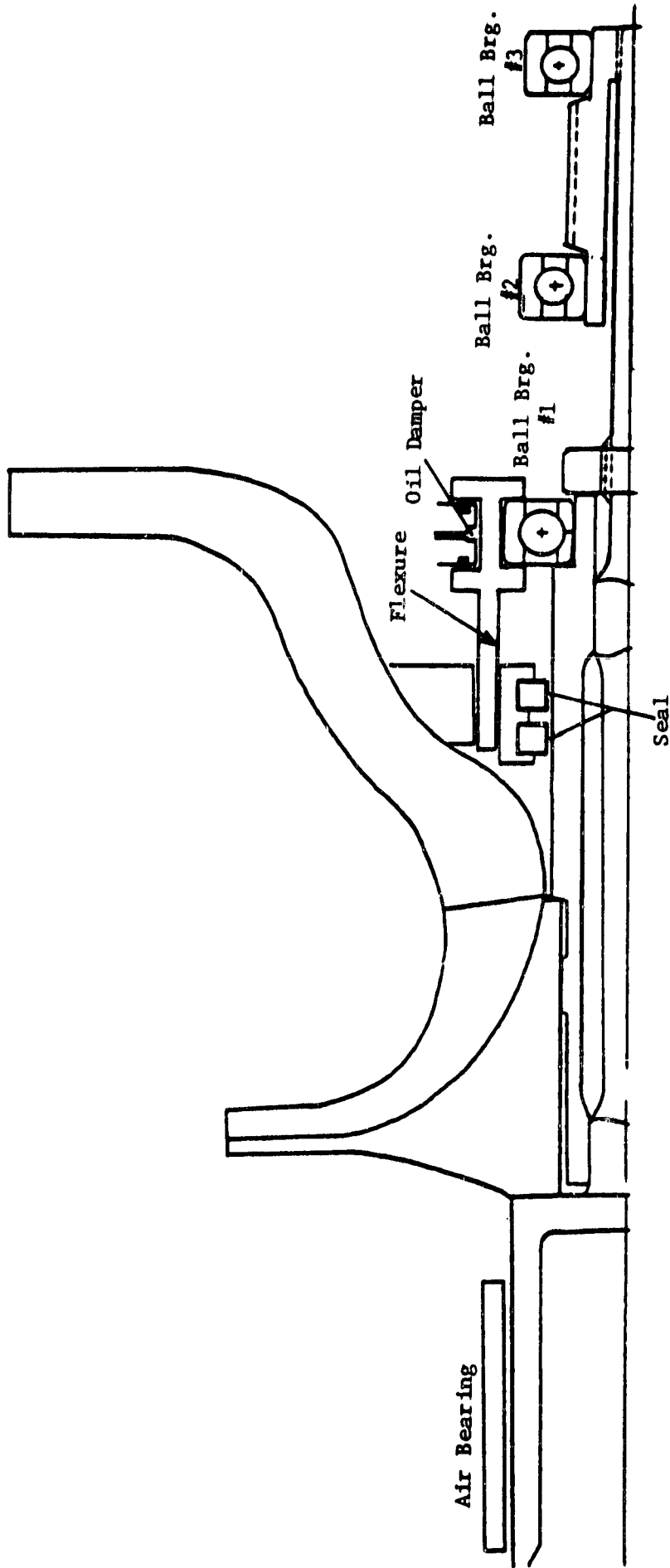


Figure 3.11 Schematic Drawing of a Four-Bearing Design (MTI 614)

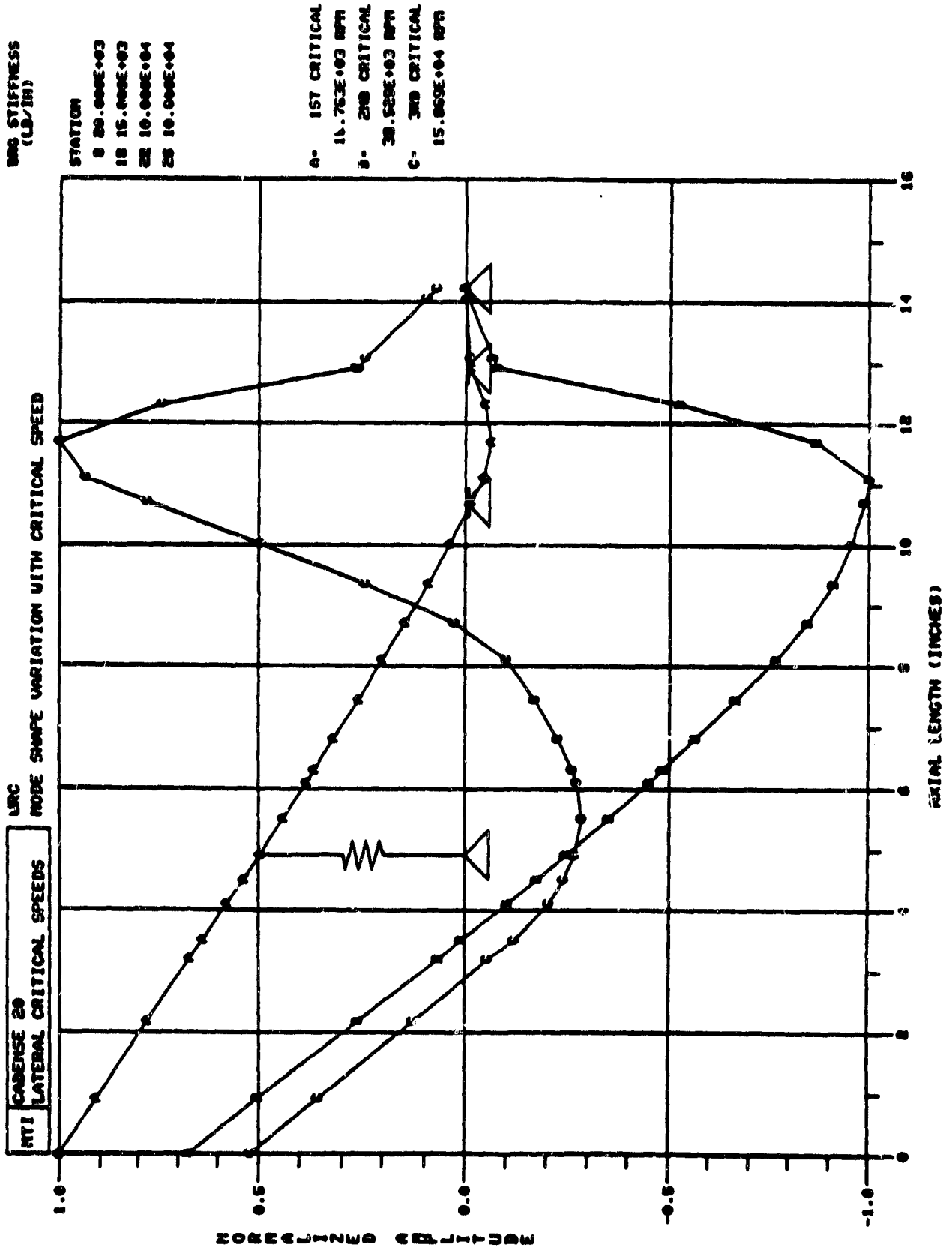


Figure 3.12 Critical Speeds of a Four-Bearing Design

STATIONS
 A - 3 TURBINE
 B - 8 AIR BRG.
 C - 12 CO. P.
 D - 18 BALL BRG #1
 E - 22 BALL BRG #2
 F - 26 BALL BRG #3

Oil Damper
 Characteristics
 B = 5 lb.S/in.
 K = 15,000 lb./in.

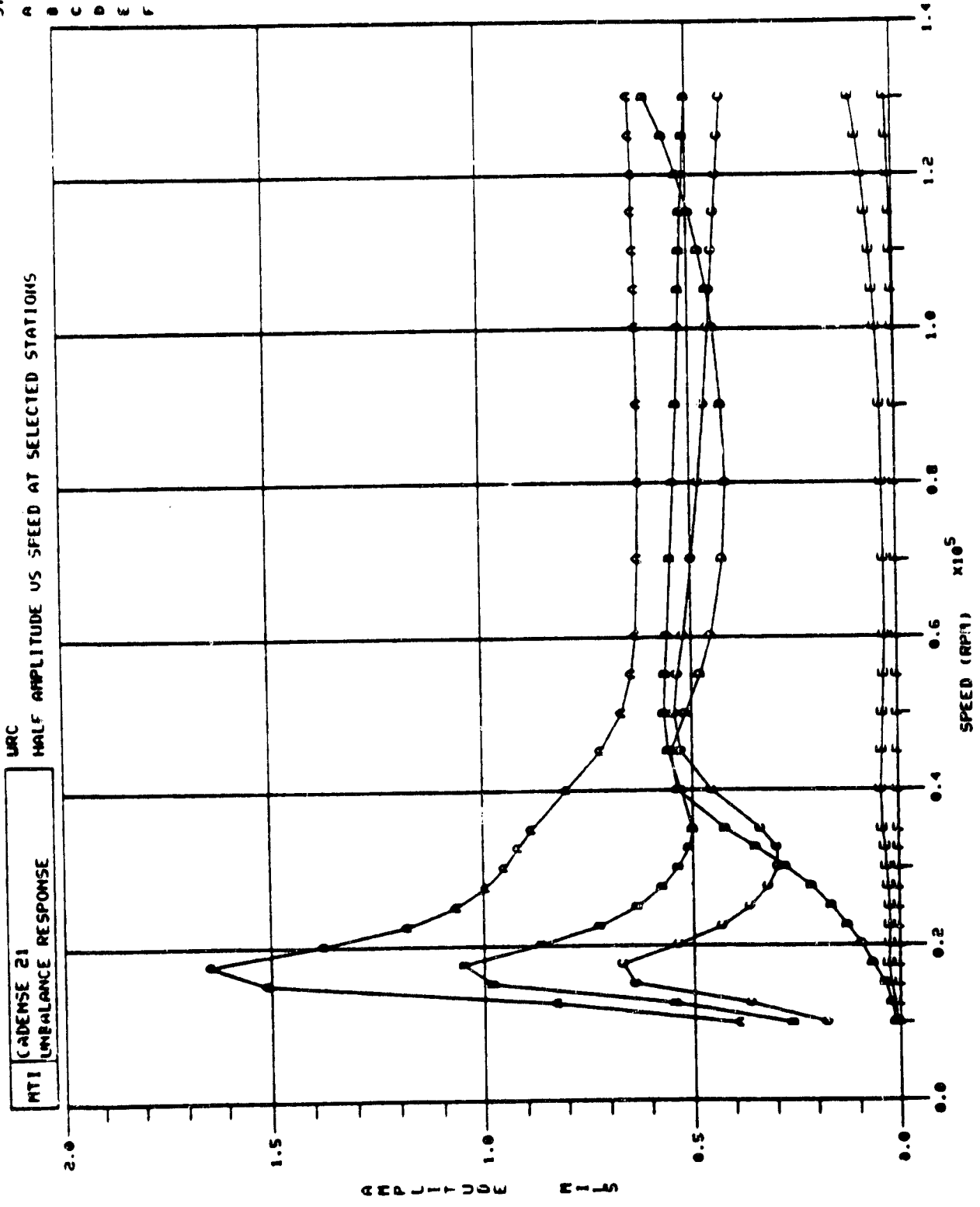


Figure 3.13 In-Phase Response of Four-Bearing Rotor

- STATIONS
- A - 3 TURBINE
 - B - 8 AIR BRG.
 - C - 12 COMP.
 - D - 18 BALL BRG #1
 - E - 22 BALL BRG #2
 - F - 26 BALL BRG #3

Oil Damper
Characteristics

B = 5 lb.S/in.

K = 15,000 lb./in.

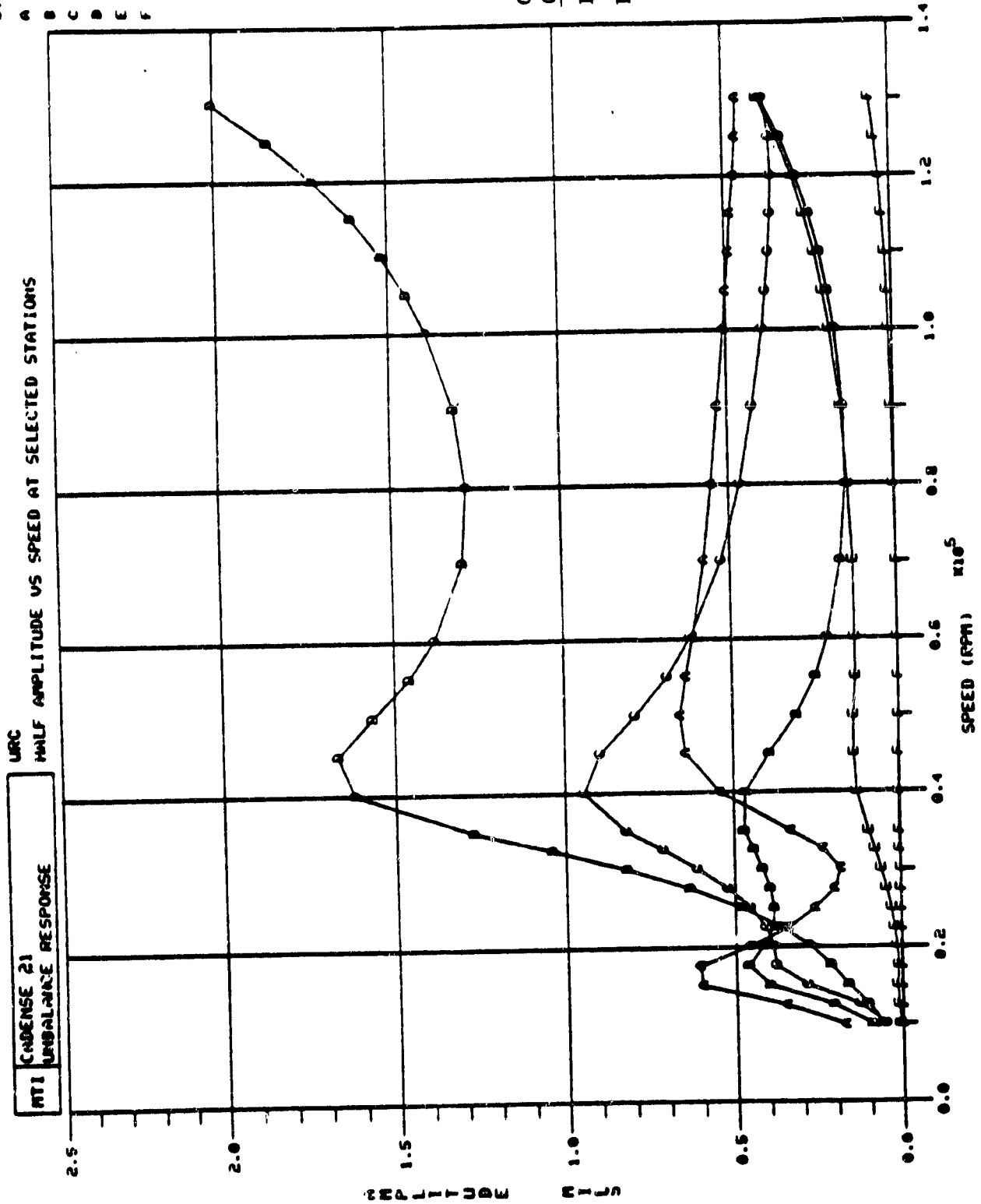


Figure 3.14 Out-of-phase Response of Four-Bearing Rotor

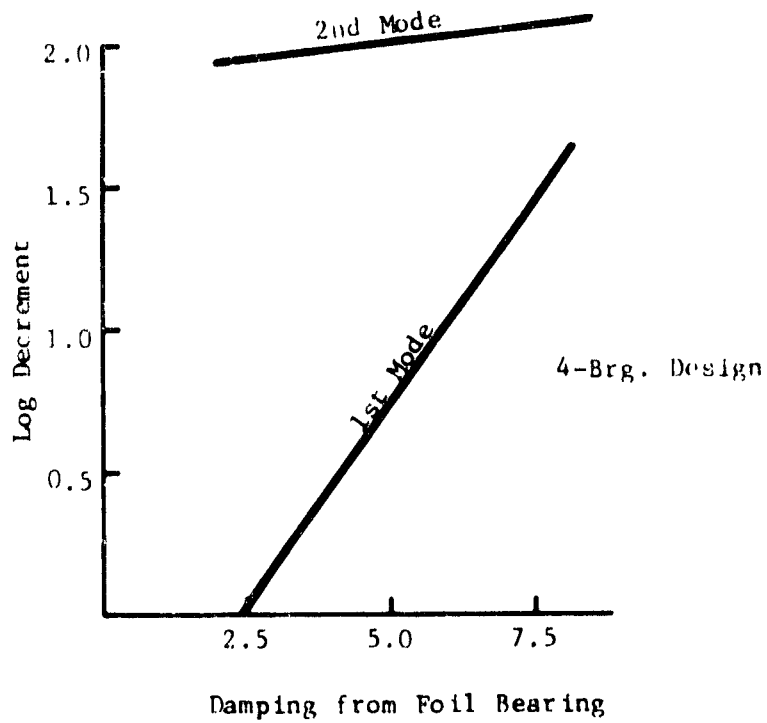
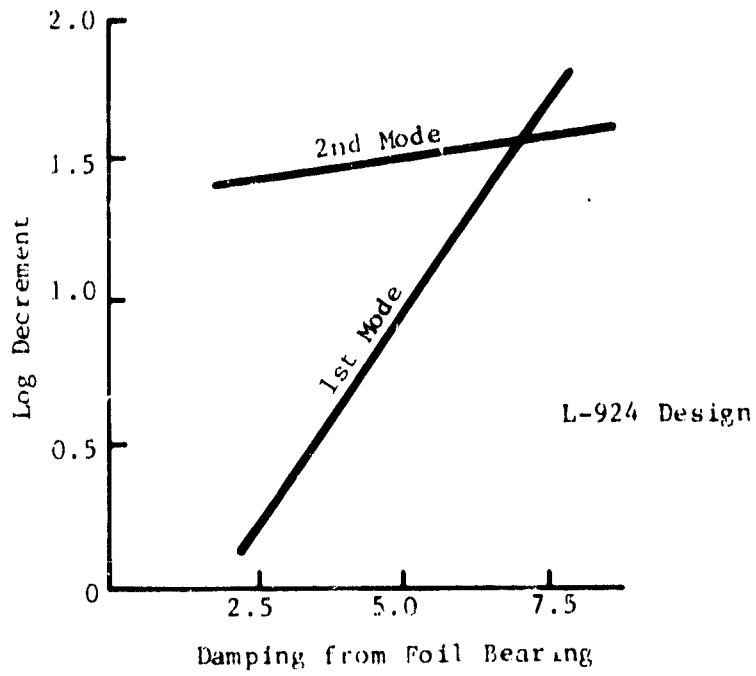


Figure 3.15 Effect of Foil Bearing Damping on Rotor Stability

TABLE 3.1
LISTING OF MODIFIED BEARING-ROTOR CONCEPTS STUDIED

<u>No.</u>	<u>Description</u>	<u>Characteristics</u>
1	WRC L-924 + Damper	<ol style="list-style-type: none"> 1. Maintains original engine configuration. 2. Traverses one rigid and one flexible mode 3. Damper is essential. 4. Power loss is increased by fluid film damper support.
2	Three Active Bearing Shaft	<ol style="list-style-type: none"> 1. Maintains original engine configuration. 2. Second critical in operating range. 3. Bearing alignment problem. 4. "Static" oil damper over ball bearings.
3	Outboard Air Bearing	<ol style="list-style-type: none"> 1. Large shaft O.D. with larger compressor wheel I.D. 2. Requires large bearing stiffness at cold end. 3. Bending mode above operating range. 4. Heat flow problem.
4	WRC Super Flexible Shaft	<ol style="list-style-type: none"> 1. Possible bending at air bearing. 2. Second critical has very small margin at idle speed. 3. Difficult high temperature air film damper requirement.
5	Rigid Shaft	<ol style="list-style-type: none"> 1. Large shaft diameter and short bearing span. 2. Large bearing stiffness required at cold end. 3. Bending mode above operating range. 4. Requires flow path #2 plus larger compressor wheel I.D.
6	Four-Bearing, Two-Shaft + Damper	<ol style="list-style-type: none"> 1. Aero package and gear package are separated. 2. Smaller ball bearings at gear package. 3. Traverses two rigid body modes below idle speed. 4. Requires flow path #2. 5. "Static" damper over ball bearing.

WRC ORIGINAL DESIGN (L-924)

FOIL BEARING STIFFNESS (LB/IN)	EFFECTIVE STIFFNESS AT COLD END (LB/IN)	CRITICAL SPEEDS (RPM)
20,000	10,000	15930. 26850. 91040.
20,000	20,000	16000. 31000. 101100.
20,000	40,000	16000. 34630. 117480.
20,000	60,000	16040. 36310. 129740.
20,000	80,000	16050. 37260. 139040.
20,000	100,000	17030. 38800. 148600.

TABLE 3.2 Critical Speed Changes Due to Different Effective Stiffness at Cold End

4. DETERMINATION OF LOAD REGIME

Loads and forces acting on the bearing were analyzed using MTI Computer Codes CAD 21 and MVL D and were the result of the weight of the rotor, the amount of unbalance, the shock loading from maneuvering conditions, pinion gear reactions and aerodynamic thrust load. Bearing loads due to unbalance of 0.01 oz.in. are plotted for both L-924 and the four-bearing shaft as shown in Figures 4.1 and 4.2. Table 4.1 also lists the bearing loads due to shock and maneuvering conditions for the two rotor arrangements.

A summary of bearing loads for both L-924 and the split-rotor four-bearing shaft at 100% full speed is listed in Table 4.2.

These resulting loads were used to determine the bearing sizes and rotor proportions used in the rotor dynamics analysis.

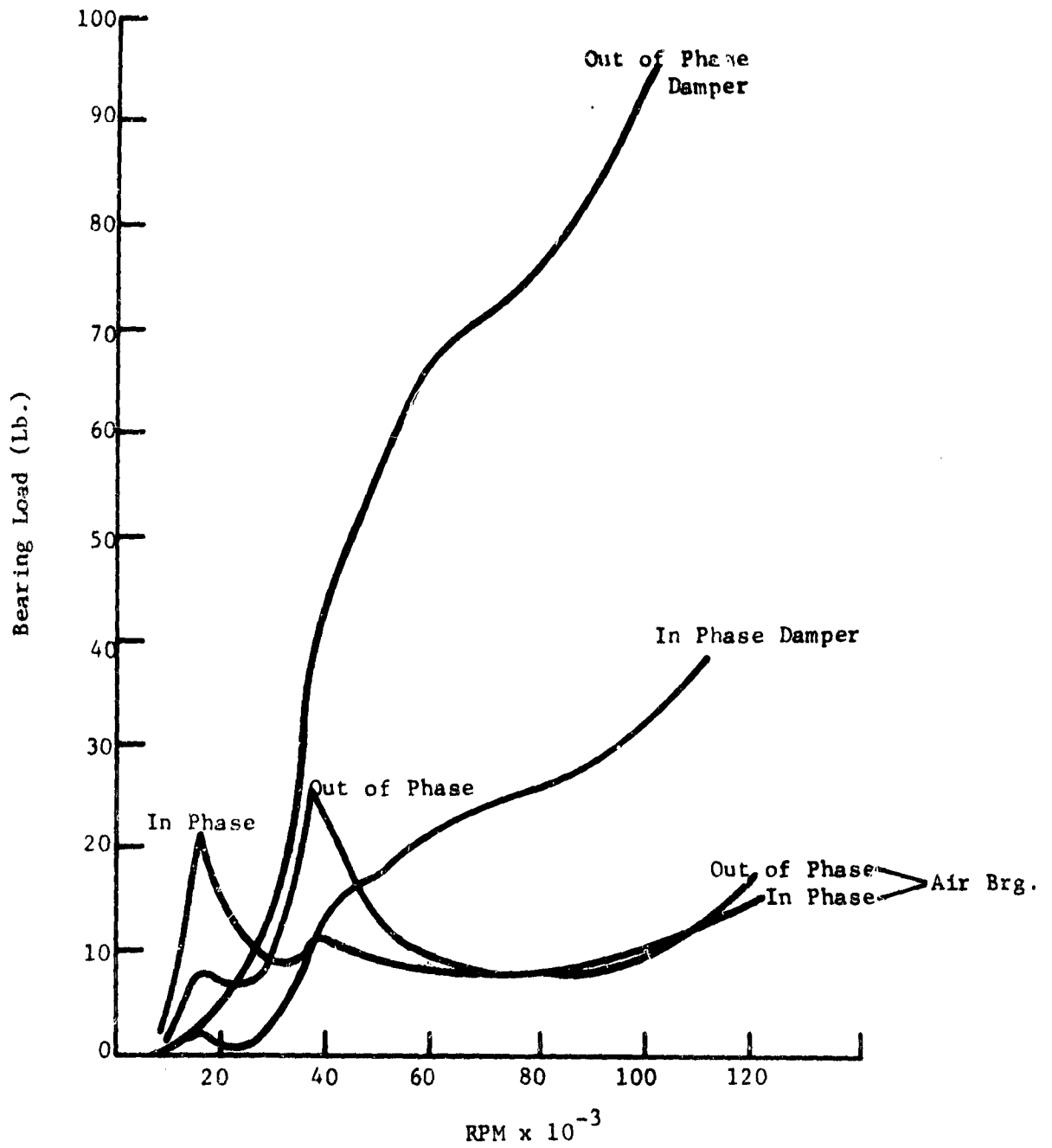


Figure 4.1 Bearing Loads at $U_B = 0.01$ oz.in. - L-924 Rotor

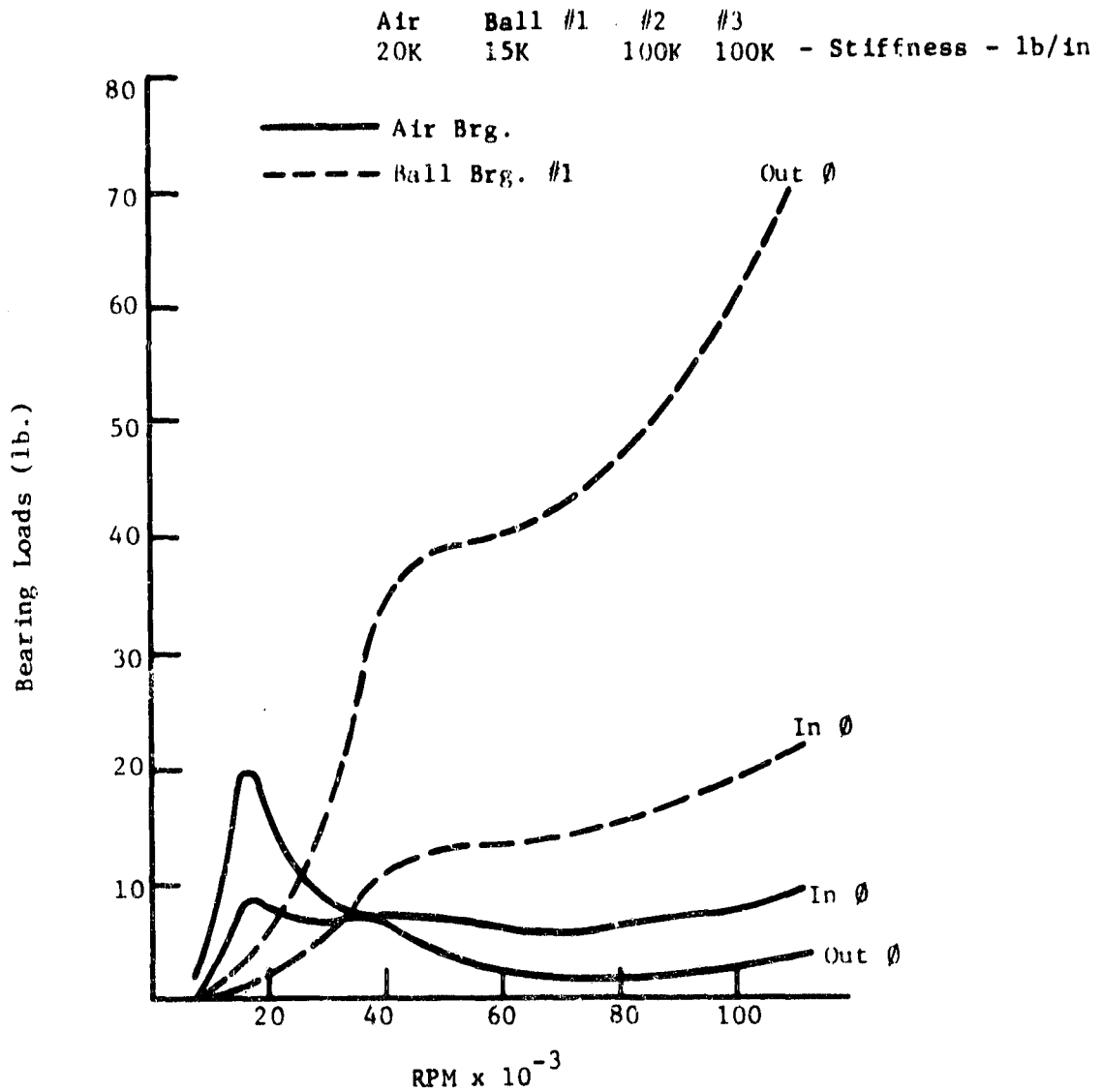


Figure 4.2 Bearing Loads Due to Unbalance at 0.01 Oz.In.
Split Shaft - Four Bearing Rotor



L 924	AIR BEARING			BALL BEARING		
	RPM	3G	2 RAD/S	3G	2 RAD/S	
50,000	6.59	6.30	0.71	3.80		
70,000	6.59	7.87	0.71	5.40		
100,000	6.59	10.33	0.71	7.95		

MTI 614	AIR BEARING			BALL BEARING		
	RPM	3G	2 RAD/S	3G	2 RAD/S	
50,000	7.11	10.68	0.50	8.10		
70,000	7.11	13.98	0.50	11.41		
100,000	7.11	18.93	0.50	16.38		

TABLE 4.1 Comparison of Maneuvering Loads for the Two Different Designs (Ceramic Turbine)

BEARING	FOIL BEARING		BALL BRG. #1		BALL BRG. #2		BALL BRG. #3	
	L-924	4-Brg.	L-924	4-Brg.	L-924	4-Brg.	N/A	4-Brg.
STEADY STATE LOADS								
ROTOR WEIGHT	2.40	2.22	0.40	0.34				
UNBALANCE $U_B = 0.01$ Oz. In.	10.0 (In ϕ)	6.0 (In ϕ)	62.0 (Out ϕ)	60.0 (Out ϕ)	8.0 (Out ϕ)	19.0 (Out ϕ)	---	1.2 (Out ϕ)
GEAR REACTION	---	---	50	0	50	50		50
THRUST (Aerodynamic) or Gear	---	---	32	32	30-40 (Assumed)	10 (Assumed)		10 (Assumed)
TOTAL STEADY STATE RADIAL LOAD	12.4	8.32	112.4	60.3	58.	69.		51.2
DYNAMIC LOADS								
SHOCK (3G)	6.59	7.11	0.71	0.50				
MANEUVER (2 RAD/S)	11.85	16.54	11.85	16.54				
COMB. STATIC AND DYN. RADIAL LOADS (WORSE CASE)	30.84	31.97	124.96	77.34				

(all loads in lbs.)

TABLE 4.2 Bearing Load Summary at 100% Full Speed (Ceramic Turbine)

5. FOIL JOURNAL AIR BEARING ANALYSIS

The preliminary analysis of the HydresilTM (see Figure 5.1 and References 2 & 3) compliant foil air bearing was performed based on a size of 1.375" dia. x 1.5" long and using the loading specified in Table 4.2. Two designs were studied which give overall stiffness levels of 11,000 lb./in. and 30,000 lb./in. respectively so that the best match to the rotor dynamic models could be established. MTI Computer Codes JSTAT and HYDRE were used in the analysis and these showed that (a) a comfortable load margin would exist and that the size of the bearing could be reduced during detailed design and (b) the final bearing size might be dictated by the loading limitation related to starting and stopping under sliding contact rather than loading at high speed.

Figure 5.2 gives plots of the minimum film thickness, eccentricity and frictional power losses for the two bearing designs at 100,000 rpm as a function of load. Table 5.1 details the stresses in the supporting bump foil and dipping of the top foil between bumps as a function of load at 100,000 rpm.

The materials selected for the foil bearing are Inconel X-750 or Inconel 718 foil material and a CdO+ graphite bonded high temperature coating for the start-stop sliding contact wear resistance of the foil. The matching rotor coating would be fine grain, flame sprayed and ground chrome carbide or possibly the ceramic turbine material for the ceramic engine. Recommendations were made on rotor configurations in the region of the foil bearing which would minimize heat flow along the shaft and limit axial temperature gradients.

A three-pad version of the foil bearing illustrated on Figure 5.1 was selected because as discussed in Section 3.3 it provides an inherently greater stability margin for a high speed rotor and the bearing design would be optimized to provide a high level of inter-foil coulomb friction for damping purposes.

TABLE 5.1

Summary of Foil Air Bearing Characteristics

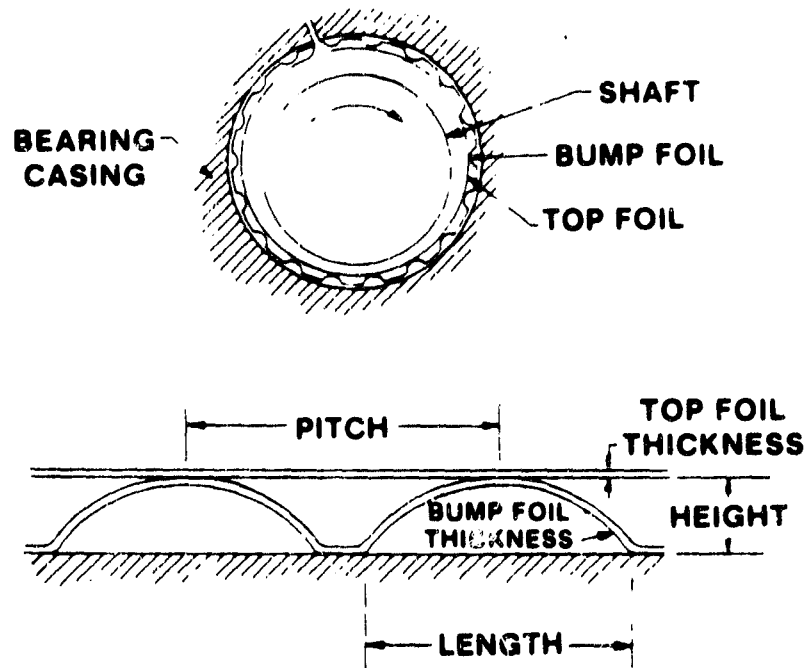
	CASE A		CASE B	
LOADING LBS	30	60	30	60
PSI	14.6	24.2	14.6	29.2
BUMP STRESS, PSI	66,420	121,320	44,740	76,870
UPPER TAPE DIP INS. BETWEEN BUMPS	.0003	.0005	.0001	.0002
MECH. STIFFNESS, LB/IN	17,200	13,900	46,670	54,330
APPROXIMATE OVERALL BEARING STIFFNESS, LB/IN	11,000		30,000	

D = 1.375

L = 1.5 INS

N = 100,000 RPM

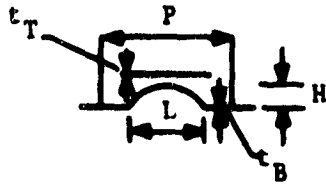
FOIL JOURNAL BEARING



TYPICAL DETAILS OF BEARING



Figure 5.1 Typical Details of Hydresil Foil Air Bearing



Dia. = 1.375"
 Length = 1.5"
 C = .0015" (Radial)
 N = 100,000 RPM
 T = 600° F
 Press. - 60 psia

Case	P	L	H	t_B	t_T
A	.165"	.125"	.020"	.003"	.004"
B	.124"	.093"	.020"	.003"	.004"

} Foil Details

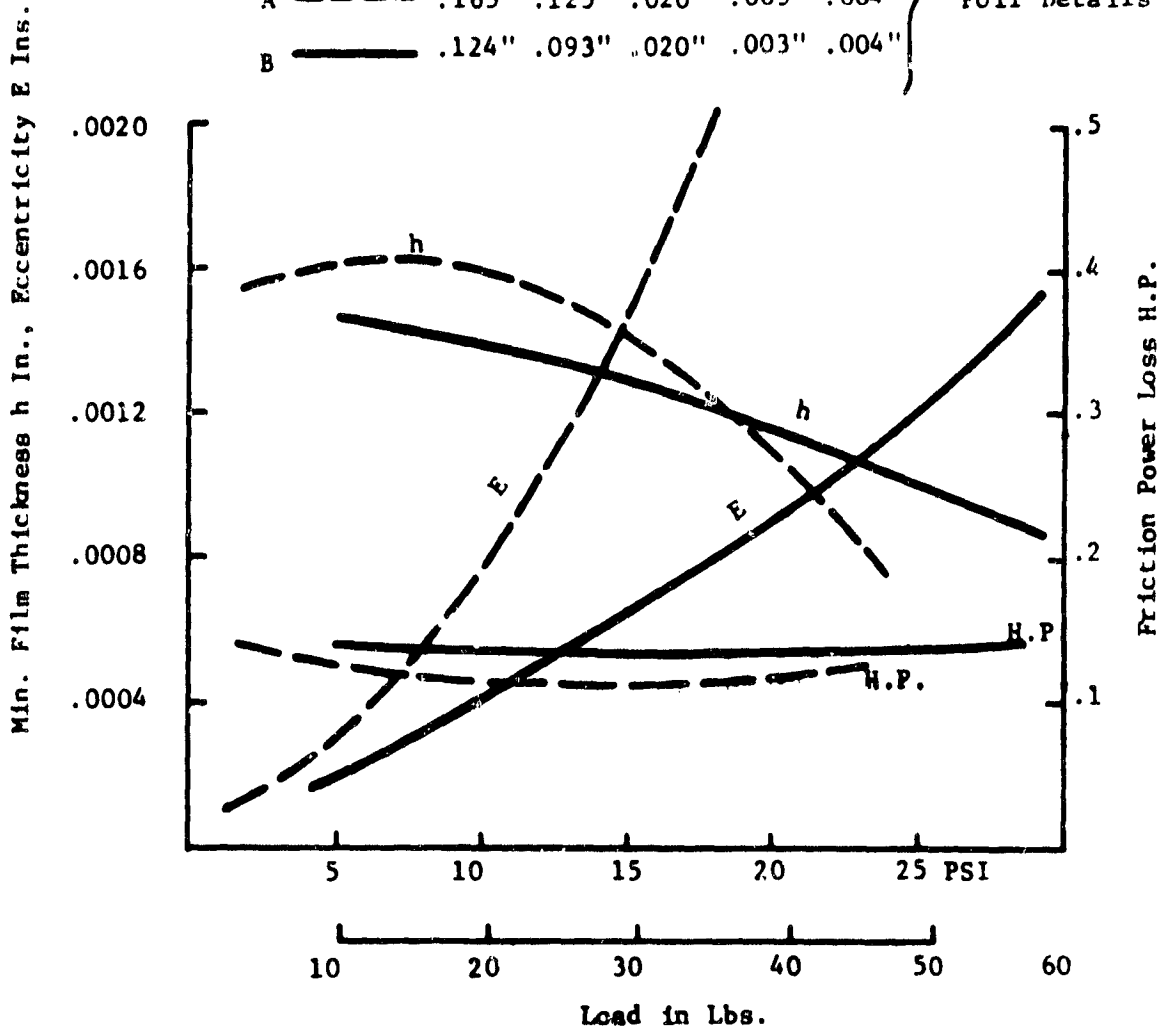


Figure 5.2 Hydresil Journal Bearing Performance (Uncorrected)

6. BALL BEARING ANALYSIS

Two basic sizes of ball bearings were studied to suit the various rotor arrangements at the cold end positions; these were a 104 (20 mm bore) and a 202 (15 mm bore) size of either angular contact or split inner race designs. At normal 100% speed, the DN values of these two bearings are 1.5×10^6 and 2.0×10^6 (RPM x mm) respectively. The MTI DREB (Dynamics of Rolling Element Bearing) computer code was used to analyze the bearing and to determine fatigue life, internal contact stress, and power losses. Bearing dimensions and characteristics used in the preliminary analysis are listed on next page. No effort was possible to optimize the designs for best performance.

Selected Bearing Characteristics

	<u>104</u>	<u>202</u>
Bore	0.7874 in.	0.5906 in.
O.D.	1.6535 in.	1.3780 in.
Shaft I.D.	0.50 in.	0.25 in.
Ball Dia.	0.25 in.	0.25 in.
Pitch Dia.	1.2205 in.	0.984 in.
Contact Angle	20 degrees	20 degrees
Outer Race Int. fit	0.0 in.	0.0 in.
Inner Race Int. fit	0.0005 in.	0.0005 in.
O.R. Curvature	0.515	0.515
I.R. Curvature	0.515	0.515
No. of Balls	13	10

The calculations made here assumed the radial and axial loads (with springs) are at 50 lb. and 80 lb. respectively. No allowance has been made for dynamic load or change of load with speed. The preliminary analysis was based on the following duty cycle and life requirement:

- (1) 10% @ 100,000 RPM
- (2) 10% @ 70,000 RPM
- (3) 70% @ 60,000 RPM
- (4) Desired L_{10} life 3,500 hours

The fatigue lifes for the above duty cycle were calculated and are listed below:

<u>Condition</u>	<u>104J</u>	<u>202J</u>
1	243 hr.	732 hr.
2	2077 hr.	3853 hr.
3	5408 hr.	8687 hr.

These were combined in accordance with the equation:

$$\frac{1}{L_{10}} = \frac{1}{L_{(1)}} + \frac{1}{L_{(2)}} + \frac{1}{L_{(3)}}$$

where L is the life of each condition, to give the following L_{10} life.

	<u>104</u>	<u>202</u>
L_{10} life	1646 hr.	3927 hr.

This preliminary analysis indicated that with appropriate optimization and refinement of the bearing designs, mounting, lubrication and cooling, satisfactory fatigue life can be achieved.

Other bearing characteristics determined from the analysis were as follows:

	<u>104J</u>	<u>202J</u>
Stiffness (lb./in.)	556,000	400,000
Max. Stress Contact (psi)	238,800	222,690

It is also found during the calculations that the axial load should be maintained at a certain level such that all the balls will be equally loaded. When the applied radial load exceeds the axial load, only a few balls will be loaded and this will significantly reduce the life of the bearing due to ball skidding. It is recommended that the ratio between applied axial and radial loads be kept at about 1.5 to 2.0 in order to have good bearing performance.

7. ROTOR FRICTIONAL POWER LOSSES

A major concern in the engine design is to ensure that the minimum total frictional power losses are achieved in the high speed bearing-seals-damper-rotor system. Table 7.1 details the power losses estimated for each of these components at 100,000 rpm for the baseline L-924 rotor with an oil film damper and the split rotor four-bearing arrangement.

The power losses related to oil lubricated components, in particular the ball bearings, are quite difficult to estimate because of their sensitivity to the oil churning part of the losses which are strongly influenced by the system design - oil feed, drain, oil quantity and viscosity, and cavity design. The estimates of probable losses for good system design given in Table 7.1, which could easily be increased by inadequate design and the gear pinion churning influence, are judgments based on the following three sources of data:

- (a) Measured power loss data at high speed available at MTI
- (b) Reference (4) ASME Paper
- (c) MTI analytical DREB computer code

Important findings from the power loss analysis are as follows:

- (a) Every effort is necessary to minimize the ball bearing sizes. The WRC integral inner race-rotor concept would be attractive in the developed engine.
- (b) The floating oil film damper, which acts as a bearing, generates significant power loss, and concepts for combining this as part of the oil seal at the compressor inlet should be reviewed.
- (c) The associated ball bearing oil system, as previously discussed, requires careful design work.
- (d) The lower power loss of the foil air bearing is very significant.

	FOIL BRG.	AIR SEALS (HOT END)	OIL BRG./ DAMPER	BALL BRG. 104J	BALL BRG. 202J	OIL SEAL (COLD END)	TOTAL POWER LOSS
WRC L-924 with oil film damper	0.15	0.06 x 2	1.21	1.8 x 2	---	0.6	5.68*
4 Brg. Shaft	0.15	0.06 x 2	---	1.8	.90 x 2	0.6	4.47*

* Pinion churning and subsequent gearbox losses not included

TABLE 7.1 Power Loss at 100% Speed (100,000 RPM)

8. CONCLUSIONS WITH RECOMMENDED CONCEPTS AND RELATED DEVELOPMENTAL RISKS

The preliminary design work which has been completed has shown that practical bearing-rotor systems for this high speed gas turbine can be achieved with both metal and ceramic turbine wheels.

A number of specific areas were identified in which careful detail design will be important in order to ensure that a reliable rotor system will be obtained. These areas are:

- The spline connection between the turbine-compressor shaft assembly and the pinion assembly for the modified L-924 rotor system must be positive to ensure achieving a rotor having the desired stiffness.
- The rotor should be designed to ensure repeatability of balance within 0.005 oz.in. at each plane in order to minimize unbalance force response.
- The oil film damper is a critical item in the rotor designs and must be carefully located and be fully effective with adequate oil supply at all times.
- The foil air bearing must be designed to minimize internal cross-coupling aerodynamic destabilizing forces and have meaningful internal coulomb friction damping to ensure an adequate rotor stability margin.

The foil air bearing mounting and associated journal section of the shaft should be designed to minimize the heat flowing along the shaft and to avoid large temperature gradients across the bearing.

Two designs are recommended for continued engineering into rotor-simulator evaluation. These are:

- (a) The basic L-924 three bearing rotor with a floating oil film damper.
- (b) The split rotor four bearing arrangement with a static oil damper at the outer race of the compressor inlet end ball bearing.

Of the two concepts, the split-rotor arrangement is considered to present the lower developmental risk because of the rigid nature of the rotor and conventional damper techniques.

REFERENCES:

1. Lund, J.W., "Stability and Damped Critical Speeds of a Flexible Rotor in Fluid Film Bearings", ASME Paper No. 73-DET-103, presented at Design Engineering Technical Conference, Cincinnati, Ohio. Sept. 9-12, 1973.
2. Gra, J., "Foil Bearings for the Chrysler Automotive Gas Turbine Engine Program - Development and Operational Experiences", SAE Preprint 790109, February 1979.
3. Gray, S., Heshmat, H., Bhushan, B., "Technology Progress on Compliant Foil Air Bearing Systems for Commercial Applications", 8th International Gas Bearing Symposium, Leicester Polytechnic, England, April 8, 1981.
4. Trippett, R.J., "A High-Speed Rolling-Element Bearing Loss Investigation", Transactions of ASME, Journal of Engineering for Power, Page 40, Vol. 100 January 1978.

APPENDIX D

Van Doorne Belt Analysis

Van Doorne has supplied a torque capacity figure for their belt at a single operating point representing the low-gear condition where stresses are generally highest. The objective of Battelle's work was to project from this limited data the torque capacity of the drive at other ratio settings and other speeds, and to predict efficiency of the belt as a function of ratio, speed, and load level. This information is needed to determine the adequacy of the Van Doorne belt, in the size available, for various possible transmission configurations, and to compare the overall efficiencies of these candidate transmissions at the more important operating points.

Since many operating conditions were to be calculated and each calculation involves tedious iteration, a computer program was written to generate capacity and internal loss maps. The development of this program was partially funded by Battelle since it also has applications in our continuing work with compression belts. Belts of either Van Doorne or Battelle design can be simulated, and the belt can be operated always at optimum tension ratio, or it can be operated at constant total tension, an approximation to the Van Doorne industrial control system. Five iterative procedures are satisfied simultaneously to define each data point.

The program provides a detailed and accurate analysis of load and deflections within the belt structure, and serves well to predict capacity. It does not include a detailed model of the interaction of the belt with the pulley, and consequently it evaluates only those components of loss that are internal to the belt: friction between the bands and between the inner band and the strut tops, creep due to introduction of ungathered gaps in the strut column to the driver, and creep due to compression of the strut column.

A detailed model of the pulley interaction would be a logical next step toward understanding steel belts. Such a program would comment upon the axial force requirements, evaluate losses associated with strut ends rubbing on the pulley faces, and provide a tool for studying the effects of pulley rigidity and lubrication dynamics. For the present, we

have taken the pulley losses to be 2.5 percent at all operating conditions if the control system is optimum.

Dimensions and weight of the Van Doorne parts were determined at Chrysler by measurements on the parts of a purchased industrial drive. Results presented here are based on assumptions that the bands are neutrally nested and coefficients of friction are .10 at all band contacts and at the pulley contacts. This pulley friction is based on experiments at Chrysler with the Van Doorne parts and is somewhat higher than we have experienced with our own belts. The band friction assumption is validated by no-load drag torque measurements made at Chrysler.

Torque and Speed Capabilities.

Discussion of Failure Modes. In order to relate capacity at one operating condition to capacity at another, it is necessary to know the mode of failure of the belt. Van Doorne has not been willing to divulge their laboratory experience in this regard. Battelle's laboratory experience was that failure of the bearing between the inner band and the tops of the struts limited belt capacity. More recent Battelle designs, not yet tested, have included changes in the strut geometry intended to ease the service of this bearing. Consequently, the failure mode of the belt is not now known, and the following modes may be considered:

- 1) Fatigue failure of the bands due to a combination of bending stress and tension.
- 2) Bearing failure between the inner band and the strut tops or between adjacent bands.
- 3) Fatigue or bearing failure of the Hertzian contacts between adjacent struts.
- 4) Fatigue or bearing failure of the Hertzian contacts between the struts and the pulley faces.
- 5) Undue slippage of the belt in the pulleys.

The fifth mode depends upon the control system that determines axial pulley force, rather than upon the strength of the belt itself.

Calculation of the Hertzian stresses in Battelle belts has indicated these to be moderate in comparison to the contact stresses commonly found in gearing and in rolling traction drives. Also, our laboratory experience has not disclosed any problems corresponding to modes three and four except where gross slippage of the belt in the pulleys was allowed. The Van Doorne belt is sufficiently similar that modes one and two are expected to limit its capacity rather than modes three and four.

Bending stress in the bands is more a function of the radius ground into the strut tops and the residual stress pattern in the bands than of the pitch radius of the pulley. Consequently, for a given belt, bending stress is not a function of operating condition, and the stress capacity remaining for carrying band tension is fixed. Failure mode one yields a capacity theory that can be expressed as follows: The limiting torque of the drive at any ratio and speed is reached when the tension in the most highly loaded single band is equal to the maximum single band tension under the operating condition specified by Van Doorne. By our calculation, this is a band tension of 180 pounds, corresponding to a tensile stress component of 36,000 psi, which seems rather low.

Failure mode two yields a second capacity theory that has been expressed for computational purposes as follows: The limiting torque on the drive is reached when the radial force on the most highly loaded single strut is equal to the maximum radial force under the operating condition specified by Van Doorne. Maximum radial force is a function of the total stack tension and the pitch radius of the smaller pulley.

Theories one and two yield essentially the same capacities at all speeds at the ratio of the Van Doorne specifications (2.236:1 downdrive). At the inverse ratio (2.236:1 updrive) they also yield essentially the same capacities at all speeds. At all ratios between these two, theory two yields higher capacities, and at more extreme ratios, theory one yields higher capacities. At unity ratio, the capacity predicted by theory two is about 65 percent higher than that predicted by theory one. Since the drive is not intended to operate beyond 2.236:1 downdrive or updrive, the more conservative result throughout the operating range is obtained by theory one, based on

maximum single band tension

The computer program can provide capacity and loss scans based on failure theories 1, 2, or 5, or can operate at a specified constant torque.

Results. Figures 1 and 2 summarize the torque capacity of the Van Doorne belt as defined by the maximum single band tension theory of failure. The axial force control system was taken to be optimized. That is, the breakaway tension ratio was evaluated for the pulley angle of wrap associated with each speed ratio setting and for a coefficient of friction of .10 between the belt and the pulley, and the operating tension ratio was then set to 75 percent of this breakaway tension ratio.

Figure 1 shows torque capacity at the input pulley while Figure 2 is for the output pulley. The torque ratio is not the inverse of the speed ratio because of losses in the belt and in the interfaces with the pulleys. In order to relate shaft torques to belt forces, the two pulley interfaces were assumed to contribute a total torque loss of 2.5 percent at all operating conditions.

In two-range transmissions, the belt transmits power back toward the engine in the lower range. It is important to keep in mind that the pulley associated with the output planetary is then the input pulley of the belt, while it is the output pulley in high range.

It can be seen that dynamic effects do cause substantial reduction in capacity when the Van Doorne belt is run faster than the 3000 input rpm at which it is rated. This belt is considerably heavier in cross section than the Battelle design. The limiting speed at full updrive ratio is approximately 7000 rpm input (15,600 rpm out). At this speed, the entire tensile capacity of the bands is needed to contain centrifugal tension.

The substantial decrease in capacity as the updrive range is entered is due to the tractive action of the bands. They always slip backwards over the struts on the smaller pulley. Hence, in the underdrive range, the bands act as flat belts to transmit a portion of the power, and the compression action transmits only the remainder. In the updrive range, however, the bands transmit power from the output pulley back to the input, and the compression action transmits all of the output power plus this returned power. The effects on band tension and strut

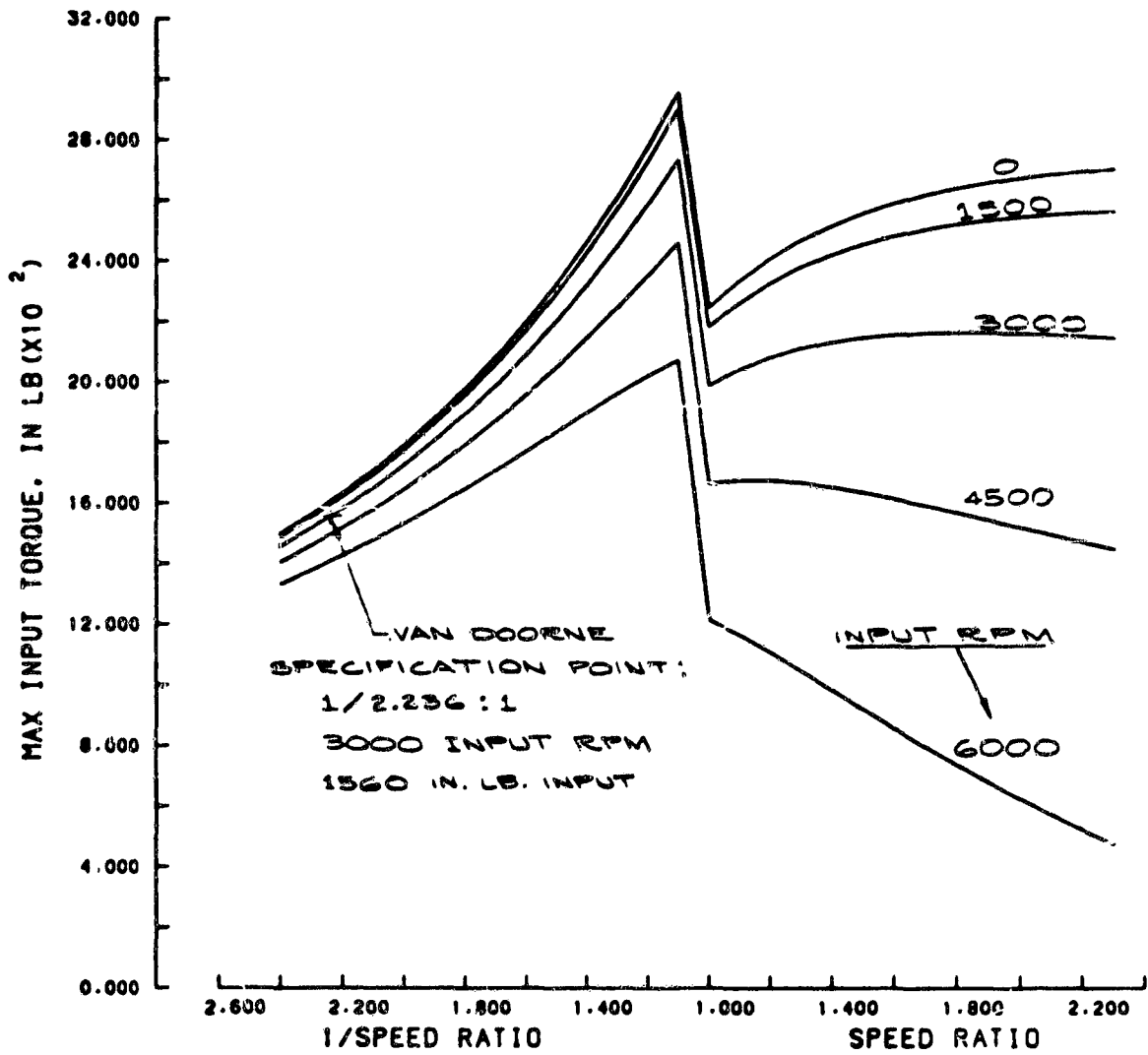


FIGURE 1. INPUT TORQUE CAPACITY AS DEFINED BY MAXIMUM SINGLE BAND TENSION

Tension ratio maintained at 75% breakaway

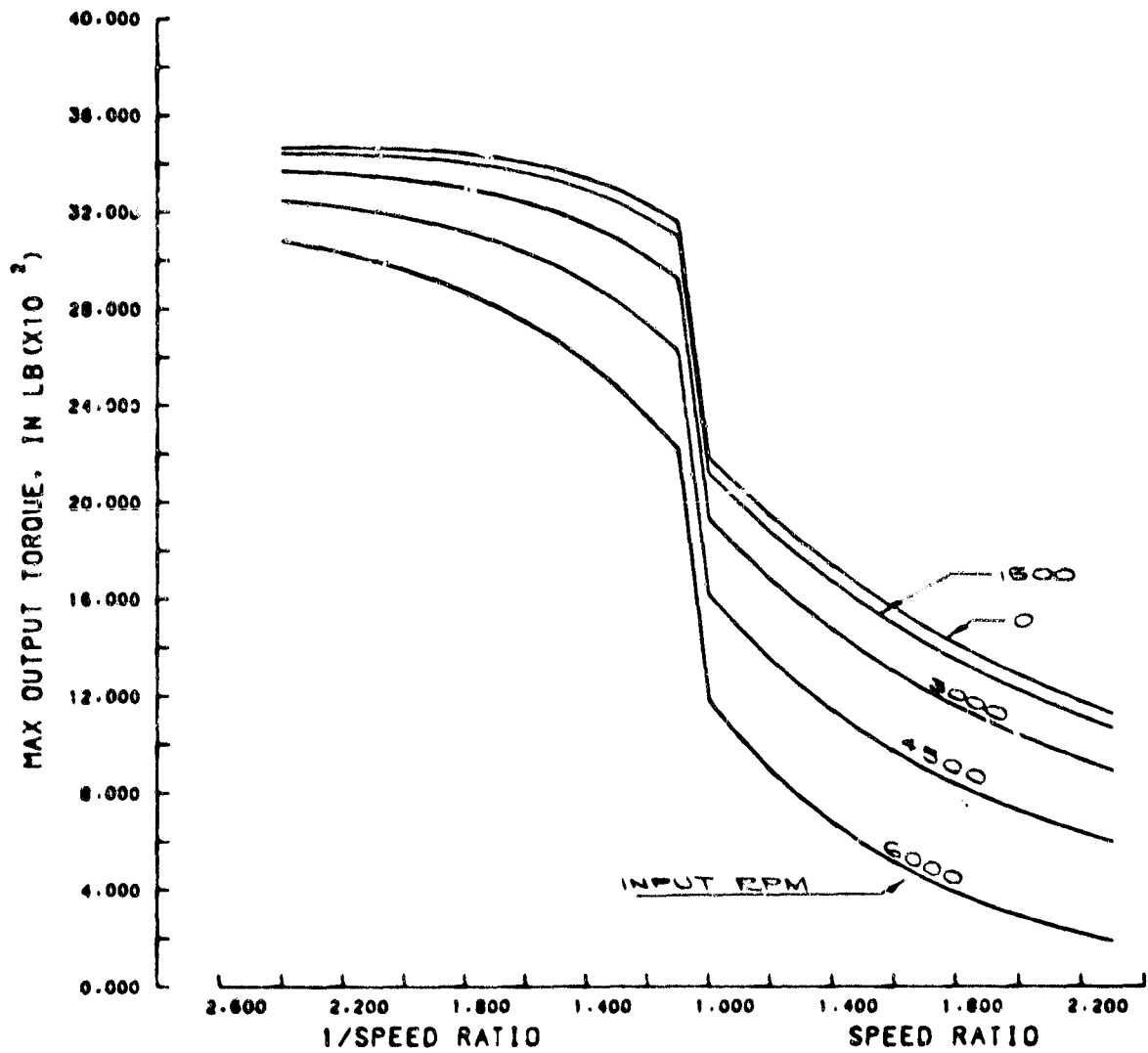


FIGURE 2. OUTPUT TORQUE CAPACITY AS DEFINED BY
 MAXIMUM SINGLE BAND TENSION

Tension ratio maintained at 75% breakaway

compression are illustrated in Table 1.

The effects of band traction vary about in proportion to the included angle of the pulleys. Since Battelle has successful experience at an included angle of 13 degrees, compared to 22 degrees for the Van Doorne design, there seems substantial potential for reducing the pulley angle.

Internal Losses

For the purpose of expressing losses as a percentage of power transmitted, full power was defined by failure theory 5 (belt slippage) so as not to bias the results by any particular theory of belt stressing. A constant total tension control system was assumed, approximating Van Doorne's. The belt was operated at a tension ratio that was 75 percent of the breakaway tension ratio. The resulting full-capacity power versus ratio curve is shown in Figure 3. Five curves at speeds from 6000 rpm to zero are actually superimposed in Figure 3, and it can be seen that speed has virtually no effect on capacity under these assumptions. Once the full load torque curve is defined as in Figure 3, efficiency scans can be made with any control system assumption that may be desired.

Figure 4 is a map of internal losses at full torque as defined by Figure 3. The shape of the curves is dominated by band friction, which goes to zero at unity ratio because there is no relative velocity between adjacent bands or between the inner band and the strut tops then, and is higher in the updrive range because of the band traction effects already discussed. The upward convexity of the 6000 and 4500 rpm curves in the region of 1.2:1 is due to failure of the belt to completely close the gaps in the strut column before they reach the input pulley. The remaining loss at unity ratio is mostly due to compression of the strut column, which causes a creep loss similar to the well-known creep of flat belts. The offset of the low point from unity speed ratio is due to creep (the pulleys must operate in an updrive configuration to achieve unity speed ratio), and is exaggerated by the computation interval of 0.1 along the speed ratio axis. The 2.5 percent pulley interface losses should be added to obtain total drive losses.

TABLE 1. SAMPLE DATA SHOWING EFFECT OF
BAND TRACTION

Van Doorne drive at 3000 input rpm.

Speed ratio	1/1.1	1.1
Tight side tension, lb	1776	1306
Slack side tension, lb	1306	1775
Centrifugal tension, lb	133	162
Tight side compression, lb	0	0
Slack side compression, lb	735	1308
Tight side net tension, lb	1643	1144
Slack side net tension, lb	438	305
Input torque, in lb	2735	2044

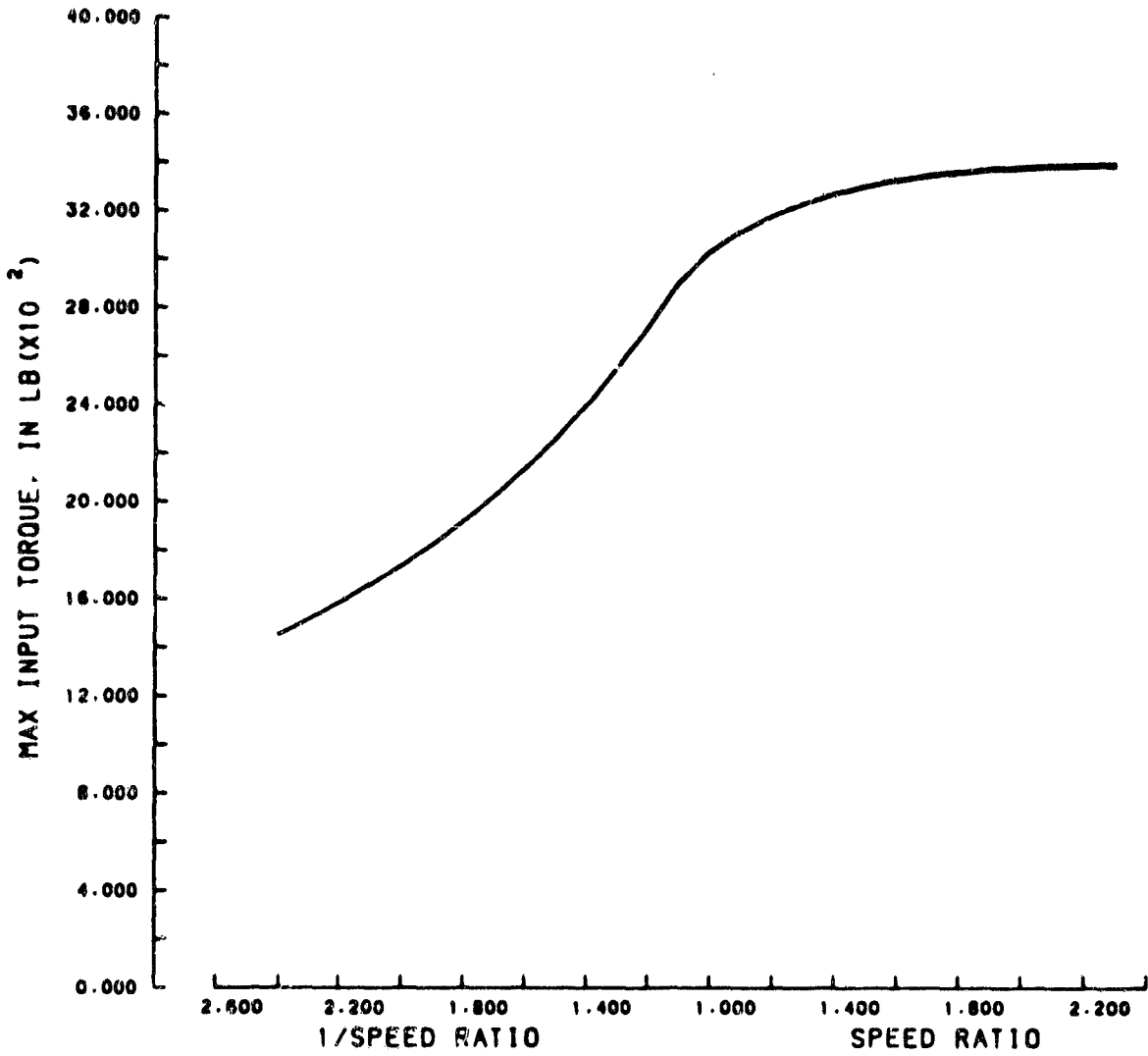


FIGURE 3. TRACTIVE CAPACITY WITH CONSTANT TOTAL TENSION CONTROL SYSTEM

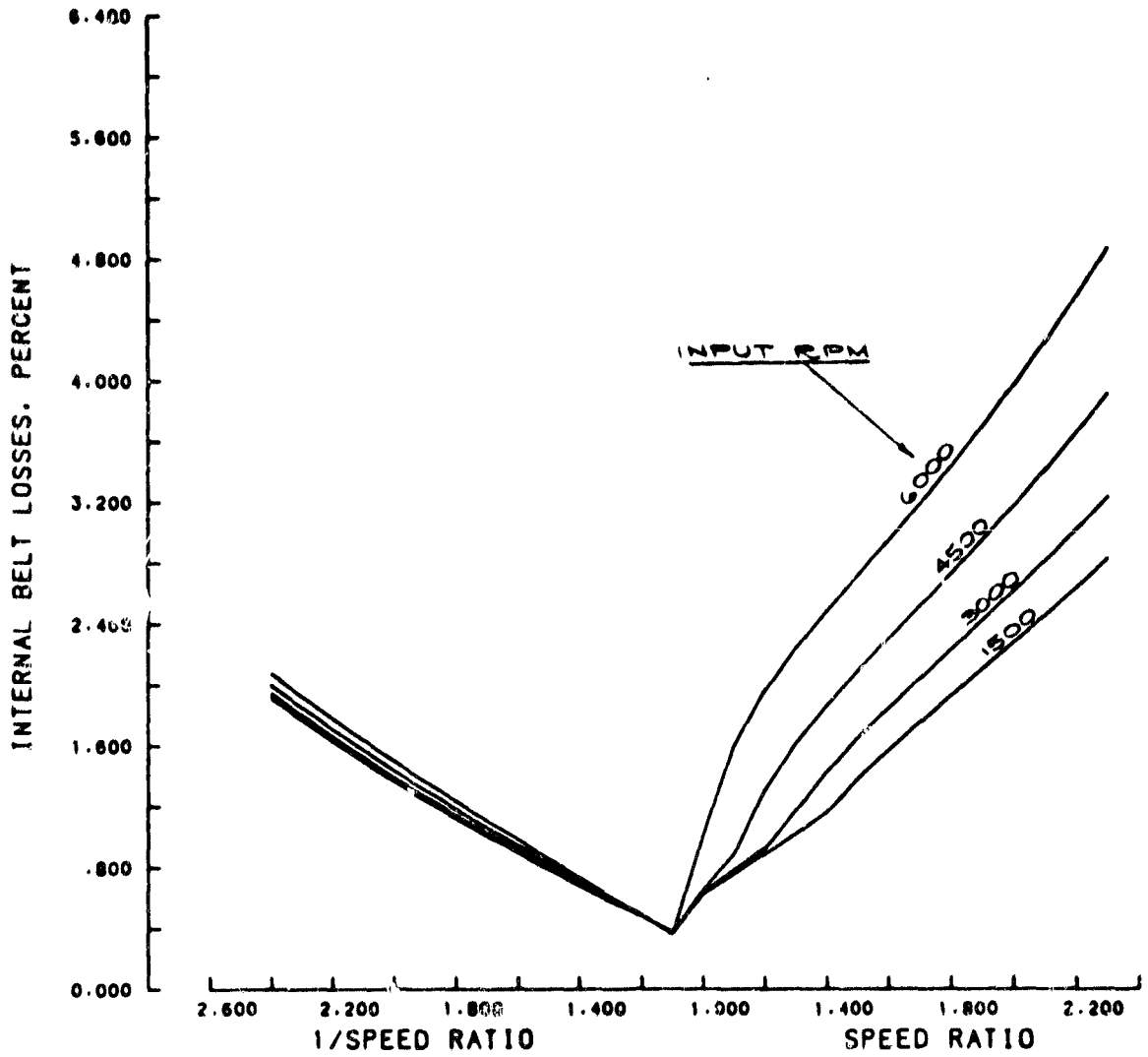


FIGURE 4. INTERNAL BELT LOSSES AT FULL LOAD

Tension ratio maintained at 75% breakaway

Figures 5 and 6 are part-load efficiency maps made on the assumption that an intelligent control system senses torque and maintains an optimum tension ratio. Figure 5 is for a torque curve at half the level of Figure 3, and Figure 6 is for one-fourth that torque level. Friction losses are somewhat higher, percentage-wise, because centrifugal tension remains the same as at full load. Gaps in the strut column are completely closed and do not cause any loss at this load level.

Figures 7 and 8 are similar part-load efficiency maps made on the assumption that a less intelligent control system, not sensitive to torque, maintains constant total tension. This is an approximation to the action of the Van Doorne industrial drive control system tested at Chrysler. At quarter load, this control system incurs substantial loss penalties in both the far updrive and the far downdrive regions. The pulley interface losses, not included in these curves, would also be greater. This is an important conclusion relative to automotive transmissions, since much of the cruising time is spent at relatively low power levels.

Figure 9 is a map of horsepower required to idle the belt with no power being delivered by the output pulley, assuming a constant total tension control system. If 2 horsepower is added everywhere to account for pulley interface losses and bearing drag, these results agree well with Chrysler's experimental data on the Van Doorne industrial drive except for one data point at maximum speed and maximum updrive ratio, where a thrust bearing in the drive apparently overheated.

Discussion of Gap Closure Loss. When a compression belt is assembled, care should be taken that the total length of the strut column not be very much shorter than the space provided by the bands. This can be accomplished by selectively fitting struts of different pitch thickness. In fact, if the belt is filled while the bands are in a circular configuration, a mild beneficial preload is induced when the belt is deformed into its ovate running configuration. In the Van Doorne belt that was examined, there was a fairly large assembly gap of .044 inch.

When the belt is under load, the gap is greatly increased by stretching of the bands and compression of part of the strut stack, and often exceeds .1 inch. This gap is concentrated in the uncompressed run

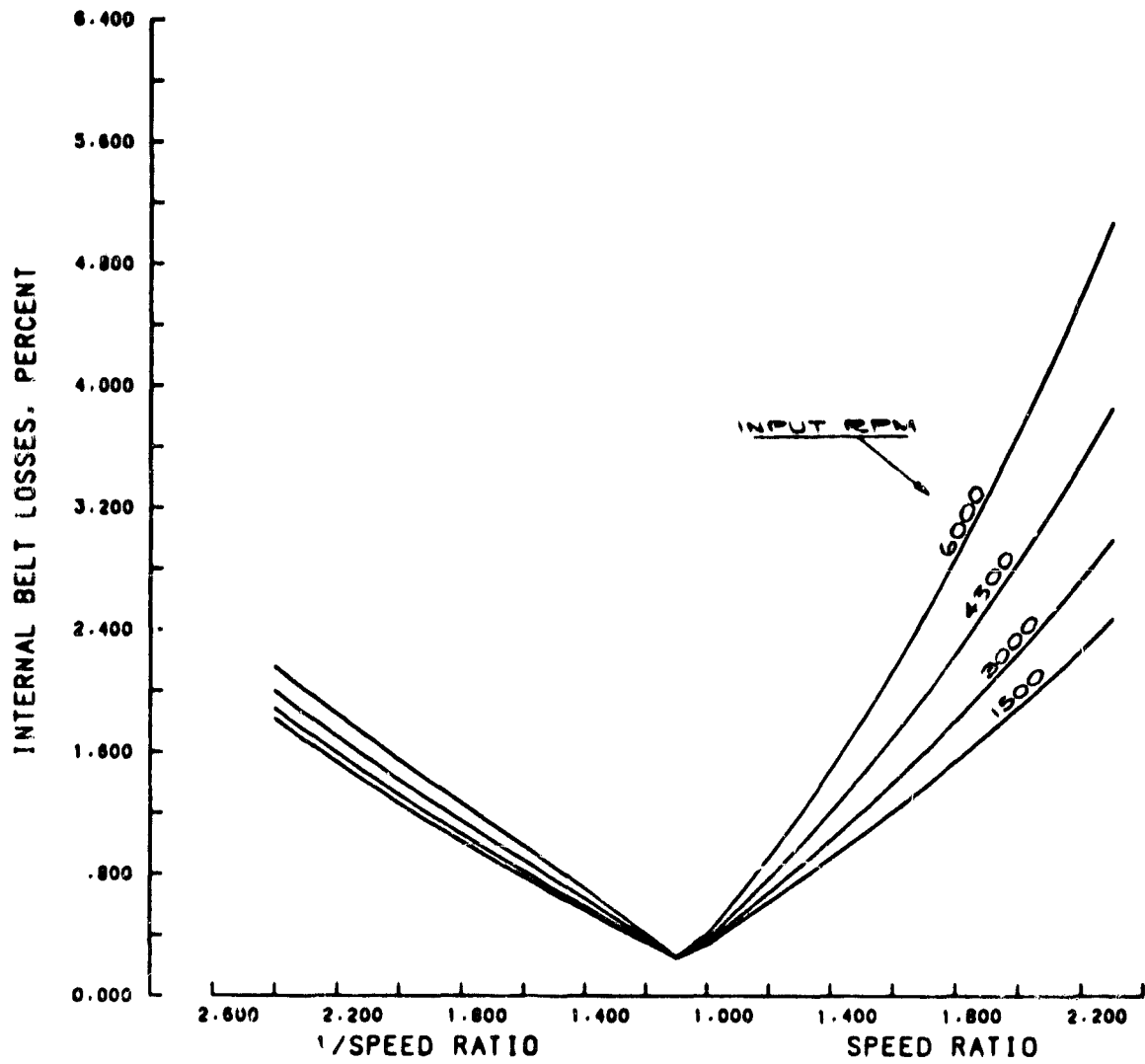


FIGURE 5. INTERNAL BELT LOSSES AT HALF LOAD

Tension ratio maintained at 75% breakaway

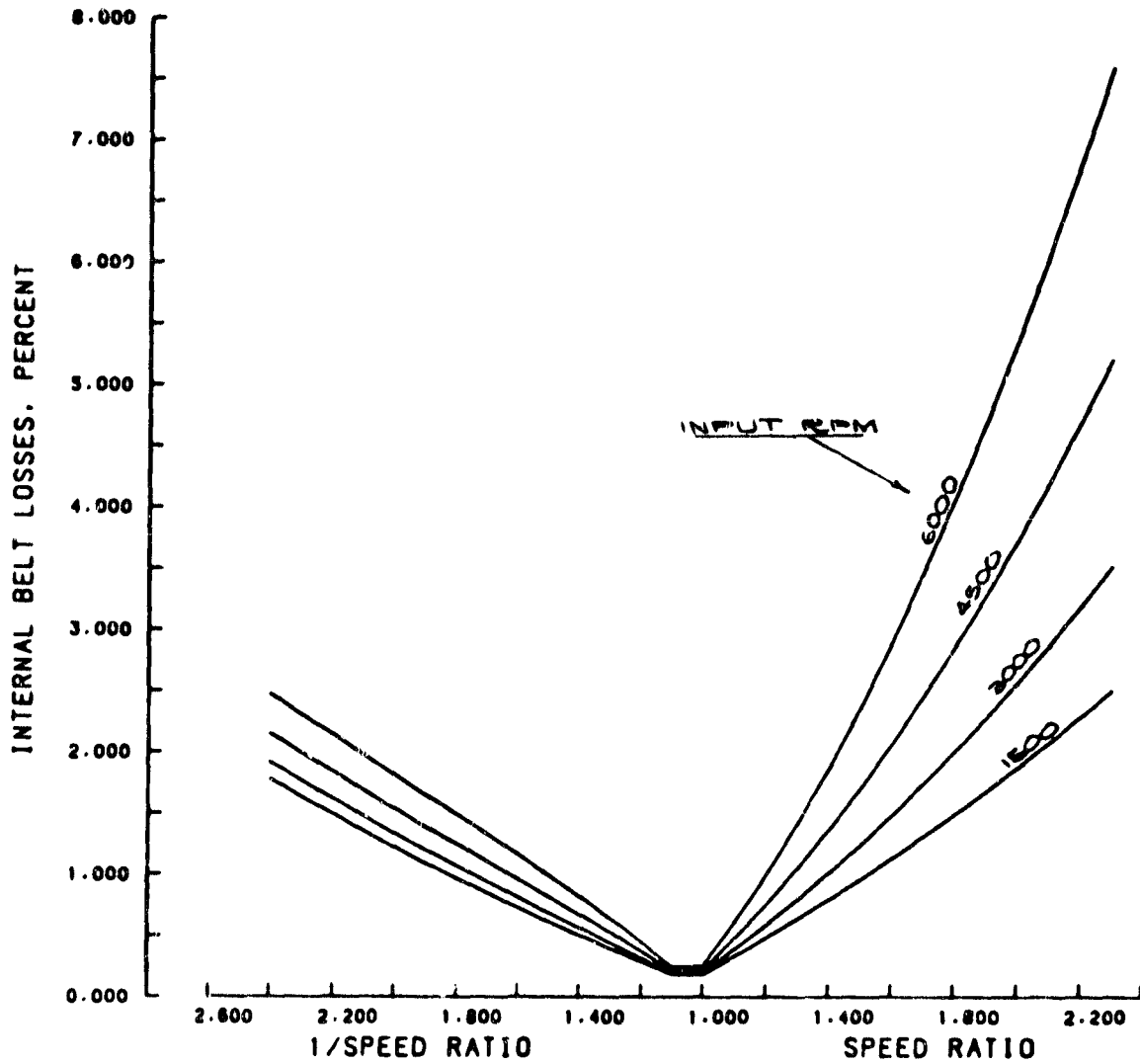


FIGURE 6. INTERNAL BELT LOSSES AT QUARTER LOAD

Tension ratio maintained at 75% breakaway

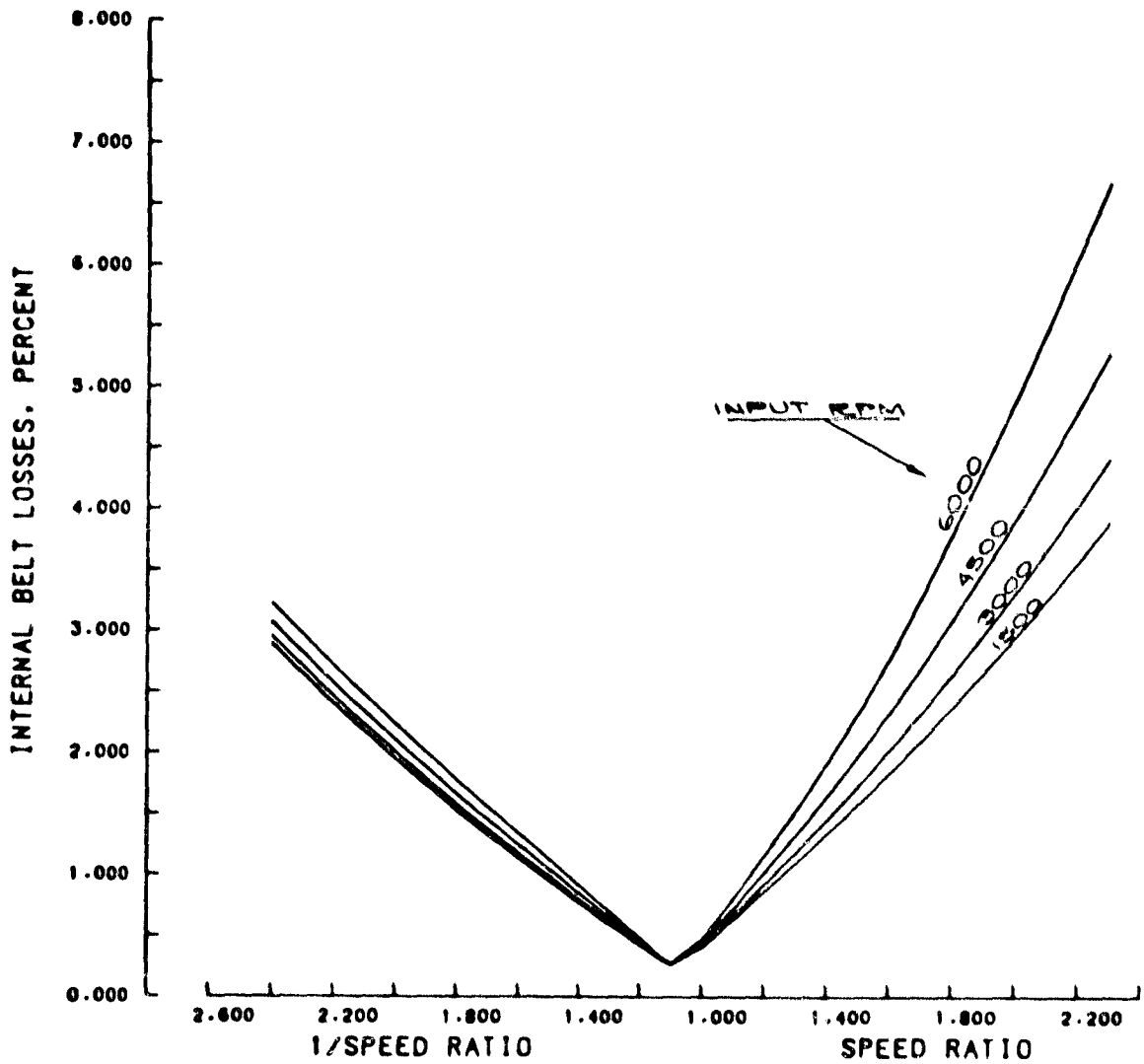


FIGURE 7. INTERNAL BELT LOSSES AT HALF LOAD

Total tension maintained constant

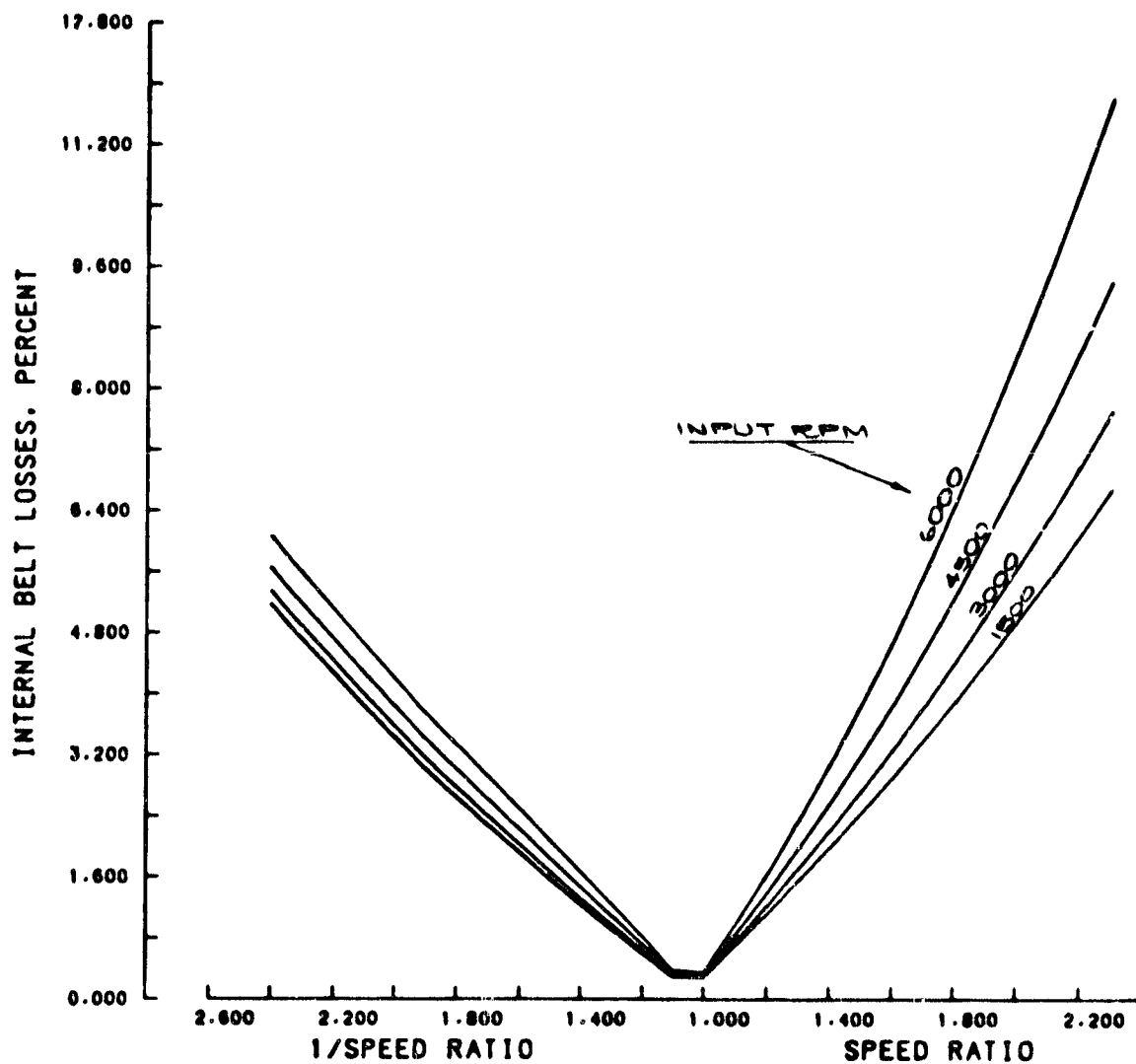


FIGURE 8. INTERNAL BELT LOSSES AT QUARTER LOAD

Total tension maintained constant

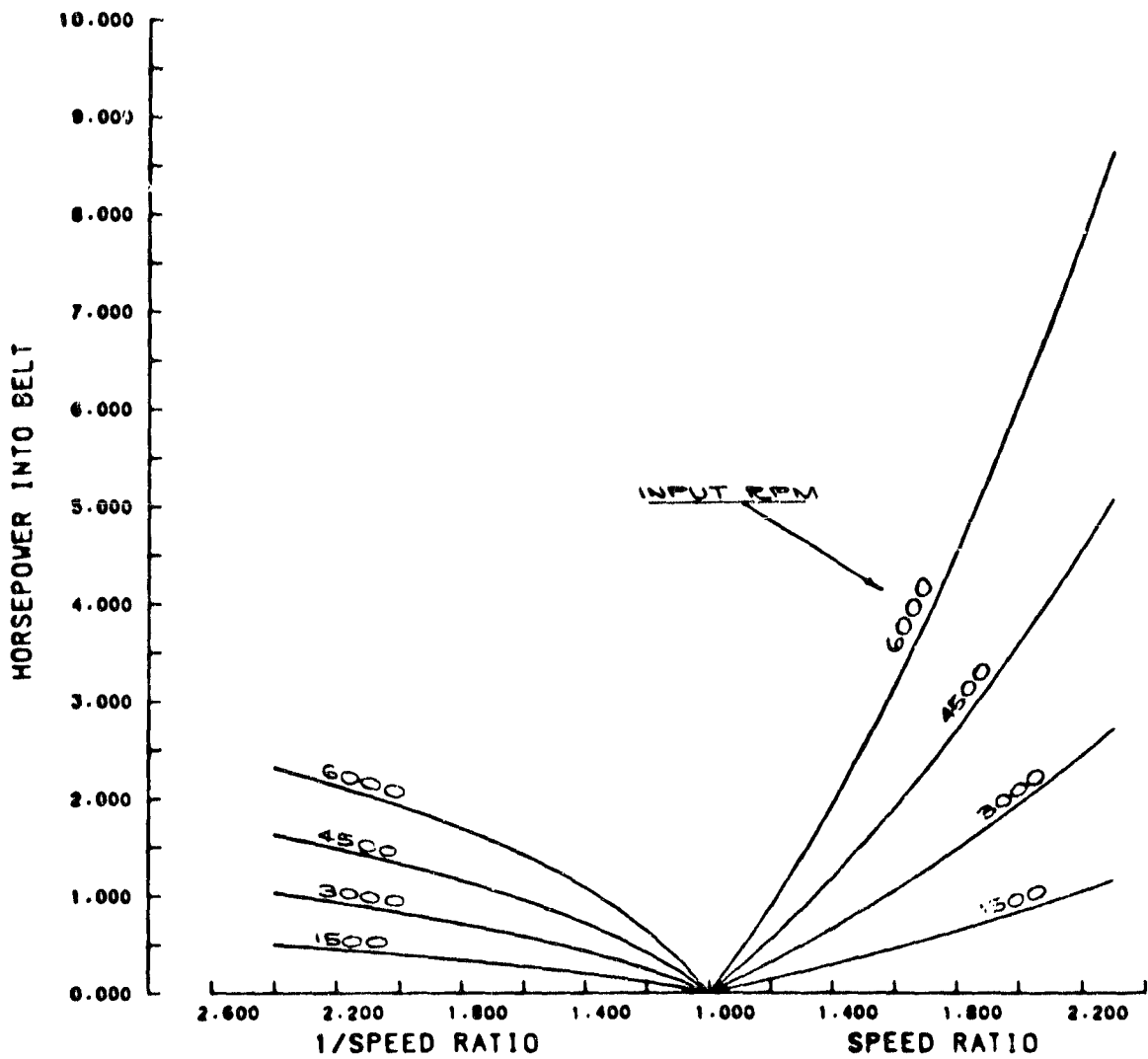


FIGURE 9. INTERNAL BELT LOSSES AT NO LOAD

Total tension maintained constant

of the belt and near the entrance of the following pulley, since the struts are pushed together elsewhere.

The struts tend to be brought into contact with one another before entering the pulley because the band stack passing through them is moving at a higher velocity than the strut stack by virtue of its greater mean radius on the pulleys. The difference in velocity is sufficient to close only a certain amount of gap, however, and this is a function of ratio setting. Any remaining gap is carried into the pulley and closed by slippage of the pulley relative to the loaded portion of the strut stack, causing a creep loss.

To the extent that a V-belt pulley can be said to have active and dormant arcs, gaps can exist only in the dormant arc. Hence, unclosed gap is distributed between the struts in the dormant arc, and the creep loss is equal to the ratio of the individual gaps to the pitch of the struts. If the tension ratio is high, which otherwise leads to good efficiency, the dormant arc will be short and the loss due to any unclosed gap will be high.

An indeterminacy exists as to the amount of gap that can be closed, because the struts are equally in contact with the inner and outer bands, and the outer band is moving at a higher velocity than the inner one. In designing Battelle belts, we have taken the pessimistic view that the struts would move with the inner band, and have designed for the gap to be closed or nearly closed under all operating conditions. In evaluating the Van Doorne configuration, however, in order not to be overly critical, we have made the more optimistic assumption that the struts move at the average of the velocities of the inner and outer bands. The data in Figures 4 through 9 are based on this assumption.

Figures 10, 11, and 12 show losses that would result if the struts were to move with the inner band, given an optimized control system. By comparison with Figures 4, 5, and 6, the gap loss can be seen to be severe at full load, moderate at half load, and negligible at quarter load. This is somewhat unfair, of course, since at unity ratio, "full load" for these curves represents a torque about 60 percent greater than the belt is able to carry by the favored theory of belt capacity. It is

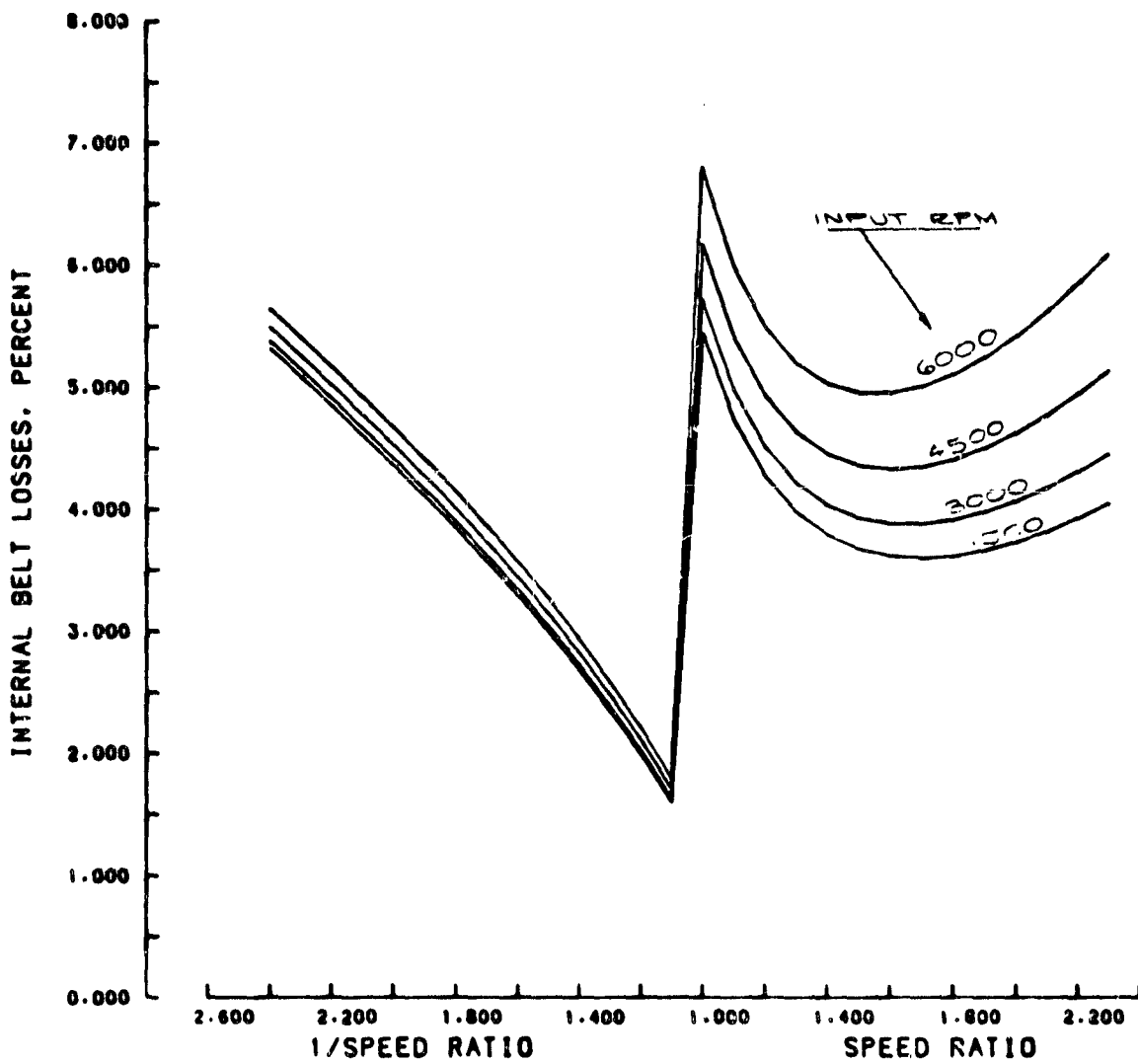


FIGURE 10. INTERNAL BELT LOSSES AT FULL LOAD WITH MORE CONSERVATIVE GAP-CLOSING ASSUMPTION

Tension ratio maintained at 75% breakaway

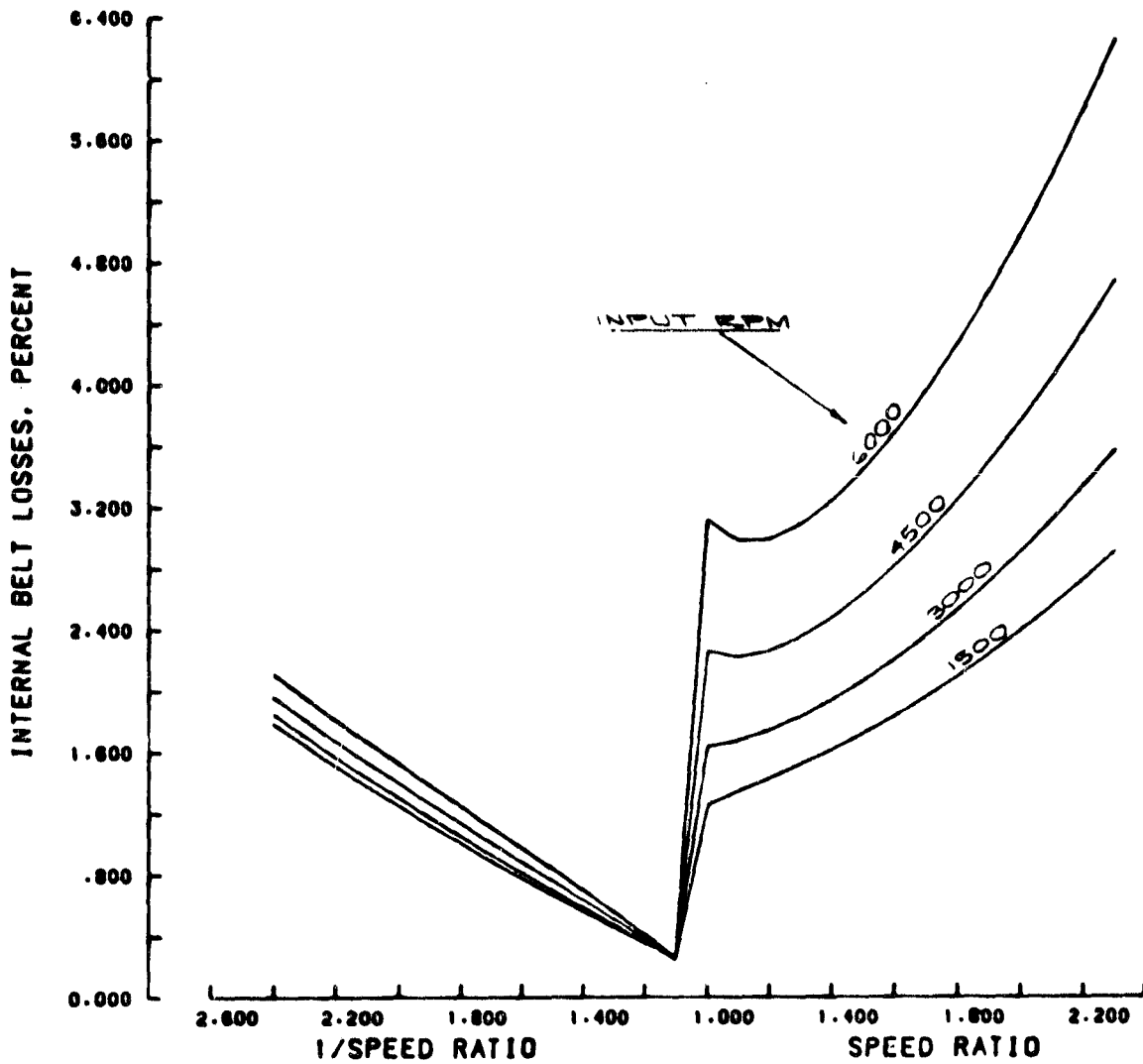


FIGURE 11. INTERNAL BELT LOSSES AT FULL LOAD WITH MORE CONSERVATIVE GAP-CLOSING ASSUMPTION

Tension ratio maintained at 75% breakaway

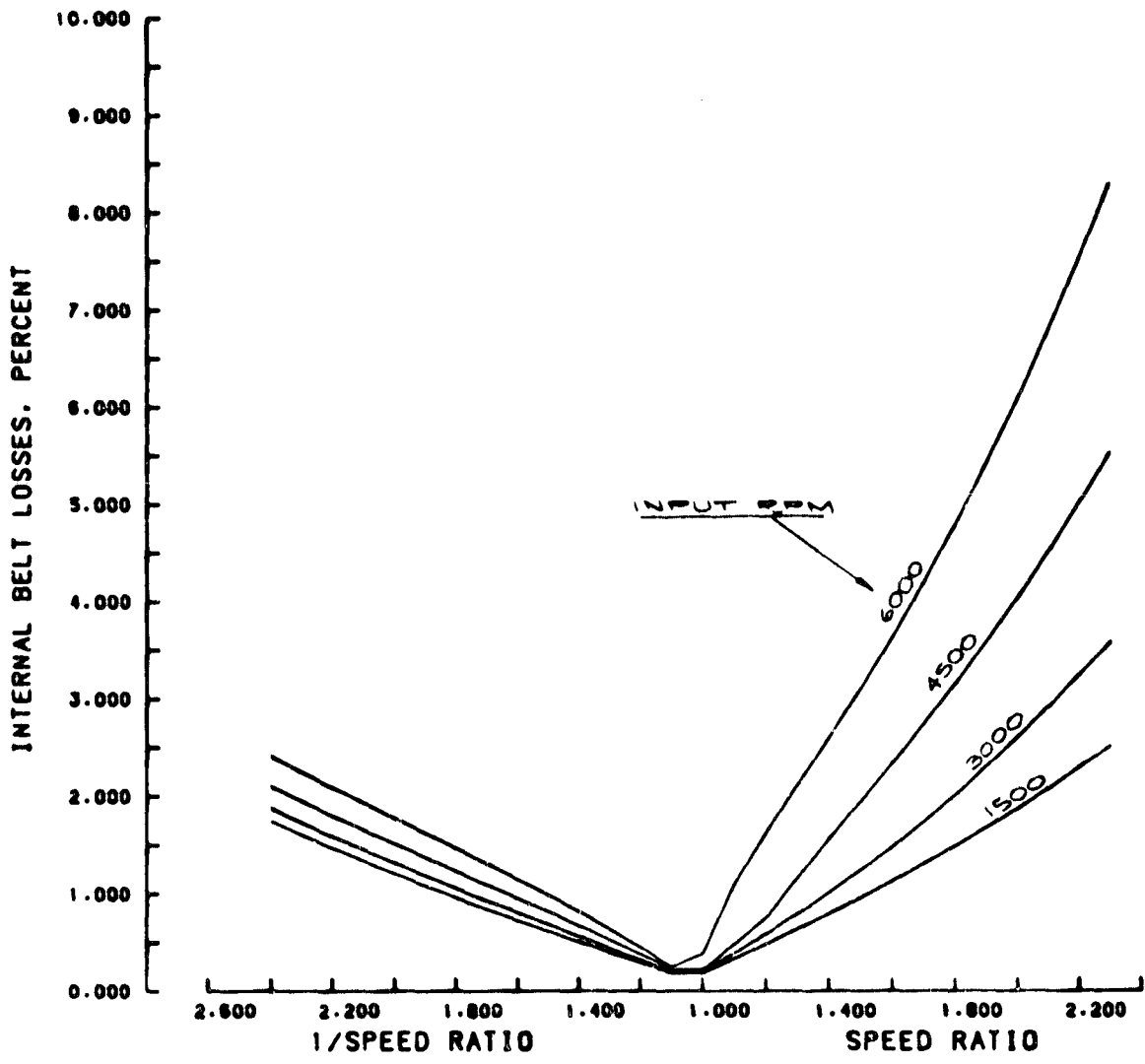


FIGURE 12. INTERNAL BELT LOSSES AT QUARTER LOAD WITH MORE CONSERVATIVE GAP-CLOSING ASSUMPTION

Tension ratio maintained at 75% breakaway

more informative to examine data for half load, unity ratio, 4500 rpm:

- Assembly gap, belt round .044 inch
- Gap in service, belt ovate, bands stretched, struts compressed .105 inch
- Unclosed gap carried into pulley .023 inch
- Resulting creep loss. 1.86 percent

Since the unclosed gap is less than the assembly gap, this loss could have been avoided by more careful assembly of the belt. At full load, unity ratio, 4500 rpm, about half the gap loss could be avoided by more careful assembly.

Clutched Flywheel Engine Response Assist

This system requires the flywheel to have access to the engine via either of two clutches arranged with different gear ratios, such that engagement of the "accel" clutch causes energy to flow from the flywheel to the engine rotor, and engagement of the "decel" clutch causes energy to flow in the opposite direction. The clutches continue to slip throughout the energy transfer, and generally do not reach a locked up condition. Considerable design flexibility is available as to the relative gear ratios of the clutches, the speed range of the flywheel, and the control philosophy for maintaining flywheel speed. The system was designed with the following objectives:

- Accelerate engine from 50,000 rpm to 80,000 rpm with no engine assist in 0.6 seconds.
- Decelerate engine from 100,000 rpm to 50,000 rpm with engine at 60 percent power in 1.0 seconds.
- Either provide enough flywheel energy for several accel-decel cycles or provide means for almost instantaneous replacement of energy dissipated in clutches.

The decel action required of the clutch is less if engine power is wasted by venting compressed combustion air, but this makes it more difficult to maintain flywheel speed in cyclical driving situations. Consequently, it has been considered worth while to attempt the more capable ERA system outlined above.

Figure 17 diagrams the way the flywheel would be used in a clutched system that appears to be fairly well optimized in its design. The wheel for this system is about 6 inches in diameter by 2 inches wide, and it operates effectively between 16,000 rpm and 27,500 rpm. Clutching events that involve simply a transfer of momentum between the flywheel and the engine appear on Figure 17 as straight lines whose slopes depend upon the gear ratio and the relative mass of the two inertias. Thus, the acceleration processes all have one slope and the deceleration processes all have another slope. If additional power is transferred by the thermodynamic action of the engine or by torque in the driveline to the wheels, the slope of the curve is altered and the clutching event does not generally

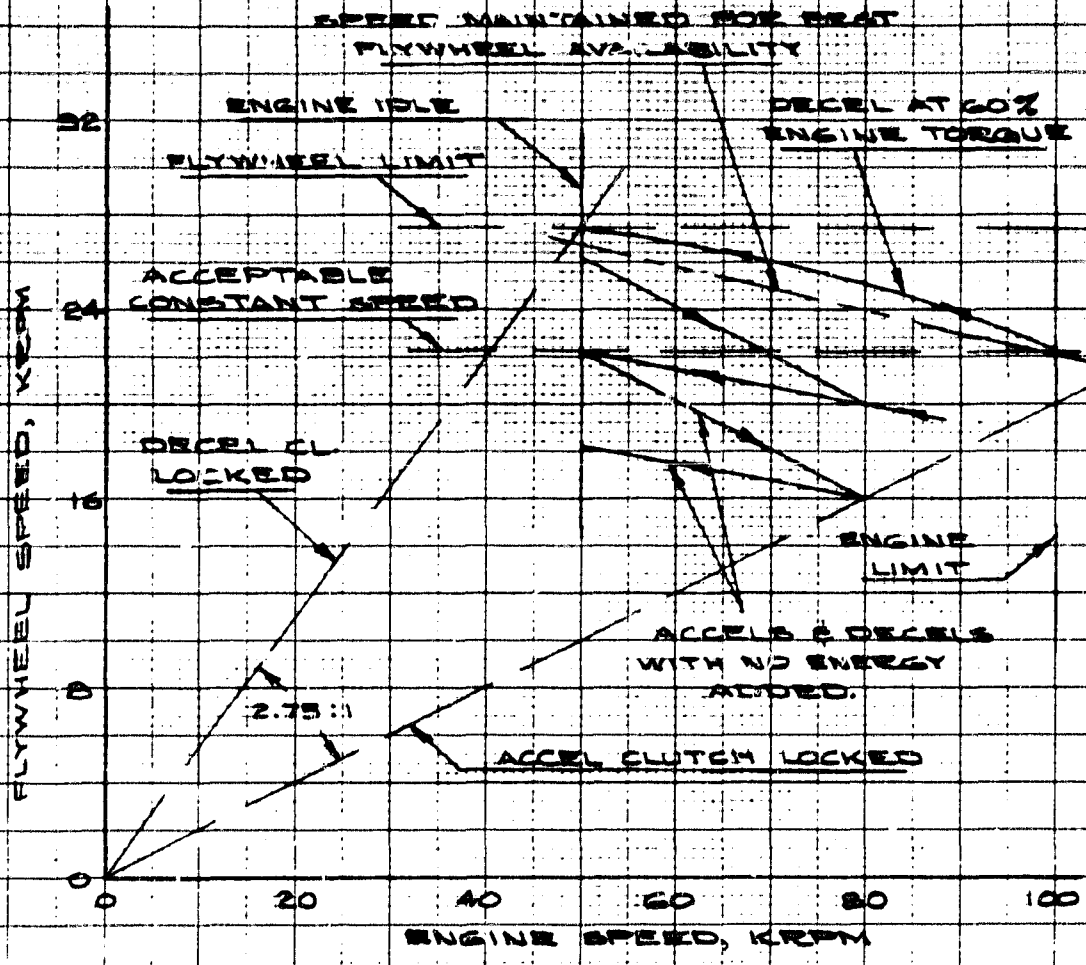


FIGURE 17
FLYWHEEL AVAILABILITY FOR
CLUTCHED ENGINE RESPONSE
ASSIST

FLYWHEEL I = 1.205 IN LB SEC²
ENGINE I = 1.0055 IN LB SEC²
DECEL CLUTCH TORQUE = 5.25 FT LB
AT ENGINE

produce a straight line on the axes of Figure 17. This is illustrated by the curve showing deceleration of the engine at 60 percent full torque.

It can be seen that the net result of an acceleration of the engine from 50,000 rpm to 80,000 rpm followed by a deceleration back to 50,000 rpm is a decrease in flywheel speed amounting to 3960 rpm, provided no energy is added to the system. More realistically, engine torque persists during the decel because of unavoidable heat storage in the regenerator, but it can be seen that the slope of the decel curve is not much affected between 80,000 and 50,000 rpm. In fact, if the engine were to be maintained at full torque throughout the accel-decel cycle, the flywheel would still "run down" rapidly. Consequently a difficult decision of policy is required: whether to allow the response assist system to become unavailable after a certain number of cycles in quick succession, or to make substantial alterations to the control philosophy in order to maintain flywheel speed.

Flywheel speed can be maintained by diverting some of the vehicle's kinetic energy into the flywheel, or by prolonging the engagement time of the decel clutch so that adequate energy is available from the engine. With the engine at 60 percent torque, the latter option would require the decel from 80,000 rpm to 50,000 rpm to be spread out over a period of 3.7 seconds, and precision would be required in the control of clutch torque. This sounds unattractive, but not as difficult as synchronizing the modulation of vehicle brakes, transmission ratio, and decel clutch torque to divert vehicle kinetic energy without producing deceleration surges that would be annoying to the driver. Also, it is not necessarily the case that vehicle deceleration is desired whenever engine deceleration is commanded.

The flywheel diagrammed in Figure 17 is heavy enough to allow some variation in control philosophy. There exists one speed (22,200 rpm) at which the flywheel is available for any accel or decel process that might be required. Since manipulation of flywheel speed via the clutches always wastes substantial portions of the energy transferred, the most efficient mode of control for a clutched flywheel is to maintain the wheel at this "acceptable constant speed" except when it is needed for rapid change of engine power. After a decel process, the wheel speed will be

higher than the acceptable constant speed and may be allowed to decay. After an accel, the wheel may be left at a somewhat lower speed until the engine is decelerated.

Another control mode, also illustrated in Figure 17, provides for better flywheel availability by always varying the flywheel speed in correspondence with engine speed, even though the flywheel may not be needed to provide a rapid change in engine speed. In this mode, two complete cycles of acceleration from idle to 80,000 rpm and deceleration back to idle are always available. This mode of control should be used if there is no provision for flywheel speed maintenance during rapid cycling of the engine power.

An earlier design iteration used a lighter flywheel that operated effectively between 16,000 and 37,500 rpm. When the clutches were sized, it was found that their diameter and weight were of more importance than the size of the wheel. By using the heavier wheel operating over a narrower speed range, the relative slip across the clutches could be reduced and their heat rates could be brought down accordingly. The size and weight of the total package was thus improved. The presently-recommended gear ratio of 2.75:1 between the decel and accel power paths is about the lowest that is convenient with a simple single-plane planetary. This ratio can be achieved with sun, planet, and ring tooth numbers of 48, 18, and 84.

Hardware for Clutched System Clutches

High performance oil cooled clutches are required for the ERA system. Relative surface speeds are high and the engagement times are long. Instantaneous heat rates are moderately high, and the total heat input per square inch of friction material is very high. Battelle has appropriate experience in the design and testing of high speed clutches wherein substantially improved heat capacity is achieved by putting most of the heat directly into the cooling oil. Some of these clutches work by shearing the oil, while others utilize inertial effects similar to those of a fluid coupling. Empirical laboratory data from these experimental clutches has been used to size clutches for the flywheel ERA system.

Battelle's experience is specifically with cone clutches of sintered bronze on steel operating at relative surface speeds from 15,000 to above 30,000 feet per minute. The technology developed includes patterns of grooving, methods of oil feed, and optimized modulation of application force. The results are presumably applicable to plate clutches as well, providing the friction surfaces are rigid and flat enough to insure the same uniformity of surface contact achieved by the cones, and providing the cooling oil is similarly constrained against being slung out by centrifugal force. These conditions are not met by plate clutches of conventional design. The plates of these high speed clutches would be much thicker than conventional plates and would be positioned to remain out of contact with one another when the clutch is disengaged. Consequently, the number of friction surfaces should be kept low, preferably not more than two.

Both cone and plate clutches have been sized for the ERA application. Since the empirical data is for cones, these are presented with greater confidence. The advantages of cone clutches are that their rigid shapes lead toward more accurate surface mating, their nearly axial flow paths lead toward better coolant retention, they provide more uniform velocity throughout the friction surface, they can be designed for more area per face of given outer diameter, and they require only about one-fourth as much axial application force. The advantages of plate clutches are that their flat surfaces are easier to make, and they tend to be more compact unless the cone parts can be packaged around other components.

Each clutch can be located at several different places relative to the parts of the planetary speed increaser. Some locations offer high relative speed and low torque, while others offer lower speed and higher torque. The thermal loading of each clutch is independent of its location. The designs were based on initial heat rates of 44 Btu/sec for the accel clutch and 50 Btu/sec for the decel clutch. Clutch sizes required for the various alternative locations are summarized in Tables 2 and 3.

Another design variable reflected in these tables is the style of grooving of the friction faces. "Groove-on-groove" clutches have both surfaces grooved, with the grooves running at different angles so that

TABLE 2

ACCEL CLUTCH SIZES FOR "HEAVY" FLYWHEEL

CLUTCHED INERTIA .0085 IN LB SEC²

ACCEL 30,000 RPM TO 80,000 RPM IN 0.6 SEC

WITH NO ENGINE ASSIST.

FLYWHEEL RANGE 27,500 RPM TO 16,000 RPM

PLANETARY RATIO 2.75 : 1 (DIRECT DRIVE IN ACCEL)

LOCATION OF CLUTCH, MAX SPEED & T	TYPE OF CLUTCH	NUMBER OF FACES	SIZE OF FACES, IN.	AXIAL FORCE REQ'D, LB.	COOLANT FLOW, GPM	
ON FLYWHEEL SHAFT 17,500 RPM 18.54 FT LB.	SMOOTH-ON-GROOVE CONE	1	4.5 DIA x 1.23 WIDE	318	1.9	
	GROOVE-ON-GROOVE CONE	1	4.0 DIA x 1.16 WIDE	313	2.7	
	SMOOTH-ON-GROOVE PLATE	1	5.75 OD x 3.50 ID	1335	2.1	
	GROOVE-ON-GROOVE PLATE	1	5.25 OD x 3.10 ID	1290	4.3	
ONE FACE BETWEEN SUN AND PLANET CARRIER, ONE FACE BETWEEN SUN & RING 27,500 RPM 7.55 FT LB	SMOOTH-ON-GROOVE CONE	2	4.86 DIA x .65 WIDE	168	3.7	MAX DIA.
	SMOOTH-ON-GROOVE CONE	2	4.00 DIA x .80 WIDE	185	3.4	MIN DIA.
	GROOVE-ON-GROOVE CONE	2	3.47 DIA. x .60 WIDE	141	3.8	
	SMOOTH-ON-GROOVE PLATE	2	4.86 OD x 2.92 ID	904	5.0	
	GROOVE-ON-GROOVE PLATE	>2				
BETWEEN PLANET CR. & RING GEAR, 10,000 RPM 32.45 FT LB.	SMOOTH-ON-GROOVE CONE	1	5.25 DIA x 1.32 WIDE	417	2.0	
	GROOVE-ON-GROOVE CONE	1	4.75 DIA. x 1.17 WIDE	492	3.0	
	PLATE	1		HIGH		

TABLE 3

DECEL CLUTCH SIZES FOR "HEAVY" FLYWHEEL"

CLUTCHED INERTIA .0085 IN LB SEC²

DECEL 100,000 RPM TO 50,000 RPM IN 1.0 SEC.

WITH ENGINE AT 60% FULL TORQUE.

FLYWHEEL RANGE 27,500 RPM TO 16,000 RPM,

PLANETARY RATIO 2.75:1 (DIRECT DRIVE IN ACCEL)

LOCATION OF CLUTCH, MAX RELATIVE SP & TORQUE	TYPE OF CLUTCH	NUMBER OF FACES	SIZE OF FACES, IN.	AXIAL FORCE REQ'D, LB	PLANT FLOW, GPM
ON 20,000 RPM SHAFT (BETWEEN PLANETARY & MAIN GEARBOX) 14,180 RPM 26.25 FT LB	SMOOTH-ON-GROOVE CONE	1	5.25 DIA x 1.27 WIDE	386	2.4
	GROOVE-ON-GROOVE CONE	1	4.75 DIA x 1.16 WIDE	373	3.2
	SMOOTH-ON-GROOVE PLATE	1	6.45 OD x 3.87 ID	1690	2.7
	GROOVE-ON-GROOVE PLATE	1	6.00 OD x 3.60 ID	1541	5.3
	SMOOTH-ON-GROOVE PLATE	2	5.00 OD x 3.00 ID	1041	3.2
	GROOVE-ON-GROOVE PLATE	2	4.50 OD x 2.70 ID	1061	3.8
BRAKE ON RING GEAR 22,290 R.P.M 16.70 FT LB	SMOOTH-ON-GROOVE CONE	1	5.25 DIA x 1.27 WIDE	344	3.9
	GROOVE-ON-GROOVE CONE	1	4.29 DIA. x .98 WIDE	247	3.8
	GROOVE-ON-GROOVE CONE	1	4.00 DIA x 1.40 WIDE	282	3.7
	SMOOTH-ON-GROOVE PLATE	2	4.60 OD x 2.76 ID	755	3.5
	GROOVE-ON-GROOVE PLATE	2	4.00 OD x 2.40 ID	760	4.7

MAX
DIA

MIN
DIA

the action remains smooth. These clutches provide optimum cooling of both friction faces and allow very high heat rates at surface speeds between 15,000 and 25,000 feet per minute. They also require somewhat less axial force and provide a softer lock-up than conventional clutches. Above 25,000 feet per minute, however, their thermal capacity decreases rapidly.

"Smooth-on-groove" clutches are of more conventional design with only the bronze face grooved. They provide better hydrodynamic support and their thermal capacity continues to increase up to the highest speeds tested. They are easier to make, particularly in the conical configurations, require less coolant, and are less sensitive to non-optimum modulation of application force.

Tables 2 and 3 provide information that can be used to make design layouts of the various alternative mechanical arrangements. The final choice between them will be based largely on packaging considerations which can be evaluated by such layouts.

Speed Increaser. Brief consideration was given to the use of a traction planetary drive, with particular reference to a small gas turbine reduction unit developed by Toyota. It was concluded that the traction drive would not be unduly large compared to the flywheel and other ERA components. It would be compatible with the nearly oil-free environment of the flywheel housing and might contribute to the support of the flywheel. Noise reduction would be the primary motivation for its use.

A geared planetary, on the other hand, is compatible with the large quantities of oil circulated through the clutches, and it allows axial motions of its parts that can be useful for engaging the clutches.

It was concluded that the transmission of torque to the planet rollers of a traction planetary has not been solved in a completely satisfactory manner, and that substantial development effort might still be required to make the traction planetary functional and reliable in this application. Consequently, a geared planetary is recommended as a more prudent approach, at least for the first generation ERA systems.

Flywheel. For the modest energy storage requirements of the ERA system, a steel disk wheel of approximately constant thickness appears obviously to be the cost-effective choice. Since effective containment of the wheel is hardly feasible because of the weight and cost of the housing that would be required, stress levels should be conservative, a tough, high strength forging steel should be used, and careful attention should be given to quality control.

A six-inch steel disk at 27,500 rpm is stressed to 22,600 psi at the center of its hub. The wheel must be designed, however, for the possibility that a malfunction of the decel clutch with the engine at max speed could drive the wheel to twice its normal speed and four times its normal stress. This means that the material must have a yield stress above 90,000 psi. Since even a small hole at the center of the disk will further double the stress, it is important to mount the disk in such a way that no hole is required. This can be done by forging it with integral stub shafts protruding on each side.

Potential Problems with Clutched ERA

The clutched system appears simple in concept, but actually its execution involves complex control intelligence because of the many situations that may arise when flywheel speed is an independent and, to some degree, uncontrollable variable. There are also some aspects of the hardware that have not yet been fully addressed. Some specific problems to be dealt with during future development are the following:

- The accel clutch comes to zero relative speed before the engine ceases its acceleration in some anticipated operating situations. Provision is needed to disengage or freewheel so that the flywheel does not hinder further acceleration of the engine under its own power.
- It has been assumed that rapid accel or decel of the engine can be followed by similarly rapid changes in transmission ratio and with such accurate control that unacceptable torque transients are not generated in the driveline. It remains to be demonstrated that this can be achieved with a steel belt transmission.

- The high performance clutches require a source of cooling oil capable of delivering 3 to 6 gpm, depending on clutch style, for the duration of the engagement. This is within the capability of the pump presently anticipated, but the parasitic losses in this large pump may be substantial. Also, the oil passing through the clutches will be highly aerated and may have to be kept separate from the oil used in the hydraulic controls.
- Aerodynamic drag on the flywheel was not evaluated as part of the work at Battelle. Since most other users of energy storage flywheels have taken the trouble to evacuate their housing, there is some concern that the losses running at atmospheric pressure may be greater than anticipated.

Steplessly Variable Engine Response Assist

In this system the clutches and 2.75:1 planetary are replaced by a steplessly variable drive, presumably a second belt. Since the power path between the flywheel and the engine is energy-conservative, this system does not tend to run down its flywheel. A one-to-one correspondence between engine speed and flywheel speed may be established such that the total kinetic energy of the system is constant and it appears "inertialess" to an external observer. The advantages of this system are:

- Safer because it always responds to driver command in the same way, while the clutched system becomes unavailable if the flywheel runs down.
- More efficient, 95 percent compared to only about 60 percent for the clutches.
- Troublesome auxiliaries such as the clutch cooling oil and heat rejection facilities are eliminated. The ERA belt can share auxiliaries already required for the main transmission belt.

- Control logic is greatly simplified since flywheel speed is eliminated as an independent variable.
- The flywheel size can be less than half that for the clutched system because the wheel operates over a wider speed range, delivers energy more efficiently, and stores enough for only one accel.

Added complexity of the driveline is an obvious disadvantage of this system. Overall packaging, weight, and cost tradeoffs are too complex to anticipate without more detailed engineering of the steplessly variable ERA.

This system was not pursued because it was regarded as outside the scope of the current project. We do believe, however, that from an engineering standpoint it is an attractive alternative to the clutched system.

A transmission concept was also proposed wherein the ERA belt provides the second power path of a single range, split power main transmission. The complexity of the second belt is thus partially offset by elimination of a chain or gearing.

The efficiency of the steplessly variable ERA system also opens interesting possibilities for the storage of vehicle kinetic energy. Mileage can be substantially improved on the urban driving cycle by saving only the energy associated with stops from 30 to 35 mph. The clutched system cannot save energy effectively because, with energy transfer only 60 percent efficient in each direction, only about one-third of the energy captured can be returned. With the steplessly variable system, however, a wheel the same size as that recommended for the clutched system, operating at 37,500 rpm, could store enough energy to accelerate the engine plus 75 percent of the energy needed to accelerate a 2950-pound car to 30 mph.